# Genesis And Consequences Of Fracturing In The Cretaceous Carbonate Reservoirs Of North Oman

Mr. SALAH HAFIDH HASHIM AL-DHAHAB

Submitted for the degree of Doctor of Philosophy

Heriot-Watt University

Institute of Petroleum Engineering

May 2010

# ABSTRACT

North Oman is underlain by Cretaceous Natih and Shuaiba carbonates, which are important hydrocarbon reservoirs. Fracturing, especially fracture clusters, contributes significantly to reservoir performance. The fractures in the Natih are strongly affected by mechanical layering, whereas the Shuaiba is less obviously layered, except in the NW, where Upper Shuaiba is present. The fracture network of the Lower Shuaiba in the central and SE region of north Oman is dominated by fault–related fractures and associated corridors. Late Cretaceous deformation created NW-WNW strike-slip faults and associated fractures, as well as activation of salt diapirs. Tertiary deformation (NE shortening) resulted in the creation of abundant NE oriented background fractures, and more importantly NE fracture corridors that act as conduits to flow. Salt diapirs, when reactivated during Tertiary events, result in more intense fracturing locally. Field scale analyses of the fracture networks for Ghaba North and Lekhwair A North (both Shuaiba), based on BHI logs, reveal a change in dominant fracture orientation between the SE and the NW parts of north Oman. The NE fracture corridors play a major role in connecting the NW-WNW fractures seen in Lekhwair A North, and the current NE oriented maximum horizontal stress may also play a role.

# DEDICATION

To my late father and my new born son

"Essentially, all models are wrong, but some are useful"

Box, George E. P

# DECLARATION STATEMENT

**Copyright and ownership:**

The work presented in this thesis originates from three sources:

a- Review of existing research undertaken by Petroleum Development Oman PDO staff, Shell Exploration and Production EP Technology Research staff and other academic or consultant researchers.

b- Review of pre-existing researches undertaken by the author either alone or with other staff, while working for PDO 1996-2002 and Shell 2002-2006.

c- Work done specifically by the author for this PhD thesis, while in Heriot Watt University Institute of Petroleum Engineer IPE, during the final year.

It is essential to note that the first three years of this PhD were undertaken as part-time, distance learning, while the author worked for Shell EP Technology. The agreement with Shell was to work as much as possible on the PhD research, hence some of the work included, especially in Chapter 2: Regional Analysis, is related to source b (above). In all chapters, a reference is quoted whenever the data or ideas presented originate from other sources (a or b sources). It is almost impossible to partition the chapters and their sub-sections by source, since it is necessary to present the thesis in a "story line" approach; however the table below provides guidance regarding the intellectual ownership of the work included:

***How to read the table?*** *N = not applicable, L: M: H is Low, Medium or High with respect to dependency or work presented origin. For a, b and c see above definition*

| Chp | Section | Title | a | b | c |
|---|---|---|---|---|---|
| 1 | 1.1 | Background | N | L | H |
| | 1.2 | Objective | N | N | H |
| | 1.3 | Fracture definition and terminology | N | N | H |
| | 1.4 | Methodology and approach | N | N | H |
| | 1.5 | SVS and other software | N | N | H |
| | 1.6 | On Fracture characterization | N | N | H |
| | 1.7 | Data availability and limitation | L | N | H |
| | 1.8 | Pre-view of subsequent chapters and main conclusions | M | M | H |
| 2 | 2.1 | Introduction | M | N | M |
| | 2.2 | Stratigraphy | H | N | L* |
| | 2.3 | Tectonic | H | N | N |
| | 2.3.1 | Tectonic: Salt Halokinesis | H | N | N |
| | 2.3.2 | Tectonic: Defining the structural grains of north Oman | L | H | N |
| | 2.3.3 | Tectonic: north Oman Faults | H | N | N |
| | 2.3.4 | Tectonic: Uplift | H | N | N |
| | 2.3.5 | Tectonic: Stress analysis | H | N | N |
| | 2.3.6 | Tectonic: Diagenesis | H | N | N |
| 3 | 3.1.1 | Regional fracture analysis: Natih Fm: Salakh Arch | H | L | N |
| | 3.1.2 | Regional fracture analysis: Natih Fm: Natih Field | H | N | M** |
| | 3.1.3 | Regional fracture analysis: Natih Fm: Fahud Field | M | M | M** |
| | 3.1.4 | Regional fracture analysis: Natih Fm: Ghubar Field | H | N | M** |
| | 3.2.1 | Regional fracture analysis: Shuaiba Fm: J. Madar | H | N | N |

| | | | | | |
|---|---|---|---|---|---|
| | 3.2.2 | Regional fracture analysis: Shuaiba Fm: Huqf | H | N | N |
| | 3.2.3 | Regional fracture analysis: Shuaiba Fm: Ghubar Field | L | M | M** |
| | 3.2.4 | Regional fracture analysis: Shuaiba Fm: Qarn Alam F | L | M | M** |
| | 3.2.5 | Regional fracture analysis: Shuaiba Fm: Ghaba North F | M | M | M** |
| | 3.2.6 | Regional fracture analysis: Shuaiba Fm: Burhaan Field | H | N | M** |
| | 3.2.7 | Regional fracture analysis: Shuaiba Fm: Saih Rawl Field | N | H | M** |
| | 3.2.8 | Regional fracture analysis: Shuaiba Fm: Musallim Field | H | L | M** |
| | 3.2.9 | Regional fracture analysis: Shuaiba Fm: Al Huwisah F | M | N | M** |
| | 3.2.10 | Regional fracture analysis: Shuaiba Fm: Yibal Field | H | N | M** |
| | 3.2.11 | Regional fracture analysis: Shuaiba Fm: Dhulaima Field | H | N | M** |
| | 3.2.12 | Regional fracture analysis: Shuaiba Fm: Lekhwair Field | H | N | M** |
| | 3.3.1 | Discussions: Fractures drivers | L | L | H |
| | 3.3.2 | Discussions: Fractures conductivity | M | L | H |
| | 3.3.3 | Discussions: Fractures indicators | M | L | H |
| | 3.3.4 | Discussion: Micro-Fractures | M | L | H |
| 4 | 4.1 | Ghaba North GN Field introduction | M | L | M |
| | 4.2 | GN Fractured data import to SVS | L | L | H |
| | 4.3 | GN Curvature data analysis -imported to SVS | L | L | H |
| | 4.4 | GN Well test and well interference test analysis | M | N | M |
| | 4.5 | GN Stress data analysis | M | N | M |
| | 4.6 | GN Sand box analogue for Ghaba North | H | N | L |
| | 4.7 | GN Fracture spacing calculations in SVS | N | N | H |
| | 4.8 | GN well by well fracture analysis in SVS | N | N | H |
| | 4.9 | GN Statistical analysis of Ghaba North Shuaiba fractures | N | N | H |
| | 4.10 | GN Testing Fracture concepts | N | N | H |
| | 4.11 | GN Building the fracture models | N | N | H |
| 5 | 5.1 | Lekhwair A North LAN Field introduction | M | L | M |
| | 5.2 | LAN Fracture related data | N | N | H |
| | 5.3 | LAN fracture characterization | M | N | H |
| | 5.4 | LAN Fracture concepts | M | N | M |
| | 5.5 | LAN Building fracture models | N | N | H |
| 6 | 6.1 | Building GN simulation model | N | N | H |
| | 6.2 | GN fracture simulation result analysis | N | N | H |
| 7 | 7.1 | ANALYSIS: Underlying Geology | N | N | H |
| | 7.2 | ANALYSIS: Fracture network genesis | N | N | H |
| | 7.2 | ANALYSIS: Flow analysis | N | N | H |
| | 7.2 | ANALYSIS: 3D modelling analysis | N | N | H |
| 8 | | SUMMARY | N | N | H |

* Map analysis of Natih thickness and porosity-permeability plots for Shuaiba presented are based on writer's work while in HW IPE ©

** For all the subsurface fields, the Bore Hole Image BHI analysis of fracture picks (objects) and observations presented is done by the author, except for Yibal field

+ For LAN field, the fracture characterization part has been done by PDO, only a review of the analysis and interpretation of the observations is done by the author

# Any interpretation of field production history is done by the author

***Acknowledgement:***

***I would like to express my gratitude to Shell EP Technology for their partial sponsorship and Petroleum Development Oman for their partial sponsorship and the use of their data for this PhD. In particular, I would like to thanks the following individuals for their support: Khalid al Khabouri, Paul Wagner, Jan-Michael Dwan, Abdullah Shizawi and Khalid al Rawahi (for their logistical support); Pascal Richard (PDO- for his technical supervision and discussions), Keith Rawnsley, Roeland Roeterdink, Ali al Sulimani, Loic Bazalgette and Simon Price (for their technical support in discussion and provision of data), Mohammed al Abri (for his help in the simulation chapter- in setting up the Eclipse model) and Peter Swaby (for his help in SVS software). In addition, I would like to express my sincere gratitude to the Heroit Watt IPE for the support during the making of this thesis, particularly to Dr. Gary Couples for his supervision.***

ACADEMIC REGISTRY
**Research Thesis Submission**

| | | | |
|---|---|---|---|
| Name: | Salah H H Al-Dhahab | | |
| School/PGI: | IPE | | |
| Version: *(i.e. First, Resubmission, Final)* | Final | Degree Sought (Award **and** Subject area) | PhD |

## Declaration

In accordance with the appropriate regulations I hereby submit my thesis and I declare that:

1) the thesis embodies the results of my own work and has been composed by myself
2) where appropriate, I have made acknowledgement of the work of others and have made reference to work carried out in collaboration with other persons
3) the thesis is the correct version of the thesis for submission and is the same version as any electronic versions submitted*.
4) my thesis for the award referred to, deposited in the Heriot-Watt University Library, should be made available for loan or photocopying and be available via the Institutional Repository, subject to such conditions as the Librarian may require
5) I understand that as a student of the University I am required to abide by the Regulations of the University and to conform to its discipline.

* *Please note that it is the responsibility of the candidate to ensure that the correct version of the thesis is submitted.*

| | | | |
|---|---|---|---|
| Signature of Candidate: | H. Salah | Date: | 4 DEC 09 |

## Submission

| | |
|---|---|
| Submitted By *(name in capitals):* | |
| Signature of Individual Submitting: | |
| Date Submitted: | |

## For Completion in Academic Registry

| | | | |
|---|---|---|---|
| Received in the Academic Registry by *(name in capitals):* | | | |
| *Method of Submission* *(Handed in to Academic Registry; posted through internal/external mail):* | | | |
| *E-thesis Submitted* ***(mandatory for final theses from January 2009)*** | | | |
| Signature: | | Date: | |

Please note this form should bound into the submitted thesis.

Updated February 2008, November 2008, February 2009

# TABLE OF CONTENTS

# LIST OF PUBLICATIONS BY THE CANDIDATE

**Dhahab**, Al Ghubar 16 HST2 End of well review, north Oman 1998, PDO internal OQP/98/003R.

**Dhahab**, Qarn Alam QA21, QA 22 & QA23 wells review, north Oman, 2000, PDO internal OQP/00/021NFF

Langhorne, Eberli, Masaferro and **Al-Dhahab**, 2000, Discrimination of effective from ineffective porosity in heterogeneous Cretaceous carbonates, Al Ghubar field, Oman, AAPG Bulletin; v. 87; no. 9; p. 1509-1529

Wei, Price, De Keijzer and Al **Dhahab**, 2005, Capturing Fracture Uncertainties in Reservoir Simulation of a Giant Mature Fractured Carbonate Field, Oman. AAPG International Conference and Exhibition presentation (September 11-14, 2005)

De Keijzer, Hillgartner, **al Dhahab** and Rawnsley, 2007, north Oman fracture system exposed: A surface-subsurface study of production-scale heterogeneities, Geol Soc London Special Publication

**Al Dhahab**, De Keijzer and Richard, Shuaiba Asset study: 2002 & 2003 Compilation Report Part 3 Structural and tectonic framework, Shell EP Technology Report EP2003-5273

Droste; Richard; **al Dhahab**; Wagner and Ochs. 2004, Shuaiba Asset study: north Oman Shuaiba regional synthesis, Shell EP Technology Report EP2004-5473

Filbrandt , **Al-Dhahab**, Al-Habsy, Harris, Keating, Mahruqi, Ozkaya, Richard and Robertson, 2006, Kinematics interpretation and structural evolution of north Oman, Block 6, since the Late Cretaceous and implications for timing of hydrocarbon migration into Cretaceous reservoirs, GeoArabia, v. 11, no. 1, 2006, p. 97-140

Richard, **al Dhahab**, Hillgartner, de Keijzer and Bettembourg,2004, Qarn Alam Steam Fracture Service Qarn Alam sequence stratigraphy and fracture analysis, Statistical Analysis, Shell EP Technology Report EP2004-5336

Rawnsley and **al Dhahab**, 2005, Qarn Alam Steam Fracture Service project: QA Reservoir 3D fracture modelling, Shell EP Technology Report EP2005-5327

**Al Dhahab**, 2002, Ghaba North Field, north Oman: Shuaiba Fmn. Geo-Statistical Analysis of Fracture, PDO internal report, OQP/02/018NFF

**Al Dhahab**, de Keijzer, Swaby, Hansen, van Heel, Bettembourg, Roeterdink, Richard, Beintem and. Warrlich, 2005, SVS Fracture Reservoir Technology Software Manual Based on SVS version May 2005, Shell EP Technology Report EP2005-5237

**Al Dhahab** and O Regan, 2006, Shell 3D fracture software manual SVS: Simple Visualization Software, Shell EP Technology Report EP2006-5306

**Al Dhahab**, 2004-2005, 3D fracture model for Khuff Formation, Qatar North Dome Field, Shell EP Technology internal presentations.

**Al Dhahab**, 2005, Review of 3D fracture model for Kashagan Field, Caspian, Shell EP Technology internal presentations.

**Al Dhahab**, 2006, 3D fracture characterization and conceptual models for Kirkuk Field, Iraq, Shell EP Technology internal presentations.

Richard, **al Dhahab** and Bettembourg, 2004, Saih Rawl Fracture Study: Fracture characterisation and Fracture modelling, north Oman, PDO internal report, Live Link Document

Zellou, Hartley, Hoogerduijn-Strating, **Al Dhahab**, Boom and Hadrami. Integrated Workflow Applied to the Characterization of a Carbonate Fractured Reservoir: Qarn Alam Field, Oman, SPE 81579-MS, 2003

Rawnsley, Swaby, Bettembourg, **Dhahab**, Hillgartner, de Keijzer, Richard, Schoepfer, Stephenson and Wei. New Software Tool Improves Fractured Reservoir Characterisation and Modelling Through Maximised Use of Constraints and Data Integration, SPE 88785-MS, 2004

Rawnsley, Hadhrami, Kok, Moosa, Swaby, **Dhahab,** Bettembourg, Engen, Richard, de Keijzer, Penney, Boerrigter, Pribnow, Koning and Hillgartner. Accelerated Understanding and Modelling of A Complex Fractured Heavy Oil Reservoir, Oman, Using A New 3D Fracture Modelling Tool, SPE 10095-MS, 2005

**Al Dhahab**, 2005, carbonate structural geology page in the Reservoir Modelling Knowledge Base RMKB in Shell EP Technology web site.

**Al Dhahab**, 2005, QA/QC for fracture studies, detailed excel spread sheet for review of fracture characterization and 3D DFN modelling using SVS, Shell EP Technology internal note – web site

Bazalgette, Beintema, Bettembourg, Swaby, **al Dhahab**, de Keijzer and Rawnsley, 2007, Fault and fracture corridor detection and fracture modelling using SVS curvature analysis tools. Shell EP Technology Journal 2007-7001•09

De Keijzer, Hilgartner, Rawnsley, **al Dhahab**, Heesbeen, Taberner, Rejas, Esteban and Alfonso, 2003-2004 north Oman Fault and Fracture exposed - Jebel Madmar study, Shell EP Technology Report EP2004-5401, 2004-5402, 2004-5403, 2004-5404, 2004-5404 and 2004-5405

De Keijzer, Hillgartner, **Al Dhahab** and Rawnsley, 2007. A surface-subsurface study of reservoir-scale fracture heterogeneities in Cretaceous carbonates, north Oman. Geological Society, London, Special Publications; 2007; v. 270; p. 227-244

Also several well proposals while working in Petroleum Development Oman PDO as production geologist from 1997 to 2002.

**Abbreviation**

| | |
|---|---|
| A | fracture aperture |
| AG NTH | Al Ghubar field Natih Formation |
| AG SHB | Al Ghubar field Shuaiba Formation |
| AH | Al Huwisah field |
| BHI | BoreHole Image -resistivity log |
| BRN | Burhaan field |
| CC | large Conductive fracture in BHI |
| CI | Induced Fracture in BHI |
| CP | small Conductive fracture in BHI |
| CT | Induced Fracture in BHI |
| DFN | Discrete Fracture Network model |
| DLM | Dhulaima field |
| EPTS | Exploration and Production Technology Services |
| ESP | Electrical Subsurface Pump |
| F | Fracture |
| FC | Fracture Corridors |
| FHD | Fahud field |
| FI | Fracture Intensity Index |
| FMI | Formation Micro Image –resistivity log |
| FMS | Formation Micro Scanner –resistivity log |
| FOWC | Fracture Oil Water Contact |
| FU | Flow Unit |
| FZ | Fracture Zone |
| g | gravity |
| GN | Ghaba North field |
| GOGD | Gas Oil Gravity Drainage |
| GWC | Gas Water Contact |
| h | height (depth) |
| HK | Not layered but high permeability streak |
| Inj | Injection |
| JM | Jebel Madmar |
| K | Permeability |
| Kf | fracture permeability |
| Kmax | Curvature maximum value |
| L | Layered |
| L | Lower |
| L | matrix block dimension |
| LAN | Lekhwair A North field |
| LAS | Lekhwair A South field |
| LKH | Lekhwair field |
| LOT | Leak off test |
| LT | Limited test |
| MH | Matrix heterogeneous |
| ML | Mechanical Layering |
| MLM | Musallim field |
| NC | large non-conductive fracture in BHI |
| NL | Homogeneous matrix not layered |
| NOCEM | North Oman Common Earth Model |
| NP | small non-conductive fracture in BHI |
| NTH | Natih field |
| Ø | Porosity |
| OFM | Oil Field Manager Production data base |
| OWC | Oil Water Contact |
| Pb | Formation break down pressure |
| PDO | Petroleum Development Oman |
| Pf | formation pore fluid pressure |
| PLT | Production Log Technology |
| QA | Qarn Alam field |
| RFT | Repeat Formation Test |
| RUI | PDO subsurface data base |
| S | fracture spacing per cell along the grid direction |
| Shmax | Principal maximum horizontal stress |

| | |
|---|---|
| Shmin | Principal minimum horizontal stress |
| SPM | Seed Probability Map |
| SR | Saih Rawl field |
| STOIIP | Stock Tank Oil Initially In Place |
| SVS | Shell EP Simple Visualization Software: 3D fracture software |
| T | tensile strength of the rock |
| TGOGD Thermal | Gas Oil Gravity Drainage |
| THSU | Top Thamama Shuaiba Formation |
| U | Upper |
| UF | Unidentified Fault in BHI |
| WFL | Water Flow Log |
| X/I | x-axis |
| Y | Yibal field |
| Y/J | y-axis |
| Z/K | z-axis (vertical) |
| ρ | Density |
| σ | Principal stress |
| σ | Sigma Factor in Eclipse |
| σH | Principal maximum horizontal stress |
| σh | Principal minimum horizontal stress |
| σv | Principal vertical stress |

# Chapter 1– INTRODUCTION

This thesis describes the fracture systems of the Cretaceous Natih and Shuaiba Formation reservoirs of north Oman, which underlie an area of approximately 300km by 250km (mainly in Petroleum Development Oman (PDO) Block 6). The thesis starts with this introduction chapter covering the objectives behind the study, the data available and their limitations, and the approach used. Chapter 2 describes the regional sedimentological and tectonic setting of north Oman in order to set the scene for the subsequent fracture characterization chapters. Chapter 3 consists of a comprehensive, descriptive fracture evaluation of most of the north Oman Cretaceous carbonate fields based primarily on a review of existing work and new geometric analysis of BHI/FMI interpretations. The main purpose of this evaluation chapter is to identify the main similarities and differences between the fracture networks in the reservoirs examined. The following two chapters (4 and 5) focus on two specific fields, which were subjected to a detailed fracture evaluation that spans from wellbore fracture characterization all the way to 3D fracture modelling at the field scale. These fields are Ghaba North (GN), located in the south-eastern region of north Oman, and Lekhwair A North (LAN), located in the north-western region of north Oman. These two fields were chosen because they represent different geographical areas, hence possibly different geological settings, and also because of PDO recent interest in their development. A short chapter (6) presents a simple implicit dual porosity / dual permeability simulation exercise performed on the 3D DFN models created for the GN Shuaiba reservoir. The objective of the simulation is to illustrate the impact of different fracture scenarios on the reservoir simulation process and to understand the main parameters that affect the results of such simulation. Chapter 7 presents a detailed critical analysis of the fracture network of north Oman. It examines the role of the underlying geology, i.e. the matrix-diagenesis-fracture interrelationship, the genesis of the north Oman Cretaceous fracture network, and the fracture conductivity flow analysis. The last chapter (8) provides a summary of the technical findings of the research.

BHI/FMI (Bore Hole Image, Formation Micro Imager) logs represent the main data sources for fracture characterization in PDO. There are many limitations associated with BHI/FMI tools and their fracture interpretations. For instance, the fractures seen in BHI are much fewer in number than those observed in core (or outcrops), which is mainly due to resolution. However, if integrated with other fracture-related data, these logs can be of substantial value to fracture network characterizations. From a conductivity prospective, at least for the examined reservoirs, it seems that the large scale fractures, those that are observed in BHI, are the ones that usually affect flow behaviour, especially if they occur in clusters either as fracture corridors or in a fault damage zone. In contrast with naive statistical approaches, this study shows that it is essential to

understand fracture type (e.g. single or cluster; conductive or non-conductive) and to split fractures per orientation, before embarking on a meaningful statistical analysis.

There will always be a large uncertainty associated with 3D fracture modelling, because of lack of data through the entire reservoir volume. Thus, it is beneficial to develop a conceptual scenario for the creation of the fracture network and to build geologically constrained fracture scenarios that reflect what is seen in outcrops while also honouring the conceptual model. Nowadays, there are several 3D software tools that allow the creation of 3D Discrete Fracture Network (DFN) models. The purpose of these DFNs is to enable explicit fracture simulation and to better illustrate the effects of the fracture network when taken to flow simulation. Extracting fracture geometrical properties (intensity and spacing) from a 3D DFN model into a 3D geo-cellular grid, for the purpose of implicit dynamic simulation (either single porosity or dual porosity), may give rise to errors associated with the method used for the spacing calculation (e.g. scan line orientation or the mathematical approach used), with the grid orientation, and with the size of the grid cells. Hence, the fracture geometrical values in a grid are relative values. Furthermore, there are many assumptions associated with such implicit simulation even with dual porosity / dual permeability simulation. For instance, predicting fracture conductivity from fracture aperture estimation or defining the transfer function used in implicit simulation, are aspects that can introduce bias. These choices may affect the flow simulation outcome; hence explicit fracture simulations which use direct 3D DFN are encouraged as a way to minimize the artefacts.

A review of existing regional stratigraphic studies for north Oman suggests that the Natih Formation should be prone to mechanical layering due to its interlayering of carbonate/shale. For the Shuaiba Formation reservoir, only those fields that occur in the NW region of north Oman are likely to show intense mechanical layering. This is due to the presence there of both Upper and Lower Shuaiba Formations. The Lower Shuaiba does not exhibit strong layering, whereas the Upper Shuaiba does. The fracture network of the Shuaiba reservoirs in the central and SE region of north Oman, where only Lower Shuaiba is present, is dominated mainly by fault–related fractures and fracture corridors, with less evidence of fractures associated with mechanical layering (as might be expressed in flexures).

A review of the existing regional tectonic studies highlights the importance of the Late Cretaceous [Alpine I] deformation on the Cretaceous reservoirs' fracture networks in north Oman. The main impact of this event is the creation of a NW-WNW set of strike-slip faults and their associated fractures, as well as the activation of the salt diapirs. Subsequently, the Tertiary deformation [Alpine II] – which consists of a NE-oriented shortening – has resulted in the creation of abundant NE oriented background fractures, and more importantly NE fracture corridors, that are perceived to act as conduits to flow. In addition, salt diapirs, wherever they occur, were reactivated during Alpine II

events, resulting in more intense fracturing in fields nearby. The geometric distribution of the Cretaceous fracture network, based on BHI investigations, shows that the NE fracture set dominates in Fahud and Natih fields (at the foot of the Oman Mountains) as well as in the eastern fields – e.g. Ghaba North and Burhaan, whereas the NW-WNW fracture set dominates in the Lekhwair field and central north Oman fields such as Musallim. Reservoir-scale analysis of the fracture network for Ghaba North and Lekhwair A North (both in Shuaiba Formation) reveals a change in dominant fracture orientation between the SE and the NW of north Oman.

To date, the impact of diagenesis on the fracture network connectivity has not been assessed thoroughly, despite the clear interrelationship between chemical processes and fracture intensity (e.g. early meteoric diagenesis impact on deposited sediments leading to mechanical changes), and more importantly on fracture conductivity (e.g. late diagenesic hydrothermal leaching or late burial cementation). Field performance reviews indicate that almost all the Cretaceous reservoirs of north Oman exhibit fracture-related flow behaviour to some extent. For example, production behaviour even of the perceived pure matrix reservoir (e.g Musallim Field) has shown water short-circuiting, especially in the case of water flooding development.

An assessment of the fracture network conductivity is hampered by the lack of well-test analysis for GN; nonetheless, interference tests shows that the fracture network can increase flow capacity from mD to Darcy scale. Only fractures that occur in clusters (either in a fault damage zone or in a fracture corridor) contribute significantly to flow. These corridors are normally spaced in the range of 50-100s of meters compared to background fractures which usually have spacing in the range of a few meters. The NE fracture corridors may play a major role in connecting the NW-WNW fractures seen in Lekhwair A North. The ratio of large conductive to large non-conductive BHI fractures in Ghaba North is 9:1 (where NE fractures dominate) compared to a ratio of 2:1 in Lekhwair A North (where NW fractures dominate). This observation, which is also valid for most of the other fields in north Oman, may indicate that the current NE oriented maximum horizontal stress might have an impact on the conductivity of the fracture network in the Cretaceous reservoirs, though the role of diagenesis cannot be ruled out.

### 1.1 Background

More than one third of Oman oil, currently produced at a rate of ~740000 bbl/day, is reservoired in the Cretaceous Natih and Shuaiba limestone Formations (Figure 1.1 & Figure 1.2). As shown in Figure 1.1, all of these reservoirs are in the northern region of Oman, mainly in Petroleum Development Oman (PDO) Block 6. Oil production started in Oman in the late 1960s. Fahud and Natih Fields produce only from the Natih Formation. Al Ghubar field has a 50:50 production rate from both Natih and Shuaiba, while all the other Cretaceous fields shown below produce from the Shuaiba Formation,

except for Qarn Alam Field and Lekhwair fields, which are producing from Shuaiba Formation and Kharaib Formation. This study focuses on Cretaceous reservoirs; hence in the regional analysis (at least the fracture analysis) it includes the Kharaib of Qarn Alam and Lekhwair fields.

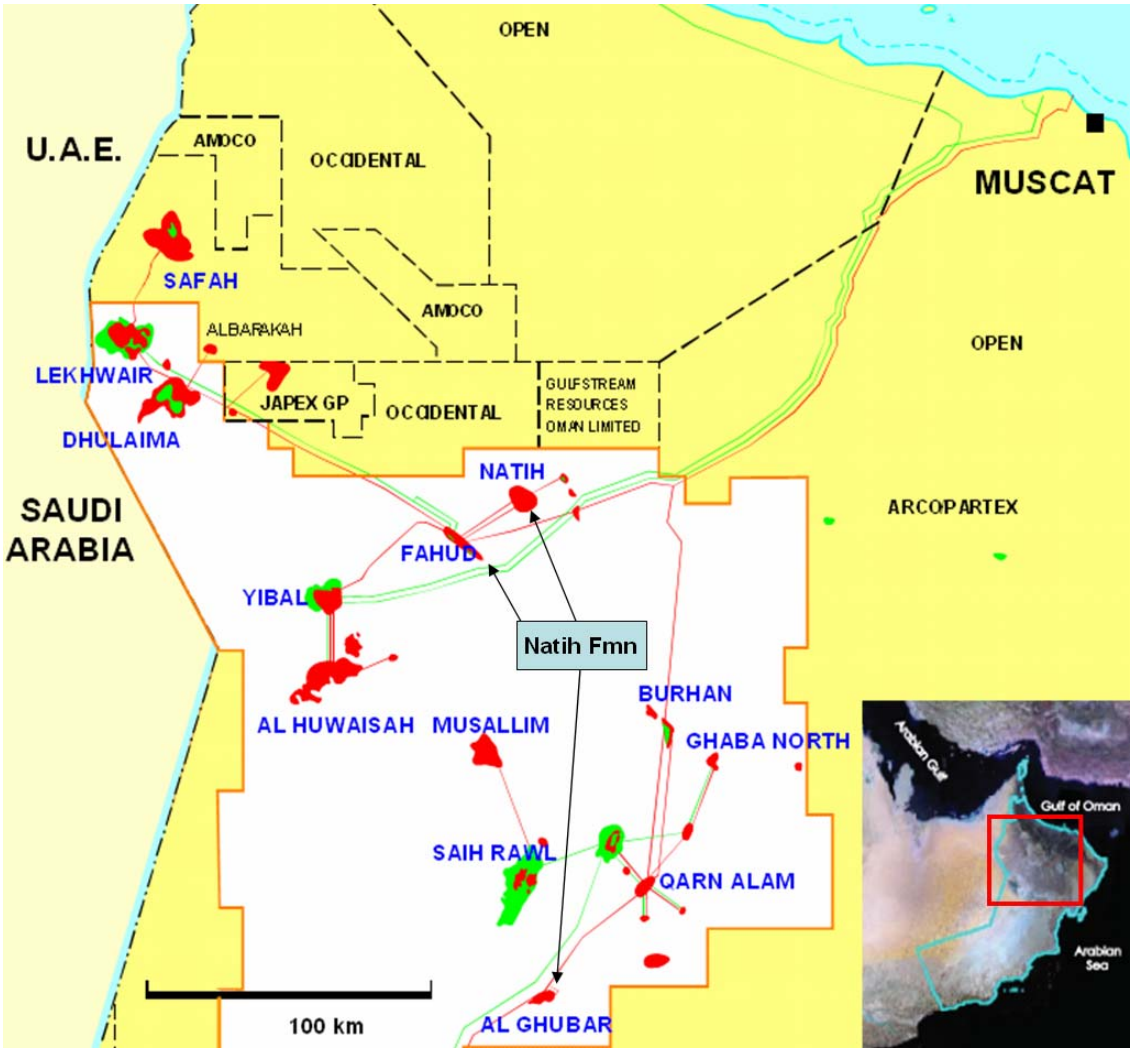


**Figure 1-1 Map of north Oman Cretaceous fields with annotation showing the fields producing from Natih Formation, all the others produce from Shuaiba except for Qarn Alam which produces from Shuaiba, Kharaib and Lekhwair Formation (from PDO internal presentation).**

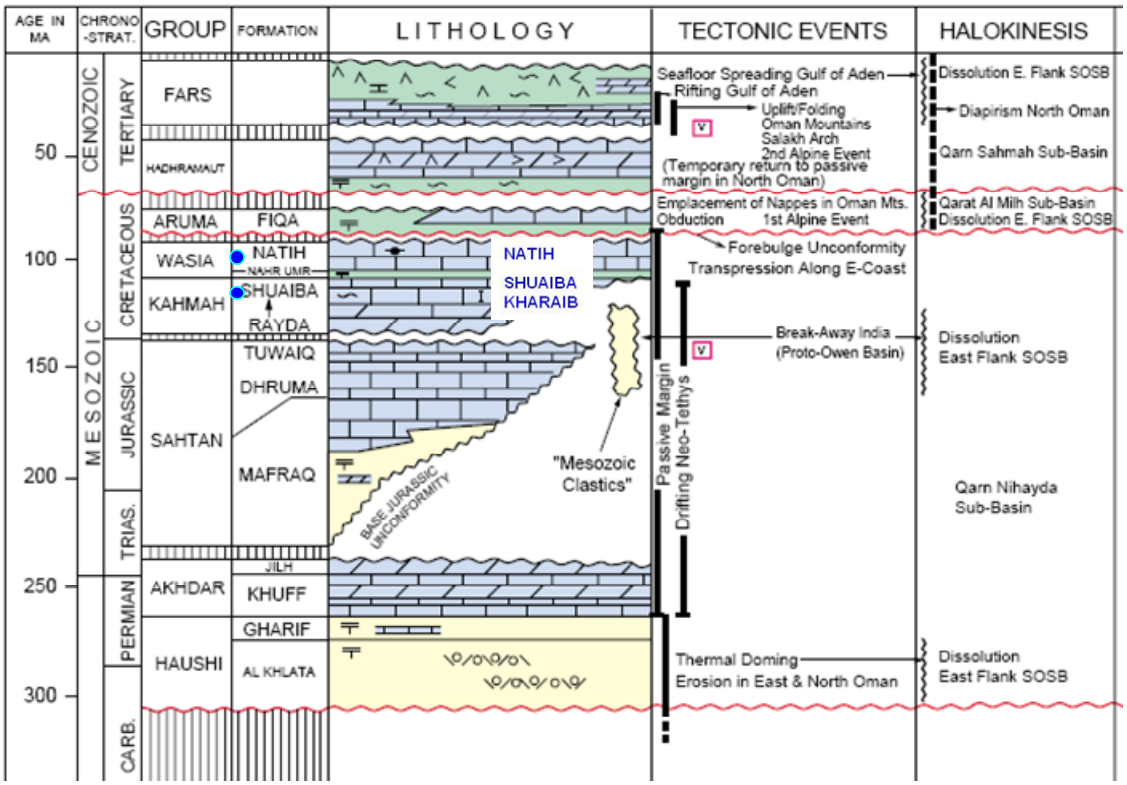


**Figure 1-2 Stratigraphy of Oman, showing the Cretaceous reservoir with annotation (right hand side) regarding the main tectonic events and halokinesis (Loosveld and Terken, 1996).**

Traditionally, the fields' reservoirs have been classified into either matrix reservoirs, such as Yibal, Lekhwair, Musallim and Saih Rawl, or fractured reservoirs (in relation to flow, see section 1.3 below on fracture definition), such as Qarn Alam, Fahud, Natih and Al Ghubar. However, almost all have shown fracture behaviour to some extent. For example, production behaviour even of the perceived pure matrix reservoir has shown water short-circuiting especially in the case of water flooding development, when the injection water pressure is high (Figure 1.3). The majority of this water fingering in such cases is attributed to fractures.

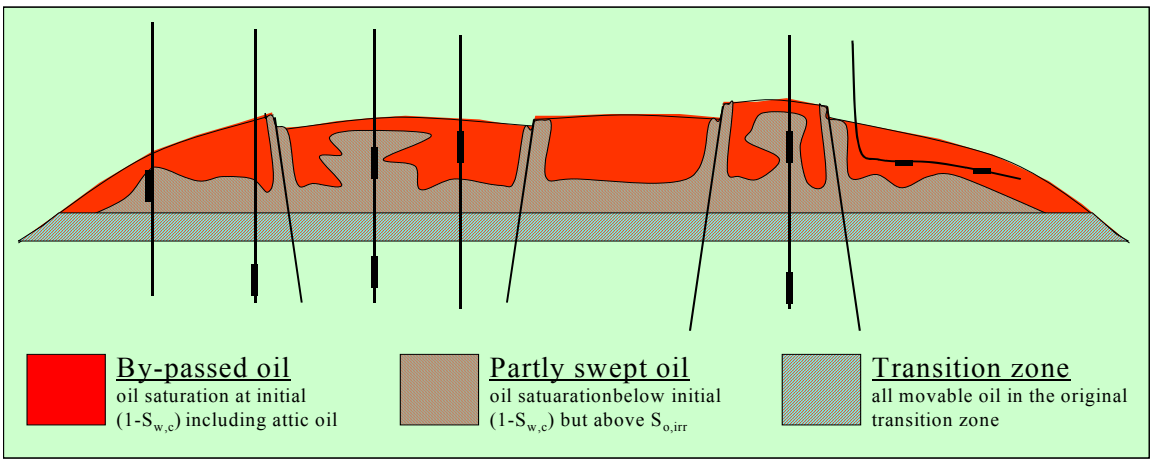


**Figure 1-3 Cartoon showing potential causes of water fingering in a perceived matrix reservoir of Yibal field (PDO internal presentation).**

The development scenarios applied to these fields (Figure 1.4) have changed over time, but in principle follow the traditional subdivision of reservoir type stated above. All of the fields started with pure depletion but were quickly assisted with gas lift due to pressure decline. In the perceived fractured reservoirs with thick oil columns, Gas Oil Gravity Drainage (GOGD) development has been applied as in the case of the Fahud Natih reservoir. This had been assisted with thermal injection where the oil is viscous as in the Qarn Alam Shuaiba reservoir (Figure 1.5). In contrast, if the reservoir is perceived to have moderate fracture intensity, then a matrix natural depletion development, with gas lift, is applied assisted with mechanical and/or chemical shut off techniques. Such shut off techniques have been applied in Al Ghubar and Ghaba North Shuaiba reservoirs, though with little success. On the other end of the spectrum, in the perceived pure matrix type fields such as Yibal, Lekhwair, Saih Rawl and Musallim, a matrix development with water injection, where the aquifer pressure support is low, has been applied. Well pattern has been either vertical infill or horizontal injection in the water window, below the matrix OWC. For the GOGD development to succeed fracture intensity has to be high to allow connectivity and the reservoir must be thick to allow gravity to work. While for the horizontal matrix development, fractures should be avoided, to allow for even sweep. Hence, the importance of the role of fractures on production needs to be carefully assessed if not already proven; and, in order to do so, the fracture network characterisation is essential.

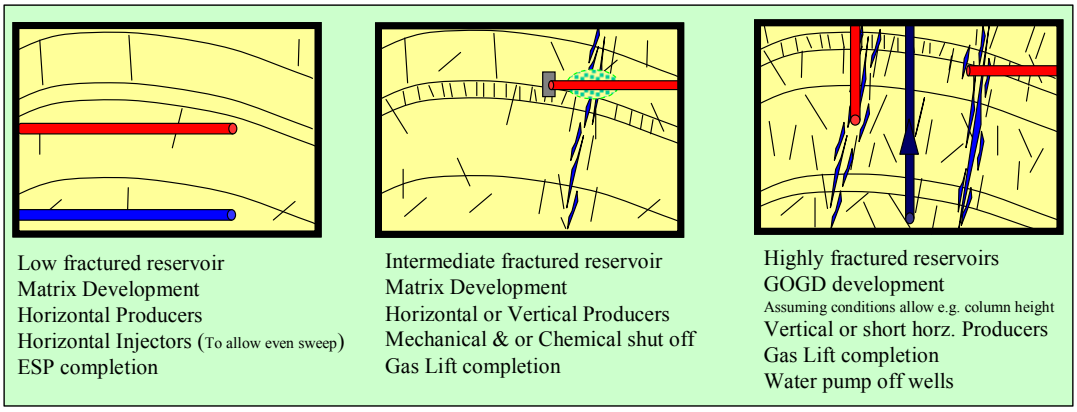


**Figure 1-4 Conceptual cartoon showing development type of PDO carbonate reservoirs (red is producer, blue is injector, dark blue is pump-off well) with possible development scenario. Left to right: matrix water flooding; nature depletion with chemical or mechanical water shut off techniques; and gas oil gravity drainage GOGD development in highly fractured reservoirs.**

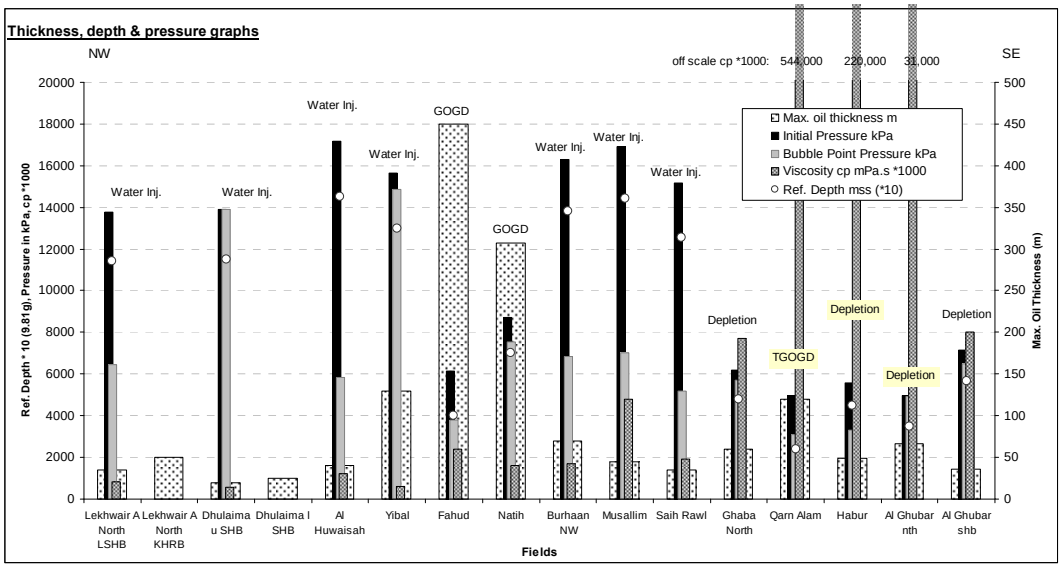


**Figure 1-5 Overview of north Oman Cretaceous fields. Reference depth in mss indicate how deep or shallow is the reservoir (in this graph * 10 to show how close is the pressure to hydrostatic) see left axis. Note the Development type annotation and how it relate to the oil viscosity (cp * 1000 for visibility) and to the reservoir thickness in m (the only variable to be read using the right hand scale).** ***Note this figure is not accurate enough for any volumetric calculations.***

## 1.2 Objectives

The objective of this PhD research is to better understand the fracture networks that occur in the Cretaceous reservoirs of north Oman, and to assess their effects on flow. This understanding covers both the geometrical and property aspects related to the fracture networks at regional, field and well scale. The emphasis of the research is on the Shuaiba Formation which is the commercial reservoir in most of the fields. The Natih Formation will be only covered in the regional analysis.

Knowledge of the regional structural geology will help primarily by improving our understanding of regional similarities and differences of the static characteristics of the fracture networks such as orientations and relative timing. This will be further refined during specific field and well scale analysis. The latter will also help in establishing the dynamic characteristics of the fracture network (flow properties). Thus, the research will cover both the geometry (areal and vertical distribution, orientation, etc.) and the property (fracture type: open or close) of the fracture network. This understanding will aid in constraining reservoir static and dynamic models.

## 1.3 Fracture definition and terminology

The term fracture refers to any natural geo-mechanical discontinuity that occurs during rock "deformation" which does not have a tangible, "measurable" displacement (modified from IFP definition, 2004). This research is focused only on natural fractures and it is not intended to describe hydraulic fractures induced either intentially or accidentally while drilling (Barree and Woodroof, 2002; Yang, 2000). However, drilling induced fractures are used as indicators of the stress direction in the rock.

There are several definitions and classifications of fractures. In the context of this research the following is adopted. When referring to "a fractured reservoir" the classification of Nelson (1999), as used in the petroleum industry, is adopted, where reservoirs are subdivided into:

- Type I: Fractures provide the essential storage capacity and permeability in the reservoir. The matrix has little porosity or permeability.
- Type II: Rock matrix provides the essential storage capacity and fractures provide the essential permeability in a reservoir. The rock matrix has low permeability, but may have low, moderate, or even high porosity.
- Type III: Fractures provide a permeability assist in an already economically producible reservoir that has good matrix porosity and permeability.
- Type IV: Fractures do not provide significant additional storage capacity or permeability in an already producible reservoir, but instead create anisotropy.

When describing a fracture as a single feature or a fracture set as a group of related fractures, the IFP classification (IFP definition, 2004), illustrated in Figure 1.6, is slightly modified and adopted: A ***fracture*** is characterised by its geometric attributes (dip, strike, length, aperture, morphology and origin). Here a fracture is referred to as a stand-alone fracture if it occurs alone. The term is independent of the size of the discontinuity. The fracture definition includes features with little or no relative displacement. A ***fracture set*** is a group of fractures that have similar attributes (Figure 1.6). In this research fracture sets are described in terms of their morphology and origin (Figure 1.7). The latter definition can be sub-divided into genetic classes, in a fashion similar to the Nelson (2001) classification, as follows:

- Dispersed, also called ***background fractures,*** which occur in a diffused distribution through the reservoir**.**
- ***Fracture corridors*** are fracture sets which occur in ***clusters*** or as a ***swarm*** and do have an effect on fluid conductivity (for their geometry distribution see Tindall and Davis, 2003). They are usually regional in extent – probably related to a regional stress state. They only differ from the above group in their high intensity "clustering" and their ability to conduct fluid in tangible amounts.
- ***Regional fractures*** are a fracture set that can be seen in several fields (i.e. at a regional scale) and probably originated from regional paleo-stress state (Lorenz et al, 1993; Engelder and Peacock, 2001; Gillespie et al, 1993; Bai et al, 1993). They can be described as background regional fractures, regional fracture corridors, regional fault related fractures or regional fault damage zones – though this last group is not very common unless the faults themselves are regional in nature. For example, in north Oman, the NW and WNW regional strike-slip faults are associated with fault damage zones that have abundant fractures in them.
- ***Fault-related fractures*** are fractures that occur in the vicinity of a fault (a geo-mechanical discontinuity with a measurable displacement), with orientations

largely the same as the fault and plausibly associated with the faulting process. Their intensity tends to decrease with distance away from the fault surface (Wilkins et al, 2001; Gross et al, 1997; Fachri, 1997).

- ***Fault damage zone*** is a local region around a fault plane that contains fractures (and potentially other deformation features), indicative of higher strain intensities (see Caine et al. 1996). Fractures in this category differ from the group above in having a sharp decline of intensity away from fault plane, often over distances of +/- a metre. Sometimes a fault damage zone contains NO physical fault (i.e. discontinuity) and it is only made up of a cluster of fractures that exhibit minor displacements, such that if the zone were treated as a single plane, there would be a measurable displacement of the rock units. Fault related fractures and fault damage zones are sometime intermingled.
- ***Fold related fractures,*** also termed here flexure or curvature related fractures are perceived to originate in high strain areas of curved horizons (Couples et al 1994; Couples and Lewis, 1998; Bergbauer et al, 2003).
- A ***fracture network*** is a group or assemblage of fracture sets. One of the important aspects of a network is its state of connectivity. The consequence of a fracture network is that all of the matrix blocks are surrounded by fractures.


**Figure 1-6 A fracture (example any of the red or white lines), a fracture set (one group: the red lines or the white lines) and a fracture network (all the white and red lines plus wavy lines seen on the rock blocks) illustration, from Bristol Channel.**

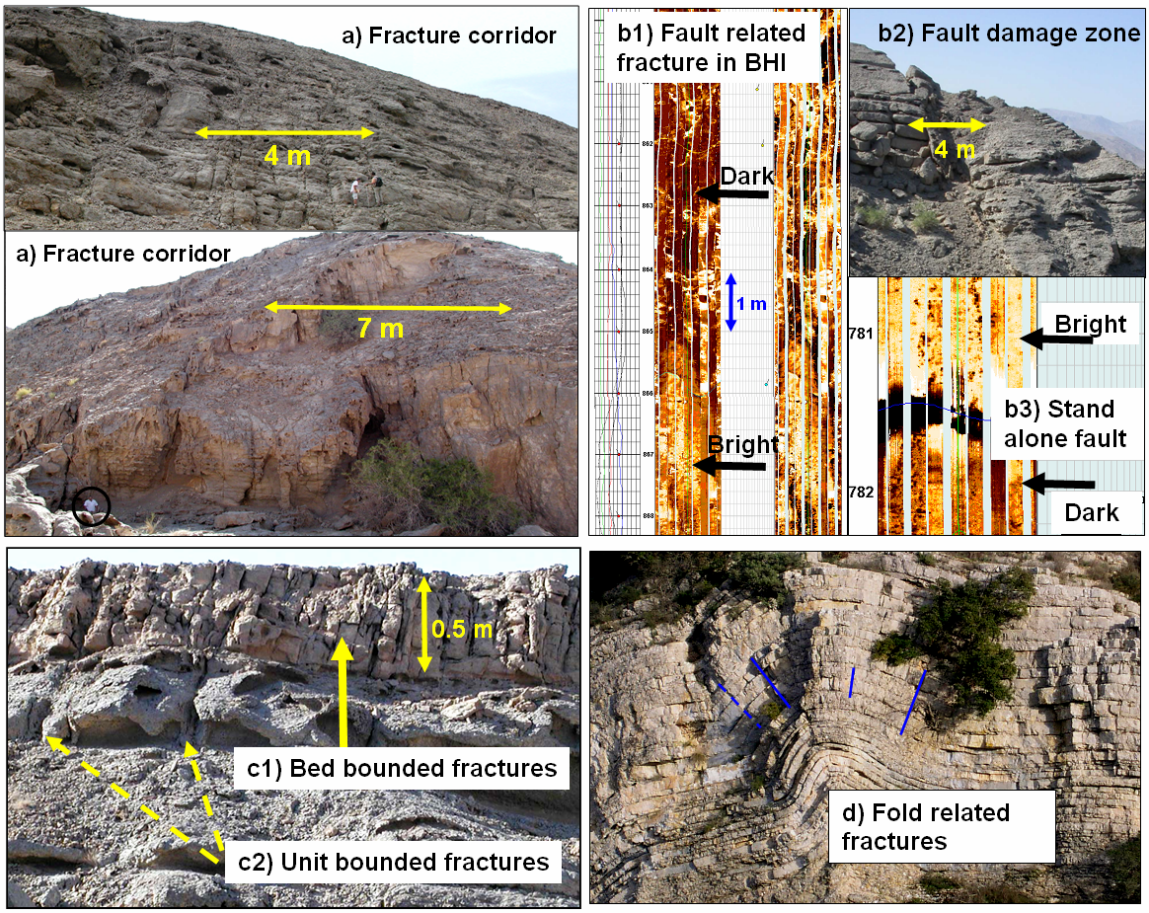


**Figure 1-7 Photos illustrating some of fracture term used in this research: a) Fracture corridor outcrop example from Jebel Madmar; b) Fault related fracture and fault damaged zone Jebel Madmar outcrop and Qarn Alam Field BHI example; c) Bed bounded fractures of Jebel Madmar Natih Formation (a-c de Keijzer et al, 2004); and d) fold related fractures outcrop example from France (Bazalgette, Shell internal presentation).**

Micro-fractures or ***hairline fractures,*** and vertical or horizontal ***stylolites*** (pressure-dissolution features related to tectonic "burial" stress), both of which can typically be seen in core, but not in BHI, are not considered in detail here. They are described only in the regional chapter and are excluded from the 3D discrete fracture network models created in Chapter 4 and Chapter 5, because they are normally modelled as part of the matrix part of the reservoir as an enhancement or degradation of porosity and permeability of the matrix.

The generic description of fracture "cracks" as mode I (tension), mode II (shear) and mode III (hybrid) is not used in this research (for further information on such description see Rao et al, 2003; Li and Sun, 1988). This thesis attempts to avoid using the term "joints" as the word has many descriptions; however it is notably used in reviewing the outcrop existing fracture characterisation work. Here (in the outcrop studies of north Oman) another terminology is introduced which is "***lineament***" to refer to structural trends (nominally the strike of planar features that intersect the ground surface, which is approximately horizontal over regional scales). The term is used here when examining satellite images to pick fractures in outcrop studies (see Figure 2.38)

for an illustration of this use. The word also arises when describing the structural grains of a seismic map or cross-section or mapped horizons.

When referring to mechanical stratigraphy, in this research the Shell EP Research and Montpellier University classification is used (shown in Figure 3.7 of Chapter 3). The most common term used is bed-bounded fracture, describing a fracture that is contained within a horizon or a bed (i.e. it does not cross the bedding plane, vertically). However some fractures may be unit bounded, i. e. constrained within a group of beds. This subject of mechanical layering and relation between rock type, bed thickness and fracture intensity, has been the subject to many detailed studies (e.g. Haiqing and Pollard, 1995). It also marked the start of the end for the usage of the fractal approach for fracture characterization which assume a homogenous rock with systematic fracture intensity relation from the low scale (bed unit) to the large scale (field faults).

Since the Bore Hole Image (BHI) data is the most commonly available fracture data in PDO (see section 1.7 on data limitations), there is a common usage in this thesis to mean a fracture picked on BHI (FMI or FMS). Such fractures are the basis for the fracture statistical analysis presented in Chapter 3. In SVS (Shell Simple Visualization Software, which was used in this study), these fractures or BHI picks are termed ***well objects.*** It is essential to note that it is unknown whether they are physically conductive or not, because they are the product of electrical logs reflecting anomalous resistivity in a well borehole. Thus, BHI fractures can be closed away from a borehole unless confirmed open by losses or production logs.

A naming standardisation of all the BHI fractures or objects has been used in PDO and adopted in this research, by applying it to BHI picks that are not standardized. This standardization refers to conductive fractures - which are possibly open - and non-conductive fractures - which are possibly cemented. The sub-grouping relates to whether they are high or low confidence (large or small) and whether they are connected or not to each other.

### 1.4 Methodology and approach

The research is divided in two main parts: regional and field scale. The first part of the thesis summarises the regional geology of north Oman, and its implication for the Cretaceous reservoirs, building on existing regional studies such as Loosveld et al (1996) and the Shuaiba Asset Study (Nichols et al, 2002-2003). The latter includes the analysis done on the north Oman Common Earth Model NOCEM: fault and horizon modelling of the north Oman region performed in gOcad $^{TM}$ software based on a combined regional 2D and 3D seismic interpretation. More specifically, that section focuses on the relationship between regional stratigraphy, diagenesis, oil migration, tectonic settings and the fractures observed in the Cretaceous reservoirs. The evaluation starts with background information on the stratigraphy of north Oman, with emphasis

on Cretaceous rocks, based on existing work that utilises both outcrop and well data (potential mechanical layering). A summary of the tectonic setting, based again on existing work, is presented. This covers the tectonic deformation history of the area: collisions, uplift, faulting, folding and salt halokinesis. A main source of data here is the published paper by Filbrandt et al (2006).

An evaluation of all the available Bore Hole Image fracture interpretation results of all the Natih and Shuaiba Formations is presented in Chapter 3. The aim of this section is to set the stage for the specific field studies and to draw conclusions regarding the similarities and differences between the Cretaceous reservoirs of north Oman with respect to geometric characteristics of the fracture networks (Figure 1.8).
The second and main part of the research concentrates on the field to well-scale fracture evaluation. Two fields of the Shuaiba reservoirs are examined, Lekhwair A North (LAN) and Ghaba North (GN), to cover regional structural variations. These fields were also chosen because of recent PDO interest in their development. Compared to the regional fracture evaluation, these two specific field chapters focus on both detailed static and dynamic characteristic of fracture networks.

During these field studies, a work flow (Figure 1.9), derived from Shell EPT best practices, is adopted. Fracture characterisation (with emphasis on well data: core, borehole images and static and dynamic logs) defines the basic information. The prime focus here is the geometry and characteristics of the fractures and their distribution. The section will start by visual inspection of the core data and BHI picks of key fields. All the existing fracture related data (static and dynamic) is loaded into the Shell fractured reservoir characterisation software SVS$^{TM}$ to be integrated and analysed from both well- to field- scale. Fracture-fault and fracture-fold relationships and regional fracture patterns are investigated. Other constraints, such as the PDO–Shell sand box digital data base and kinematics analysis of the structural setting of each field, will be presented based on existing work of PDO and other researchers. 3D static discrete fracture network DFN realizations are generated for these fields. The 3D DFN models are based on conceptual scenarios and constrained using seismic data, outcrop analogues, conceptual models, well data (both static and dynamic), regional constraints (such as in-situ stress), lab experiments, etc. These 3D fracture models consist of either sector models or full field models. As a demonstration, a 3D flow simulation model, based on the 3D fracture/static models for one field, is presented and discussed. This is a simple model at the well and/or sector scale, created using Eclipse$^{TM}$. The aim is to analyse the impact of different realisations of fracture networks on the flow response of the reservoir. The matrix grids are either created straight in the simulator or created in SVS or imported from existing models created by PDO/Shell using Petrel $^{TM}$. The individual field studies end by summarising the findings and drawing conclusions regarding the role of fracture networks in each field.

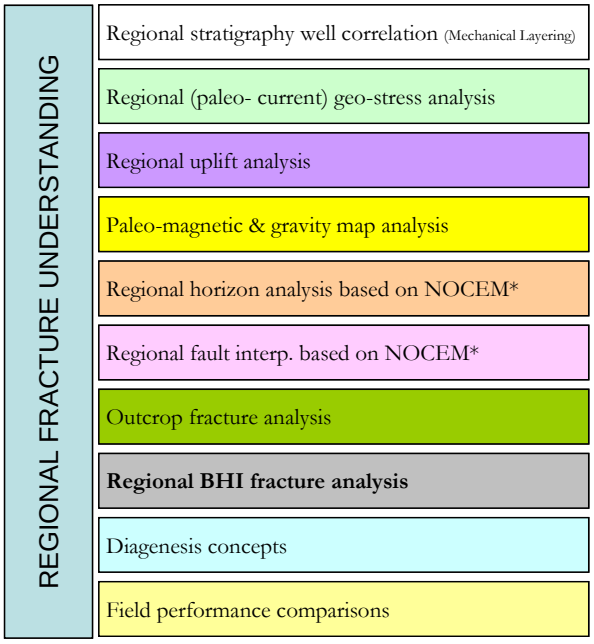


**Figure 1-8 Tools used for regional fracture understanding, emphasis is on integration of fracture related data to arrive at a coherent story. NOCEM stand for North Oman Common Earth Model.**

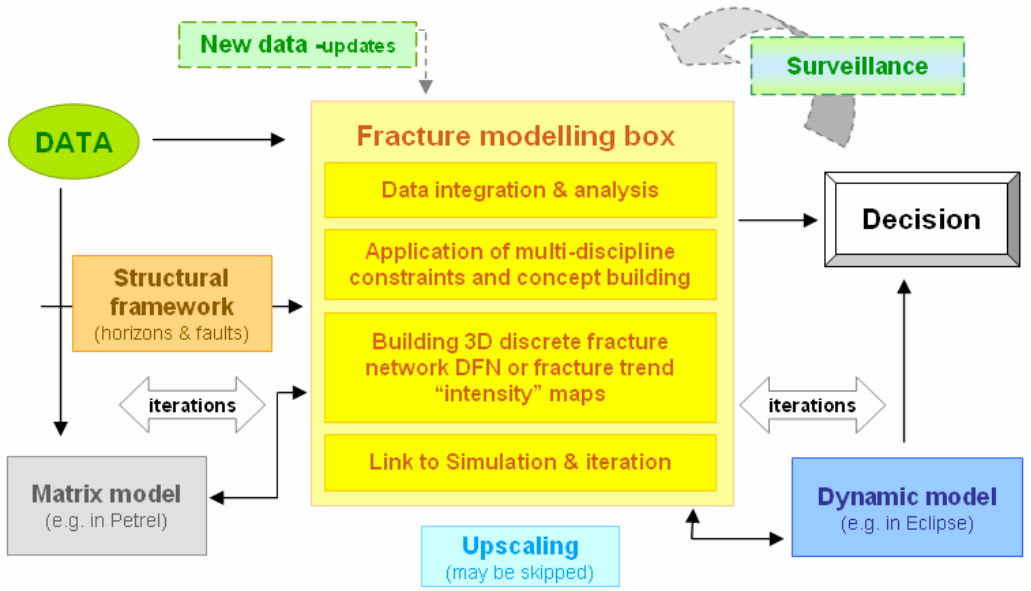


**Figure 1-9 Shell fracture modelling workflow (yellow box), showing route used in this study.**

The results from the regional fracture evaluation and the two specific field studies are sysnthesised in Chapter 7 to arrive at a coherent picture for the significance of fracture networks of the Oman Cretaceous reservoirs. This chapter also provides an opportunity to generate recommendations for further work that is needed to advance our understanding of the impact of fracturing for north Oman.

## 1.5 SVS and other fracture modeling software

There are several types of commercial software that aid in fracture characterization and 3D fracture modeling, i.e. discrete fracture network (DFN) generation. Shell Simple Visualization Software (SVS) is one of them. The main strength of SVS is in its visualization aspects and integration of fracture related data. In addition, it generates 3D

DFNs based on conceptual models and hence the generated models can be independent from the input data (i.e. there is no automated relationship between the 3D DFN and the input data, and fractures created are usually not data driven unless forced so by the user). This independency of the DFN from specific data allows users to use SVS for fracture characterization alone (remembering that it is very strong on data integration) or to simply go straight to creating multiple realizations of DFNs based on conceptual models where there is NO data, as is the case for the exploration stage. SVS has also a geo-mechanical plug-in that enables analysis on fault planes. The main data at the well scale is fracture picks either from BHI or core; these are termed "well objects" in SVS. I decided to use the software simply because I am familiar with it, as there are many other types of software that do have more or less similar functionalities. Below is an attempt to list the main software commonly used, but note that the list might not be comprehensive.

**Golder Associates FracMan**:
http://www.fracman.com/
The FracMan software suite provides an integrated set of tools for discrete feature network (DFN) analysis of fractured and non-fractured heterogeneous rock masses. FracMan includes tools for discrete feature data analysis, geologic modelling, spatial analysis, visualization, flow and transport, and geomechanics. The software is broken into modules that cover data analysis (FracSys), with a strength in dynamic related data evaluation, 3D DFN generator (FracWorks XP), which is usually data driven stochastic in nature as shown in Figure 1.10 below. There is also a matrix and fracture interaction code (MAFIC) that uses the finite element method to solve for flow and transport through generated DFNs. The fourth module is called PAWorks / FraCluster. This basically analyses flow behaviour of discrete feature networks and evaluates fracture clusters to arrive at block size determination.

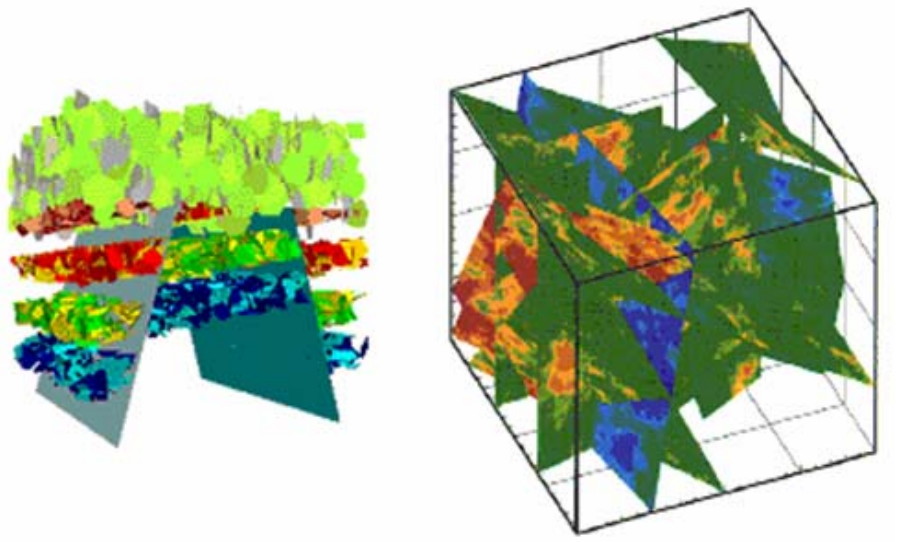

**Figure 1-10 Snapshot showing an example of 3D DFN created by FracMan (left) and one of MAFIC illustration for flow analysis (Golder Associate FracMan web site).**

**Schlumberger Petrel Software**
http://www.slb.com/content/services/software/geo/petrel/fracture_modeling.asp?entry=ad_google_petrel_fracture_modeling&gclid=CJ_4q8X4pZECFQwwlAodzGhRWQ
Petrel had incorporated a plug-in 3D fracture characterization and modelling software with the cooperation of Golder Associates. Hence their plug-in to Petrel uses more or less the same principles as FracMan.

**Midland Vally 3D Move**:
http://www.mve.com/3DMOVE2/
This is a 3D structural tool that enables 3D structural restoration incorporating geological time in the modelling process. The software is not specific to fracture (their fracture version is called FrcMV which is a cooperation with Earth Decision). It validates a fault network and predicts compartmentalisation issues based on fractures generated according to user-supplied rules. It has an emphasis on a kinematics approach.

**Earth Decision FracMV**:
http://www.earthdecision.com/products/reservoirmod_fracmv.html
This software was developed based on cooperation between Midland Valley and Earth Decision. It generates geologically constrained discrete fracture networks using seismic attributes, volume strain, other 3D data and wellbore data, providing a method to generate flow properties directly from the fracture network (Figure 1.11).

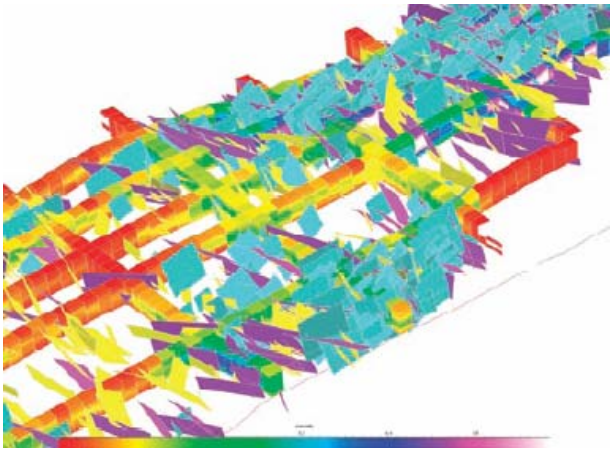

**Figure 1-11 Example of a 3D DFN with a 3D grid extracting fracture properties from FracMV (Earth Decision web site). Note how the fractures, though generated stochastically, showing a uniformity that reflect geological constraints.**

**IFP – Beicip Inc FRACA**:
http://www.beicip-inc.com/portal/alias__Rainbow/lang__en-US/tabID__3341/DesktopDefault.aspx
This is the French Institut de Petrole fracture software. FRACA is a fracture permeability modelling solution for faulted and fractured reservoirs. FRACA is a commercially-available package that permits the user to calibrate the fracture model to dynamic field data. Again it is modular software split into data analysis, 3D DFN creation and dynamic fracture analysis. Thus it synthesizes a large variety of data to characterize fracture networks (borehole imagery, logs, cores, flow meters, seismic

attributes). FRACA offers a number of variably-constrained stochastic techniques to generate fracture models at various scales (wellbore, grid block, full field). FRACA calculates the equivalent dynamic characteristics of the fractured reservoir (fracture permeability, matrix block size) for either single or dual media simulation. Its main strength is the latter (dynamic simulation analysis such as well tests with the objective of understanding the fracture network). Its workflow is shown below (Figure 1.12) together with a view of a typical 3D DFN network.

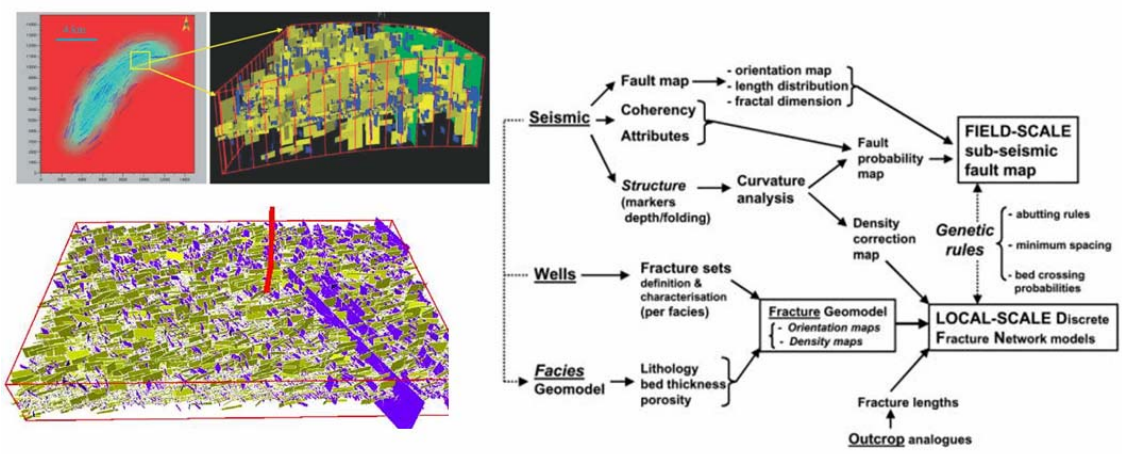


**Figure 1-12 Typical example of 3D DFN generated using FRACA and the geological multi-scale workflow used for fracture characterization (Biciep Inc Website & Bourbiaux et al, 2005).**

**Roxar FracPerm**:
http://www.roxar.com/category.php?categoryID=651
Roxar has also recently introduced fracture software to their geological modelling tools (RMS). It uses both geo-mechanical and dynamic information to constrain the generated DFN via the usage of density maps that may relate fracture density to fault proximity, curvature or stress/strain models. The software contains its own stress calculator.

**ResFrac - NAPSAC:**
http://www.napsac.co.uk/
This software is no longer available as its licence has been bought by Veritas (see CGG below). It used to characterize fracture networks based on so-called fracture indicators and drivers (e.g. seismic faults are drivers while losses are indicators). The creation of the 3D DFN was done by collaboration with another company called NAPSAC. NAPSAC generates fractures as a combination of deterministic and random fractures. For random fractures a classification into sets is used. The basis for classifying these sets can be according to orientation, spatial location or flow properties.

**CGG Veritas FractAL**
http://www.veritasdgc.com/bins/content_page.asp?cid=5-946-2642
This is a future generation of ResFrac that has an emphasis on estimating fracture density and orientation from variations in AVO with Azimuth. The input to FractAL is conventional P-wave 3D gathers that have been processed with an Azimuthal AVO-

preserving flow. It is not clear to me whether the software uses the fractal concept but I do not think so.

**Stanford Uni Poly3D**
http://pangea.stanford.edu/research/geomech/Software/Software.htm
This 3D-boundary element method uses triangular dislocations in a linear-elastic, homogeneous, isotropic, whole- or half-space to solve linear inverse problems such as slip inversion for earthquake study. It relates to fracture characterization by identifying highly strained areas. Thus, it is a geo-mechanical tool in the realm of fracture characterization more than 3D DFN generation. One of the main challenges for this approach is when a fractured area had been subjected to multi-phase deformation which usually makes geomechancial analysis very complex.

### 1.6 On Fracture characterization

In this thesis, the fractures are characterized based primarily on a geometric description that arises from BHI interpretation analysis as well as outcrop evaluations. This description is supported to some extent by kinematics (strain) as well as stress analysis. The regional fracture evaluation chapter provides a brief preview of this work as the objective there is to set the scene for specific field scale evaluations and to describe the geometry of the fracture network.

The field scale evaluation, however, presents a detailed fracture characterisation that is based on combination of fracture indicators such as seismic and dynamic data as well as fracture drivers related to mechanisms, such as curvature assessment, fault analysis and simple stress analysis derived from regional tectonic geology as well as pressure data (leak off or interference tests) together with borehole elongation data. These are termed fracture constraints in the SVS workflow shown in Figure 1.9, and they are used to enable the creation of fracture concept models for the reservoirs studied.

Other approaches of fracture characterisation such as fractal analysis (La Point, 1988; Boad and Long, 1994) are disregarded in this research since the matrix or stratigraphy description indicates high rock heterogeneities which result in anisotropic and heterogeneous fracture distributions that do not fit the fractal concept. One example of fractal methodology assumes that the large scale features (seismic faults) and small scale features (fractures seen in wells) have a geometric relationship, and by plotting their intensity versus frequency in a log-log plot, sub-seismic features can be estimated. It is shown herein that there is no such simple relationship between faults and fractures in north Oman.

Poly3D analysis, a stress analysis of force to predict areas of high strains hence high fracture intensity zones, is also disregarded in this research as regional tectonic geology

indicated that the north Oman reservoirs have been subjected to multi-phase deformations (many uplifts/collisions), which would make such analysis very complex.

## 1.7 Data availability and limitations

This section gives a summary of the data availability and limitations of the data used.

### *1.7.1 Regional data*

**Stratigraphy data:**

The summary presented in the first section of the regional stratigraphy is from reference papers that used subsurface well correlation panels and outcrop descriptions of Oman Mountains, Jebel Madmar in the North and Huqf area in the SE. The thickness map for the Natih formation was created in SVS using well data obtained from RUI (PDO subsurface data base). The porosity–permeability versus depth for the Shuaiba fields are based on core data from RUI, analysed in Excel. Only vertical wells are used as the deviation data were not available, data were not scrutinised for quality and from experience, core samples are normally biased, as samples are usually taken only from competent "not-friable" sections of core. The net result is to get lower porosity and permeability averages compared to the log porosity average.

The outcrop description data used were extracted from the following studies, table 1.1:

| Location | Formation | Described by | Year | Remarks |
|---|---|---|---|---|
| Oman Mountains | Natih/Shuaiba | Buchem et al | 2002 | |
| Jebel Madar | Shuaiba | Heesbeen | 2002 | Vrije Uni. of Amsterdam |
| Jebel Madmar | Natih | Dekeijer et al | 2004 | Shell EPT research |
| Salakh Arch I | Natih | Jones & Loosveld | 1994 | PDO research |
| Salakh Arch II | Natih | Kindi | 2006 | Leeds Uni PhD |
| Central Oman | Salt | Peters et al | 2003 | PDO field trip work |
| Huqf | Shuaiba | Immenhaouser et al | 2004 | PDO – Vrije Uni research |

**Table 1-1 Main studied Cretaceous outcrops of Oman used in this research. For the location of these outcrops see Figure 2.1, except for the salt outcrops which are shown in Figure 2.25**

**Tectonic data:**

The regional tectonic analysis is based on an integration of the data from NOCEM, primarily horizons and faults. These are based on regional 2D/3D seismic which was interpreted in 250m by 250m bins, and hence was not suitable for detailed field scale analysis. The faults and horizons were cleaned up using gOcad modelling. In addition, the data was further refined by PDO and the faults were split per time horizon going from the basement to the surface level. Furthermore, while defining the tectonic domains for north Oman (domains are areas that cover more than one field which have more or less the same tectonic history), more detailed sub-regional fault interpretation were used.

The salt outlines and the basement fault trend maps are mainly based on gravity-derived maps of the basement. The resolution of the data used is not very detailed; however, it is sufficient for drawing conclusions regarding the main trend in the basement and the salt

locations. Moreover, outcrop and seismic studies of salt diapirs in the region are presented. The paleo and current geo-stress data is mainly based on drilling Limit Test data and a few Leak Off Test data. Also, some BHI elongation data, which are scarce, especially for the Shuaiba Formation, were used, together with the induced fractures, for estimating stress orientation.

The main outcrop data used are from the Salakh Arch NE of Natih field. In this area the main outcrop is the Natih Formation and not Shuaiba. Also, recent studies have shown that local tectonics, such as uplift, have more impact on the fracture characteristic of the outcrop compared to regional effects. Recent study has shown that the majority of the fractures seen there are related to local doming (curvature). Thus, the data is used as analogue only with caution. In addition, that fracture density "spacing" calculation from outcrops, should be used with caution as it might be biased due to lack of sampling area exposed, and possibly due to scan line orientation issues, parallel or perpendicular to fracture set orientation, and also is it a 1D line, 2D box or even a circle (Terzaghi, 1965; Rohrbaugh, 2002); and there is also a scale issue: Outcrop fractures are equivalent to core fracture and hence tend to be much more intense than BHI fracture. Field experience had shown that if a fracture is not seen in a BHI, it will not be flowing (i.e. no losses or no potential path for water break through).

Curvature analysis has been used in this research with the following objectives:

- To highlight areas of high curvature (proxy for strain) using multi-direction (azimuth) with large wavelength,
- To highlight areas of possible faults using multi-direction small wavelength analysis, curvature discontinuities to visualize fractures in damaged zones, and
- To highlight hidden structural strain oblique to dominant fault direction using uni-direction (azimuth) small wavelength to see FC or small faults.

In this research the curvature calculation is done in SVS and the Kmax value is used, which calculates and maps the maximum curvature value. The quality of a curvature map is highly dependent on the resolution of the input horizon map and how it was created. Thus, where the seismically interpreted horizon is of low quality (e.g. the regional-scale top Shuaiba map of north Oman, which was based on regional 2D/3D seismic acquired at 250m bins grid), the measured maximum curvature value (Kmax) might be in-accurate. In contrast, for field-scale seismically interpreted horizons, the value might be good enough to use especially if integrated with other fracture related data (e.g. BHI fracture interpretation and dynamic fracture indicators such as losses).

The BHI data (this is applicable for both regional and field scale data) has its own issues (Narr, 1996). The resolution of the log is less than for the cores. It has been reported (Lekhwair field – see existing work: report not available) that BHI logs see about 7% of the fractures reported/seen in core. The quality of the resistivity log run is dependent on borehole state (in-gauge or not) and on type of mud used (water or oil). In Oman, water

based mud is used, but borehole diameter enlargement is very common in fractured reservoirs, and it has even been used as an indicator of fractured intervals. Moreover, there is a blind zone associated with the BHI tool. It is normally about 5 degree in each direction away from the well strike. So any fracture striking within +/- 5 degree of the borehole will not be seen by the tool. Furthermore, inconsistency in the fracture picks may arise due to having more than one interpreter (i.e. which fracture to be called large conductive and which ones to call small non-conductive differ from one interpreter to another). Most recent north Oman BHI data were interpreted by the same person (Ismail S Ozakaya -Baker Atlas), which resulted in better consistency. The BHI fracture data had been subjected to standardization (the naming was changed to reflect that of PDO convention) as part of this research, thus allowing better comparison between each field. It is essential to note that despite the fact that these fractures are conductive in the image log, they might be closed to flow. Not all the conductive fractures seen in BHI conduct fluid**.** A good test is to calibrate BHI fractures against WFL or PLT production logs. In addition, there is also a lateral and vertical coverage issue: the fracture picks (objects) are sufficient enough for regional and sub-regional statistical analysis; however, in some fields where the data is scarce such as Al Ghubar, caution should be applied when drawing conclusions based only on this data. From the vertical coverage prospective, most fields in north Oman have their wells either drilled in the upper most part of the reservoir (producers) or below the OWC (injector) as the case for Musallim, Burhaan and Saih Rawl fields. This results in a lack of sampling for the intermediate parts of these reservoirs. Furthermore, the main fracture orientations in north Oman is NE and NW, hence wells running parallel to these directions will be biased in their coverage. More critically in some fields due to their development (as the case for Saih Rawl) the wells are orientated in only one direction which results in obtaining biased data.

**Diagenetic data:**

The diagenesis history of the region has not been studied in detail yet. There are some emerging concepts based on Shell recent work on the Fahud field. Also there are a few observations that suggest diagenesis effects, such as the tilting of the Shuaiba reservoirs and the fracture cementation with depth. There is limited work done to understand the uplift history of north Oman. The main conclusions are drawn from sub-crop maps and density vs. depth plots.

**Production data:**

The production data used for the field performance analysis were obtained from oil field manager OFM data-base from PDO. There is always error associated with the human interface. However, annotations, wherever possible, are used to explain these actions, for instance onset of water injection or start of drilling horizontal wells or just closure due to shut down. More importantly the recent production data from central Oman Ghaba North and Al Ghubar has an allocation issue due to a failure in metering.

### *1.7.2 Field scale data*

For the field scale analysis of Lekhwair A North (LAN) and Ghaba North (GN), the main fracture data used are BHI fracture picks. For LAN this data is sufficient enough (orientation wise, and with good areal coverage, though limited vertical coverage) to make a statistical analysis, whereas for GN it is much more limited, hence, the same issues mentioned above apply. Core data are extremely limited and thus are used only for qualitative analysis. Analogue information from other fields such as Qarn Alam is also used.

The dynamic well scale data is also very limited. The losses data are few and their magnitude or depth is seldom identified. More importantly there are few production logs (PLT or water flow logs WFL) which are crucial for defining the fracture properties. However, there is a well drop-off test for a LAN injector and an interference test for GN which will be examined. Well by well production data has been used again for qualitative analysis, as these data are not robust enough especially in case of GN.

Furthermore, the seismic volumes are used as qualitative data and their value is primarily in the integration with other data. All the faults interpretations have been done outside this study (in most cases by PDO seismologists). For the specific fields section of this research, all the latest interpretations are used. Top Shuaiba seismic reflector is very weak, hence seismologists tend to interpret top Kharaib and then isochore upward, since top Shuaiba is conformable with top Kharaib and normally Shuaiba has a uniform thickness (unless distorted by fault cut out). The interpretation at a field scale is further refined using well tops (well-tie). The top reservoir horizons and faults interpretation of both fields are thought to be robust enough and the analysis done on them (e.g. curvature for the horizons) has helped in defining a better picture of the fracture network, although there is no sub reservoir horizons mapped seismically.

## 1.8 Pre-view of subsequent chapters and main conclusions

Chapter 2 covers the tectonic setting, the stratigraphy (with emphasis on aspects related to mechanical layering), outcrop analysis, fault distribution, uplift and stress analysis. It is based primarily on a review of existing work ("literature"), including work done by the writer while working for PDO and Shell EP Technology, as well as work done by the writer specifically for this thesis. The objective is to set the scene for the fracture characterization. Thus, it is quite lengthy and **the reader may opt to skim through it**. The related Appendix A presents a screening of the total production history of each of the Cretaceous fields, with the objective to draw any conclusions regarding the connectivity of these reservoirs and how that links to fractures.

Chapter 3 examines the fracture geometrical distribution, based on BHI image interpretation analysis, seen in all the investigated reservoirs, which is perceived to be important to the understanding of the Cretaceous fracture network of north Oman. It also includes a review of existing fracture studies carried out in these fields.

Chapters 4 and 5 provide a detailed fracture characterization for two specific fields: Ghaba North (GN) and Lekhwair A North (LAN), respectively. A descriptive approach is used, coupled with the integration of all the fracture related data available for the two reservoirs. For the LAN, the work presented depends to some extent on existing fracture analysis done by PDO. For both fields, examples of 3D discrete fracture network (DFN) models were built based on conceptual scenarios which were derived from field fracture related data evaluations.

Chapter 6 presents a simplified 3D Eclipse$^{TM}$ simulation exercise executed on a sector scale model extracted from the 3D geo-cellular static (both matrix and fracture properties) models for GN Shuaiba reservoir. The objective of the simulation is to show that the candidate understands the impact of each fracture scenario on the reservoir simulation process. It does not go into detailed dynamic analysis, as no history matching exercise is attempted. However, dynamic calibration of the static fracture scenarios used, were done in Chapter 4 and Chapter 7.

Chapter 7, the analysis chapter, is a critical analysis of the fracture related data of north Oman Cretaceous reservoir with the objective of creating a regional synthesis for the genesis of these fractures. In addition, it presents further detailed fracture flow evaluations, as well as dynamic calibrations “history matching” of two examples of 3D DFN from Ghaba North Shuaiba reservoir.

Chapter 8 presents a summary of the findings of both regional scale and field scale fracture analysis, i.e. the conclusions. In addition, it presents some ideas concerning ways forward such as: further refinements of the fracture network characterization approach, more investigation into the genesis of the fracture networks that have been interpreted, using mathematical stress-strain approaches, and some recommendations with regard to new data acquisition.

The main conclusions are presented here to assist the reader in identifying the main points while reading the subsequent chapters:

The dynamic data available from north Oman carbonate fields (e.g. well tests, PLT logs, losses data, etc) are scarce and only useful for qualitative characterization of the reservoirs’ fracture network.

Calculating fracture intensity based only on dynamic data (e.g. well production rate) tends to result in overestimation of the fracture network present in the Cretaceous reservoirs of north Oman. This is because diagenesis in these reservoirs tends to enhance connectivity by either leaching the matrix or even part of the fracture network in the vicinity of major faults or fracture corridors. Diagenesis may also have negative effects, such as degradation of fracture connectivity due to cementation processes, which has been observed, for instance, close to the OWC in Qarn Alam Field.

PLT logs have shown that it is mainly those fractures that occur in clusters which contribute to flow. These occur in fault damage zones or as fracture “swarms” or corridors.

The core data (from Qarn Alam field where a detailed structural interpretation had been undertaken on core data) tend to show more intense fracturing than BHI. This is entirely due to the scale of resolution. In cores the small scale fractures (even the hairline and stylolite fractures) are very visible. In the majority of Shuaiba fields, the core is friable and only available for vertical wells hence its coverage is very limited. Nonetheless, the presence of damaged core can be used as an indicator of fracture occurrence in cases where the caliper log is erratic.

There are three types of fractures seen: a) Fault related fractures, these are the NW-WNW fault related fractures seen clearly in the Makarm High around Musallim field and Lekhwair area, and the NE fault related fractures attributed to local deformation such as salt in Ghaba North Basin; b) a dominant NE regional fracture system, which occur as either dispersed background fractures or in fracture corridors; an c) fold “curvature” related fractures in Natih field and in the eastern part of the area, such as Ghaba North and possibly Al Ghubar.

The NW/WNW fault related fractures are usually non-conductive except in the area of Lekhwair field. The fractures in the latter case are running opposite to the perceived present day regional in-situ stress that is orientated NE, though locally it had been reported to be running NW, as shown in compilation figure of the regional stress section. They occur as minor clusters or full fracture corridors mainly when their trace follows a deep seated basement fault. The ratio of conductive to non-conductive fractures here is 2:1. On the other hand, the N to NE fracture set occurs as background fractures sometimes related to existing local faults (as the case for the salt deformed area around Ghaba Basin). They tend to occur in clusters. In order to obtain a more accurate calculation of their spacing, the data has to be split into clusters spacing and background spacing. Conductive fractures dominant in these fields.

The schematic below (Figure 1.13) highlights the geometric distribution and BHI fracture counts, split per type, seen at the regional scale, superimposed on top of the

perceived structural-stratigraphy-diagenesis domains with salt outline and basement fault outlines.

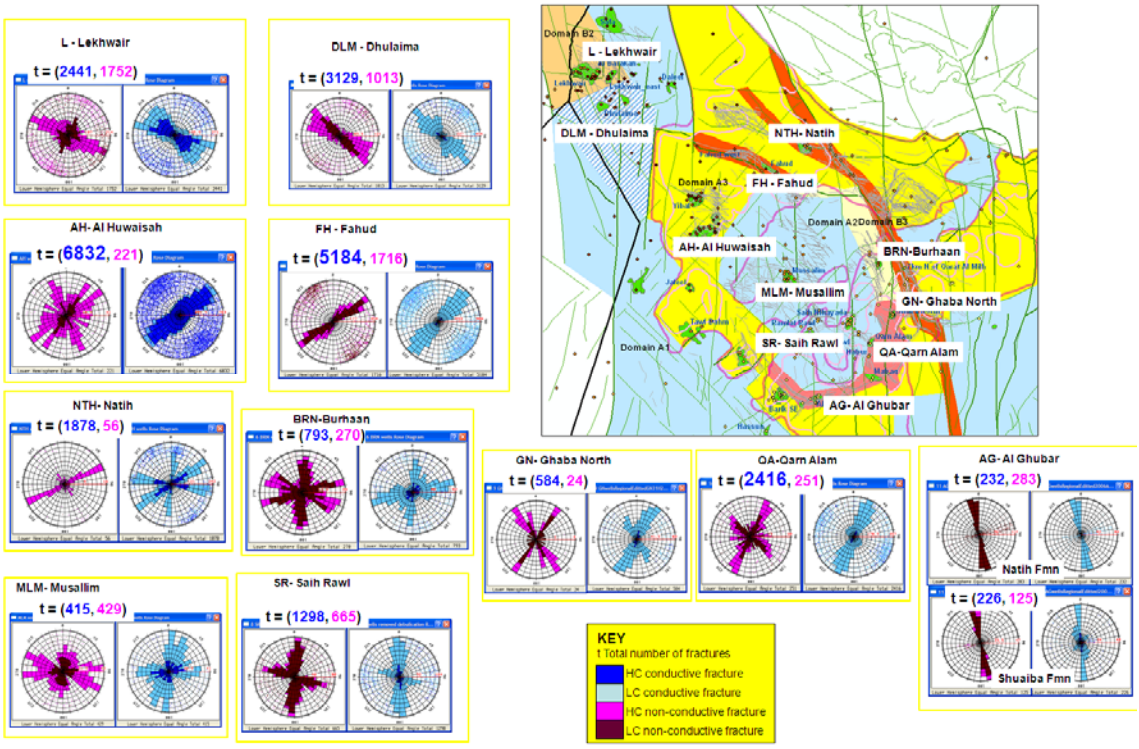


**Figure 1-13 Map view of north Oman (compare to figure 1.1 for orientation) showing the BHI fracture rose diagram per type (dark blue large conductive, light blue conductive, dark pink large non conductive, pink small non conductive) with total count of number of fractures (t). The inner map is showing the structural domains (areas of similar tectonics) of north Oman, for further detail on structural characteristic of each domain see section 2.3.2; Also shown are the salt outline in pink and basement faults (structural grains) in green as well the Cretaceous Faults in grey.**

The schematic cartoon drawing below (Figure 1.14) is an attempt to summarise the fracture network characteristics in north Oman, showing a block diagram per area (Al Huwisah is not included because existing report were not available to this study to integrate the BHI data with other field related data). These are like a mid case scenario per field showing both the geometrical distribution and the fracture mechanism driver. No quantitative data were included (For an enlarged A3 picture of this figure see APPENDIX 1).

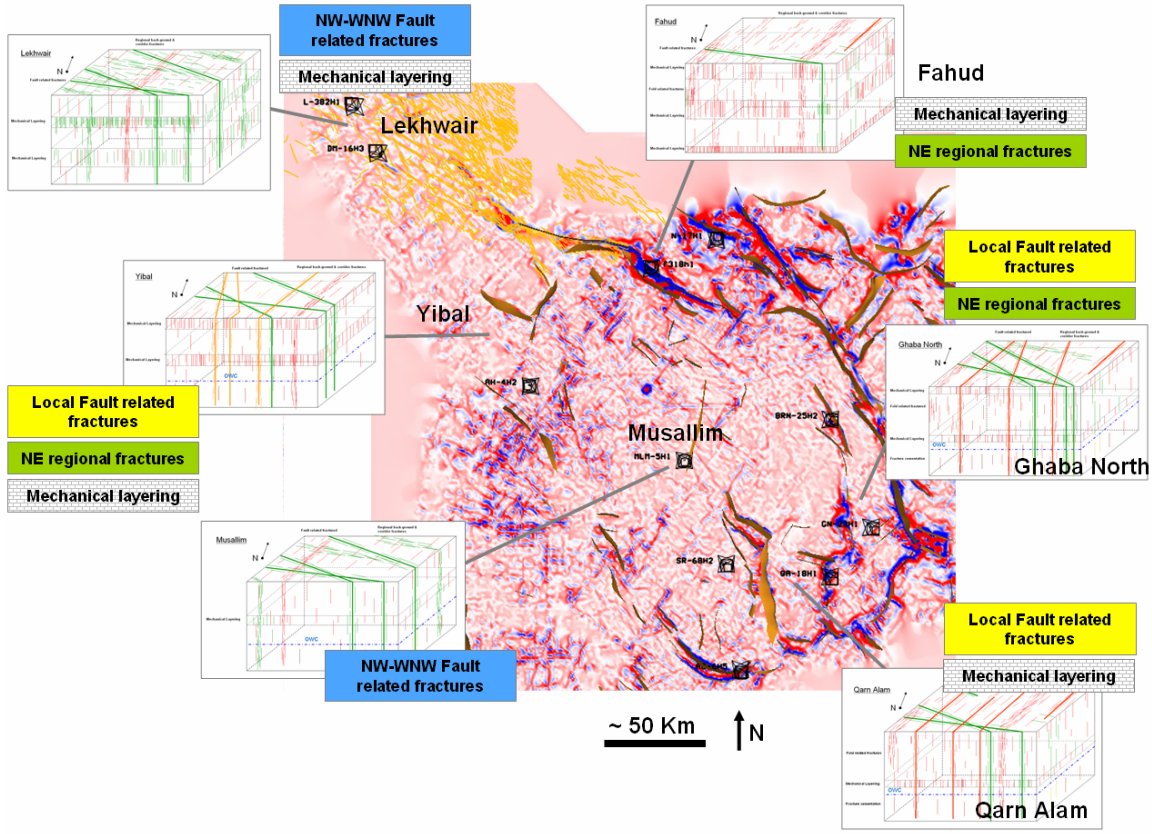


**Figure 1-14 Schematic block diagrams showing a possible mid case conceptual fracture scenario per each area of north Oman. Green line relate to NW to WNW trending fault-fracture, while orange line relate to faults and their associated fracture running N to NE; Red line relate to background NE fracture and NE fracture corridors. Map in the middle is a multi-directional curvature map (Kmax) of top Kharaib of NOCEM at 500m scale, shown together with regional fault planes (light brownish) and sub-regional-scale seismic faults striking WNW to NW (dark yellow fish net line). These fish-net faults are believed to extend all the way to Saih Rawl field and even to the SE part of north Oman. *See graph below an insertion of what is believed to be the main driver for fracture in each field: LKH = Lekhwair, DLM = Dhulaima, AH= Al Huwisah, Y= Yibal, FHD= Fahud, NTH= Natih, MLM= Musallim, SR= Saih Rawl, BRN= Burhaan, GN= Ghaba North, QA= Qarn Alam, AG NTH= Al Ghubar Natih Formation, AG SHB= Al Ghubar Shuaiba Formation.***

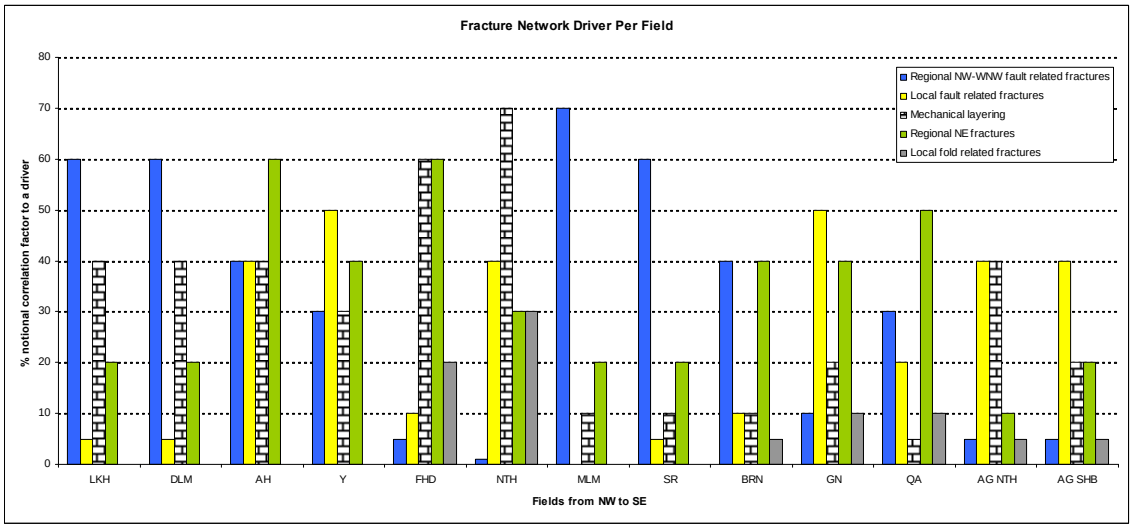

# Chapter 2– SETTING THE SCENE

## 2.1 Introduction

The regional geology of Oman has been the subject of many integrated studies, spanning from Lee (1928), Glennie et al (1974) and Clarke (1988) to more recent studies such as Loosveld et al (1996), Stuart-Smith et al (2003; 2004), and Filbrandt et al (2006). The majority of the studies have been based on descriptions of the north Oman Mountains outcrops, with some covering the Eastern Oman Masirah Huqf area outcrop. The Glennie et al (1974) study of the Oman Mountains, with reference to the Oman Interior (subsurface fields), was the earliest comprehensive regional geology description of Oman. It resulted in the establishment of the Oman stratigraphy shown in Figure 1.2 above, its relation with the wider Gulf region, as well as the creation of the first ever structural sketch map of Oman. An updated map for north Oman is shown in Figure 2.1. The stratigraphy of the interior of Oman was further refined by Hughes Clarke (1988).

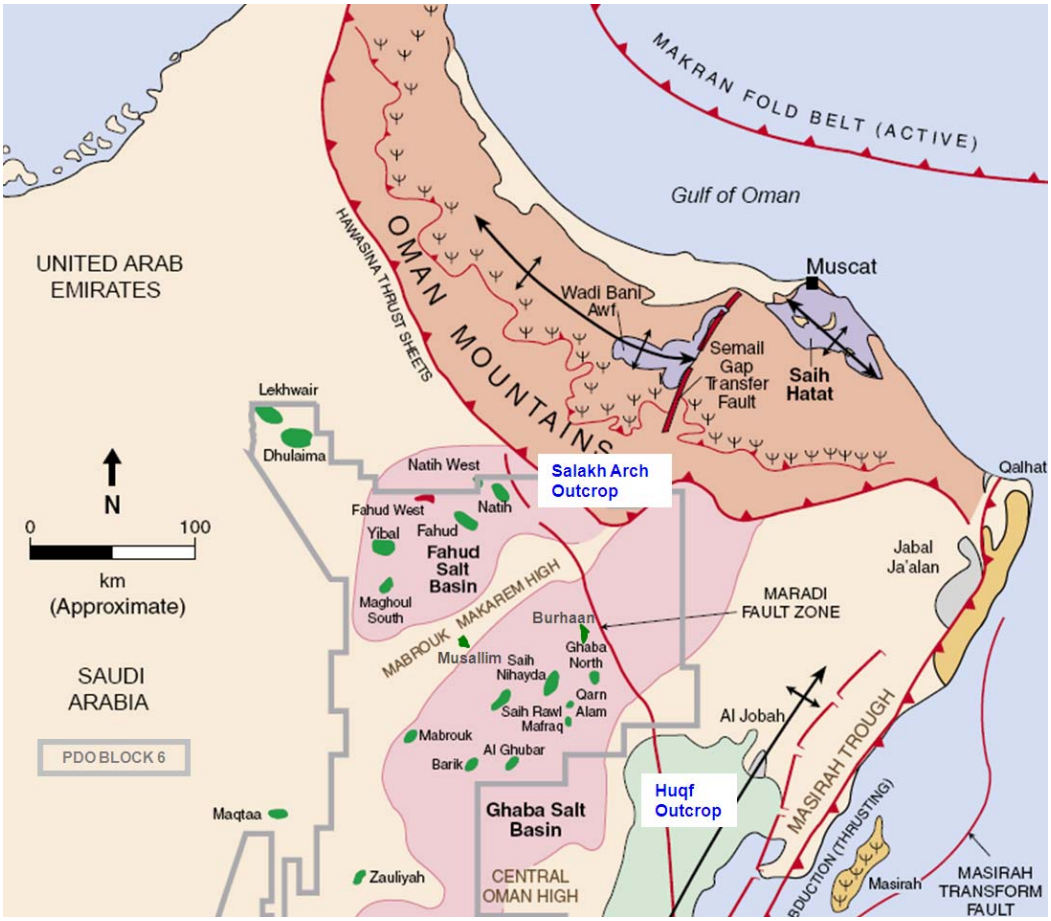


**Figure 2-1 Structural map of Oman (Filbrandt et al, 2006). Slightly modified to add in Musallim and Burhaan fields and highlight the location of Cretaceous outcrops in blue font. Main features are the light brown Oman Mountains bounded by thrust; the green Huqf outcrop west of the Masirah thrust to the SE and the Salakh Arch outcrop in NE of Fahud salt basin; pink salt basins and the red Maradi Fault zone.**

A summary of the main tectonic studies related to this research is presented below in a section concerned with the regional structural setting. These studies focused on a description of the major structural aspects, with two of them (e.g. Loosveld et al; 1996 and Filbrandt et al; 2006) **focusing on the interior of Oman**, where the oil and gas fields reside. In addition, there have been many new integrated studies on the stratigraphy of the Cretaceous Shuaiba and Natih Formation in Oman, including Droste and van Steenwinkel (2004) and Droste (2002-2003). This chapter will summarise the key stratigraphic findings that are related to fracture distribution.

In contrast, detailed fracture characterization studies are predominantly reported based only on a single subsurface field or single outcrop basis. For instance, Jebel Madmar, north Oman fracturing was described by de Keijzer et al (2004); Jebel Nihayda by Mercadier and Makel (1989), Qusaybah by Jones and Loosveld (1994) and Salakh Arch by al Kindi (2006). There is a recent attempt to use the Huqf outcrop as an analogue to Shuaiba reservoir by Immenhauser et al (2004).There have been few attempts to correlate between outcrops in the foreland of the Oman Mountains and nearby subsurface fields.

The map view sketch of Oman (Figure 2.1) together with a schematic cross section (Figure 2.2) show the main structural features of north Oman geology. The following elements are the main aspects; these will be further described in this chapter: The NW-striking Oman Mountains occur in the NE part; the foreland Salakh Arch outcrop trends southwesterly away from the Oman Mountains; the Huqf outcrop and Masirah Island occur in the SE; the salt basin (pink colored) underlies most of the interior and is very strongly linked to the basement structural arrangement; and the Maradi Fault Zone running from the Salakh Arch at the base of the Oman Mountains in the north all the way to the SE Huqf outcrop. The stratigraphic intervals of primary interest in this thesis consist of the Cretaceous Natih Formation, which is generally characterised by layer-bound fractures, while the slightly older Shuaiba Formation is more homogenous, from a mechanical layer prospective. However, in the northern part of North Oman (such as in the Lekhwair and Dhulaima fields), where the upper Shuaiba Formation exists, there are signs of fractures being controlled by layering.

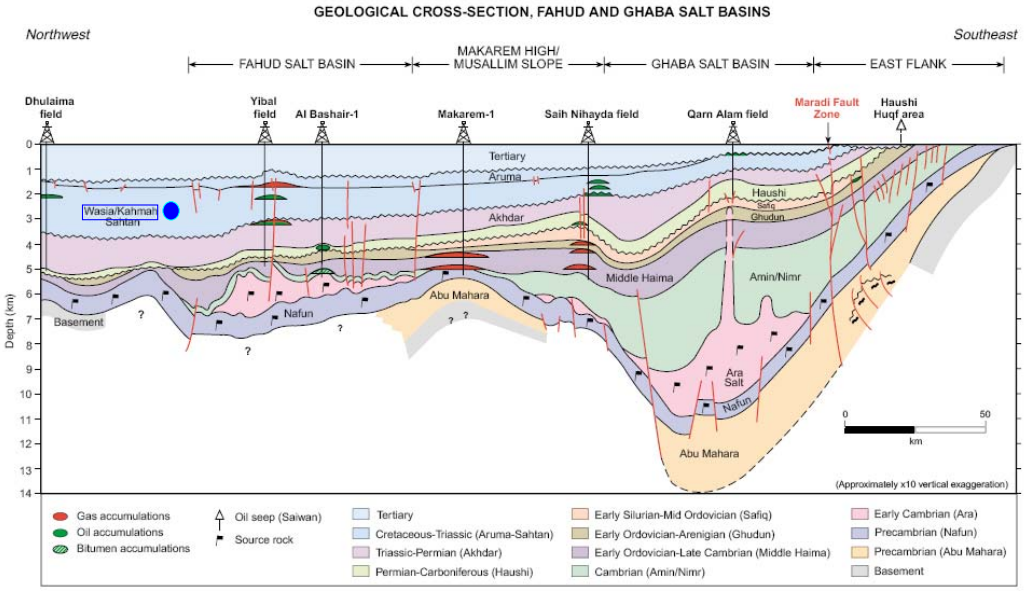


**Figure 2-2 Schematic cross section of north Oman (Peters et al, 2003). For stratigraphy see Figure 1.2, highlighting the position of the salt basins and Maradi Fault zone.**

The oil charge for the Cretaceous reservoirs has been studied by Terken (1999) and more recently by the Geo-Solution team of PDO (Ochs et al, 2004). The oil types of north Oman (Figure 2.3) are: Tuwaiq and Natih oil [named the Mesozoic oil], Q oil and Huqf oil (split between North and South Oman). The Natih Formation is made up of both reservoir and source rock (Figure 2.4). However, the reservoir fluid of the Natih field comprises a mixture of oil types with Natih oil making up 75%. The Natih oil is perceived to have originated in the deep foreland basins, south of the Oman Mountains (Terken, 1999).

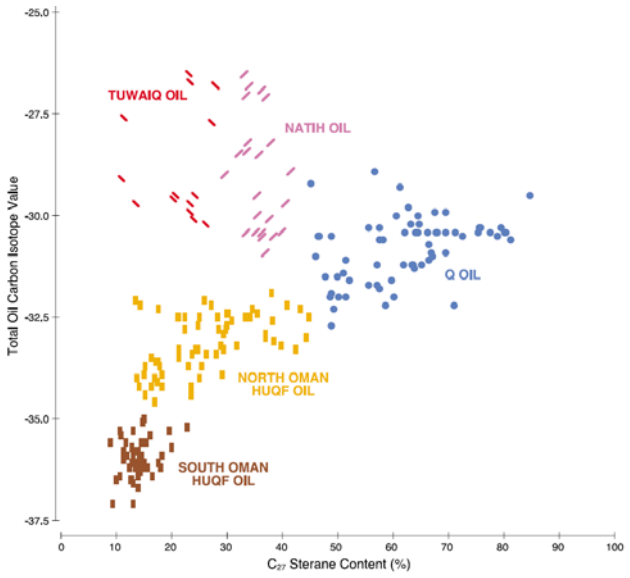


**Figure 2-3 A cross-plot of the % C27 steranes and total oil carbon isotope of all Oman oil types, (Terken, 1999). Note that Tuwiq and Natih oil also named Mesozoic oil.**

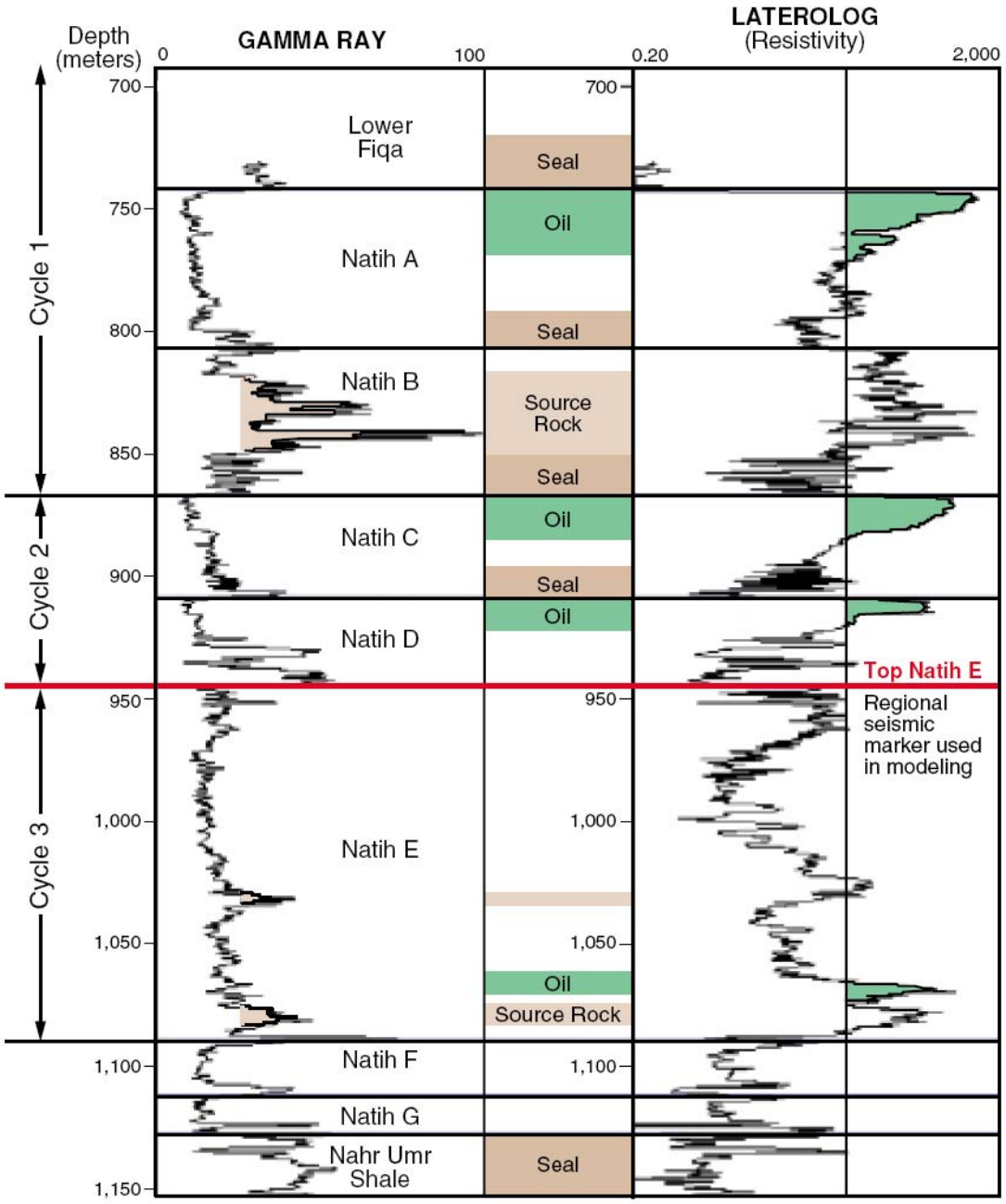


**Figure 2-4 Natih Field type log (Natih 3), with oil bearing reservoir, seal and source rock highlighted (Terken, 1999). For the stratigraphic subdivision see next section.**

Faults appear to act as conduits for hydrocarbon migration to most –if not all – the fields of North Oman (Figure 2.5) for both Natih and Shuaiba oil. This highlights the inter-link between oil charge and tectonic evolution of north Oman.

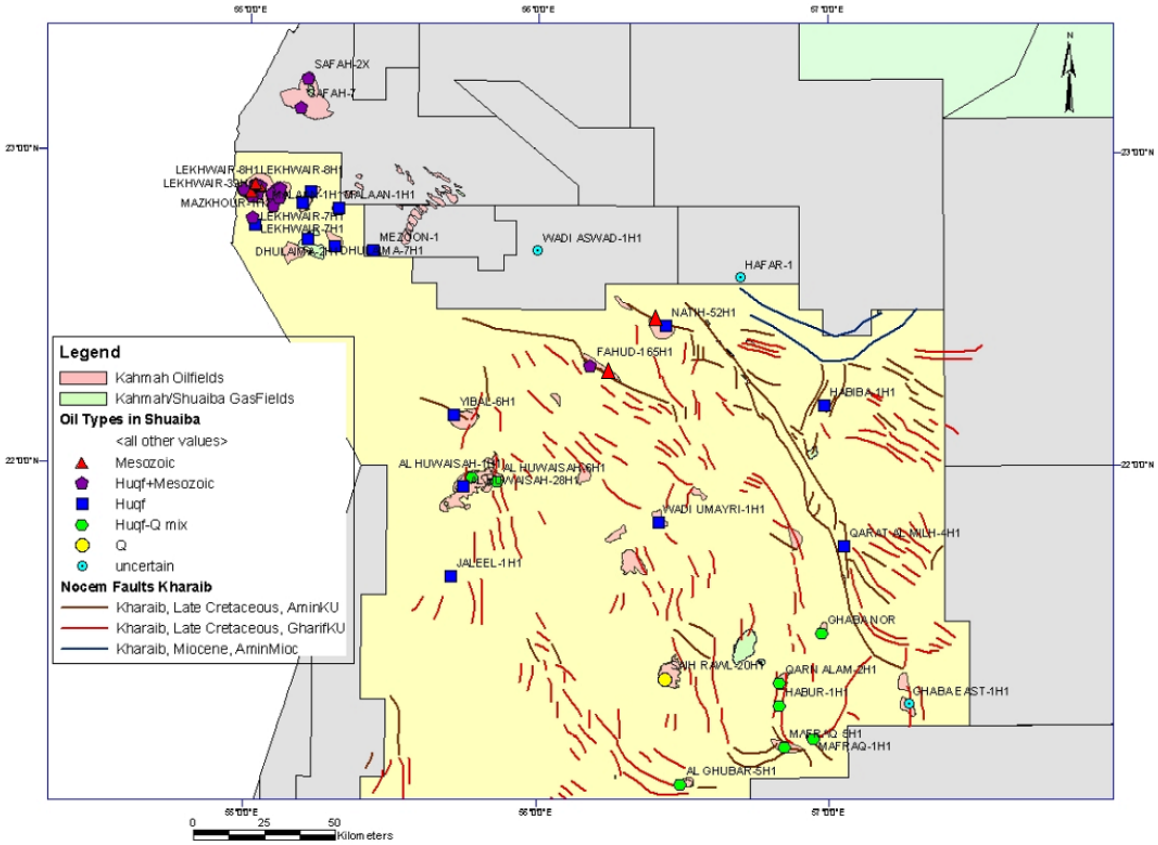


**Figure 2-5 HC type in the Cretaceous reservoirs of north Oman (Ochs et al, 2004 – modified to show only the Wasia Gp (Natih) as well as Kahmah Gp (Shuaiba) fields). Note the coincidence between the mapped faults and oil fields locations.**

## 2.2 Stratigraphy

The objective of this section is to provide only a general description of the stratigraphy of the Cretaceous reservoirs of north Oman. The reader is referred to Hughes Clarke (1988), Droste and van Steenwinkel (2004) and Terken (1999) for general information on the Cretaceous carbonate platform as well as the Natih Formation description and to Hughes Clarke (1988), Droste and van Steenwinkel (2004), Droste (2002-2003), and Immenhauser et al (2004), for detailed descriptions of the Shuaiba Formation stratigraphy and sedimentology. This section aims to highlight the main elements of the Cretaceous stratigraphy that are related to the fracture networks present in them.

Natih and Shuaiba are the main oil bearing formations for the Cretaceous fields of north Oman. However, in fields such as Qarn Alam, the Kharaib Formation and even Lekhwair Formation are considered part of the reservoir due to pressure and fluid communication via faults across them to the Shuaiba Formation. The Cretaceous of north Oman (Figure 2.6) is made up of two groups (Droste and van Steenwinkel, 2004):

- The Kahmah Group (late Berriasian to Aptian) consisting of:
  1. Habshan Formation
  2. Lekhwair Formation
  3. Kharaib Formation (Hawar member is believed to belong to it)

4. Shuaiba Formation (Incl. Hawar and divided into upper and lower)

- The Wasia Group (Aptian to Maastrichtian) consisting of:

5. Nahr Umar Formation
6. Natih Formation (Divided into members G to A)

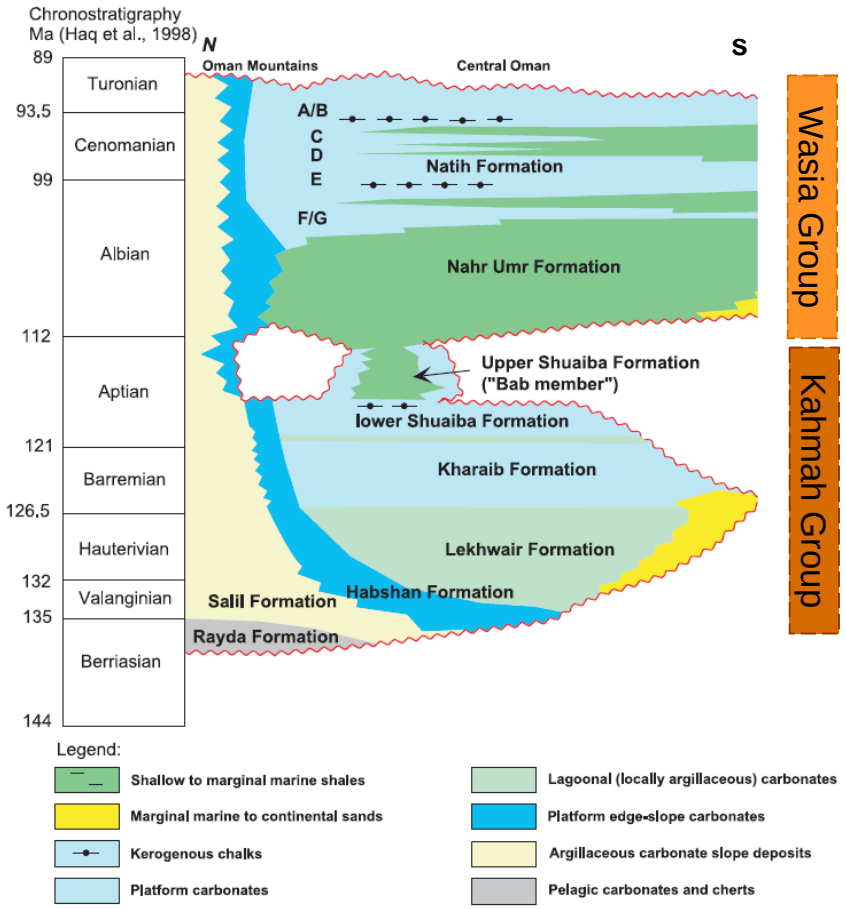


**Figure 2-6 Detailed stratigraphy of Oman Cretaceous (Droste and van Steenwinkel, 2004).**

The Cretaceous rocks of North Oman were deposited in a carbonate platform (Figure 2.7) complex that is up to 1200 m thick and 1000 km wide (Droste and van Steenwinkel, 2004). It unconformably overlies Jurassic and older strata, which were tilted, uplifted, and eroded in late Jurassic. The interior parts of this platform is commonly visualized as consisting of undifferentiated, extensive shallow-water deposits, where carbonates accumulated by aggradation. This view is based on the fact that individual shoaling-upward carbonate packages are laterally extensive (Droste and van Steenwinkel, 2004). The carbonate deposition was regularly interrupted by subareal exposure and the influx of fine-grained clastic material from the south. The largest interruption was a relative sea level fall in the late Aptian which can be recognized as a regional unconformity associated with major leaching and erosion (at the top of the Shuaiba). It was followed by a widespread influx of fine-grained clastic of the Nahr Umr Formation from the south. The Cretaceous platform was terminated by a regional phase of uplift and subareal exposure in the Turonian.

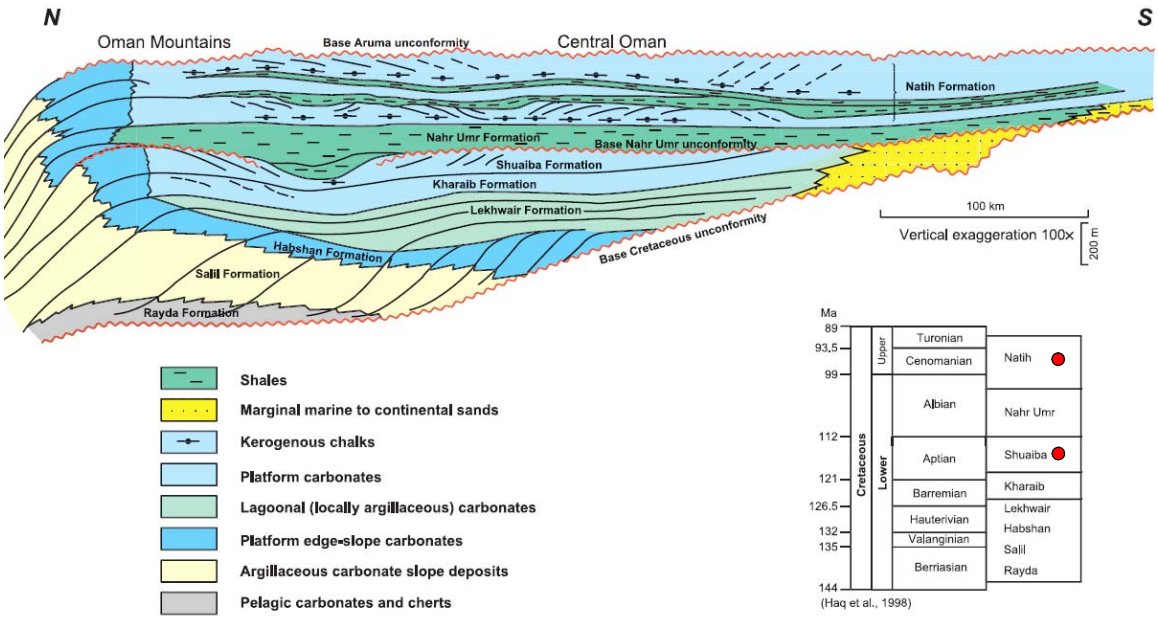


**Figure 2-7 Schematic geological cross section based on seismic, well and outcrop data of the Cretaceous platform (Droste and van Steenwinkel, 2004).**

### *2.2.1 Natih stratigraphy*

The Natih Formation is made up of seven members in the interior of north Oman; these are named A to G, with A being the shallowest (Figure 2.4). These members represent sedimentary cycles which start with thin mixed carbonate and shale that is then overlain by a thick carbonate. Each cycle consists of a relatively thin succession representing deepening, and a much thicker shoaling-upward interval. The coarser-grained sediments at the top of the cycles have commonly been subareally exposed and leached (Figure 2.8). The top of the Natih has been disrupted by faulting shortly after deposition, and has been truncated, leached and incised by extensive subaerial channel systems. The Natih thickness ranges from 0 to 400m (as in Natih Field), based on well penetrations. It thins toward the E to SE (Huqf) area, too (Figure 2.9). The oil bearing zones are indicated in Figure 2.4. The porosity and permeability distributions in the Natih Formation are strongly controlled by the prominent layering as shown in Figure 2.10. These characteristics suggest that the deformation of the Natih should be affected by its mechanical stratigraphy.

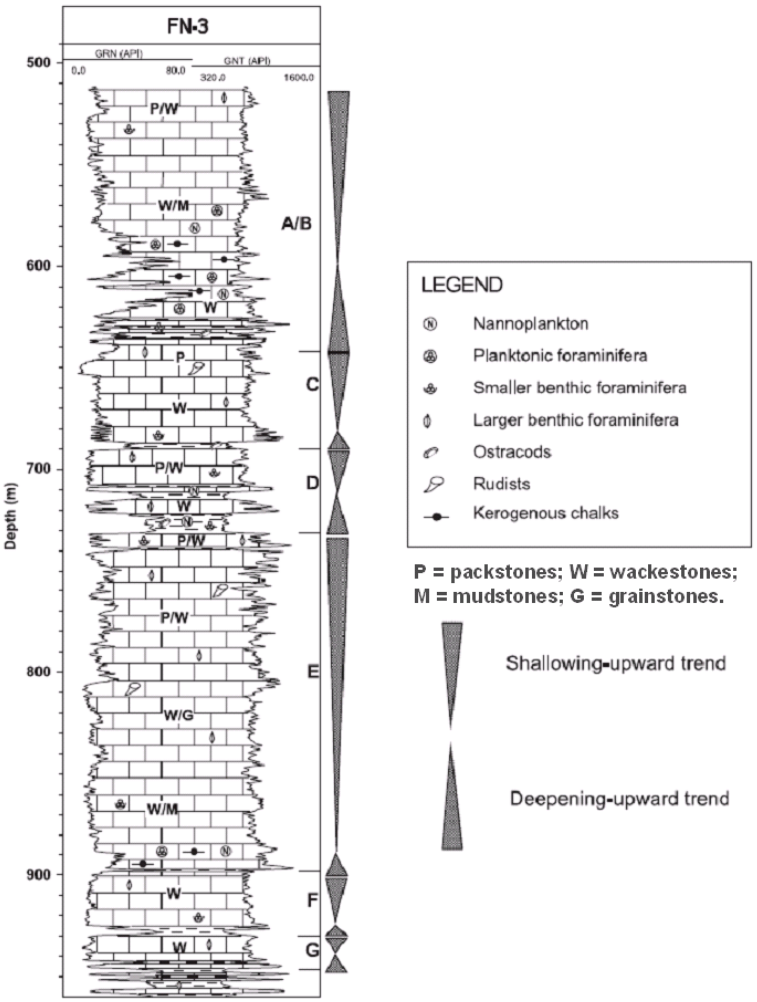


**Figure 2-8 Fahud field type log (Droste and van Steenwinkel, 2004).**

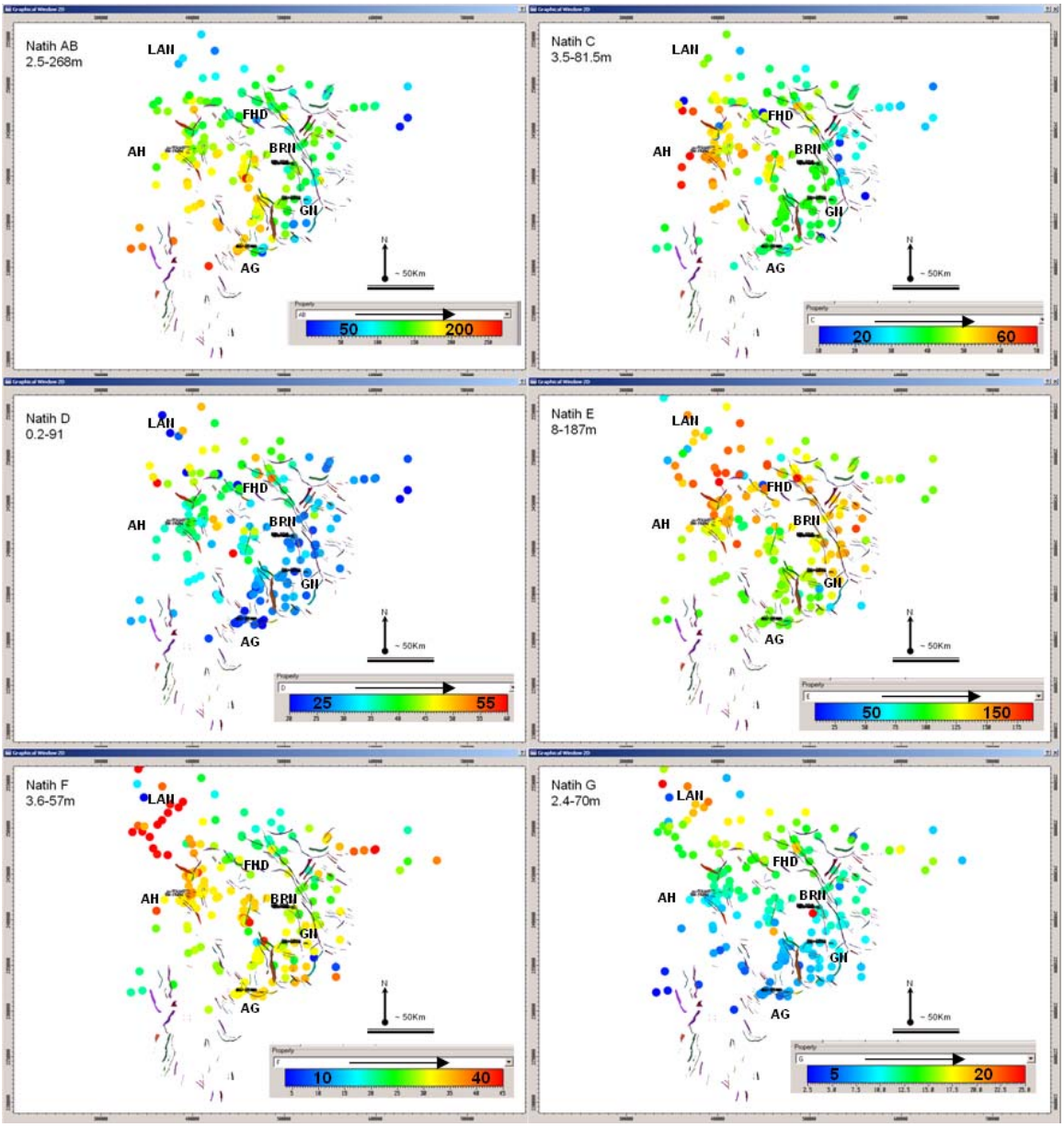


**Figure 2-9 Natih members thickness of north Oman fields, based on well data, shown in SVS. Note thinning toward E & SE. LAN = Lekhwair A North, AH = Al Huwaisah, FHD = Fahud, BRN = Burhaan, GN = Ghaba North and AG = Al Ghubar field.**

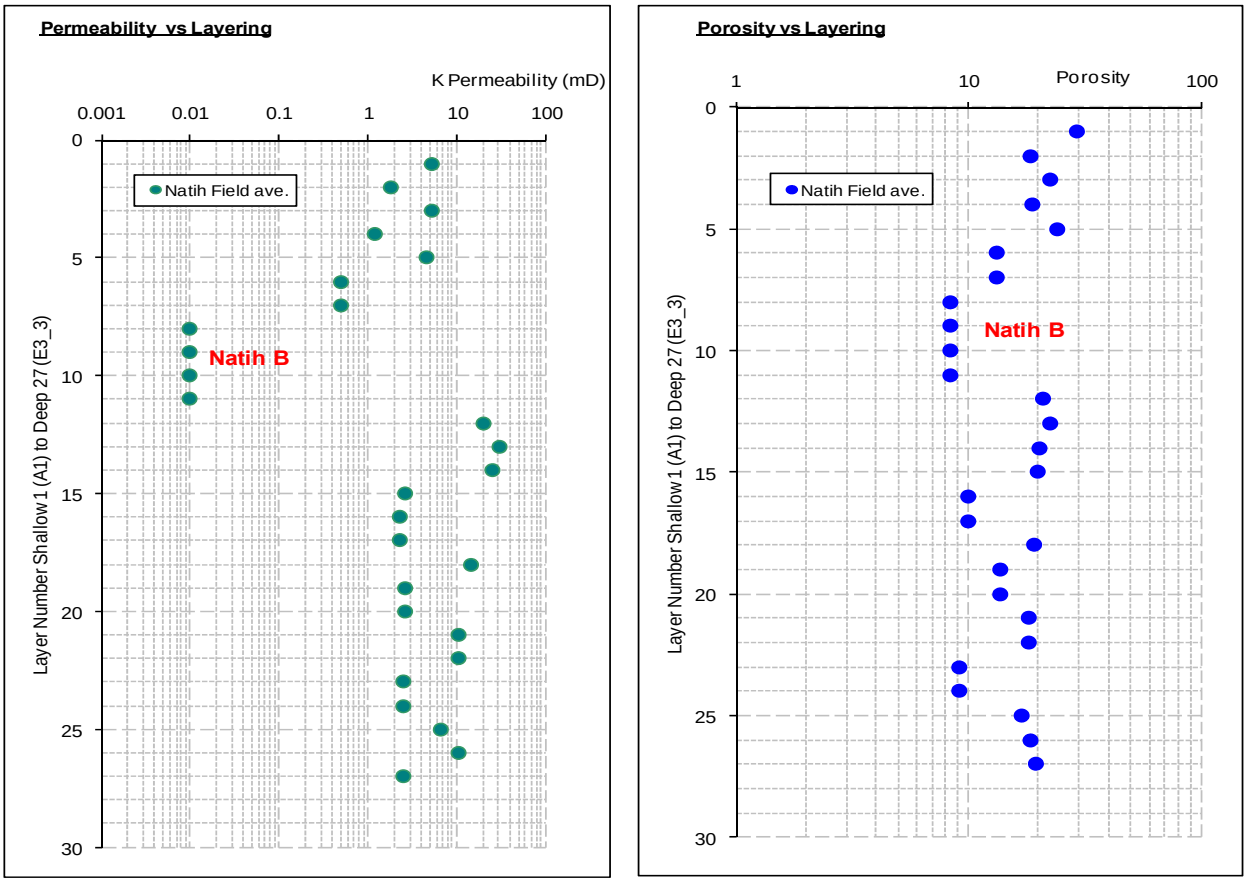


**Figure 2-10 Natih Field average Permeability (mD) and average porosity versus layering (depth). This can be used to predict zone of mechanical layers.**

A detailed study that helped in understanding the stratigraphy of the Natih was focused on the Oman Mountains and foreland area with links to the Interior of Oman (van Buchem et al, 2002). The main conclusions are similar to those based on sedimentological analysis: namely that the Natih Formation was built up by the alternation of two types of depositional systems: (1) a flat-bedded, mixed carbonate-clay ramp, dominated by benthic foraminifera, and (2) a carbonate-dominated ramp bordering an intrashelf basin, with abundant rudists in the mid-ramp environment and organic-rich basinal facies. In addition, the Natih Formation is organized in a long term shoaling upward sequence. Moreover, there are three fully developed third-order sequences distinguished in Natih Formation (Figure 2.11)

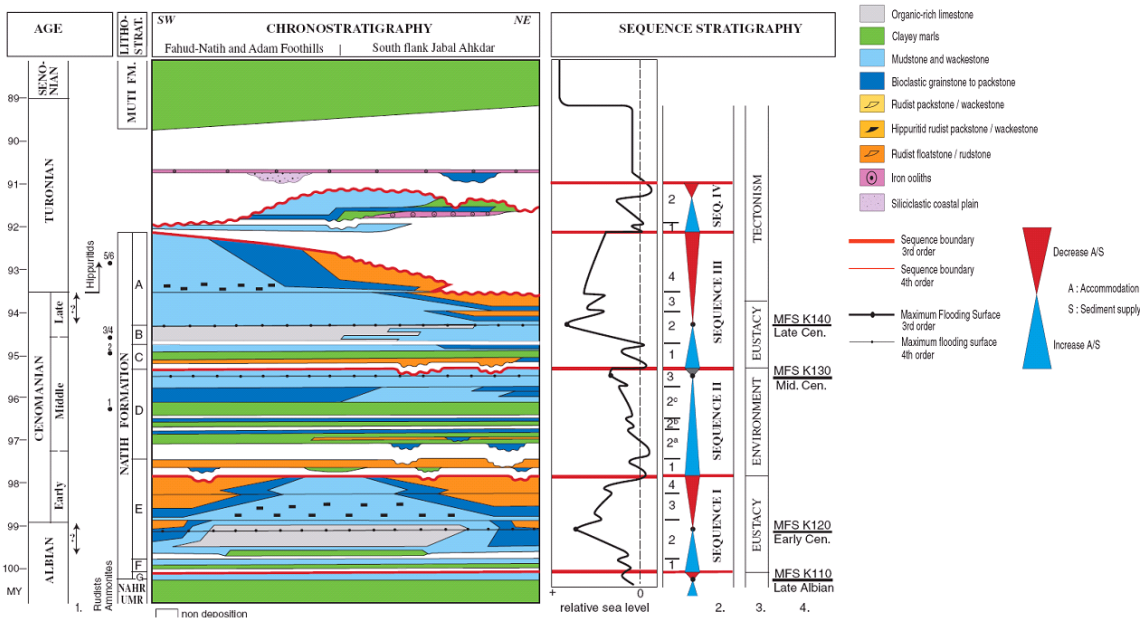


**Figure 2-11 Chrono-stratigraphic cross section of Natih Facies. Key at bottom numbered (1) Arrows indicating age uncertainty in dating, (2) 3rd Order and 4th order sequences, (3) dominant controlling factors on sedimentation pattern and (4) correlation of sequences with MFS as defined for the Arabian Plate by Sharland et al, 2001 (van Buchmen et al, 2002).**

### *2.2.2 Shuaiba stratigraphy*

The Shuaiba Formation is the uppermost unit of the Kahmah Group (also termed the Thamama Group in UAE & Saudi Arabia) and consists of an Aptian interior carbonate platform complex of some 100 m thickness. It is separated from the clean carbonates of the underlying Kharaib Formation by an easily recognizable marker bed of tight limestone (Hawar Member). In north-western Oman (Lekhwair and adjacent areas) the Shuaiba can be subdivided into a Lower and Upper Member (Figure 2.12). In other parts of Oman the calcareous clays are not present and the Shuaiba cannot be subdivided into members according to the official PDO lithostratigraphy. However in several fields (e.g. Al Huwisah and Yibal) an informal Upper and Lower Shuaiba subdivision has been applied locally usually with reference to gamma log profiles. The boundary between these members (Figure 2-13) is usually defined at a high gamma spike between a generally increasing and decreasing log trend (Droste, 2002-2003). Overall the Formation indicates a shoaling upward sequence. Detailed analysis of log and core well data, together with outcrop data, allowed Droste (2002-2003) to pose a schematic sequence stratigraphic model (Figure 2.14).

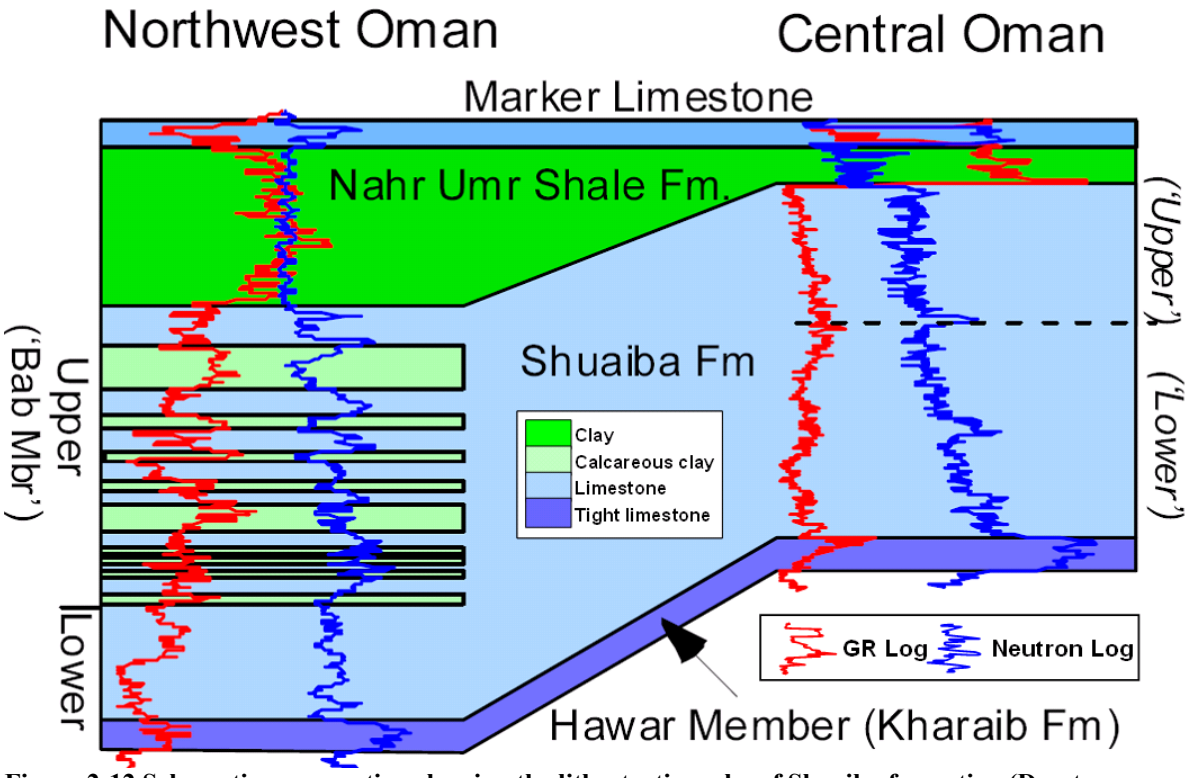


**Figure 2-12 Schematic cross section showing the lithostratigraphy of Shuaiba formation (Droste, 2003). Note that Shuaiba is more homogeneous toward SE (Central Oman), this will impact mechanical layering.**

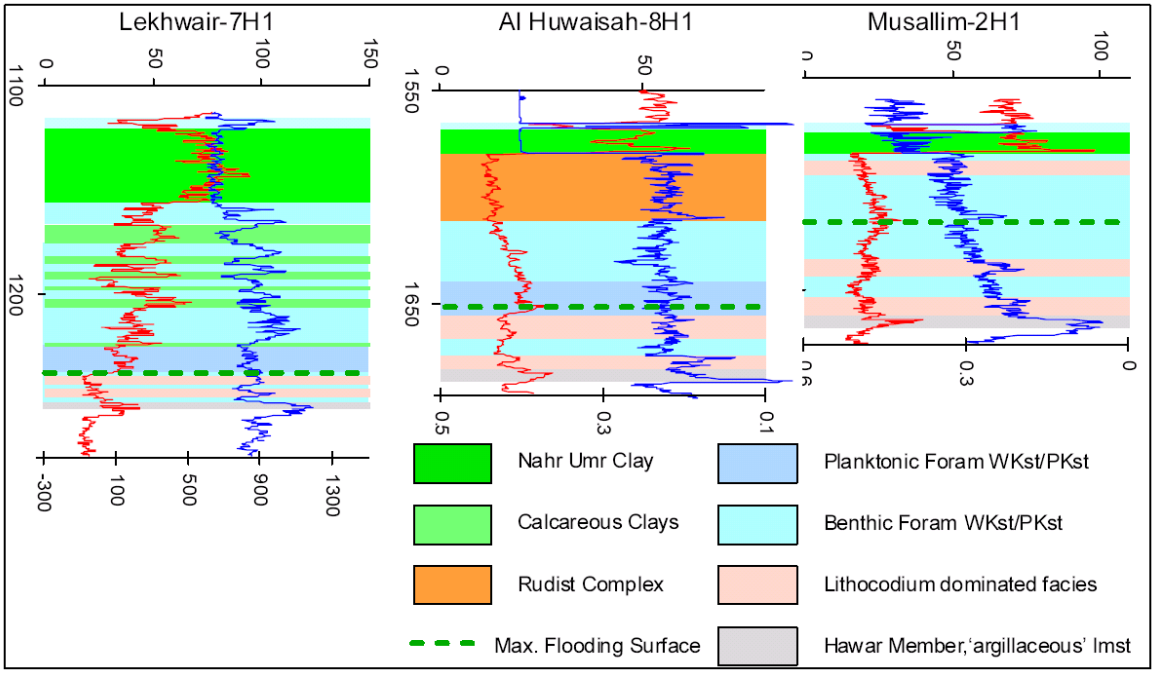


**Figure 2-13 0Shuaiba field type logs from NW to Central Oman (Droste, 2003). GR red line and Neutron blue line.**

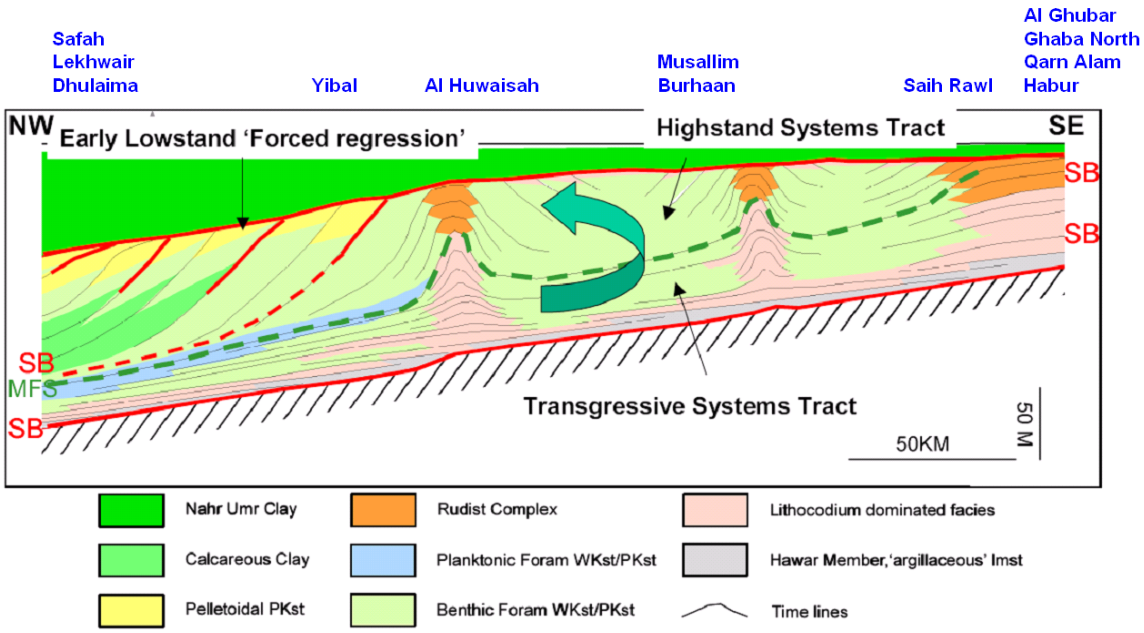


**Figure 2-14 Shuaiba sequence stratigraphy model with fields locations in blue (Droste, 2003). The green dashed line represents a maximum flooding surface**

Quoting from (Droste, 2002-2003):

> *The Shuaiba Formation consists of two third-order sequences. The lower sequence starts with a Transgressive Systems Tract (TST) consisting of laterally extensive very shallow marine to intertidal sediments of the Hawar Member followed by shallow marine algal limestone transgressing over the exposed and karstified shallow marine limestone of the Kharaib Formation. During the late TST, the development of algal mound complexes led to a differentiation on the platform. Between these mounds fine-grained, nannoconid dominated, sometimes organic-rich deeper water sediments (water depths up to some 80 m) were deposited. The Maximum Flooding Surface (MFS) is characterized by a regionally developed high gamma spike. During the early Highstand Systems Tract (HST), prograding rudist biostrome and shoal complexes colonized the mounds. During the late HST, the rudist growth decreased as the platform interior became more restricted and the shoals started to experience more frequent subareal exposure. During this phase, the intermound depressions are filled in by open lagoonal to distal ramp sediments, and the mounds develop into a larger platform surrounding an intra-shelf basin ('Bab' basin). A regional drop in sea level and a sequence boundary associated with subareal exposure terminates deposition on the platform and karst is formed. The second sequence starts with early Lowstand Systems Tract (LST) deposits of offlapping carbonate wedges into the intra-shelf basin. As sea level continues to fall, erosion on the mainland leads to repeated influx of clays resulting in a lateral stacking of carbonate and clay wedges. Within the carbonate wedges, reservoir-prone rudist shoal complexes are present. Ultimately, the whole platform interior is exposed and a late Lowstand Systems Tract wedge is deposited as a fringing carbonate platform along the ocean margin, which is exposed in the northern Oman Mountains. The basal shales of the Nahr Umr Formation form the TST of the upper sequence and a Marker Limestone Bed within the shales represents the maximum flooding surface.*

The Shuaiba is nearly everywhere overlain by clays of the Nahr Umr Formation which form a regional seal. The exceptions are the parts of the Lekhwair High where the Shuaiba is unconformably overlain by clays of the Palaeocene Shammar Formation and along the western flank of the Huqf area and above salt domes in the eastern Ghaba Salt Basin where younger Tertiary strata may overly the Shuaiba because of local post-Shuaiba erosion. As suggested in Figure 2-14, the Shuaiba exhibits depositional

thickening from the southeast towards the basin centre (Figure 2.15) where it reaches about 130m of thickness in the NW but thins to 0 in the SE. Note that, from hydrocarbon perspective, the oil column in the Shuaiba fields is normally 20-50m thick, with Lekhwair fields having oil shows in both Upper and Lower Shuaiba, while central and south of north Oman fields have oil shows in Lower Shuaiba.

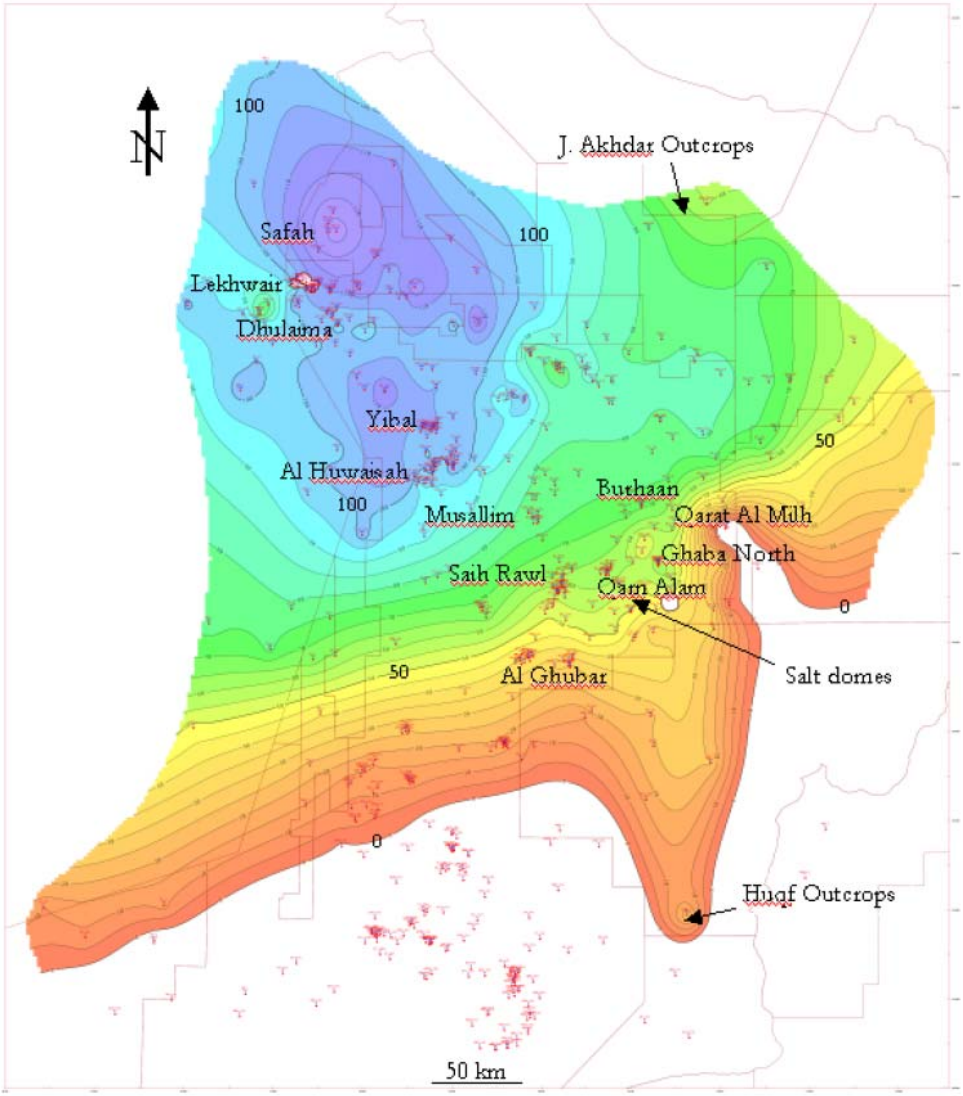


**Figure 2-15 Shuaiba thickness map based on well data in north Oman (Droste, 2002-2003).**

A recent study of Wadi Jarrah and Wadi Baw in the Huqf area was undertaken by Vrije University of Amsterdam, Shell EPT and PDO (Immenhauser et al, 2004). The study describes the limestone of the middle Cretaceous Qishn Formation (Figure 2.16), thought of as an outcrop analogue for the Upper Kharaib and Lower Shuaiba oil reservoir. This study shows that the Qishn formation consists of shale, open platform carbonates, high energy and intertidal platform-top deposits, with a thickness of 75 m in Wadi Jarrah and of about 65m in Wadi Baw, capped by a regional unconformity that represents an approximate 5 Ma hiatus. Figure 2.17 illustrates the facies of Qishn based on sequence stratigraphic analysis done by Immenhauser et al (2004).

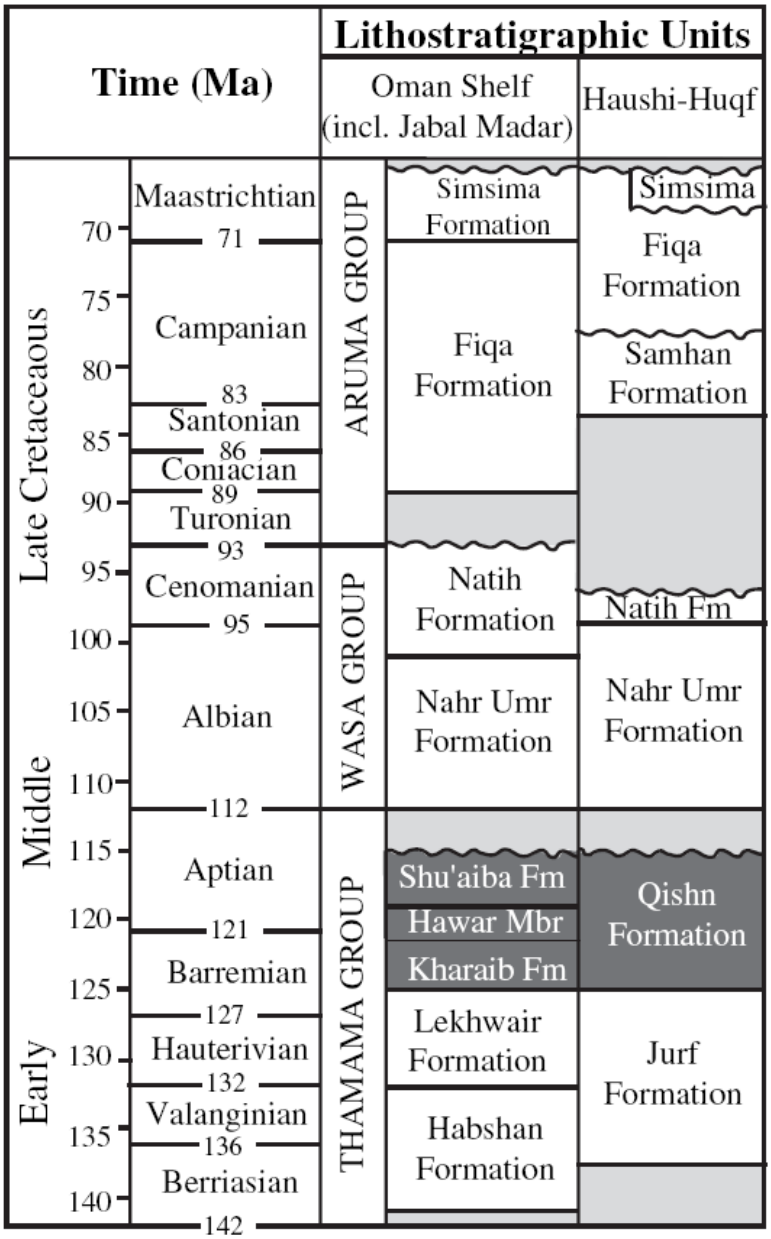


**Figure 2-16 Cretaceous chrono-stratigraphy of Oman comparing north and interior Oman with Huqf area outcrop (Immenhauser et al, 2004).**

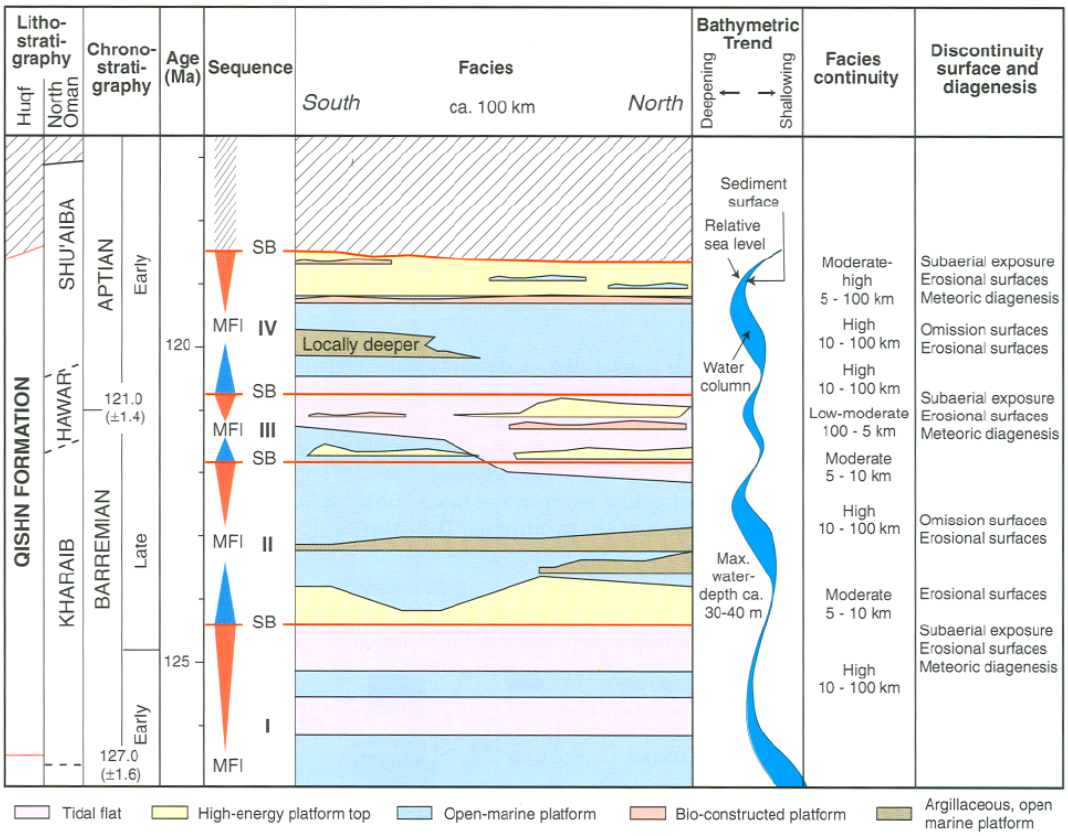


**Figure 2-17 Schematic overview of facies distribution of Qishn Formation in Huqf (Immenhauser et al, 2004).**

Outcrop plug sample porosity and permeability plots of Qishn Formation (Figure 2.18) have been analysed by Vrije University of Amsterdam, Shell EPT and PDO (Immenhauser et al, 2004). On average, porosity is 10-20% and permeability averages 1 to 10 mD. The porosity plot shows no dramatic changes with depth within the Shuaiba outcrop analogue, which support the fact that the Shuiaba reservoir is quite homogenous in the south east of Oman.

A similar analysis of porosity and permeability variation with depth is presented below for the Shuaiba subsurface fields (vertical wells). The original data were obtained from PDO RUI (subsurface data). The porosity and permeability values were extracted from core data (Figure 2.19, 2.20 and 2.21) with the objective being to assess the occurrence of significant mechanical layering. Examination of the porosity log with depth indicates that the rock competence is more or less of same magnitude in the south and SE fields compared to the N and NW, where trends and scatter of porosity data are seen such as in Yibal and Lekhwair.

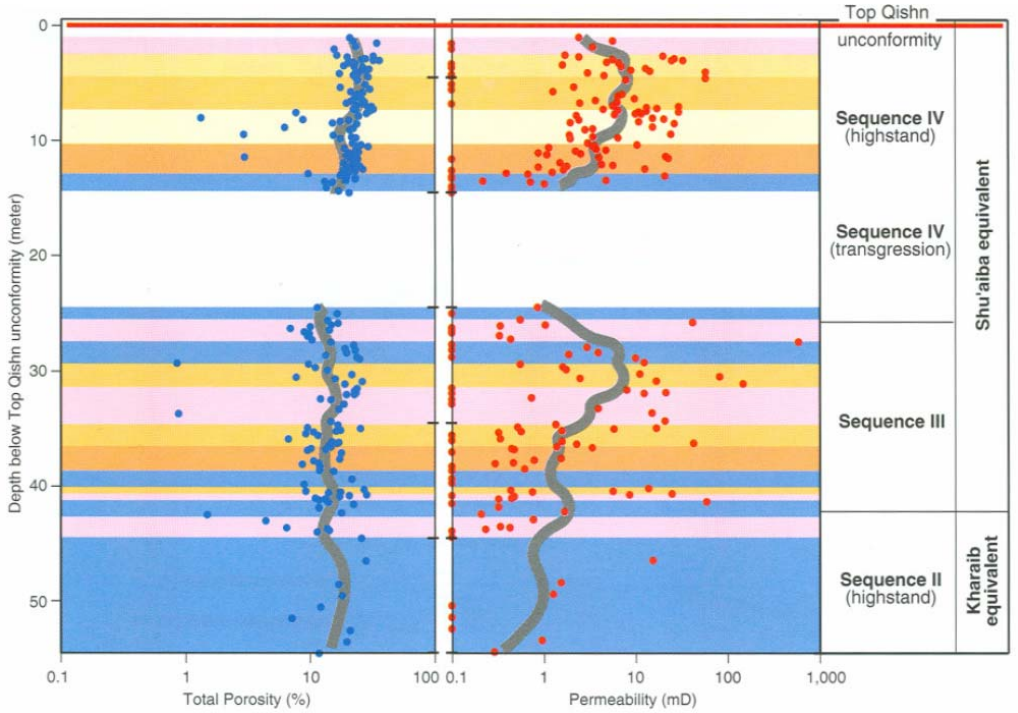


**Figure 2-18 Overview of total porosity and permeability data from Qishn Formation, Dark grey lines is calculated 5-points moving average of all data (Immenhauser et al, 2004).**

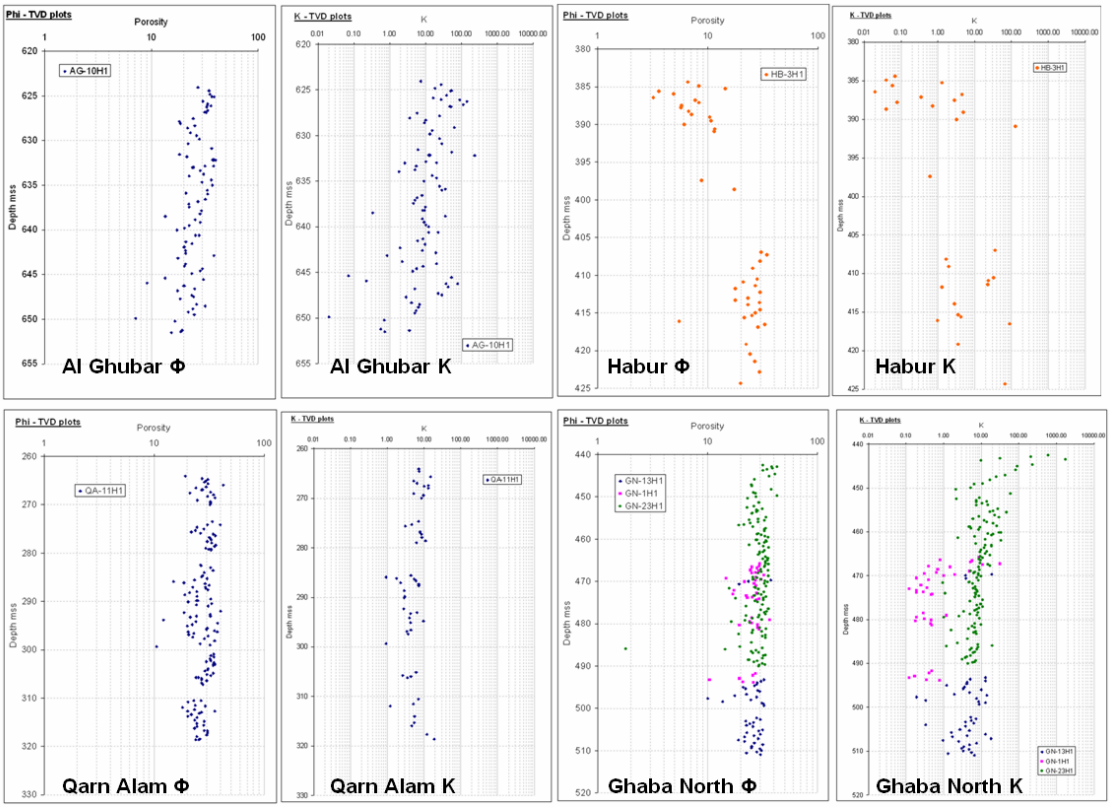


**Figure 2-19 Core porosity – core permeability plot versus depth in south and SE fields (Shuaiba Formation), see well name to note the field name.**

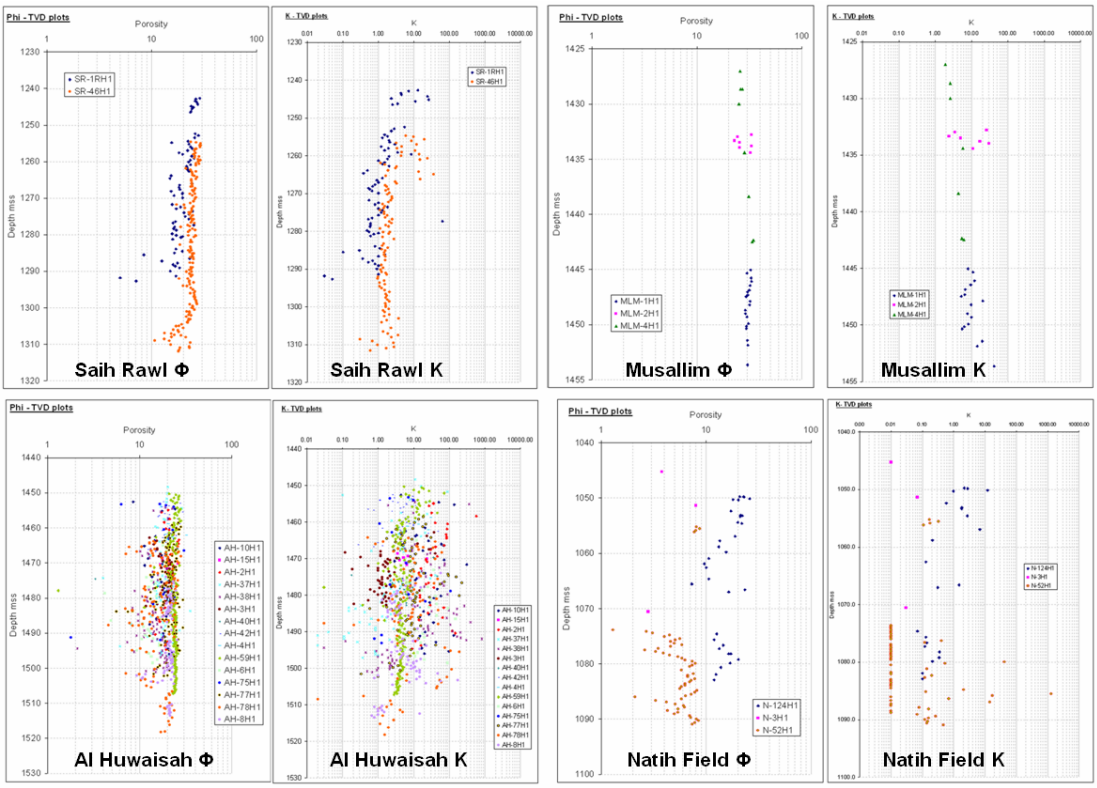


**Figure 2-20 Core porosity – core permeability plot versus depth central fields (Shuaiba Formation), see well name to note the field name.**

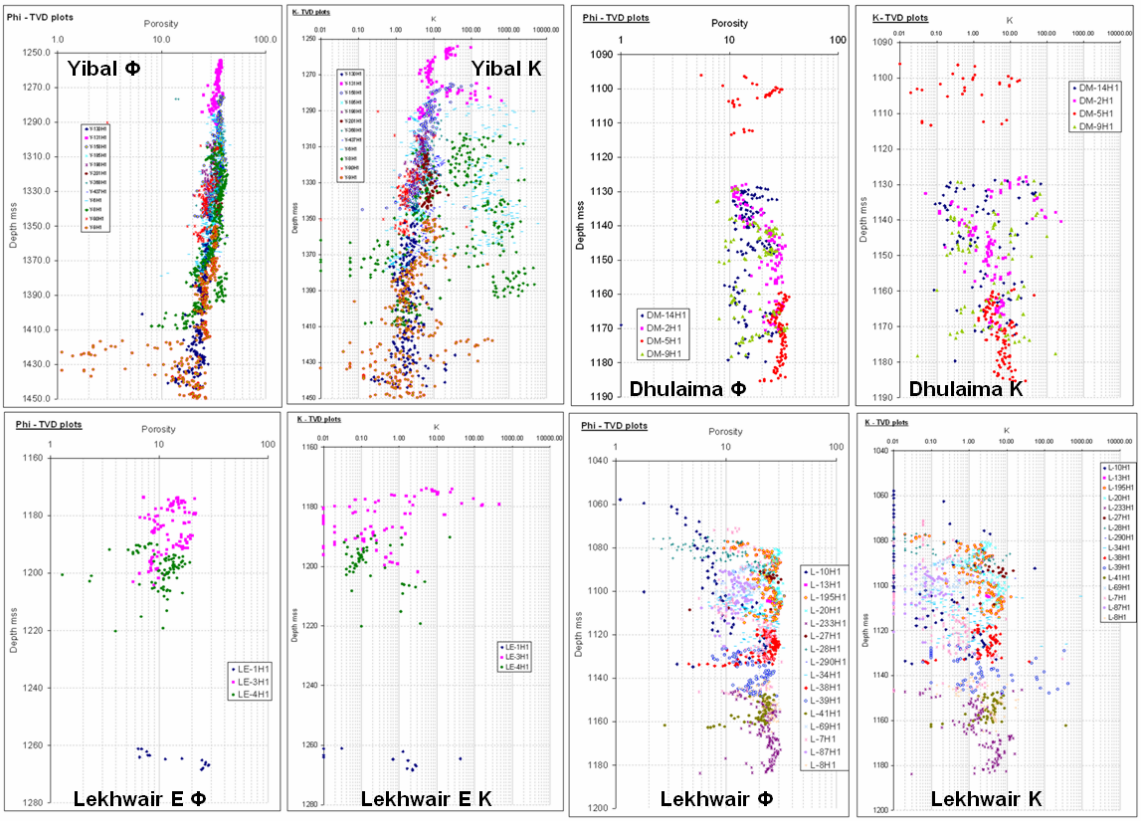


**Figure 2-21Core porosity – core permeability plot versus depth northern fields (Shuaiba Formation), see well name to note the field name. These are within the Bab basin where both upper and Lower Shuaiba is present. Note the spread in the porosity range seen in the matrix.**

## 2.3 Tectonics

Loosveld et al (1996) describe six tectono-stratigraphic units in Oman from the late Precambrian to Present day:

**Unit I**: Precambrian basement representing continental accretion (Figure 2.22).

**Unit II and III**: Infracambrian to Ordovician, may reflect two periods of rifting possibly related to Najid movements in western Saudi Arabia. The NE-SW trending salt basins formed during this time interval. A classical "steer's head" basin geometry is developed in north Oman, whereas a less complete rift-sag sequence is preserved in South Oman. Of the entire time-span from Late Silurian to Mid-Carboniferous, only little Devonian (Emsian) sediment is preserved. Hence, it was followed by a long period of erosion and little or no deposition.

**Unit IV**: Late Carboniferous to Mid Cretaceous, reflect the breakup of Gondwana and the creation of NE and SE passive margins of the Arabian Plate. Quoting from (Loosveld et al, 1996):

> *During the Late Jurassic-Early Cretaceous, a new phase of westerly tilt and uplift of the eastern high resulted in a similar, if less pronounced, eastward onlap of shallow marine sediments. This phase of uplift of eastern Oman may testify to the - now successful - separation of India-Madagascar-Antarctica from Africa-Arabia, and is related to the formation of the Masirah oceanic crust (= now the Eastern Ophiolite Belt of Oman), which has been dated at ~150 M.*

**Unit V**: documents intra-plate deformation related to Late Cretaceous continent-ocean obduction in the north and transpresssional movements of the Indian Plate in the east (Alpine Phase I). Quoting from Loosveld et al (1996):

> *Around 110 Ma, the Atlantic Ocean started to open, leading to closure of the Neo-Tethys between the Afro-Arabian and Eurasian plates. NE dipping intra-oceanic subduction zone developed, accompanied by back-arc spreading and the formation of the future Semail Ophiolite. At ~93 Ma, this subduction complex collided with the continental crust of Oman .Uplift and partial erosion of the Natih Formation during the earliest Turonian (Wasia-Aruma forebulge unconformity), and the development of a major hardground throughout the carbonate shelf area, signaled the onset of this first Alpine event. Around 80 Ma, the relatively hot oceanic crust of the Semail was emplaced over the deep-water Hawasina sediments and Arabian continental margin. This phase of NE-SW compression and loading led to SW stacking of thrust sheets in the area of the future Oman Mountains and the generation of a Campanian to Maastrichtian foredeep. Thrusting continued until the Late Santonian, but the foredeep continued to subside into the Late Campanian (i.e. much later) as it was partly supplied by sediment derived from the emerging Hawasina and Semail ophiolite thrust sheets. Loading of thrust sheets resulted in the down-warping of the continental crust and its flexural extension. The extension south of the Oman Mountains is largely accommodated by a set of evenly distributed NW-SE trending normal faults, all with minor throws.* [N.B.This explanation for the nature of the NW-SE trending faults, was described differently in the recent study by Filbrandt et al, 2006]. *Around 84 Ma, greater India, including the Seychelles micro-continent and the oceanic crust of present-day Masirah Island (and minor outcrops at Ras Jibsch and Ras Madrakah), separated from Madagascar and drifted northwards. Associated with this drift was a component of compression along the*

*eastern continental margin of Oman. Thus, simultaneous to the NE-SW extension south of the thrust sheets of the Oman Mountains, the eastern continental margin of Oman suffered from sinistral transpression. The western margin of the Ghaba Salt Basin suffers minor inversion as a result. The Late Cretaceous was a period of pronounced salt movement in the Fahud and Ghaba Salt Basins.*

**Unit VI**: spanning the Tertiary, represents a return to quiet conditions followed by continent-continent collision in the north. Following Late Eocene uplift, the Gulf of Aden rift developed in the south in the early Oligocene, with sea-floor spreading from the Late Miocene onwards (Alpine Phase II). Quoting from Loosveld et al (1996):

*Due to a global eustatic fall in sea level at the end of the Cretaceous, north Oman became emergent again leading to the Base Tertiary regional unconformity. Completion of the mountain building process was in the second (Oligocene-Pliocene) Alpine event. The Oman Mountains were broadly uplifted, subsequent to which their culminations collapsed and large extensional structures developed (Mann et al., 1990). In a narrow zone south of the Salakh Arch, many normal faults were inverted, including the main Natih Field fault and the northern parts of the Maradi Fault Zone. East Oman remained strongly influenced by tectonics in the proto-Indian Ocean. In the late Campanian early Maastrichtian, a rift developed between the Seychelles and India. This rifting culminated in the Deccan volcanic event at approximately 64 Ma, when a new oceanic spreading zone, the present-day Carlsberg Ridge, developed. This in turn resulted in continued northwards drift and anti-clockwise rotation of India. At the Cretaceous/Tertiary boundary, intra-oceanic north-over-south thrusting between the lower and upper ophiolitic nappes of Masirah Island occurred, immediately followed in the Paleocene by the oblique obduction of the Masirah Ophiolite complex onto the Arabian continent. Seismic and well data suggest that obduction has been active from Late Cretaceous to at least Eocene (PDO, unpublished data). Even Miocene rocks are folded, along north northeast-south southwest trending axes, near Jebel Ja'alan. Along the east coast of Oman, i.e. largely offshore under Masirah Bay and Sawqrah Bay, a narrow, gently folded, Late Cretaceous to Miocene foreland basin, the Masirah Trough, developed. The western margin is bounded by normal faults reactivating Mesozoic rift-related faults. On its eastern margin, a wedge of ophiolitic and probably continental slope sediments is largely under-thrusted below the eastern and uplifted part of this foredeep basin. Even Eocene sediments are tilted above this wedge. This eastern basin margin thus appears to overlie a passive roof thrust.*

The above tectonic evolution is summarized below (Figure 2.23) in a simplified plate-tectonic time chart.

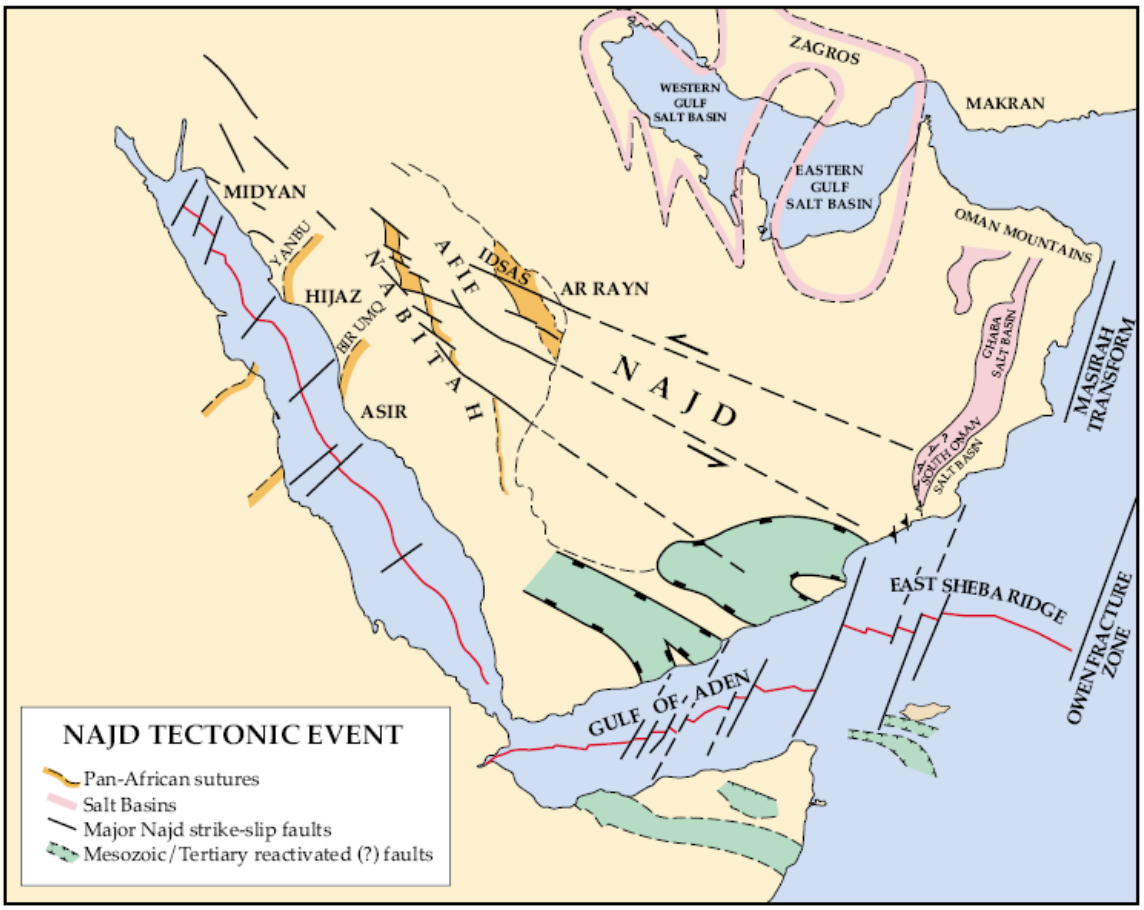


**Figure 2-22 The Arabian Peninsula, with Precambrian terrenes in the Arabian Shield area of western Saudi Arabia and the Infra-Cambrian sinistral Najd tectonic event, which occurred 600-530 Ma ago (Loosveld et al, 1996).**

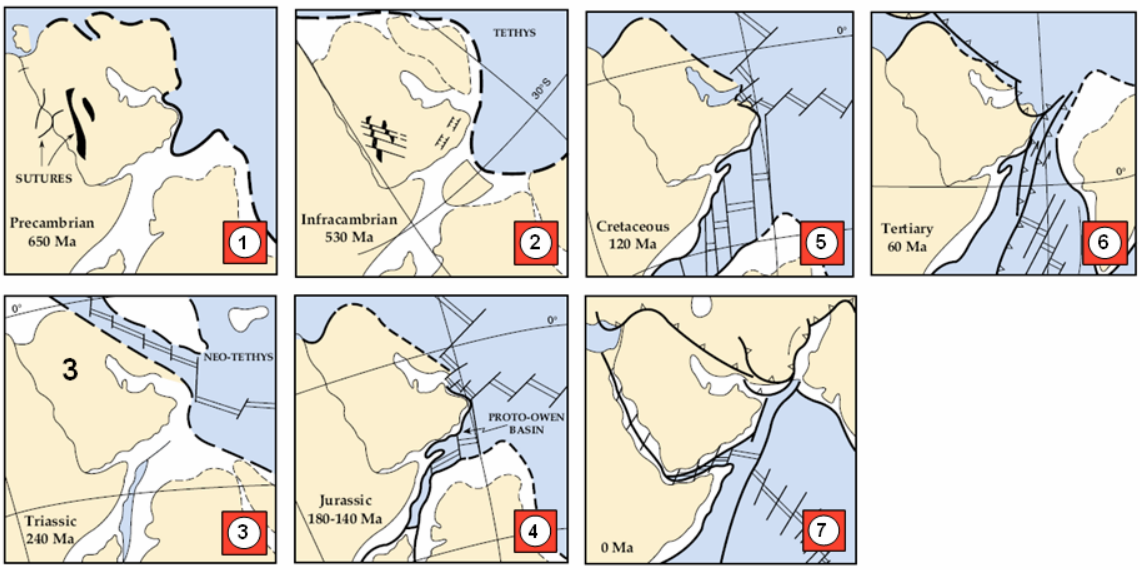


**Figure 2-23 Simplified plate-tectonic evolution of Oman (Loosveld et al, 1996).**

### *2.3.1 Salt Halokinesis*

Salt dissolution, salt doming and the three types of diapirism, i.e. passive (down building), reactive (to normal faults) and active (forceful intrusion), all play a major role

in the configuration of most intra and post-salt traps in Oman. Halokinesis is episodic and is related to tectonic events (Loosveld et al, 1996). In the Ghaba Salt Basin, early growth of salt domes was concentrated on the margins of the basin. Fault-initiated down building was the dominant mechanism. This growth can be dated from unconformities, onlaps and rapid thickness variations of the Haima sediments. It continues up to Middle Haima and Safiq times, i.e. when halokinesis in the South Oman Salt Basin had already come to an end. It is probably related to normal faulting at the end of the second rift cycle. A simplified history of the halokinesis is presented in Figure 2.24.

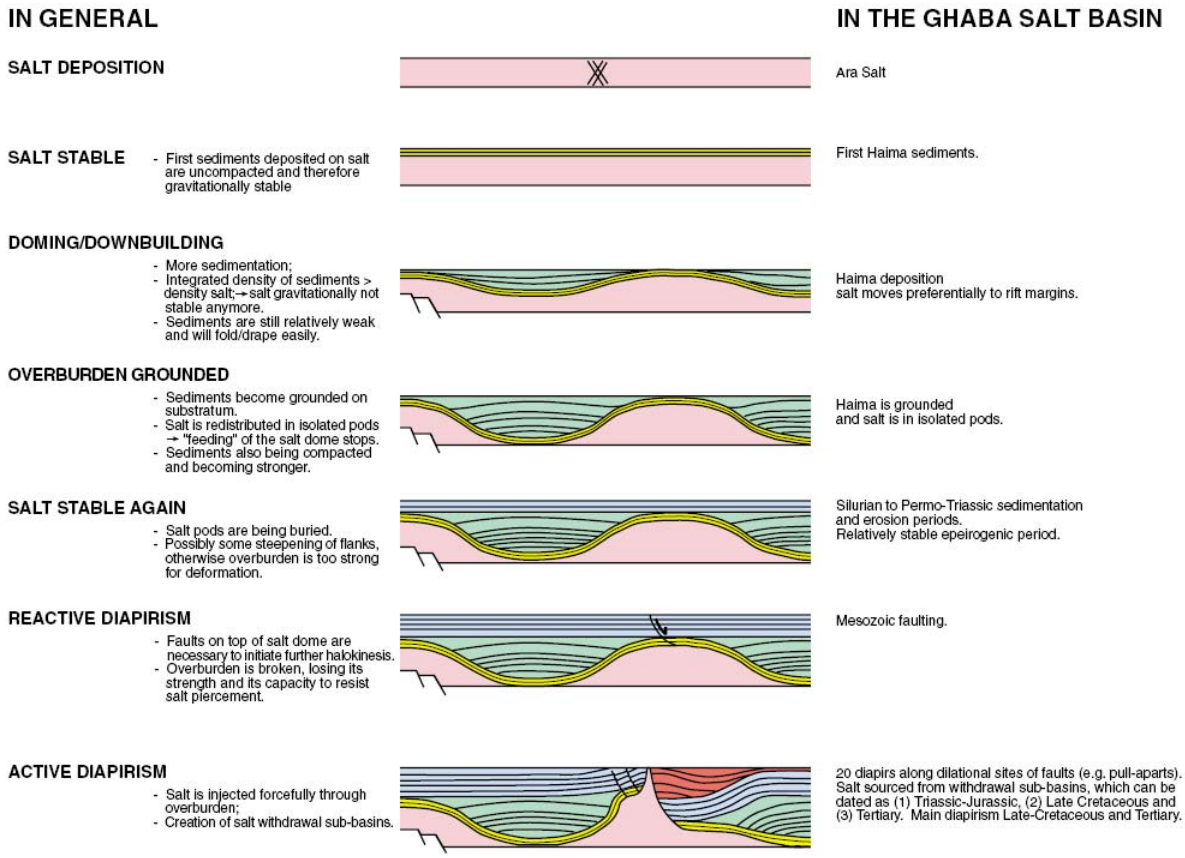


**Figure 2-24 Simplified history of salt halokinesis in Ghaba Salt Basin (Loosveld et al, 1996).**

In north Oman, renewed halokinesis was triggered by various phases of Mesozoic and Cenozoic deformation. About 20 diapirs and some non-piercing domes were formed, most of them initiated by transtensional faulting along Maradi-parallel fault zones, and subsequently forcefully injected in the faulted overburden. Most diapirs were active until the second Alpine event. Some of the salt diapirs are capped by the base of the Fars Group. Flow to surface in several other diapirs continues to the present day.

Salt halokinesis has been the subject of many detailed studies. The reader is referred to Richard (1997) and Peters et al (2003) for a comprehensive description of Oman salt domes based on seismic, well data and outcrop analysis. Their main findings are that in total there are 29 salt structures that have been identified in the Ghaba Salt Basin, ranging in type from eight relatively low relief, deeply buried salt pillows to twenty-one

narrow, high-relief salt diapirs. The diapirs are limited to the deepest part of the Basin, with six surface-piercing salt domes that crop out in the desert of the interior of north Oman (Figure 2.25). Furthermore, structurally, the salt diapirs are extremely high-relief features (as much as 9 km) that pierce the entire stratigraphic post-Ara Group sedimentary succession in the Ghaba Salt Basin. The surface-piercing diapirs have elevations of only 100 m or less above the surrounding areas but they are prominent features in an otherwise flat and strongly deflated desert setting. Their domes are roughly circular to irregularly oval in shape, with the largest (Qarn Sahmah) being over 8 km in circumference at the surface. Their irregular topography reflects the strong contrast in rock hardness between the very resistant exotic carbonate blocks and the enclosing evaporite matrix. In addition the nature and volume of the exotic blocks varies from dome to dome. North Oman salt diapirs are compressive in origin: QK and QANE occur in a compressional fault overlap, and Qarn Alam is a salt cored compressional fold. Their evolution can be summarised in three phases (Figure 2.26):

1 - Passive down building,

2 – Burial, and

3 - Reactivation in compression.

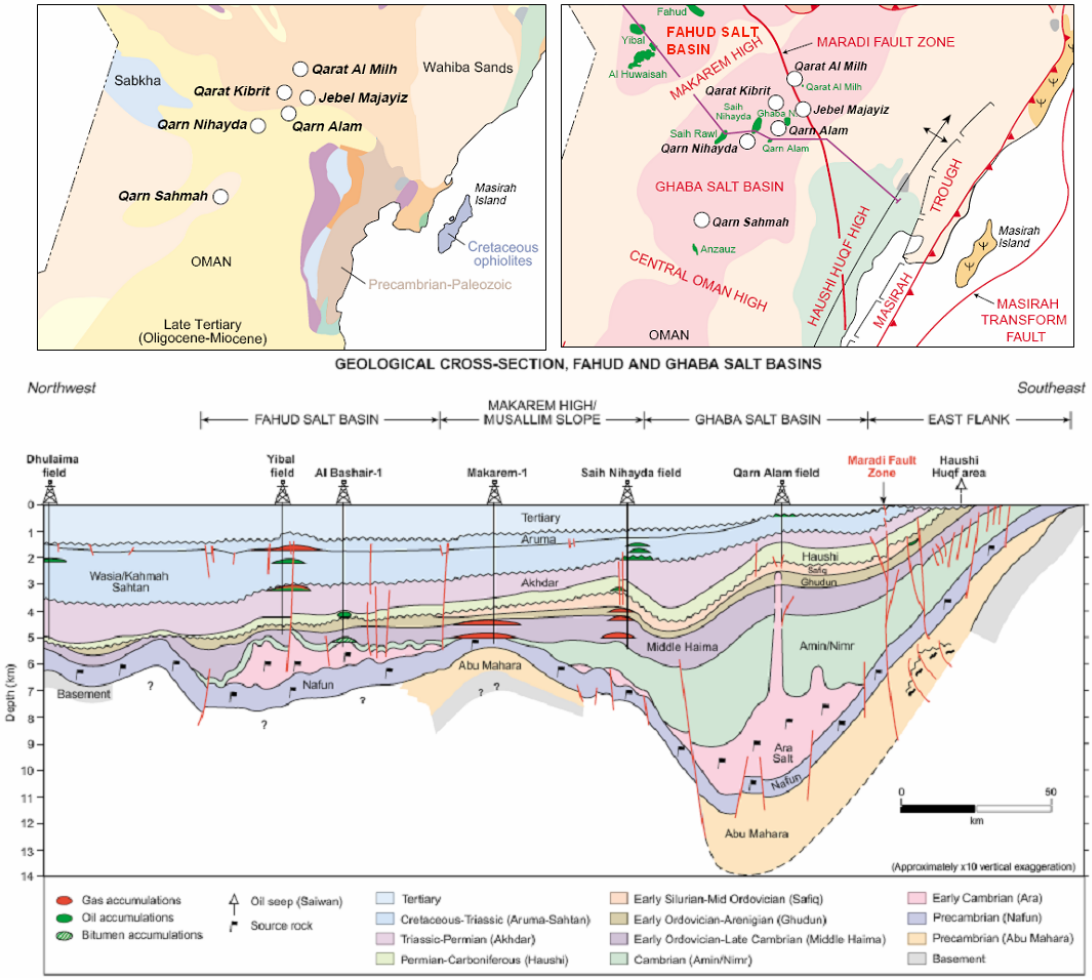


**Figure 2-25 Simplified geological cross section of north Oman (NW to SE), showing the Ara Salt (pink). Top left insert map is of surface geology showing location of the 6 piercing salt domes. Top**

**Right insert map is of structural grains (same as in Figure 2.1), with salt dome location as dark pink lines; and cross section line (Peters et al, 2003).**

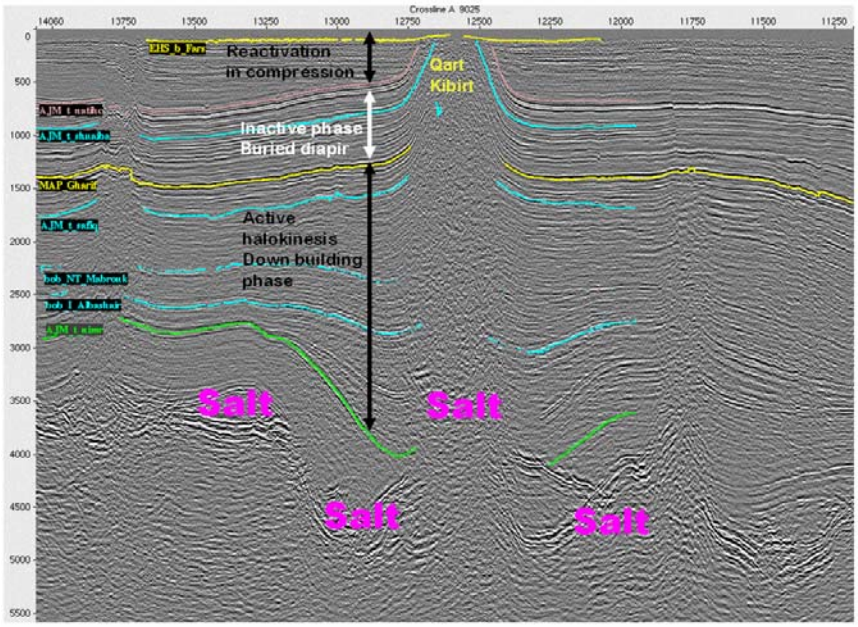


**Figure 2-26 Cross section of Qart Kibrit salt dome highlighting time interval for salt activities (Richard, 1997).**

### *2.3.2 Defining the structural trends of north Oman*

In 2002-2003, as part of the Shuaiba asset study Phase I (Nichols et al, 2002-2003), an attempt was carried out (Dhahab et al, 2003) to subdivide north Oman into regions (domains) of similar tectonic geology, based on the following criteria:

- Amount of halokinesis (salt related deformation)
- Amount of uplift/burial
- Fault signature (intensity and orientations)

The study used the north Oman Common Earth Model NOCEM which was created in gOcad$^{TM}$ (a model of regional faults and key horizons based on regional 2D/3D seismic of 250m grid spacing). The horizons (Figure 2.27) were, from bottom to top: Base Salt, Top Salt, Top Amin, Top Gharif, Top Akhdar, Top Kharaib, Top Natih E, Base Tertiary, and present day surface horizons (the present day surface was created on a 40m grid spacing from PDO geo-matic). The faults were interpreted as traces on each horizon and then modelled as (converted to) planes (Figure 2.28). The analysis was based primarily on isochore maps of the above horizons.

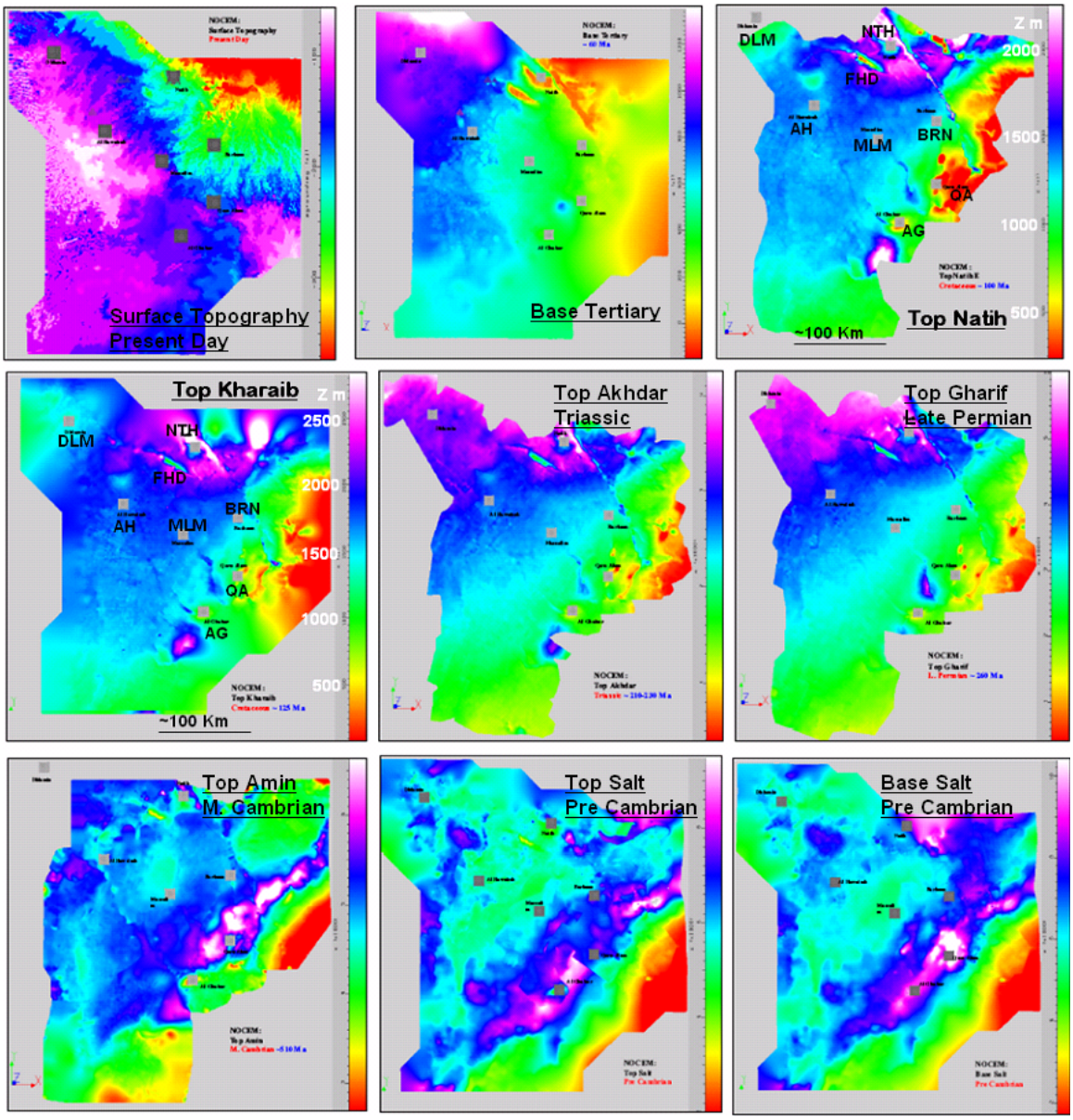


**Figure 2-27 NOCEM depth maps for all the horizons from base salt at bottom right to surface horizon at top left with field abbreviation. Note the changes in structural pattern from one layer to the other (Dhahab et al, 2003).**

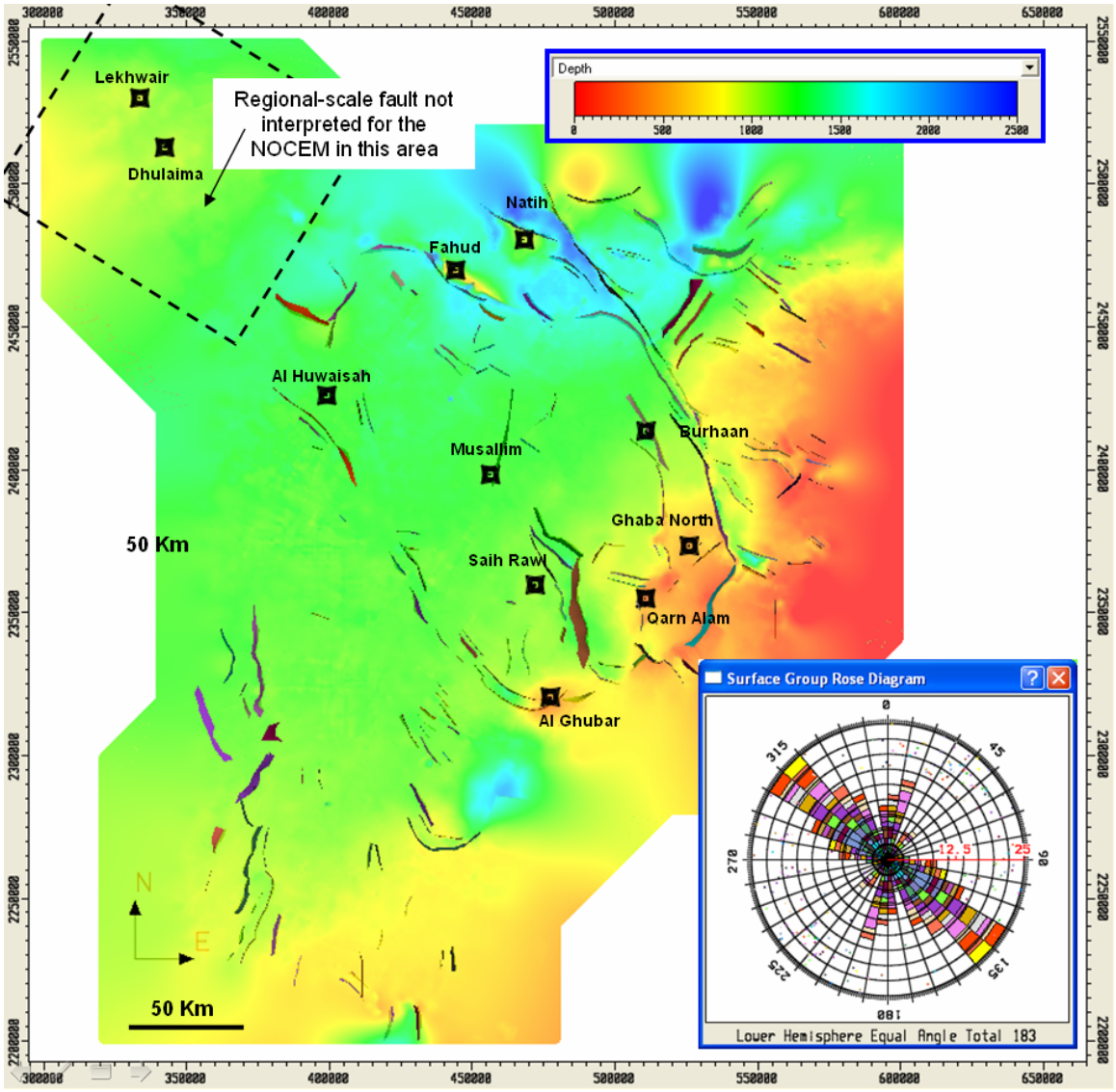


**Figure 2-28 North Oman regional faults of NOCEM overlain on top Kharaib map, with rose diagram showing the strike orientation of the faults and their total number (Dhahab et al, 2003).**

The base salt to Amin isochores are very noisy (Figure 2.29), probably due to salt and depth conversion problems, though one can see a thick salt in the centre and the SE, probably related to the initiation of Fahud and Ghaba North Salt Basin. A variation of thickness is seen across the eastern (NW to SE striking) Maradi Fault Zone, which may indicate the fault was active. Furthermore, there is a lot of thickness variation. This is probably due to low seismic quality and also due to clastic sediment depositing on salt basins creating depo-centres. But the structural grain indicates changes in thickness along lineaments striking N and NW, which are possible basement faults.

The isochore map from top Amin to top Akhdar (Figure 2.30) shows that more sediment was deposited in Ghaba Basin compared to the NW Dhulaima / Lekhwair area or the SE-Huqf (SE of Al Ghubar). Also, the Fahud and Natih structures are more defined. There are small salt diapirs “bulls-eyes” seen scattered in the vicinity of the Maradi Fault Zone, though no thickness variation is observed across the fault. In addition, there is an offset SW of Al Huwisah running NW (see also Tertiary time, Figure 2.32). There

is a change in the thickness increase direction from SE "Ghaba Basin" to NW from top Gharif, possibly due to sedimentary activity more than to tectonic activities.

The isochore map from top Kharaib to top Natih, representing the Cretaceous time, (Figure 2.31) shows a dramatic change of thickness in NW (Lekhwair/Dhulaima area). This may indicate a very strong tectonic activity. In contrast, there is zero to little offset across Maradi Fault Zone. There is still the thickness increase direction toward the NW, but probably due to depositional processes. Furthermore, salt bulls-eyes disappear in the Kharaib to Natih isopach. There is a potential uplift and erosion around Dhulaima and Huqf area (SE of Al Ghubar).

The isochore map from top Natih to base Tertiary (Figure 2.32) shows a change in thickening direction toward the NE in the Natih-Tertiary isopach. This could be related to the Oman Mountain weight creating a depo-centre ahead of it which in turn resulted in high elevation around Natih and possible uplift/erosion in the NW and SE. There is a clear offset along parts of the Maradi Fault Zone, which mean the fault is active. Local thickening occurs south of Al Ghubar (see also Gharif time, north of Al Ghubar Figure 2.30). This could be attributed to differential weighting of sediment on the salt basin. Furthermore, the salt bulls-eyes are very clear north of Qarn Alam and in Al Ghubarm, which indicate active salt halokinesis. There is also a change in thickening direction back to the NW seen in the isochre map of base Tertiary to present day surface, probably due to combined tectonic and depositional processes.

Based on the above analysis the north Oman region was subdivided into regions "domains" of similar tectonic activities (Figure 2.33).

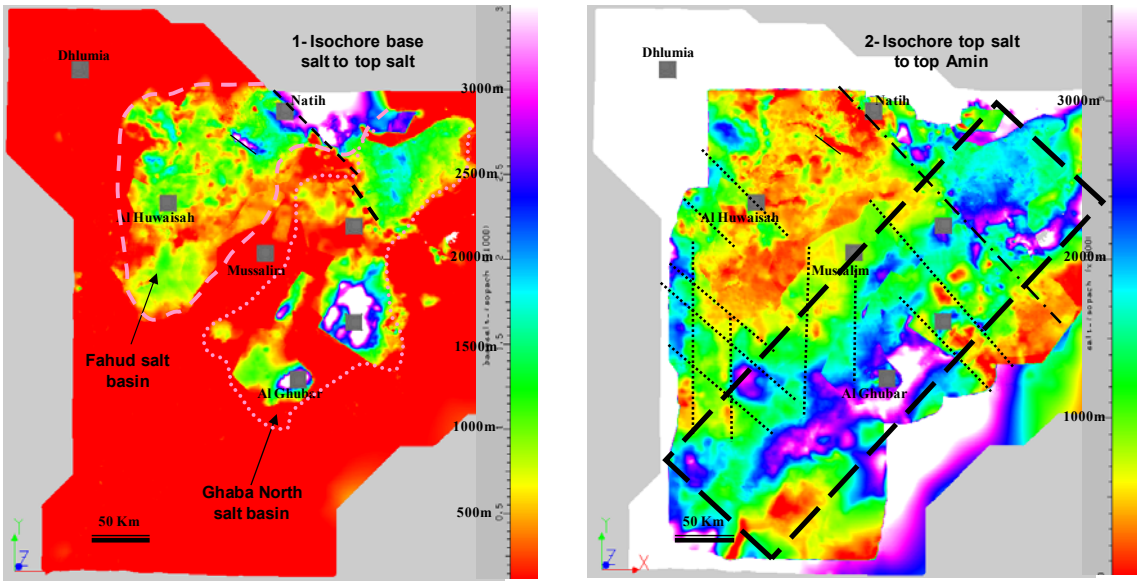


**Figure 2-29 Isochore maps of base salt to top salt and from top salt to top Amin Formation, north Oman (Dhahab et al, 2003).**

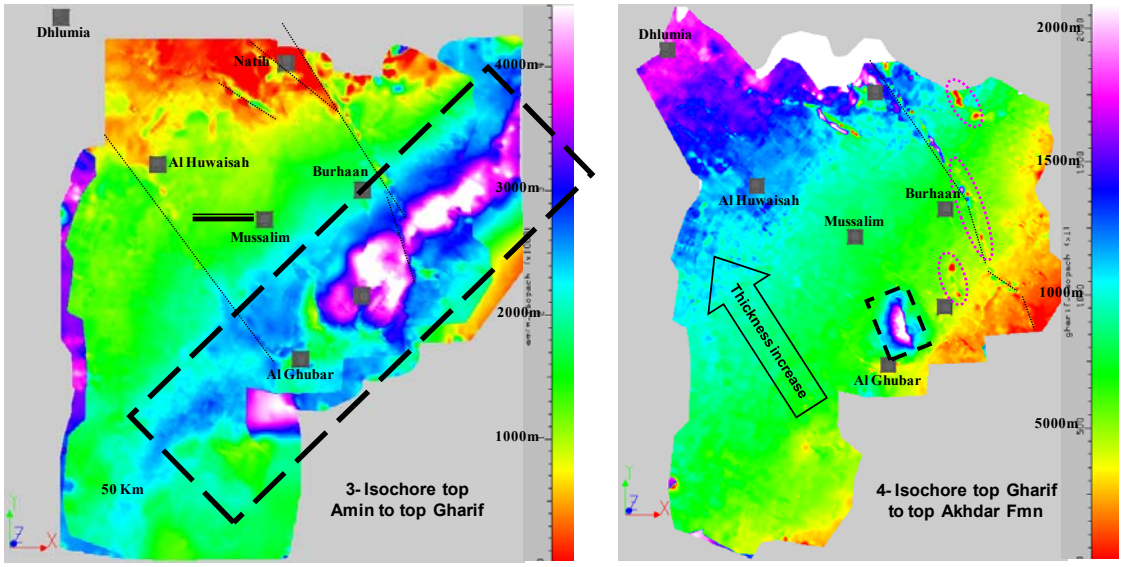


**Figure 2-30 Isochore maps of top Amin to top Gharif and from top Gharif to top Akhdar, north Oman (Dhahab et al, 2003).**

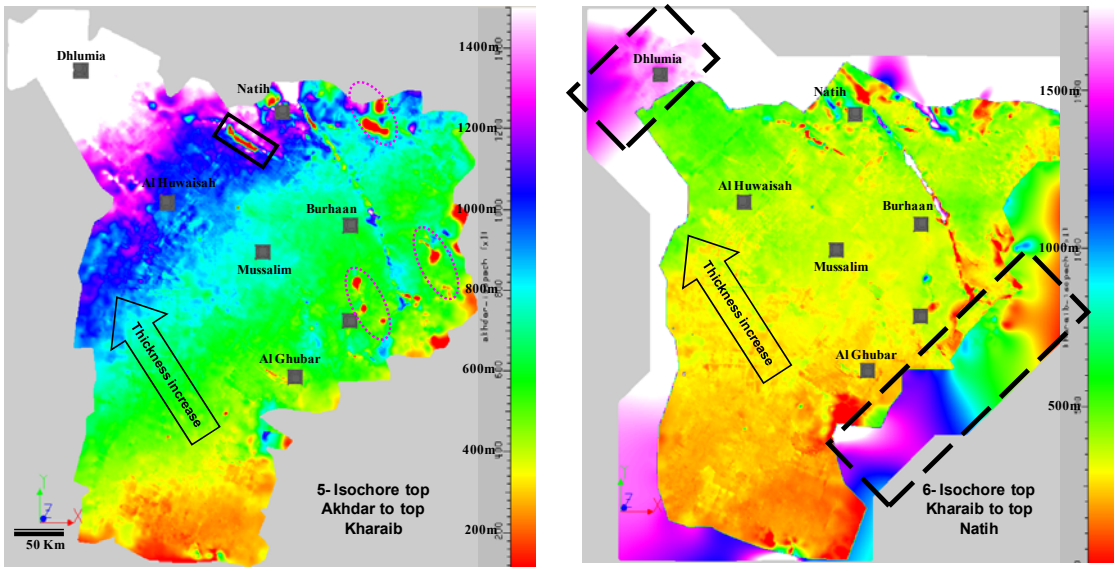


**Figure 2-31 Isochore maps of top Akhdar to top Kharaib and from top Kharaib to top Natih, North Oman (Dhahab et al, 2003).**

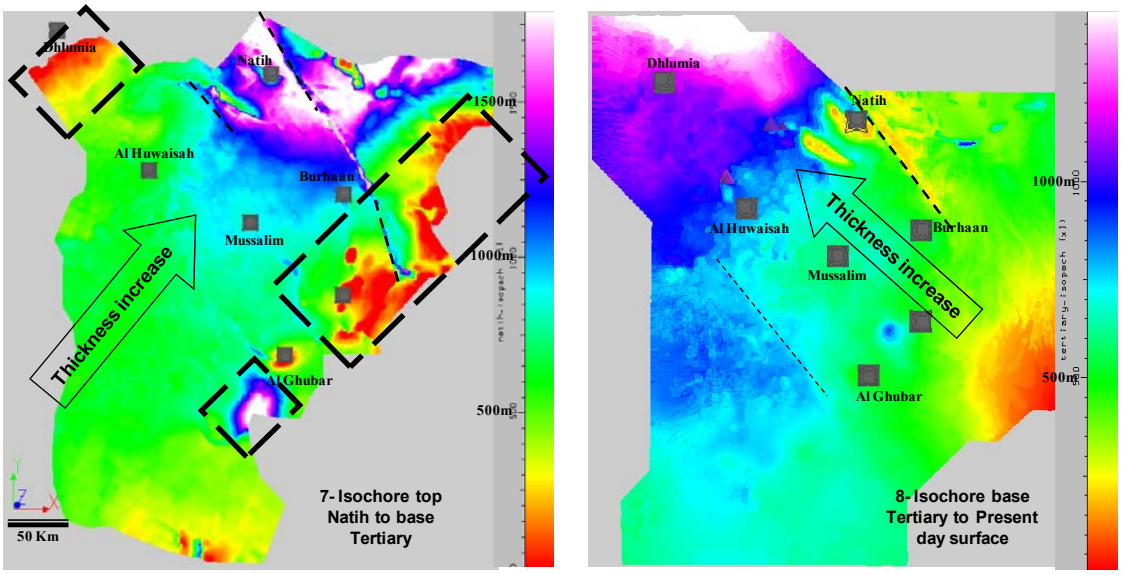


**Figure 2-32Isochore map of top Natih to base Tertiary and from base Tertiary to Present day surface, north Oman (Dhahab et al, 2003).**

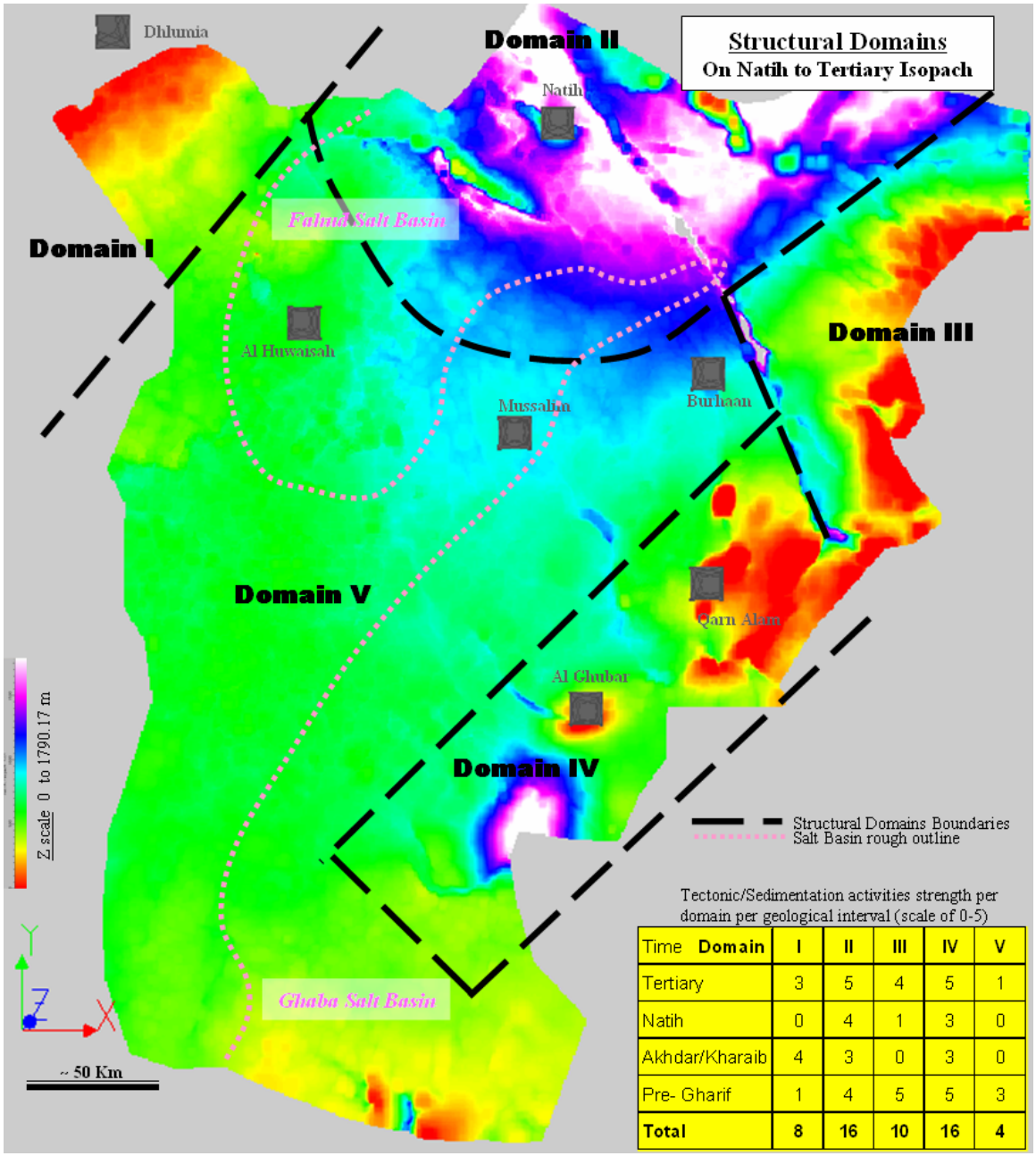


| Time Domain | I | II | III | IV | V |
|---|---|---|---|---|---|
| Tertiary | 3 | 5 | 4 | 5 | 1 |
| Natih | 0 | 4 | 1 | 3 | 0 |
| Akhdar/Kharaib | 4 | 3 | 0 | 3 | 0 |
| Pre- Gharif | 1 | 4 | 5 | 5 | 3 |
| **Total** | **8** | **16** | **10** | **16** | **4** |

**Figure 2-33 North Oman region divided into domains of similar tectonic. The inserted table highlight strength of tectonic and sedimentation activity (Dhahab et al, 2003).**

In phase II of the Shuaiba asset study (Droste et al, 2004, the structural domains for the Shuaiba Formation were defined. This is based on the deformation history post-Shuaiba deposition only, which is different from the above where the entire geological history was considered. More importantly, the knowledge of detailed fracture analysis of several Shuaiba reservoirs had been used implicitly in defining those domains. The post-Shuaiba deformation history is applicable to the Natih Formation, too. The key elements used in defining the Shuaiba structural and fracture domains are: Influence of regional basement faults; amount of salt halokinesis; present day salt thickness outline (based on SRK study); amount of uplift; and intensity of post deposition faulting. The present-day salt thickness contours and the basement lineaments interpretation of the SRK team (Stuart-Smith et al, 2004), based on gravity and magnetic maps, were used to

help delineate the boundaries of the individual domains (Figure 2.34). The domains are grouped into two categories based on the impact of fractures on production behaviour (Dhahab and Richard in Droste et al, 2004): **Type A- Domains** with fields characterised by absence of dense background fractures and presence of fracture corridors. **Type B-Domains** with fields characterised by the presence of dense background fracture and fracture corridors.

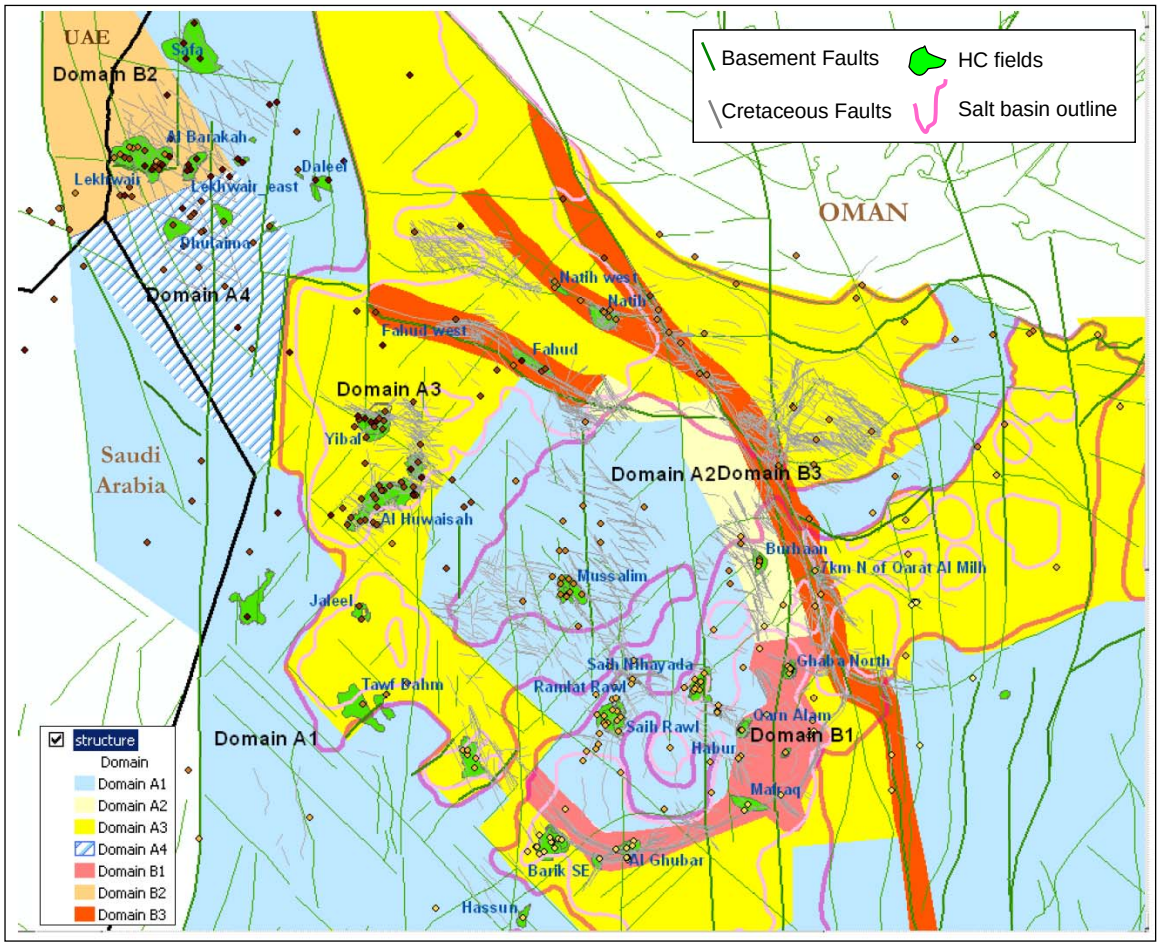


**Figure 2-34 Shuaiba structural fracture domains, Domain A are characterized by absence of dense background fracture and absence of fracture corridors, while Domain B are characterised by the presence of both regional fractures and fracture corridors (Droste et al, 2004).**

Domain subdivisions:

**A1** (Musallim area): no influence of regional basement faults; thin salt (less than 50 m) or absence of salt; no uplift; and overall minor reservoir scale Cretaceous faulting.

**A2** (Burhaan area): influence of regional basement fault (parallel to Maradi fault); little influence of salt; no uplift; and dense reservoir scale Cretaceous normal faulting.

**A3** (Al Huwisah area): little influence of regional basement faults; medium salt thickness (50 m to 300 m?); no (or minor) uplift after Shuaiba deposition caused by passive salt movement associated with fault displacement; and medium to intense Cretaceous faulting.

**A4** (Dhulaima area): little influence of regional basement faults; absence of salt; medium uplift post-Shuaiba and pre-Tertiary deposition (*c.f.* Lekhwair); and passive transtensional Cretaceous fault pattern.

**B1** (Al Ghubar to Ghaba North): Indirect influence (control on localisation of deformation) of regional basement faults; intense halokinesis (passive salt doming and active diapirism); little to medium uplift; and intense Cretaceous faulting.
**B2** (Lekhwair area): little influence of regional basement faults; absence of salt; important uplift after Shuaiba deposition (before Tertiary deposition); and pervasive transtensional Cretaceous fault pattern.
**B3** (Fahud and Natih area): strong influence of regional basement faults (Maradi fault and branch faults); little salt influence (passive salt movement associated with fault displacement); uplift post-Shuaiba; and medium to intense Cretaceous faulting.

### *2.3.3 North Oman Faults*

**Faults in the subsurface**

The faults in north Oman regions are extracted from three sources:

1. Basement trend faults (interpreted by SRK –green lines in Figure 2.34).
2. Regional faults of NOCEM (Figure 2.28). These were further split into choronlogical type (Kharaib faults, Gharif faults and so on), all derived from seismic data.
3. Sub-regional and field-faults: same as group 2, but some are also supported by well data (fault cut-outs), BHI data, core data, etc.

As stated earlier, the post-Cretaceous (Shuaiba and Natih Formation) deposition tectonism is thought of to be the most relevant indicator of the structural characteristics of the Cretaceous reservoirs, though it is believed that the basement faults did impact the deposition of the Shuaiba Formation. The kinematics interpretation and structural evolution of the north Oman region, since the Late Cretaceous (Filbrandt et al, 2004), examined the geometric characteristics of these faults and the Gharif fault set (Figure 2.35 & 2.36). Based on this analysis, it was proposed that the dominant tectonic control on the formation of faults in the subsurface area of north Oman is an oblique “collision” of the Indian Continent with the Arabian Plate (84 Ma) in the SE Huqf area, compared to the perceived cause of the compression from the Oman Mountains in the NE. However, there are some faults observed with an average NE orientation, in Natih and Fahud fields, and these are believed to be associated with the later deformation.

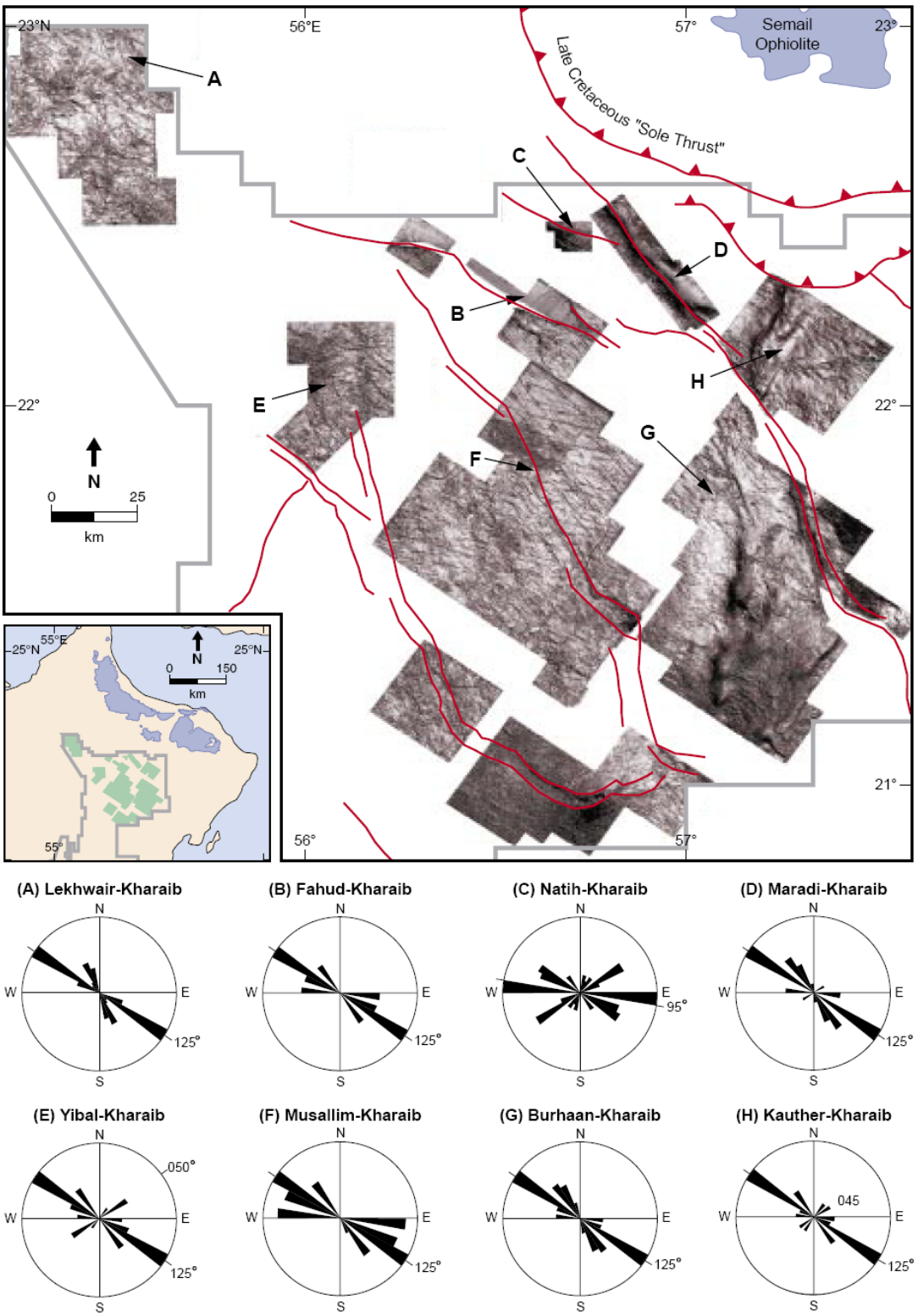


**Figure 2-35 Surface illumination at near-top Kharaib Formation based on 3-D seismic data only. Fault families have been created to highlight fault orientations in accompanying rose diagrams (Filbrandt et al, 2006).**

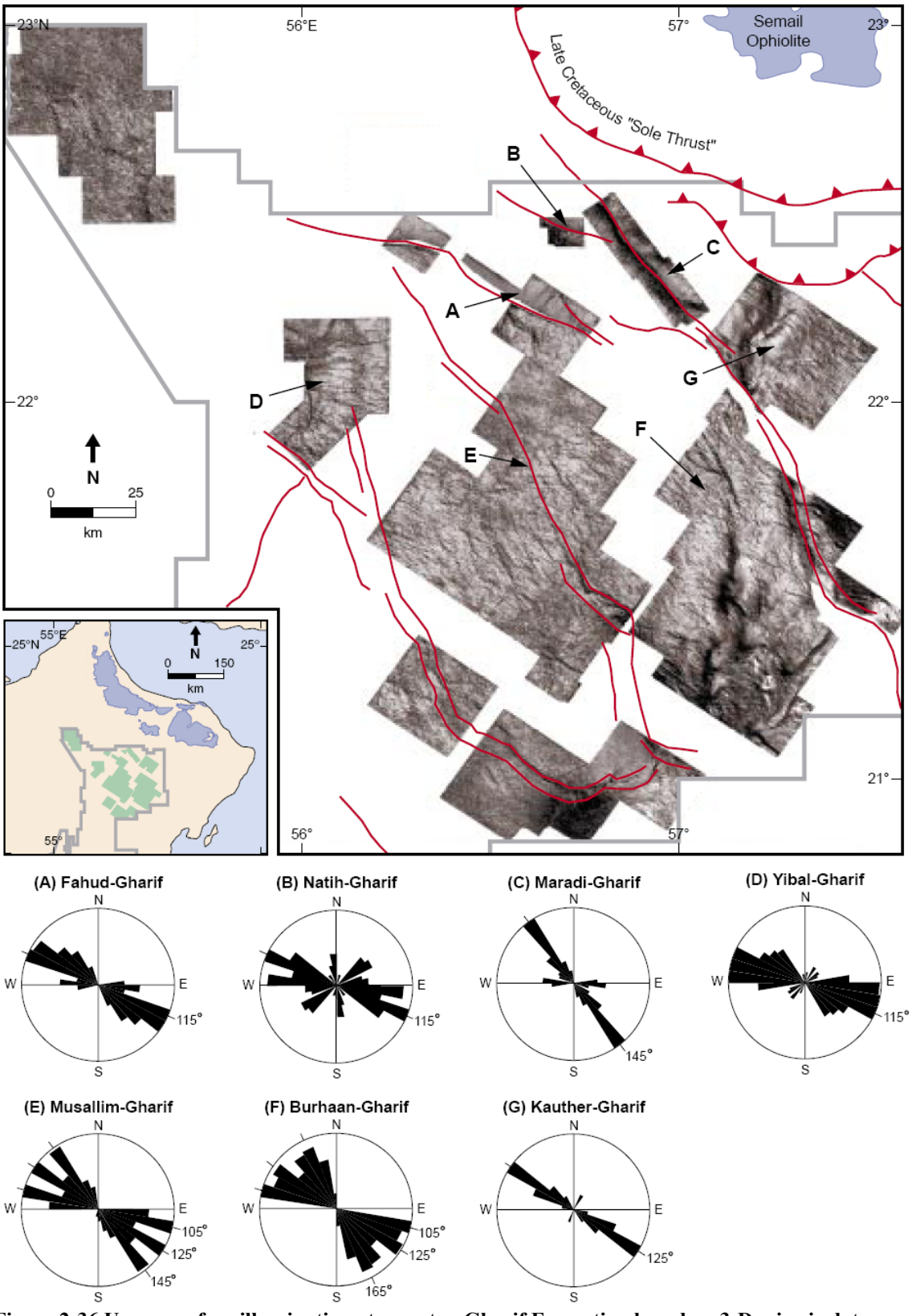


**Figure 2-36 Upper surface illumination at near-top Gharif Formation based on 3-D seismic data only. Fault families have been created to highlight fault orientations in accompanying rose diagrams (Filbrandt et al, 2006).**

**Faults in outcrops:**

The faults observed in Jebel Akhdar, Oman Mountains (Filbrandt et al, 2004) show that there are two main strike orientations - NW at 130 degrees and WNW at 100 degrees - similar to those observed in the subsurface fields (Figure 2.37), with faults cutting down from the top Natih Formation to the base of the Mesozoic carbonate section. In contrast, a similar analysis on satellite Quick Bird images in Jebel Madmar, Salakh Arch Natih Formation outcrop (de Keijzer et al, 2004 –Part 4) shows that the majority of the large lineaments (equivalent of faults) are dominantly running NE, NW and WNW (Figure 2.38). However, the faults interpreted in Huqf outcrops in the SE also indicate that the NW is the dominant strike direction (Figure 2.39) (Montenat et al, 2003). Most of the observed faulting in outcrops tends to have damaged zones associated with them that range from less than a meter up to 25m in width.

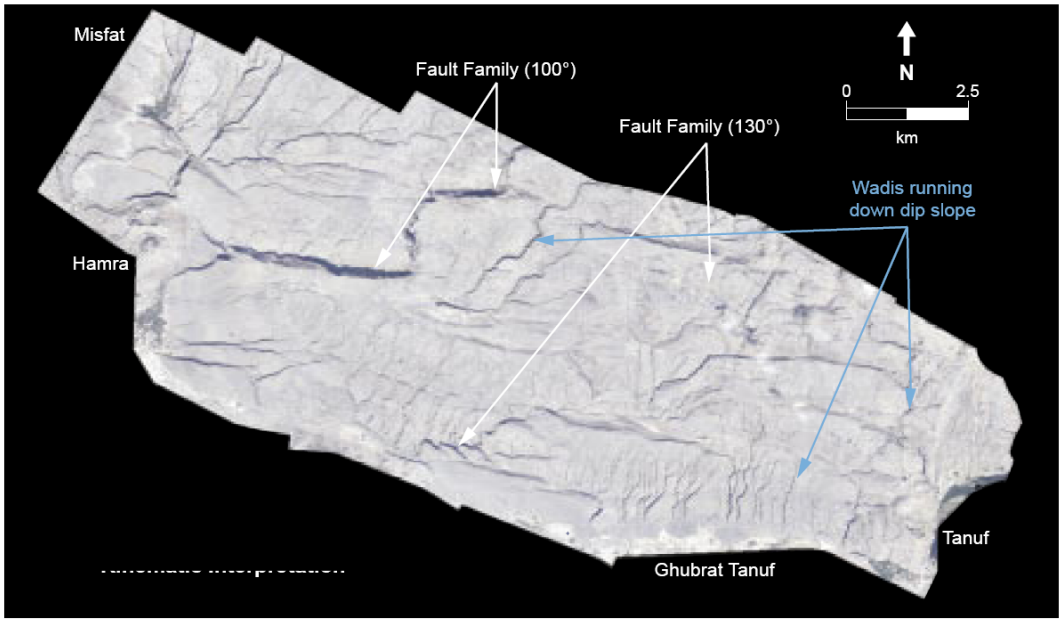


**Figure 2-37 Arial photograph of fault planes intersecting the top of the Natih Formation on the southern slopes of Al Jabal al Akhdar (Filbrandt et al, 2006).**

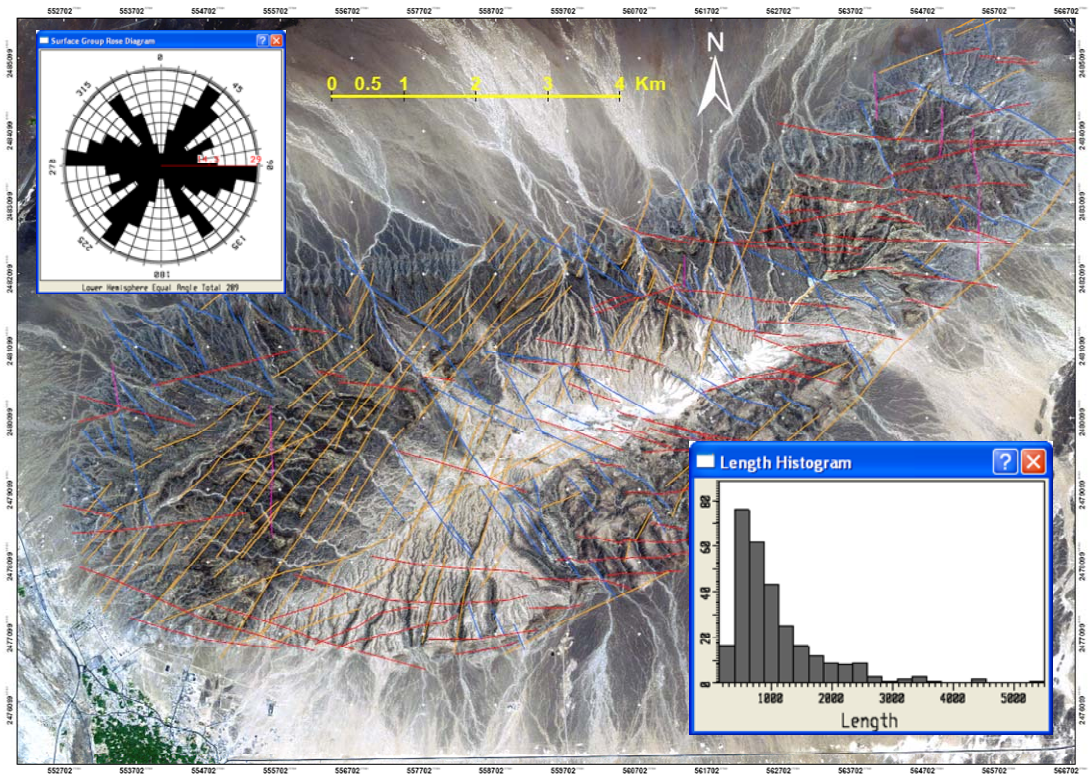


**Figure 2-38 Lineament interpreted on Quick Bird Image of Jebel Madmar (modified from de Keijzer et al, 2004) showing strike of the large lineaments (possibly faults) divided into different set using color (blue –NW; red –E; and orange NE).**

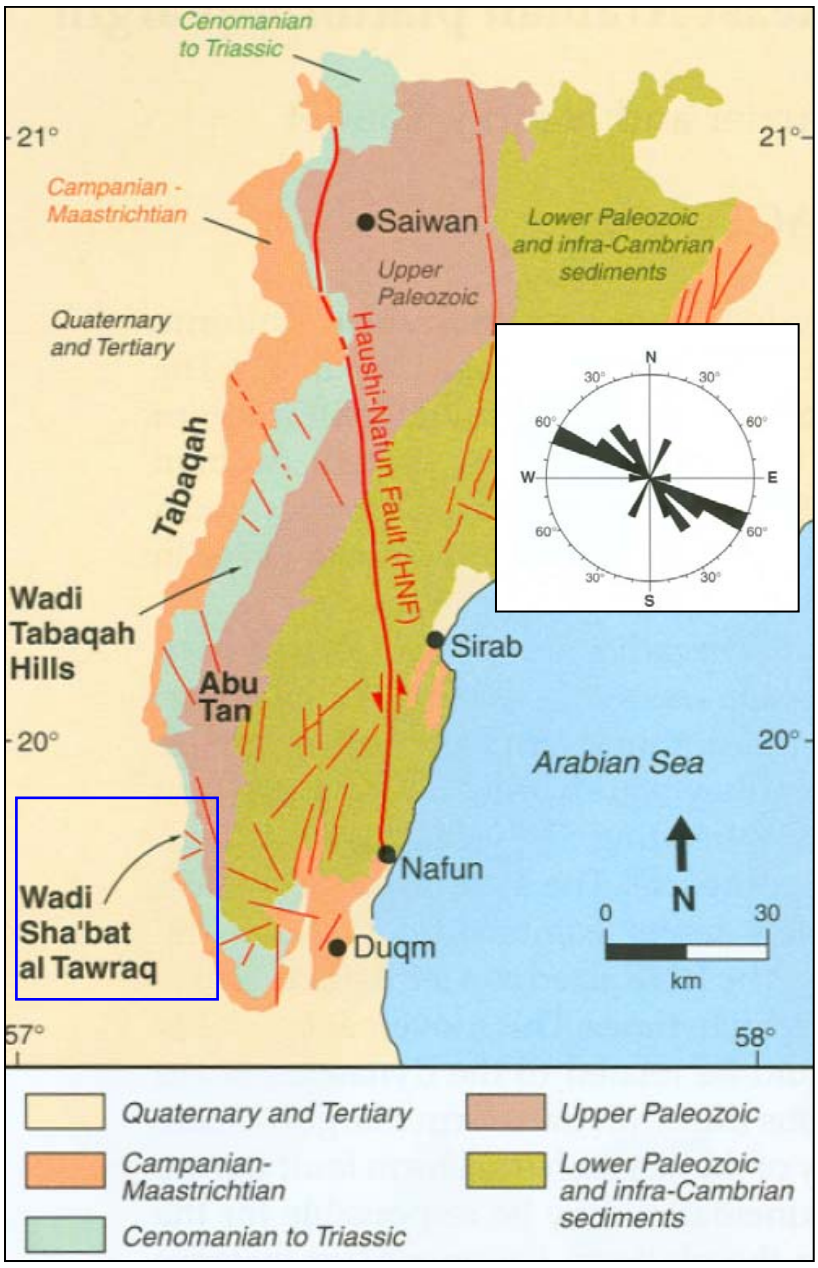


**Figure 2-39 Geological sketch map of Huqf outcrop, SE Oman: major faults, together with an insert rose diagram of syn-diagenetic fault directions in Wadi Sha'bat al Tawraq: normal faults affecting the Qishn limestone prior to complete lithification (Montenat et al, 2003).**

### *2.3.4 Uplift*

As stated above, the uplift map was one of the main elements used to determine the domains of similar tectonic characteristics. There are few (to none) integrated, detailed uplift studies done in the Interior of north Oman. The current understanding of north Oman uplift history is based on the following analysis: subcrops of Formation based on seismic analysis (unconformity), combined with well tops (thickness) data; and velocity trends with depth to highlight any anomalies. For the purpose of this study, the combined "net" uplift map (Figure 2.40) together with the uplift at the end of the Cretaceous (Figure 2.41) were used.

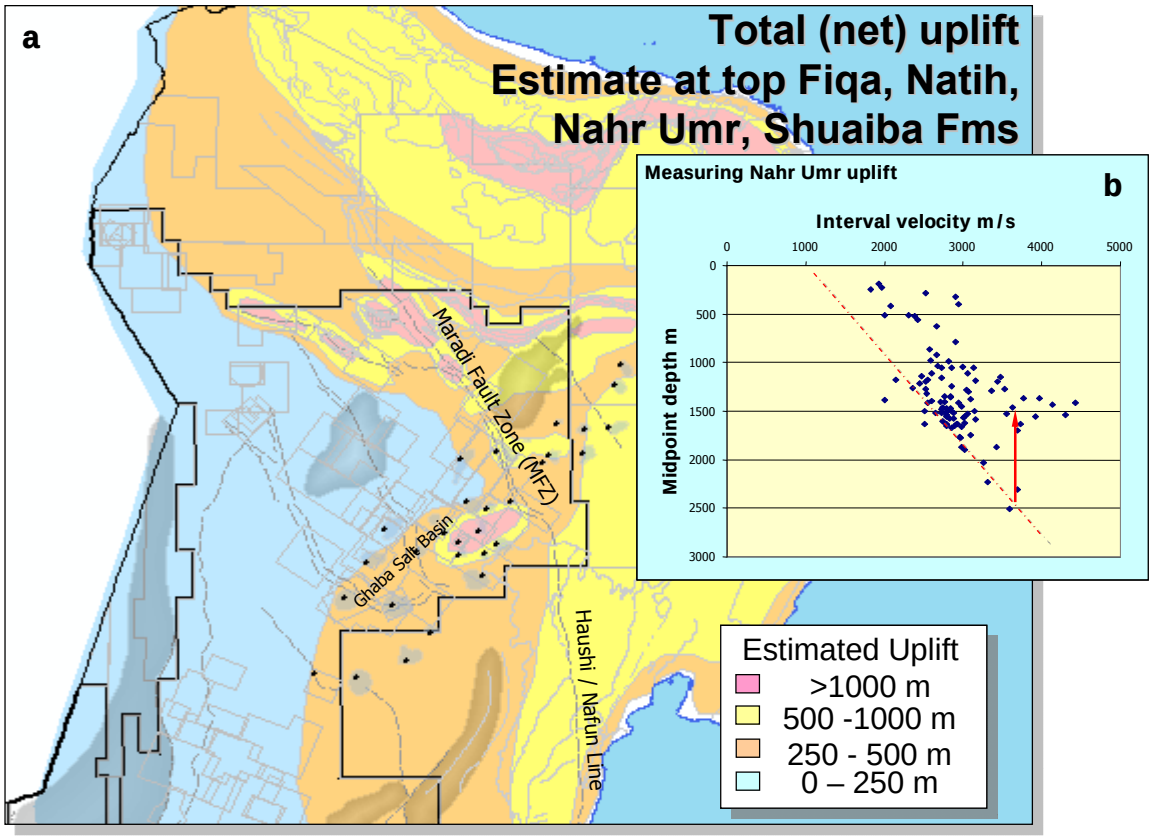


**Figure 2-40 Total net uplift of the Interior of north Oman (PDO exploration team internal presentation, 2004).**

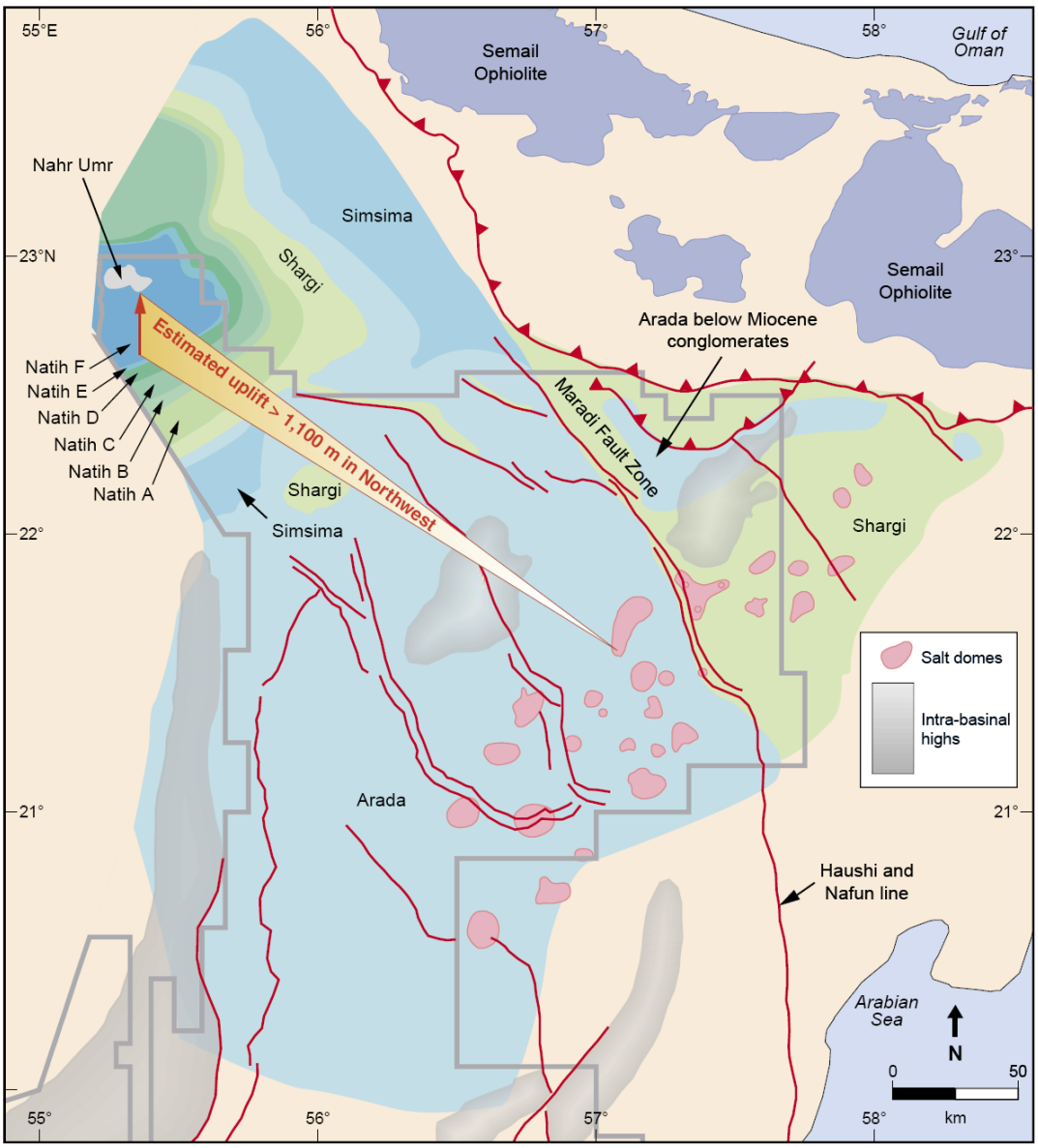


**Figure 2-41 Base Shammar (Base Cenozoic 60-65 Ma) subcrop map highlighting estimate of uplift at the end of the Cretaceous (Filbrandt et al, 2006).**

From both figures above, it is clear that the scale of uplift in the Interior of north Oman is much less compared to that of the eastern (Huqf) and NE (Oman Mountain) margins of the Arabian Plate, which were uplifted well over 3000m. A narrow zone (less than 5km) of uplift can be defined along the Maradi Fault Zone, Salakh Arch, and localized areas associated with the salt domes in the eastern part of the Ghaba Salt Basin (Filbrandt et al, 2006).

### *2.3.5 Stress analysis*

Borehole breakouts and induced fractures in Oman suggest that the orientation of the present-day first-order maximum horizontal in-situ stress is oriented NE-SW, (Hoogerduijn Strating, 2002; Filbrandt et al, 2004; and compilation of PDO data from Schlumberger and Baker Atlas). Note that the borehole breakout data are obtained from various depths (Figure 2.42). This subject is further discussed in detail in Chapter 4 and also in Chapter 7. The average magnitudes of the present-day stresses in north-central

Oman are 24.3 kPa/m for vertical stress (σV), 19.4 kPa/m for minimum horizontal stress (σh) and 34.3 kPa/m for maximum horizontal stress (σH) (PDO-GMI Internal Report, 2004). This means that the present-day regional tectonic stress regime in north-central Oman is strike-slip (maximum and minimum stress horizontal; intermediate stress vertical). The carbonate reservoirs in north-central Oman are at hydrostatic pressure (See Figure 1.5). Hence, the fluid pressure (Pf) gradient is assumed to be ~10.0 kPa/m.

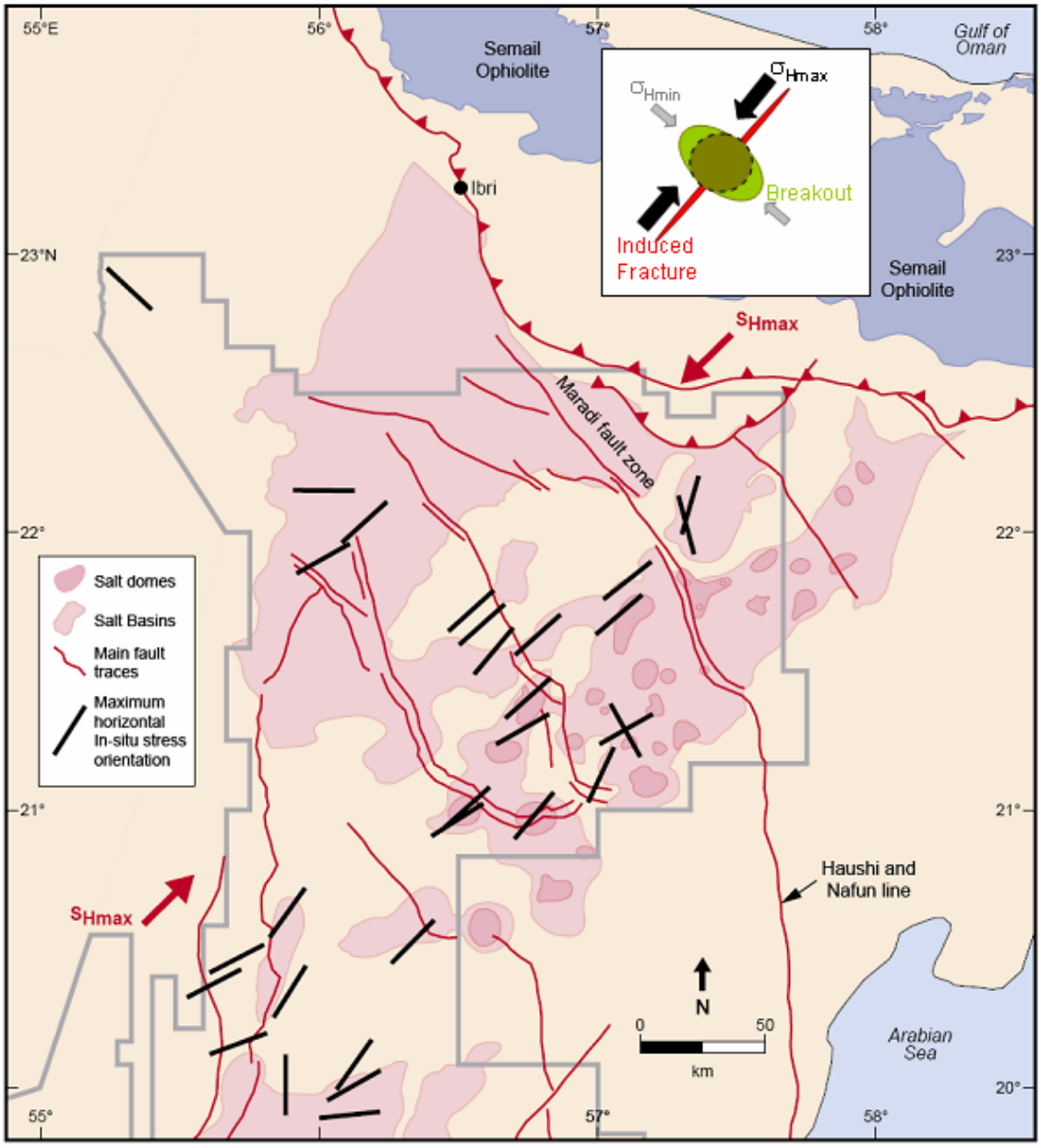


**Figure 2-42 In situ stress direction in north Oman (Filbrandt et al, 2006). Note the anomaly at Lekhwair area in the NW.**

The kinematics analysis of both the subsurface and surface faults (shown in Figures 2.35 to 2.37) indicates a paleo-stress (or shortening axis) of NW-SE (~135 degree) orientation during the Alpine Phase I (Filbrandt et al, 2004), Figure 2.43. This trend of NW-WNW strike slip "wrench" faults seen in most of north Oman, best example close

to Lekhwair, were also reported in the United Arab Emirate's fields (Marzouk and Sattar, 1993; Johnson et al, 2006).

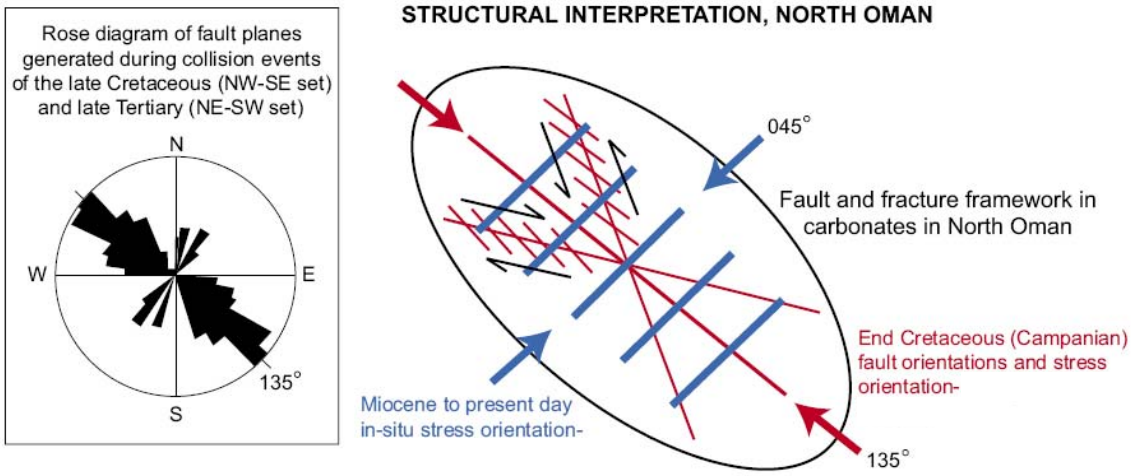


**Figure 2-43 Schematic drawing for the stress directions (current and paleo) based on fault kinematics (Filbrandt et al, 2006).**

### *2.3.6 Diagenesis*

The north Oman Shuaiba regional synthesis study, Phase II of Shuaiba Asset Study (Droste et al, 2004), also describes regional trends in Shuaiba diagenesis inferred from available reports, literature and data files (Figure 2.44). A summary of the diagenesis section is presented below:

**Subthrust compaction domain**. This domain is limited to northern portions of north Oman that were overthrust during the Late Cretaceous. The Subthrust compaction domain is characterized by extreme levels of chemical compaction and associated burial cementation. It's postulated that Shuaiba reservoir potential is very poor to nonexistent below the thrust.

**Foredeep leaching domain**. This domain is characterized by a net benefit of compaction water leaching in areas where thrusting-induced chemical compaction might otherwise have substantially degraded the reservoir section.

**Bab Basin leaching domain**. This domain is characterized by the same benefit of burial leaching associated with basin dewatering as described above, but the source of fluids is inferred to have been the Bab Basin. The mechanism of fluid expulsion was normal loading-induced compaction. Lateral reach of this leaching system was broader compared to the thrust front domain because of proximity of high permeability facies rimming the basin edge, and possibly to the existence of uncemented NW-SE trending fault conduits trending into northern Oman (assuming a later timing for cementation of these faults).

**Tectonic/salt-withdrawal fault and burial leaching domain**. This domain is proposed to exist based on a very small database; more work should be done to confirm its existence. The domain is characterized by aggressive leaching associated with salt-withdrawal and larger tectonic faults that ring the Makarim High.

**Meteoric leaching and erosion domain**, including the Makarim High (Musallim area). This domain is characterized by greater effects of meteoric leaching and early mechanical erosion - especially towards the south and east. Lower levels of chemical compaction are also observed – especially in coarser textured facies that exist in hydrocarbon-charged intervals. Coarser textured facies associated with structural-influenced highs (Al Huwisah, Safah) benefited from more meteoric leaching and a degree of meteoric cementation that helped armour the intervals against effects of later chemical compaction.

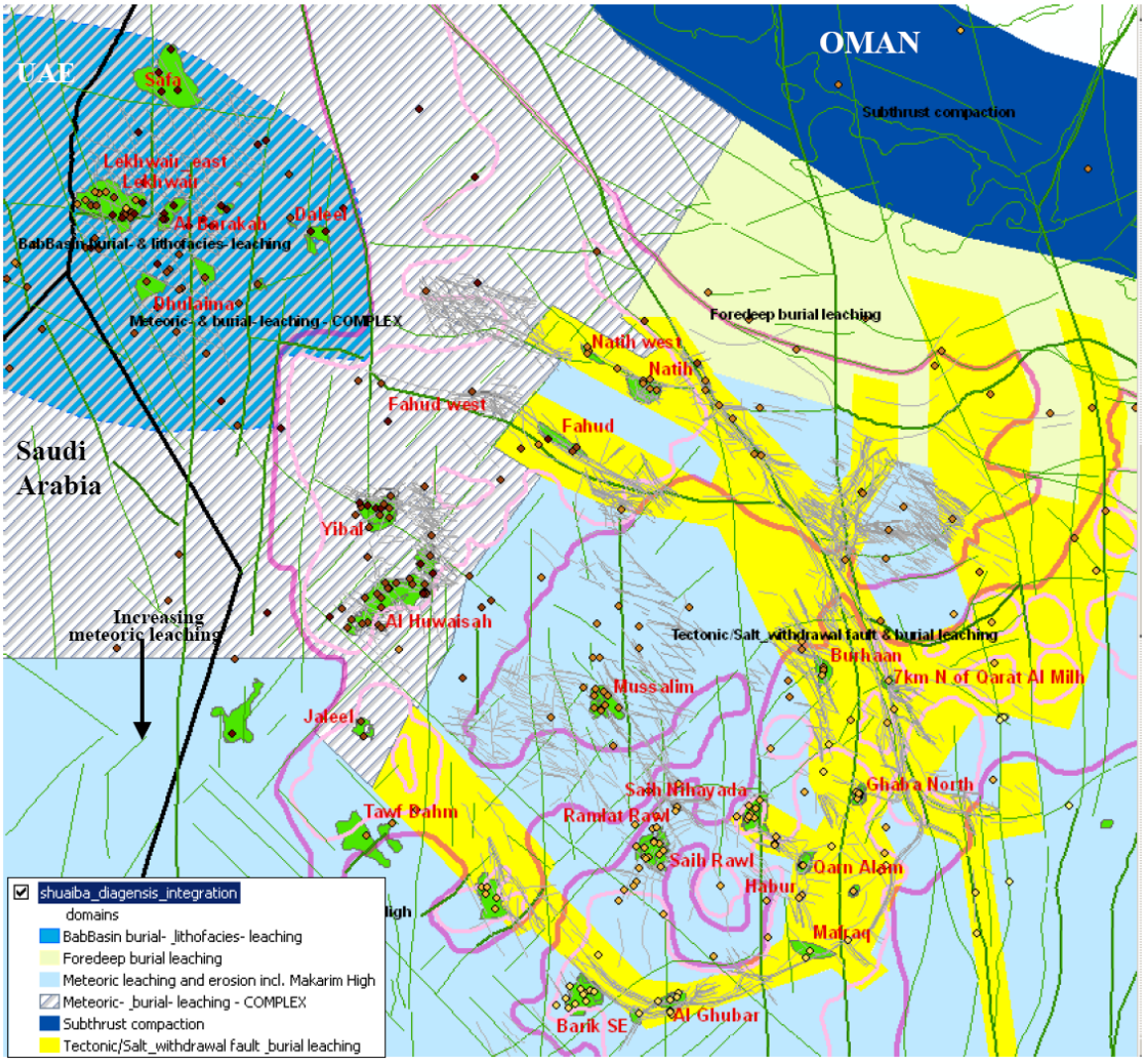


**Figure 2-44 North Oman Shuaiba diagenesis trend: see key for type (Droste et al, 2004).**

Diagenesis of the Cretaceous reservoirs is the least studied subsurface aspect. The above work is a notional draft based on regional analysis and it has to be confirmed by detailed field scale studies. Recently, a schematic conceptual model for the diagenesis in the Fahud field (Natih Formation) has been created by Shell EPT for PDO based on thin-section analysis. The results were not available for this thesis.

# Chapter 3– REGIONAL FRACTURE EVALUATION

This chapter focuses on the geometric and static properties of fracture data seen in the Cretaceous reservoirs and in outcrop analogues. The main input data is the BHI fracture picks, as there are limited core fracture data available. An attempt to link the fracture distribution to the associated mechanism is presented. The results of existing fracture studies per fields are reviewed and summarized.

## 3.1 Natih Formation

As has been shown in Chapter 2, the stratigraphy of this formation is characterized by interbedded carbonate and shale layers (see Figure 2.4). The fracture data available for this formation are obtained from the outcrops of the Salakh Arch area, from Natih Field, Fahud Field and Al Ghubar Field.

### *3.1.1 Salakh Arch Natih outcrop*

This outcrop in the foreland of the Oman Mountain was the subject of many studies because it is thought to be an analogue of the nearby Natih and Fahud fields (Figure 3.1), and even to the Shuaiba Formation Fields to some extent. The outcrop is made of Jebels ("hills") that make an arch at the SW edge of the Oman Mountains (Figure 3.2). Also see Figure 2.1 for regional location.

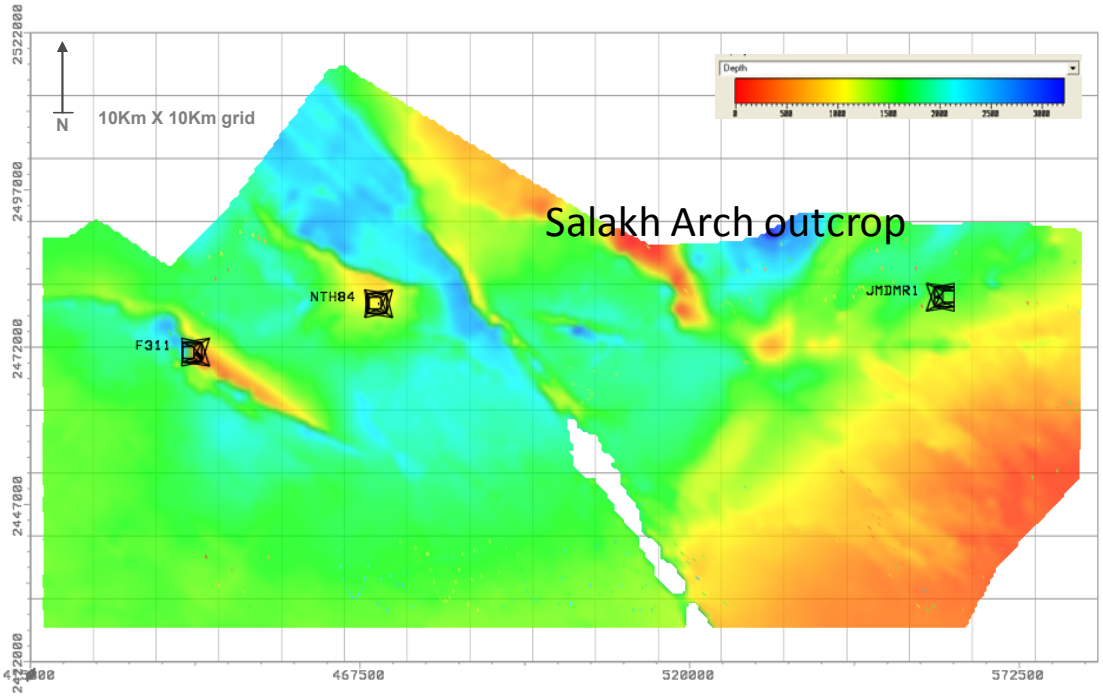


**Figure 3-1 Location map of Fahud field (F311 well), Natih field (NTH84) and Jebel Madmar (JMDMR1) on top of top Natih NOCEM structure map, showing the proximity between the outcrop of Salakh Arch and the producing fields of Fahud and Natih.**

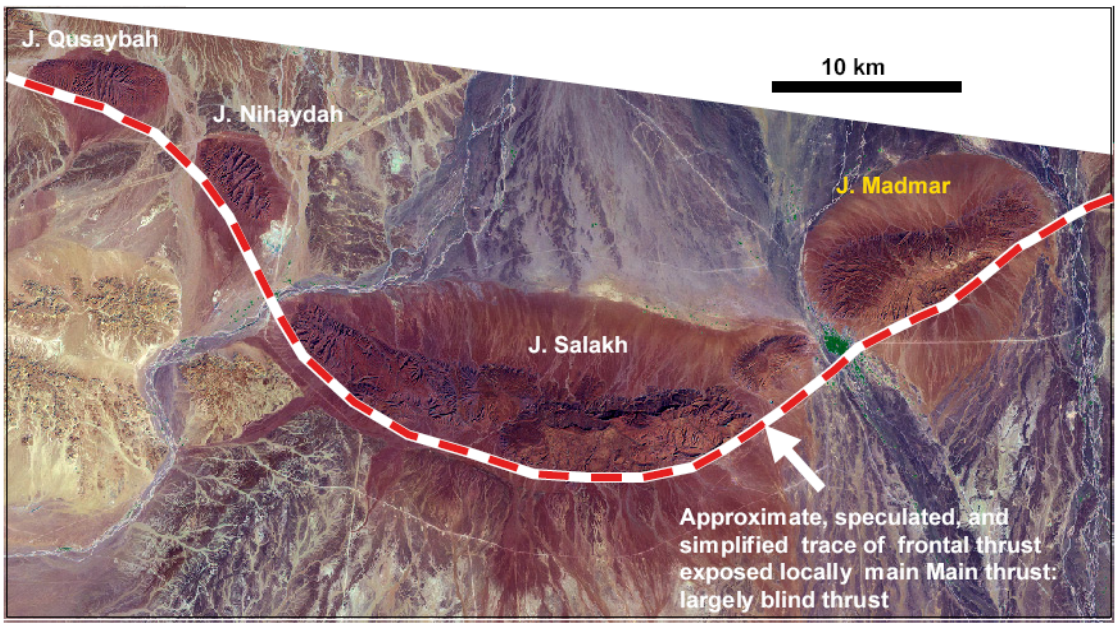


**Figure 3-2 Quick bird satellite image of Salakh Arch showing Jebels "hills" locations from de Keijzer et al, 2004.**

A summary of the findings reported in the main existing studies of these outcrops is presented below:

Mercadier and Makel (1989) main findings:

The field work was undertaken on Jebel Qusaybah, Jebel Nihayda and Jebel Salakh. Two families of fractures were identified: cross-axial fractures that strike roughly perpendicular to fold axis, and longitudinal fractures that strike roughly parallel to the fold axis, i.e. fold-related fractures. All the fracture types are (sub) vertical and may occur as extensional or shear fractures. For the cross–axial group, the extensional fractures have a spacing of 1 to several tens of meters, while the shear fractures, with 0.1 to 2m spacing, are more numerous. For the longitudinal group the spacing is more variable over the structure, depending on lithological variation, bed thickness and more importantly dip change. The fractures seen in these outcrops are fold-related fractures, as their orientation changes from one outcrop to another depending on the local orientation of the fold axis. They also change (orientation and intensity) with structural position (i.e. flank or crest) on those anticlines. Small scale (1-10 cm), sub vertical fractures have been noted in the argillaceous limestone intervals, with no preferred orientation, but these fractures do terminate at bed boundaries. These are interpreted to be hydraulic fractures that formed at an early burial stage. A length to height ratio of about 10 is observed for fractures in both the clean limestone and the argillaceous limestone. Almost all fractures are calcite cemented and fracture apertures vary from less than 100 microns to up to 5 cm.

Jones and Loosveld (1994) main findings:

The field work was undertaken on Jebel Qusaybah, Jebel Nihayda, Jebel Salakh and Jebel Madmar. They distinguished four fracture generation mechanisms, in order of

abundance: regional tectonic fractures running NE (Figure 3.3); uplift or stress release fractures occur in orthogonal patterns and abut against the regional fractures, the majority of which run NW-SE. These were absent when compared to the Natih Field, hence supporting the uplift interpretation. The ten-fold increase in the intensity of the NE regional fractures is attributed to the strength of the uplift compared to its impact on the field (Figure 3.4). Faulting has a small effect upon the outcrop structure, perturbing the fracture pattern over a limited area in the immediate vicinity – around 25m – of the faults (Figure 3.5). Folding or curvature is thought to have a limited effect upon the surface structure, increasing the fracture intensity only in areas of high curvature, in contrast with the Mercadier and Makel (1989) interpretation.

de Keijzer et al (2004) main findings:

This study was based on a combination of field observations and lineament picks on high resolution Quick Bird satellite images, as well as comparison with subsurface fracture data (mainly BHI data). The lineament picks were done at different satellite image resolution: 1:100 000, 1:25 000 and 1:2 000) of Jebel Madmar, and then were grouped per orientation (Figure 3.6). NE and NW fractures comprise a multi-scaled, nested system of strata-bound fractures and fracture corridors (Figure 3.7). NE fractures are most pervasive; however NW fractures are also locally abundant or even dominant. NE fracture corridors (Figure 3.8) up to ca. 150 m wide have been mapped in which internal layering (i.e. mechanical stratigraphy) has been largely destroyed. Faults are either (i) genuine faults such as WNW normal faults, (ii) reactivated faults such as inverted WNW faults, or (iii) reactivated fractures and fracture corridors (especially NE). N-trending faults are least numerous and still largely enigmatic. Some have latest strike-slip motion. With regard to the Natih Formation, outcrop work had shown that (Figure 3.9): mechanical boundaries that stop fractures up to bed-scale are generally sharp discontinuities with a textural or mineralogical change; mechanical boundaries that stop fractures up to unit-scale are characterised by a significant change in texture and/or chemistry, and additionally a change in bedding style across the boundary; and mechanical boundaries that stop fractures up to formation-scale are determined primarily by a change in clay content and thickness of the clay/marl interval adjacent to the boundary (of the order of 10's cm or thicker).

Al Kindi (2006) main findings:

The field work was undertaken on Jebel Qusaybah, Jebel Nihayda, Jebel Salakh and Jebel Madmar, as part of a PhD study. The fractures seen in outcrop are inferred to be mainly related to folding ("curvature") (Figure 3.10), though regional fractures were seen in the eastern part of the area running NNE-SSW and ESE-WNW. The fold–axis parallel fractures in tight hinge zones are usually confined within competent thick units or homogeneous thinner beds that behave as a single massive bed, indicating mechanical layering. Field data indicate that the density of fracturing is inversely proportional to the bed thickness. In general, the extensional fractures trend mainly

perpendicular and parallel to the fold axis, however the shear fractures formed conjugate sets with a bisector perpendicular to the fold axis. The direction of the regional maximum compressional stress which produced Salakh Arch was uniform in the inner and outer parts of the arc as determined from the orientations of fold axes and stress analyses. The trend of the regional transport direction was N03° E.


**Figure 3-3 Regional fractures form parallel planes exposed in Jebel Nihayda (2 486 000 – 514 000) from Jones and Loosveld, 1994.**

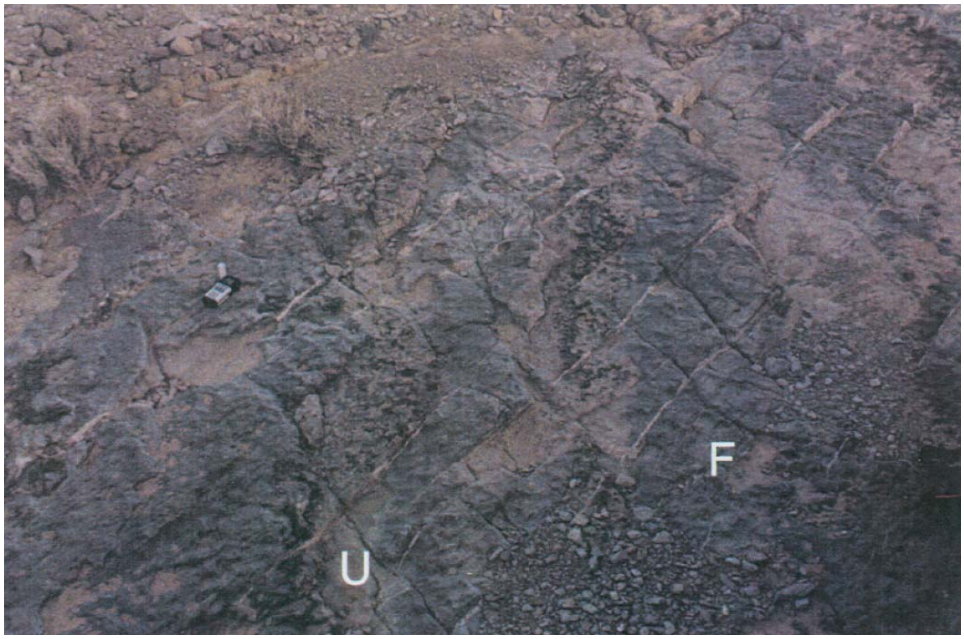


**Figure 3-4 Uplift related fractures abutting against regional fractures (cemented) exposed in Jebel Nihayda (2 486 000 – 514 000) from Jones and Loosveld, 1994.**

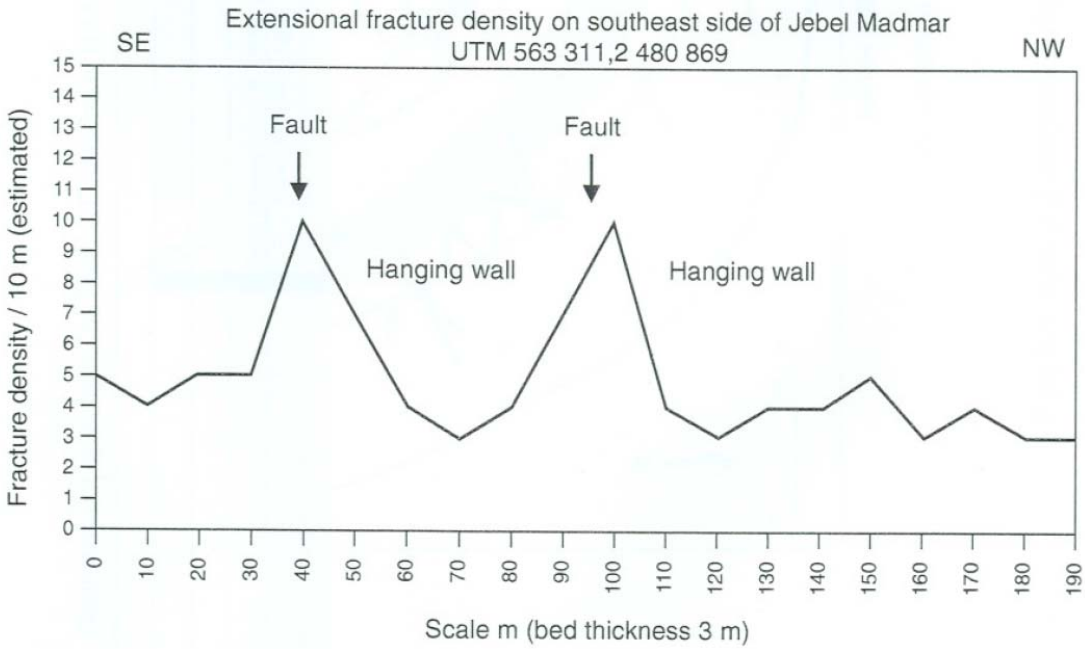


**Figure 3-5 Normal faults with throw <5m in Jebel Madmar, looking SW, together with a plot of fracture intensity with distance away from faults (Jones and Loosveld, 1994).**

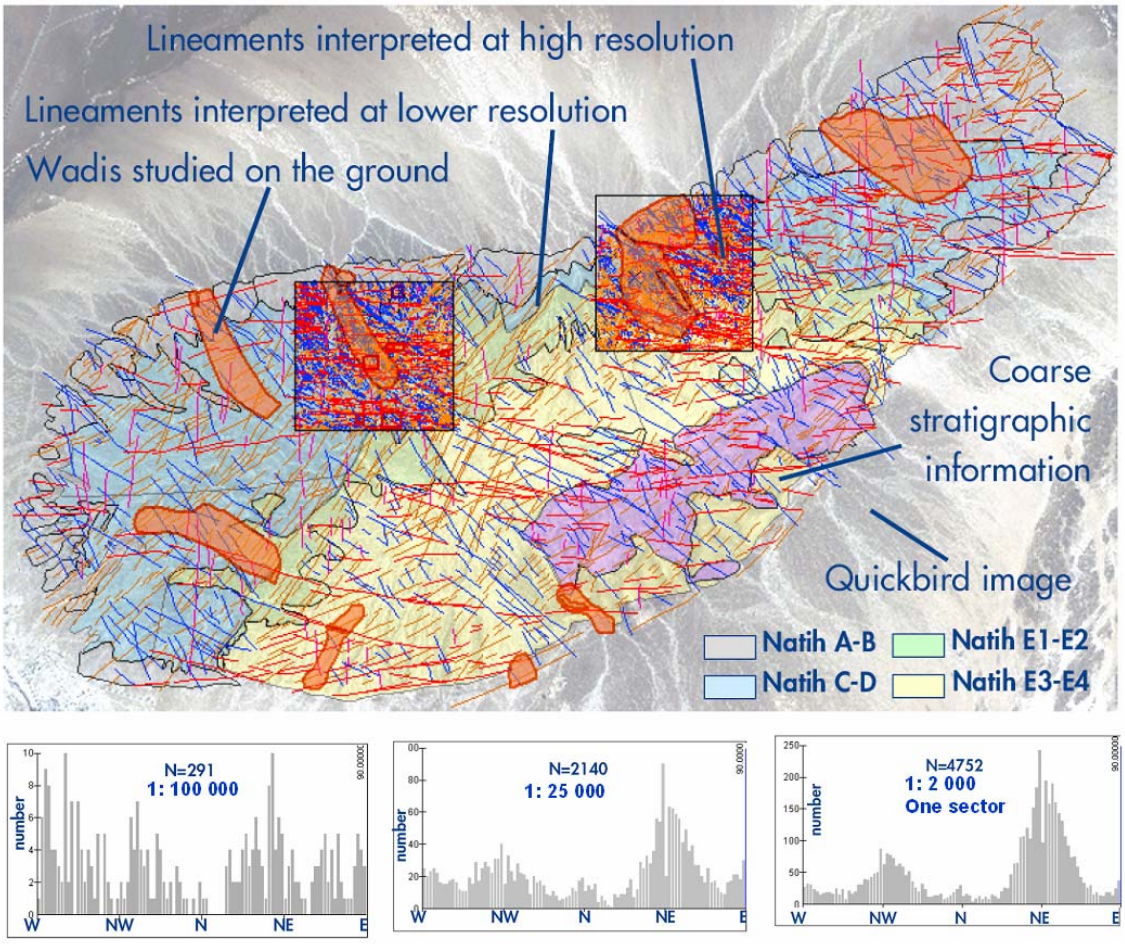


**Figure 3-6 Jebel Madmar lineament interpretations based on satellite images, the histogram are showing the intensity (frequency) per orientation per resolution (de Keijzer et al, 2004).**

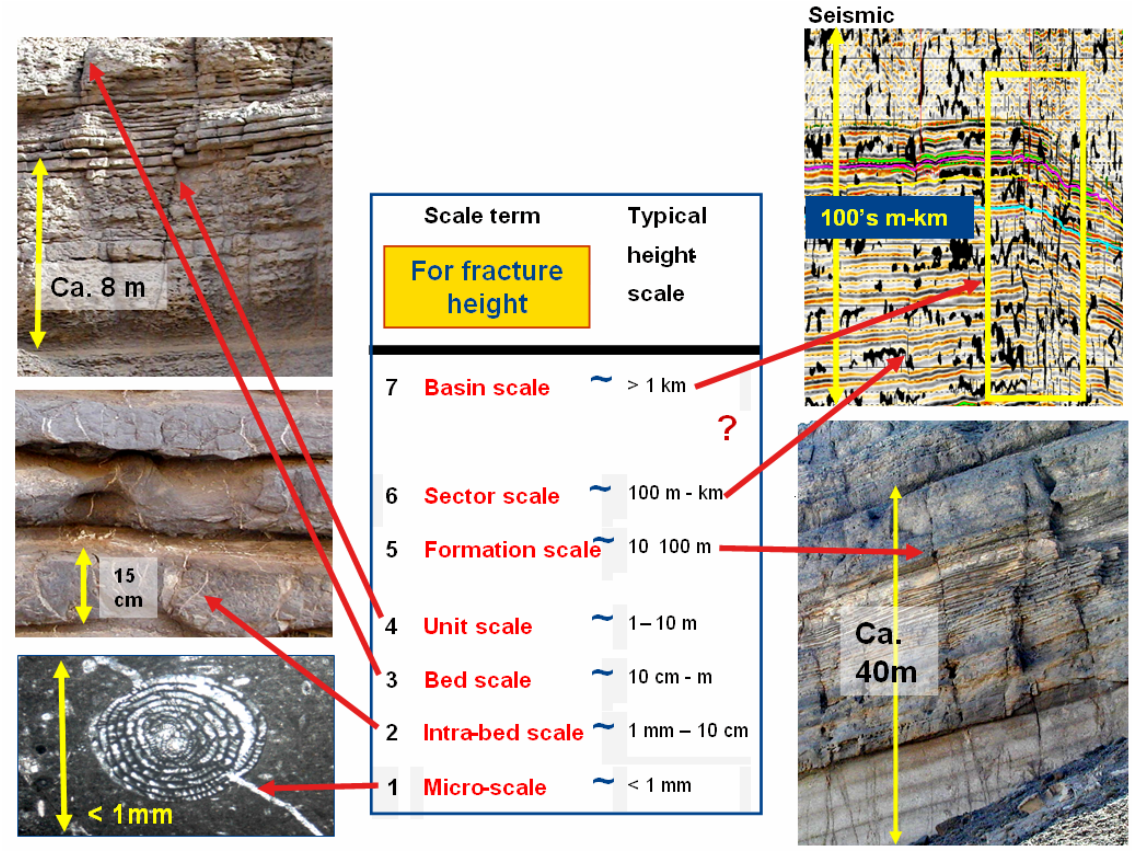


**Figure 3-7 Classification of fracture classes used for J. Madmar (de Keijzer et al, 2004).**


**Figure 3-8 Fracture corridors view in cross section in Natih E3 and in map view cutting Natih, see man standing for scale (de Keijzer et al, 2004).**

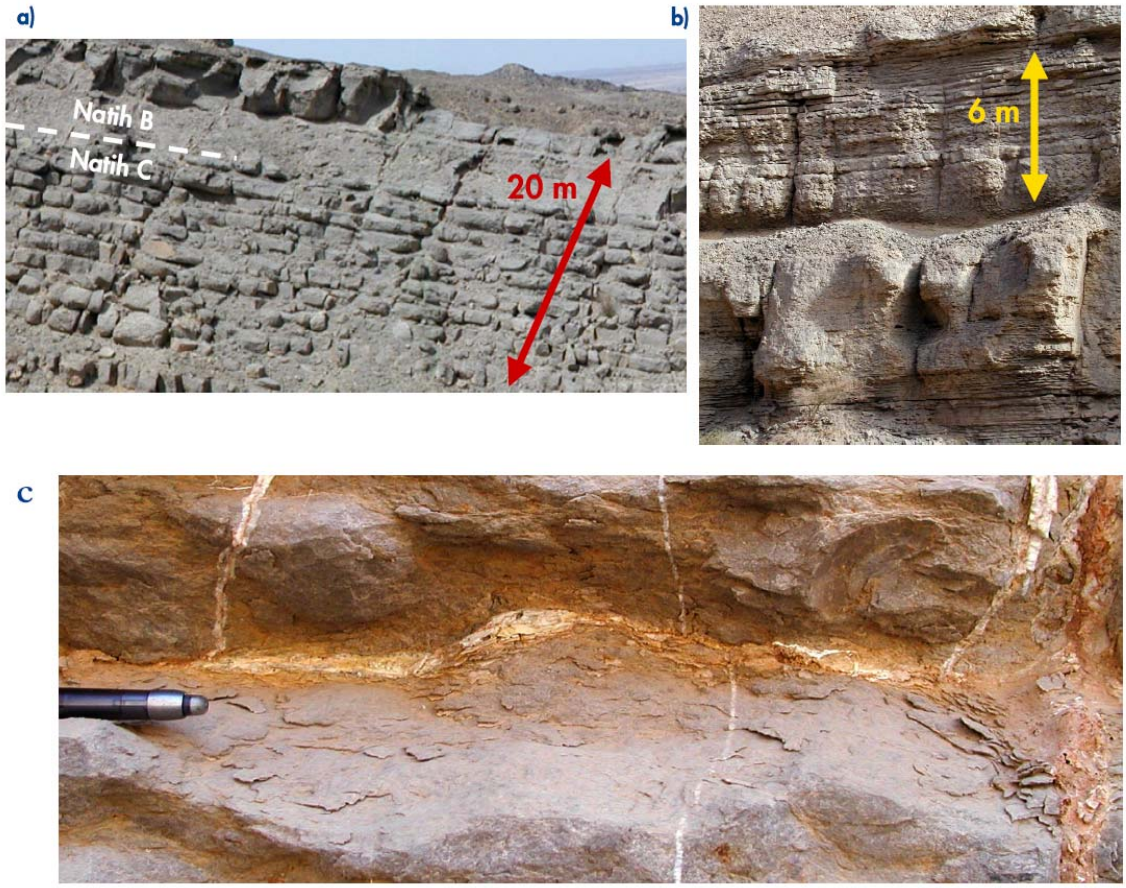


**Figure 3-9 Bed-scale and unit-scale NE joints (a) Natih C – Lower Natih, note the continuity of unit-scale joints between Natih C and Natih B. Typical spacing of these is 5-15 m compared to 0.5-1 m for bed-scale joints, and they tend to have wider apertures (up to 20 cm, cemented). (b) Top Natih E4. (c) Example of cm-thick calcite filled fractures parallel to bedding discontinuity in Natih E4 (de Keijzer et al, 2004).**

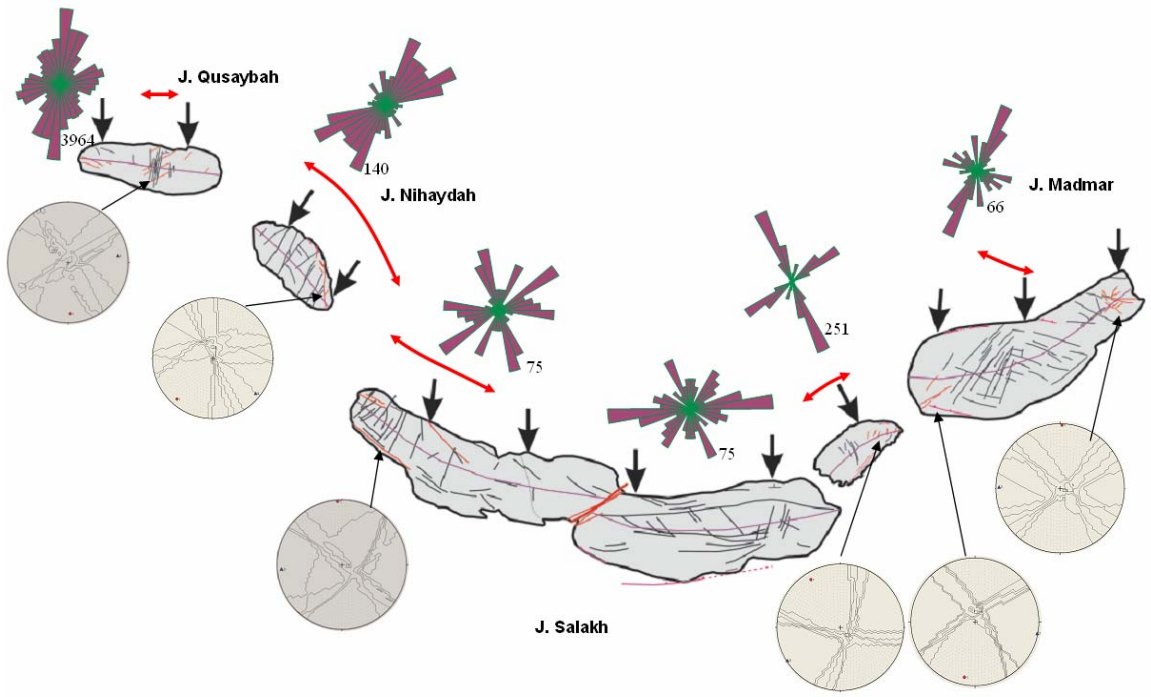


**Figure 3-10 A summary of fracture's strike orientations in various Jebels. The figure also highlights the areas with arc parallel or oblique extension (red arrows). The black arrows show the orientation of the maximum compression in various parts of the Arch as suggested by the fold-axis orientations and/or the paleostress analyses of σ-1 from the kinematics of strike-slip faults (al Kindi, 2006).**

### *3.1.1 Natih Field – Natih Formation*

This is the closest field to the Salakh Arch and, as mentioned above, its tectonic history is believed to be similar to that of the outcrop described above, after reducing the effect of the uplift. The field is produced using the GOGD concept from a highly faulted reservoir of the Natih Formation.

#### *Existing work*

The Natih field's natural fracture network was subjected to several studies in the past. A summary of the findings reported in these existing studies is presented below:

Hitchings (2000):

The study was based on integration of static (mainly seismic and BHI data) and dynamic data (mainly production data) in 1997, partly published in 2000. According to the study, there are three types of fractures seen, listed in order of importance (Figure 3.11): NE-trending fractures produced by regional tectonics; folding or curvature-related fractures; and fault-related fractures. The field was subdivided into domains based on fracture intensity using combined BHI & seismic fault data together with productivity index (PI) data (Figure 3.12). An update of Hitchings study was carried out by Baker Atlas (Ozkaya, 2002). This update resulted in a proposed fracture model for the field based BHI intensity, type and orientation (Figure 3.13).

Roeterdink (2004):

Roeterdink fracture analysis work was part of an integrated reservoir study intended to optimise the reservoir management strategy for producing the remaining Natih oil rim reserves. In addition to using newly acquired data (compared to Hitchings), it focused on fracture distribution vertically (i.e. within the Natih Formation), utilizing a detailed sequence stratigraphy analysis based mainly on data from eight cores: Core, BHI and outcrop data indicate that fractures follow the rules of mechanical layering: certain beds are more prone to fracturing than others (Figure 3.14). Natih A, especially the lower part, seems most fractured. Natih B is a possible baffle to flow, although certainly not to pressure. Alternatively, flow may only cross at certain places, e.g. at major faults. Top Natih C has multi-Darcy permeability in the matrix.

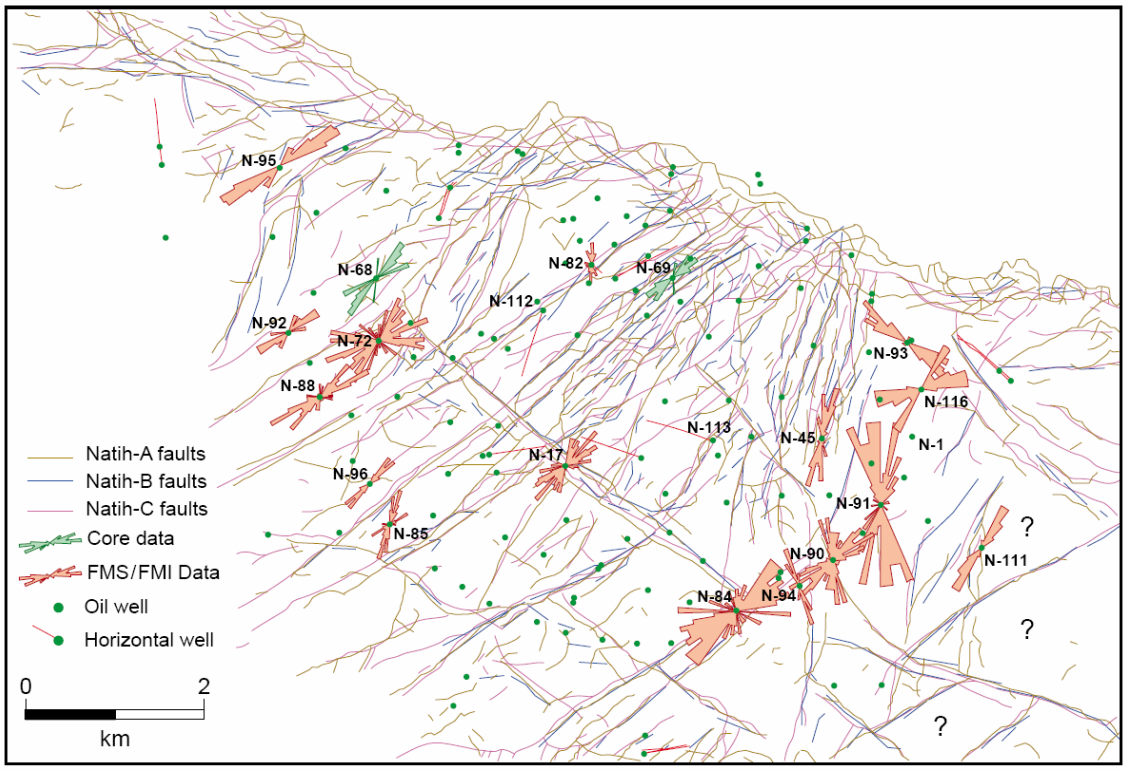


**Figure 3-11 Natih Field core and BHI fracture orientation (Hitchings, 2000).**

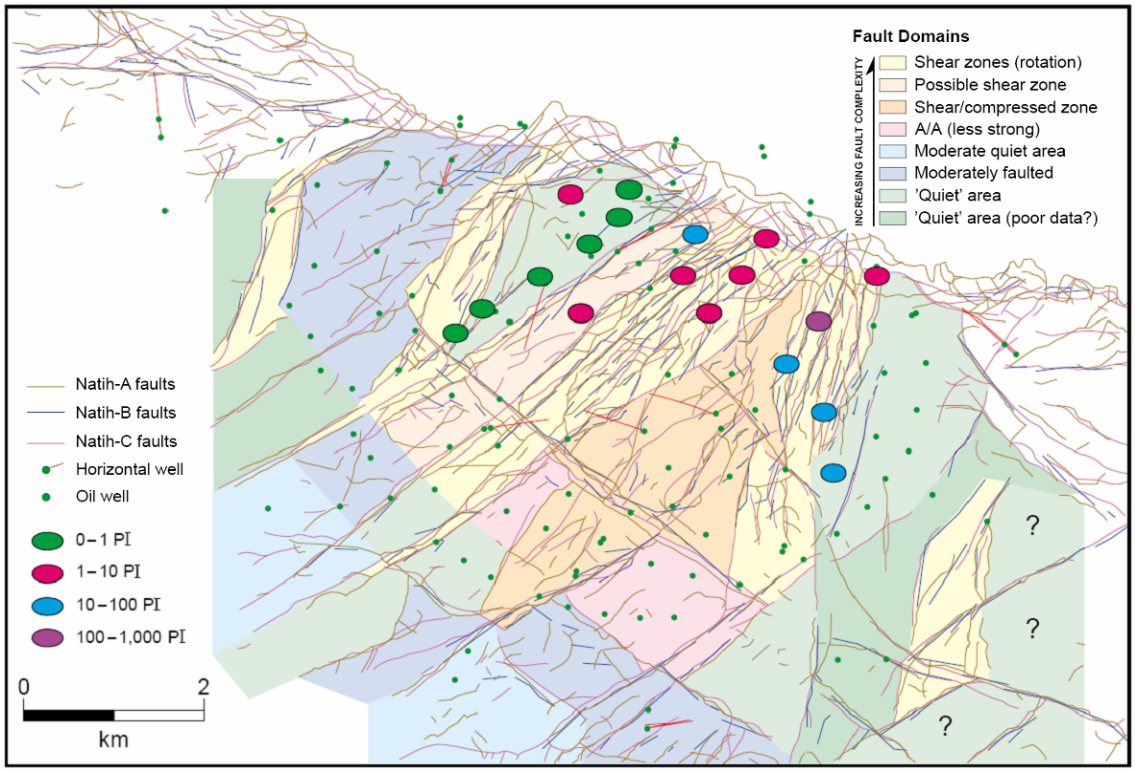


**Figure 3-12 Natih crest well Productivity Index, superimposed on top of Natih field divided into domains based on fault/fracture intensity and orientation (Hitchings, 2000).**

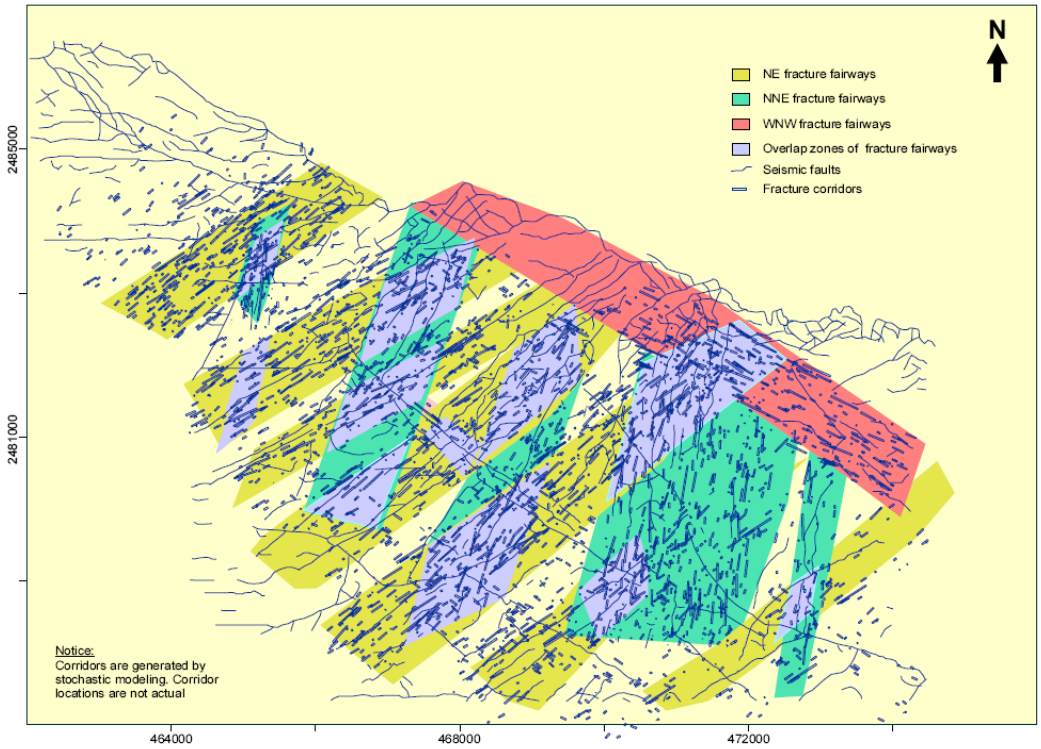


**Figure 3-13 Baker Atlas proposed model for the fractures of Natih Field (Ozkaya, 2002).**

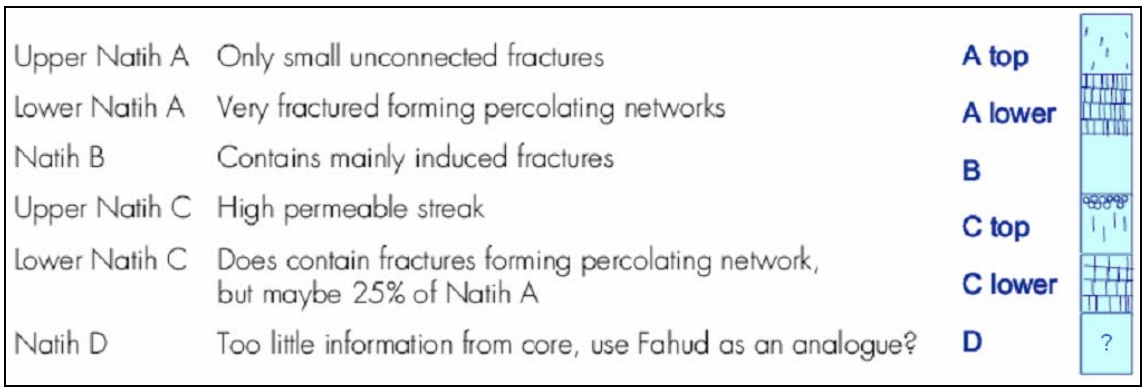


**Figure 3-14 Schematic concept diagram of the fracture intensity in the Natih formation (Natih field) based on core analysis combined with BHI data (Roeterdink, 2004).**

### *Natih field fracture data evaluation*

This section presents the result of Natih BHI fracture picks analysis, which I undertook in SVS. A plot of all the fractures picks in Natih formation (1808 fractures and 38 faults), superimposed on top of a multi-direction curvature map of top Natih, curvature wave length scale is 50m (shown in Figure 3.15 created in SVS), indicates the following: The dominant fracture orientations are NE, WNW and N. Note that a composite summary of all BHI data orientation (rose diagram inserted in the corner of the figure) does not reflect the real distribution. This is because the N-116H1 (in the north east side of the field) fracture picks show high intensity of fractures running WNW, which affects the total calculation. In contrast, the well by well roses diagrams indicate that the WNW fracture set is not present everywhere. Correlation is low between the occurrence of BHI fractures and high curvature areas (see circled N-88H1 & N-17H1 in Figure 3.15). The majority of the fractures are conductive (blue and light blue). Only 56 non-conductive fractures exist all striking NE (Figure 3.16). Majority of the wells TD within the shallow Natih AB member (Figure 3.17), thus it is very hard to evaluate mechanical layering concepts for the whole Natih Formation in Natih field. However, the cumulative plot of fracture frequency versus depth hints toward an influence of mechanical layering (Figure 3.18).

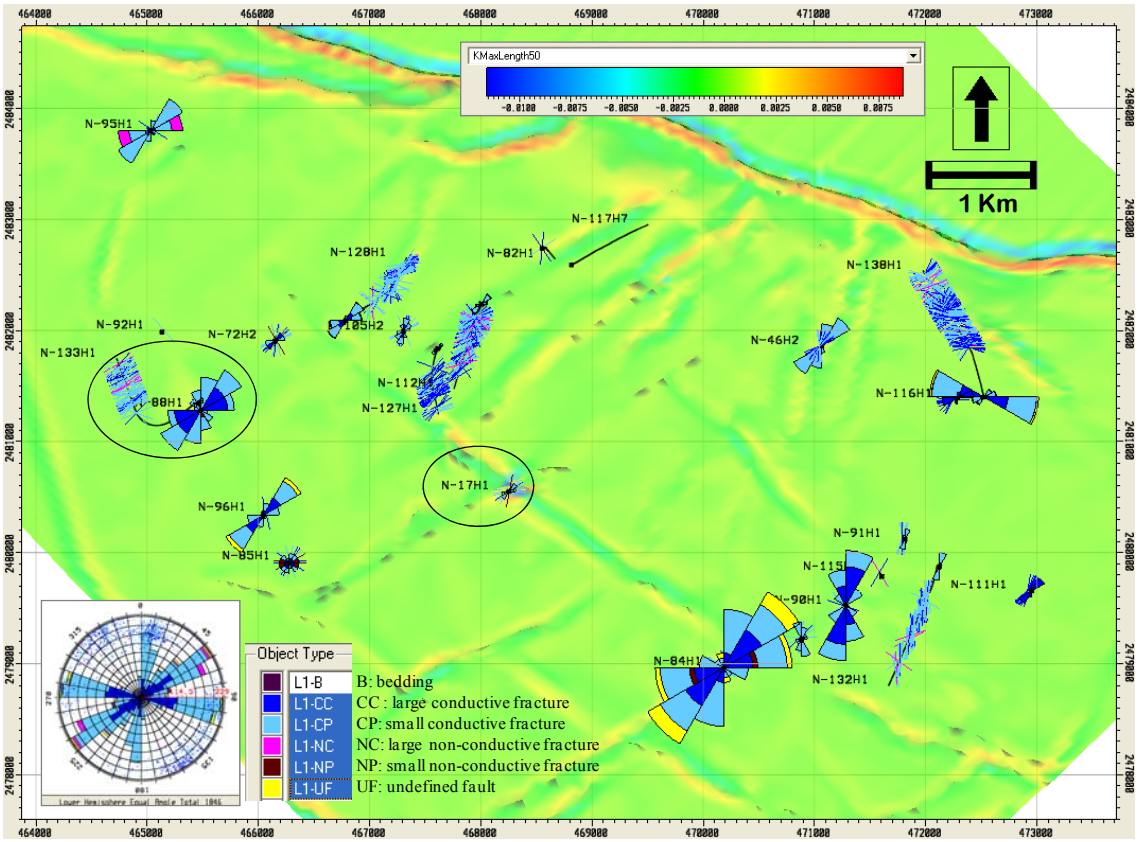


**Figure 3-15 Natih field BHI fracture picks, shown in SVS with both well rose diagram (size is proportional to standardize fracture count –i.e. frac/m) and full field rose diagram (bottom left corner insert), superimposed on top of a curvature map (Kmax with wavelength of 50m scale) of top Natih. Note how N-116H1 (in the north east side of the field) fracture picks show high intensity of fractures running WNW, which affects the full field rose diagram.**

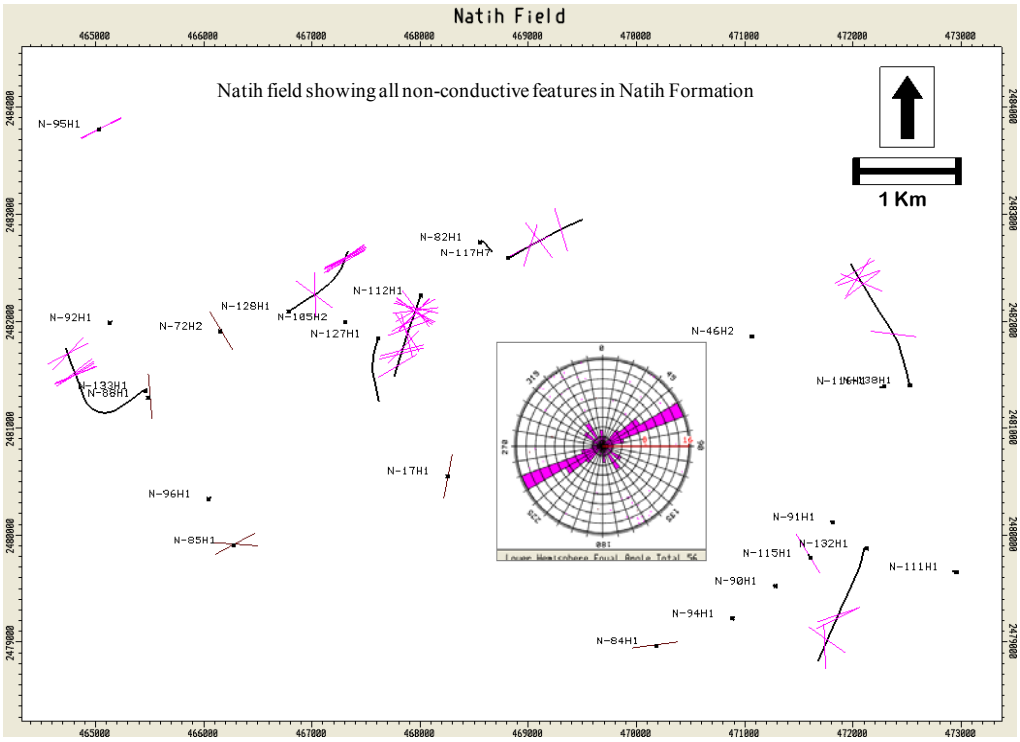


**Figure 3-16 Non-conductive BHI fracture picks of Natih field, majority striking NE.**

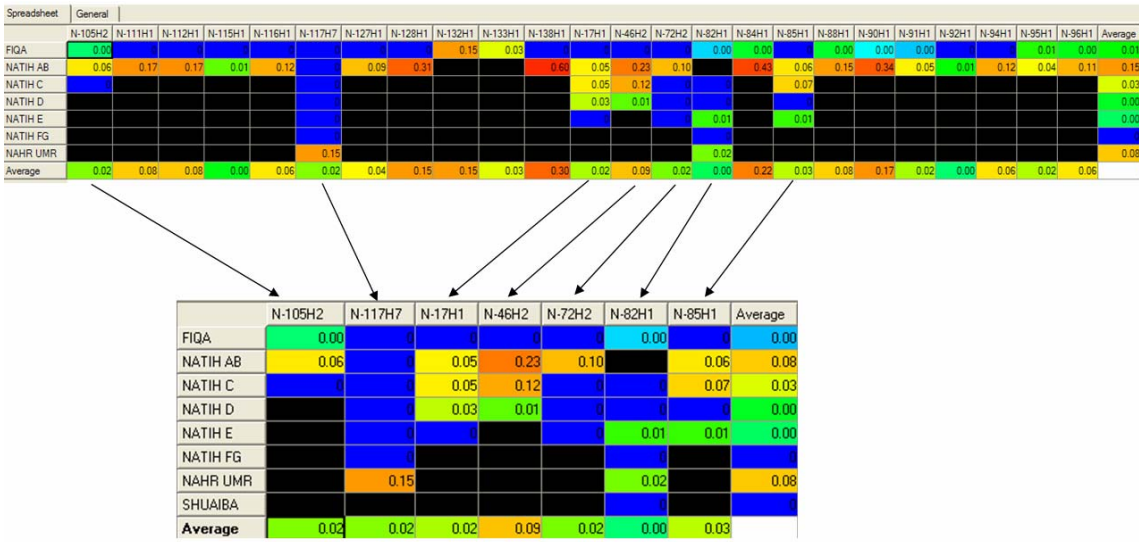

| | N-105H2 | N-117H7 | N-17H1 | N-46H2 | N-72H2 | N-82H1 | N-85H1 | Average |
|---|---|---|---|---|---|---|---|---|
| FIQA | 0.00 | | | | | 0.00 | | 0.00 |
| NATIH AB | 0.06 | | 0.05 | 0.23 | 0.10 | | 0.06 | 0.08 |
| NATIH C | | | 0.05 | 0.12 | | | 0.07 | 0.03 |
| NATIH D | | | 0.03 | 0.01 | | | | 0.00 |
| NATIH E | | | | | | 0.01 | 0.01 | 0.00 |
| NATIH FG | | | | | | | | |
| NAHR UMR | | 0.15 | | | | 0.02 | | 0.08 |
| SHUAIBA | | | | | | | | |
| **Average** | 0.02 | 0.02 | 0.02 | 0.09 | 0.02 | 0.00 | 0.03 | |

**Figure 3-17 SVS spread sheet of BHI fractures "objects" standardize (divided by BHI length) number per well per layer group (Natih member). Lower table focused for wells with BHI coverage beyond Natih AB. Note how most of the wells were TD within Natih AB member.**

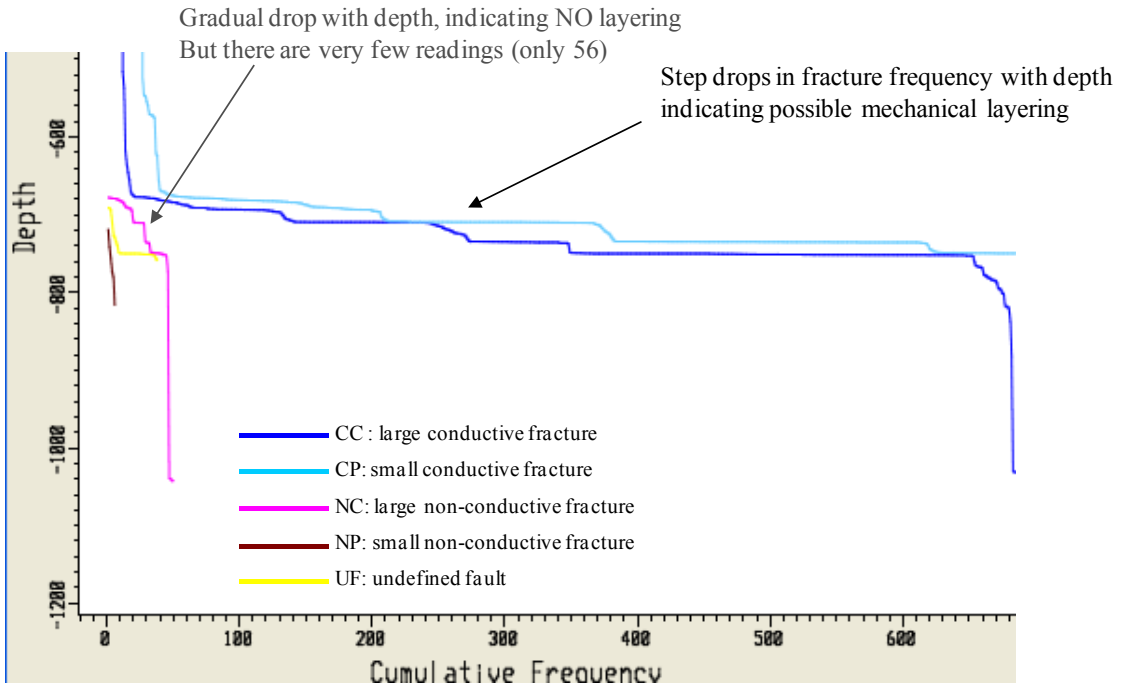


**Figure 3-18 Cumulative fracture frequency versus depth plot of Natih field's BHI fractures per type, indicating mechanical layering.** ***How to read such a plot? The Y axis is showing vertical depth, while the X axis is showing the cumulative frequency of BHI objects "fractures" per type (blue is conductive, while pink is non-conductive), basically like adding up the number of fractures. A drop indicates a possible layer with NO fracture, whereas a long horizontal section indicates a layer with lots of fractures. In addition, one can check if fracture type's frequency varies with depth. For instance, if the OWC depth is known then one may check whether the non-conductive fractures increase as the OWC is approached. Note it is per well so when wells are very shallow and very deep in same field, caution should be applied as layering will be at different vertical depth.***

### *3.1.2 Fahud Field – Natih Formation*

This mature GOGD field does not show many faults in seismic, yet many fractures are recorded by BHI and core, supporting the observation noted in the neighbouring Natih field that the majority of the fractures are regional in nature and few are related to faults.

***Existing work***

A summary of the latest fracture studies on this field is presented below:

Rawnsley (2001):

This study focused on the Natih E member in the north western area of Fahud Field, as part of Fahud Asset Study carried out by Shell EPT in 2001. Evaluation had shown that very few faults are present in the crest of the field (Figure 3.19). Integrated dynamic data, together with fracture data (Figure 3.20), were used to define areas of high fracture intensity, i.e. fracture corridors. Core fracture analysis, coupled with High Resolution Sequence Stratigraphy and outcrop observation, indicate that there is a mechanical stratigraphy present. The regressive units ($4^{th}$ order scale) are potentially more fractured than the transgressive units. FMI data analysis was used to identify the main fracture trends and tie them to the layering scheme. Despite the extensive FMI data set, most layers were insufficiently sampled to uniquely characterise the layer-bounded fracturing. The main fracture trend is NE, with less frequent N-S orientated fractures. NE-SW trending lineaments of productive fractures cross the reservoir units and have greatest permeability at the top of the Natih E.

De Keijzer (de Keijzer and al Dhahab, 2004):

This was a continuation of the above asset study, but covering the whole field as part of Fahud Field Development Plan and EOR screening. Correlation with Jebel Madmar was the main driver, combined with the integration of the BHI data and the other dynamic data. A simplified fracture intensity histogram hints toward mechanical layering (Figure 3.21) though the majority of the wells are biased in sampling because of the field structure (see Figure 3.20), with wells drilled in a specific member of Natih Formation, for example GOGD wells in E while matrix wells in B, resulting in under sampling of other Natih members. The field was split into Representative Area Model, RAM, areas of similar static and dynamic behaviour. An experimental design approach was used to assess fracture parameters impact on reservoir simulation: history matching and forecast (Figure 3.22). Several 3D discrete fracture network DFN model realizations were built and assessed (Figure 3.23).

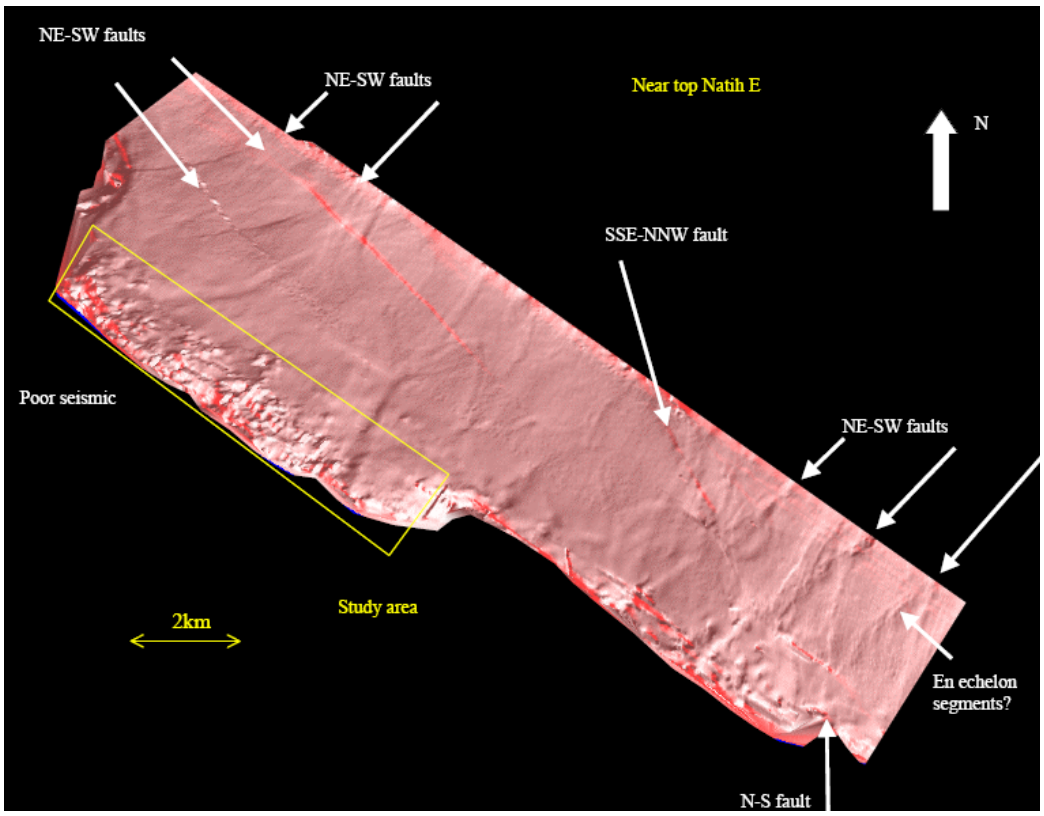


**Figure 3-19 Top Natih E illumination map of Fahud field. The wavy features running across the field away from the main western NW-SE bounding fault are channels (Rawnsley, 2001).**

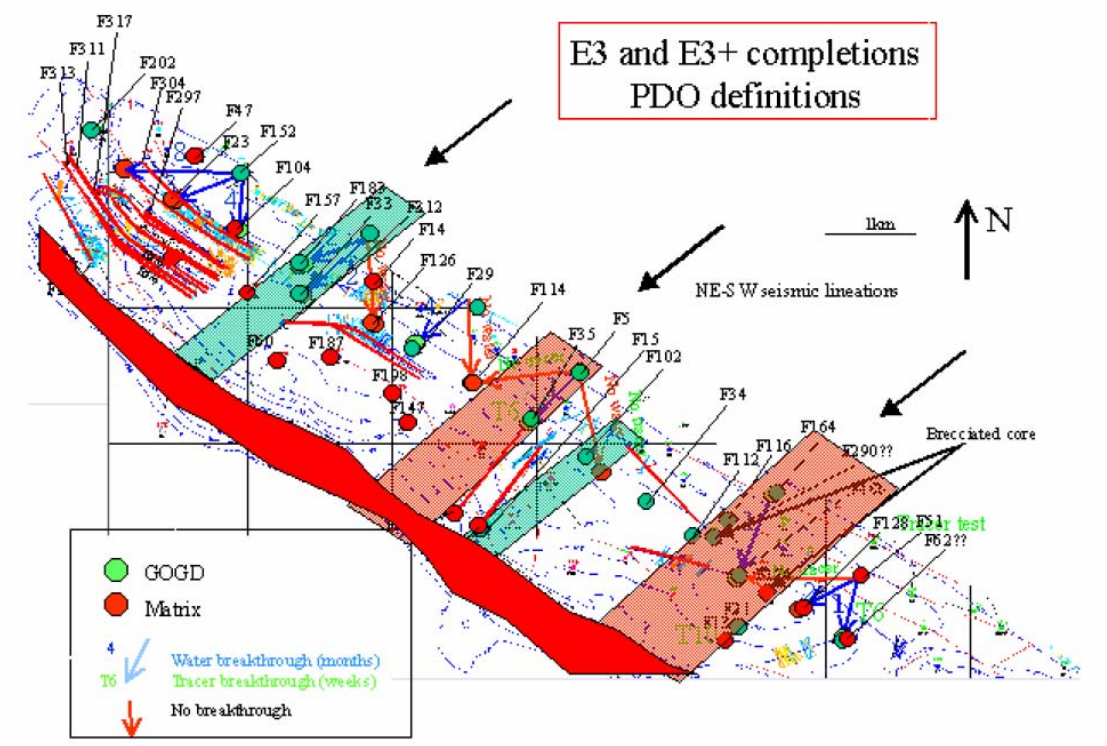


**Figure 3-20 Integration of BHI, core, tracer, water-breakthrough, production behaviour (matrix, GOGD) and seismic lineation. Solid red block is the main bounding Fahud fault and its associated damage zone. Transparent red zones are main seismic lineaments which best correspond to production behaviour in E3. Transparent green zones correspond to lower confidence lineaments, partly derived from seismic and production data (Rawnsley, 2001).**

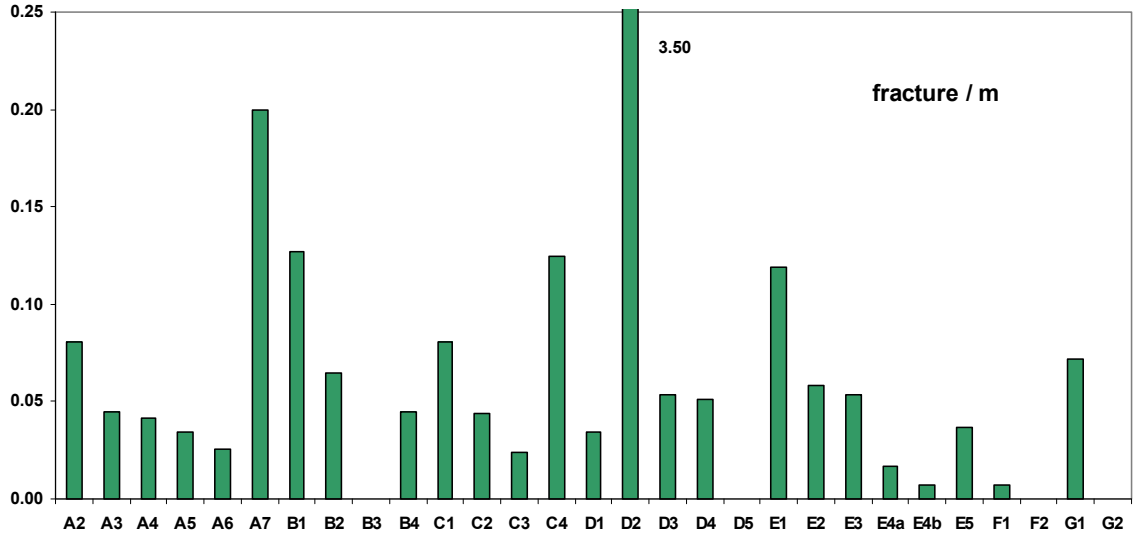


**Figure 3-21 Standardize BHI fracture counts per Natih sub-members for the Fahud field indicate potential mechanical layering.**

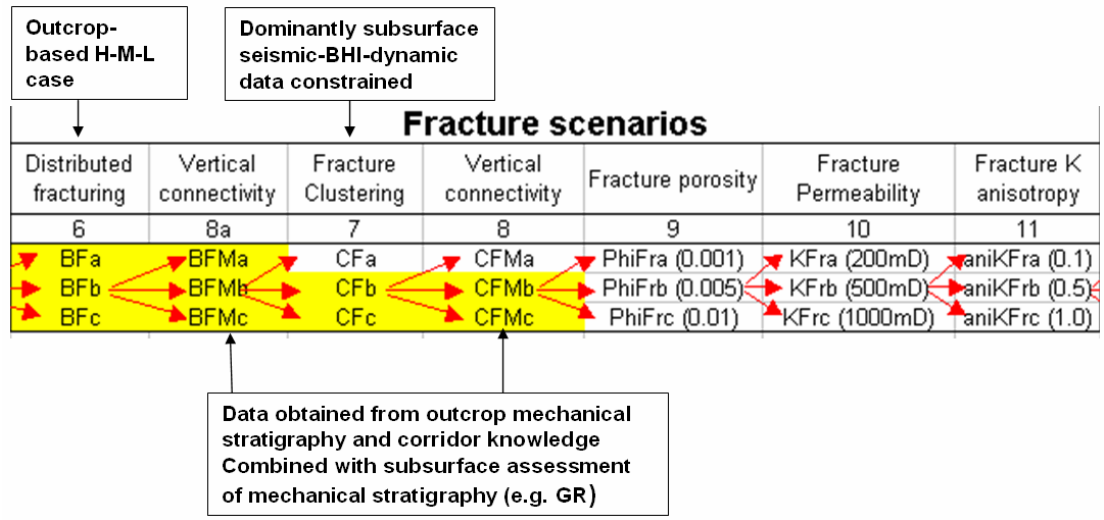


**Figure 3-22 Fracture parameters used for the experimental design simulation analysis (de Keijzer and al Dhahab, 2004).**

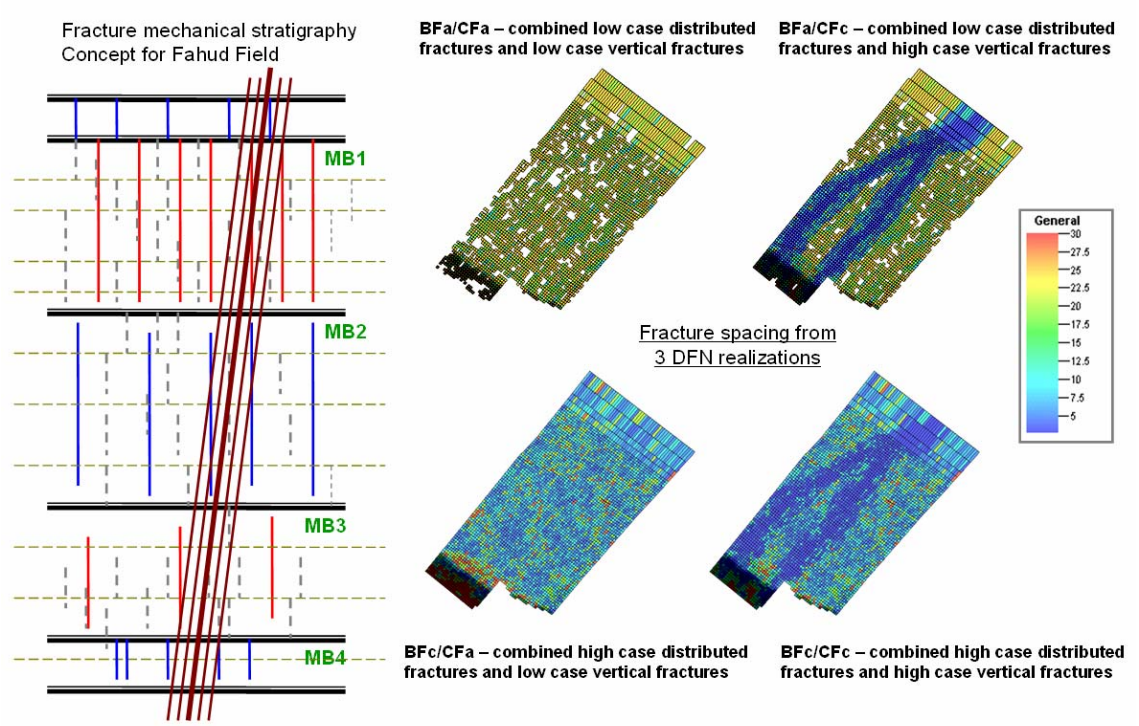


**Figure 3-23 Conceptual model for the fracture network in Fahud (left) together with extracted fracture spacing from 3 DFN models for RAM in Fahud field (de Keijzer and al Dhahab, 2004).**

### *Fahud fracture data evaluation*

In this section, a static analysis of the Fahud BHI data, done in SVS, is presented to validate the statements mentioned in the existing work above. Based on a plot of the entire BHI data, faults and fractures in Natih formation (6899 fracture and 73 faults) superimposed on top of multi-direction curvature map of Natih formation (Figure 2.87) and uni-directional curvature map running NW (Figure 3.24) (in both cases, curvature wave length scale is 50m created in SVS), the following is deduced: The majority of fractures are running NE in both full field rose diagram and individual well rose diagrams except for a few wells (F287H1, F331H1 & F316H1) which are either vertical or running NE and contains few picks. The multi directional curvature highlights NW structural grains ("faults") running parallel to the Fahud main fault. In order to see any lineaments running NE a uni-directional curvature was needed. This highlights few features that may coincide with the fracture corridors running NE (compare Figure 3.25 with Figure 3.20). The majority of the fractures are conductive or partly conductive, 5184 in total; with almost all the large features running NE (Figure 3.26 and Figure 3.27). A cumulative BHI frequency versus depth plot shows a step change supporting the concept of mechanical layering for Natih Formation (Figure 3.28). This analysis also hints toward a rise in non-conductive picks "objects" as the FWL is approached.

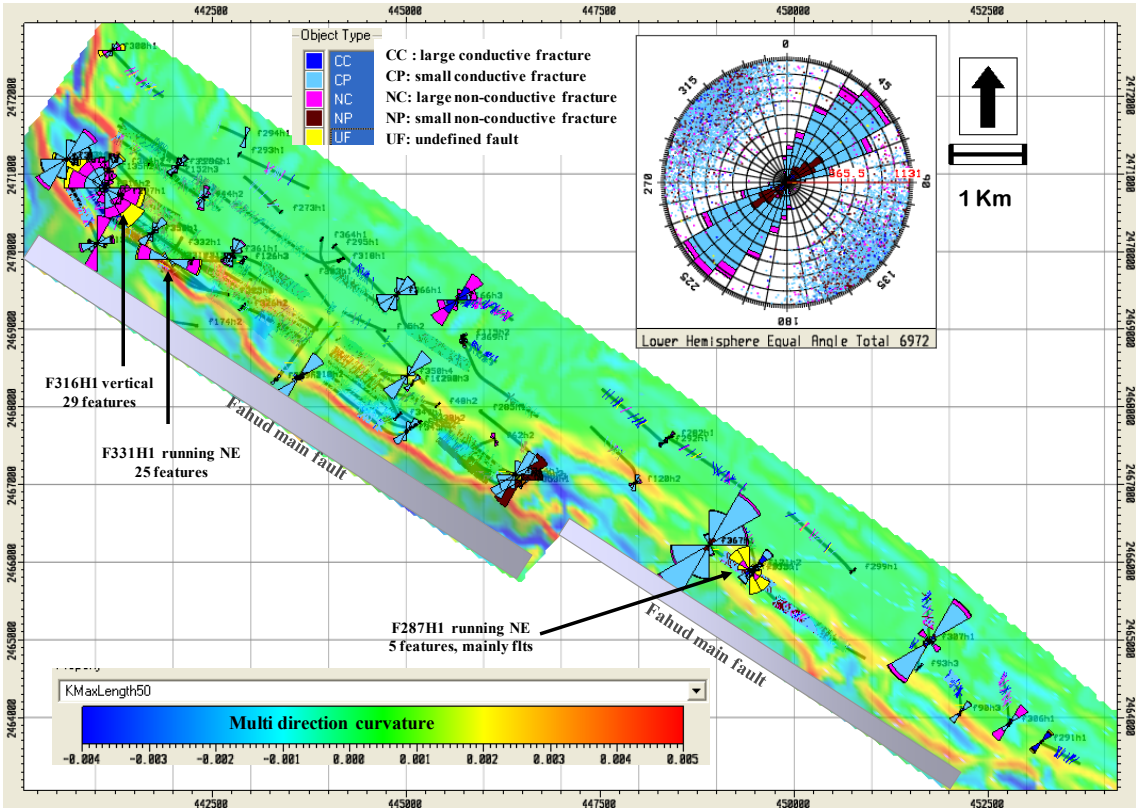


**Figure 3-24 Fahud BHI picks superimposed on top of Natih Formation multi-direction curvature map (K max at small wavelength) with both full field BHI picks rose diagram (top right insert) and individual wells rose diagrams. Most BHI fractures are striking NE, though curvature hint toward features running NW, that could be either sub-seismic faults or bedding effects.**

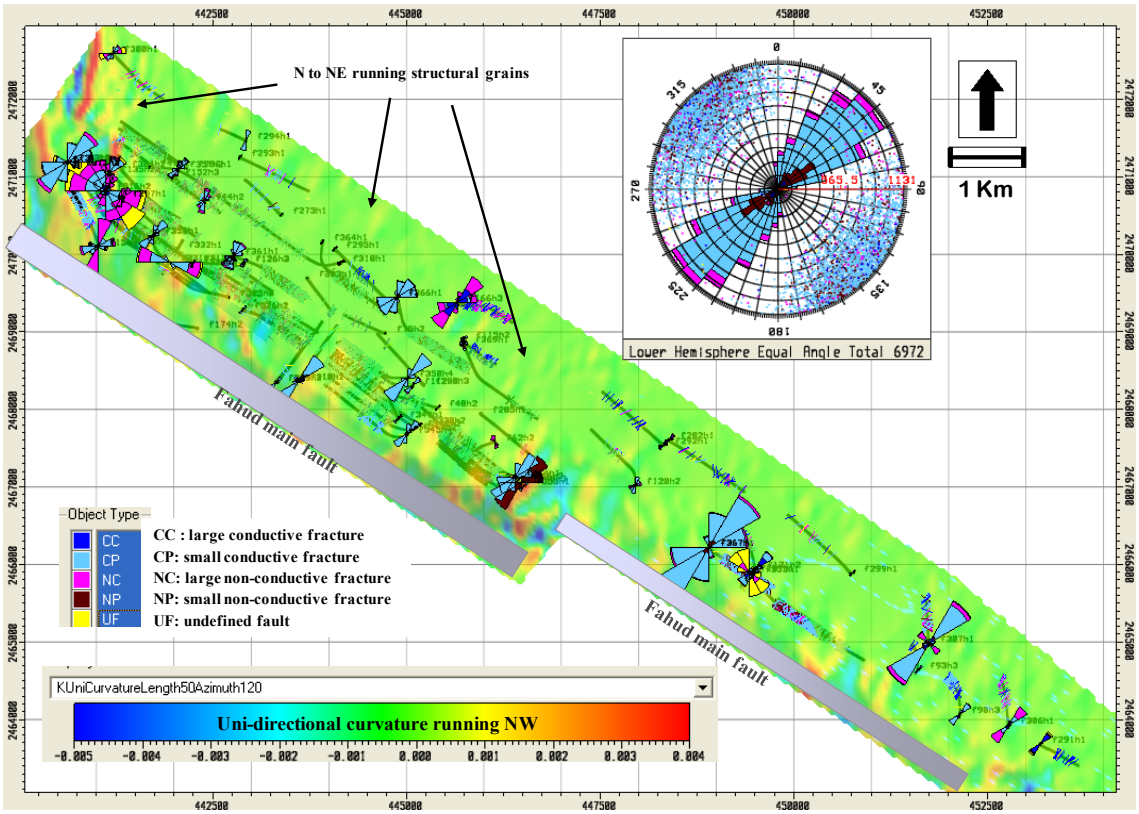


**Figure 3-25 Fahud BHI fracture superimposed on top of Natih Formation uni-direction curvature map (Kmax at small wavelength), with the fracture rose diagram. Indicating possible sub-seismic feature running parallel to BHI fracture with NE strike direction (possibly fracture corridors).**

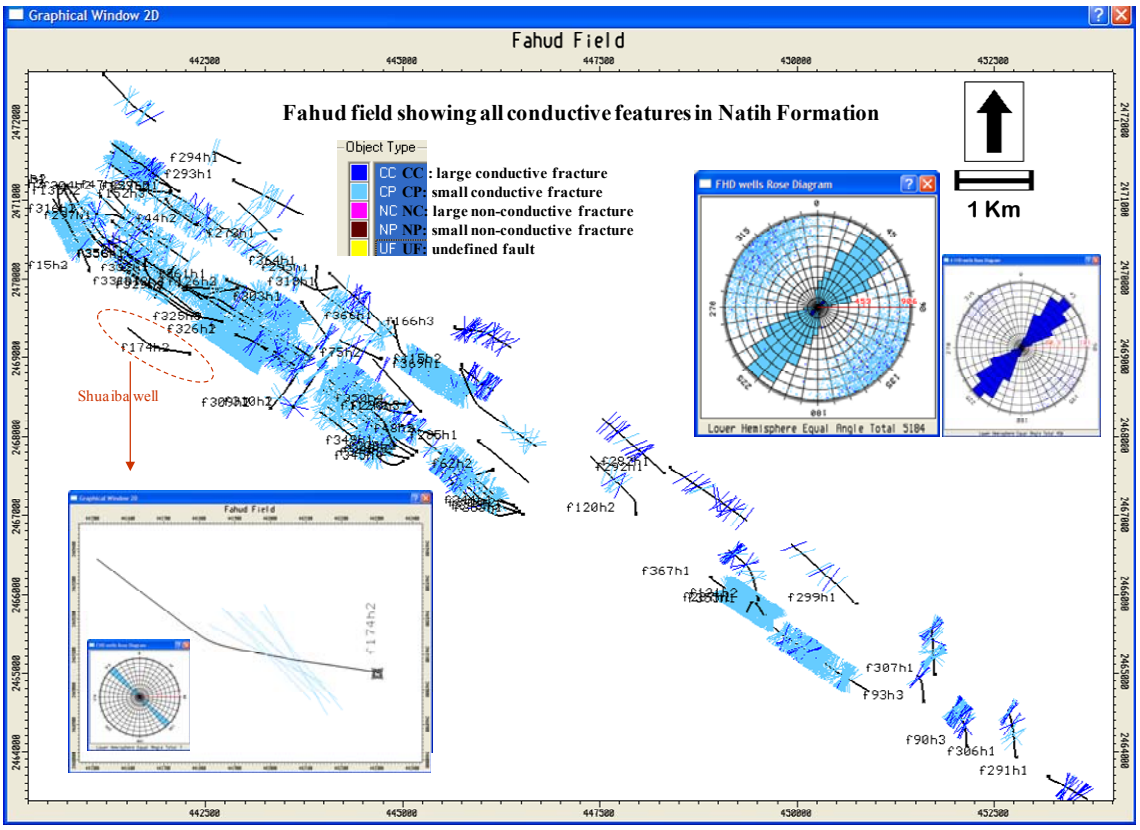


**Figure 3-26 Fahud field, Natih Formation large & small conductive BHI objects ("fractures").**

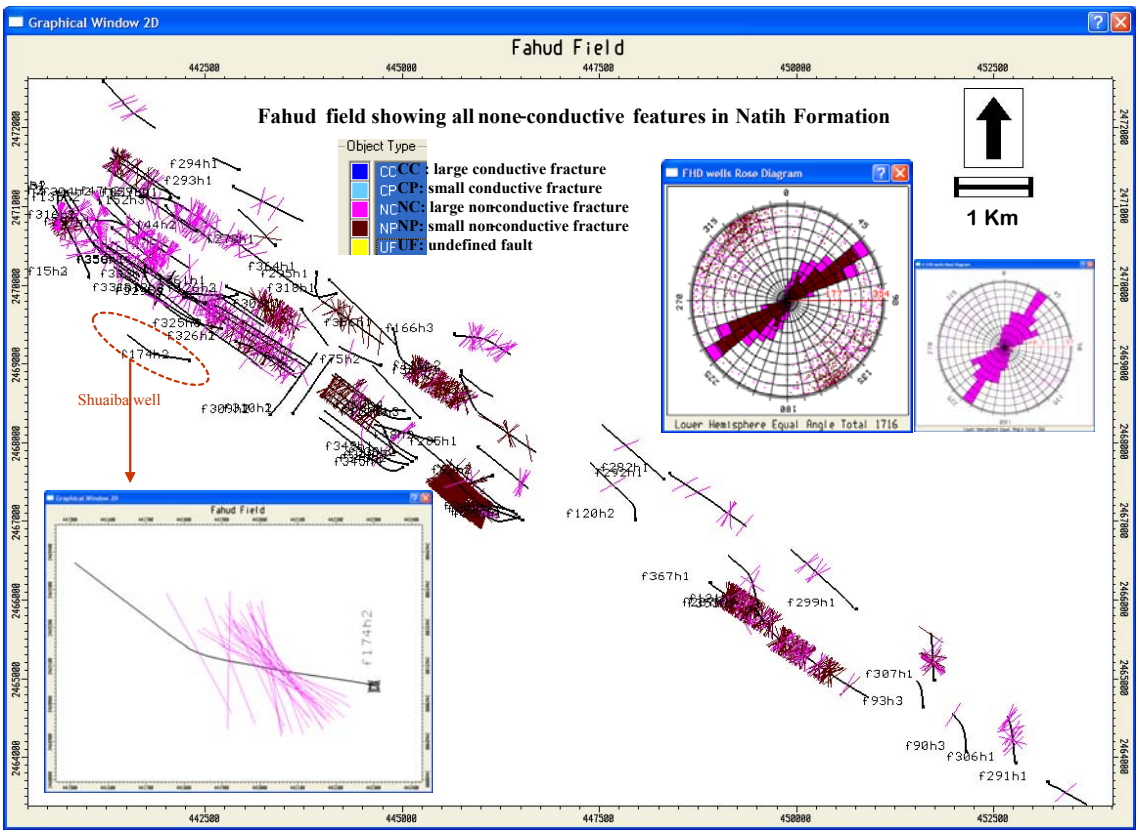


**Figure 3-27 Fahud field, Natih Formation large & small none-conductive BHI objects ("fractures").**

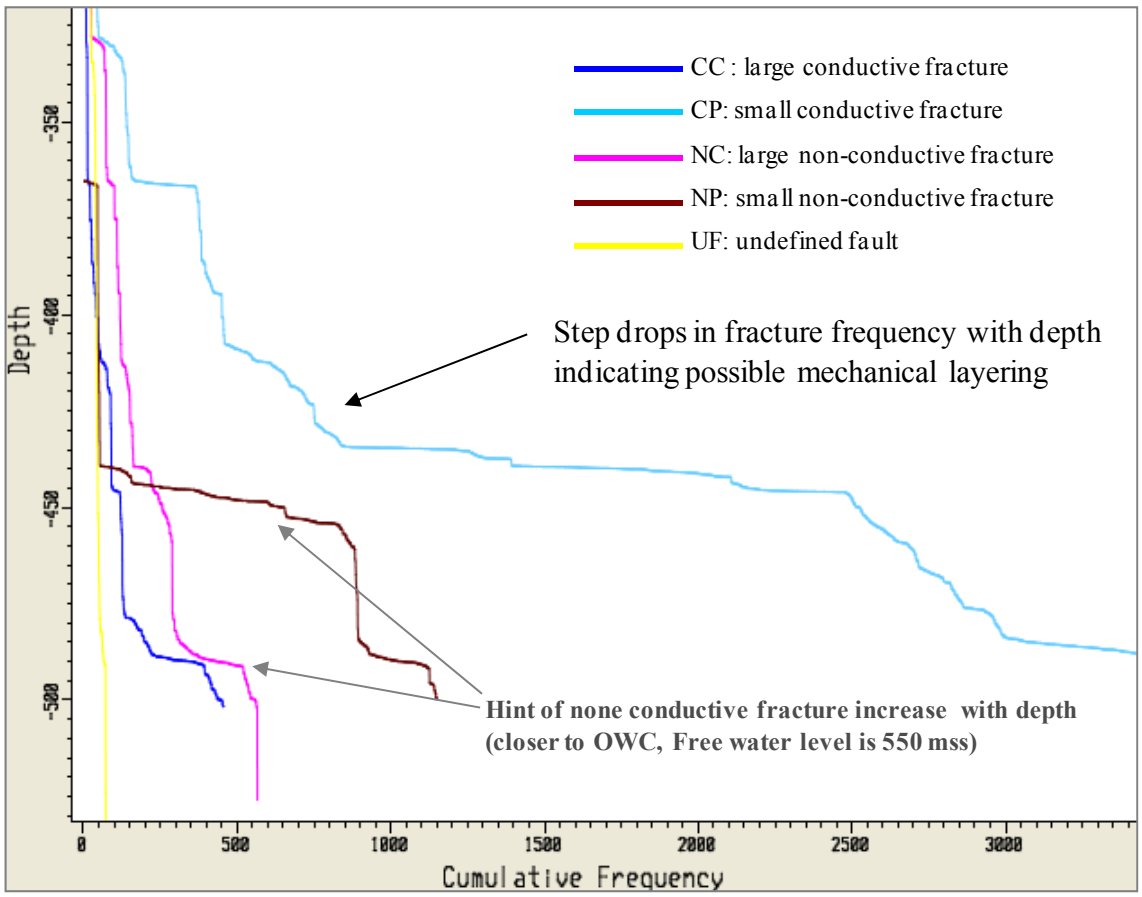


**Figure 3-28 Fahud field, Natih Formation BHI objects cumulative frequency plot, indicating potential mechanical layering.**

### *3.1.3 Al Ghubar field -Natih Formation*

The Natih E of Al Ghubar field (Figure 3.29) is still producing via pure depletion due to the complexity of this reservoir: stratified with moderate reservoir thickness, hence GOGD is not a very viable development scenario, yet the field is moderately fractured and to produce the matrix reservoir, water shut-off techniques are required.

***Existing work***

The Shell EPT carbonate team has undertaken a major asset study of Al Ghubar Natih E in 1998. Since then no further work was done for this field until the recently on-going PDO-Shell EPT study for the whole Al Ghubar field, addressing both Shuaiba and Natih formations.

Konijnenburg (Konijnenburg et al , 1999):

When this study was done all the wells were verticals. Based on core observations and characteristic log responses, the Natih E was subdivided into five depositional cycles. Diagenesis was found to play an important role in the Natih E of Al Ghubar field. Throughout the oil-saturated part of the Natih E, cemented streaks are encountered with varying degrees of fracturing on a cm to a dm-scale. These cemented streaks are thin (20-70cm) and probably areally extensive although they can rarely be correlated between wells. Two main types of fractures have been identified based on the

interpreted relationship to bedding in cores. First of all, steeply dipping background fractures occur throughout the section. Secondly, bed-bounded vertical fractures, observed on BHI, occur within thin, cemented tight streaks (Figure 3.30). Overall, the number of fractures intersected by the vertical wells in the Natih-E is small. The fractures do not clearly cluster near faults, nor have a distinct relationship with different units except for the bed bounded fractures related to thin tight streaks, where they enhance permeability of the matrix. Due to the strong mechanical layering of the sequence, the majority of the background fractures are expected to have a vertically segmented nature (as observed with the seismically imaged faults). Thus these fractures are expected to have a limited vertical continuity, and not run from the top of the reservoir into the water leg (Figure 3.31). Background fracture spacing in Natih E is estimated to be in the range 5 to 10 m, (i.e. similar to what is observed on one horizontal well in the Shuaiba). In contrast, the fracture spacing of the bed-bounded fractures is estimated to vary between 20cm to 50cm (Figure 3.32).

Price (Price et al, ongoing):

The study team had passed VAR2 (Value Assurance Review – subsurface part) in Q3 of 2006. So far only the petrophysical report has been issued. The study benefited from the drilling of three appraisal wells:

- AG6H5: Highly deviated leg (1000 m) in Shuaiba, running SSW,
- AG21H1: Vertical hole in Natih D,
- AG21H2: Slightly deviated hole in Natih E,
- AG21H2: Slightly deviated hole in Shuaiba,
- AG22H1: Highly deviated leg (700 m) in Natih E, running NW, and
- AG22H2: Highly deviated leg (900 m) in Natih E, running SW.

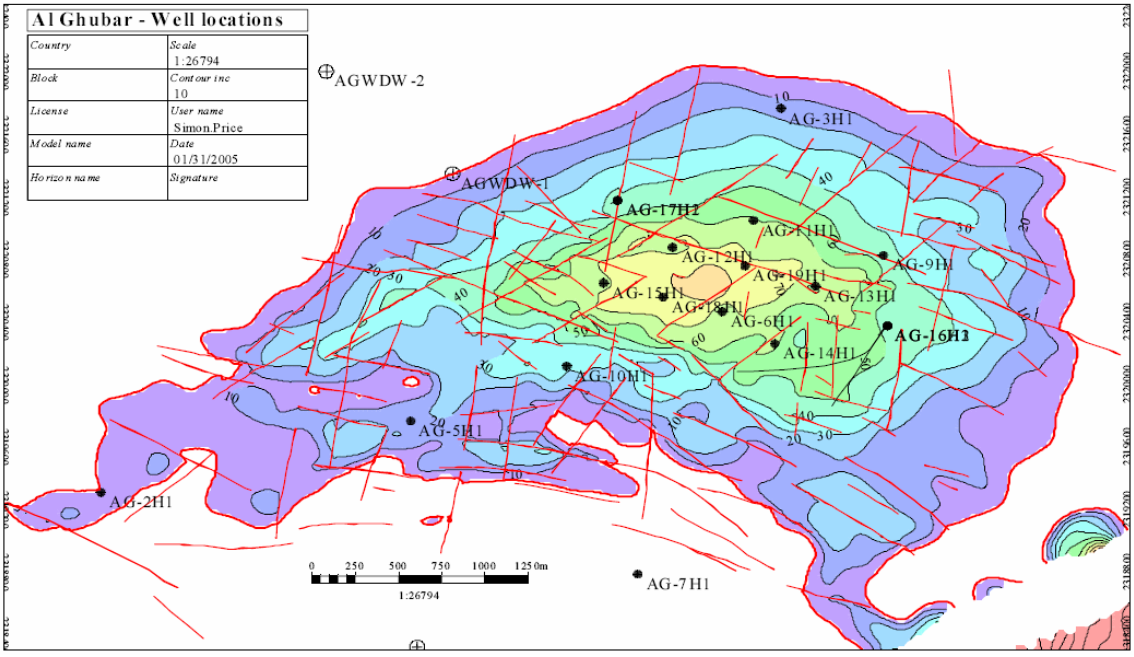


**Figure 3-29 Natih E oil thickness map (from Price - Shell-PDO internal report, 2006) with the latest fault interpretation (red lines).**

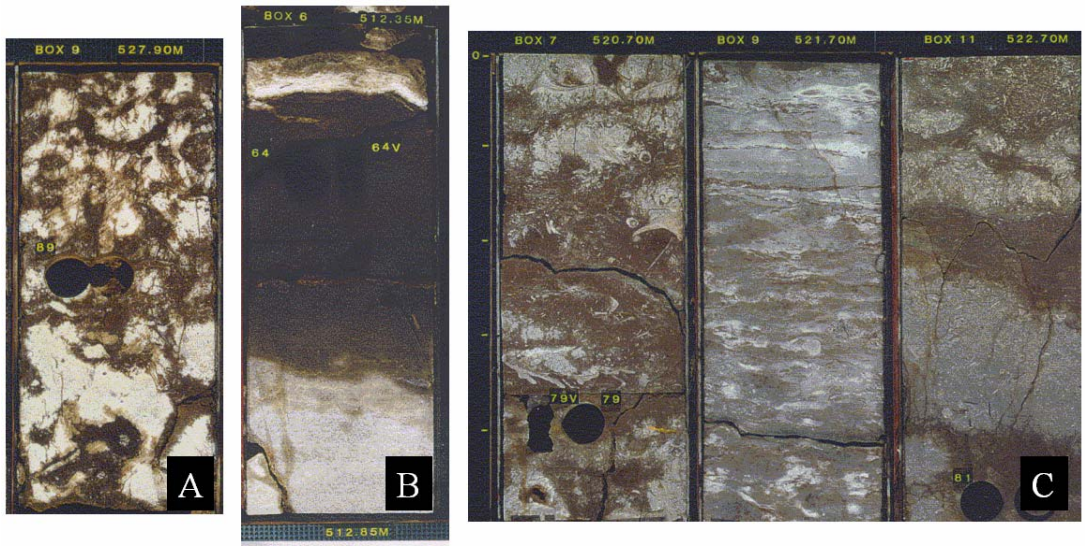


**Figure 3-30 AG-15 core photos, Natih Formation. A) Example of patchy cemented streaks; B) Pervasively cemented streak in a grainstone interval. The large fracture in the lower left part of the streak is mineralized along the fracture plane. C) Part of the correlatable layered cemented bed, note the occurrence of patchy and pervasively cemented parts as well as oil stained fractures (Konijnenburg et al, 1999).**

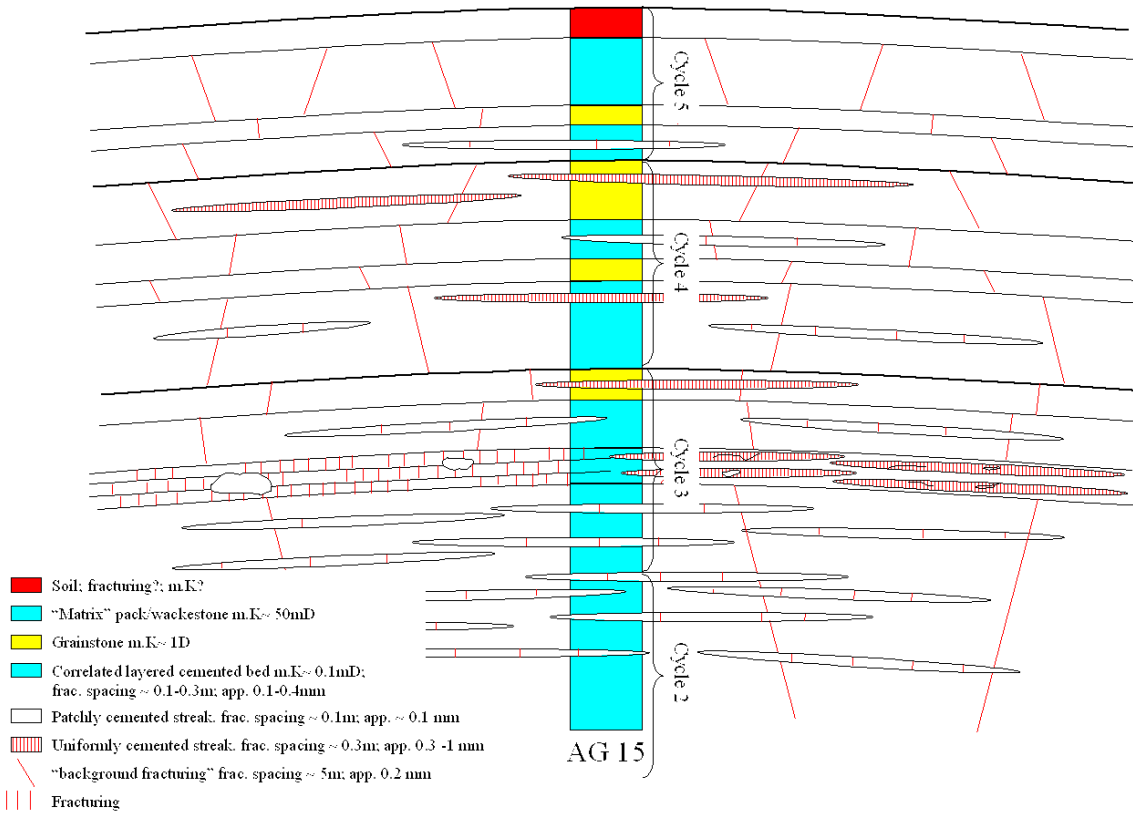


**Figure 3-31 Conceptual fracture model for AG15, based on core & logs (Konijnenburg et al, 1999).**

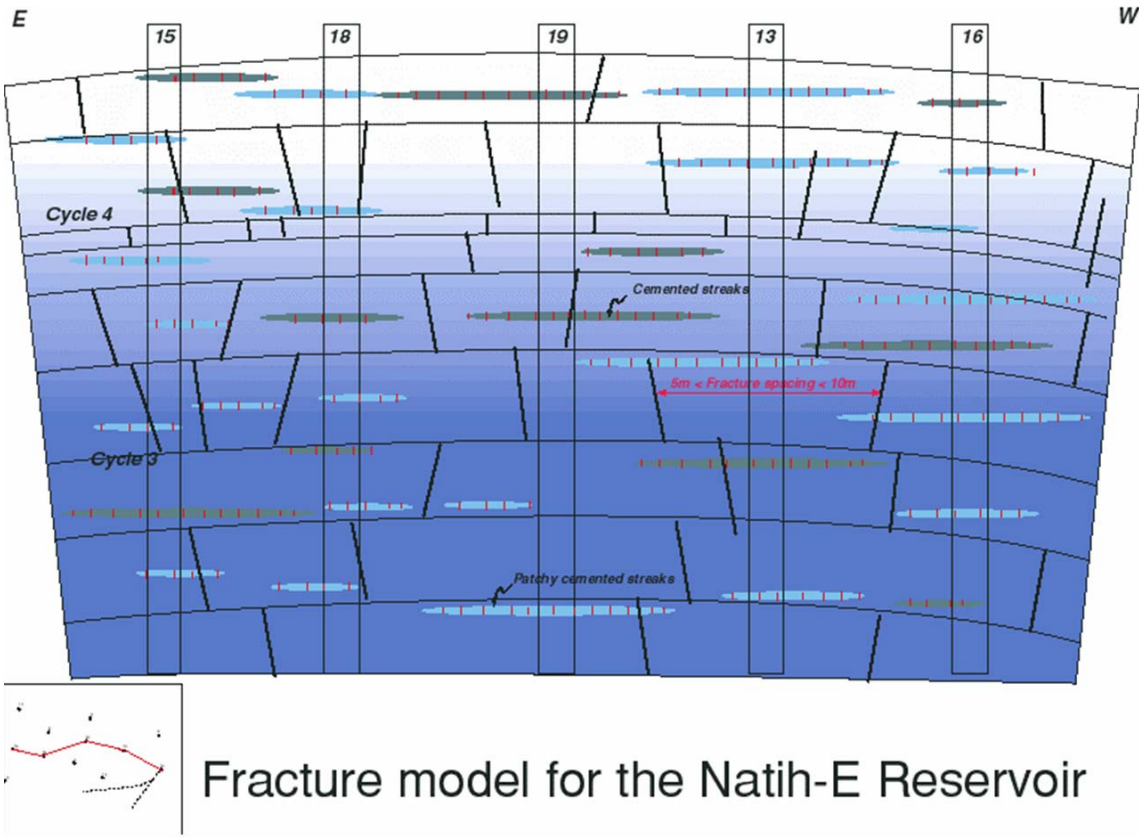


**Figure 3-32 Conceptual fracture model for Al Ghubar field Natih Formation, number correspond to wells (Konijnenburg et al, 1999).**

### *Al Ghubar Natih fracture data evaluation*

In this section, a static analysis of the Al Ghubar Natih E BHI data, done in SVS, is presented to validate the statements mentioned above by the existing work. Note that for the vertical wells, old BHI data were not used in this analysis (as the data could not be found), with BHI information available only for the new appraisal wells. However, in the Konijnenburg (1999) report a figure was found showing a rose diagram for the fractures interpreted from the vertical well BHI information (Figure 2.33).

The main observations, from the BHI of those vertical wells, are as follow: there is no preferred orientation; the fractures were reported by Konijnenburg to be parallel to faults. Non-conductive fracture seems to dominate.

A plot of all the BHI faults and fractures picks in Natih formation shows: 510 fractures, with 13 BHI faults and 24 induced fractures CI (Figure 3.34). The majority of the fractures are small non-conductive (283), or small conductive (231) running mainly NNW to N (Figure 3.35). AG22H2 shows induced fractures, light green in Figure 3.36, which are running NNW together with BHI faults. The BHI objects cumulative frequency versus depth plot, together with cross section view of the two appraisals Natih well, at X4 vertical exaggeration, does not readily show a potential mechanical stratigraphy in the Natih Formation of Al Ghubar field (Figure 3.37).

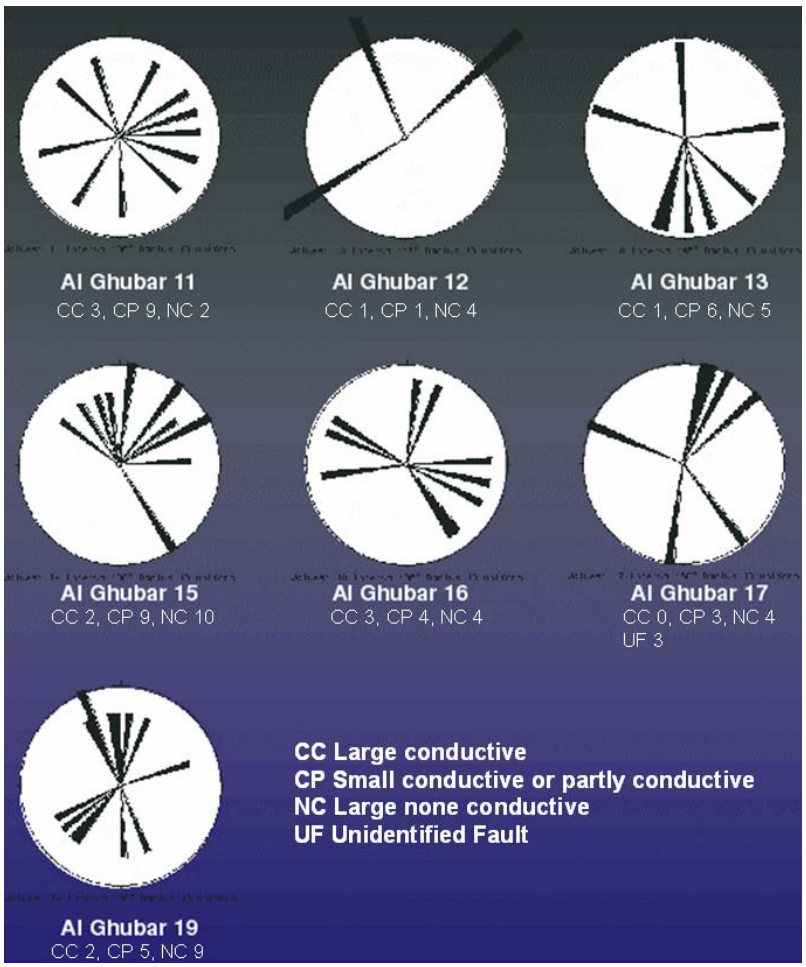


**Figure 3-33 Al Ghubar Natih E BHI fractures orientations (Konijnenburg et al, 1999). Figure was modified to include fracture counts per type.**

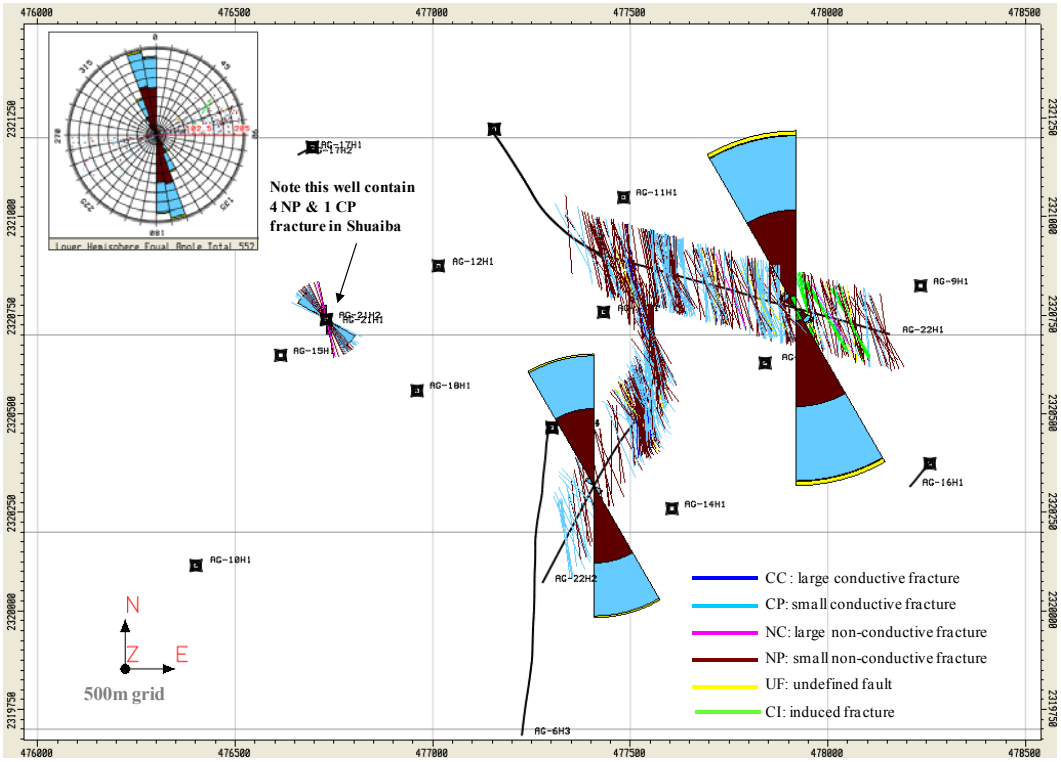


**Figure 3-34 Al Ghubar Natih E appraisal wells BHI fracture evaluation (light blue are small conductive picks, while light brown to dark pink are small non-conductive fracture picks).**

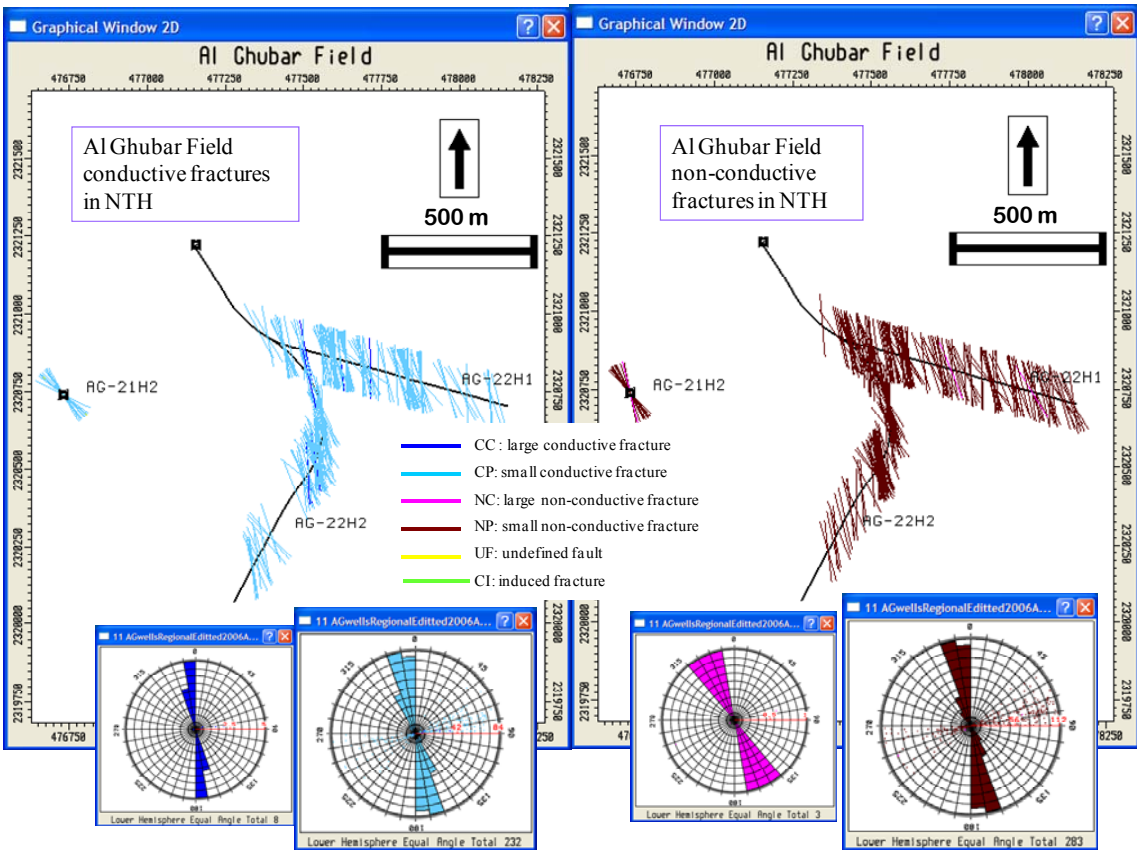


**Figure 3-35 Map view of al Ghubar Natih BHI fractures with rose diagram showing strike orientation per type.**

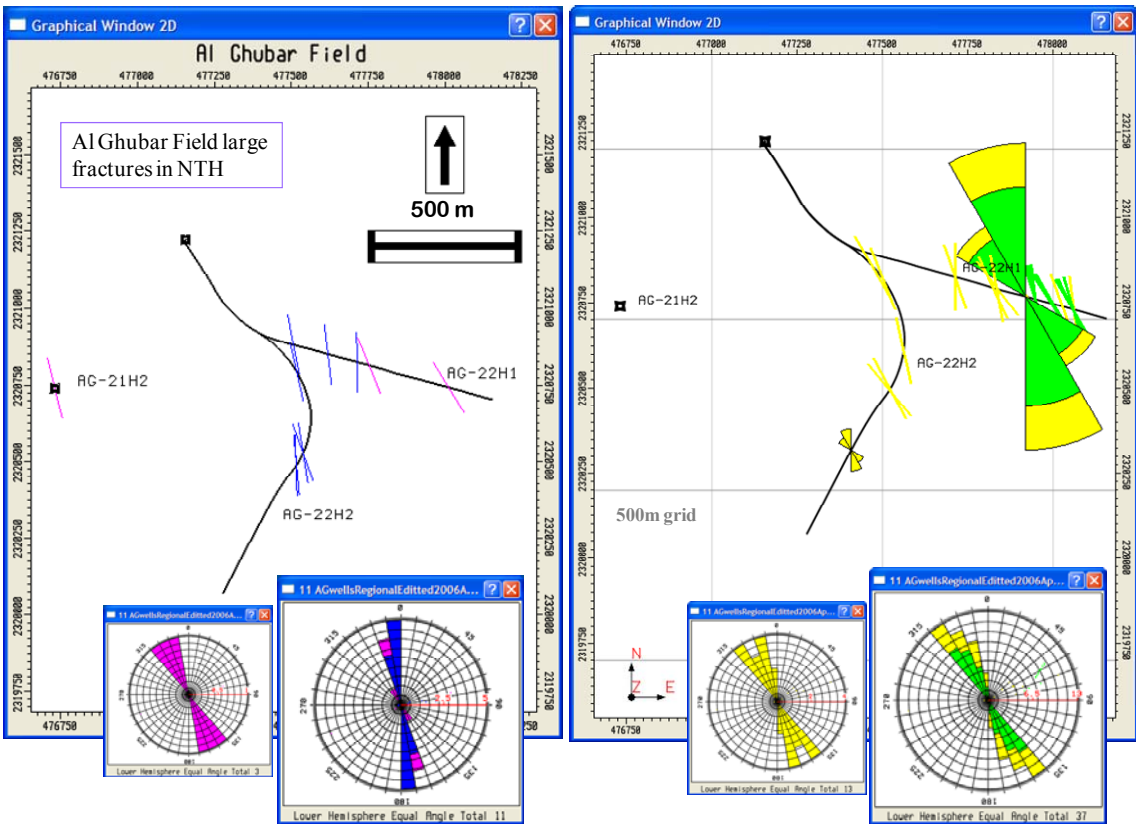


**Figure 3-36 Al Ghubar Natih BHI large fractures (left); BHI faults and induced fractures (right).**

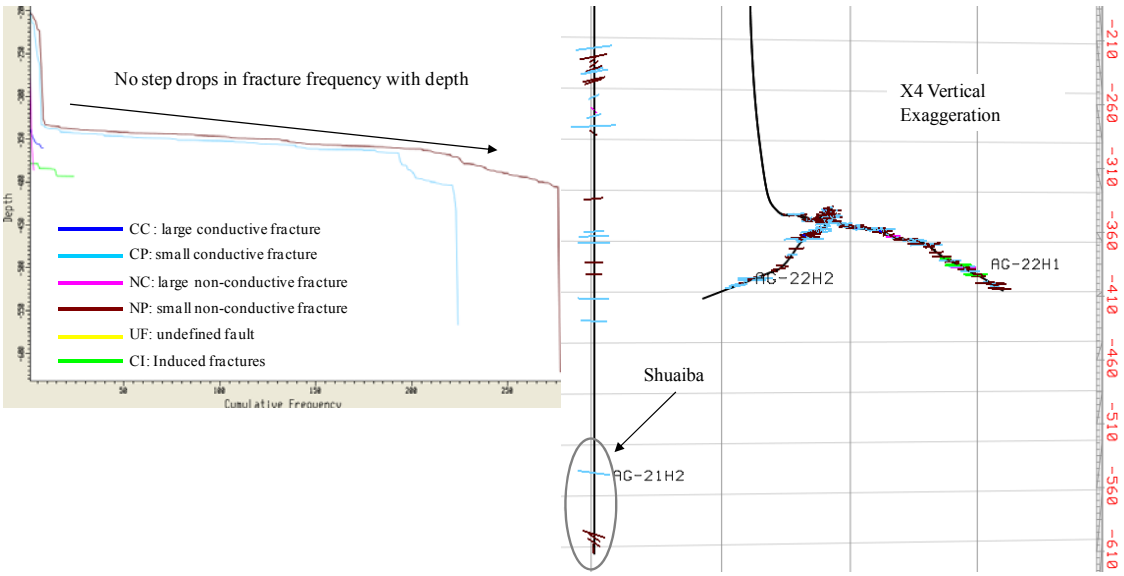


**Figure 3-37 Al Ghubar Natih Formation BHI fractures cumulative frequency versus depth plot (left); a cross section showing fractures with depth, FWL is at 410mss in Natih E (right).**

## 3.2 Shuaiba Formation

### *3.2.1 Jebel Madar Shuaiba outcrop*

This outcrop in the foreland of the Oman Mountains (Salakh Arch area) is located about 60km west of Jebel Madmar and represents the most northerly series of the diapiric structures within the Ghaba salt basin (see Figure 2.1). The Jebel fracture network was studied by Heesbeeen (2002).

The main findings of Heesbeen (2002) outcrop study are summarized below:

Madmar is a Permian through Cretaceous salt cored dome structure, with an elevation of ~ 500m above the surrounding terrain (Figure 3.38). A carbonate unit about 70m thick, mainly of Lower Aptian age, Shuaiba Formation, is exposed. Fractures form (sub) vertical sets to the bedding or conjugate systems. JM1 (Jebel Madmar Station 1), see Figure 3.38 for location, in the east of the field area, shows heterogeneous spreading of fracture poles for restored bedding with three different sets, in total 56 fractures: JM1a striking NW, JM1b striking N and JM1c striking NE parallel to fold axis (Figure 3.39). JM2, in the NE of the field area, shows a trend of EW to ENE-WSW fracture set, total fracture count 45. JM3 in the SW of the field show two pronounced fracture sets, 37 fracture count, striking NW and NE, the later parallel to fold axis. Normal faults in the east, JM1 & JM2 area, have similar orientation and make steep angles to the bedding, with several meter wide fault zones. Hawar member shows large differences in spacing, compared to Shuaiba. The study attempted to analyse the fracture network using a fractal approach but failed due to data limitation, but most likely also due to scale variance attributed to both facies change and location change.

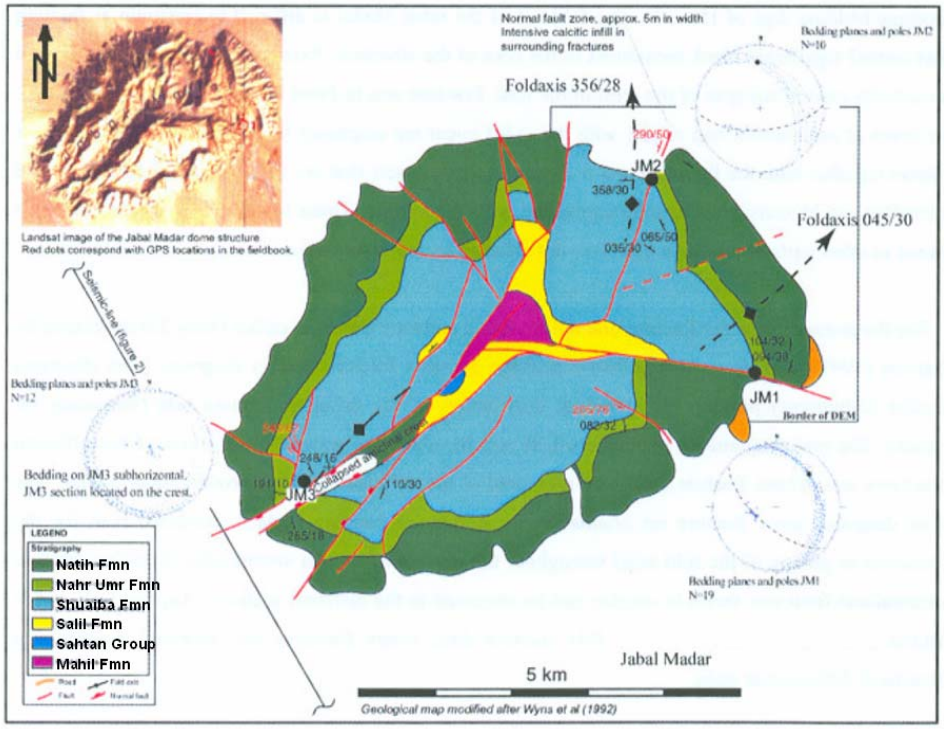


**Figure 3-38 Geological map of Jebel Madar showing study location (Heesbeen, 2002).**

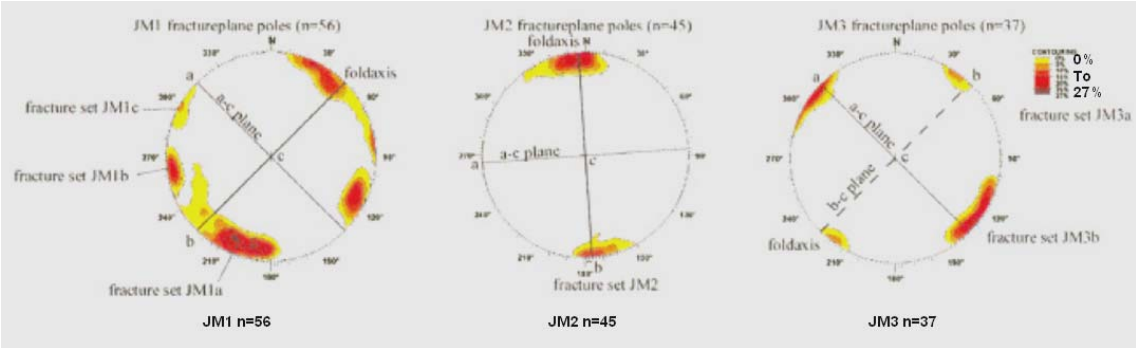


**Figure 3-39 Contour plots of fracture poles, showing varying strike orientation from one location to another, the exact location of each JM is shown in the above figure (Heesbeen, 2002).**

### *3.2.2 Huqf Shuaiba outcrop*

The fault and fracture network of the Shuaiba Formation equivalent "Qishn" Formation in the Huqf area (see Figure 2.1 for location) was examined, the summary of the main outcrop works is presented below:

Montenat (Montenat et al, 2003):

This group found out that the Qishn carbonate was subjected to pre-lithification normal faulting. A thick ferruginous crust (hard ground) covered the top surface before the unit was buried under the Albian Nahr Umr marls. The faults are mostly NW trending, SW facing, normal faults. These faults are of various sizes: from 1-100s of meter long, from one decimetre to ten of meters of vertical throw. The fault damage zones vary from none to several meter in width, showing mechanical stratigraphy based on the facies.

Immenhaauser (Immenhaauser et al, 2004):

The rocks of the Qishn Formation are affected by widespread faulting and fracturing and to a much lesser degree by folding. The most common strain-related features are widespread "regional" systematic joints, which form homogeneous sets with regard to their morphology, distribution in space and their orientation (Figure 3.40). Fractures normally develop in fully lithified layers, possibly post-Cretaceous meteoric diagenesis, forming the top of Table Mountains built by Qishn Formation or being linked to intensively dolomitized intervals at top Jurf (top Lekhwair) or base Qishn Formation. The joints are usually straight and long, 1m to few 10s of meters, showing a systematic NW-SE to WNW-ESE orientation, with a second joint family running perpendicular to the first set, the later one is irregular noted only in few locations compare to the NW set. NW set spacing shows a systematic distribution averaging 6-18m (Figure 3.41). Vertical sections show that systematic fractures or joints are present in specific beds, with an abrupt termination at layer boundaries. However, their orientation and spacing is quite constant throughout. NW set is found in four interval within Qishn Formation, from bottom to top: A 50cm thick bundle of bioclastic limestone at top of sequence I; a 1m thick of thinly bedded tidal flat deposited of top of sequence III; and a 1.5-2 m thick, cross bedded rudstones at very top of sequence IV. No significant modification of joints density was noted approaching fault zones (normally 10-20 m thick).

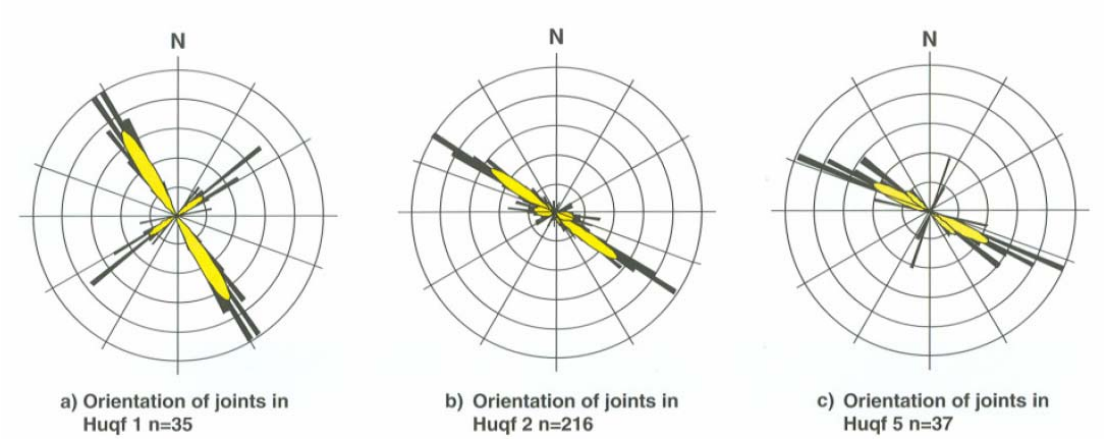


**Figure 3-40 Orientation of joints in three structural station of Wadi Baw in southern part of Huqf - see Figure 2.39 for location, close to Wadi Sha'bat al twarq, ~ 5km west of Duqm – showing similar strike orientation toward the NW (Immenhauser et al , 2004).**

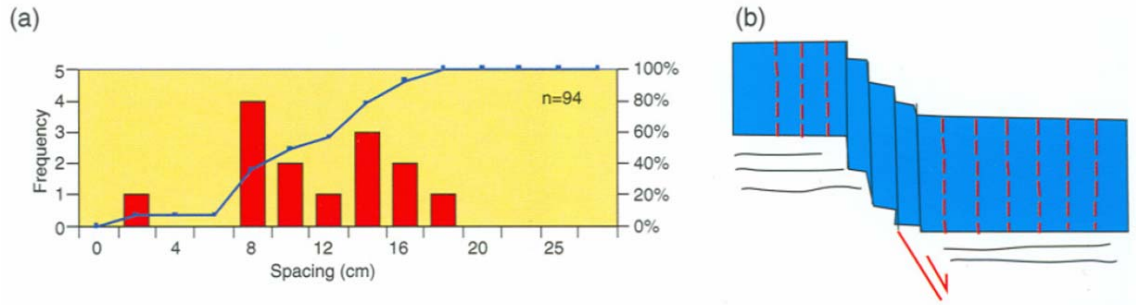


**Figure 3-41 a) Distance between systematic joints in a structural station in Wadi Baw. Distance is measured perpendicular to the trend of the dominant set, on bedding plate. b) Cartoon illustrating the widening of fault zones where they cross pre-jointed layers (Immenhauser et al, 2004).**

### *3.2.3 Al Ghubar field - Shuaiba Formation*

The Shuaiba of Al Ghubar Field is still produced via pure depletion due to the complexity of this reservoir: stratified with moderate reservoir thickness, hence GOGD is not a very viable development scenario, yet the field is moderately fractured and to produce the matrix reservoir, water shut-off techniques are a must for a successful matrix development (Figure 3.42).

***Existing work***

Al Dhahab (1998):

This study was an end of well review report for AG-16 ST2, in which the first ever chemical shut-off technique was undertaken in Oman. The report examined the whole reservoir with the following main findings, with respect to the fractures in AG16 ST2: AG16 horizontal side track 2 provides lots of fracture data, as it represents the first horizontal well (over 800m) with a BHI log in the reservoir. However, the vertical reservoir coverage was low because the well was drilled in the upper part of the reservoir to be as far away as possible from OWC (Figure 3.43). Large and small conductive fractures dominated the hole with only 4 possible non-conductive fractures seen in the BHI. Few BHI faults were picked at 922, 1110, 1209, 1340(?), 1509(?), 1518, 1530 and 1558 MD with the intensity of fracture increasing toward the tail of the open hole and close to these faults. The fractures occur in clusters as seen from the normal frequency plot -showing higher fracture frequency of < 5m spacing (Figure 3.44). Fracture cluster locations do not coincide with seismic fault locations, though this lack of correlation could result from uncertainty related to the fault location picks in seismic (Figure 3.45). The dominant strike direction is NNW to N. The chemical shut off test provided hints about the strength of the non-conductive fractures, as the pressure profile indicates opening of closed fractures due to pressure applied (Figure 3.46).

Price (Price et al, ongoing):

This work is still ongoing. The study team had passed VAR2 (Value Assurance Review – subsurface part) in Q3 of 2006. So far only the petrophysical report had been issued. For the Shuaiba reservoir the study benefitted from the drilling of AG-6H5 side track and AG21 H2 slightly deviated hole in Shuaiba.

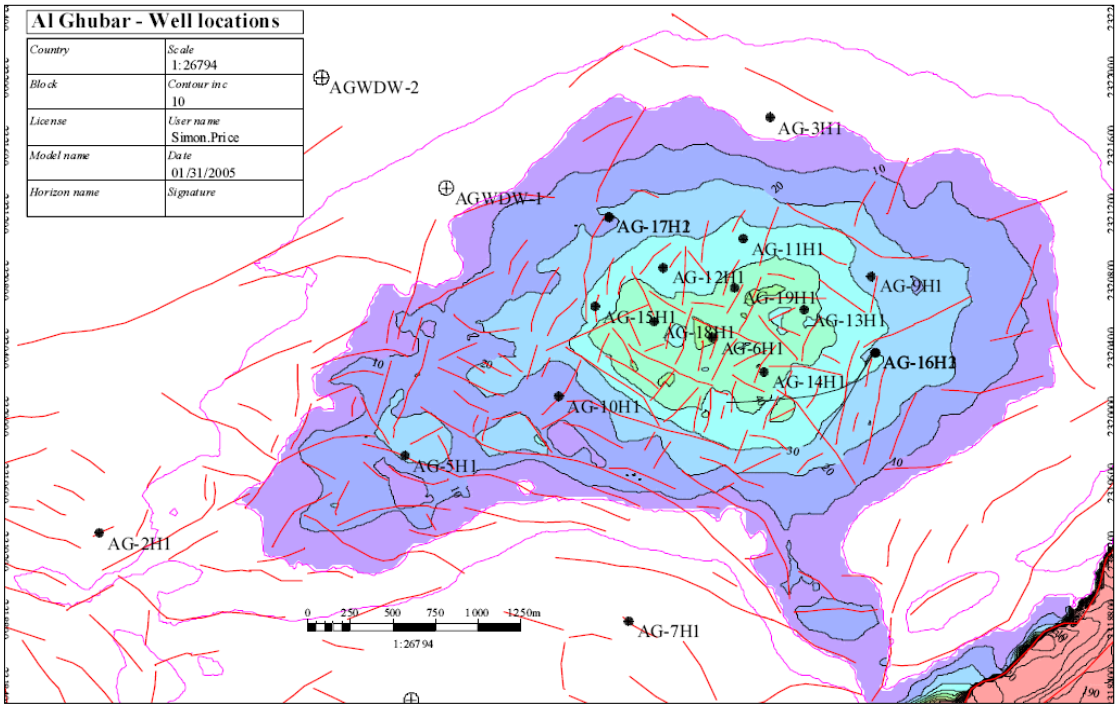


**3-42 Al Ghubar Shuaiba thickness map, with only one horizontal well AG16 drilled before 2006 (Price - Shell-PDO internal report, 2006).**

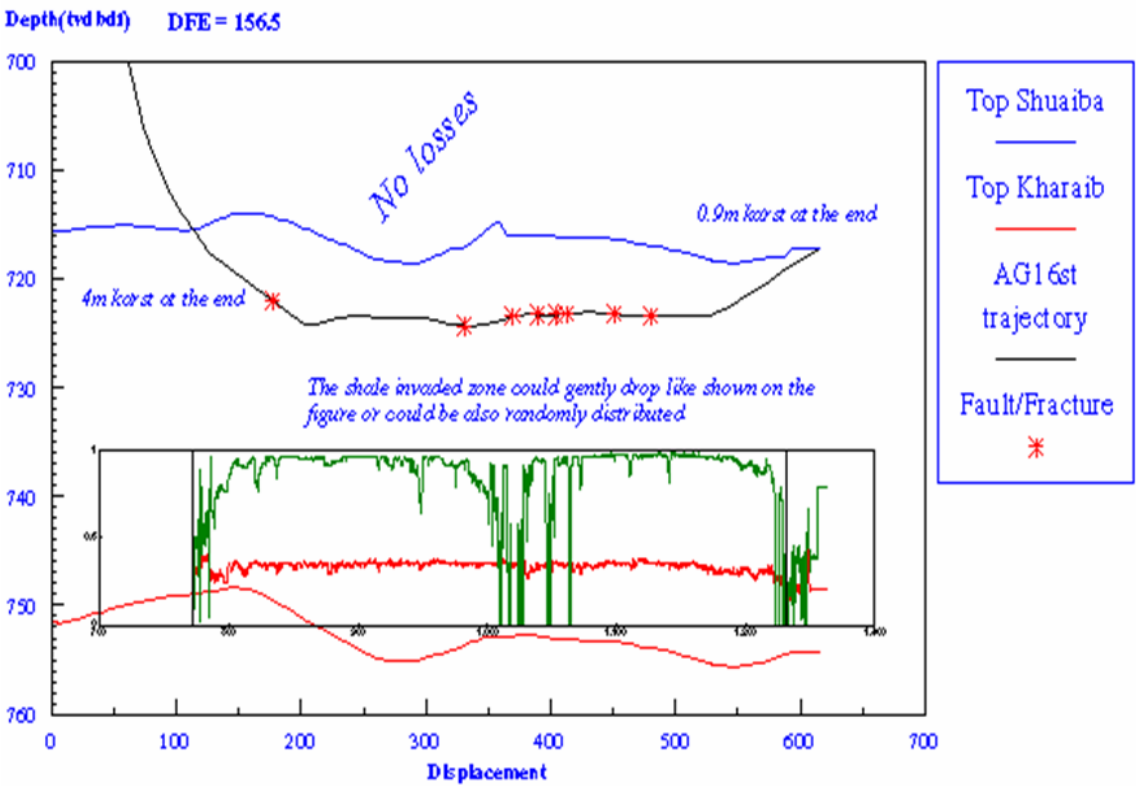


**3-43 Cross section showing AG16 ST2 well bore with location of major fractures/faults. Note the well is very shallow –OWC at 762 mTVDbdf (al Dhahab, 1998).**

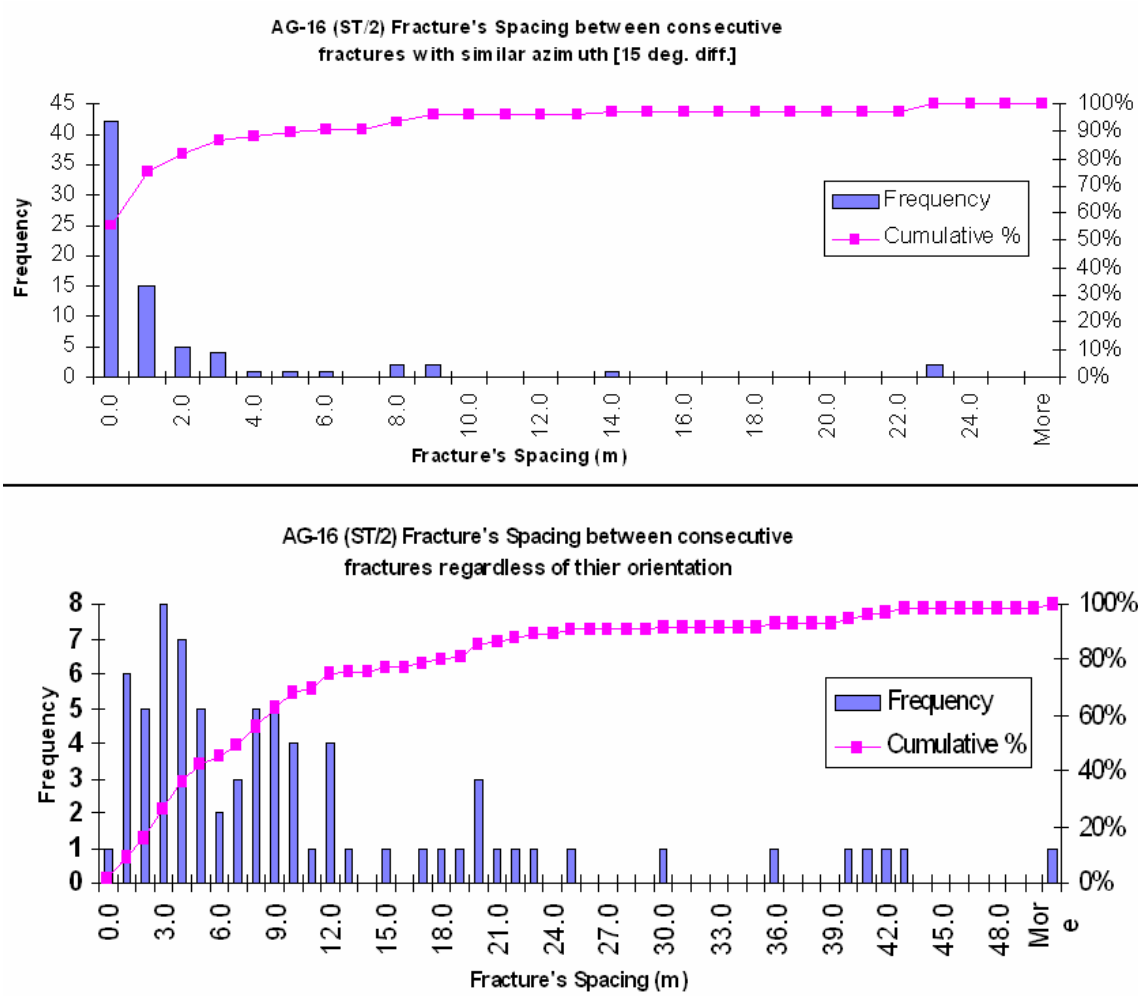


**3-44 AG16 ST2 BHI fracture occur as clusters as shown from spacing histogram (al Dhahab, 1998).**

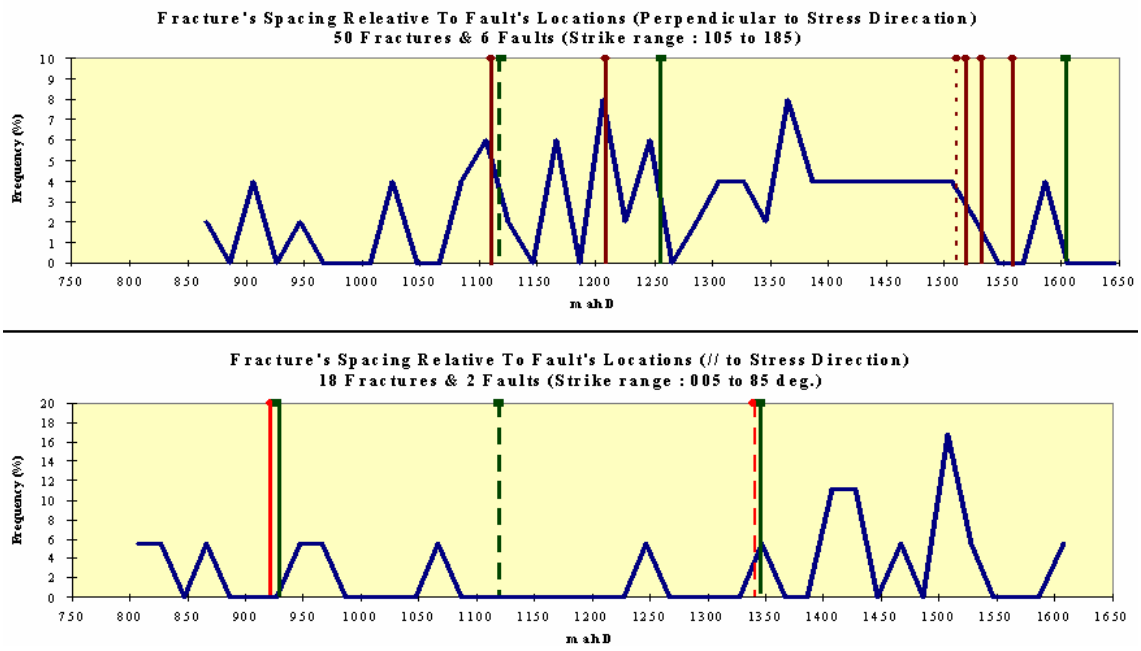


**3-45 Fracture cluster (frequency) plotted against measured depth, after being split into two groups // and perpendicular to stress direction (perceived to be running NE). Also plotted seismic fault locations (again after splitting them into two groups) in green lines (dotted line indicate possible fault) and BHI fault location red lines (al Dhahab, 1998).**

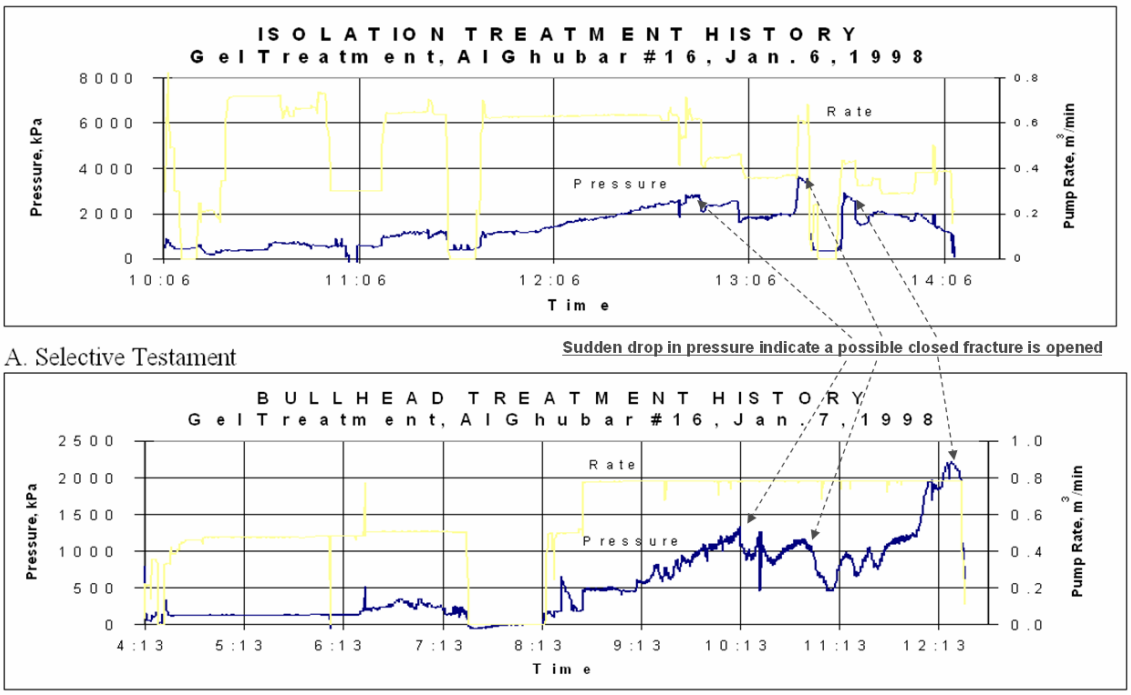


A. Selective Testament

B. Bull heading Treatment

**3-46 Plot of pressure (blue) and rate (yellow) of AG16 ST2 fracture chemical shut-off treatment. The sudden drops in pressure profile are perceived to represent fracture opening strength. The two graphs represent both a selective treatment (a zone in the leg closed in by packers) and a simple bull heading in the open hole (al Dhahab, 1998).**

### *Al Ghubar Shuaiba fracture data evaluation*

A geometric analysis of the BHI fracture of Shuaiba Formation of Al Ghubar is presented below. The majority of the fractures are conductive running NNW in AG6 side track, but NE and NW in AG16 ST2 (Figure 3.47). AG6 is orientated N-S, which is an unfavourable orientation to see these trends, suggesting that the observed pattern is significant. Large non-conductive fractures are only seen in the tail of AG6 ST (Figure 3.48). Faults are predominantly running NW (Figure 3.49). The fracture frequency plot versus depth indicates step changes in fracture counts, which may indicate mechanical layering. However, this could also be related to the presence of faults, which are even picked by the BHI (yellow features in Figure 3.50). The induced fractures in AG6 ST are running NNW, indicating a stress direction running NNW to NW compare to the perceived regional NE direction. This observation could be due to a local change in stress related to a local fault presence, for instance, or it could suggest that the notion of a regional stress is not as useful as might have been assumed.

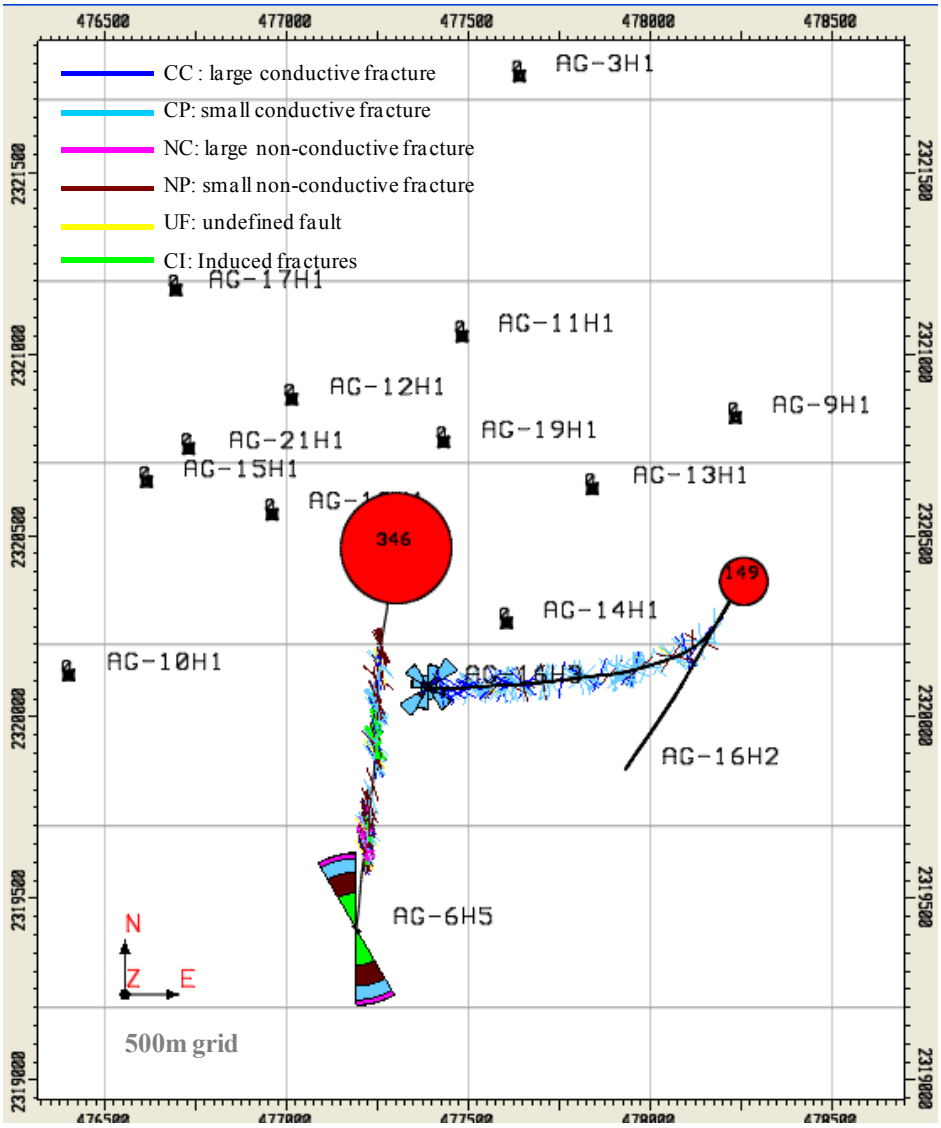


**Figure 3-47 Al Ghubar Field Shuaiba Fmn BHI map view, with BHI counts in red.**

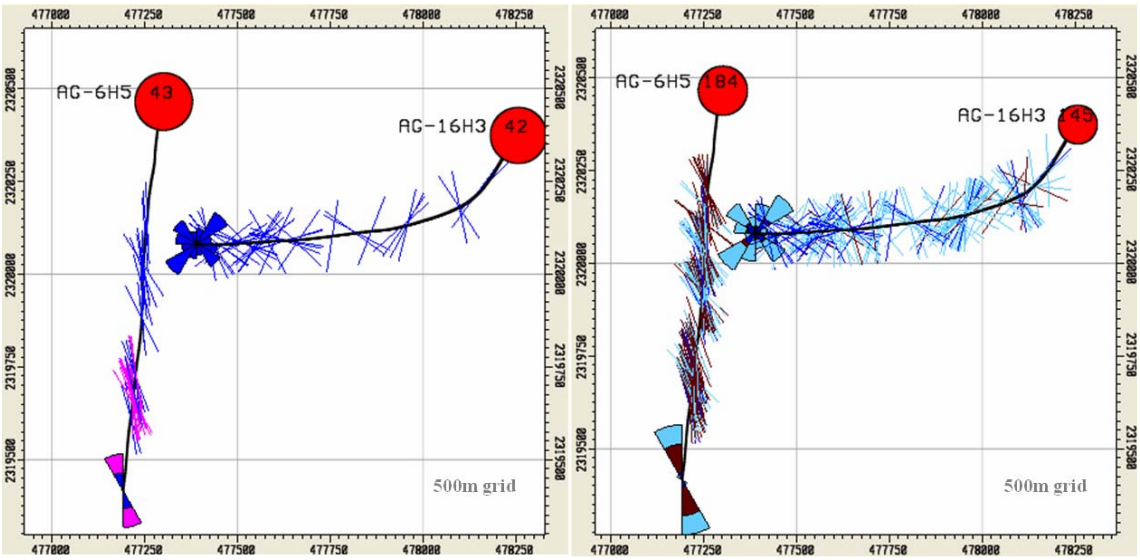


**Figure 3-48 Al Ghubar Field Shuaiba BHI fracture distribution, large (left) and small (right).**

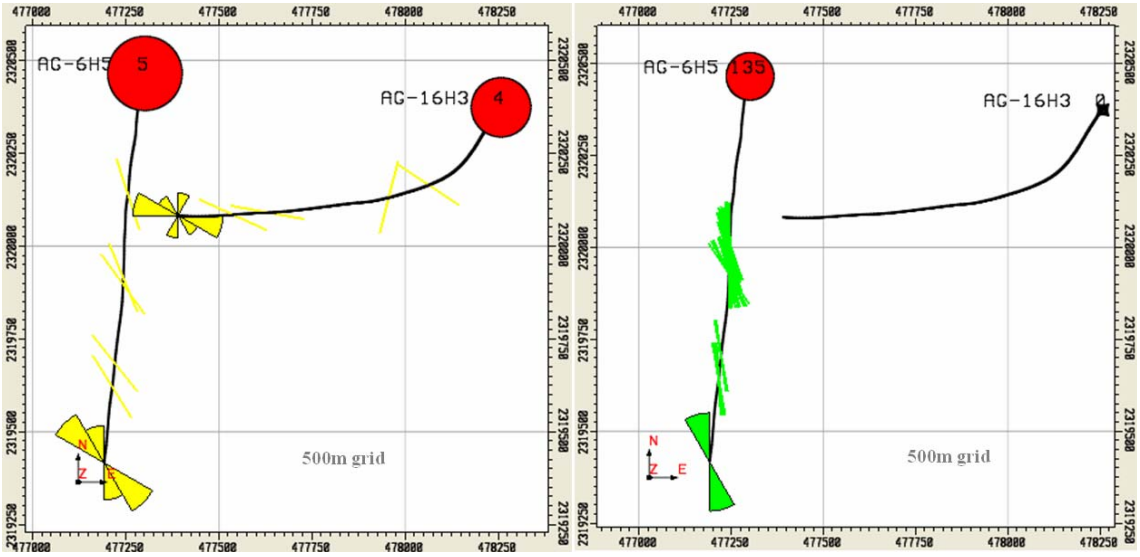


**Figure 3-49 Al Ghubar Shuaiba BHI features (yellow faults, green induced fracture) distribution.**

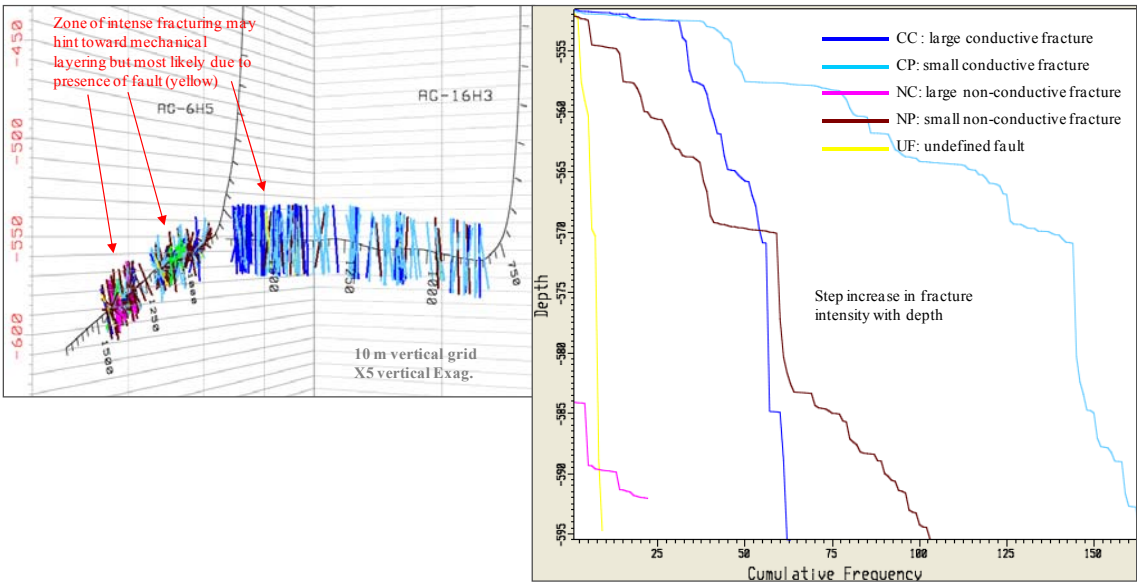


**Figure 3-50 Al Ghubar Shuaiba BHI fracture cumulative frequency plot and cross section.**

### *3.2.4 Qarn Alam field - Shuaiba Formation*

The Qarn Alam field in the southern part of the Ghaba North Salt basin is a naturally fractured carbonate reservoir, primarily producing from the Cretaceous Shuaiba and Kharaib Formations. The field-scale structure is defined by a ca. 3 x 6 km anticline, which formed as a result of compression (due to the Tertiary deformation) of a deeper-seated salt dome. The anticline is cut by transtensional and normal faults. It is a shallow field with very heavy oil scheduled for the first ever steam injection in a fractured carbonate reservoir "TGOGD" development in the Middle East (Figure 3.51).

#### *Existing work*

Because the fracture network is so critical to the success of the Thermal GOGD development, the field has been subjected to a very detailed fracture study. The fracture characterization of Qarn Alam started in 2000 and ended in 2005 with 3D discrete

fracture network scenarios, which will be updated ("basically a live model", as the drilling will commence in 2008/2009 for the development). The fracture studies which had been carried on this field benefitted from a recent sub horizontal appraisal wells that were drilled. These studies are: De Keijzer (de Keijzer and Richard, 2000), with wells up to Q20, Richard (Richard et al, 2003), with wells up to QA23, new 3D high resolution seismic and re-processing of old 3D seismic, Rawnsley (Rawnsley and al Dhahab, 2005), with wells up to QA34.

The main findings of the above reports are listed below:

The majority of the BHI fractures are conductive, striking NE-SW. Fault damage zone widths vary from 0 to more commonly 20-25m (Figure 3.52). Core & BHI inspections show leaching of some of the NW, N and NE fractures (Figure 3.53), as well as leaching of originally cemented fractures. Water Flow Logs (PLT) analysis from several wells indicate that not all of the BHI fractures seen contribute to the flow (Figure 3.54). Non-conductive "mineralized or cemented" fractures increase dramatically as the OWC is approached (Figure 3.55). Substantial numbers of fractures occur in clusters ("swarms"), thus probably related to faults or fracture corridors. No systematic areal trends are observed in BHI fractures– i.e. from crest to flank or from one flank to another, though the western flank shows a bit more fracture intensity. Mechanical stratigraphy: observed at the small/BHI scale (fractures abutting at layers) and at a large scale through analysis of QA27 and QA29 legs; also limited correlation possible vertically for various types of fractures across reservoir. A detailed statistical analysis of the BHI data was done to predict fracture spacing. Despite the high number of total BHI fracture data, their coverage is insufficient for a systematic statistical analysis on a "per well – per type – per FU flow unit– per orientation". A conceptual 3D fracture model was created for the field (Figure 3.56). Several 3D DFN realizations were created for this field based on different geological scenarios and their geometric properties, e.g. fracture spacing, and were extracted into simulation grids (Figure 3.57).

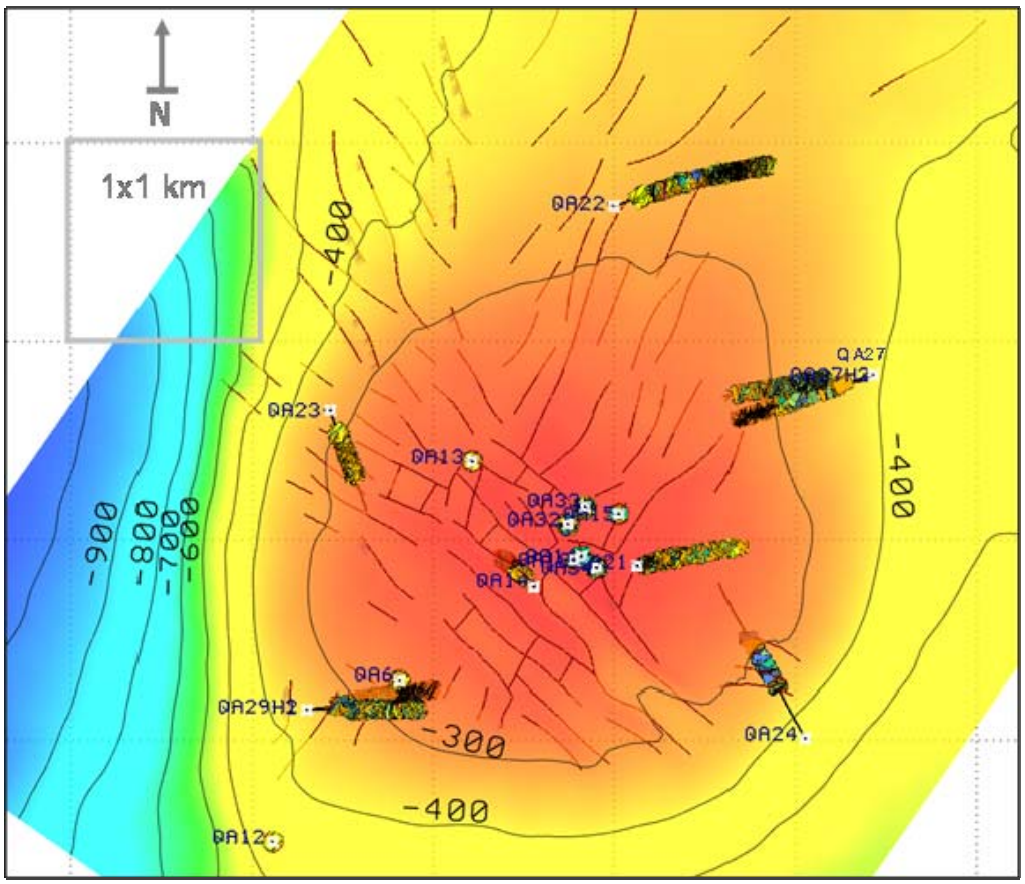


**Figure 3-51 Qarn Alam field, top Shuaiba map, with faults and BHI fractures (Rawnsley and al Dhahab, 2005) showing location of appraisal wells at the flanks.**

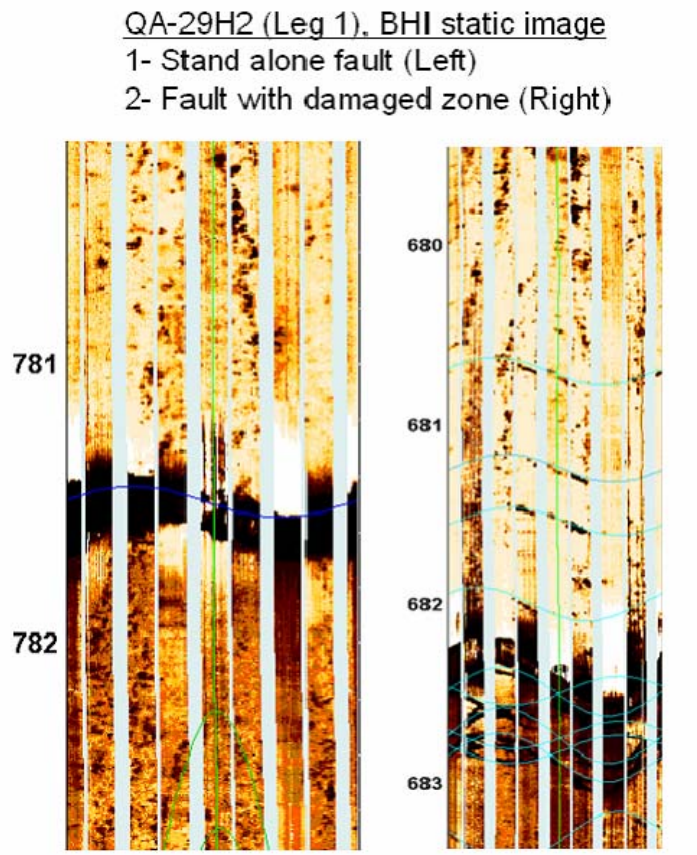


**Figure 3-52 BHI of QA29H2 showing faults imaged in BHI (Richard et al, 2003). Left is a stand alone fault, while in the right a fault with damaged zone is seen.**

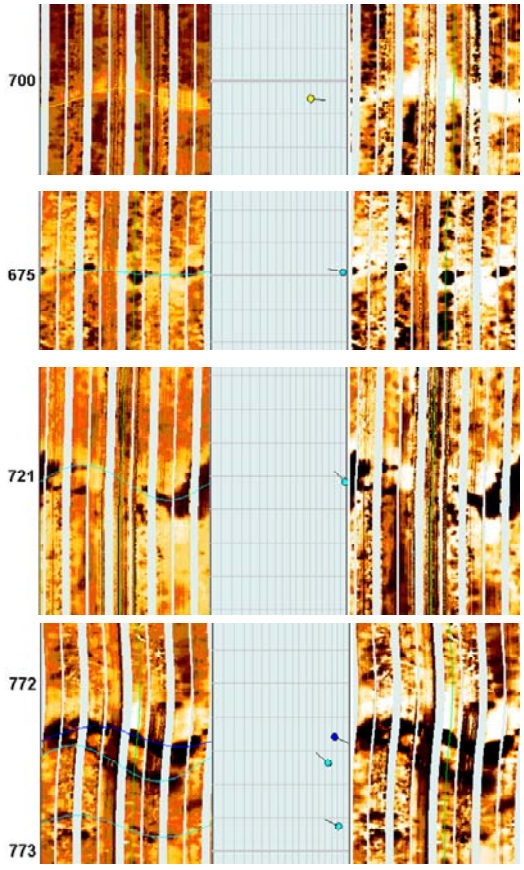


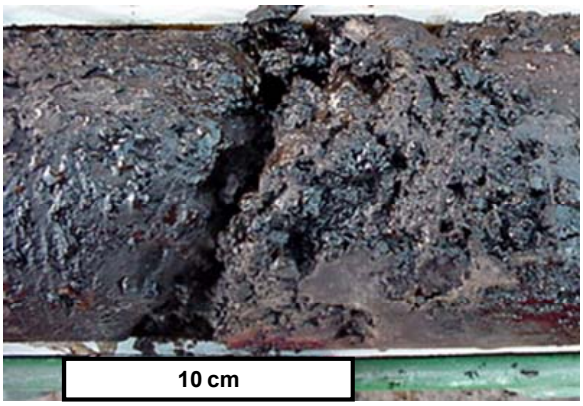


QA22 horizontal core showing a fracture with leaching (right), from al Dhahab 2000- OQP/00/021NFF

QA27H3 Leg2, horizontal well, BHI image
Fracture showing different stage of leaching and cementation

From Richard et al, 2003

**Figure 3-53 Example of different fracture diagenesis seen in Qarn Alam field.**

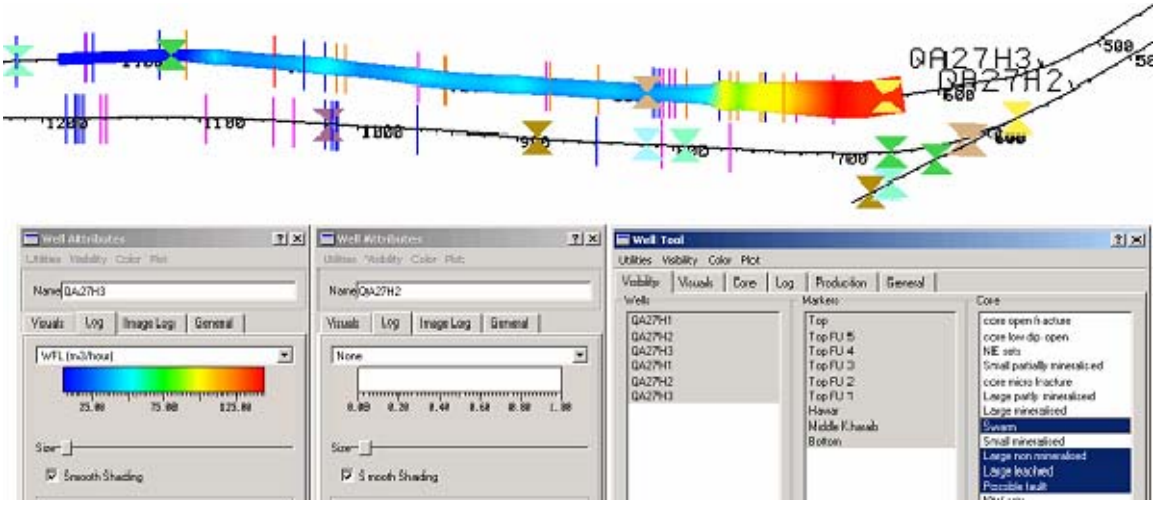


**Figure 3-54 Water Flow Log WFL/PLT on QA27H3 (colored log alonge the well bore), showing that not all the BHI fractures (vertical lines) contribute to follow (Richard et al, 2003).**

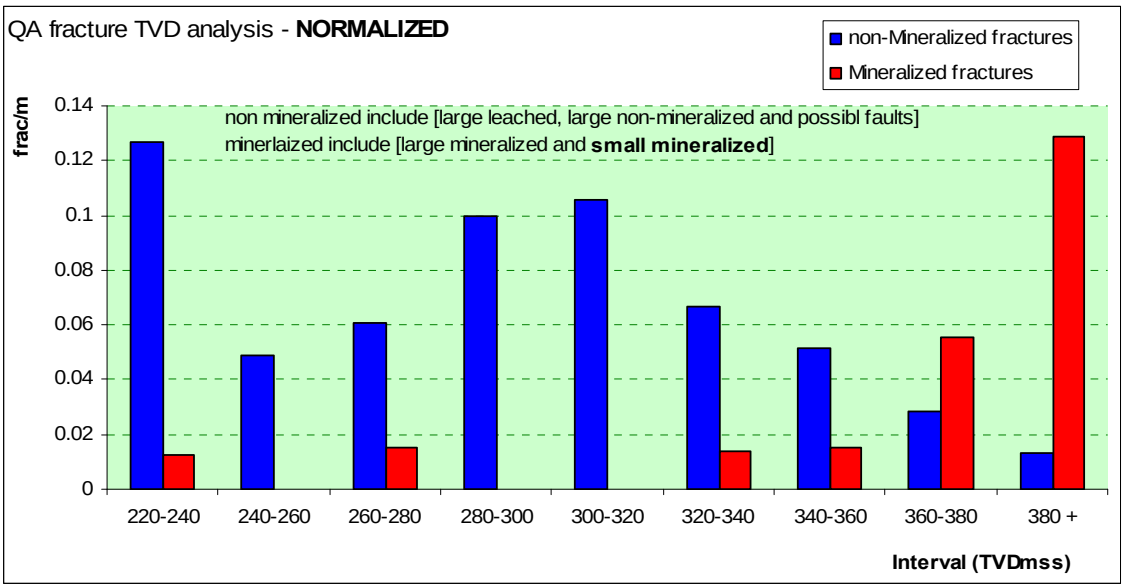


**Figure 3-55 Qarn Alam BHI data plot of standardised "normalized" fracture intensity (frc/m) versus 20m bins of TV depth in mss intervals, plot of conductive "non mineralized – blue" and non conductive "mineralized - red" (Richard et al, 2003). Note how the non-conductive fractures intensity increases as the OWC is approached at 376mss.**

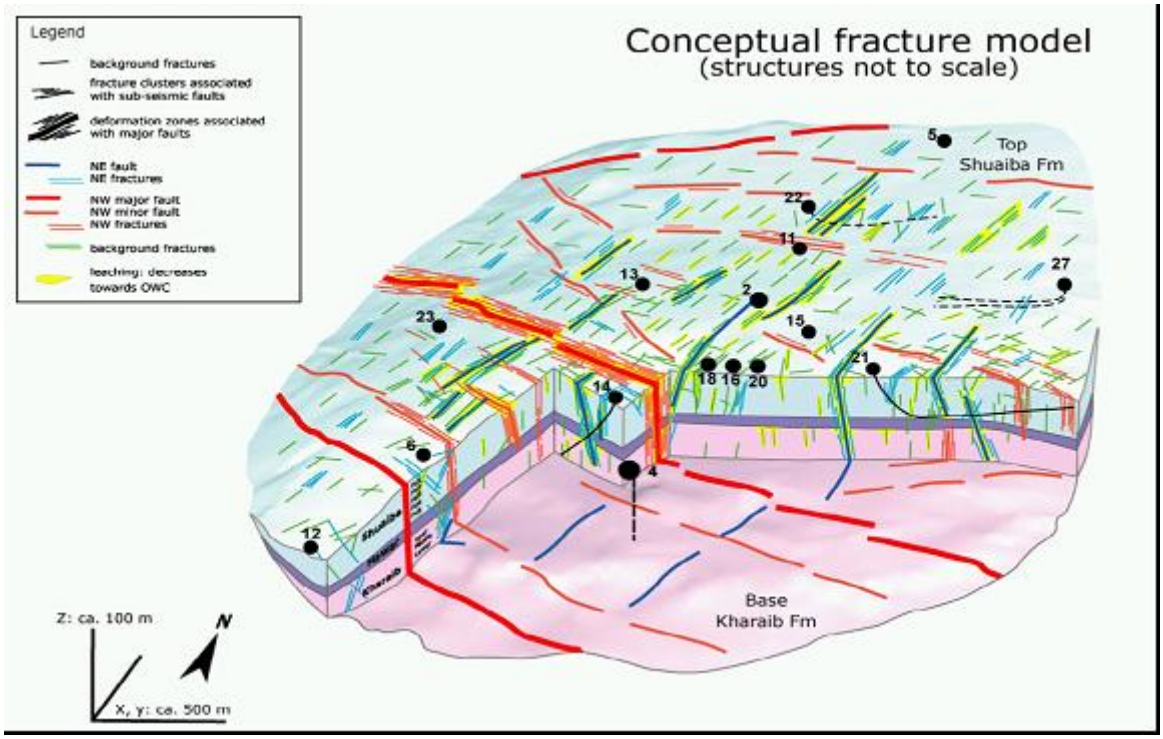


**Figure 3-56 Conceptual model of Qarn Alam Shuaiba, Hawar and Kharaib reservoir showing the fault and fracture characteristics (Richard et al, 2003). Yellow patches are thought to be diagenesis effect on fractures and faults.**

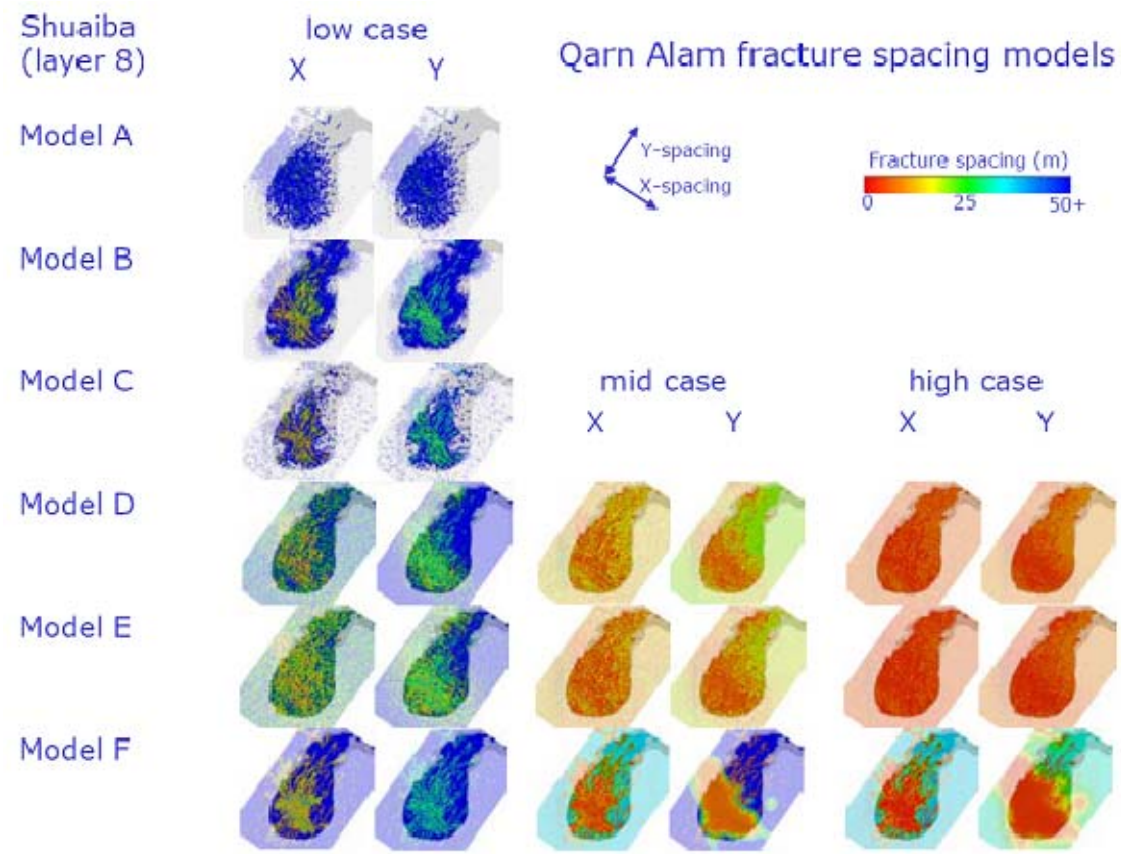


**Figure 3-57 Qarn Alam field 3D grids showing fracture spacing of the top layer only for different geological models: from A crest only, B fault only to F fault cluster and background fractures (Rawnsley and al Dhahab, 2005).**

### *Qarn Alam fracture data evaluation*

The Rawnsley and al Dhahab (2005) report is very comprehensive; the comments here provide a synopsis that is intended to highlight the main geometrical aspects of the Qarn Alam fracture network, so that this information can be used in understanding the regional fracture scheme. My evaluation of the BHI data shows that: Both individual wells and total BHI fracture rose diagram indicate that the N to NE direction is the most dominant fracture trend (Figure 3.58). The NW direction is stronger in the non-conductive set (Figure 3.59). Multi-directional curvature map of top Shuaiba at large scale 1000m shows slight hint of correlation with BHI fracture intensity (Figure 3.60). Cumulative frequency plot of BHI versus depth and vertical view of the wells (Figure 3.61), show that: non-conductive fractures increase as OWC is approached; and there is slight stepping indicating possible mechanical layering.

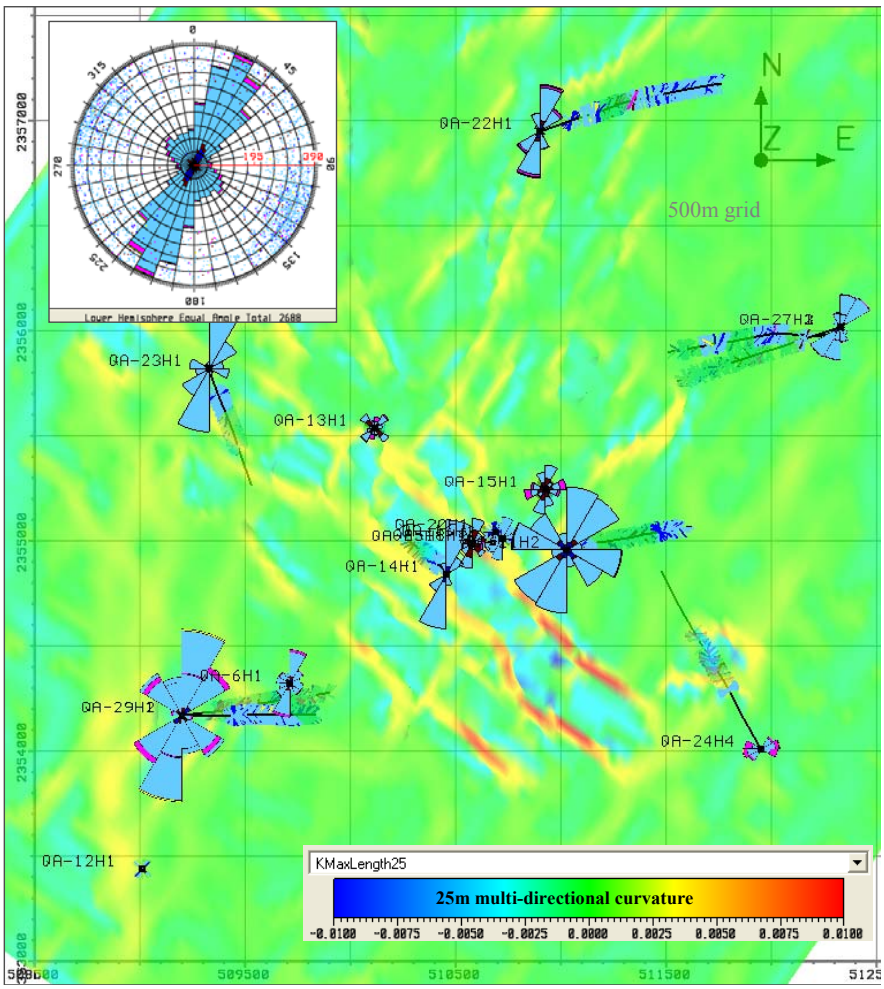


**Figure 3-58 Qarn Alam top Shuaiba multi-direction azimuth curvature map (Kmax at 25m scale wavelength) with BHI fracture rose diagram. Note how the majority of the fractures strike NE.**

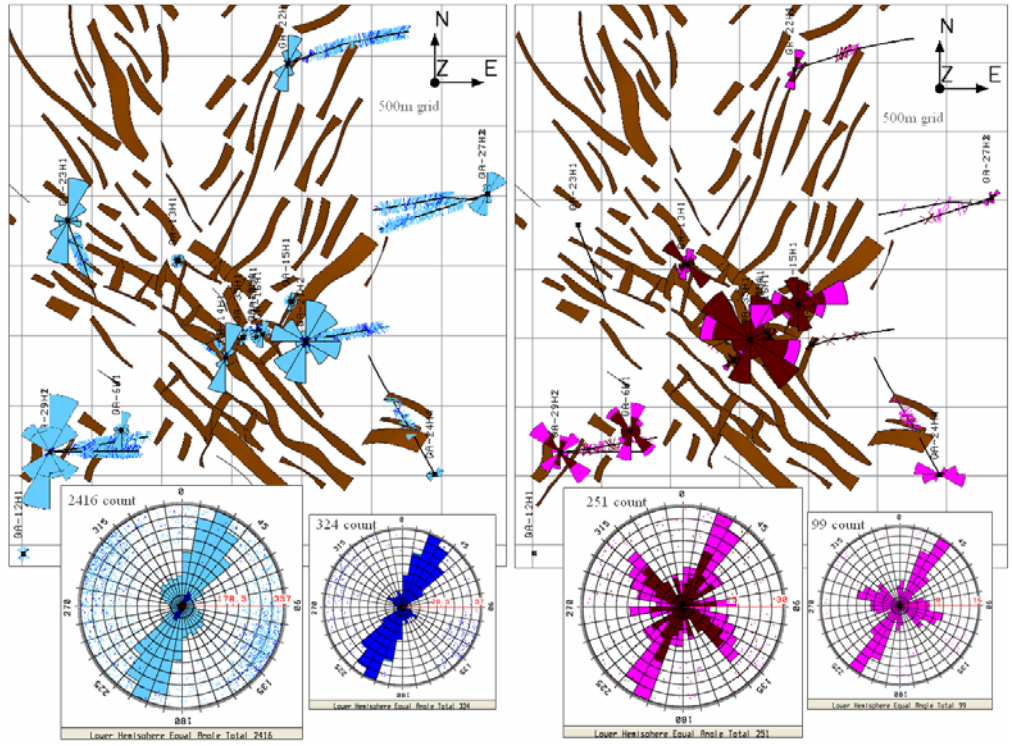


**Figure 3-59 Map view of Qarn Alam BHI fractures (Blue is large conductive, light blue is small conductive, Pink is large non-conductive, dark pink is small non conducive) with faults.**

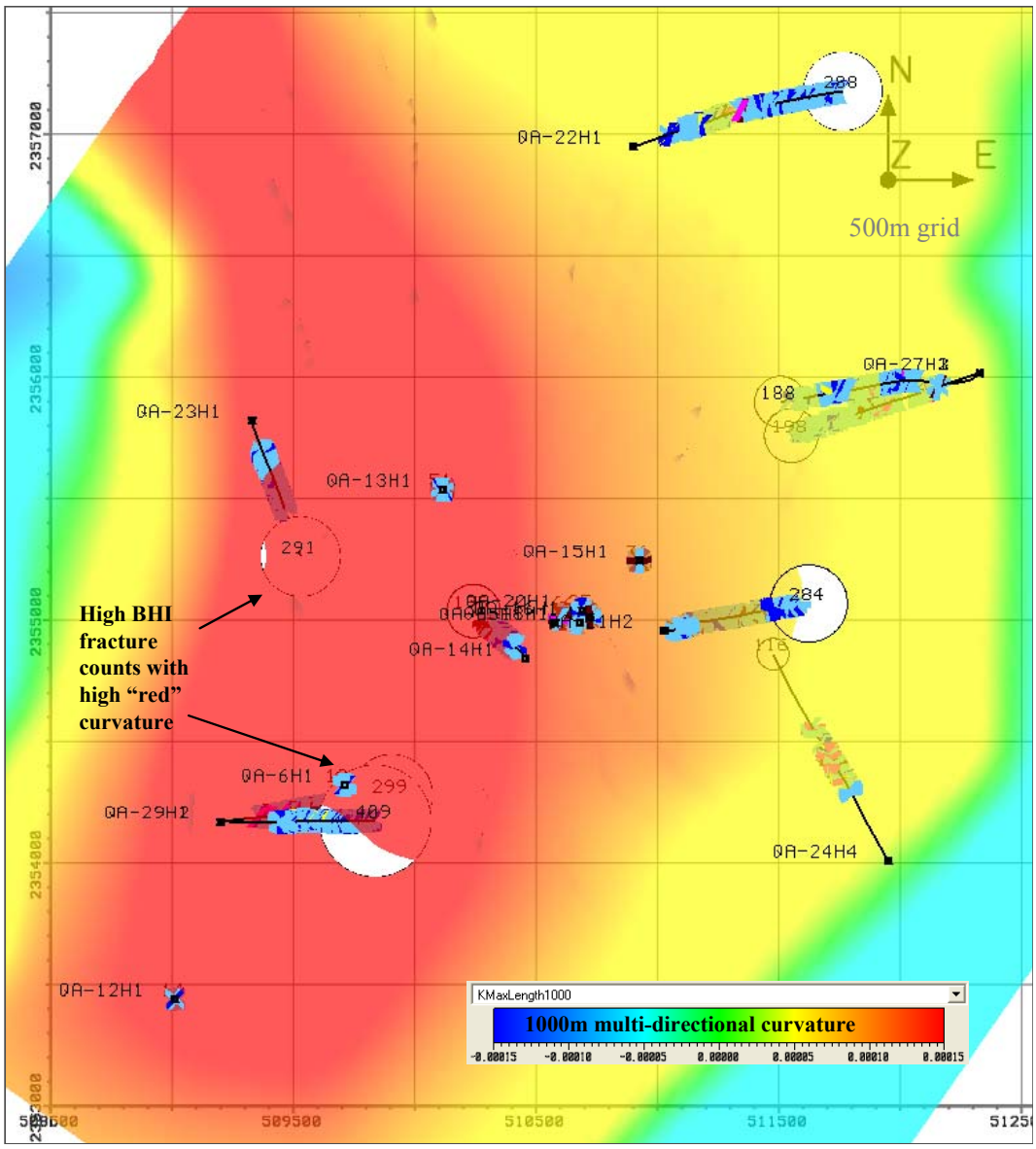


**Figure 3-60 Multi-directional curvature map (Kmax) of top Shuaiba at 1000m scale (red = high curvature) with BHI fracture counts (white circles with numbers).**

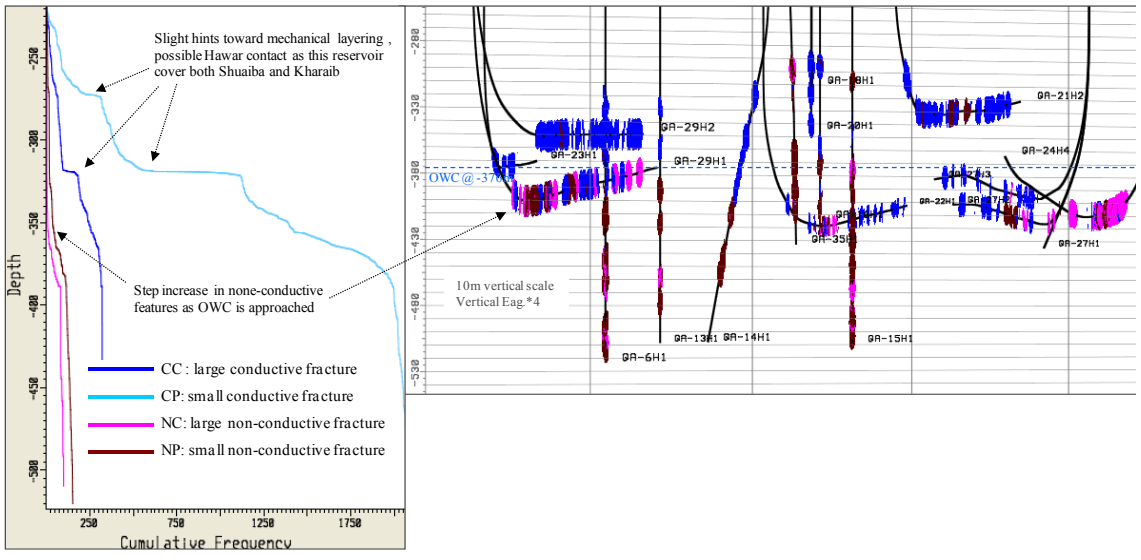


**Figure 3-61 Qarn Alam BHI fracture cumulative frequency plot versus depth (Left) and cross section showing large conductive fractures with all –large & small- non conductive fractures.**

### *3.2.5 Ghaba North field - Shuaiba Formation*

The Ghaba North field, about 22km NE of QA (see Figure 1.5 and 2.1), is formed by a four-way dip closure above a salt diapir. The field is oil-bearing in the Shuaiba and gas-bearing in the Natih E formation. The deep Gharif Formation is oil bearing. This field will be studied in detail in the next chapter. Up to 2004, there were only two horizontal wells in this field: GN25 and GN26 (Figure 3.62).

***Existing work***

Dhahab (2002): Up to GN26

This was a geo-statistical analysis of the existing BHI fracture data. It showed that there are three main fracture sets: NW, NNE and NE striking fractures. Most of the fractures seen (>90%) are open in all sets, even with depth, though GN25 & GN26 were only drilled in the upper parts of Shuaiba. Fractures do occur in clusters "fracture corridors" with a width of 0.5-6m and a spacing of 15-28m for all the sets seen in the field.

Ita (Ita and Richard, 2001-2003): Up to GN26

In this study, seismic analysis (coherency cube analysis – Shell stopper voxel) was applied on the 3D seismic volume of the field, to pick up structural patterns. A 3D structural model was constructed in gOcad$^{TM}$ for the Shuaiba reservoir. This resulted in a new fault interpretation (Figure 3.63). Several scenarios of 2D fracture conceptual models were created (Figure 3.64).

Price (Price et al, ongoing): Up to GN31H2

This work is still ongoing. The study team had passed VAR2 (Value Assurance Review – subsurface part) in Q3 of 2006. So far only the petrophysical report has been issued.

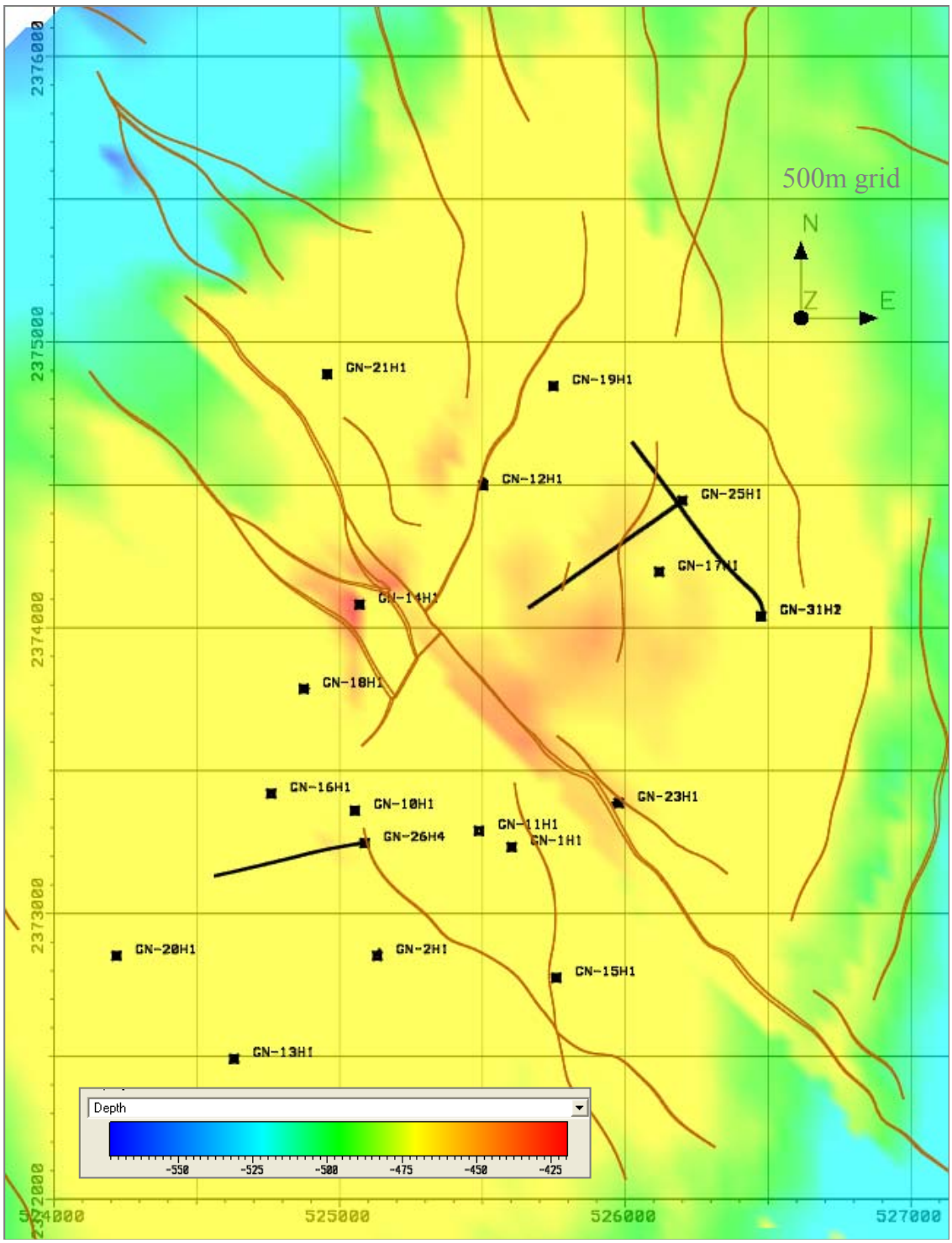


**Figure 3-62 Ghaba North Shuaiba top map with wells (GN31H2 was drilled in 2006). Faults shown are pre 2001 fault interpretation.**

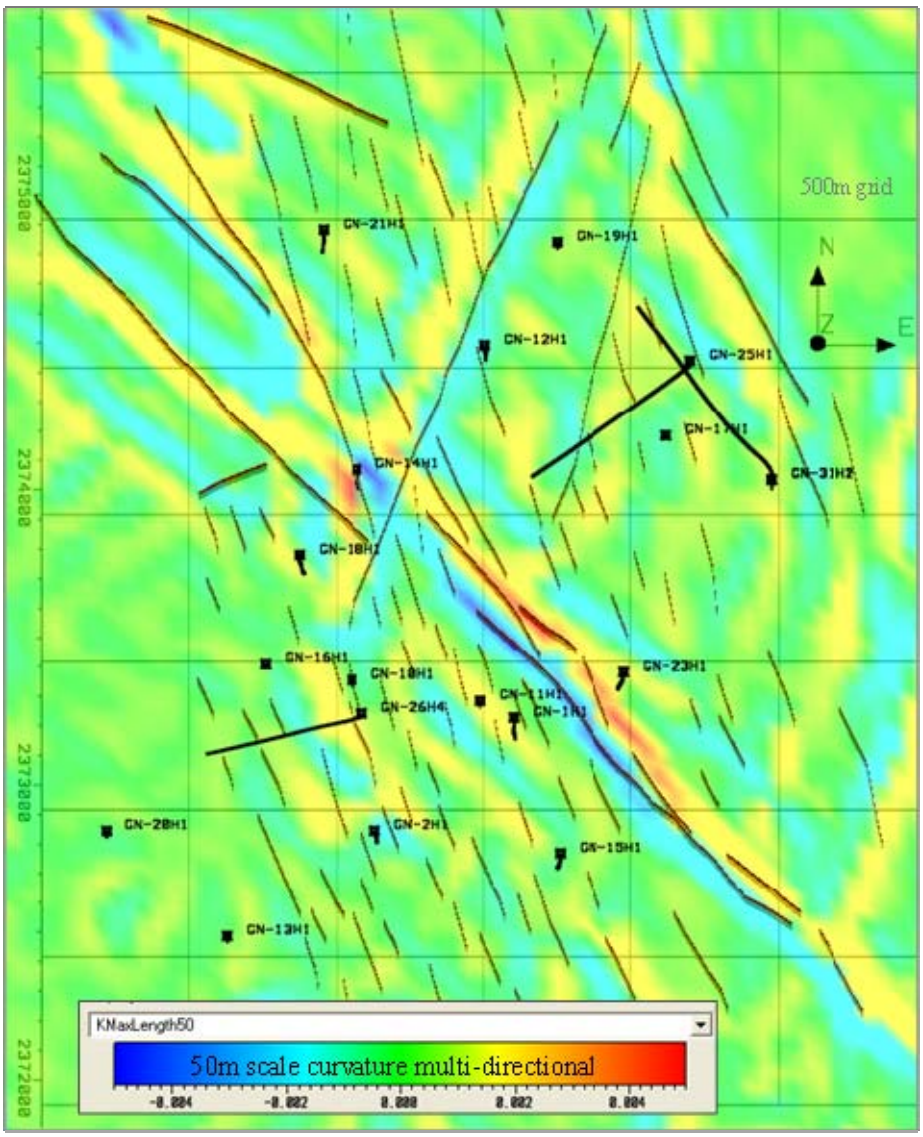


**Figure 3-63 The 2001 fault interpretation by Ita and Richard (2003) superimposed on top of a 50m scale wavelength curvature map (Kmax) of top Shuaiba.**

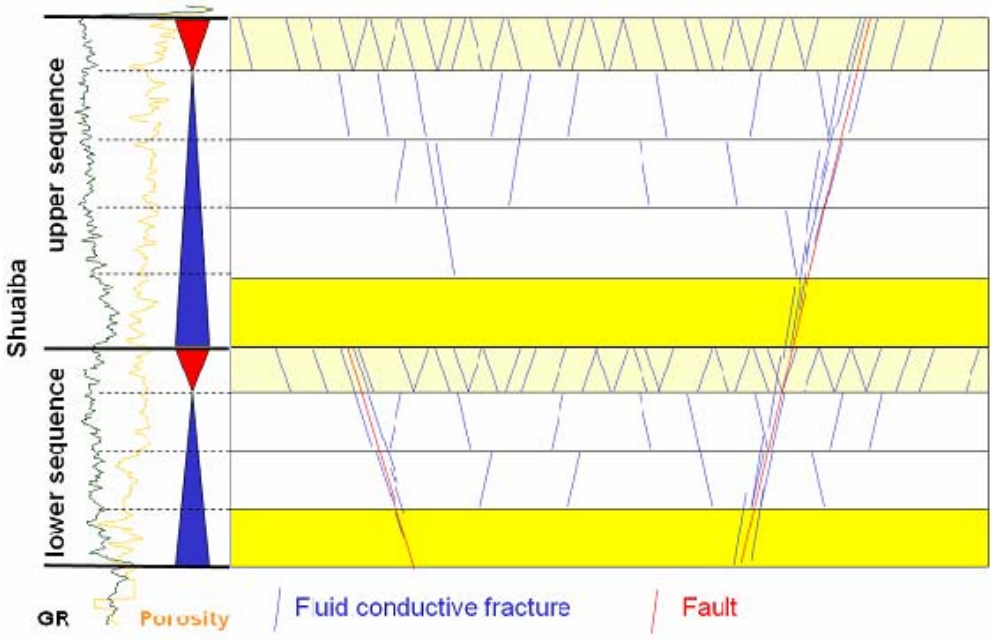


**Figure 3-64 One scenario of Ghaba north 2D conceptual fracture model (Ita and Richard, 2003).**

### *Ghaba North fracture data evaluation*

As mentioned above, this reservoir will be subjected to further detailed fracture characterization work in the next chapter, hence in this section I present only geometrical aspects of the fracture network that are important in regional understanding, as well as validating the interpretation presented in the existing work. Even with the new horizontal appraisal well running in a direction oblique to GN25 & GN26, the dominant fracture direction is NE (Figure 3.65). GN25 is the most fractured well, and it also shows induced fractures that are running NE (compare to that of Al Ghubar, Figure 3.49 above). The conductive BHI fractures are dominant > 90% (Figure 3.66). Since all the wells, including the appraisal well, (GN-31H2 which has a vertical coverage of about 20m into the reservoir) were drilled in the upper half of Shuaiba, is still difficult to predict the fracture variation with depth (Figure 3.67).

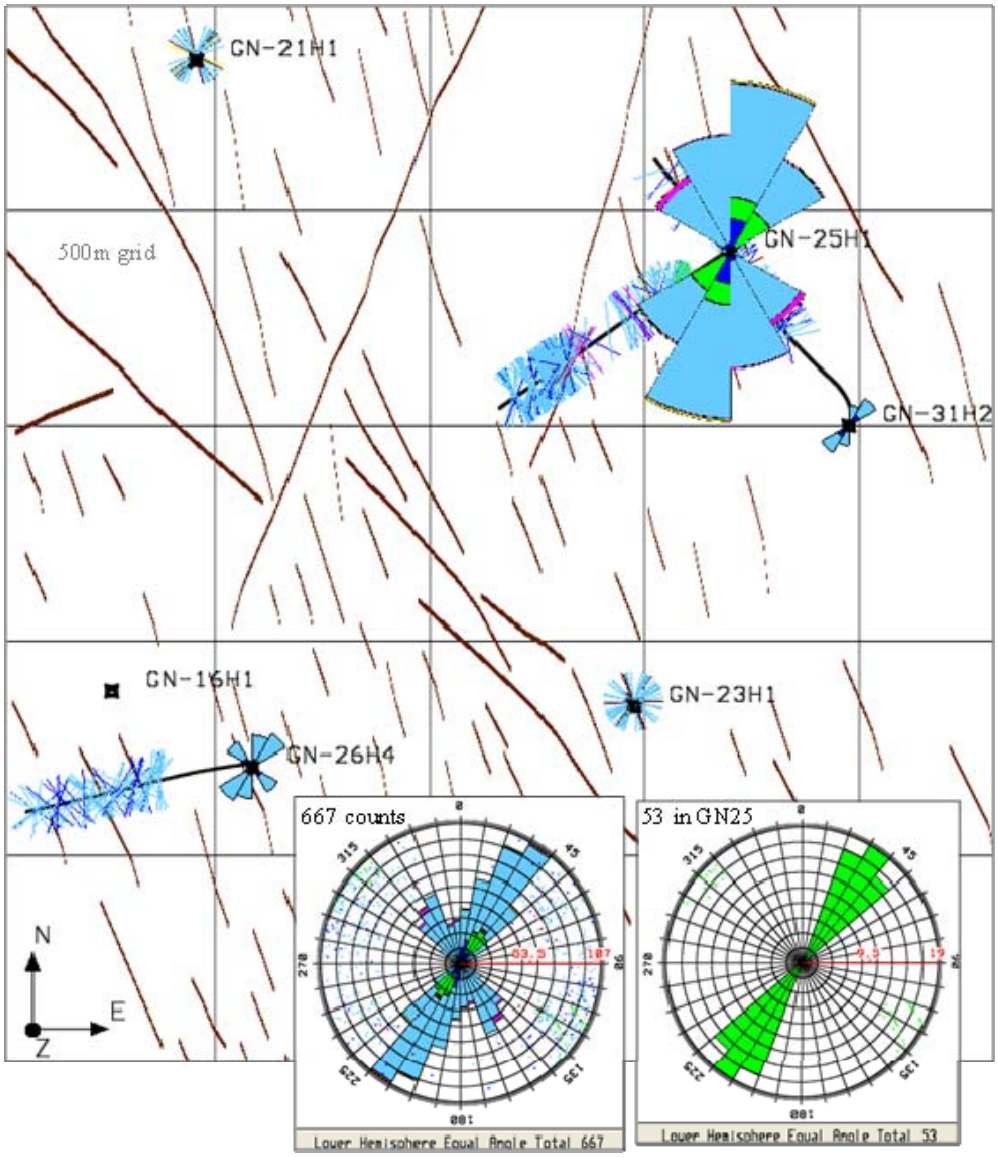


**Figure 3-65 Ghaba North Shuaiba BHI fractures, small conductive fractures are dominant (light blue). Greens are induced fractures seen only in GN25.**

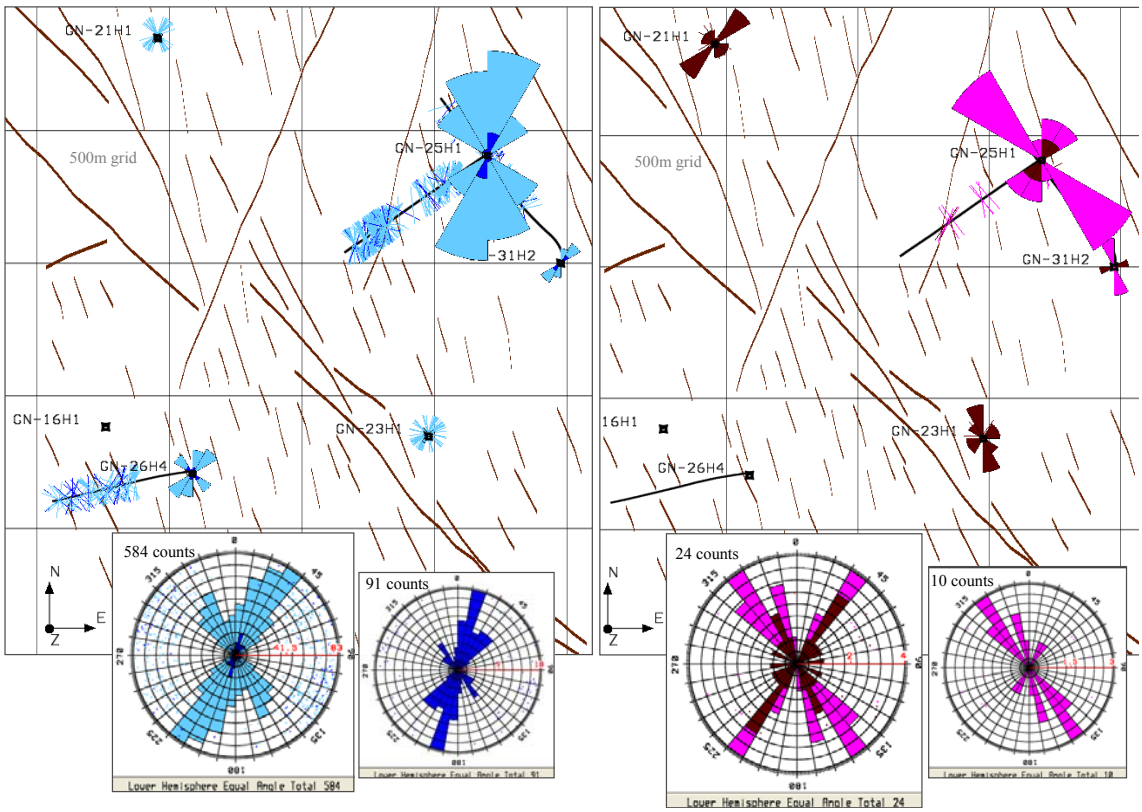


**Figure 3-66 Conductive BHI fractures (Left) are more dominant than non- conductive (Right).**

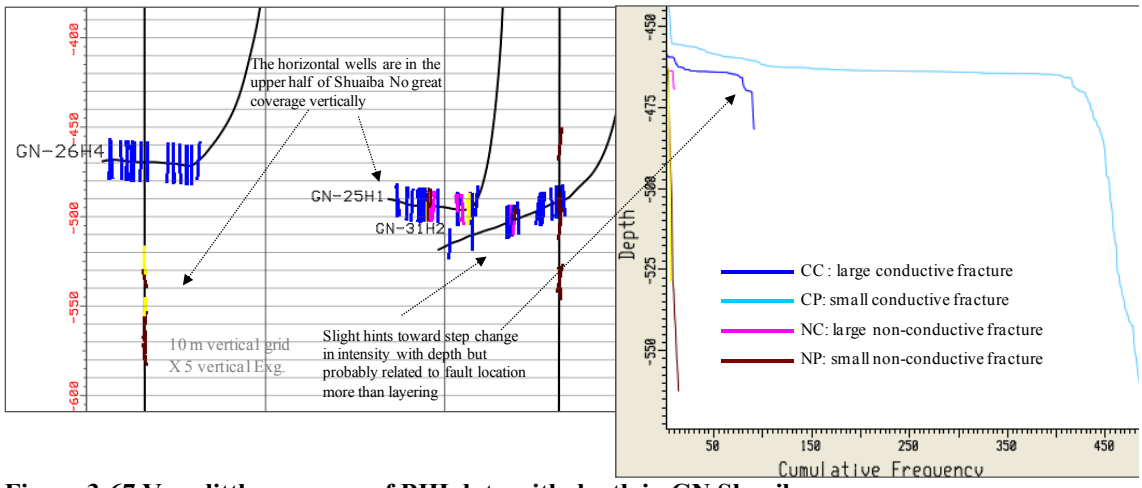


**Figure 3-67 Very little coverage of BHI data with depth in GN Shuaiba.**

### *3.2.6 Burhaan NW field - Shuaiba Formation*

Although this field was discovered in 1988, full field development started only in 2000. The field is the closest to Maradi Fault Zone. The field is produced with water injection, using pairs of multi-lateral producer–injector wells with a spacing of about 120m (Figure 3.68), which make fracture network characterization very important to avoid short circuiting between injector– producer pairs. The field is divided into two areas separated by a potential sealing fault, as the pressure regimes differ between these areas. The whole region from Saih Rawl to Musallim and Burhaan going NW all the way to Lekhwair area is associated with a fish-net fault pattern indicative of a regional transtensional tectonic regime at the time of the fault generation (Figure 3.69).

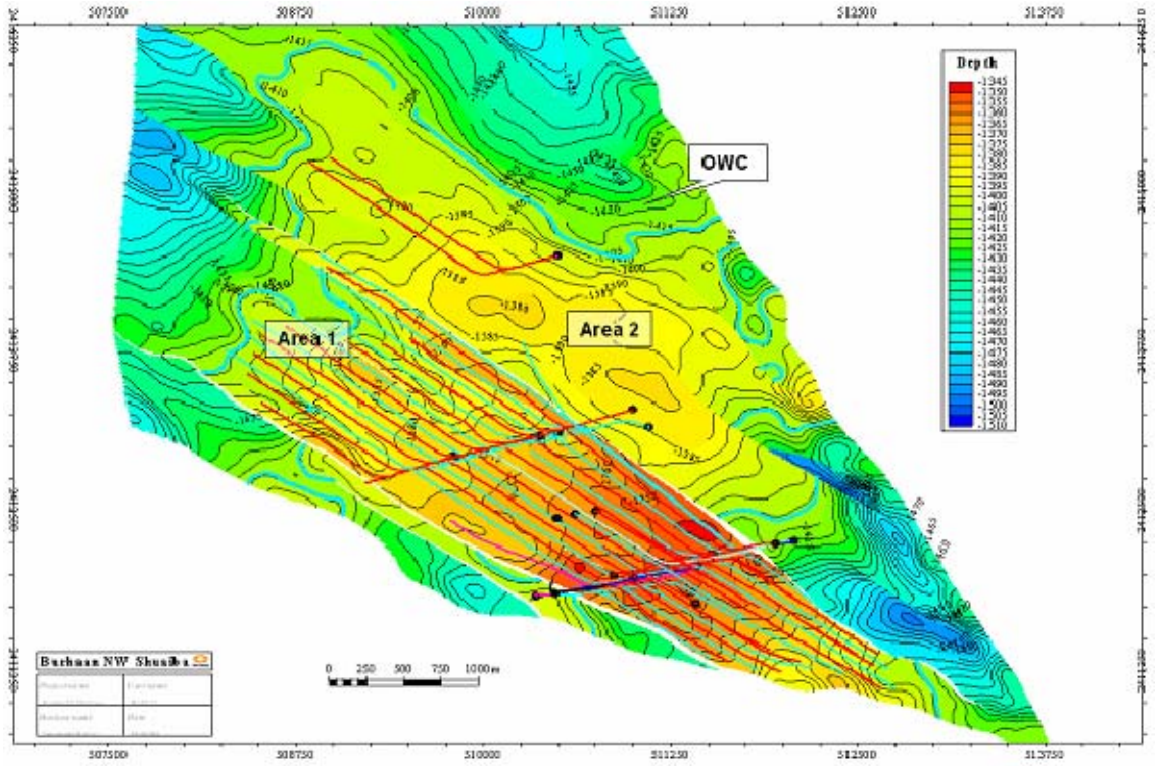


**Figure 3-68 Burhaan NW Shuaiba top map, with producers (red) injectors (blue/cyan) multi-lateral pair water injection development (Burhaan Team, PDO field note strategy).**

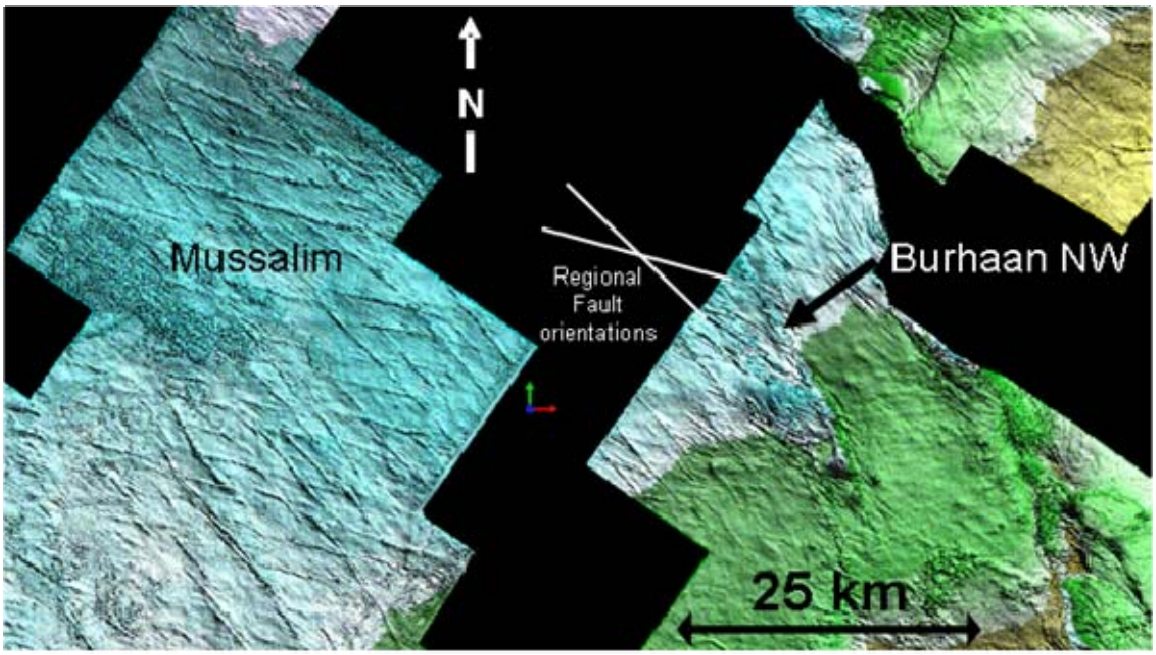


**Figure 3-69 Regional seismic of top Kharaib (Robertson, PDO internal report, 2003). Note the fish-net NW & WNW striking faults covering the whole region from Burhaan to Mussalim.**

### *Existing work*

A fracture modelling study was carried out on this field by Richard (2003), based on a detailed BHI fracture interpretation by Baker Atlas (Ismail Ozkaya). The main results are as follow: A simplified kinematics analysis presented for the field's fault (Figure 3.70). Analysis of BHI fractures indicates that fracture corridors (fracture clusters) occur only within the north eastern half of the field. The south western sector is devoid

of fracture corridors. In addition, most fracture corridors strike NE even though the fault direction is NW. There are several non-conductive fracture corridors and some corridors have cemented walls running sub parallel to the fault in the field. Background dispersed layer bound fractures, observed in all layers, are not interconnected and far below percolation. They have no influence on reservoir dynamics. The small permeability enhancement by conductive dispersed fractures is cancelled by non-conductive fractures. Hence, the fractures have only negligible positive effect on reservoir permeability, but fracture corridors may cause early water breakthrough in the Burhaan NW. Production data were insufficient to be used as constraints for 3D fracture models, however, other dynamic data such as PLT and saturation logs were used to better understand the fracture network (Figure 3.71). A conceptual model is proposed for the field (Figure 3.72). A 3D DFN models with several realizations were built.

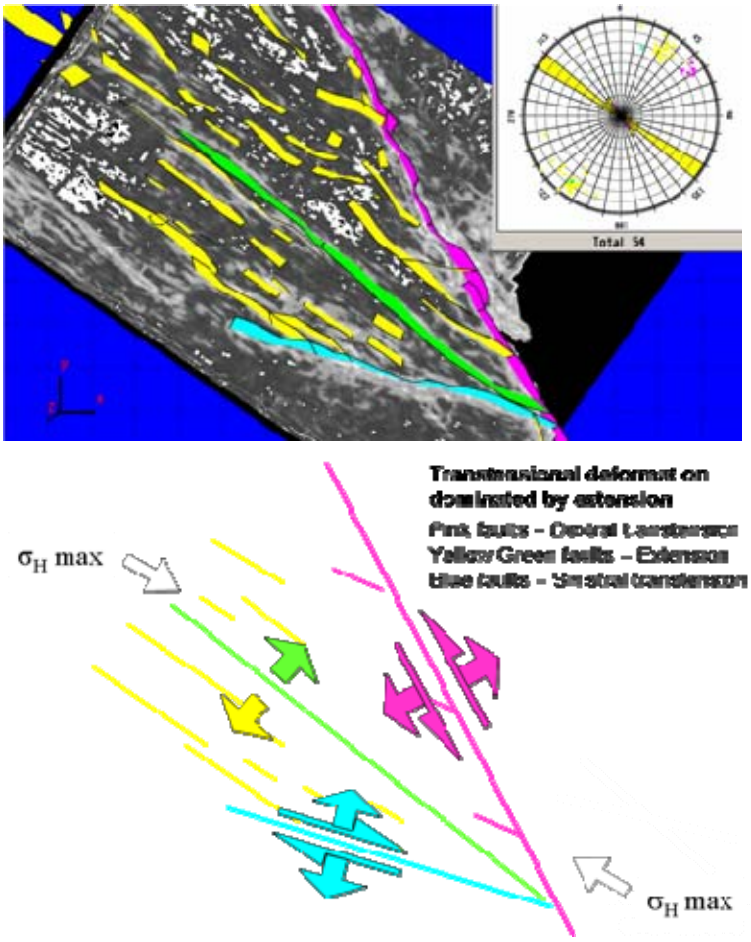


**Figure 3-70 Simplified kinematics interpretations of Burhaan NW (Richard, 2003).**

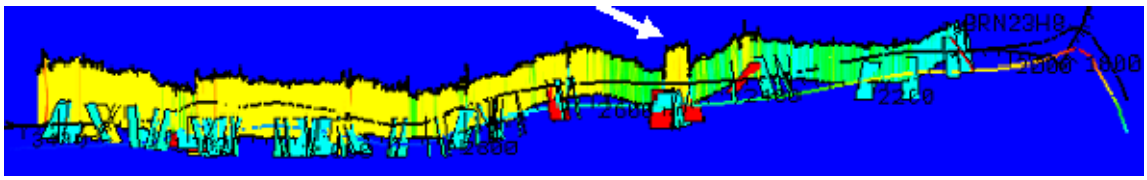


**Figure 3-71 Example of BHI fracture analysis with dynamic logs: large conductive fracture (blue planes) and fault (red planes) interpreted from BHI with the porosity attribute and the Sw log along BRN23H8. The white arrow indicates a fault which shows higher Sw (Richard, 2003).**

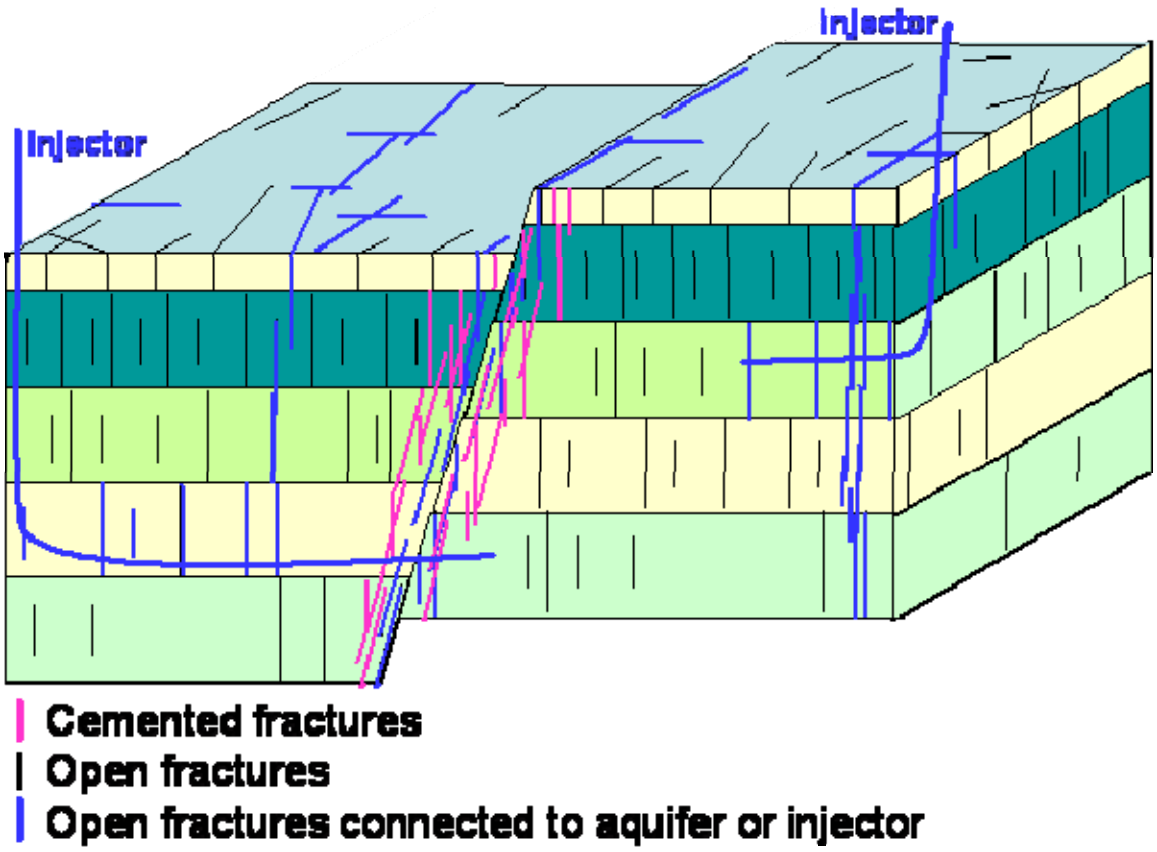


**Figure 3-72 Burhaan NW Shuaiba conceptual fracture model (Richard, 2003).**

### *Burhaan NW fracture data evaluation*

Analysis of existing BHI logs of Burhaan NW Shuaiba, indicate that the majority of the fractures are striking ENE to N (Figure 3.73). The conductive fractures are more dominant, compared to non-conductive fractures, by more than a factor of 2. More importantly, the conductive fractures seem to be striking NE to N while the large non-conductive fractures strike NW (Figure 3.74). BHI faults are parallel to major faults in the field running NW (Figure 3.75). There are possible hints toward mechanical layering when examining the BHI fracture intensity with depth (Figure 3.76).

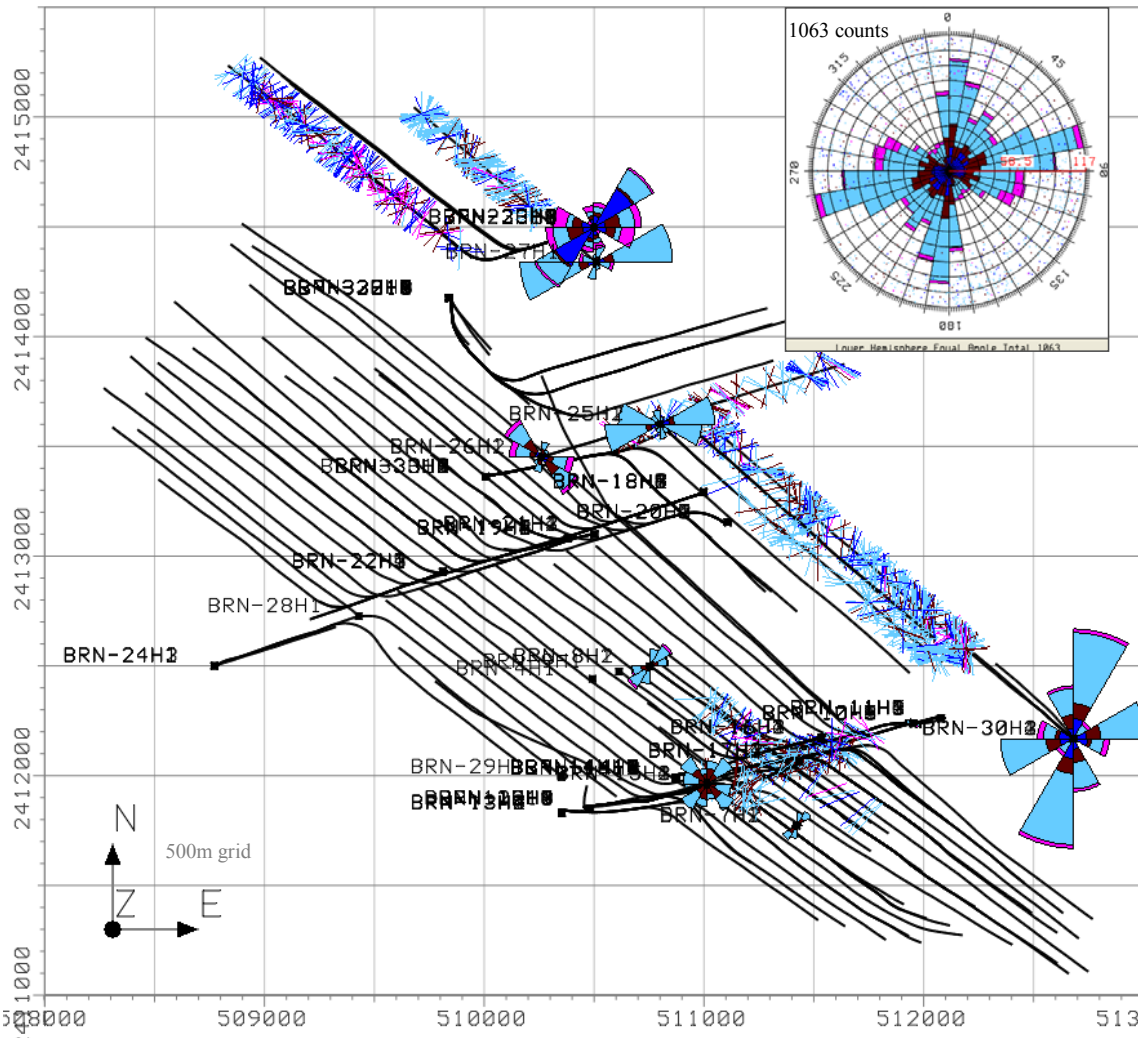


**Figure 3-73 All BHI fracture data for Burhaan NW wells.**

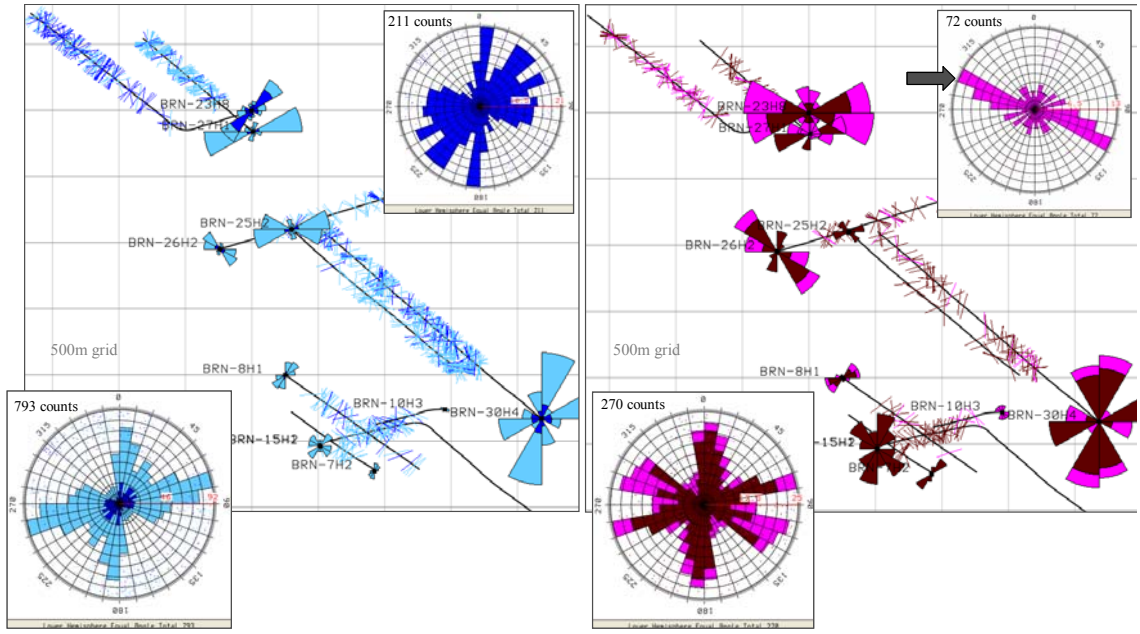


**Figure 3-74 Burhaan NW Shuaiba BHI fractures split per type (Conductive – blue & non-conductive pink). Note the large non-conductive "pink top left rose diagram" striking NW parallel to the fish net regional faults which are cemented faults.**

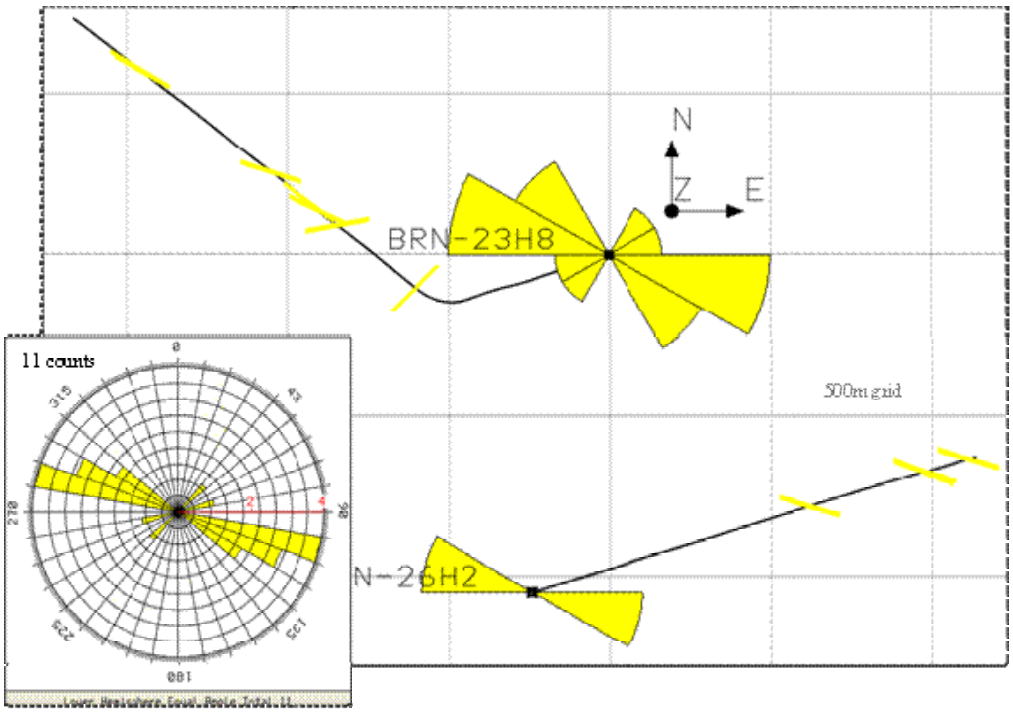


**Figure 3-75 Burhaan NW Shuaiba BHI faults striking NW.**

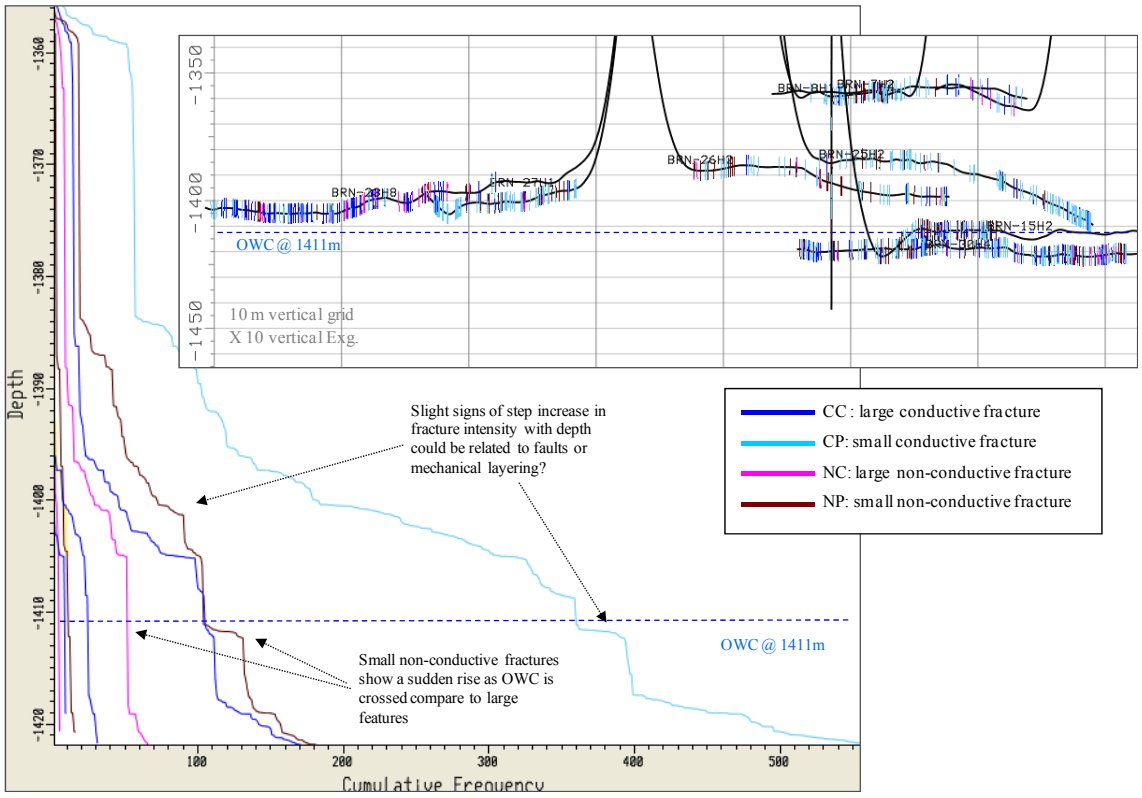


**Figure 3-76 Burhaan NW BHI fracture cumulative frequency versus depth plot and vertical cross section, indicating a major rule of mechanical layering.**

### *3.2.7 Saih Rawl field - Shuaiba Formation*

This field has two hydrocarbon reservoirs: the oil-bearing Shuaiba and the deeper gas bearing Gahrif. The Shuaiba reservoir has long been described as a “matrix” reservoir with development by multi-lateral produce-injector pairs. Musallim and Burhaan NW development was based on Saih Rawl. The water is injected below the OWC so it is a

bottom up drive in all those matrix fields. The fracture network was considered unconnected but with time the areal distance between the producer-injector pairs had become shorter (Figure 3.77), resulting in short circuits and water breakthrough, which already had been seen in few wells (Figure 3.78).

### *Existing work*

A fracture modelling study was carried out on this field by Richard (Richard, Dhahab and Bettembourg, 2002-2003), the main findings are: The BHI fracture sampling of this reservoir is bias because most of the horizontal wells were drilled in a NE-SW direction as shown below; and were targeting only the upper part of the reservoir. However, there are few vertical wells that cut through the whole Shuaiba. These were used to deduce vertical fracture distribution (Figure 3.79). The BHI fractures seem to be independent of both the Shuaiba faults and/or the deeper Gharif faults (Figure 3.80). Dominant fractures strike NE, WNW and NNW with most of the non-conductive fractures in the WNW set, and most of the fractures occurring in clusters. Some of the WNW set occur close to the boundary fault and dominate the area there. No bed bounded fracture has been clearly observed on FMI, as the vertical log coverage is limited. Undifferentiated fracture spacing varies areally from one fracture every 3 to 34 m. A conceptual model was created for the field (Figure 3.81). Several 3D DFN model realizations were built.

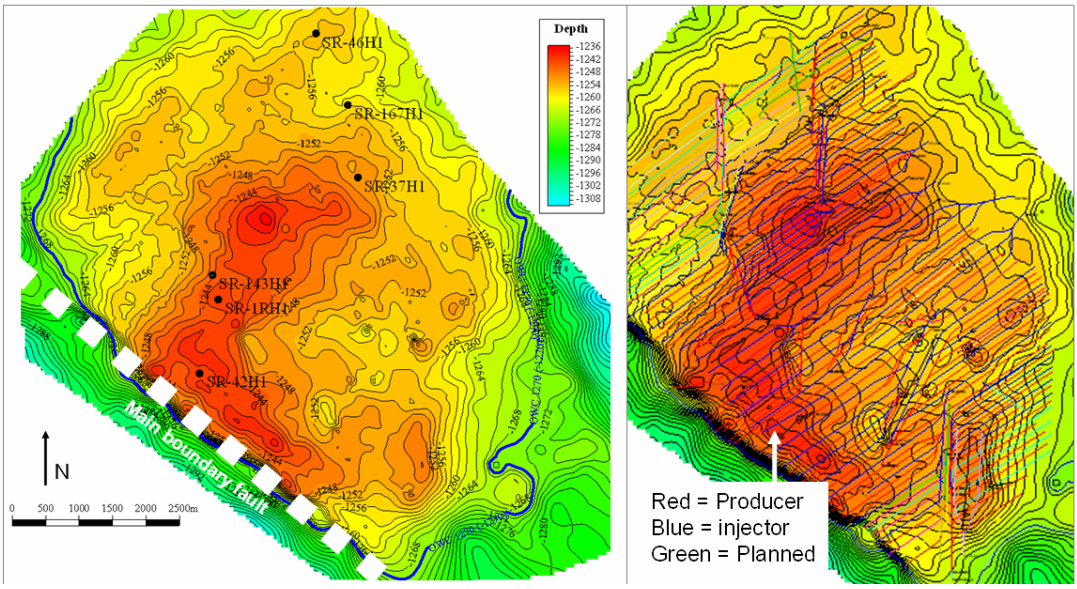


**Figure 3-77 Saih Rawl top Shuaiba map, with boundary fault (Left) and wells (Right). Note how most of the wells are striking NE-SW (Amthor, PDO internal report, 2002).**

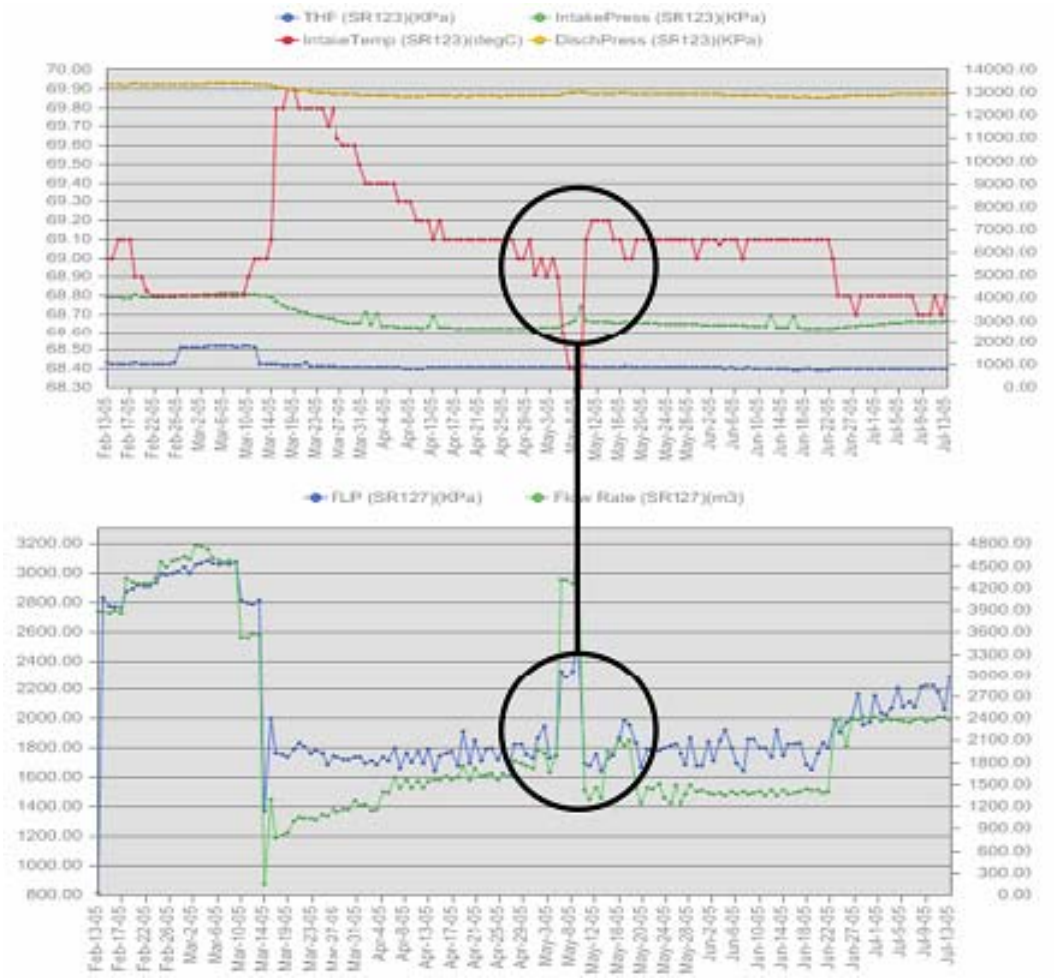


**Figure 3-78 Example of short circuiting between producer-injector pair, deduced from increase in flow rate which coincide with drop in intake temperature as injected water is at lower temperature than the reservoir (Qarn Alam matrix fields subsurface team, PDO presentation, 2002).**

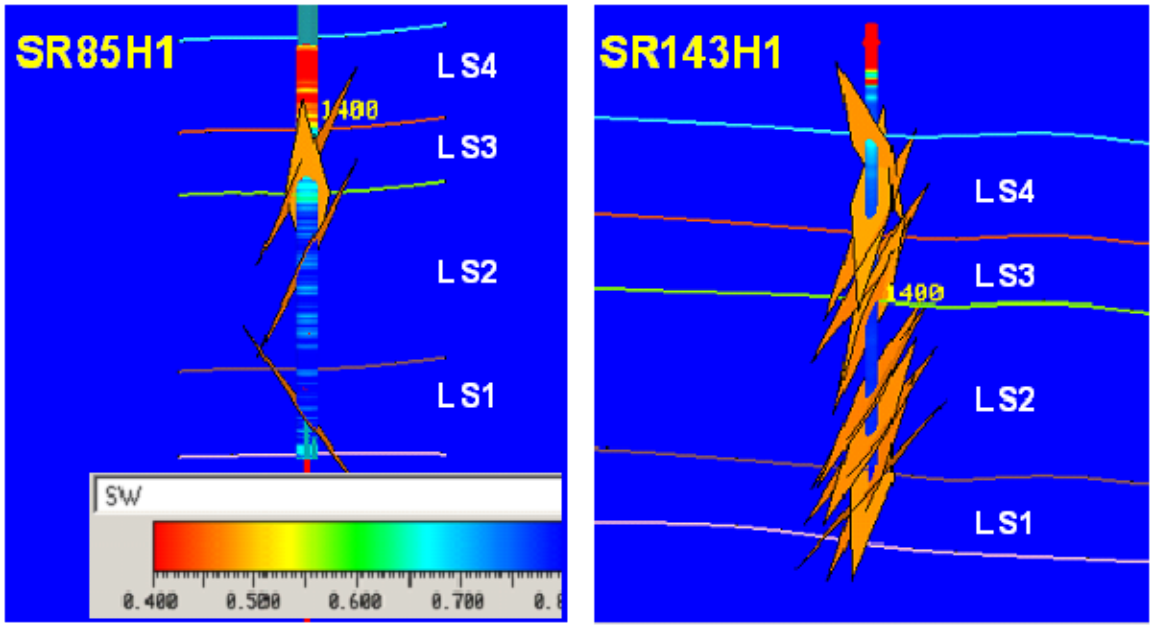


**Figure 3-79 Vertical wells showing partly conductive fractures crossing all the matrix layers of Shuaiba Formation in Saih Rawl (Richard et al, 2003).**

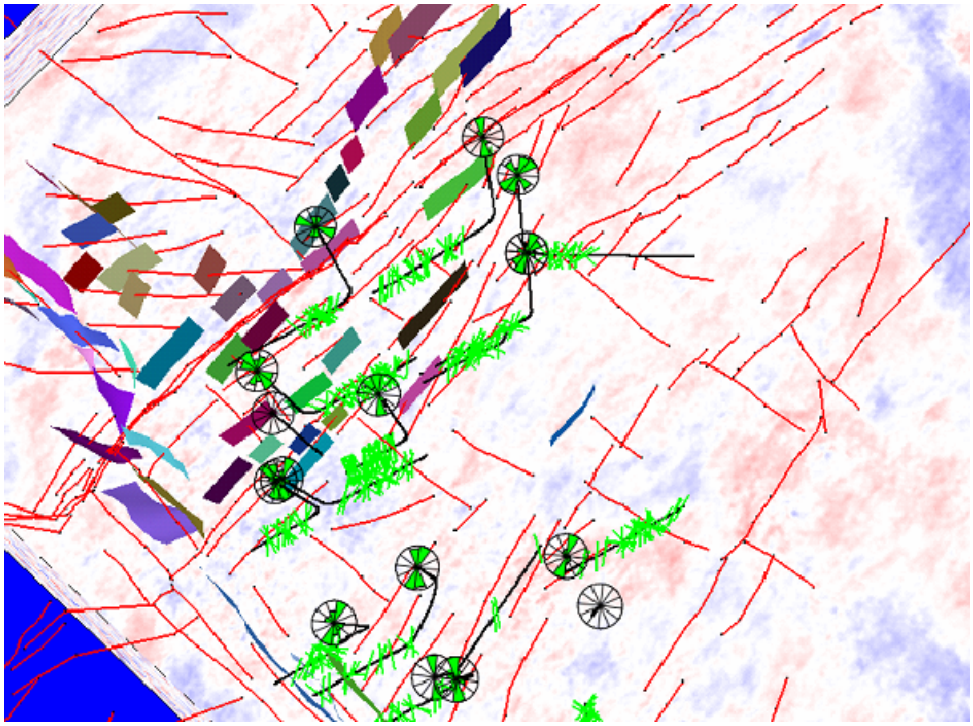

**Figure 3-80 BHI high confidence fractures "mega fractures – green" superimposed on seismic reflection of Saih Rawl Shuaiba (colored background surfaces) and the deeper Gharif fault (red lines) picks (Richard et al, 2003).**

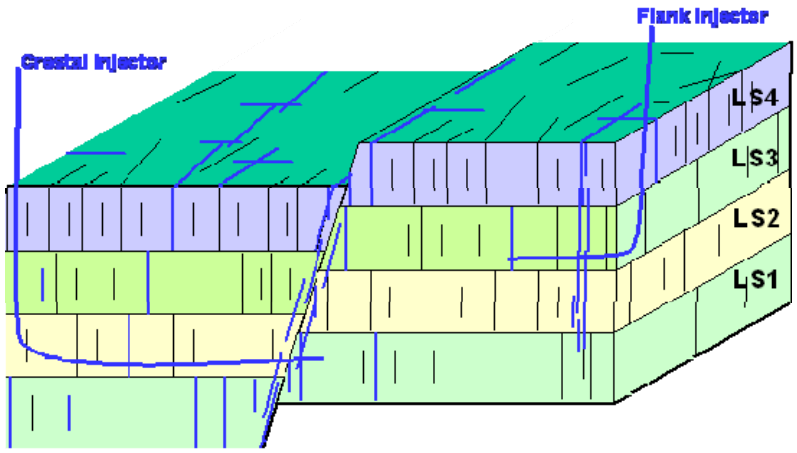


**Figure 3-81 Conceptual model for the fracture network of Saih Rawl Shuaiba (Richard et al, 2003).**

### *Saih Rawl fracture data evaluation*

A geometric analysis of the BHI data in Saih Rawl was done, to validate what presented above and to derive any regional observations. The areal coverage of BHI is relatively sufficient, but directional coverage is biased (Figure 3.82). Also vertical coverage is very low (see Figure 3.85). BHI faults are striking mainly NS and NW-SE (Figure 3.83). Conductive (large & small) fractures dominate. Similar orientation is noted for the conductive and non-conductive fractures. Though the large non-conductive pink are dominantly striking NW (Figure 3.84). All the BHI data are from the top interval of the reservoir (bias sampling vertically), hence the fracture intensity frequency versus depth plot indicate no mechanical layering (Figure 3.85).

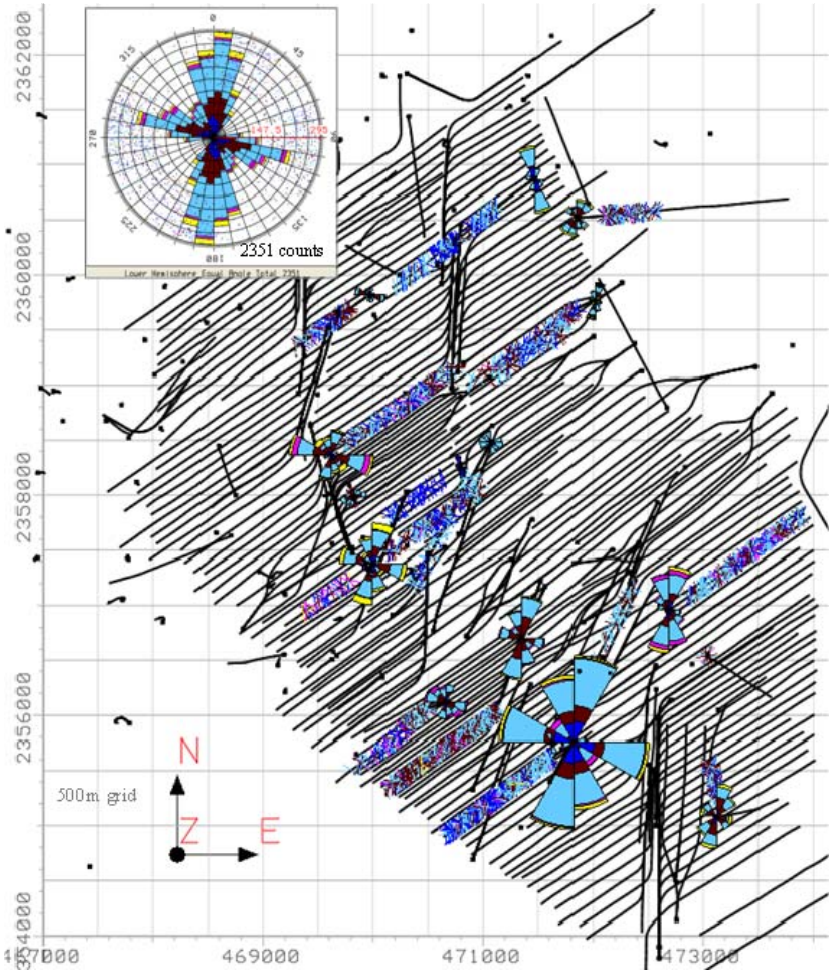


**Figure 3-82 Saih Rawl BHI fracture objects in map view a midst all the wells.**

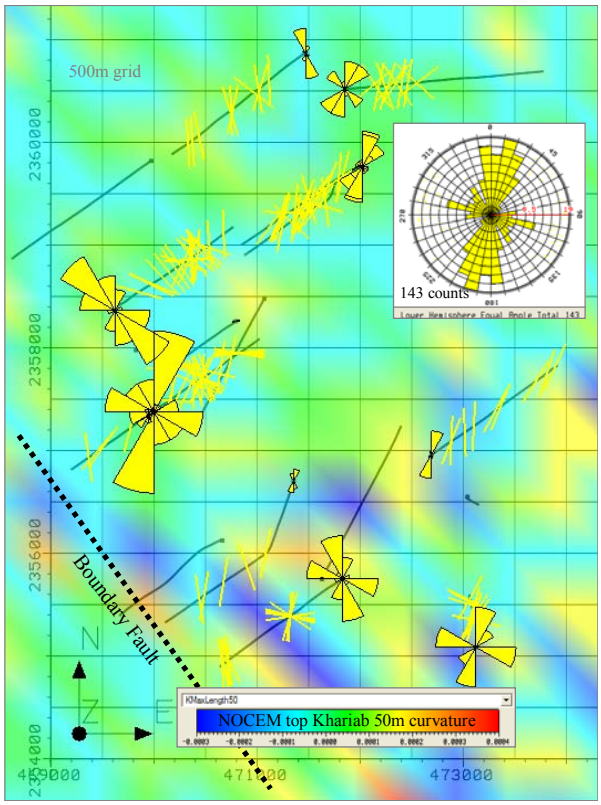


**Figure 3-83 Saih Rawl BHI fault superimposed on top of a 50m scale wavelength curvature map (Kmax) of the NOCEM regional top Kharaib. There is a hint of correlation, thus it would be useful to run another comparison between the two but using a detailed top Kharaib map.**

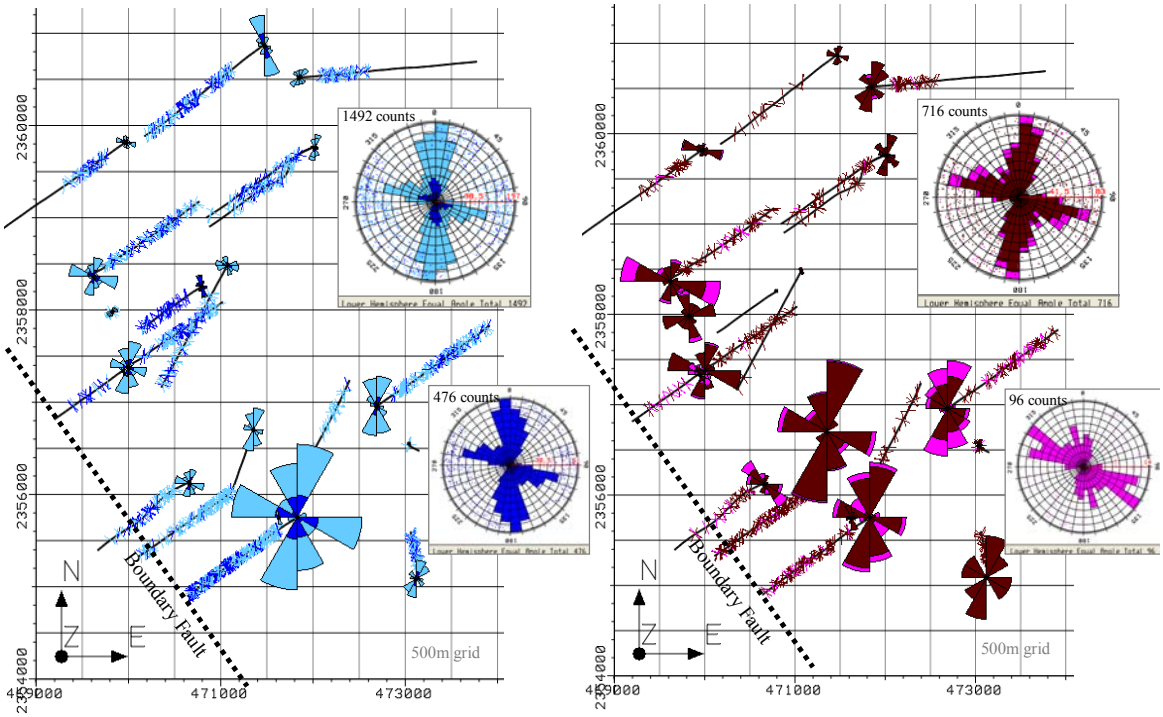


**Figure 3-84 Saih Rawl BHI fractures split into conductive (blue) and non-conductive (pink) note the large non-conductive (pink 96 counts) are striking NW in well close to the boundary fault.**

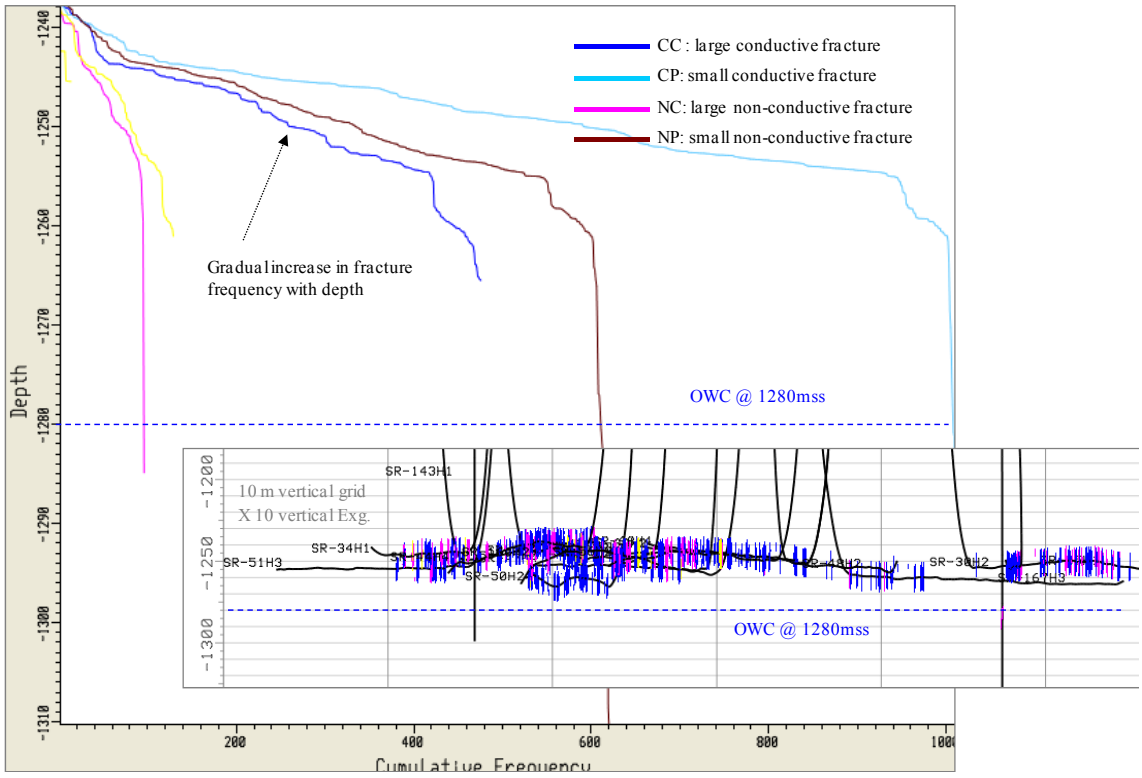


**Figure 3-85 Saih Rawl BHI fracture frequency plot with depth and cross section with BHI fracture along wells (small conductive fracture were not included as they overwhelm the data). It is hard to deduce any relationship due because the wells are confined to the top layer.**

### *3.2.8 Musallim field - Shuaiba Formation*

Musallim field is one of the matrix pancakes (though at a very large scale there are signs of clinoform indicating a depositional dip) in central Oman, located about 40 km NW of Saih Rawl. The field has a thin oil window and is situated in the Makarm High in between the Fahud and Ghaba north salt basins. The development pattern of the field is similar to that of Saih Rawl and Burhaan NW Shuaiba with multi-lateral producer–injector pairs, with ~120m areal separation and the water is injected in the water leg. The wells are drilled in NW direction sub-parallel to the fault orientation (Figure 3.86), however there is a concern that the wells may intersect open fractures – which may cause water short circuiting between producers and injectors – as they are perpendicular to the current regional maximum horizontal stress direction perceived to be running NE. MLM2 HST has two appraisal legs which were drilled in NE and NW direction, unfortunately, the BHI data for the NE well which crossed one of the major NW fault in the field is not available, though drilling information is available.

***Existing work***

Warrlich (Warrlich and Richard, 2004):

Wells with a low matrix porosity (Figure 3.86), have a higher density of fully conductive fractures (3 orientation sets) such as MLM4H2. Wells with high porosity have a lower density of full conductive fractures, e.g. MLM-2, -5. When crossing a major fault mapped on seismic, this type of wells waters out within a few months (MLM-9). Based on all the data a base case fracture model was defined with 3 orientations of background fractures: N, E and NE strikes; positive correlation between lower porosity and higher fracturing; and larger seismic faults creating short circuit between the aquifer and the reservoir. There are two set of faults NW and WNW, supported by stopper voxel "coherency" analysis on seismic volumes. When crossed by NE MLM2 leg #3, the NW set had a damaged zone of about 200m and the zone was cemented, high resistivity peak in the MWD (from Dhahab, 1998, PDO drilling report, Figure 3.87). The large non-conductive fractures are striking parallel to the main faults. The small BHI fractures are striking N, E and NE. The present day maximum horizontal in-situ stress in the field is NE-SW orientated, based on break-out trends seen in MLM-4H1, -5H1, -8H1 and MLD-1H1. Investigation of fracture patterns on a Petrel layer by layer basis shows no evidence for mechanical stratigraphy, based on the BHI data alone. However, the porosity decreases with depth, which may result in more intense fracturing in the lower part of the reservoir, which is not sampled by the horizontal wells located in the upper reservoir. Dominance of N35 background fracture set in the south and of N0/N90 in the north. A conceptual model with three sets of background fractures, a dependence of the fracture density of matrix porosity and an increased fracture density around conductive seismic faults is taken as the base case (Figure 3.88).

Ozkaya (Ozkaya, Swindells and Ghezai, 2004):

The Musallim Field has three main fracture types, similar to both the Saih Rawl and Burhaan Fields: (i) small dispersed fractures, (ii) large conductive (mega) fractures, and (iii) fault related fracture corridors. Fractures occur as conductive or non-conductive on resistivity image logs. Dispersed fractures have two dominant trends: N/S and E/W. E/W and WNW striking fractures are mostly non-conductive, and N/S fractures are mostly conductive suggesting a difference in age. Based on regional knowledge, it appears that faults and fault parallel E/W fractures formed first. The N/S and ENE fractures including the conductive fractures were generated later. The density-depth plots in some wells show that 1-2 m thick, highly fractured layers may be present within the Shuaiba reservoir in the Musallim Field. The vertical fracture permeability of these layers may reach 150mD (Figure 3.89). The height of dispersed fractures from borehole image logs is estimated to be 0.22 m based on geometrical/statistical analysis. Average fracture length is 1m. Stochastic models were created based on the above observations.

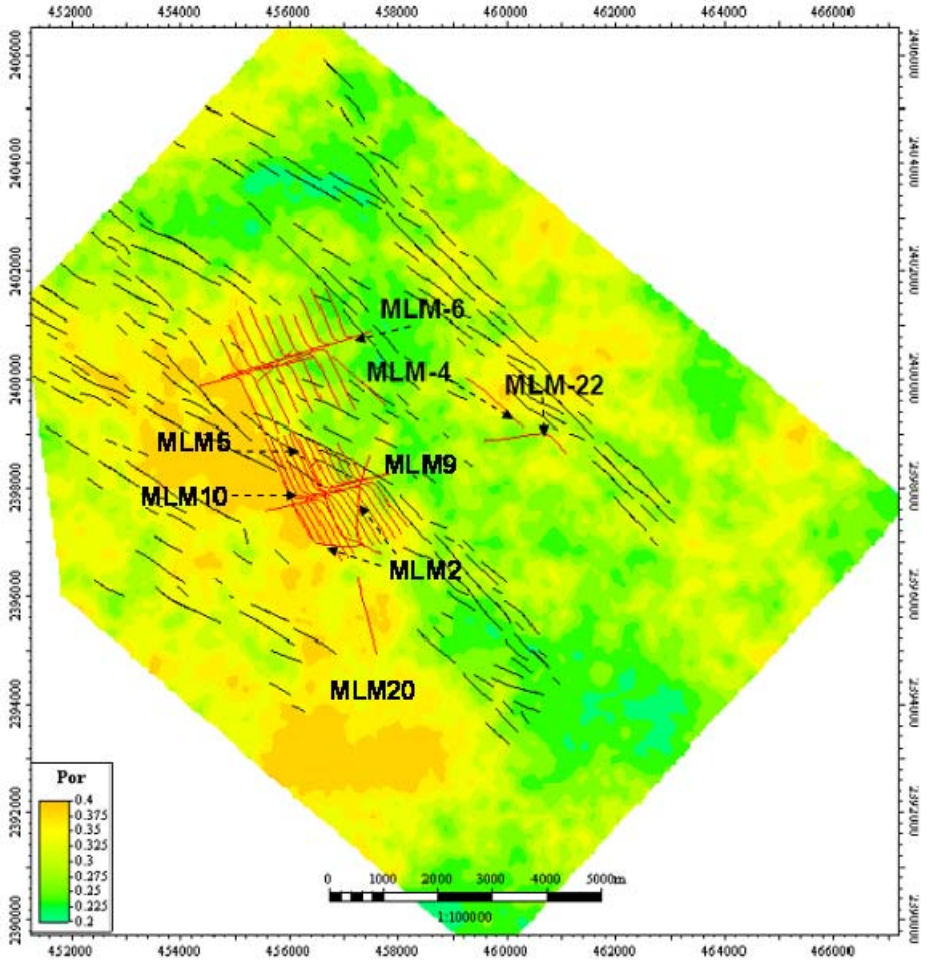


**Figure 3-86 Musallim Field, average porosity of the top 5m of Shuaiba reservoir, showing the NW-WNW faults (Warrlich and Richard, 2004). Note the location of MLM2 appraisal legs.**

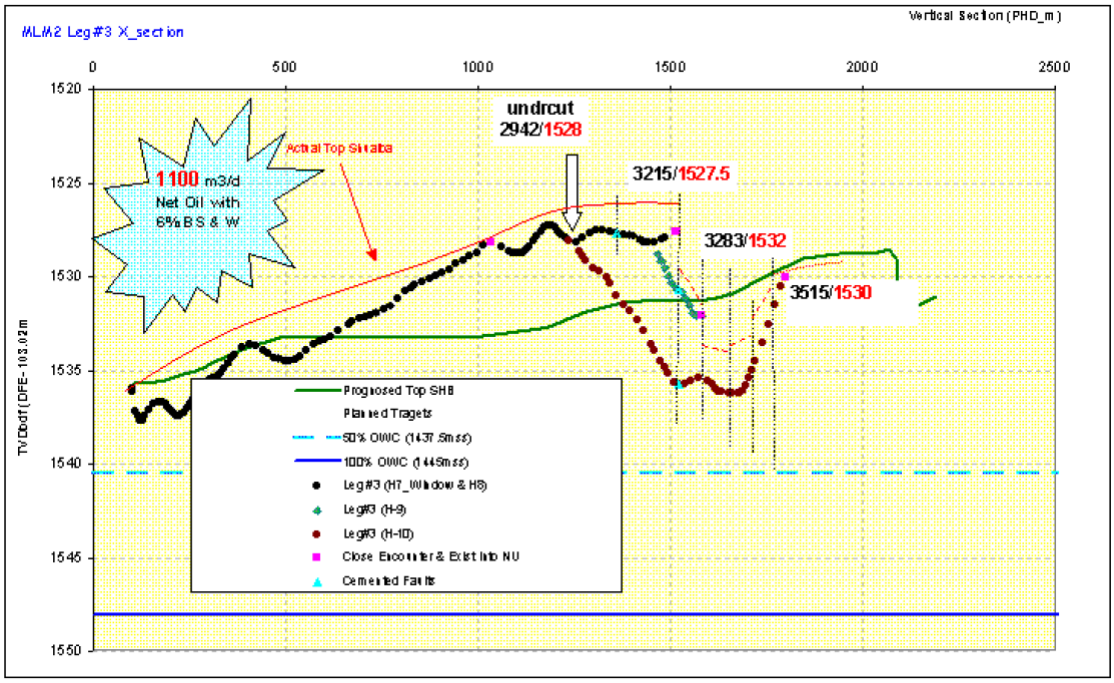


**Figure 3-87 MLM2 Leg # 3 running NE, see above figure, cut a main NW fault at its tail, dotted points indicate actual trajectory, dotted vertical lines >> interpreted fault zone (Dhahab, 1998). Cuttings and logs while drilling indicate that the fault zone is cemented.**

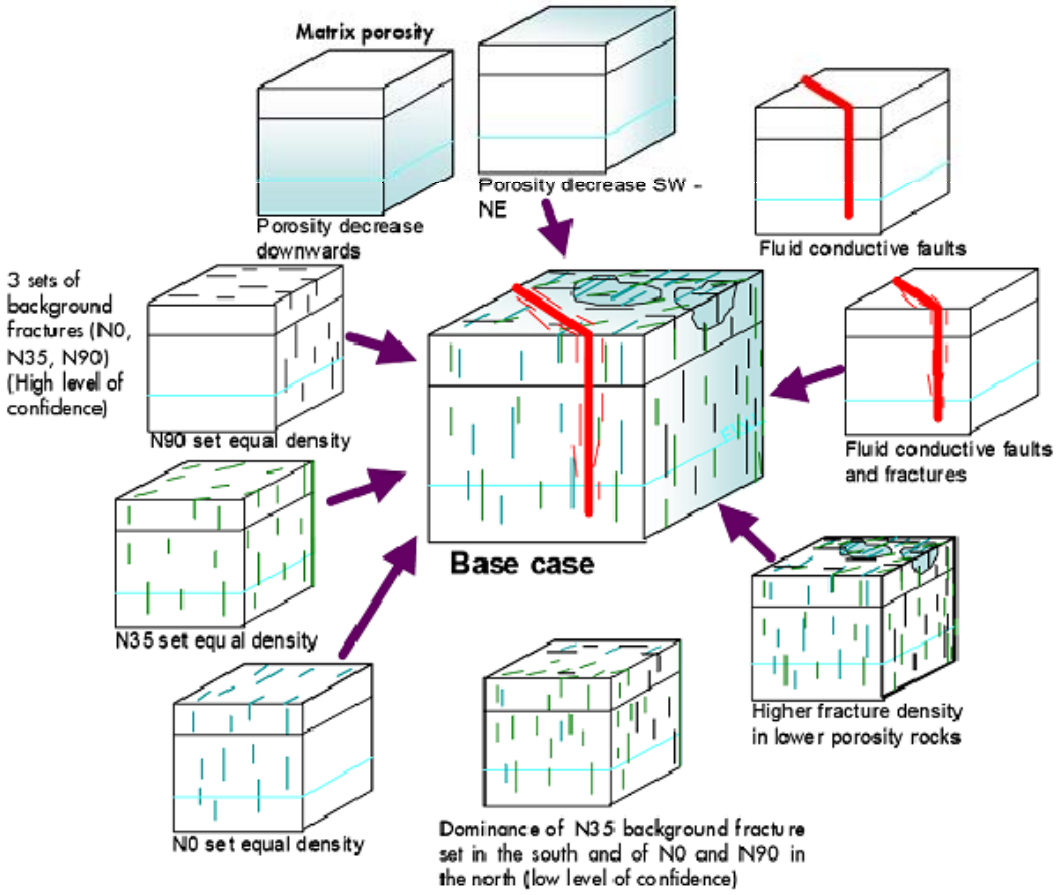


**Figure 3-88 Conceptual fracture model for Musallim Shuaiba (Warrlich and Richard, 2004).**

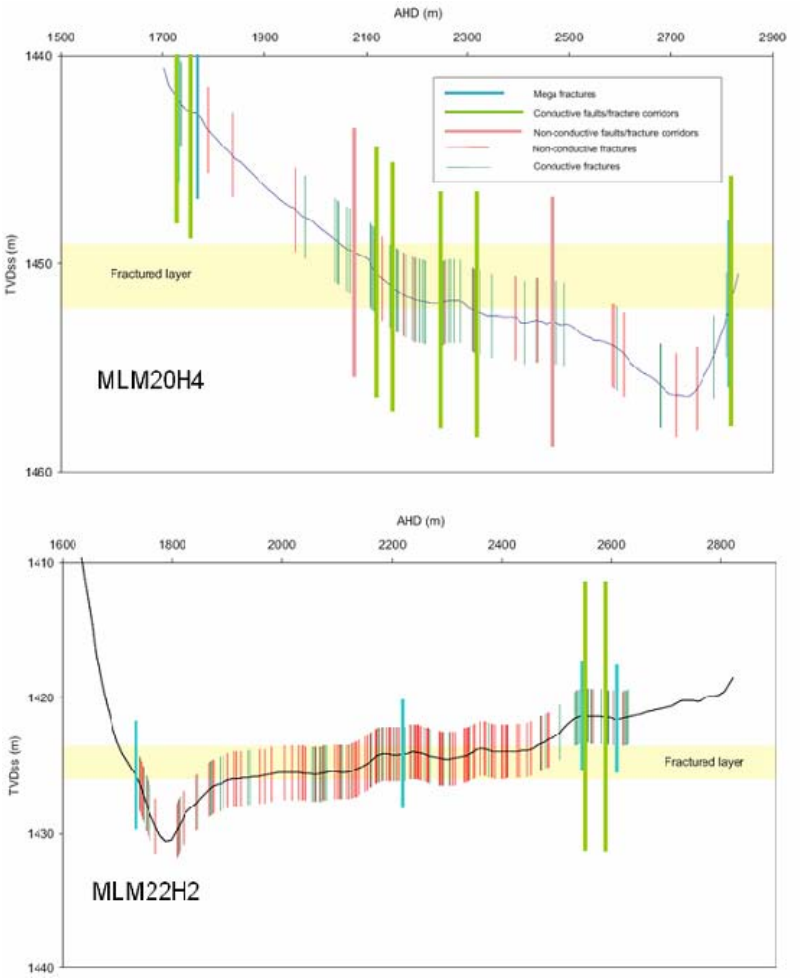


**Figure 3-89 Potential presence of a thin fractured layer in Musallim Shuaiba (Ozkaya et al, 2004).**

### *Musallim fracture data evaluation*

The geometric analysis below of the BHI data is aimed to draw conclusion regarding the regional fracture network and to validate the existing work presented above. The areal distribution of BHI coverage is not sufficient, northern area is not covered, also directionally and vertically biased as most well drilled in the upper part of the reservoir in aNW strike (Figure 3.90). BHI faults don't coincide with seismic faults or curvature grains in the field, and the only induced fracture found in MLM8 is striking NE (Figure 3.91). There is a variation in the areal distribution between the large conductive (blue) fractures and the large non-conductive (pink) fractures. For instance MLM4 is dominated by conductive features, while MLM22 by non-conductive. In addition, the dominant direction is NW for non-conductive and ENE for conductive (Figure 3.92). **This the only field so far where the large non-conductive fractures are more dominant than the large conductive BHI fractures** (see Figure 3.92). For the small conductive fracture (light blue) the N to NE is the dominant strike, whereas the small non conductive strike NW and N (Figure 3.93). BHI fractures cumulative frequency plot versus depth and cross section of the field show that: 1) there is a lack of sampling of the whole Shuaiba interval and 2) Possible hints to intense fracture zones, these could be tight layers but equally could be related to fracture corridors or sub-seismic faults seen as high curvature zones (Figure 3.94).

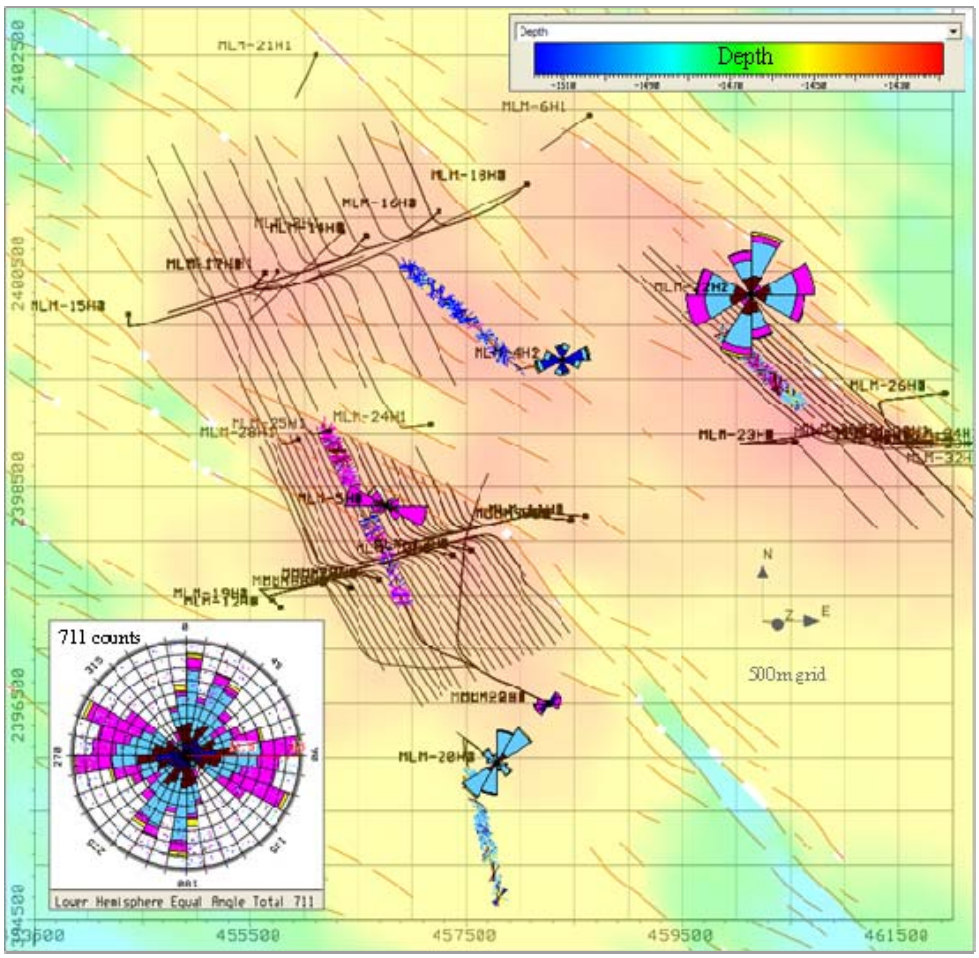


**Figure 3-90 Musallim Field BHI fracture picks superimposed on top Shuaiba map.**

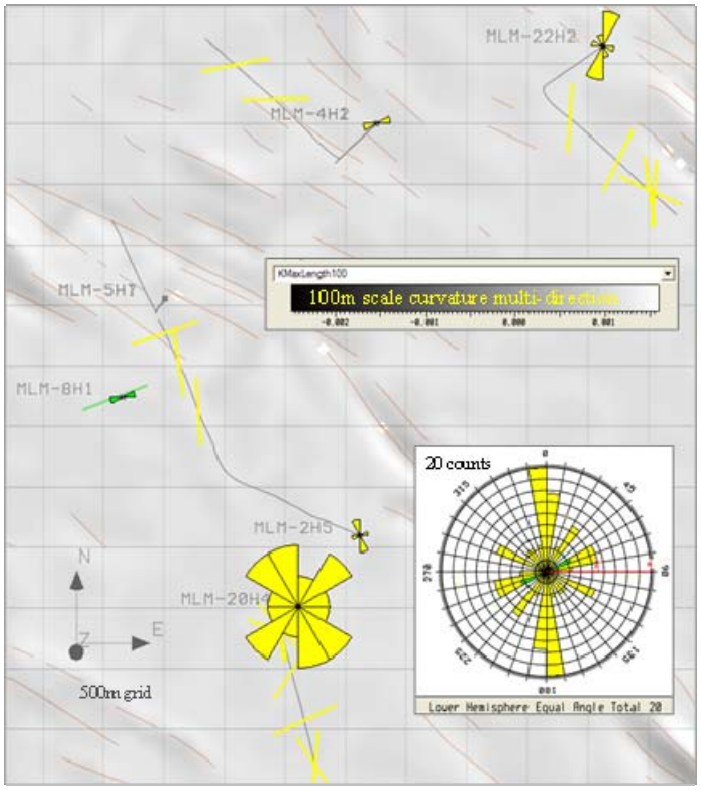


**Figure 3-91 BHI faults and induced fracture superimposed on curvature map (Kmax – with 100m scale wavelength) of top Shuaiba. See how the BHI faults do not coincide with seismic faults.**

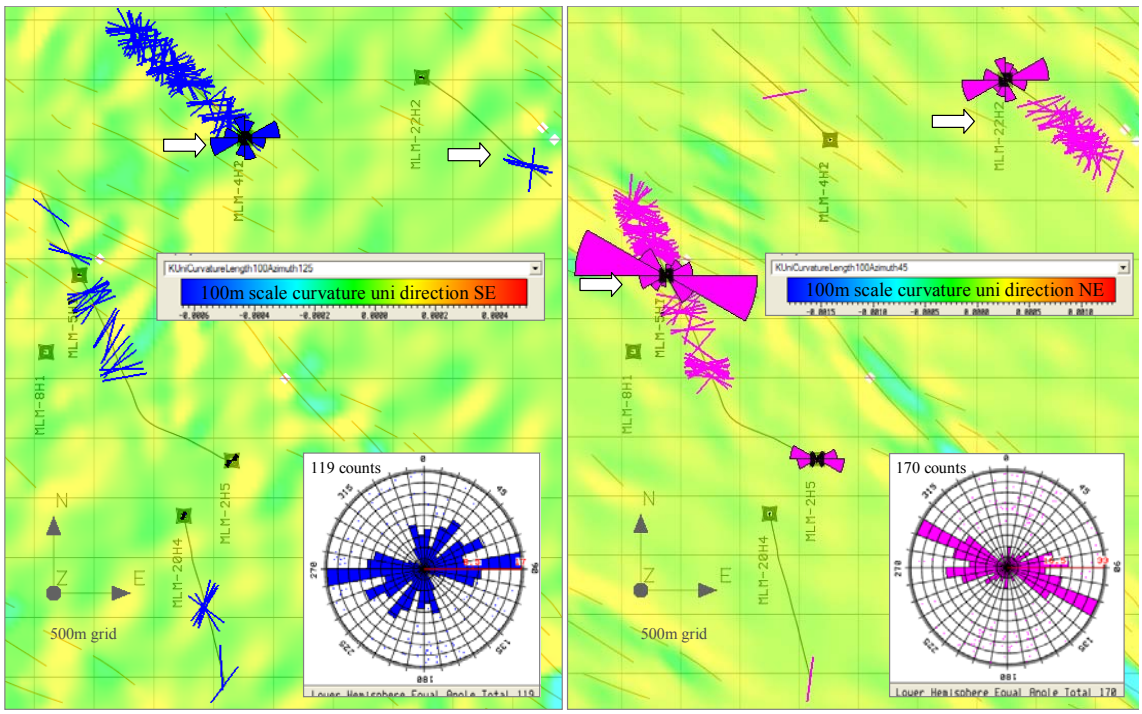


**Figure 3-92 large BHI fractures conductive (left) and non-conductive (right) superimposed on 100 m scale wavelength uni-directional curvature map (Kmax) of Shuaiba (SE Left, NE Right). Note how the varaiation in the fracture type & intensity from location to another.**

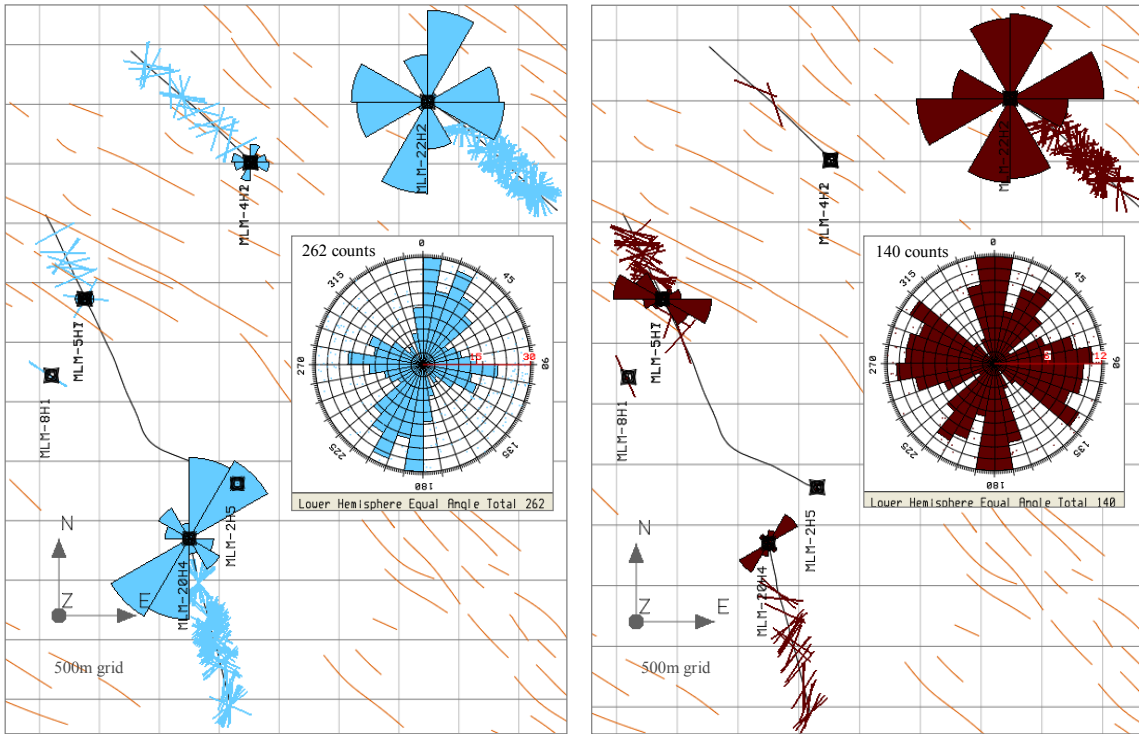


**Figure 3-93 small BHI fractures conductive (left) and small non- conductive (right) with faults.**

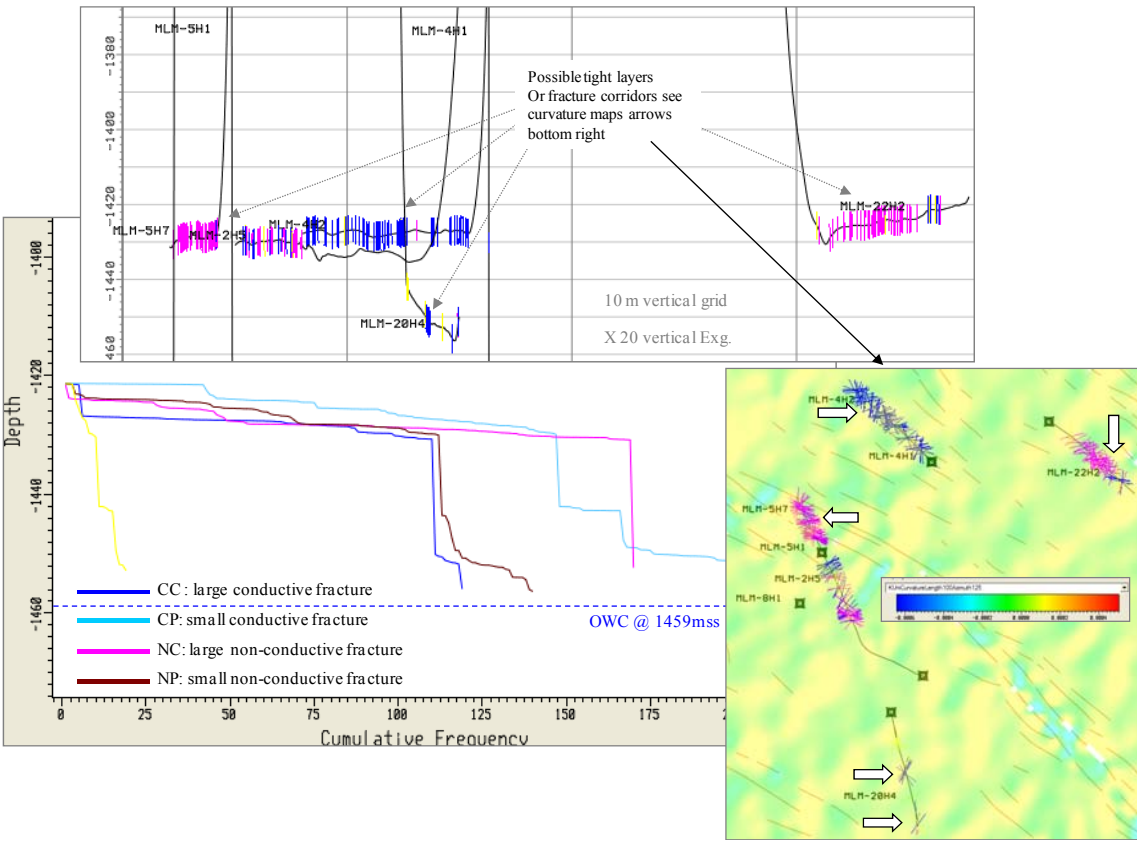


**Figure 3-94 BHI cumulative fracture frequency plot and cross section. Also (right down hand corner) map view of SE uni-curvature map (Kmax) of top Shuaiba, white arrow pointing to intense fracture zone based on BHI that coincide with the curvature grains.**

### *3.2.9 Al Huwaisah field - Shuaiba Formation*

Al Huwaisah field is one of the most mature and complex Cretaceous Shuaiba fields. It produces from the Shuaiba and its rock has been subjected to strong meteoric and burial diagenesis.

#### *Existing work*

Since the field is developed via water injection as a matrix reservoir, the presence of fractures can cause short circuiting and water break through. Hence, the asset team put up a mitigation plan to appraise the fracture network while producing, through collection of BHI data, PLT analysis and interventions with shut off when applicable. A recent study was carried out by Brown (Brown et al, 2002), with the fracture study part being done by Nelson. The following are main findings:

Al Huwaisah Field is heterogeneous and anisotropic due to both the fracture system and reservoir architecture. Al Huwaisah Shuaiba reservoir has a rich database of static descriptive data and a general lack of the dynamic quantitative data needed to define the flow properties of the reservoir. The basic fracture data for the field comes from image logs (primarily Formation Micro Image logs, FMI) run in 62 horizontal wells. A plot of the first 6,000 non-mineralized fractures analyzed shows a field-wide fracture trend of 50 degrees azimuth. This NE trend of the fractures was a surprise as seismic interpretation indicated mostly NW trending faults. In terms of fracture intensity, the

rudist grainstone had the greatest fracture intensity at an average of 0.19 fractures per meter of FMI log with the field-wide average for all rock types at 0.11 fractures per meter (Figure 3.95). Based on stress analysis from nearby field, the NE trending fractures are more open and more permeable than the NW set. A total of 141 fracture swarms were recorded in Al Huwaisah fracture dataset. A Fracture Intensity Height values were calculated and summed for each well and the wells ranked by their summed Fracture Intensity Height per Well to represent fracture permeability, as it is thought that the swarm "corridors" are the really conductive fracture in the reservoir. In order to correlate well performance to fracture, all the wells were grouped based on fracture frequency histogram splits in 7m bin size. Results indicate that horizontal wells drilled to the northwest had higher measured fracture intensities because they drilled across the dominant NE trending fractures (i.e. there is a calculation bias due to well trajectory orientation). Fracture intensity values were qualitatively correlated with losses data, PI index, production logs and well rate. Wells drilled later in the field did not experience as many drilling losses as earlier wells, probably due to reservoir depletion resulting in lower fracture permeability. Matrix-only wells can produce up to 70 % water and that fractures progressively increase the percent water produced to over 90%. Average cumulative liquid production for wells in which bedding strike and fracture strike are perpendicular is twice that of the wells in which bedding strike and fracture strike are parallel. In this field, few, if any fractures, are related to folding while the majority is related to normal faulting of seismic to sub-seismic scale. Based on a PLT log of AH-22H2 and using an equation from Joshi (Joshi, 1991) a fracture K of 1080mD was calculated. This $K_{frac}$ was applied in an equation from Nelson (Nelson, 2001) along with fracture spacing measured from FMI, which resulted in calculating an average apparent hydraulic fracture aperture (e) of 0.580 cm. This perceived to be a maximum value for aperture as the spacing was calculated from FMI (see more than 3 fold less than actual fracture in reservoir) and for a NE set. A Static Conceptual Model (SCM) for the fracture network of AH was created.

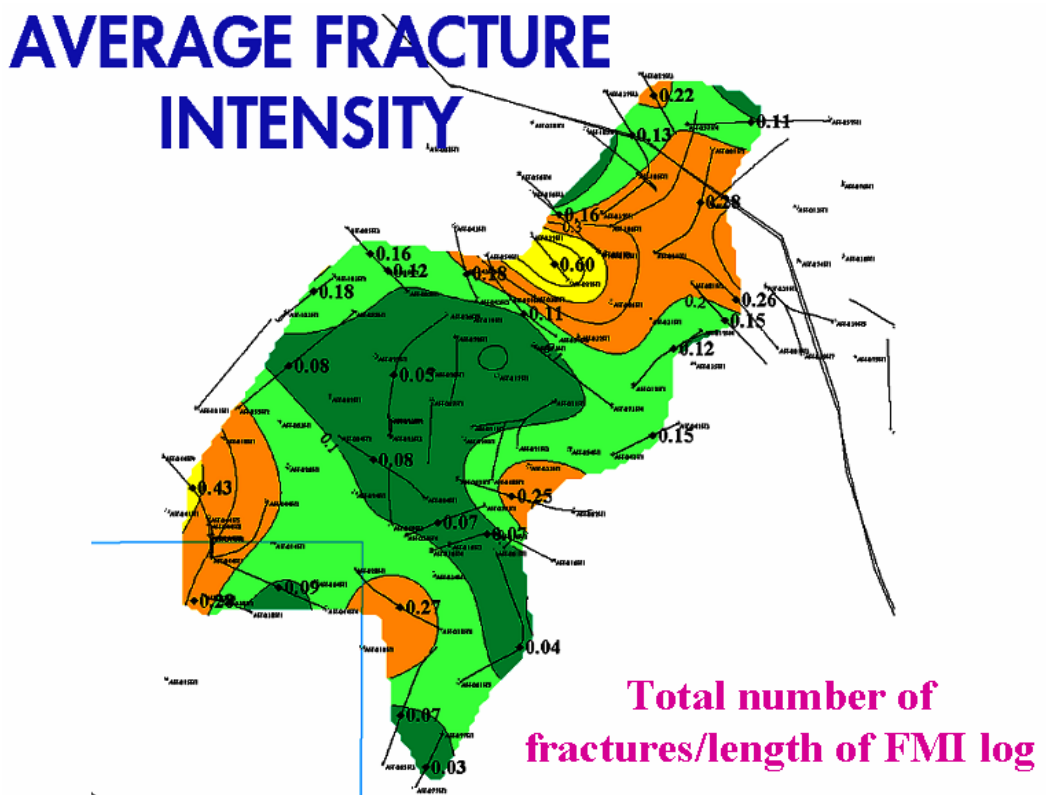


**Figure 3-95 Snap shot showing Average Fracture Intensity per well for Al Huwaish field (Nelson in Brown et al, 2002).**

### *Al Huwaisah fracture data evaluation*

Neither the Shuaiba field scale seismic faults, nor lithofacies or porosity maps are available electronically to be loaded to SVS. Hence, it is difficult to assess the impact of the fault on the fracture network seen in the field. The relationship between BHI fracture distribution and sediment porosity can NOT be assessed. The latter may well control fracture distribution as areally the sediment has different rock strength. Only BHI geometric analysis was done with the following findings:

The field is very large areally and the BHI coverage is good areally (Figure 3.96). No relationship seen between curvature at regional scale and BHI fractures. Over 85% of the BHI fractures are large conductive, mainly striking NE, though some wells shows NW strikes (grey arrow in Figure 3.97). Small conductive fractures show better the existence of a NW strike (Figure 3.98). Dominant BHI fault orientation is NE (Figure 3.99). The non-conductive fractures are mainly striking NE, though few wells shows a NW strike too (Figure 3.100). There is no indication of step changes in BHI fracture cumulative frequency plot versus depth, however, all the wells are within the very upper part of the reservoir, and thus mechanical layering cannot be ruled out (Figure 3.101).

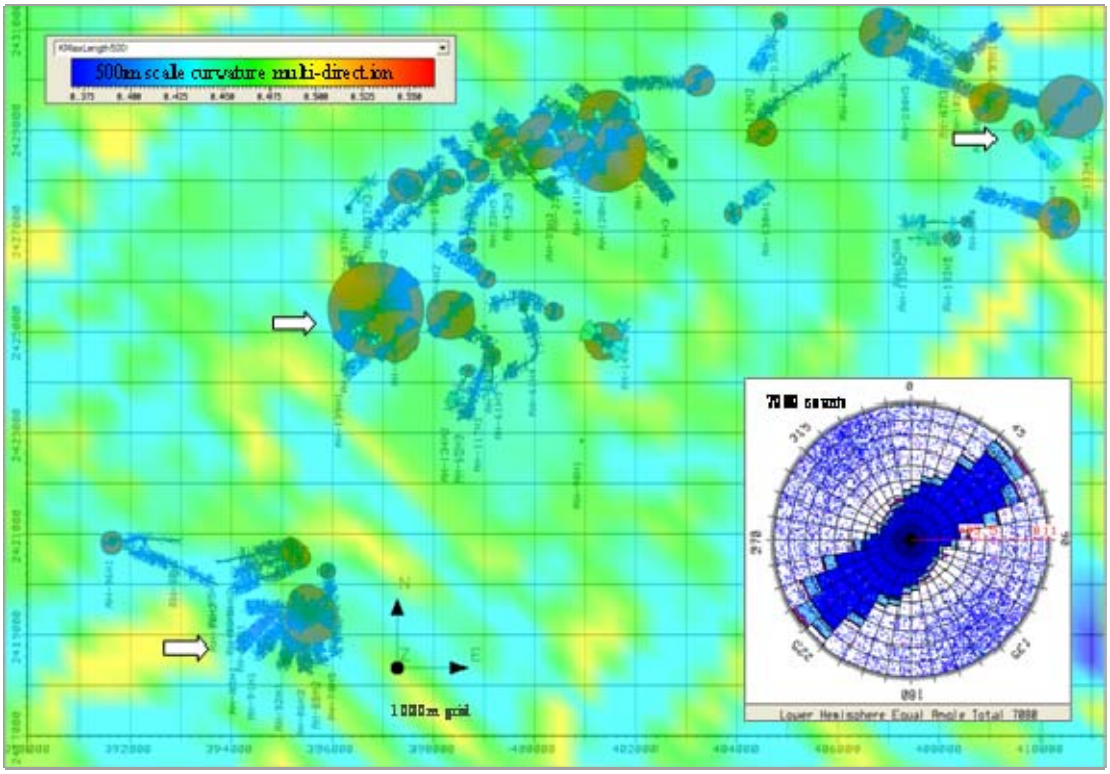


**3-96 Al Huwaisah all BHI fractures, red circles are total fracture counts per well, superimposed on top of a multi-direction - at 500m scale- wavelength - curvature map (Kmax) of the NOCEM regional top Kharaib. There is a slight hint of relationship, hence would recommend repeating this excersise but with the curvature map of a detailed –field scale- top reservoir.**

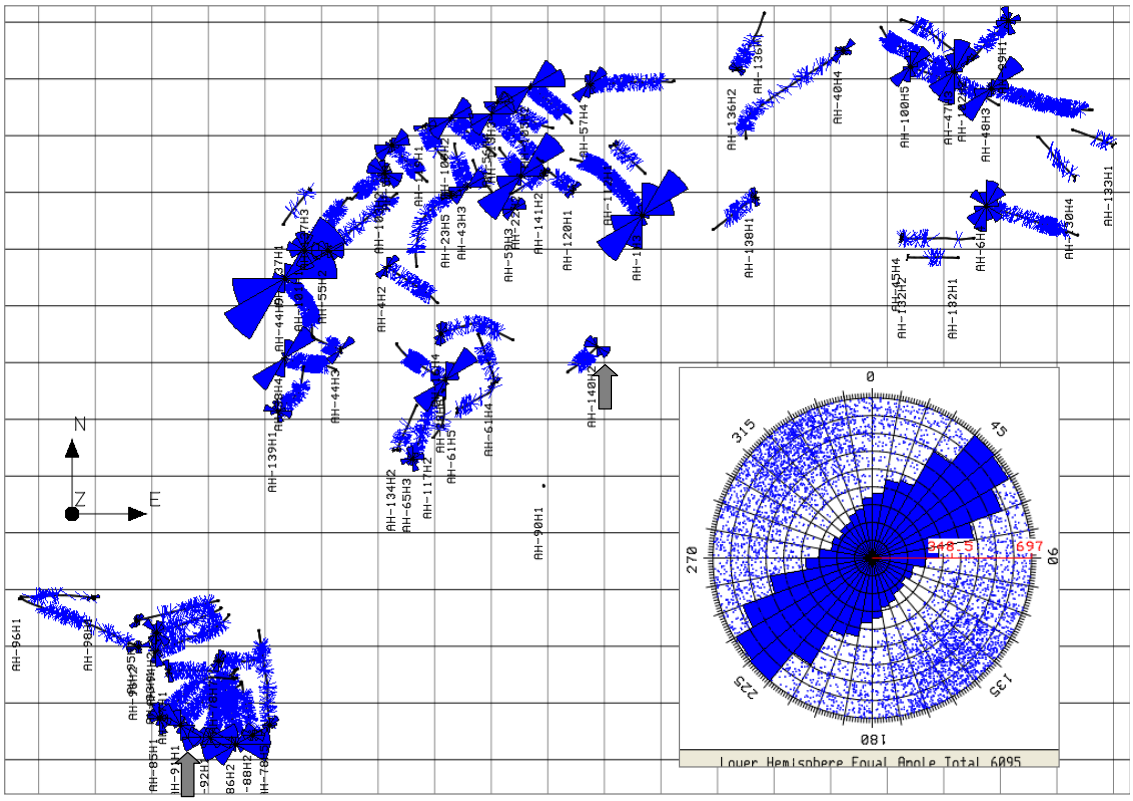


**Figure 3-97 Al Huwaisah large conductive fractures, grey arrow point to wells with NW strike.**

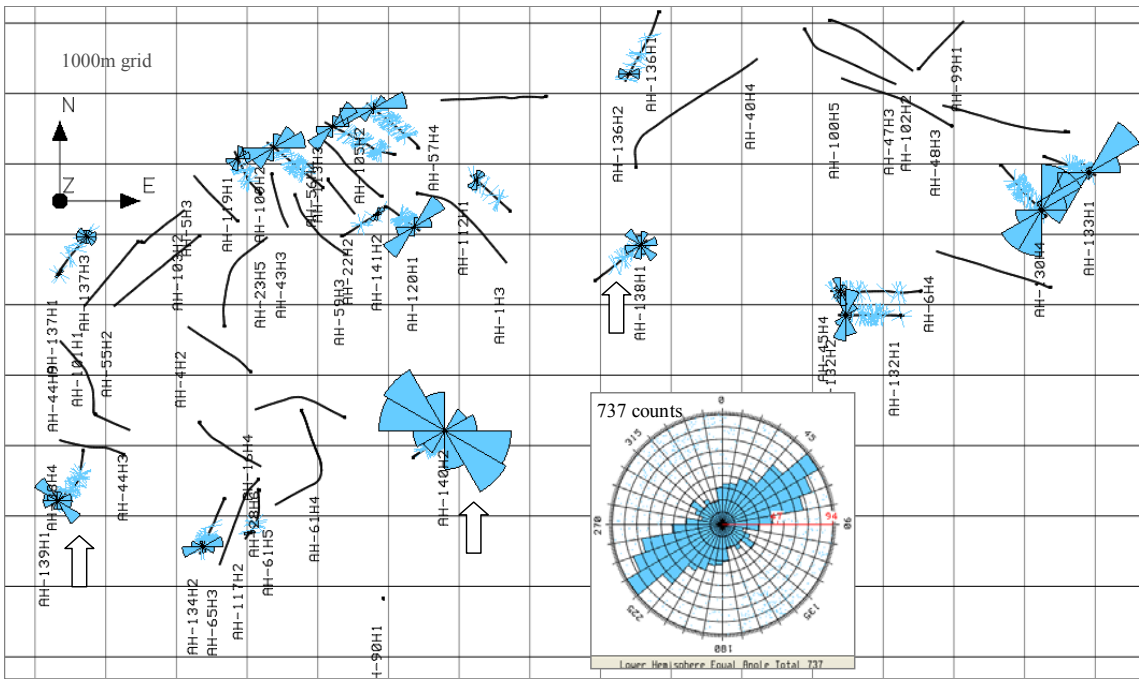


**Figure 3-98 Al Huwaisah small conductive BHI fracture, with a zoom in image at the northern part of the field as the south west wells have no small conductive BHI fractures.**

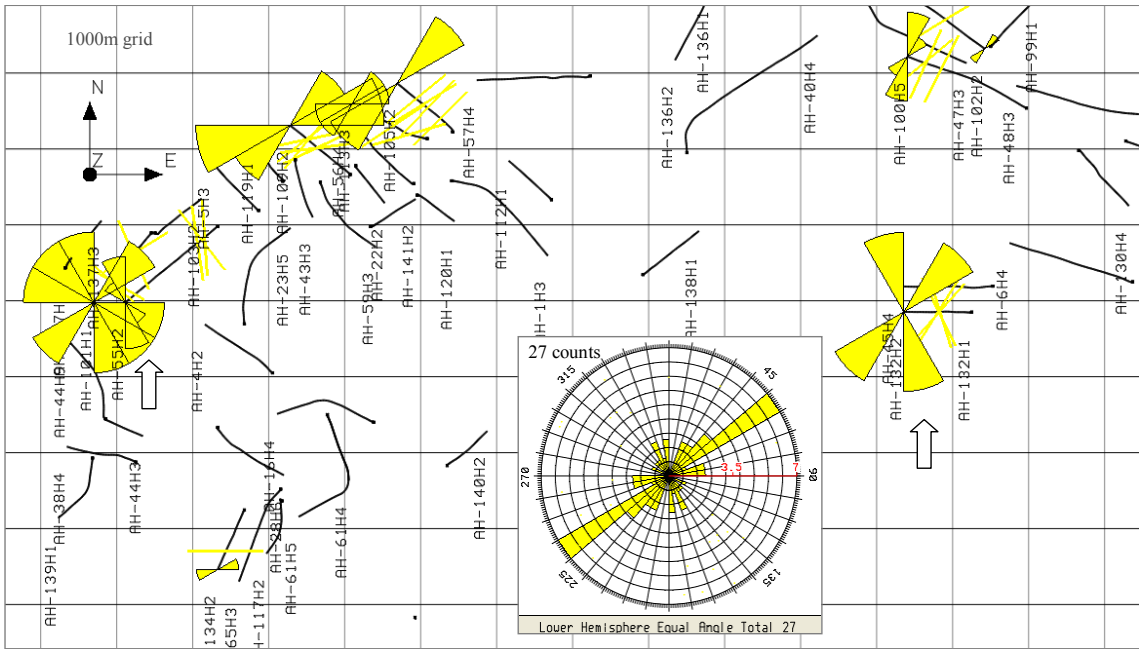


**Figure 3-99 Al Huwaisah BHI faults, the snapshot show a zoom in on the northern part of the field as the south west wells have no BHI faults picked in them.**

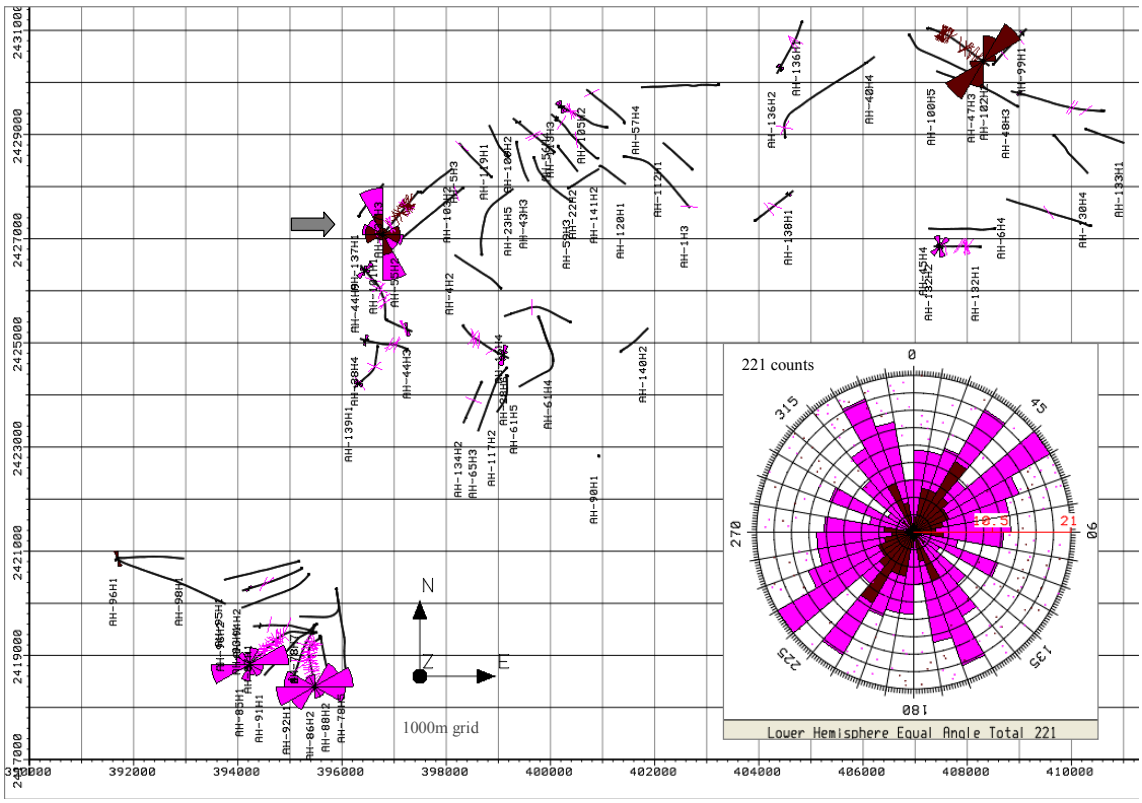


**Figure 3-100 Al Huwaisah large non-conductive fractures, grey arrow point to wells with NW strik fractures which are few compare to the dominant NE strike.**

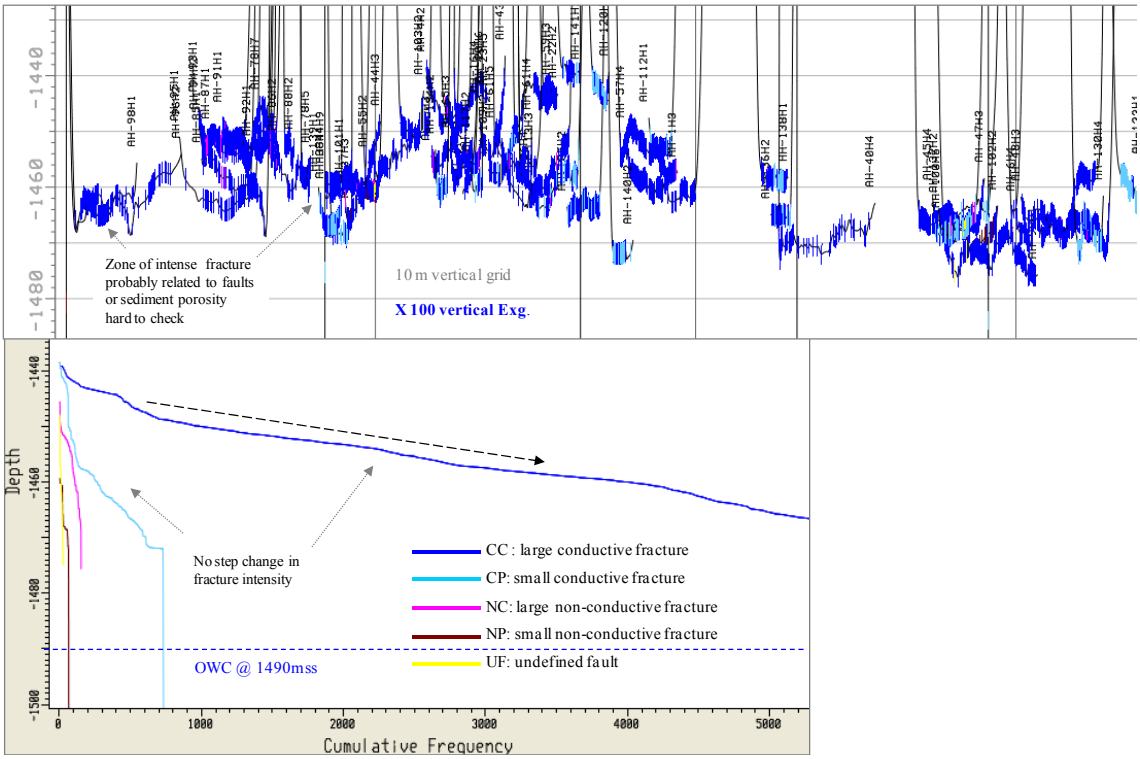


**Figure 3-101 Al Huwaisah BHI fracture cumulative frequency versus depth and cross section.**

### *3.2.10 Yibal field - Shuaiba Formation*

Yibal field is located about 50km southwest of Fahud field. Its structure is heavily faulted (Figure 3.102), low relief anticline with a productive area of 10 km long by 7 km wide. The field had incurred 4 development scenarios:

- 1969 to 1972 Primary depletion,
- 1972 to 1981 Injection in the oil leg,
- 1981 to 1993 Aquifer injection, and
- 1993 to 2000 Horizontal infill drilling.

Though the field recovery is the best recorded in Oman, recently the oil production is dropping down, thought to be due to the efficiency of the reservoir, the field is also suffering from pressure depletion (Figure 3.103). Fault and fracture played a negative role in the development of the field as they resulted in water fingering.

***Existing work***

The fault and fracture network of the field had been subjected to many detailed studies ranging from geo-mechanical to pure BHI geometrical fracture analysis.
Seismic stopper voxel (coherency) analysis had been applied on Yibal field by Koning (Koning, 2004) to test a work flow from seismic to Petrel. The report highlight the Shuaiba fault interpreted manually –based on well data and seismic and those derived from seismic Fault World$^{TM5}$ via stopper voxel (Figure 3.104). In addition, a similar analysis at a small scale, fracture scale was performed (Figure 3.105).

***How does Stopper voxel and Fault World work?***
*Stopper voxel is a mathematical seismic filter developed by Shell to highlight area of dissimilarities between consecutive seismic nodes, similar to coherency cube approach. These areas reflect discontinuities and could well be related to faults and fracture network or sudden depositional change in the sediment of a reservoir. Fault world allows the creation of surfaces out of these features, which if analysed geometrically (basically split into orientation) will help in picking out sub seismic features*

Detailed BHI fracture geometrical analysis had been done in the field by Muller (Mueller, 2001) (Figure 3.106) indicating that the majority of the fractures are striking NW and NE, though ENE and NNW had been also recorded. Stress direction is perceived to be striking NE to NNE.

Ozkaya (Ozkaya, 2003):
The field is characterized by an interconnected network made up of fault/fractures and high K matrix layers. Fractures occur as either layer bounded fractures (closely spaced average every 6m striking NW and NE with half of them being cemented) or in fracture corridors (related to faults with 1/3 of the fractures being cemented and the number of open fractures – spaced every 1.75m- correlate well with the length of the associated fault). Two high-K thief zones are known to exist, one at the top of the Shuaiba and the

other 30 meters below the top. They together with the conductive faults are responsible to water fingering.

A recent study has been undertaken internally by PDO (Richard and van Alebeek, May 2007) to understand the kinematics and structural evolution of Yibal field. This study highlighted the importance of three main phases of deformation: early salt halokinesis (Haima to Mafraq approximately); Late Cretaceous tectonic phase (transtension); and Late Tertiary tectonic phase (compression).

### *Yibal fracture data evaluation*

Unfortunately NO Yibal BHI data were available for this research. Thus, the only information available is that of Figure 3.106 and the summary of the findings of Ozkaya (Ozkaya, 2003).

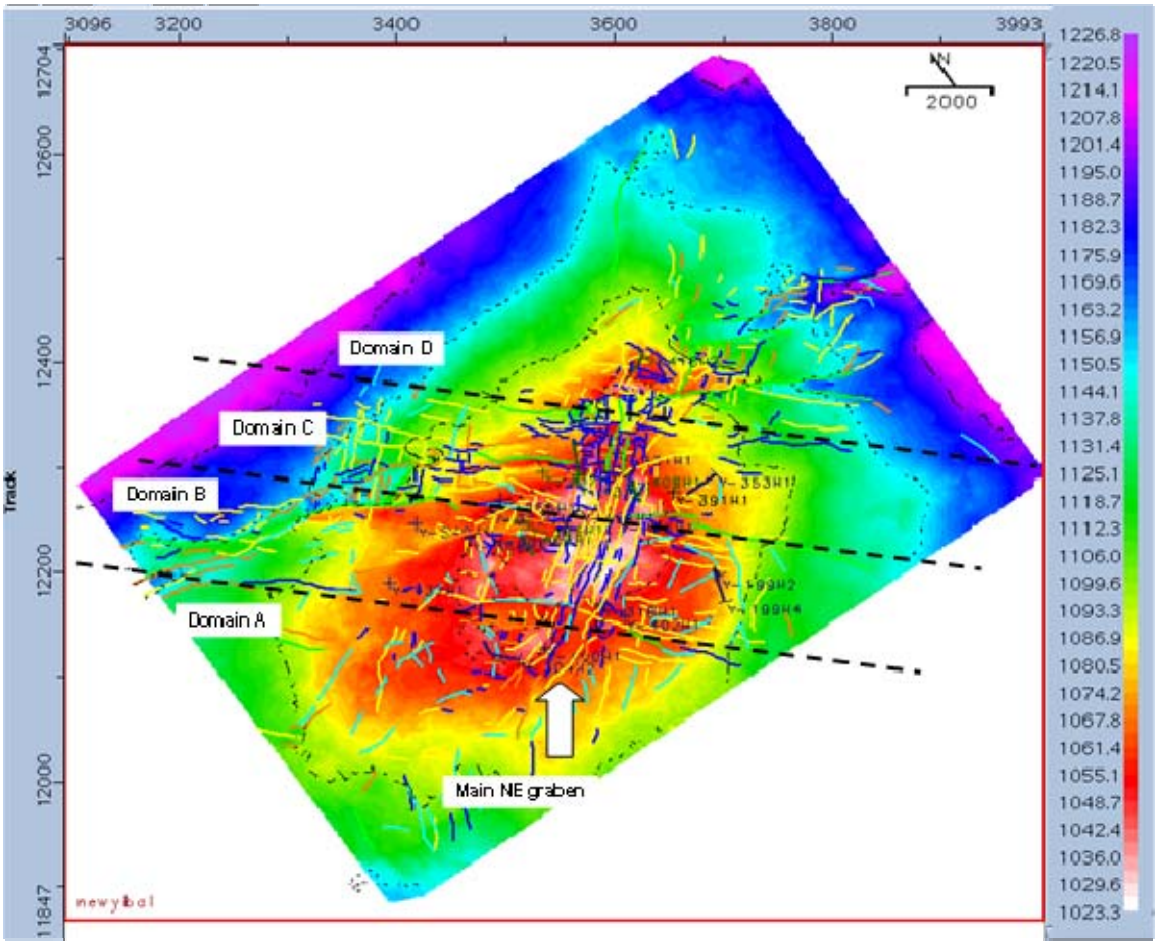


**Figure 3-102 Seismic map of top Shuaiba, Yibal field. Dominated by NW faults cutting the field into 4 possible domains. The field is split by a NE graben (modified from PDO internal report).**

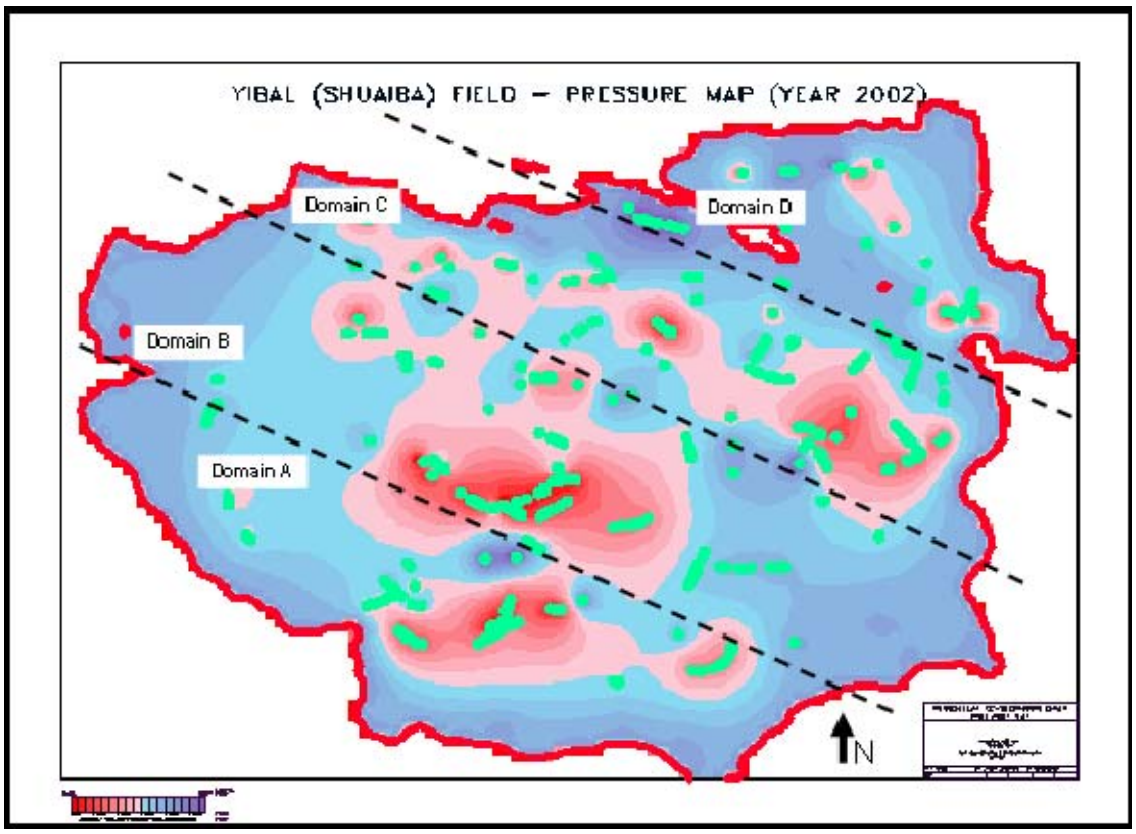


**Figure 3-103 Pressure depletion (red high, blue low) in Yibal field, modified (annotated with the potential domains division compare to the figure above) from PDO field strategy note.**

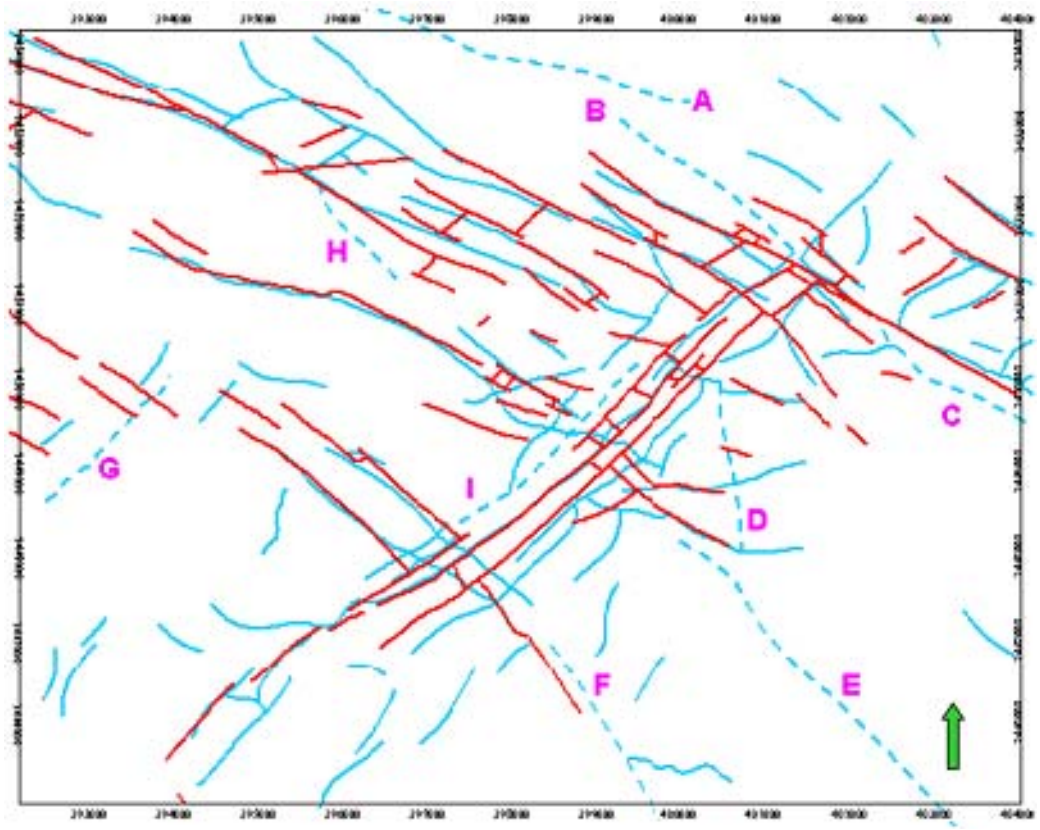


**Figure 3-104 Fault map of Top Shuaiba. Red lines: manually interpreted faults, based on seismic and on well data. Blue lines: Faults obtained via the FaultWorld procedure. Dotted blue lines: differ from manual interpretation annotated with letters A to H (Koning, 2004).**

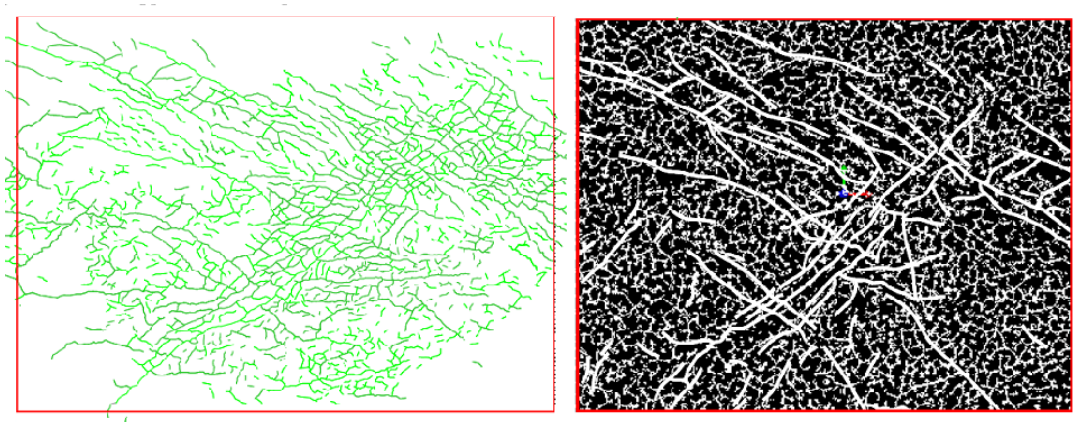

**Figure 3-105 Fracture "subseismic features" patterns on Top Shuaiba. Left) hand picked fractures, right) FaultWorld approach. Also the Petrel faults –long lines- are shown as well (Koning, 2004).**

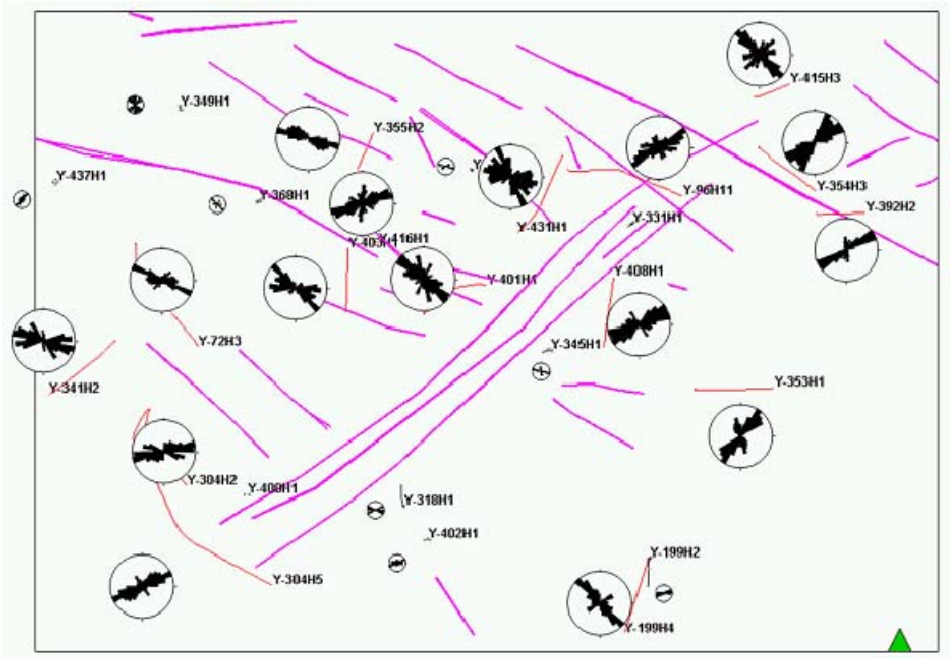


**Figure 3-106 Yibal top Shuaiba map with rose diagram of BHI fractures, superimposed on fault traces (pink) (from Mueller, PDO report, 2001).**

### *3.2.11 Dhulaima field - Shuaiba Formation*

Dhulaima field is regarded as part of the Lekhwair cluster of matrix reservoirs as it is located south of Lekhwair (Figure 3.107). This field is one of the largest fields in areal dimension; however it has a thin oil rim in both upper and lower Shuaiba. The field is characterized with NW and WNW faults, the regional fish net seen in north Oman all most evident in seismic around Mussalim area (Figure 3.108).

The main reservoir is the Lower Shuaiba. An oil bearing zone was encountered in the Upper Shuaiba in the Dhulaima C structure with DM-07. A small scale water flood pilot involving wells DM-08, DM-09 and DM-10 was not able to demonstrate an economically viable development. A direct short circuit between water injector DM-09 and producer DM-08 was evident. DM-09 was kept on injection to support producer DM-10, which continued to produce albeit at low rates (<70m3/d). The low rates are thought to be indicative of a matrix rather than fracture producer.

***Existing work***

A BHI statistical analysis of the Lower Shuaiba "the main reservoir" had been carried out in 2004 by Dhulaima subsurface team. It showed that the majority of the fractures are striking NW (Figure 3.109).

Nelson (Nelson, 2004):

This was a detailed fracture network characterization for the whole of the Lekhwair cluster including Dhulaima. A summary with the main findings related to Dhulaima is presented hereafter. The study was based on BHI and core fracture description. A statistical analysis was presented for the fractures showing fracture intensity. The Dhulaima data set consists of 9 FMI logs; 5 in or near area A, 1 in area B, and 3 in area C. The wells in area C sample the Upper Shuaiba while the wells in area A and B sample the Lower Shuaiba. Over all the combined orientations show both NW-SE and NE-SW trends (Figure 3.110). Dhulaima is the least fractured of the Lekhwair/Dhulaima areas but also the least cemented of the major productive areas. Comparison with the other field in the cluster is presented with respect to fracture orientation (Figure 3.111) and intensity per fracture type per layer (Figure 3.112). When observed in common wellbores, Upper Shuaiba & Lower Shuaiba displays common fracture orientations. Significant fracturing occurs in swarms "corridors" that have affected production rates and bottom/edge injection water movement. There is a change in fracture orientation and intensity across the Cluster Area, decreasing in intensity and rotating from NW-SE to NE-SW from west to east. In general, there is no apparent seal between the Upper Shuaiba & Lower Shuaiba reservoirs in the Cluster Area. Locally, they appear in communication through fractures.

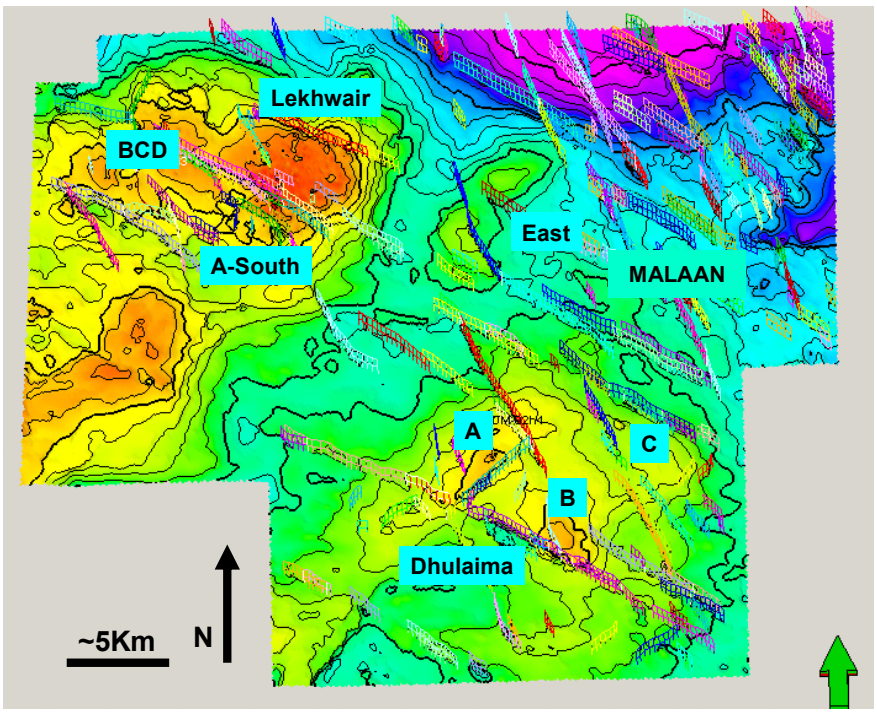


**Figure 3-107 Lekhwair matrix cluster fields locations (Dhulaima Team, PDO report, 2004).**

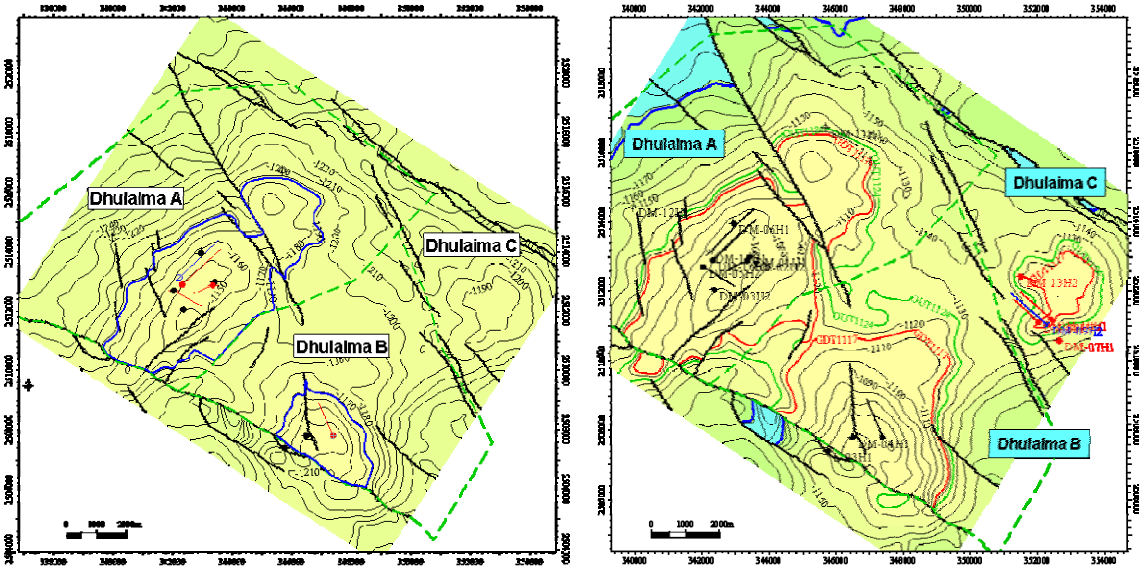


**Figure 3-108 Dhulaima structural map for top Lower Shuaiba (left) and top Upper Shuaiba (right), split into three areas A, B and C (Dhulaima team, PDO field strategy note, 2005).**

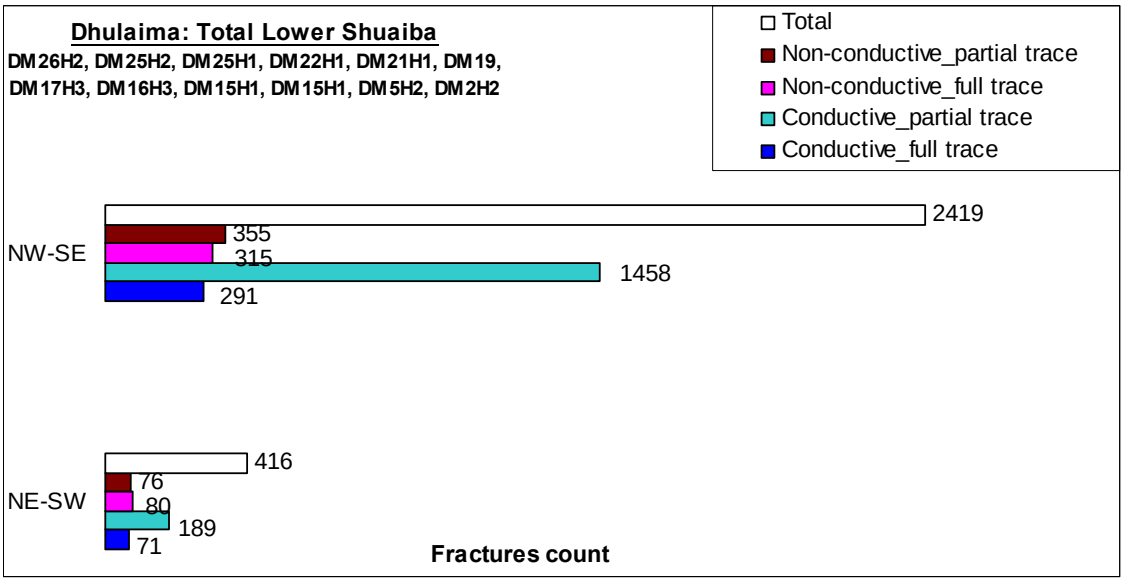


**Figure 3-109 Dhulaima Lower Shuaiba BHI fracture statistical analysis, from PDO internal report. From the well number it seems that this analysis postpone that of Nelson see the figure below.**

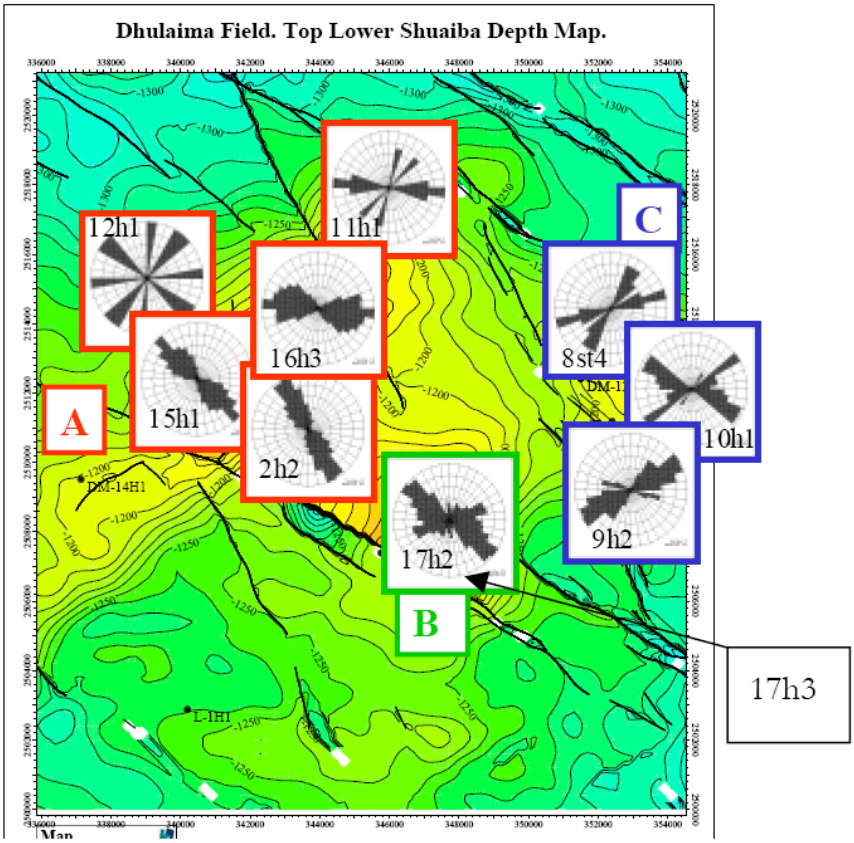


**Figure 3-110 BHI fracture orientation in Dhulaima areas A-red, B-green and C-blue, with well names (Nelson, 2004).**

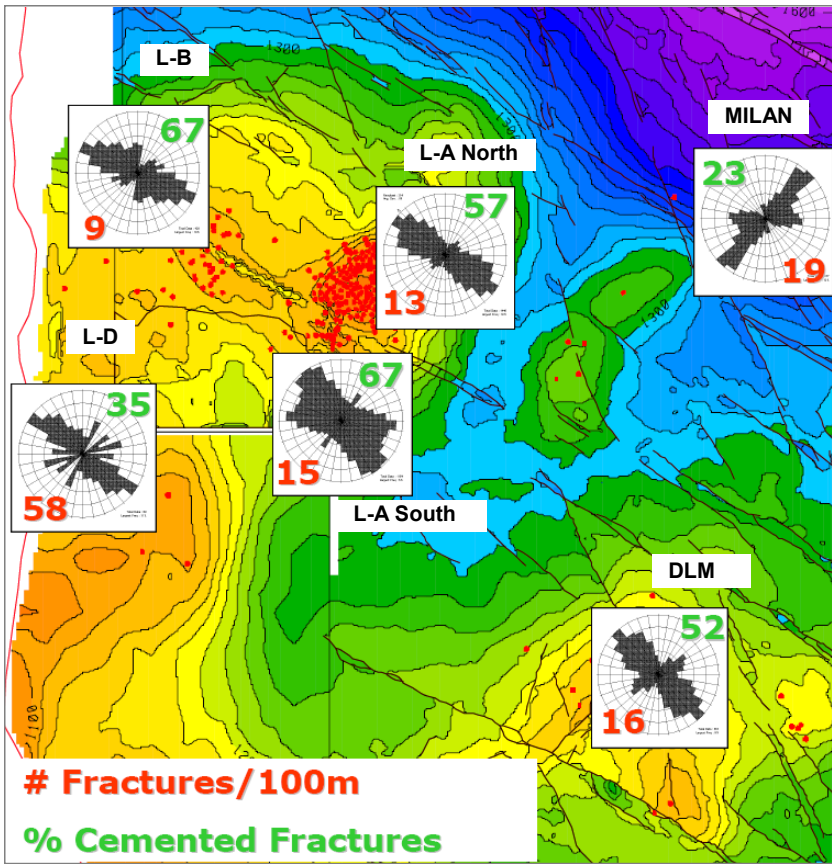


**Figure 3-111 Lekhwair cluster BHI fracture strike orientation and intensity per field for both upper and Lower Shuaiba reservoirs (Nelson, 2004).**

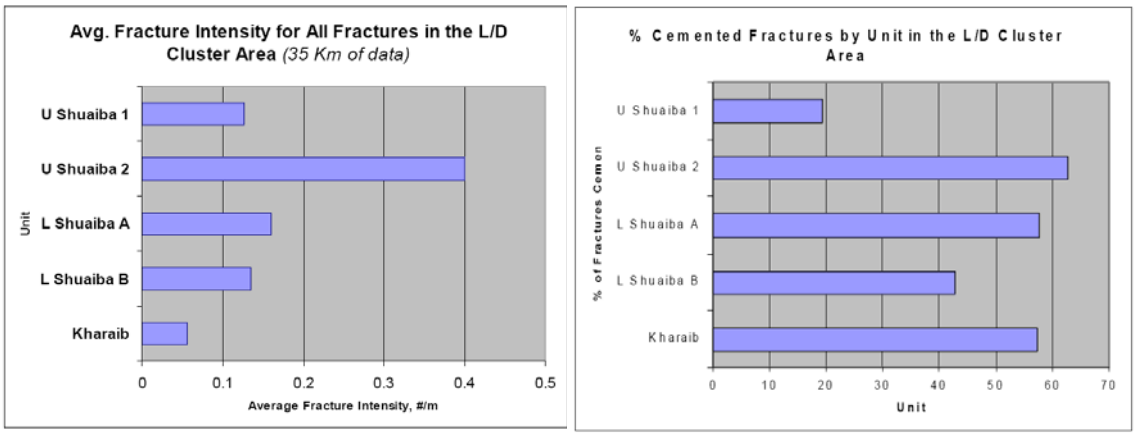


**Figure 3-112 Average fracture intensity of BHI fracture data in Lekhwair cluster per reservoir unit (Nelson, 2004).**

### *Dhulaima fracture data evaluation*

The Nelson report (Nelson, 2004) is quite comprehensive with regard to the analysis of BHI fractures in the Lekhwair cluster. Hence, the objective here is to only extract regional learning from BHI geometrical analysis and to validate the above existing work in light of the new added data. The main findings are as follow: Mechanical layering is not tested here I could not split the BHI picks per reservoir unit. Dominant fractures are striking NW, even in areas where teh wells are drilled in NW direction (e.g C area). The well trajectory of DM17H3 is sub-parallel to NW and yet lots of fractures were picked striking NW (Figure 3.113). Locally there are some variations in fracture strike direcation (e.g.NE fracture strike are seen in area C and even in area A). There seems to be a slight correlation between the regional NOCEM top Kharaib uni curvature map and the BHI fracture count seen in the field (Figure 3.114), this needs to be further refined using a local top structure map. BHI faults are running parallel to the regional faults, the "fish net" NW and WNW set seen in the Mussalim area (Figure 3.115). Only two induced fractures are picked in the BHI/FMI logs (although termed borehole breakout they are annotated with CT abbreviation for induced fractures) in DM26H1 and their strike is NE and NW at similar depth. These picks will need further review to be confirmed. The conductive BHI fractures are striking NW and WNW but mainly small in size (low confidence conductive instead of large conductive). A NE strike small conductive fracture is seen in DM5H2 (Figure 3.116). There are more of the large non-conductive BHI fractures than large conductive fractures (Figure 3.117), again most of the non-conductive are striking NW. BHI fracture frequency plot indicate that there is step change in fracture intensity with depth. When plotting BHI fracture in cross section view there is NO trend of increasing non-conductive fracture with depth (Figure 3.118).

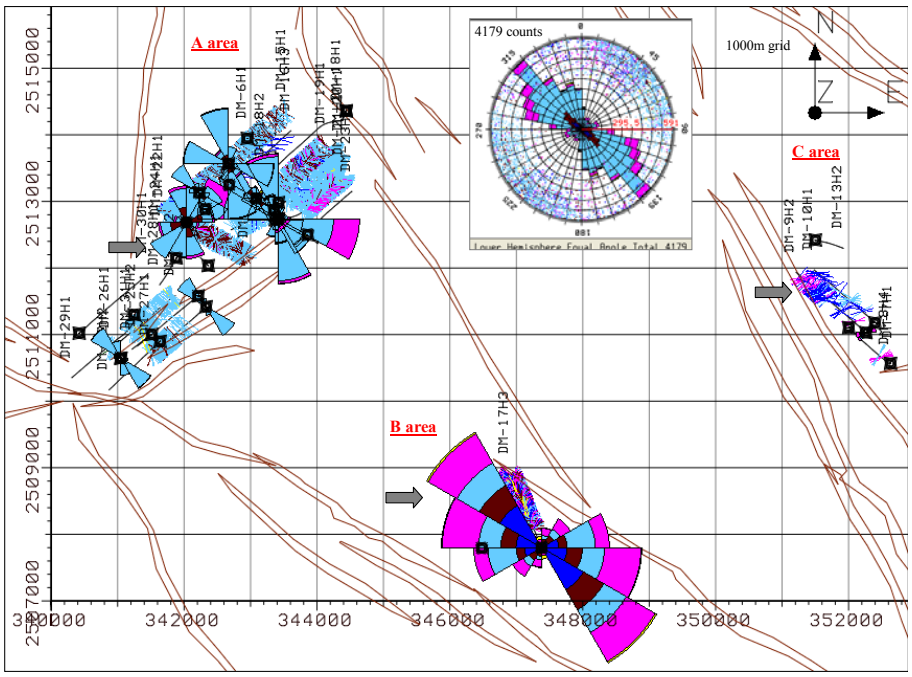


**Figure 3-113 BHI fractures of Dhulaima with regional faults, grey arrows are pointing to change in fracture strike direction from one area to another.**

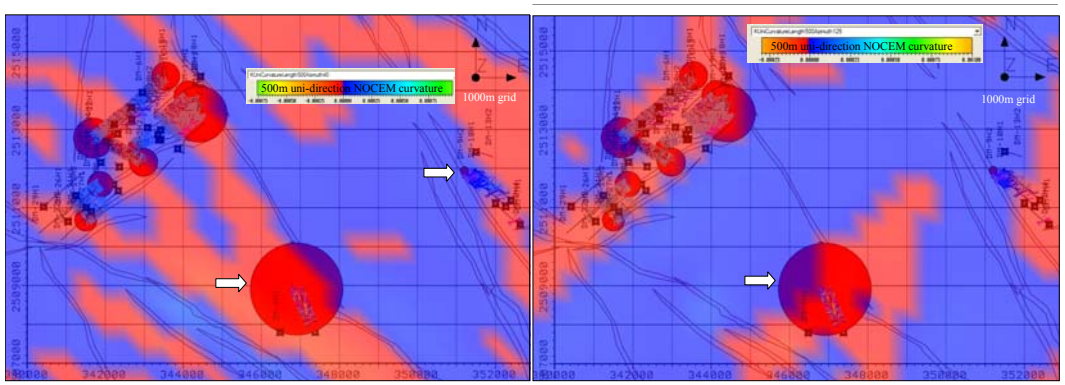


**Figure 3-114 BHI total fracture count per well (red circles) superimposed on uni-direction curvature maps (Kmax) at 500m scale wavelength of NOCEM top Kharaib (left NE and right SE oriented uni-directional curvature map), showing slight correlation with BHI fracture intensity.**

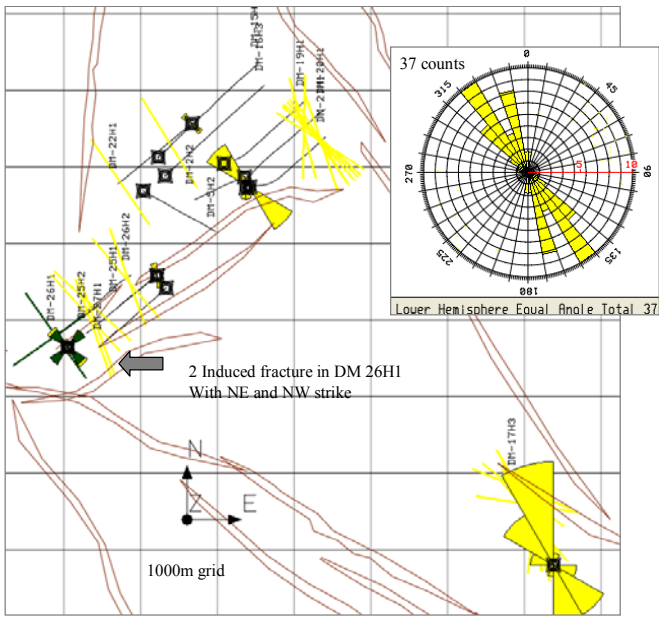


**Figure 3-115 BHI faults (yellow) and induced fractures (green) of Dhulaima, zoomed in at area A & B, as no record of BHI fault is found in area C.**

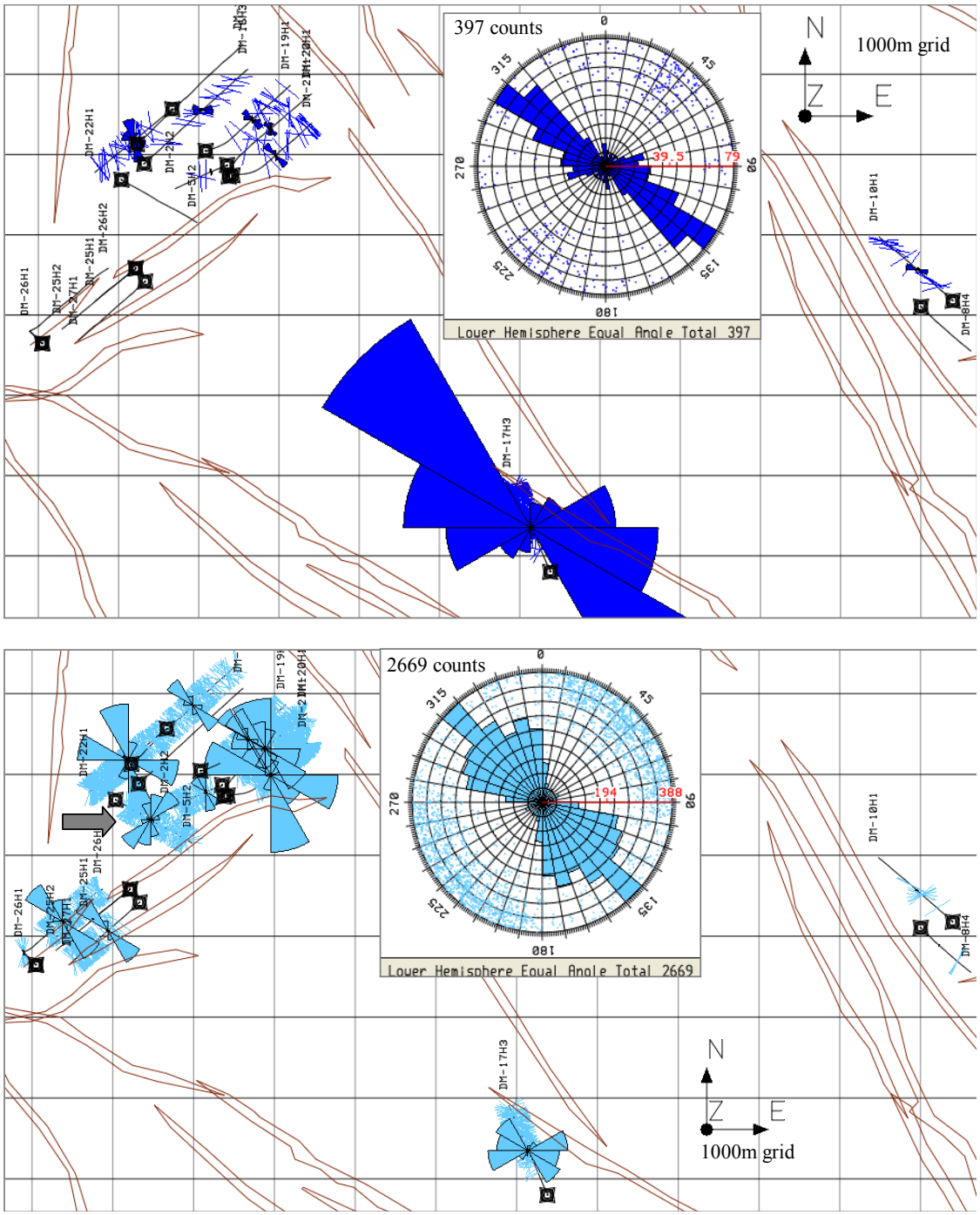


**3-116 Large conductive BHI fractures (dark blue) and small conductive fractures (light blue) with rose diagram in Dhulaima field. Grey arrow points toward wells with NE striking fractures**

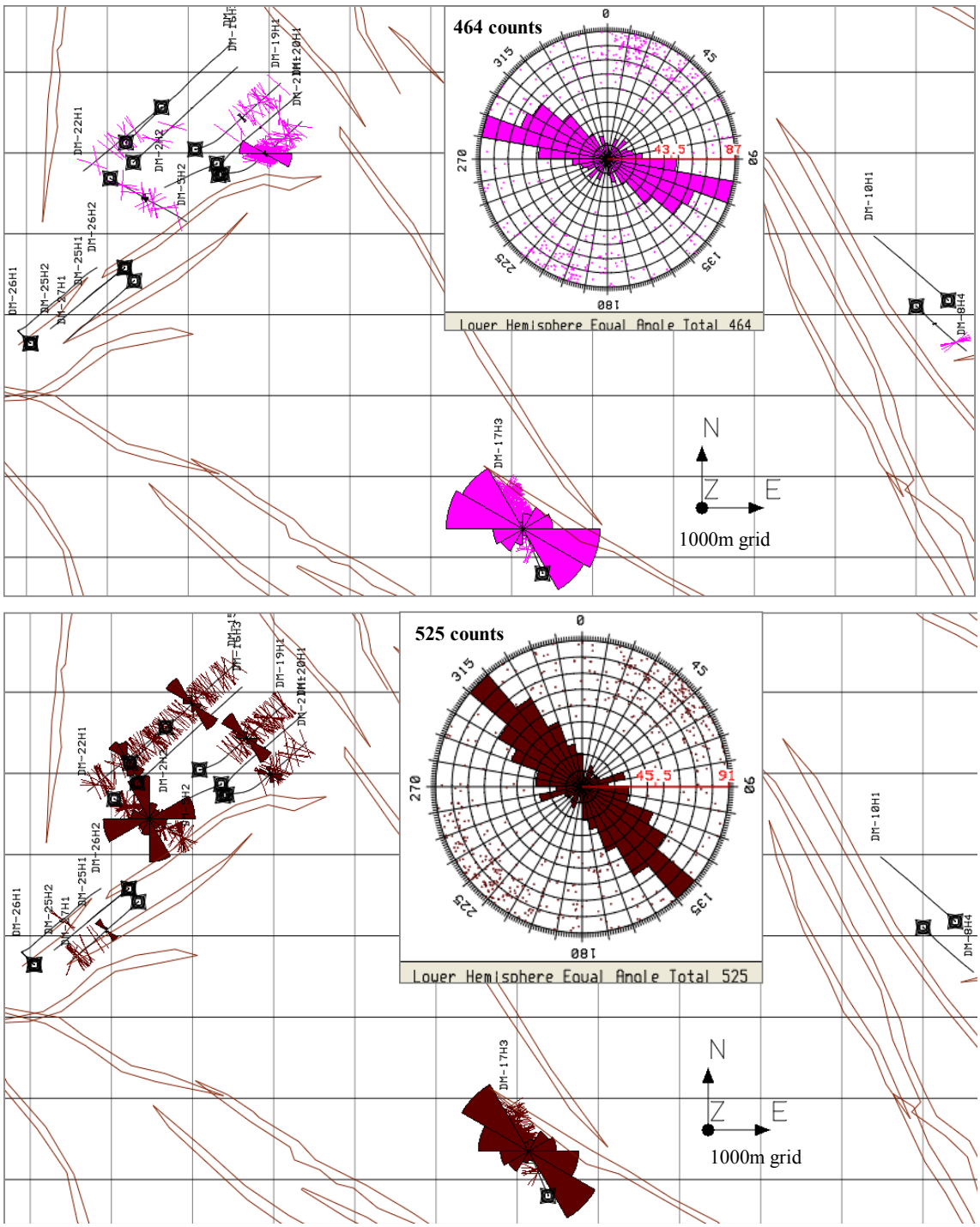


**Figure 3-117 Large non-conductive BHI fractures (pink) and small non-conductive fractures (dark pink) with rose diagram in Dhulaima field.**

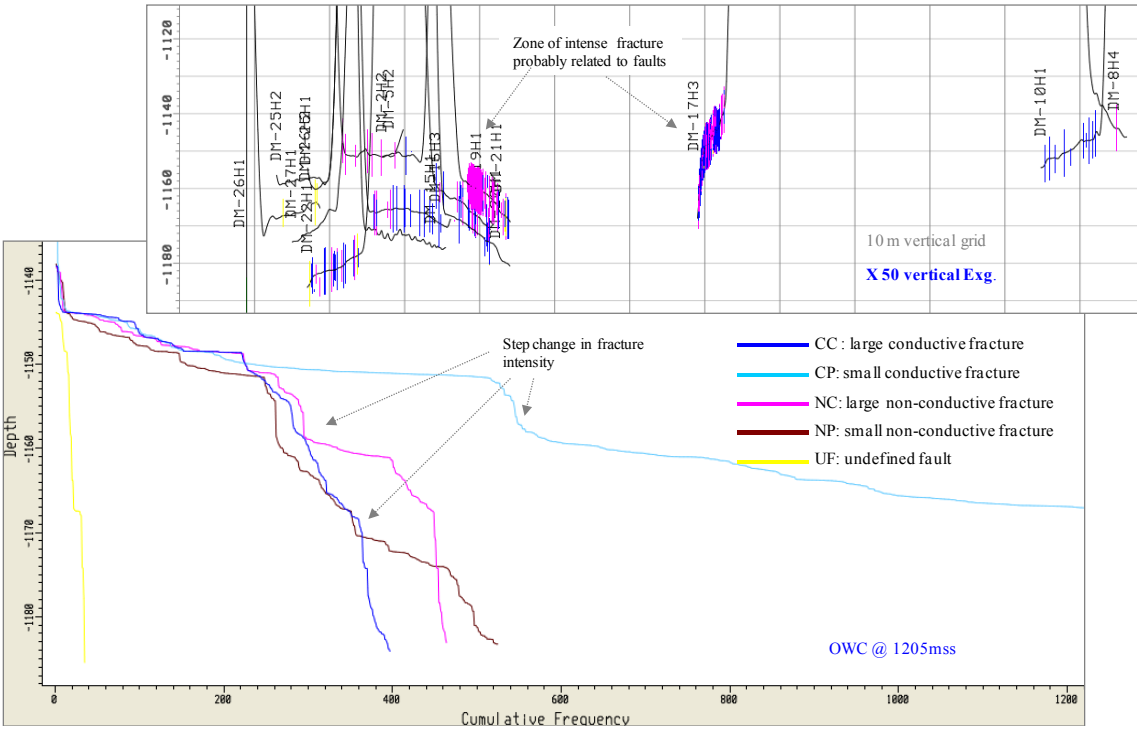


**Figure 3-118 BHI fracture cumulative frequency plot versus depth for all the BHI fracture picks; and cross section (top) with only the large BHI fracture seen in Dhulaima.**

### *3.2.12 Lekhwair field - Shuaiba Formation*

Lekhwair field is located NW of Dhulaima, close to the UAE border. This field is split into different areas: A north donated LAN, A south, B, C, D and Lekhwair East, which is a field on its own. The field has 3 oil bearing reservoirs: Upper Shuaiba split into 1 & 2, Lower Shuaiba split into A & B and Kharaib, with the Lower Shuaiba and Kharaib being the main commercial reservoir (Figure 3.119). The cluster is developed with water injection with LAN being the most matured area. This area will be discussed in detail in Chapter 5. LAN development is summarised by the following stages:

- Pure depletion from 1976 to 1984,
- 5-inverted spot water flooding pilot from 1984 to 1992,
- 9-inverted spot water flooding with injection close to matrix fracture condition,
- 1992-1996, followed by a line-drive water injection ,
- Line drive infill producer and injectors from 2001 to 2003, and
- Onset of A-North infill campaign; infilling the producer and injector lines with vertical wells at c. 100m spacing from 2003 onward.

As shown in figure 3.119 the well pattern for this field was parallel to the structure with peripheral water injection (edge water injection), whereas for LAS and LB/C/D fields the well pattern is parallel to the fault direction. The objective of the change in well strike is to avoid encountering fracture corridors which causes water breakthrough, which are perceived to be striking NW to WNW.

***Existing work***

Lekhwair field had been subjected to many fracture studies since the late 1990s, when water breakthrough became an issue in LAN. The findings of most of these studies are presented below:

Menton 1997, BHI fracture characterization in LAN: This report is not available.

Evernts (Evernts and Leinster, 1997):
Natural fractures occur as clusters in inter-connected hybrid/tensile network. BHI data suggests that individual clusters are about 2m wide, within which average fracture spacing is 0.8m and outside the cluster isolated fractures have a mean spacing of 5m. The calcite cemented fractures may act as barrier to flow; however those cemented fractures, which were observed in core occasionally, have a conductive BHI response. It is suggested that they opened during drilling and thus, likely to close once the pressure is lowered. Fault damage zones are intensively fractured (up to 45 fracture/m) with an average width of 10-20m, with NO relationship between fault damage zone width and throw. The occurrence of tightly cemented matrix around the damaged zone suggests that the fault zones will have limited connectivity with the matrix and may compartmentalize the reservoir.

Ozkaya (Ozkaya, 2002 -both Lekhwair and Dhulaima):
Two main types of features occur, fracture corridors and joints (the former are fault-related, and the latter are layer-bound). The main fracture orientation is WNW-ESE to NW-SE, with a minor population oriented NE-SW. The vast majority of fractures are joints, the remaining occur associated with fracture corridors. Only a small amount of fractures are open. Fracture spacing and size, and fracture corridor spacing, are dependent on layer thickness. Joints are unlikely to have flow potential. Fracture corridors have considerable flow potential, because half of the open fractures are found in fluid conductive fracture corridors. The transmissivity of fracture corridors has an upper boundary of 40 Darcy, with an average of 10 Darcy. Fluid conductive fracture corridors commonly have cemented walls, reducing the flow into the matrix. All fractures are cemented except the ones that were formed within the oil leg, probably formed after oil emplacement in Mid-Tertiary. Open fracture corridors are confined to the crestal parts of the structure, being cemented in the flanks.

Bizarro, 2004 – both Lekhwair and Dhulaima: This report is not available

Nelson (Nelson, 2004)– Lekhwair and Dhulaima
As mention in Dhulaima section a fracture network characterization for the whole of the Lekhwair cluster was carried out by Nelson. Specific findings related to Lekhwair are: Comparison between core fractures and BHI fractures in L193H1 indicate that the two data sets display similar fracture orientations and position of greater fracture intensity. However, the FMI-based interpretations saw only 7% of the fracture numbers

interpreted from the core. Fracture statistics were presented (see Figures 3.111 and Figure 3.112 in Dhulaima section above).

Bizarro (Bizarro, 2005) – both Lekhwair and Dhulaima, U. Shuaiba

The Upper Shuaiba reservoir has the highest fracture intensity, and the highest percentage of cemented fractures, within the Lekhwair cluster. Significant fracturing occurs in swarms or corridors, 50 to 100 m wide, that effect production rates and injection water movement. The predominant fracture orientations are NW and NE (same as in the Lower Shuaiba), in line with the structural pattern of the area. There is no orientation distinction between conductive and cemented fractures. Fractures play a role in boosting production from a very tight reservoir, as indicated by well L-323 in the Lekhwair A-south field (Figure 3.120). Thus, fractures may be necessary for the reservoir to produce under drainage. A conceptual fracture model is presented for U. Shuaiba (Figure 3.121).

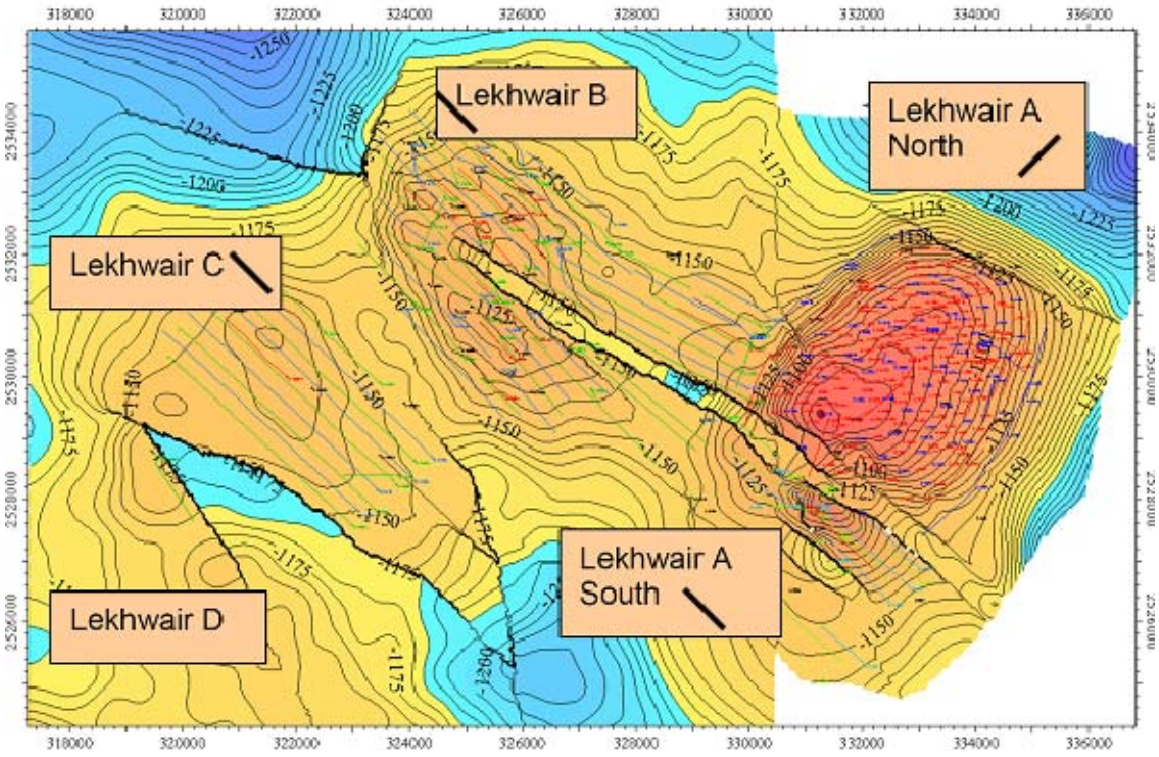


**Figure 3-119 Lekhwair Lower Shuaiba map showing field locations and dominant well direction (black line) in each area (Poyser et al, 2005).**

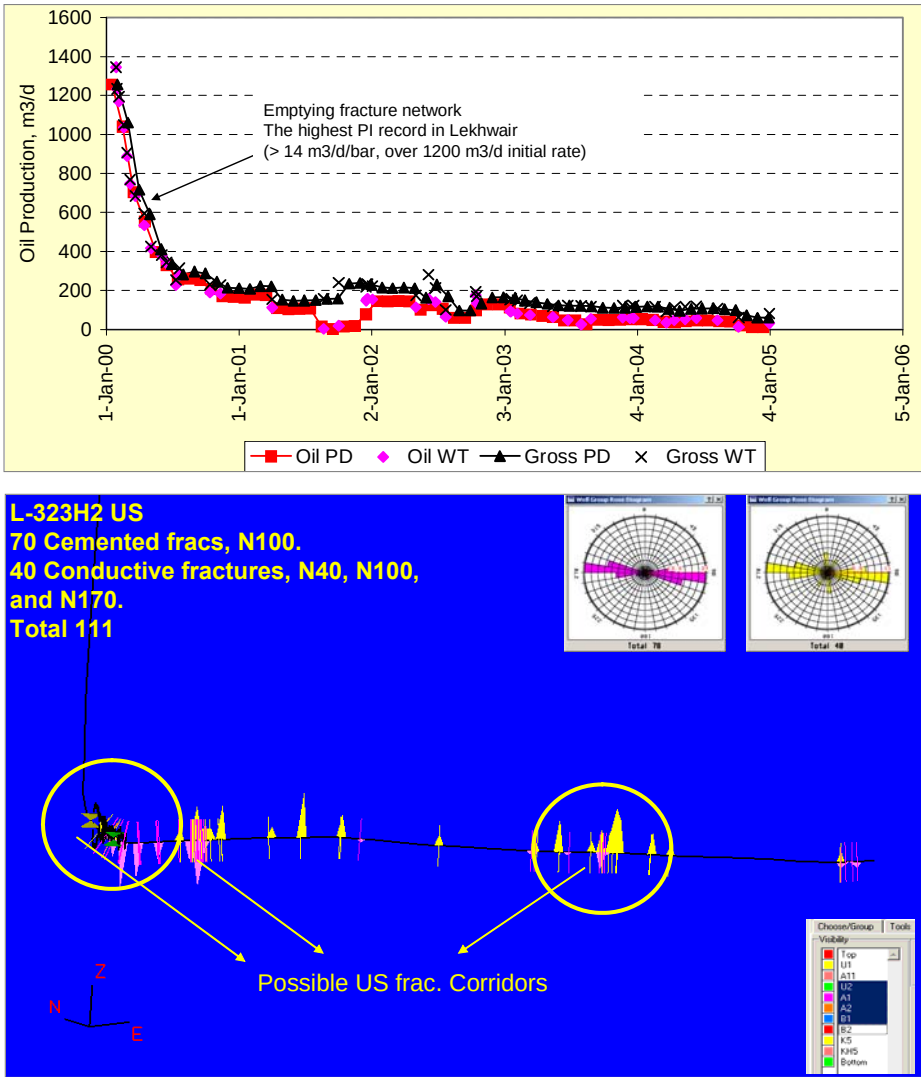


**Figure 3-120 L323H2 upper Shuaiba producer in LAS oil rate with time (top) indicating fracture behaviour; BHI fractures of the same well (bottom) seen in SVS (Bizarro, 2005).**

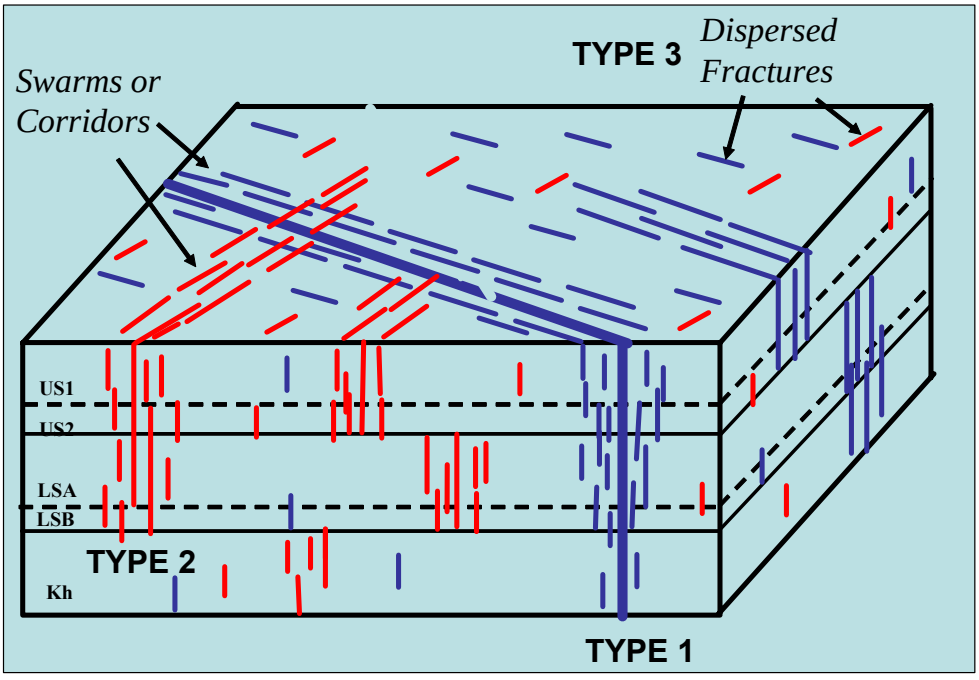


**Figure 3-121 A conceptual model for the U Shuaiba fracture network. Blue are NW fracture set while red are NE fracture set (Bizarro, 2005).**

### *Lekhwair fracture data evaluation*

The summary of the geometric analysis on Lekhwair BHI fracture data here is intended to validate the above observations and interpretations, and to draw regional correlation regarding the fracture network. Note that the fracture network characteristics of LAN area are analysed in detail in Chapter 5.

Lekhwair A is more areally covered by BHI logs than B, C or D (Figure 3.122) but there is bias sampling with regard to orientation. There is very little correlation between BHI fracture intensity and curvature "folding" at large scale calculations (Figure 3.123). BHI faults are mainly striking NW to WNW, but few wells show a NE orientation as seen in Lekhwair D area (Figure 3.124). Note induced fractures seen in LAN are striking NW, NE and N. Large conductive and non-conductive fractures are striking NW to WNW and their ratio is close to 2:1 (Figure 3.125). Small conductive and non-conductive fractures are also striking NW to WNW mainly, Lekhwair D show local variation toward NE probably related to local presence of a NE fault (Figure 3.126). BHI cumulative fracture intensity versus depth graph show step change with depth and also increase in non-conductive fractures frequency with depth (Figure 3.127).

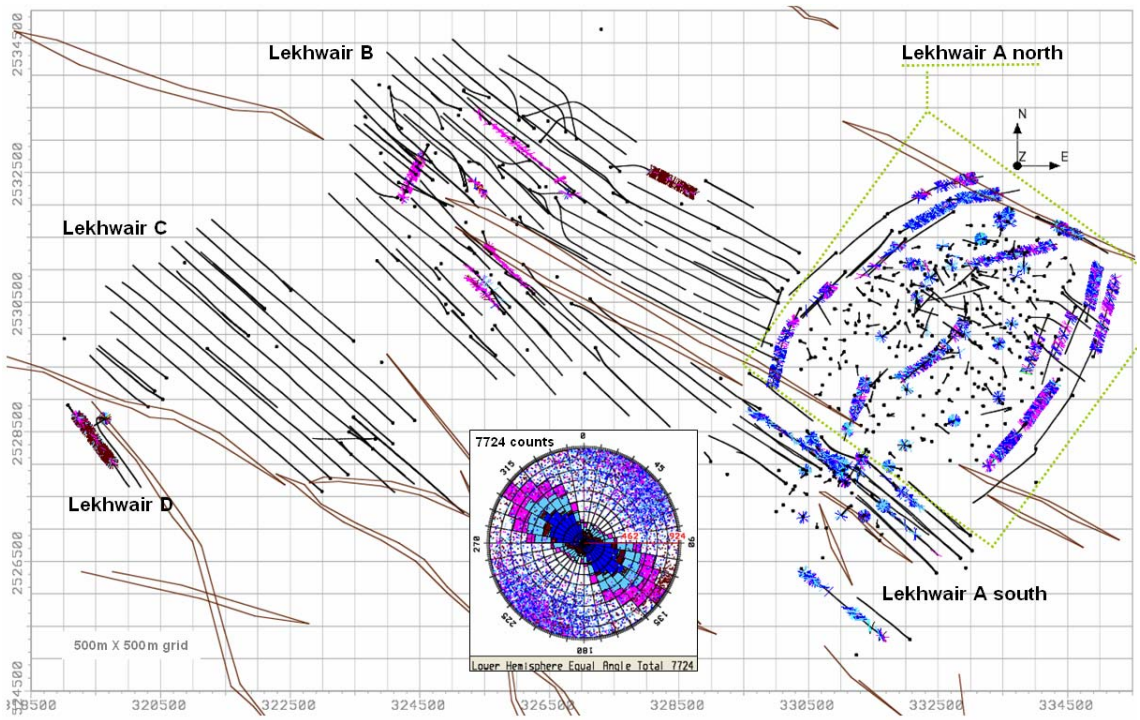


**Figure 3-122 BHI fracture coverage in Lekhwair field, with rose diagram showing BHI fracture strike orientation and count.**

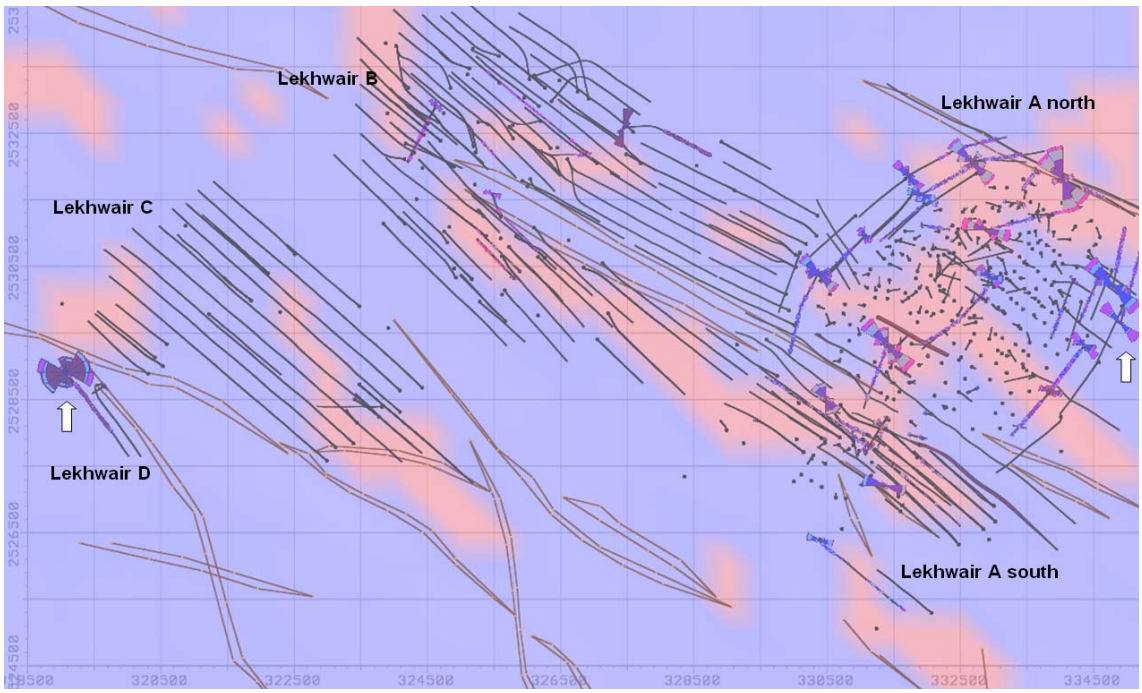


**Figure 3-123 Low correlation between the multi-direction -500m scale wavelength- curvature map (kmax) of the regional top Shuaiba NOCEM and the BHI fracture intensity. The rose diagrams per well (white arrows) are standardized to intensity. Note potential relation between the curvatures and the BHI fractures. This correlation should be refined with field-scale map comparison.**

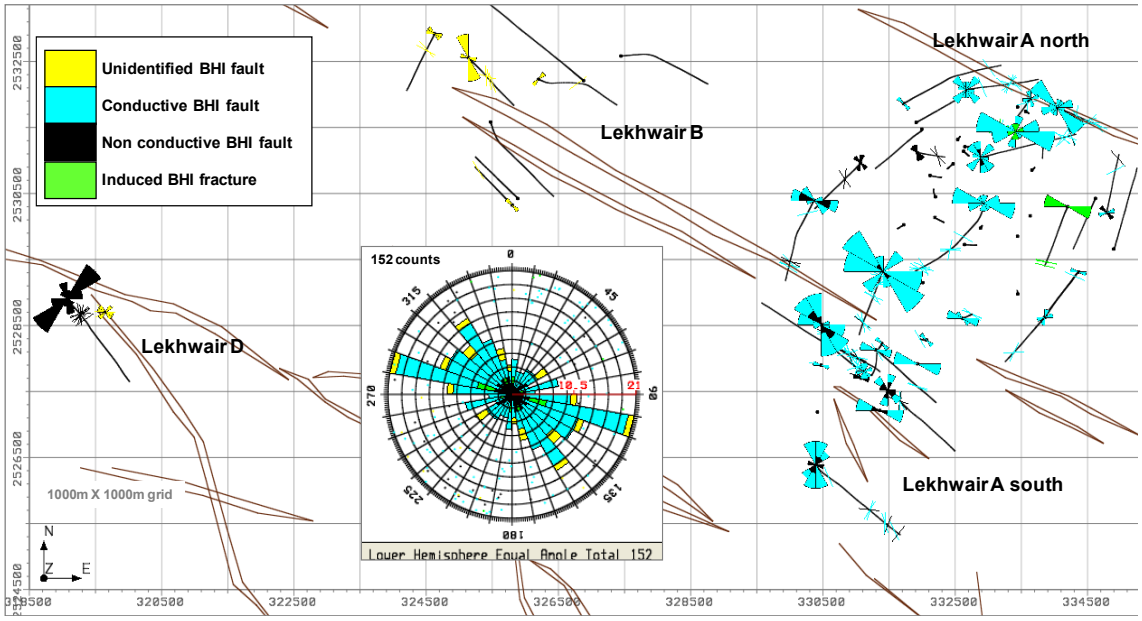


**Figure 3-124 BHI faults and induced fractures (cyan) in Lekhwair field, together with seismic fault lines (brown) indicates high BHI fault intensity close to major faults. Induced fracture direction is NW and also seen as NE in LAN. Note change in color code for fracture type.**

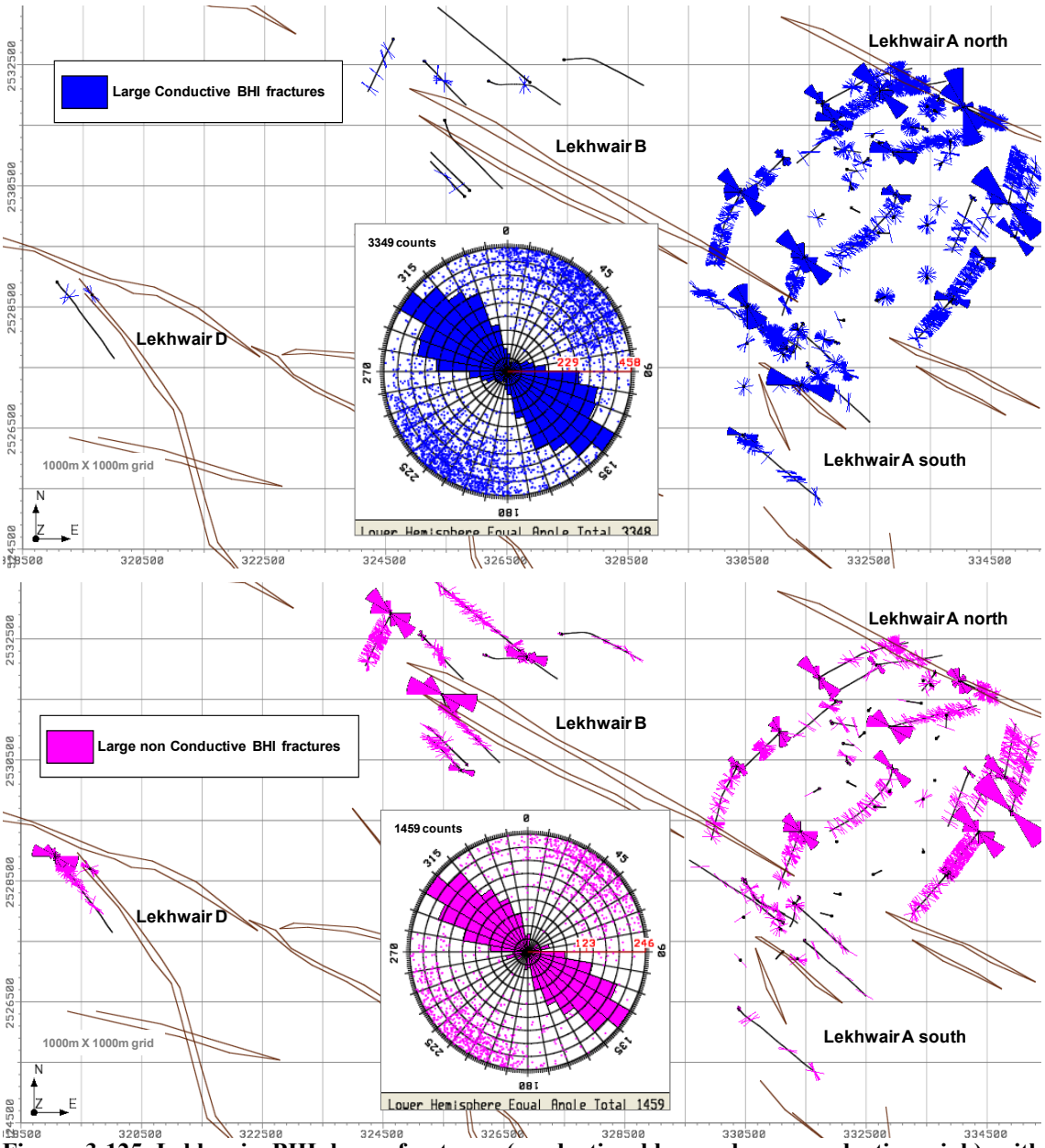


**Figure 3-125 Lekhwair BHI large fractures (conductive blue and non-conductive pink) with normalized rose diagram per well and per field (insert) showing a NW dominant strike direction.**

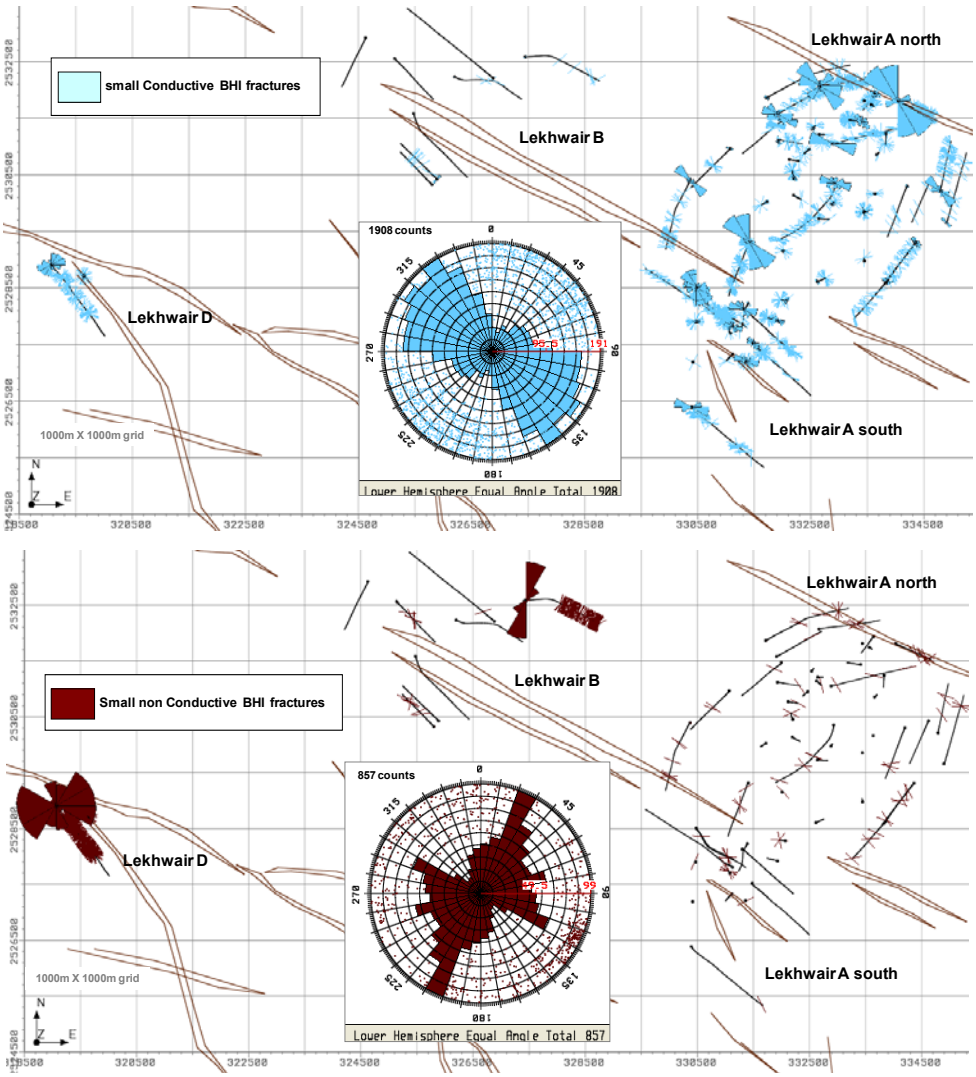


**Figure 3-126 Lekhwair BHI small fractures (conductive light blue and small non-conductive dark pink) with normalized rose diagram per well and per field (insert) showing a NW dominant orientation, except for Lekhwair D area and Lekhwair B area.**

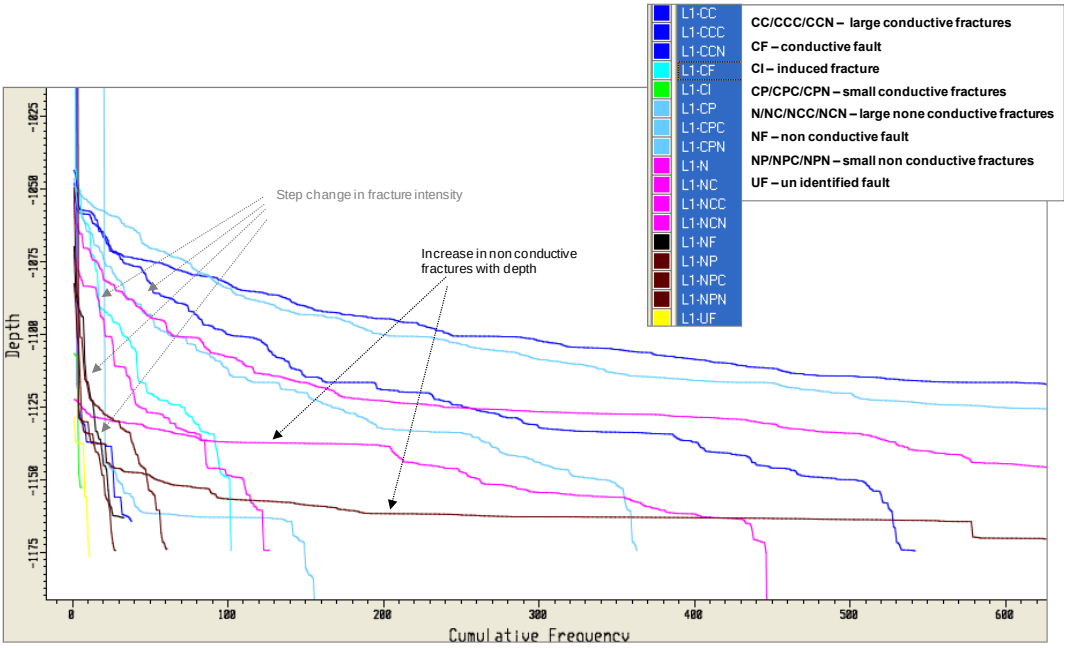


**Figure 3-127 Lekhwair BHI fractures cumulative frequency versus depth, hints toward potential vertical mechanical layering highlighted in fracture intensity variation.**

## 3.3 Discussions

This section offers some interpretations and summary to the observations mentioned above. A detailed analysis will be presented in Chapter 7.

### *3.3.1 Fractures Drivers*

There are four main parameters that control the static distribution of the fracture network of the Cretaceous reservoirs of north Oman:

1. Sedimentary depositional characteristics (basically reservoir lithofacies) combined with diagenetic processes (pre and post fracturing), impacting mechanical layering,
2. Regional and local stress orientation and magnitude (paleo- and current),
3. Fault network related to both regional and local tectonism (e.g. Salt Halokinesis), and
4. Local folding.

The matrix characteristics control the intensity of the fractures seen as well as their vertical distribution ("mechanical layering"). It is very interlinked to the diagenesis process. In general, the Natih Formation, which is made up of inter-bedded layers, shows signs of mechanical layering related to both layer competency and bed thickness. The fractures tend to be either bed or unit bounded as seen in Fahud field, Natih field and Natih Formation outcrops.

For the Shuaiba Formation, mechanical layering is very distinct in the NW part of north Oman (Lekhwair Area), which is linked to facies differences associated with depositional processes, since Upper and Lower Shuaiba exist in NW Oman and only Lower Shuaiba exists in central and SE Oman. However, central Oman shows an intermediate case where mechanical layers are observed as the case for Musallim and Saih Rawl Field, though it plays a minor role in the fracture conductivity. Since most of the wells drilled in central north Oman (around Musallim and Saih Rawl) did not encounter the whole section of the Shuaiba reservoir, there is a high uncertainty in the prediction of mechanical layering in this area.

The regional stress impact on the fracture network can be divided into two groups related to regional tectonic history: a NW orientated paleo-stress related to the Cretaceous deformation and which resulted in NW to WNW striking regional fractures, most of them associated to regional faults and more dominant in the western to north western region of north Oman, as well as the SE region (Huqf outcrop area). The second is the Tertiary compression, and its current in-situ stress orientated NE, which resulted in the NE striking regional fracture and their associated fracture corridors or swarms. Its effects are shown distinctively in the Fahud Field (in the foothills of the Oman Mountains) as well as Al Huwaisah (and probably Yibal field) and Qarn Alam field where the NE fractures dominate.

Fault related fractures in north Oman can be divided into two types. The first type is the dominant NW-WNW fishnet regional faults, seen clearly in Saih Rawl and Musallim all the way to Lekhwair Fields in the NW (they had been also reported in the neighbouring UAE), which are normally associated with fault damage zones with fracture clusters. These fractures are predominantly cemented as seen in Musallim Field, though conductive fractures have also been seen in the Lekhwair Area. This type is – as mentioned above – related to regional stress or regional tectonic deformation.

**A question that arises here is what makes those Lekhwair NW-WNW fractures conductive? This can be either attributed to recent mechanical re-activation of those faults or possible recent diagenesis process that leached those fractures.**

The second type of fault related fracture is linked to local faulting as seen clearly in Ghaba North and Al Ghubar Fields in the east to southeast. These are probably related to salt Halokinesis (which in turn was re-activated by regional tectonic deformation) and are characterised by not having a dominant strike direction.

Fold ("curvature") related fracturing is not wide spread in north Oman. The only two fields where it has been observed distinctively are Natih Field and Fahud Field. In Fahud these fractures are seen at the edge of the fields either in the NW or in the SE. Qarn Alam shows slight correlation with folding in the SE part, as large scale (500m) curvature analysis has shown.

The chart below (Figure 3.128) is an attempt to show the main driver of the fracture networks in each field. This will be further analysed in Chapter 7.

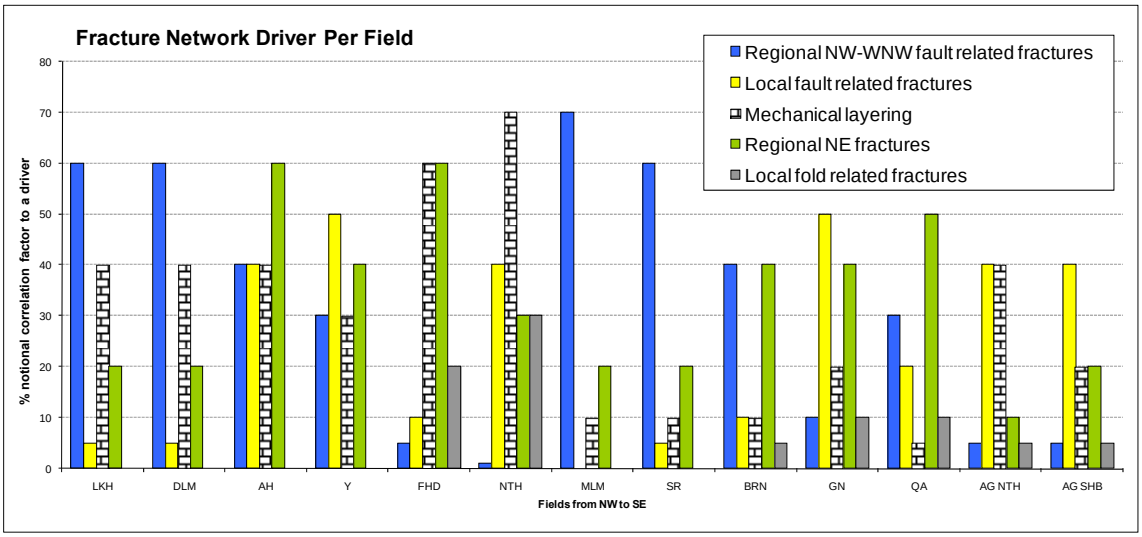


**3-128 A chart plot of fracture drivers per field: LKH = Lekhwair, DLM = Dhulaima, AH= Al Huwisah, Y= Yibal, FHD= Fahud, NTH= Natih, MLM= Musallim, SR= Saih Rawl, BRN= Burhaan, GN= Ghaba North, QA= Qarn Alam, AG NTH= Al Ghubar Natih Formation, AG SHB= Al Ghubar Shuaiba Formation.**

### *3.3.2 Fractures Conductivity*

In general most of the NE oriented fractures are conductive. This is distinctively clear in Al Huwaisah, Fahud, Natih and Qarn Alam. This conductivity is probably attributed to the present day maximum horizontal in-situ stress in north Oman (perceived to be trending NE). Several literature studies in north Oman had shown that since the reservoir depth of most of the north Oman fields is relatively shallow, geo-mechanical analysis suggests that the vertical stress is less than the maximum horizontal stress, thus resulting in a strike slip regime.

In contrast, the majority of the NW to WNW fractures is non-conductive as seen in Saih Rawl and Musallim. However, some of the NW-WNW fractures occur as conductive fractures in the Lekhwair cluster, opposing the current regional perceived NE in-situ stress direction. The conductivity of those NW-WNW fractures in Lekhwair could be attributed to post deformation diagenesis resulting in their leaching, though this has to be confirmed. Or possibly it could be due to a local variation in maximum horizontal stress direction, attributed to local faults or simply due to tectonic re-activation.

Moreover, the majority of the fault-related fractures and fracture corridors, basically fractures that occur in clusters are conductive. This could be attributed to hydrothermal leaching phase of diagenesis that may had occurred in the most tectonically disturbed areas (e.g. close to salt location as in Al Ghbuar field). Furthermore, signs of post charge diagenesis are clearly seen in Qarn Alam field. This resulted in possible cementation of the fractures in the water leg, as indicated by rapid increase in non-conductive BHI fractures as the OWC is approached. In north Oman, local fault related fractures and fold related fractures tend to be conductive in general. Again the fracture flow characteristics and relation to diagenesis will be discussed in Chapter 7.

### *3.3.3 Fractures indicators*

From a fracture indicator prospective, the following parameters can be used to better understand the fracture network in NW Oman Cretaceous fields: Understanding the lithofacies characteristics: logs such as GR, Calliper and Density are the best to use together with core descriptions and analysis of the static image of the BHI log. Combining this with the cross-section distribution of BHI fracture picks, as well as outcrop analogue work, can aid in understanding the mechanical genesis of fractures in these fields. Understanding the geometric orientation distribution of the fractures: the BHI fracture picks rose diagram plot (strike orientation) is one of the easiest available indicators to be used in these fields. Seismic coherency cubes (map view) can help in identifying fault related fractures, whereas curvature analysis (multi-scale and multi-orientation) can aid fold and fault related fracture determination. The dynamic data: well production profile, dynamic logs such as PLT and mud losses data provide a qualitative tools to analyse fracture conductivity in these fields.

### *3.3.4 Micro -Fracture*

Stylolites have been seen in the cores of the Shuaiba reservoir both in Qarn Alam field in the SE and Lekhwair field in the NW. These pressure dis-solution features appear to be linked to micro-variation of lithofacies in the reservoir. Very few analyses had been undertaken to understand their impact in the flow of hydrocarbons in these fields. The current approach is to model them as enhancement (in case they are leached or opened mechanically) or as a degradation of the matrix properties (as they are normally cemented, hence act as baffles to flow), thus they are not modelled explicitly like the other natural fractures.

In addition, micro- hairline fractures had been seen in Qarn Alam core. Those too are thought to be associated with certain rock types (i.e. they occur in certain layers in Shuaiba reservoir), but there is limited data available to further investigate their significant on hydrocarbon flow. Nonetheless, for the time being, they too are modelled as causing an increase in matrix properties during reservoir 3D simulations.

# Chapter 4– GHABA NORTH SHUAIBA

## 4.1 Field introduction

Ghaba North GN field is located in the NE-SW trending Ghaba North Basin, on the western side of the Maradi Fault Zone (Figure 4.1). At Shuaiba level the Ghaba North field is a 6 km by 4 km NE-SW trending four-way dip closure divided into two parts by a NW-trending graben. The shallow (crest depth 433 mss) Shuaiba reservoir is located above a "hammer" shaped salt diapir (Figure 4.2).

Hydrocarbons are present in three formations in Ghaba North Field: A thin gas column occurs in the Cretaceous Natih E carbonate, an oil column in the Cretaceous Shuaiba carbonate (only Lower Shuaiba Formation is present here -focus of this chapter) and another oil column in the deeper Permian Gharif sandstone reservoir. As mentioned in Chapter 2, only Lower Shuaiba is present in SE Oman and it has been recently divided into flow units (FU1 to FU5) based on regional correlation between the Huqf outcrop and Qarn Alam Field (Figure 4.3), so NO LSA or LSB as in Lekhwair clusters. GN Shuaiba FWL is at 546mss (crest depth at 433mss), while the OWC ranges from 490 to 520 mss giving a maximum gross oil column of 64m. Core plug average matrix porosity is 30% and average matrix permeability is 8 mD (Figure 4.4).

GN Shuaiba is currently developed using natural depletion with vertical producers. An attempt to perform GOGD by creating a secondary gas cap in the crest (injecting gas in GN3 & GN5 between 1990 and 1995) failed due to strong aquifer influx replenishing the reservoir. In addition, horizontal well development was attempted with the drilling of GN25 & GN26 in 1995 and 1997, but also failed due to the presence of a well-connected fracture network, resulting in very early water breakthrough despite drilling those wells in the upper part of the reservoir. GN Shuaiba is producing with high water cut (Figure 4.5). The GN Shuaiba reservoir has relatively light oil (7 cp viscosity and 867 kg/m3 density at reservoir temperature of 53ºC), and its pressure is close to hydrostatic: Initial reservoir pressure is 6190 kPa, while current pressure stands at around 5800 kPa with the Bubble Point pressure at 5715 kPa, (Figure 4.6).

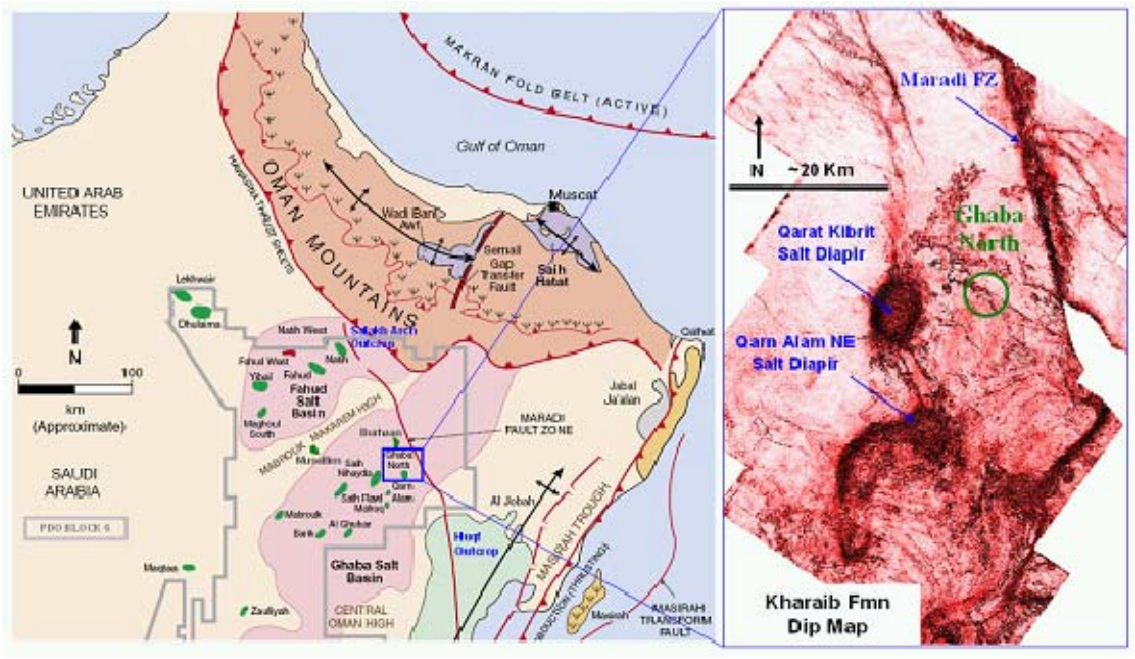


**Figure 4-1 Ghaba North field is located in the Ghaba Salt Basin (pink area in the left) in the western side of the Maradi Fault zone (right - a dip map), modified from Filbrandt et al, 2006.**

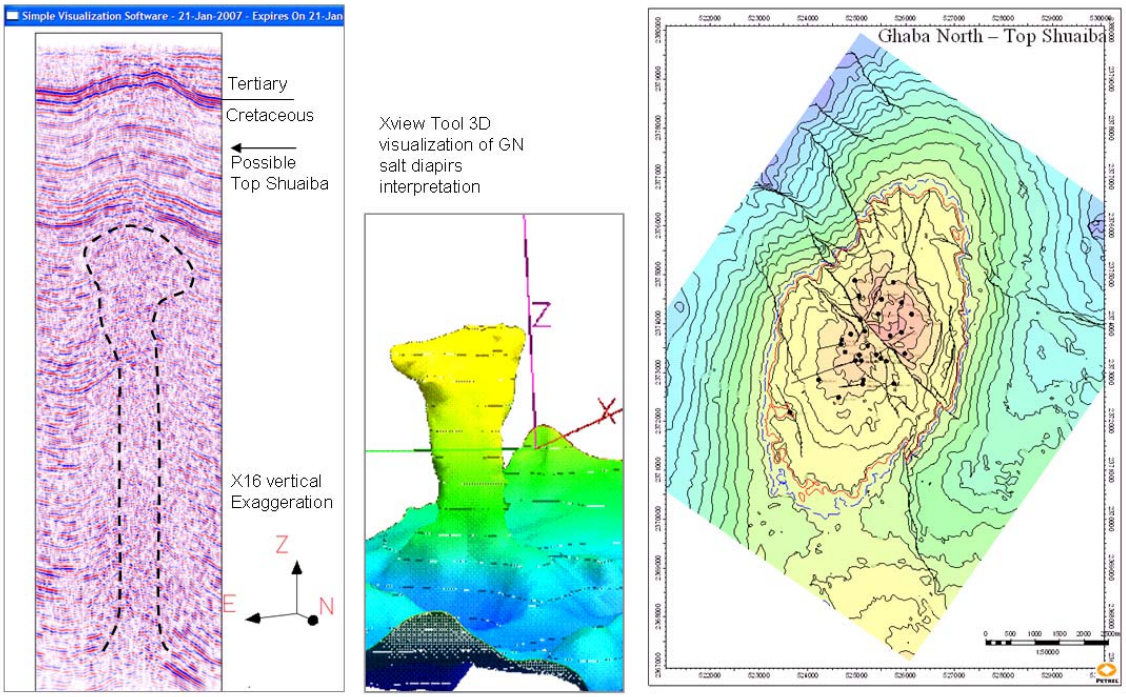


**Figure 4-2 Seismic cross section showing GN field; interpreted salt horizon (Richard, 2004); and top Shuaiba map with faults (Harwijanto, 2005).**

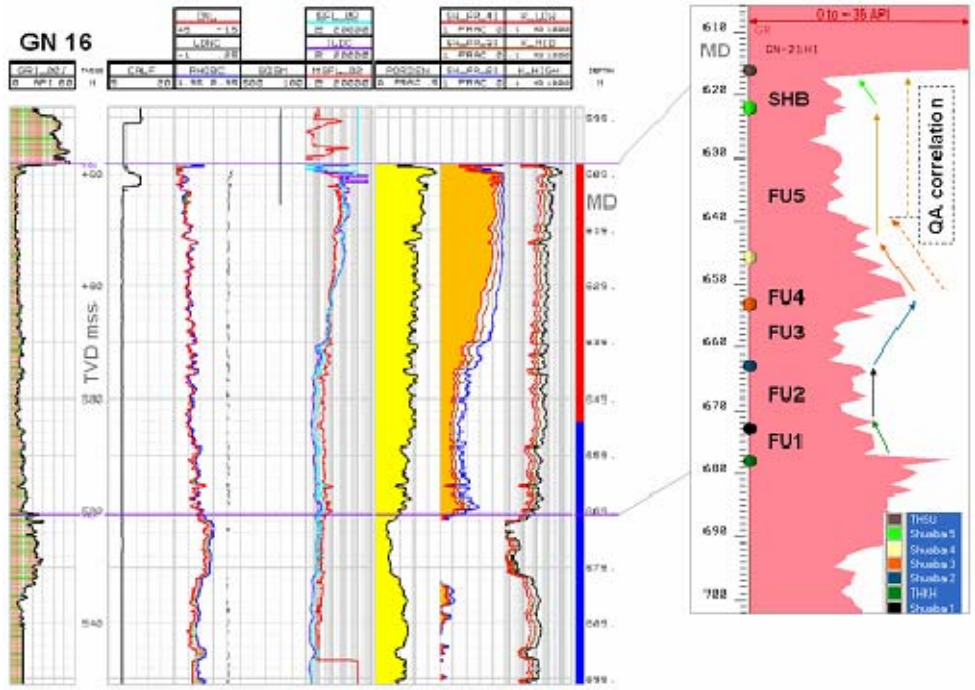


**Figure 4-3 GN Shuaiba typical log of GN16 (left, Frese, 2006); recent attempt to subdivide the Shuaiba into several flow unit layers of GN21 (right) based on GR and outcrop correlation.**

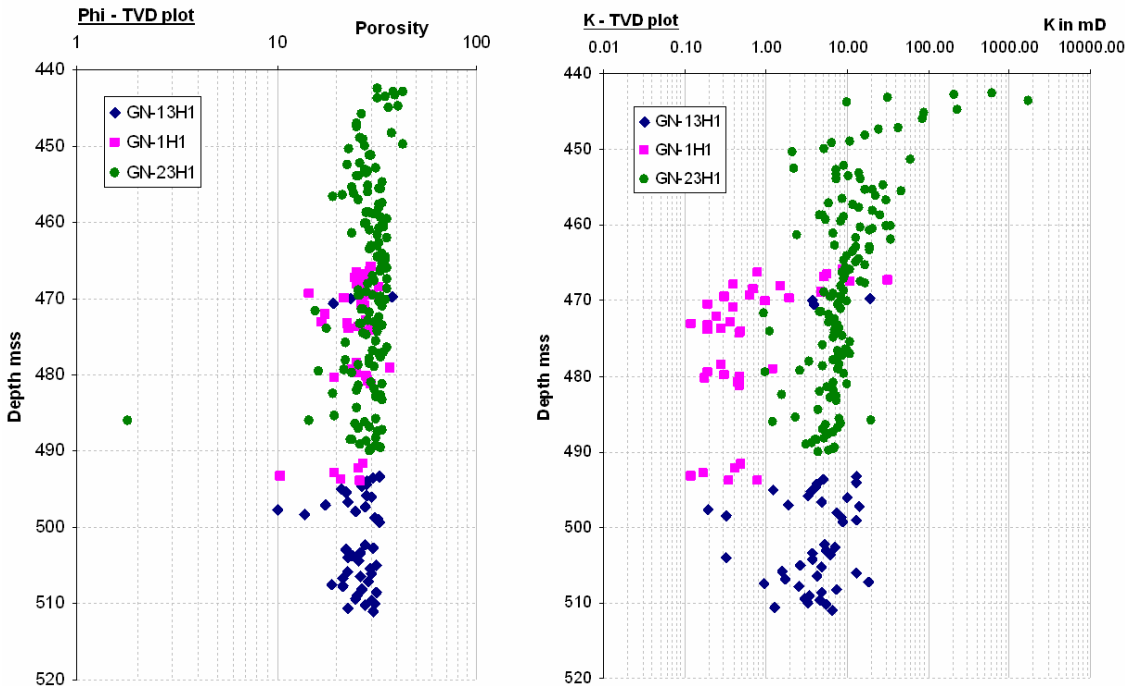


**Figure 4-4 GN Shuaiba core plug: porosity and permeability measurements. Note very little porosity changes with depth indicating minimum change in matrix property with depth.**

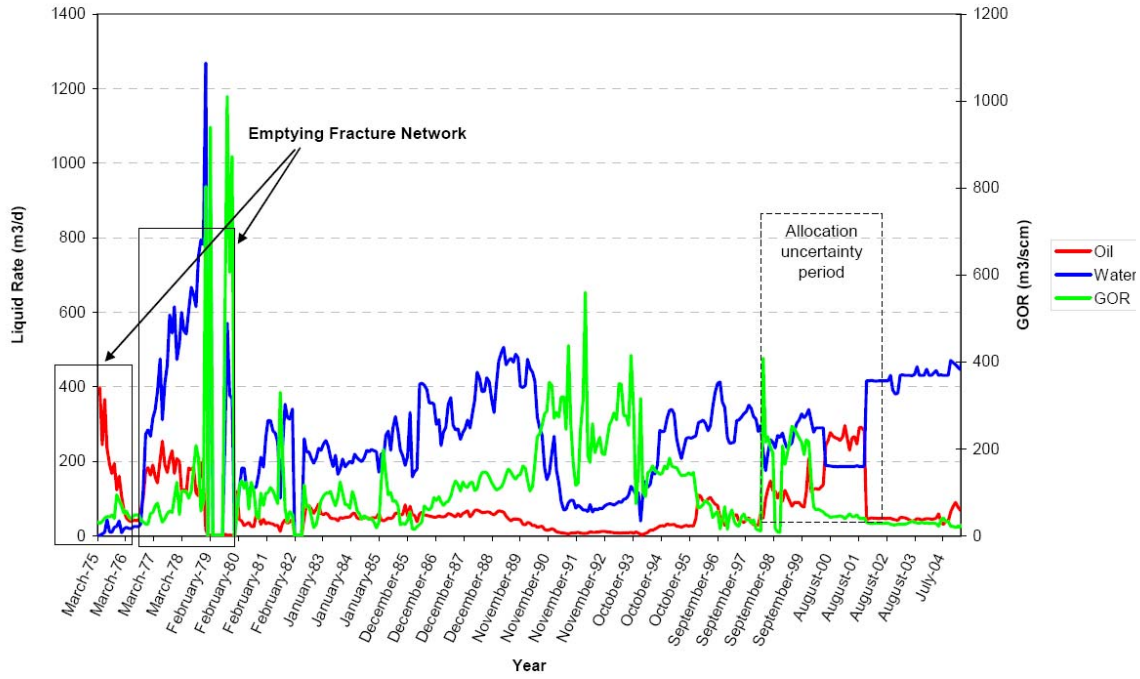


**Figure 4-5 GN Shuaiba full field production rate, water rate and GOR.**

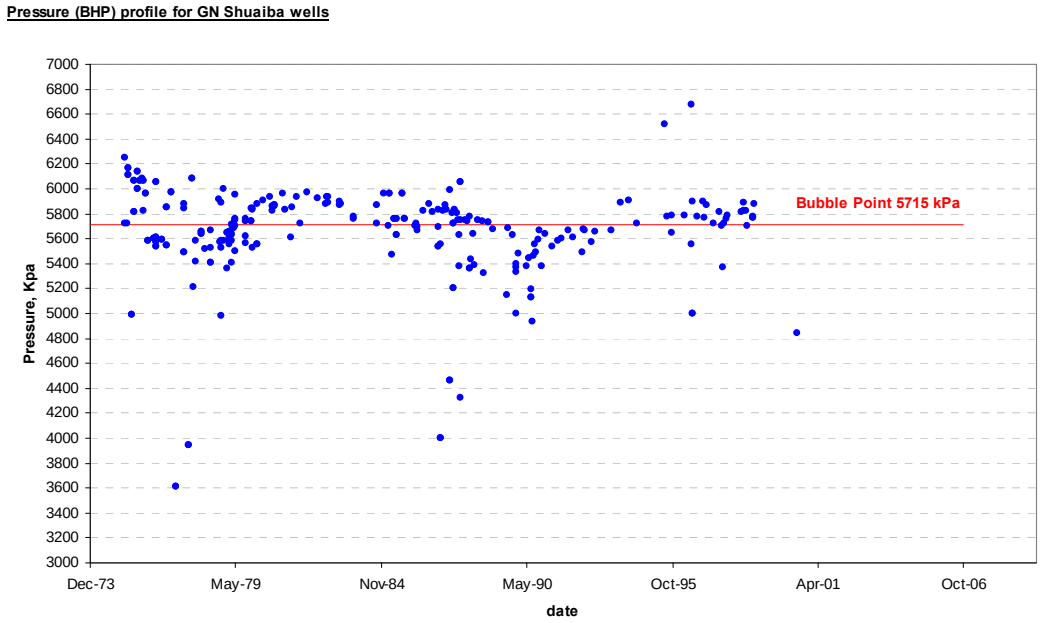


**Figure 4-6 GN Shuaiba wells average pressure profile with time, based on BHP static measurements out of PDO RUI data base.**

## 4.2 Fractured data import to SVS

The workflow approach used in this study is as described in Chapter 1. Figure 4.7 (a duplicate of Figure 1.9) sets out that workflow in a graphical fashion. This chapter documents the application of this workflow to GN Shuaiba, and describes the resulting DFNs. Also included is a description of the transformation of the DFNs to create the input model for a dynamic flow simulation.

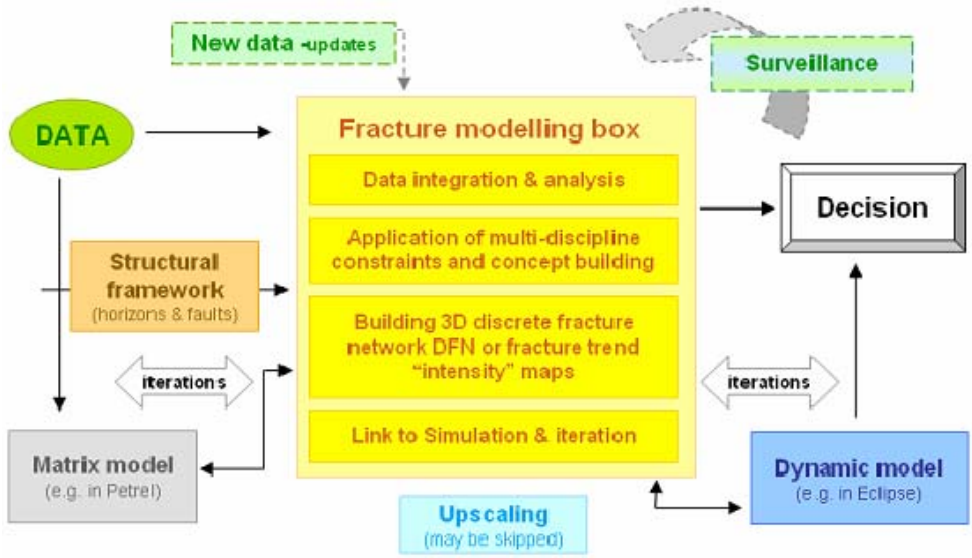


**Figure 4-7 Workflow showing elements of fracture characterization and modelling (yellow box).**

Ghaba North field has in total 31 wells (up to 2007), targeting both Shuaiba and Gharif reservoirs (Figure 4.8). Table 4.1 provides a summary for the GN Shuaiba wells, highlighting the data available to this study. The research reported in this thesis benefited from the on-going Ghaba North / Al Ghubar Shuaiba subsurface study carried out by Shell EPTS for PDO, which provided the following: A detailed seismic analysis and construction of top Shuaiba and base Shuaiba (top Kharaib) horizons (Harwijanto, 2005); creation of a 3D Petrel model for Shuaiba reservoir: This provided the startigraphic layering, the fault planes, as well as the conventional wire-line logs (Frese, 2006); and a detailed fracture interpretation ("listings") of all the BHI by Baker Atlas. Thus, for each well there is a list with measured depth (MD) at which the fracture was encountered along the borehole, fracture's type (e.g. large conductive fracture or small non-conductive fracture –donated with PDO convention of fracture naming, i.e. CC, CP, NC, NP, etc), fracture's dip direction and fracture azimuth.

<u>The following fracture related data had been uploaded to SVS:</u>

1- **Well deviations** as obtained from PDO subsurface data base called RUI.
2- **Well tops** obtained from RUI but via Petrel edited to include the new layering scheme of the Shuaiba: subdivided into flow units (Figure 4.9). Top Shuaiba was cross compared against drilling data and GR logs (Figure 4.10).
3- **Horizons** (top and base Shuaiba) and the layers in between. Obtained by extracting surfaces out of imported 3D Petrel binary grid into SVS (Figure 4.11). The basis of the vertical subdivision is not known but in total there are 15 surfaces in the fine-scale 3D model including top Shuaiba and top Kharaib.
4- **Faults**- Three sets were available (Figure 4.12): the "ZHarwi" sub-regional seismically interpreted lineaments (orange), the 2001 GN Shuaiba study conceptual interpretation (green) and faults extracted from the geo-cellular model of the current study (blue).

5- **Seismic volumes** reflection and semblance (16 bits format) in time. These volumes were used only for qualitative analysis. Since the SVS seismic attribute window does not have the functionality to see TWT values once a SEGY volume is imported, it was not possible to know which reflector is top Shuaiba exactly (top Shuaiba is around 500ms TWT). Hence the volumes were moved manually down to fit what is perceived to be top Shuaiba reflection based on visual inspection and comparison with Harwijanto's interpretation (Harwijanto, 2005) and using the clear reflection of top Natih, Tertiary unconformity, as a marker (Figure 4.13).

6- **BHI (FMS/FMI) fracture interpretation picks** (called objects in SVS) with standardized names as in Chapter 3, though added picks for GN16 & GN17, which were not included in Chapter 3, see Table 4.2 and Figure 4.14. Note that the vertical wells' BHI logs were also loaded to SVS, but it is hard to pick the fractures in it as SVS does not allow for scale manipulation of the image.

7- **Well losses** indicators from drilling data, imported as log-las files (Figure 4.15).

8- **Well Normalized Gross Rate**, imported as log-las file (Figure 4.16).

9- **Well conventional logs** available, imported from the Petrel 3D model.

10- **Well production history**, as fracture constraints, using PDO Oil Field Manger (OFM) data combined with an excel file that was produced by the recent Shell GN study to correct for the production miss-allocation between 1998 and 2002. As SVS dynamic functionality so far does not include a gas injection variable, it was decided to use the water injection tab to be an indicator of the gas injection for GN3 and GN5 since there is NO water injection in this field (Figure 4.17).

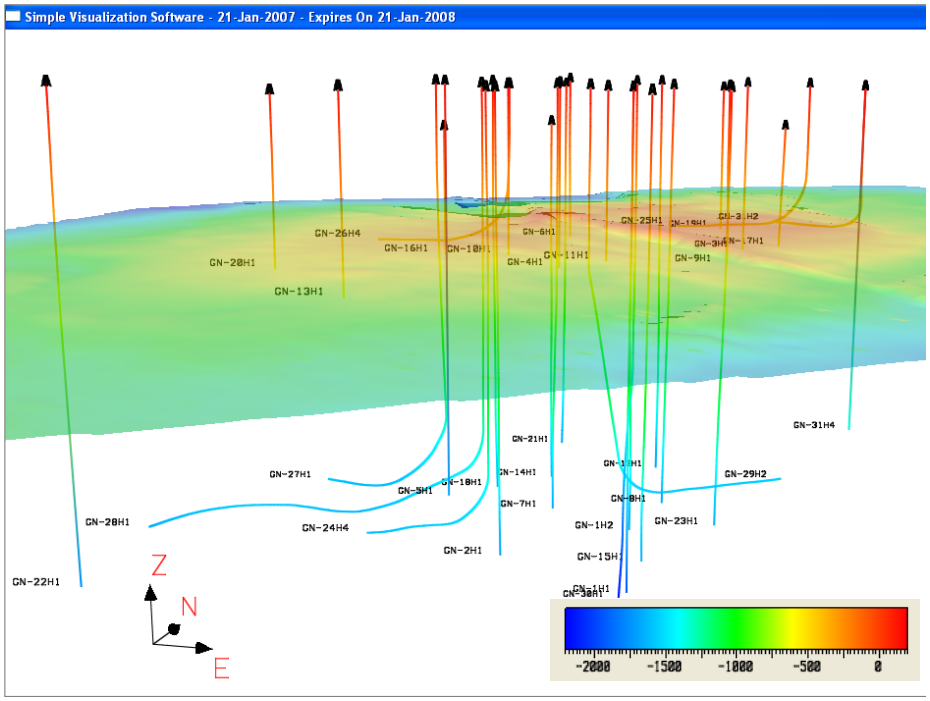


**Figure 4-8 SVS snap shot showing GN wells with well-bore coloured by depth, targeting both Shuaiba (horizon is top Shuaiba) and deep Gharif reservoir.**

| Well | Easting | Northing | Type | Spud Date | Status | Normalized Gross Rate | Core m | BHI m | top SHB mss | OPDE Losses | LOGS |
|---|---|---|---|---|---|---|---|---|---|---|---|
| GN-3H1 | 525915 | 2374430 | vertical | Sep-72 | Shut-in 1990 | 335.8 | | | 447 | | |
| GN-4H1 | 525162 | 2373845 | vertical | Sep-73 | Shut-in 1980 | 347.9 | | | 459 | | |
| GN-5H1 | 524692 | 2373671 | vertical | Dec-73 | Shut-in 1990 | **684.8** | | | 461 | | |
| GN-6H1 | 525048 | 2374563 | vertical | Mar-74 | Shut-in 1996 | 115.0 | | | 462 | | |
| GN-8H1 | 525682 | 2373748 | vertical | Apr-74 | Shut-in | | | | 436 | | |
| GN-9H1 | 525913 | 2373821 | vertical | Oct-74 | Producing | 210.1 | | | 442 | | |
| GN-10H1 | 525053 | 2373360 | vertical | Nov-75 | Producing | 395.5 | | | 455 | | |
| GN-11H1 | 525488 | 2373289 | vertical | Nov-75 | Shut-in 1997 | 88.8 | | | 465 | | |
| GN-12H1 | 525502 | 2374498 | vertical | Mar-78 | Producing | 257.4 | | | 456 | | |
| GN-13H1 | 524631 | 2372491 | vertical | Aug-80 | Shut-in 1990 | 311.4 | | | 470 | 18 | |
| GN-16H1 | 524760 | 2373419 | vertical | Nov-85 | Shut-in -obs | | 20.4 | 76 | 458 | | |
| GN-17H1 | 526121 | 2374196 | vertical | Dec-85 | Shut-in -obs | | | 98 | 450 | 0 | |
| GN-19H1 | 525748 | 2374846 | vertical | Dec-86 | Shut-in 1996 | 367.4 | | | 460 | 100 | |
| GN-20H1 | 524219 | 2372852 | vertical | Dec-86 | Shut-in 1994 | **24.9** | | | 471 | 0 | |
| GN-21H1 | 524956 | 2374888 | vertical | Nov-87 | Shut-in 1994 | **21.0** | | 99 | 464 | 25 | |
| GN-22H1 | 523629 | 2372190 | vertical | Jul-89 | Shut-in | | | | 504 | 0 | |
| GN-25H1 | 526200 | 2374445 | horizontal | Nov-95 | Producing | **598.3** | | *465* | 449 | Total | |
| GN-26H4 | 525088 | 2373246 | horizontal | Jan-97 | Shut-in 1998 | 477.9 | | *310* | 455 | Total | |
| GN-31H2 | 526475 | 2374040 | horizontal | Apr-06 | Shut-in | | 79.6* | *492** | 459 | | ROP/WFL |
| GN-23H1 | Gharif well | | vertical | | | | 50.3 | 110 | 442 | 0 | |
| GN-1H1 | Gharif well | | vertical | | | | 16.4 | | 467 | | |
| GN-2H1 | Gharif well | | vertical | | | | 6.4 | | 466 | | |
| | | | | | | | * GN-31H1 | * GN-31H1 | | | |

**Table 4-1 Summary of data available for GN Shuaiba wells: Well abbreviation, E/N, well type, spud date, status, normalized gross rate (total gross production/number of production days), core recovered in m, BHI interval in m (outlined in black >> image available), top Shuaiba depth, OPDE losses (as recorded from drilling report) and conventional log availability (light blue few logs).**

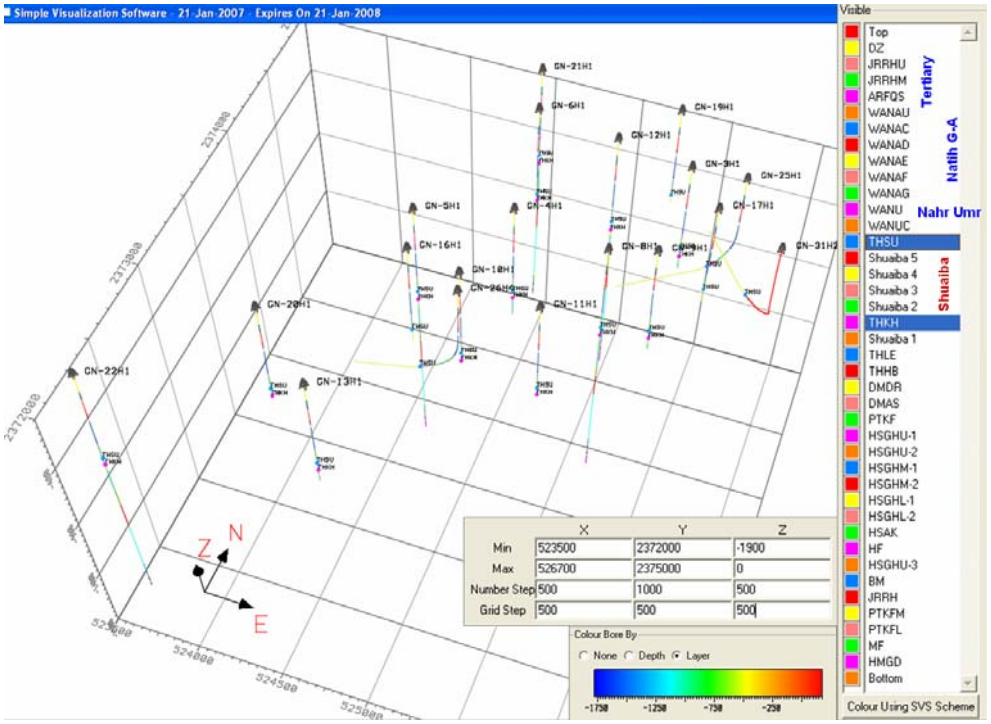


**Figure 4-9 SVS snap shot showing GN Shuaiba wells, with their bore coloured as per the layering scheme of the field. Top Shuaiba and Top Kharaib markers are shown.**

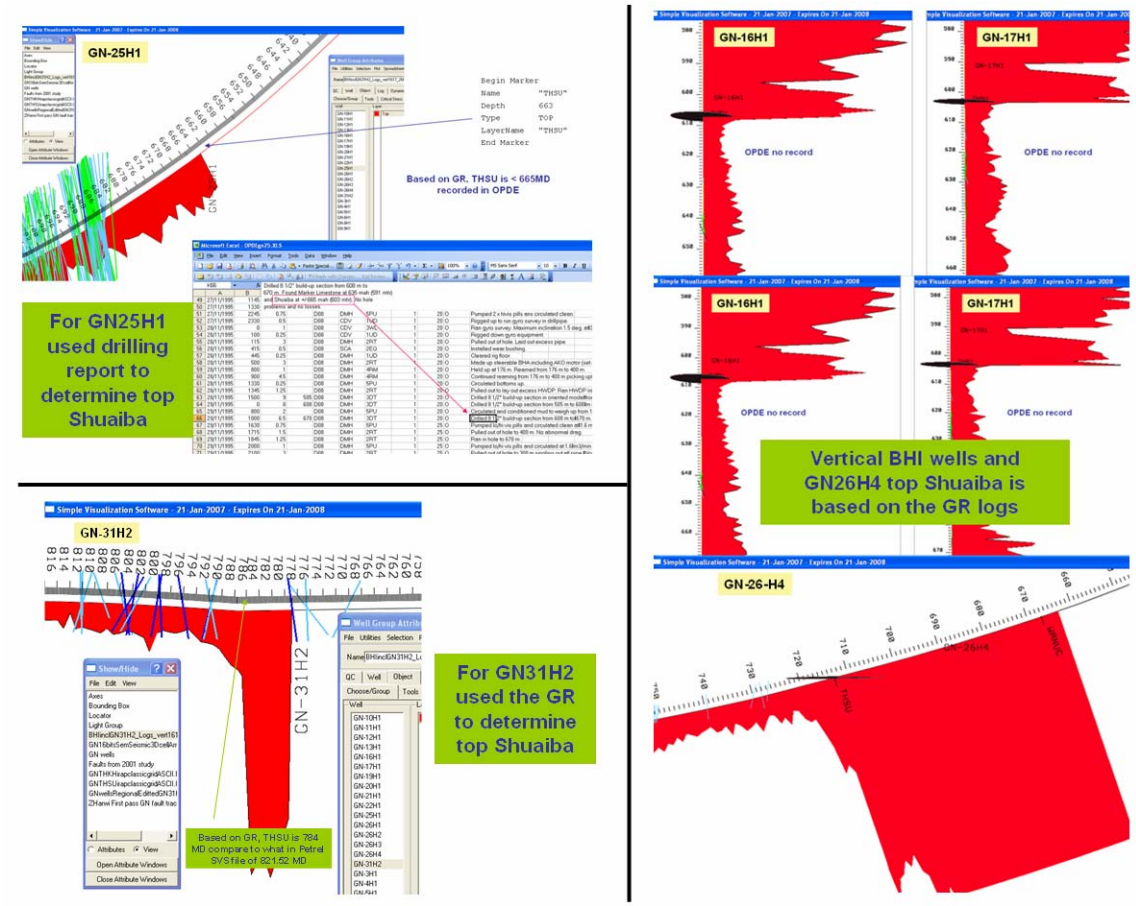


**Figure 4-10 Using drilling report and GR logs to cross checked top Shuaiba for the main BHI wells.**

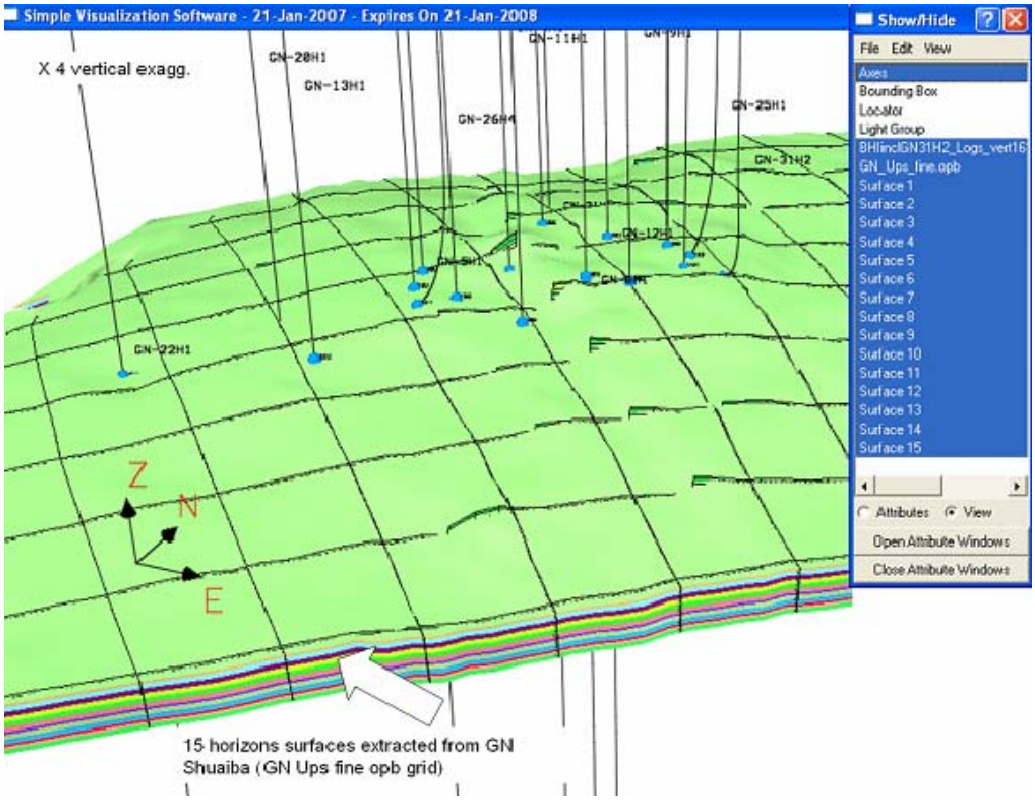


**Figure 4-11 SVS snap shot showing a fence diagram of GN Shuaiba fine scale grid together with GN wells and the horizon surfaces extracted from the grid. Blue circles are top Shuaiba markers.**

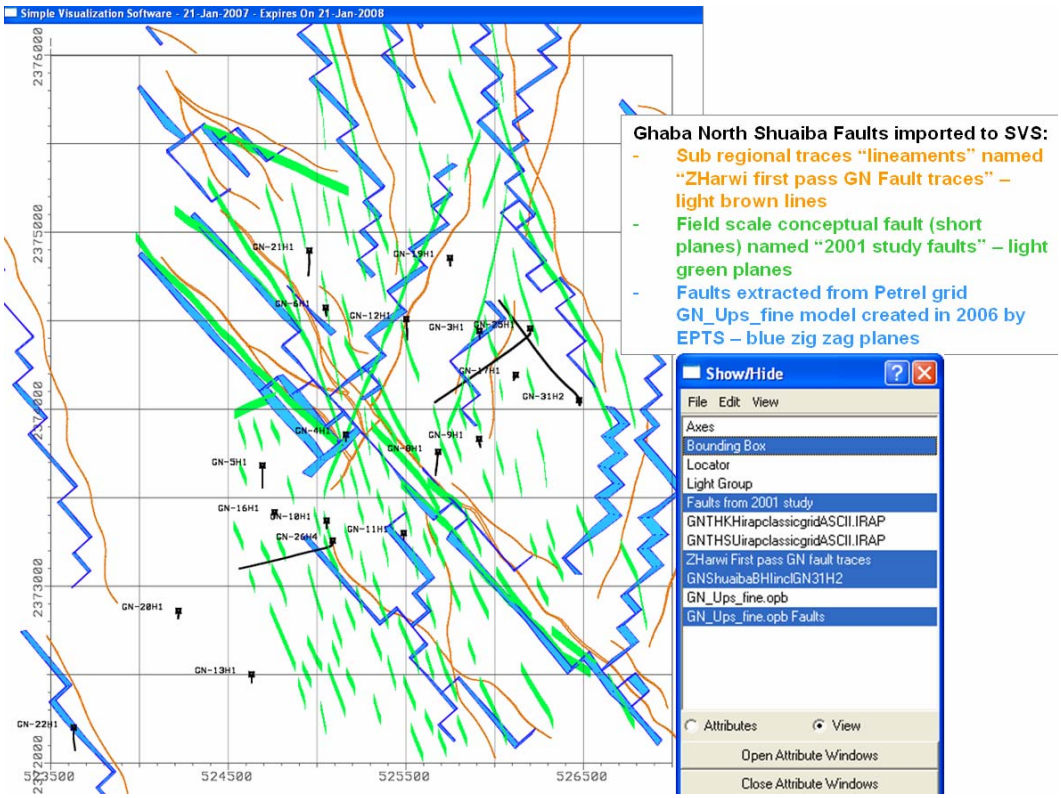


**Figure 4-12 SVS snap shot showing GN Shuaiba available fault interpretations.**

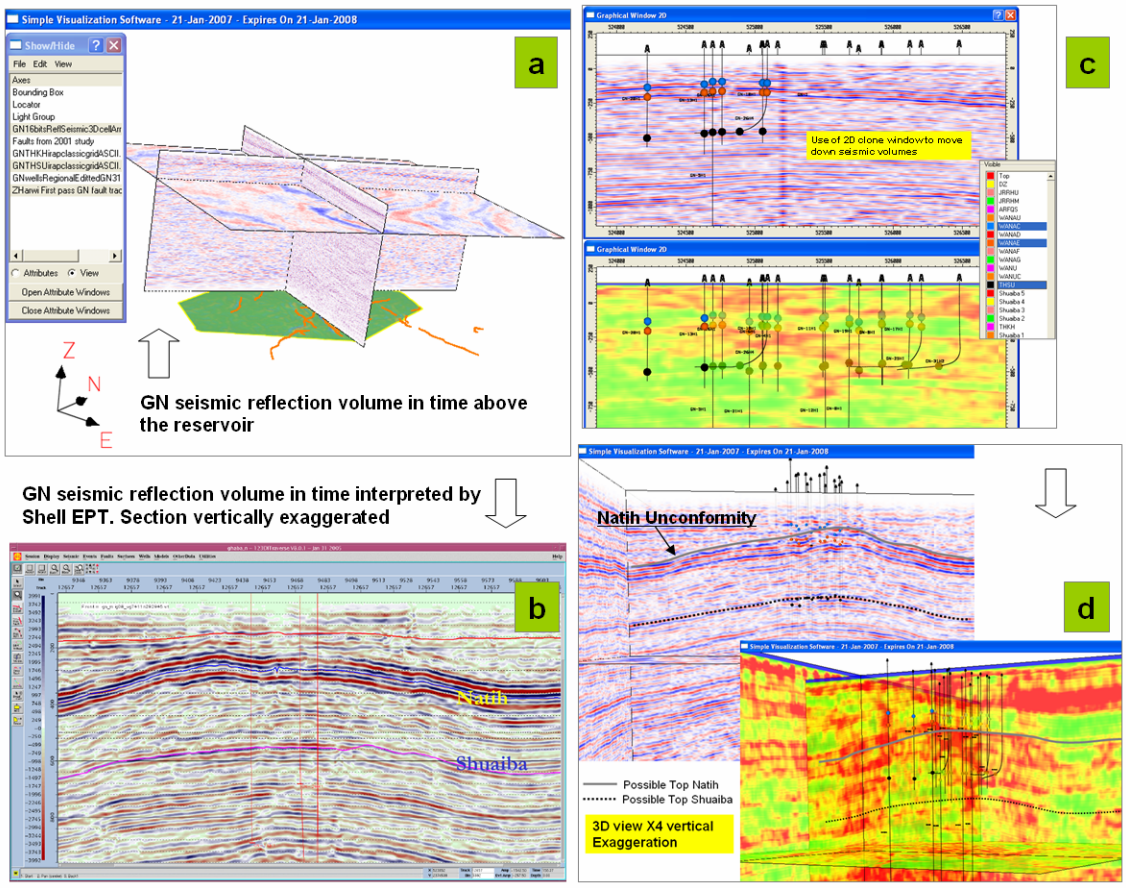


**Figure 4-13 Uploading GN seismic volumes to SVS: a) volumes in time above the reservoir, b) used Shell EPT interpretation as a guide, c) moved the volume in 2D window to ensure only vertical translation; d) confirmed translation by examining volume in 3D view exaggerated utilizing the Tertiary unconformity above Natih Formation reflector as a marker.**

| Well | CC | CI | CP | CPN | NC | NCN | NP | NPN | UF | Total | BHI m |
|---|---|---|---|---|---|---|---|---|---|---|---|
| GN16H1 | | 3 | | 2 | | | | 1 | | 6 | 76* |
| GN17H1 | | 18 | | 3 | | 1 | | 3 | | 25 | 98* |
| GN21H1 | | | 29 | | | | 6 | | 2 | 37 | 99* |
| GN23H1 | | | 38 | | | | 5 | | | 43 | 110* |
| GN25H1 | 47 | 53 | 304 | | 8 | | 2 | | 4 | 418 | 465 |
| GN26H4 | 19 | | 65 | | | | | | | 84 | 310 |
| GN31H2 | 25 | | 57 | | 2 | | 1 | | | 85 | 492 |
| Total | 91 | 74 | 493 | 5 | 10 | 1 | 14 | 4 | 6 | 698 | 1650 |

**Table 4-2 BHI fracture picks per well: CC large conductive; CI induced; CP/CPN small conductive; NC/NCN large non-conductive; NP/NPN small non-conductive; UF undefined fault. With BHI length in m. * Well cover both Shuaiba and Kharaib.**

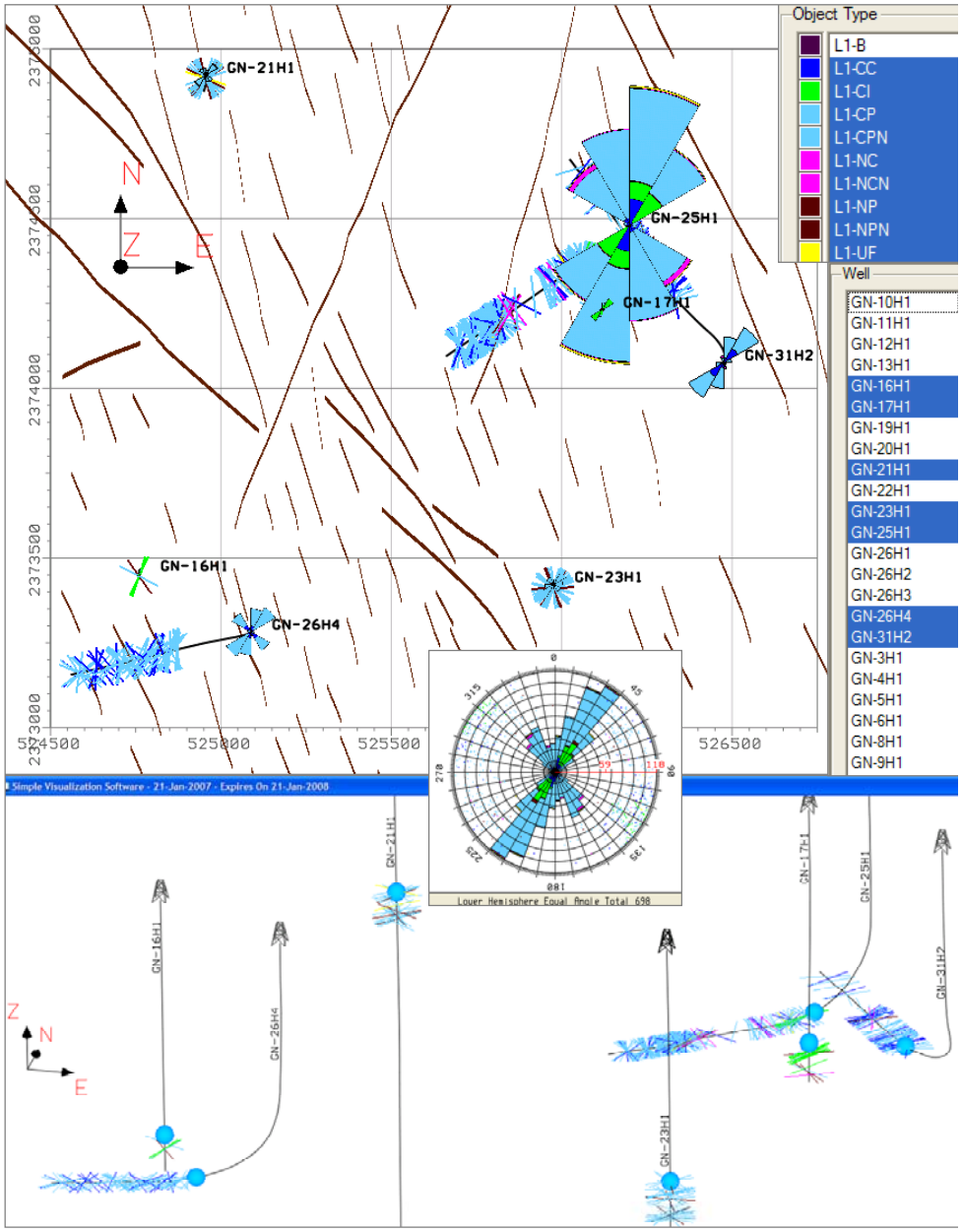


**Figure 4-14 SVS snap shot showing a map view and cross section of GN BHI wells only. Note that GN23H1 is not a Shuaiba well but has been logged with BHI to appraise Shuaiba reservoir.**

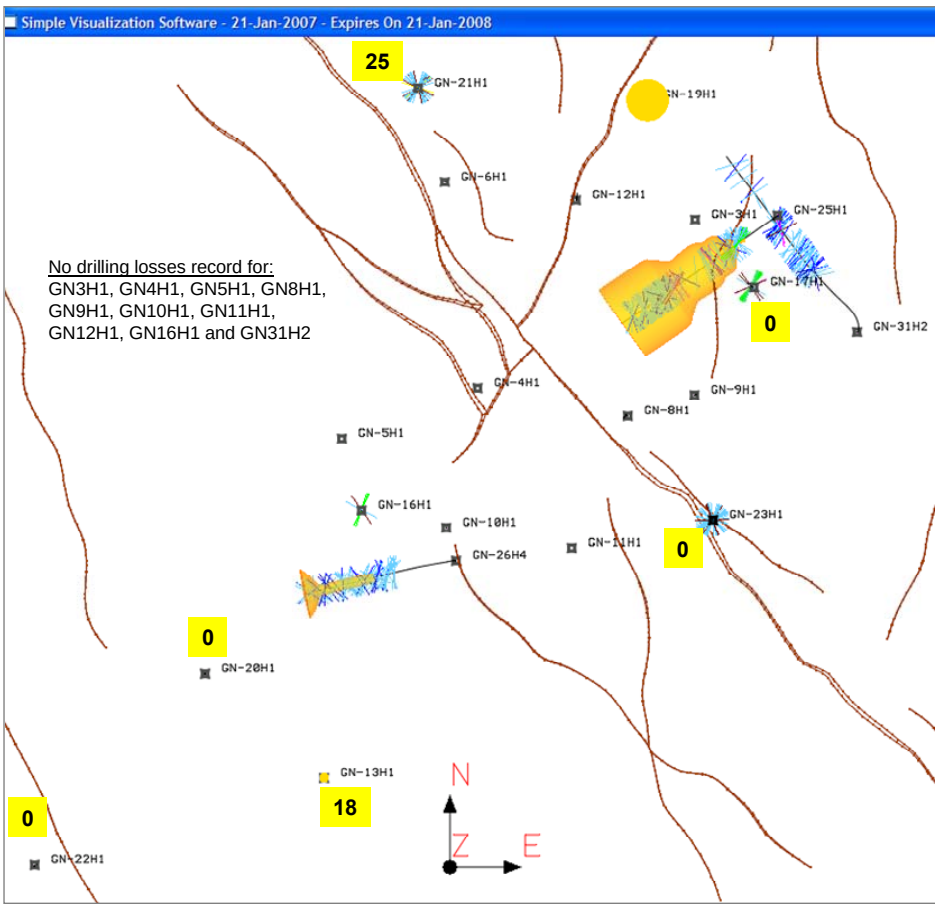


**Figure 4-15 SVS snap shot showing GN Shuaiba wells with drilling recorded losses- annotated with losses value for wells with 0 or partial losses. No drilling record for early wells and for GN31H2.**

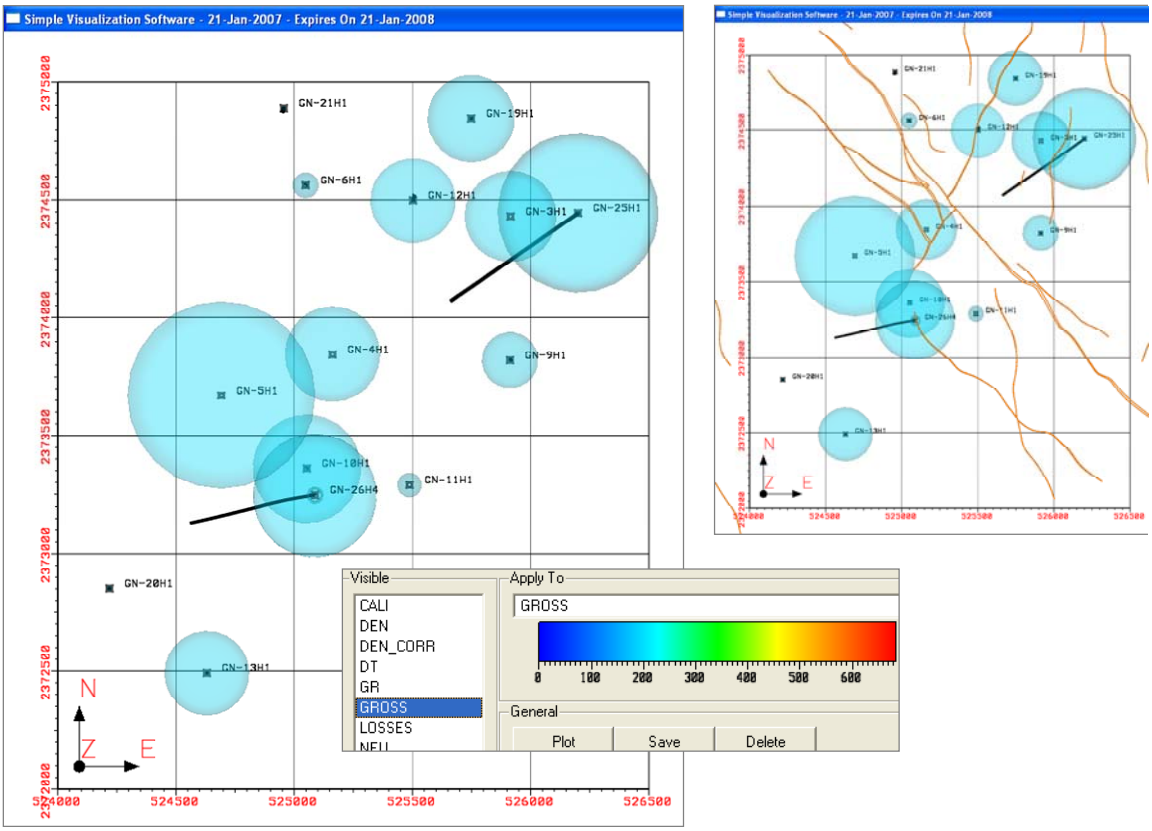


**Figure 4-16 SVS snap shot showing GN Shuaiba wells with normalized gross rate (total gross rate/number of days well on production) as log. Right hand side same with GN faults.**

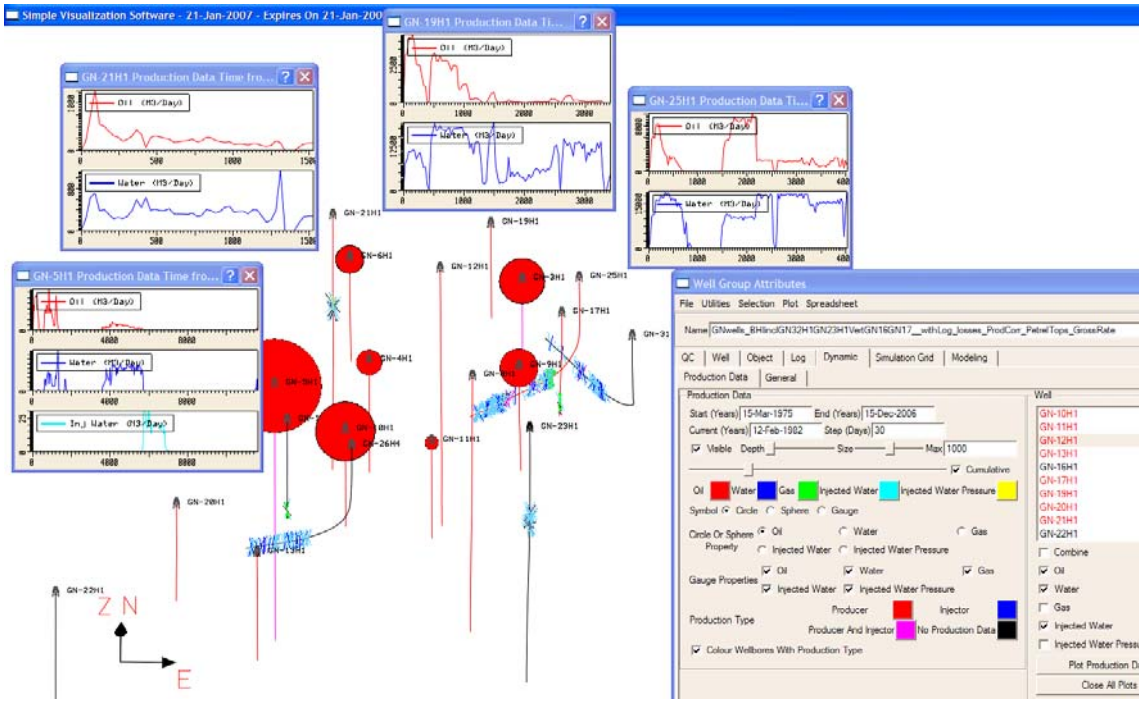


**Figure 4-17 SVS snap shot showing GN wells (wellbore coloured by type -red producer, pink injector –producer converted to gas injector, black – no production data) with examples of production plots in SVS for each wells. Note early high net oil/gross in most of the wells.**

## 4.3 Curvature data analysis -imported to SVS

Under certain conditions, the intensity of curvature affecting a rock unit (layer or group of layers) may reflect the degree of strain of this unit. For rocks deformed under brittle conditions, this strain can be proportional to fracture intensity (Bazalgette et al, 2007). Therefore, curvature analysis can be used in SVS to constrain fracture models.

The value of this method is increased by combining it with an analysis of other fracture-related data. It is essential to mention that the quality of a curvature map is highly dependent on the resolution of the input horizon map and how it was created. If the horizon is based only on well tops or on a coarse seismic bin interpretation, then the interest of curvature analysis is limited.

As mentioned in Chapter 2, the top Shuaiba seismic reflector is very weak, hence seismologists tend to interpret top Kharaib and then isochore upward, since top Shuaiba is conformable with top Kharaib and normally Shuaiba has a uniform thickness (unless distorted by fault cut out). The interpretation at field scale is further refined using well tops (well-tie). Hence, at field scale the top Shuaiba horizon created outside this study is of sufficient quality to perform meaningful curvature analysis.

In SVS the user is encouraged to perform multi-directional curvature analyses at different wavelength scales, since at different scales, the analysis highlights different structural characteristics ranging from emphasising local strain at field scale to finding minute curvature discontinuities (possible faults) at small scale. In addition, SVS allows

for uni-directional curvature analysis. This method allows filtering the curvature intensity along a single orientation. This facility has been shown to be particularly efficient in identifying quite subtle lineaments (usually small-scale) which can correspond to small-offset faults or to fracture corridors (Figure 4.18).

The top Shuaiba horizon has been subjected to curvature analysis in SVS with the objectives being to highlight:

- Areas of high curvature (proxy for strain) using multi-direction (azimuth) large wavelength analysis (Figure 4.19) to predict background fracture intensities.
- Areas of possible faults using multi-direction small wavelength analysis, curvature discontinuities (Figure 4.20) to visualize fractures in damaged zones.
- Hidden structural strain oblique to dominant fault direction using uni-direction (azimuth) small wavelength (Figure 4.20) to see FC or small faults.

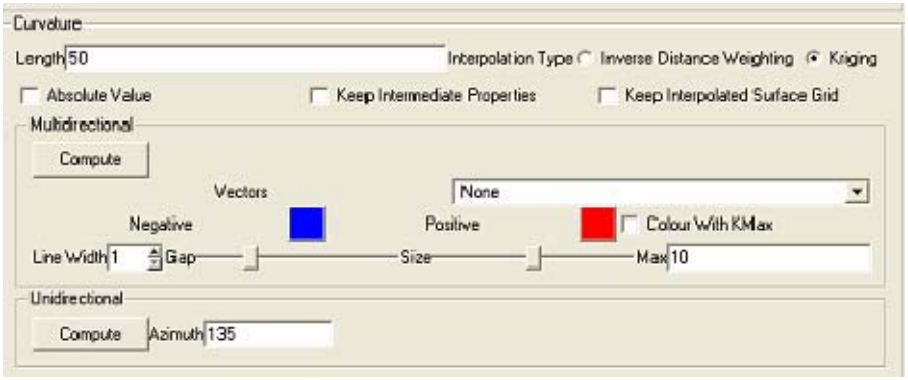


**4-18 Snap shot showing the curvature box in surface attribute window in SVS, giving user options to perform curvature at different length scale using multi- or uni- directional analysis.**

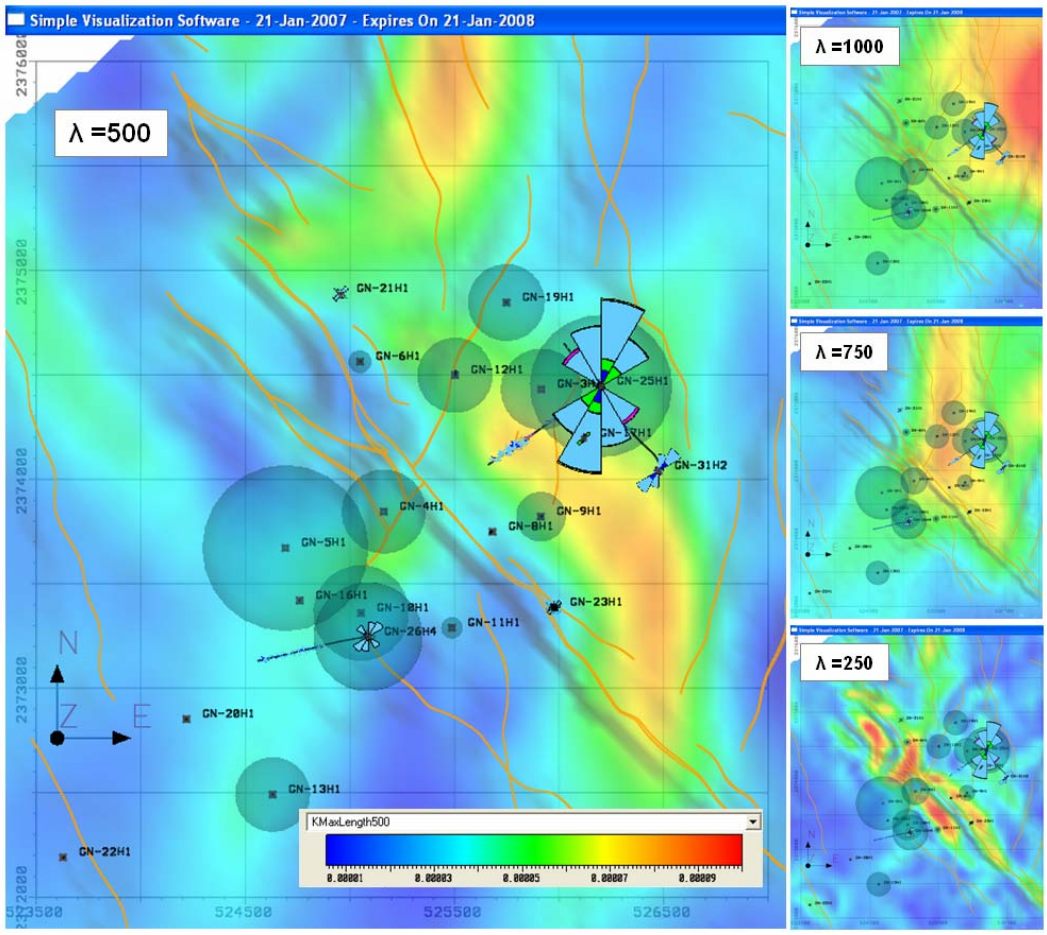


**Figure 4-19 Multi-directional curvature (Kmax – maximum curvature value) at different wavelength for GN top Shuaiba indicates that the NE side of field is more strained. This is in line with the BHI fracture picks with GN25H1 having maximum number, also with Gross rate analysis. GN5H1 is an exception probably related to local faults or due to diagenesis effects.**

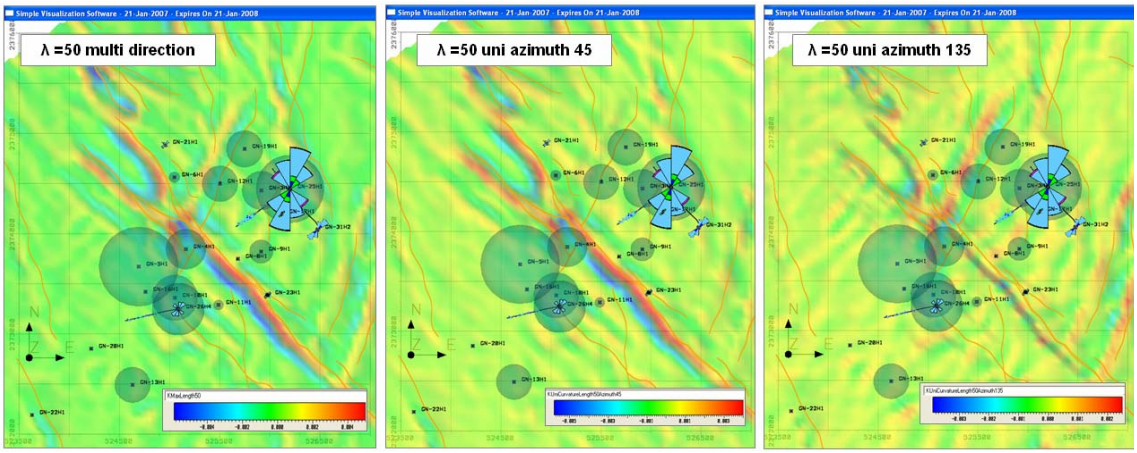


**Figure 4-20 SVS snapshot of a 50m scale wavelength curvature map (Kmax) of GN top Shuaiba to highlight discontinuities: multi-directional; uni-directional @ 45 degree azimuth; and uni-directional @ 135 degree azimuth. Superimposed are fault lines, BHI fracture picks and gross rate values as blue circles.**

## 4.4 Well test and well interference test analysis

No well test data is available to import to SVS, however, recently an interference test was done on GN5, GN8, GN9, GN10, GN13 and GN20. The preliminary observations and interpretations of the result were obtained from Shell EPT in April 2007, which can

be summarised as (Figure 4.21): GN-9H1 build up: Perm height not indicative of highly connected fracture network; GN-9H1 to GN-8H1: Signal consistent with matrix response (effective perm in the range of 10mD to 190mD); GN-9H1 to GN-5H1: No pulse detected; GN-10H1 to GN-5H1: Effective perm in the range of 25mD to 1500mD; GN-10H1 to GN-13H1: Strong pulse indicating high effective fracture permeability (1000mD to 60000mD); and GN-10H1 to GN-20H1: No pulse detected.

Interpretation:

Shell EPT study team preliminary interpretation: There is either a **heterogeneous fracture system -** with some strongly fractured areas (GN-10/13), some moderately fractured areas (GN-10/5) and some poorly or un-fractured areas (GN-9/8). Or a **strongly directional fracture system** - fractures observed in all directions on FMI but only those parallel to Shmax (NE-SW) have a significant contribution. GN-10/13 is on this trend but all other signal pairs are off it.

The Shell EPT team second interpretation is in line with the geometric distribution of the BHI fracture intensity (see figure 4.14). I.e. there is a strongly direction fracture system toward the NE. These fractures could be related to local faults and more importantly to fracture corridors created by the Tertiary compression deformation. The NE fractures, which dominate, are possibly also enhanced by being parallel to the maximum horizontal stress direction, though the role of diagenesis in having them open cannot be rule out.

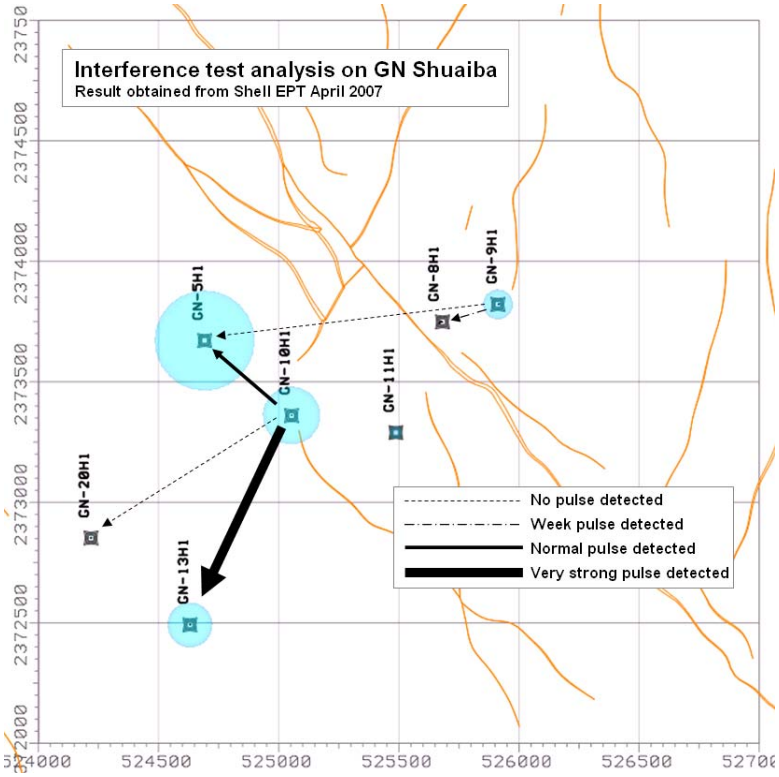


**Figure 4-21 SVS snapshot of GN vertical wells with their interference test results, superimposed are fault lines and gross rate values as blue circles.**

## 4.5 Stress data analysis

### *4.5.1 Background on stress analysis:*

*This section is also applicable for next chapter.*

Stress magnitude and stress orientation analysis is perceived to be valuable in determining the effectiveness of fractures in a reservoir by identifying the likely conductive orientations. Other factors, though, may also be important. For example, actual observations of subsurface fractures, primarily from BHI images, show that in carbonate reservoirs the impact of diagenesis (chemical dissolution or precipitation) is very critical in controlling the conductivity of a subsurface fracture network.

The three main principal stresses (**σv, σh** and **σH)** can be directly and in-directly derived from subsurface data (Hickman and Zoback, 1983). The effective vertical stress (**σv**) is obtained by multiplying the overburden rock density by the depth

$$\sigma v = \rho g h - P_f \qquad (4.1)$$

Where **ρ** is overburden rock density**, g** is gravity**, h** is depth and $P_f$ is the formation pore fluid pressure, which can be obtained from RFT data.

The minimum horizontal stress (σh) is estimated from the break-down pressure or approximated from a leak off test, while the limit test (normally required by the driller to establish if the casing and rock strength can retain a minimum required pressure for safe operations) indicates a lower limit to the actual σh. The theoretical basis for estimating the minimum stress is related to the notion that a hydraulic fracture can be initiated by raising the fluid pressure (as occurs in the leak-off test), and propagates perpendicular to σh. The magnitude of σh, therefore is determined from the pressure in the hydraulic fracture immediately after pumping into the well is stopped and the well is shut in (Figure 4.22).

Estimation of the maximum horizontal stress (σH) is again based on assumptions about the processes operating, and is largely derived from elasticity concepts. These ideas predict the development of a stress concentration around a vertical circular borehole, due to the creation of the opening itself. The parameters necessary to calculate a value are obtained from a full leak-off test or (mini) frac test.

$$\sigma H = 3\,\sigma h - P_b + T \qquad (4.2)$$

Where $P_b$ is the formation breakdown pressure, $P_f$ is the formation pore fluid pressure and **T** is the tensile strength of the rock.

Alternatively, **σH** can be qualitatively estimated from determining the present-day tectonic regime (i.e. extensional, compressional, strike-slip). The most direct source of information is from earthquake source mechanism that allows determining if the maximum horizontal stress coincides with the maximum principal compressive stress (σ□) or not (Figure 4.23).

In the other hand the stress orientation might indicate the likely direction to encounter conductive fractures. Induced (i.e. hydraulic) fractures tend to be parallel to σH, faults or fractures orientated at a high angle to σH may be preferentially closed/sealing and are the least likely to be reactivated if ambient reservoir stress conditions change during development, and borehole stability problems are least expected in deviated sections with an azimuth parallel to σh (Hoogerduijn-Strating, 2002). Borehole elongation information from calliper logs and the presence of induced fractures from BHI data, are good indicators for σH direction (Figure 4.24).

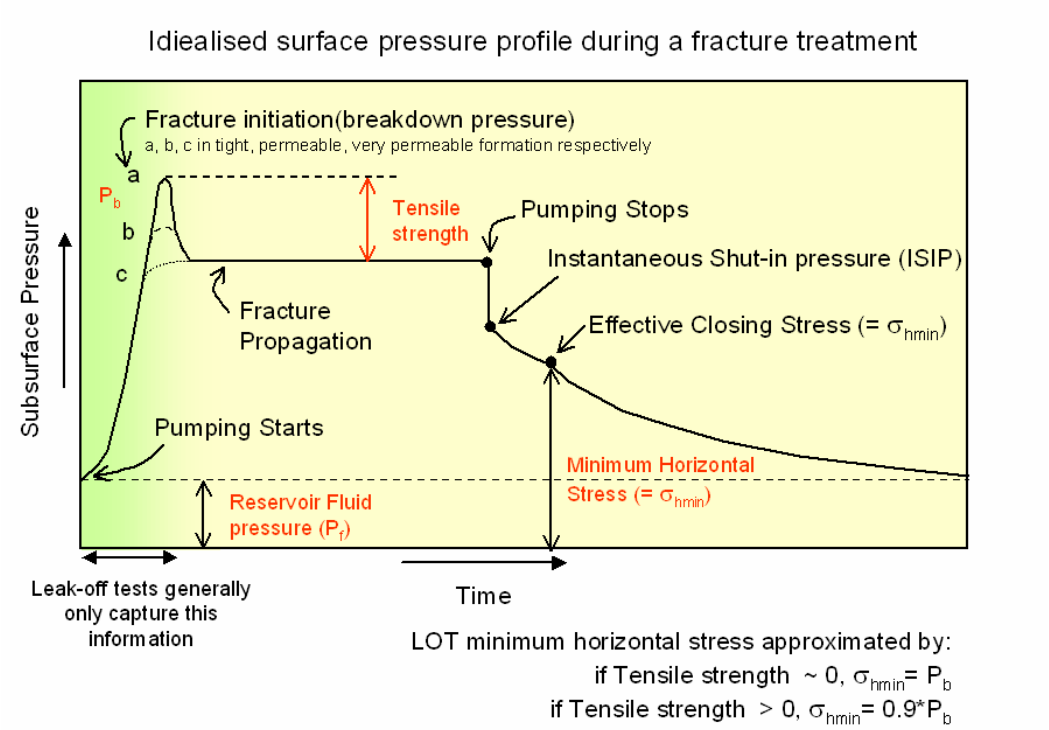


**Figure 4-22 Illustration showing pressure profile during a leak off test and the approach used to obtain minimum horizontal stress (Hoogerduijn-Strating, 2002).**

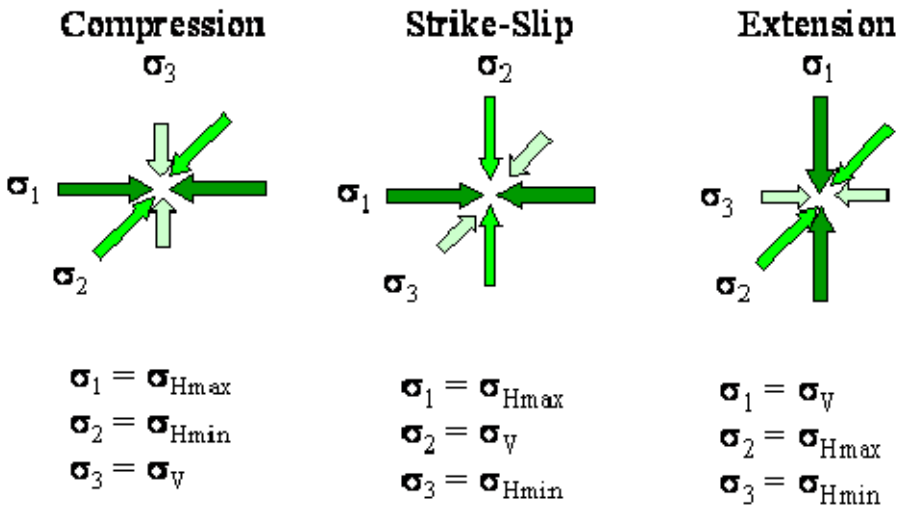


**Figure 4-23 Tectonic regimes and their associated principal stresses (Hoogerduijn-Strating, 2002).**

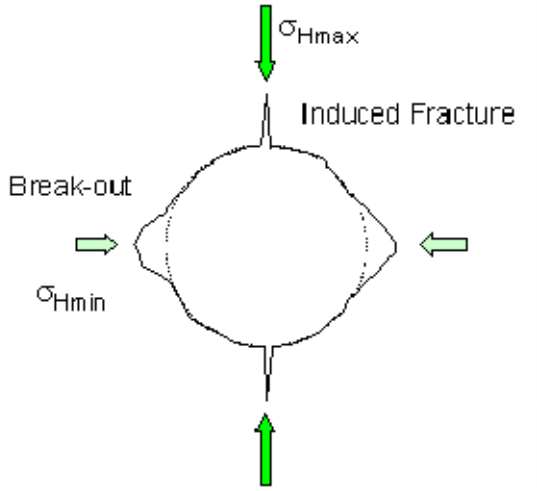


**Figure 4-24 Indicators used to determine stress orientation: induced fractures and borehole breakout (Hoogerduijn-Strating, 2002).**

### *4.5.2 Ghaba North Shuaiba stress analysis:*

Stress-strain detailed analysis for the Cretaceous reservoirs is beyond the scope of this research. However, simplified calculations are presented here to check the tectonic regime found in these reservoirs. As noted in Chapter 2, there have been only a few detailed studies in PDO to determine the stress magnitude in north Oman reservoirs. A relevant example is the study of Hoogerduijn-Strating (2002), which covers the central region of north Oman including Ghaba North. Note that the principal stresses noted in Chapter 2 were calculated for the deeper Amin Formation by GMI. Here a similar attempt is done but for the Cretaceous Shuaiba Formation to see if the likely tectonic regime is strike-slip (**σH > σv > σh**).

Ghaba North Shuaiba reservoir crest depth is at 433mss (585mbdf- below derrick floor-DFE ≈ 152m), and the overburden rocks are mainly carbonates with a density average of 2300 kg/m$^3$. Hence, the overburden pressure is

$$\sigma v = \rho g h = 2300 * 9.8 * 575 \approx 13 \text{ MPa} \quad (4.3)$$

A few measurements of leak off test data from Ghaba North and surrounding fields (Figure 4.25) were used to calculate the value of the minimum horizontal stress (**σh)**. At a depth of about 600m, the minimum horizontal stress (**σh**) value is ≈ 9 MPa.

For the maximum horizontal stress, assuming the breakdown pressure (**Pb**) equals the minimum horizontal stress (**σh**), then

$$\sigma H = 2\,\sigma h + T \quad (4.4)$$

It follows, that the maximum horizontal stress ≥ 18 MPa. Regardless of what is the value of T, a strike slip tectonic regime exists here, i.e. (**σH > σv > σh**). This transtensional tectonic setting is likely to be complicated by the impact of a rising up ("dome") salt diapirs in GN.

Borehole breakout data from nearby (< 40 Km SW of Ghaba North) Shuaiba reservoir of Qarn Alam field from 5 vertical wells gives an average azimuth of 117 degree, hence, **σH** direction of NE. In addition, this direction is also supported by induced fracture orientation seen in the BHI log (see Figure 4.14). In contrast, recent kinematics interpretation by Richard and Filbrandt, of the fault geometry at a sub-regional scale around GN (Figure 4.26) indicate a NW direction for the **σH**. This contradiction in **σH** direction and its impact on field-scale fracture may only be understood, if a detailed stress-strain analysis is to be done in north Oman Cretaceous reservoirs and all existing assumptions and current approaches are examined carefully.

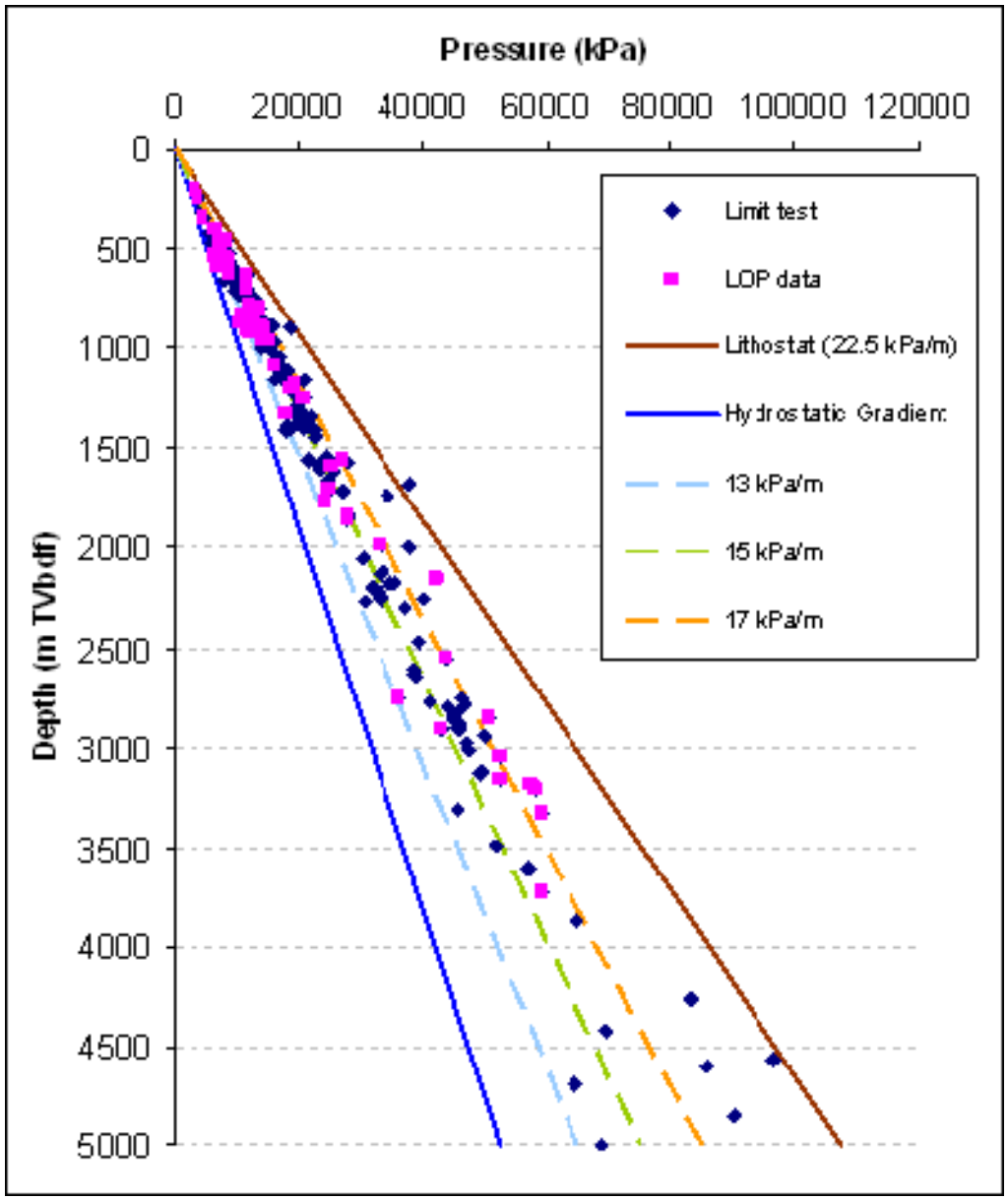


**Figure 4-25 Plot of pressure gradient with minimum horizontal stress (inferred from LOT and LT) for north Oman carbonate reservoirs (Hoogerduijn-Strating, 2002).**

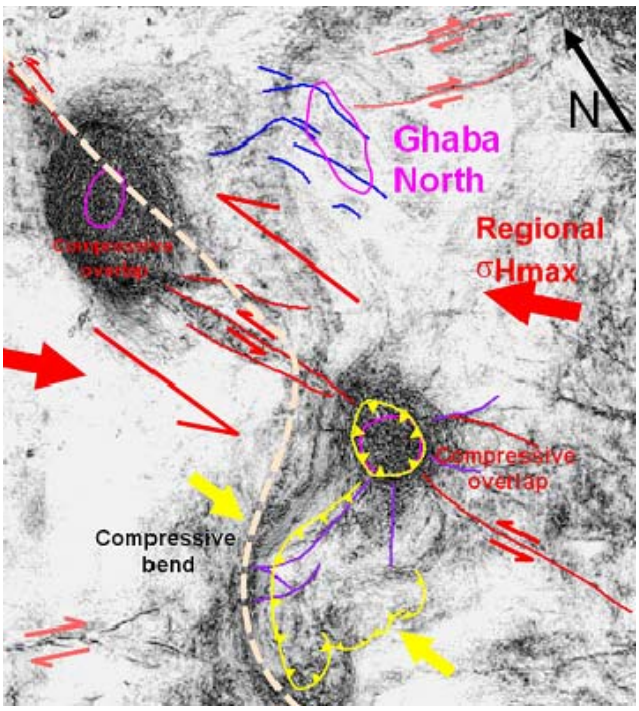


**Figure 4-26 A sub-regional kinematics analysis for the area around GN field, by Richard (2005). It indicates a possible NW direction for the maximum horizontal stress.**

## 4.6 Sand box analogue for Ghaba North

A sand box analogue for the Ghaba North Shuaiba reservoir is presented, based on Shell-PDO sand box data base (Richard, 2005) and a perceived analogue field on offshore UAE. Clay-cake physical models used to investigate interaction of far-field stress [$Sh_{min}$ (σ□) = NE-SW], and uplift bending strains and tangential extension associated with salt diapirism. It highlights complex fault interactions as a result of interaction between doming-related and far-field-related processes (Figure 4.27).

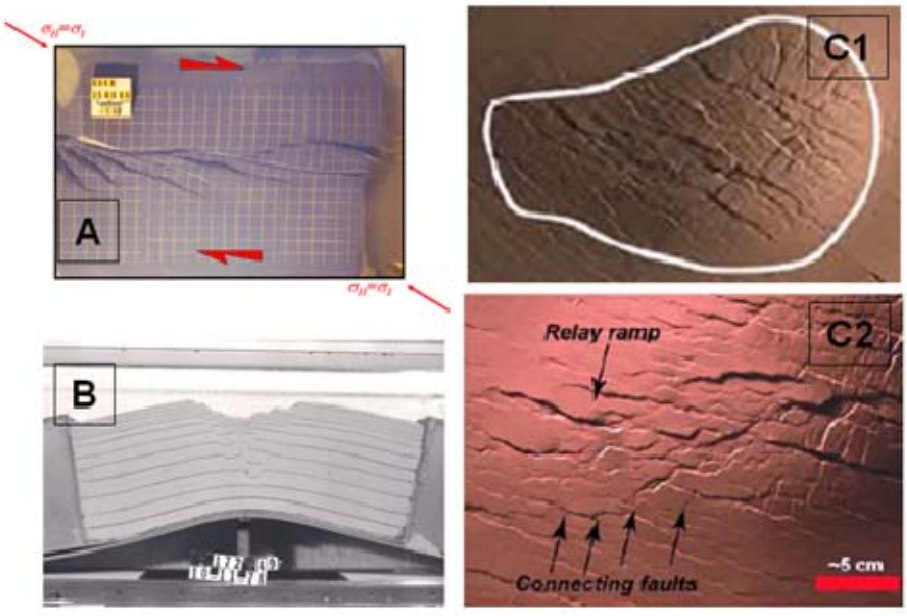


**Figure 4-27 Sand box model scenario for Ghaba North field aligned with the kinematics analysis. [A] map-view; [B] cross-section; [C1/C2] analogue model made for offshore field in the UAE (Richard, 2007).**

## 4.7 Fracture spacing calculations in SVS

*This section is also applicable for next chapter.*

The spacing between two fractures is the shortest distance between them, i.e. the normal distance between consecutive fractures. SVS measures both the distance along the borehole between consecutive fractures termed ***down-hole spacing*** and the normal distance "spacing" between consecutive fractures termed ***normal spacing*** using the borehole as a scan line and accounting for fracture orientations. Calculation starts from the first fracture encountered in a well.

In the hypothetical situation, where the fractures are perpendicular to the well's trajectory, the down-hole spacing is equal to the normal spacing (Figure 4.28, b3). But in reality, fractures tend to be running at an angle to the well's trajectory. In such cases the down-hole spacing is larger than the normal spacing (Figure 4.28, b1&b2). This situation is exemplified in the case where the well is vertical and the fractures are sub-vertical (Figure 4.28, d1 & d2). Thus, the intensity of sub-vertical fractures tends to be underestimated when sampled by vertical wells**.**

In most cases consecutive fractures tend not to be parallel, for instance because they were created by different phases of deformation. In such cases, there are two methods in SVS, to calculate or approximate their spacing (Rawnsley and Dhahab, 2005):

- By projecting a normal to each fracture from the point of intersection with the well, until it reach an extrapolated plane of the adjacent fracture (Figure 4.28, a).

- By grouping the fractures by orientation using the selective interactive rose diagram in SVS (Figure 4.28 b1/b2/b3). In this approach the accuracy of the spacing is highly dependent on the bin size and on their total population number. A 10 degree bin size will ensure that consecutive fractures of a set are sufficiently sub-parallel to allow a good estimate of their spacing, however there may not be enough of them to be representative. A bin size of 90 degrees will produce an erroneously high spacing value. In this study, a bin size of 45 degrees is used for most analysis, but bins of 15 and 90 were considered.

SVS also allows the calculation of spacing between fracture clusters. These may represent fracture corridors in a reservoir. The approach involves the creation of a ***fracture intensity log*** along a well trajectory (Figure 4.28 c1/c2) after splitting the fractures by orientation into different sets. See below for further information. Once a fracture intensity log is created, then the user can create in SVS (in well group attribute window/ log tab / curve sub tab / object box) a central object (SVS term for fractures is well objects) which will be added to the existing well objects for statistical or visual analysis (Figure 4.29).

*In SVS, the fracture intensity log is a very useful tool for fracture characterization as it can be used to calibrate fracture distribution with other fracture related data such as production logs or wire line conventional logs or even seismic logs (SVS allows to paint seismic image into a well trajectory as a log). The user can pick in between two options of intensity: average where the number of fractures is divided by the step (bin) used; or total fracture intensity log where the number of fractures in each step (bin) is used. The user decides on the size of the bin after reviewing/plotting the fractures (usually not more than few meters).*

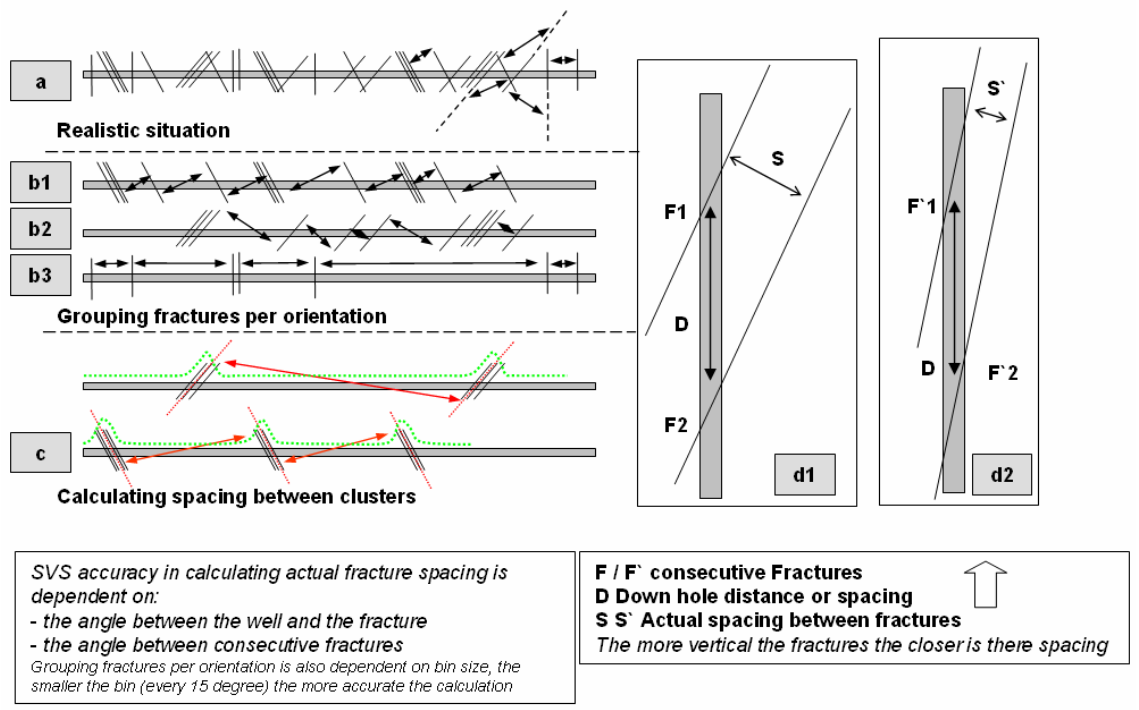


**Figure 4-28 an approximation approach, is used to calculate normal spacing between consecutive fractures in SVS (a), otherwise fractures "well objects" have to be splits per orientation into sub-groups of similar strike (b). Clusters can be analysed in SVS as single fractures (c) using fracture intensity logs to determine fracture corridors spacing for instance. Vertical wells tend to sub-sample fracture intensity when fractures are sub vertical (d).**

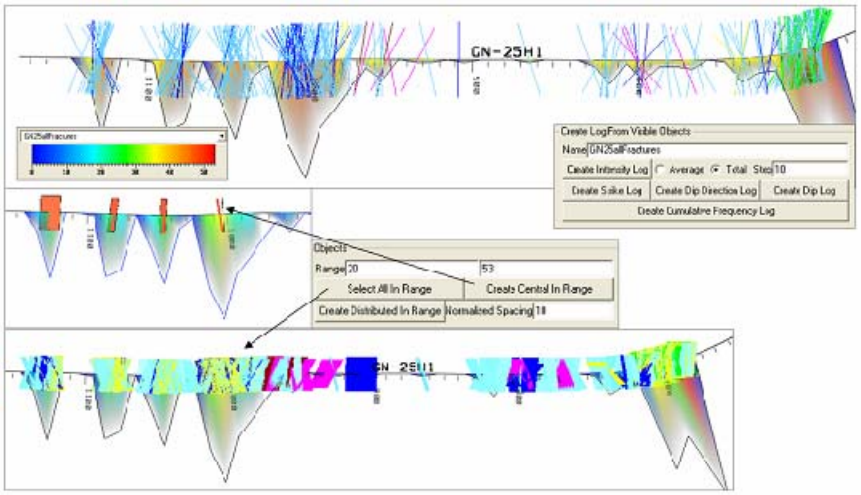


**Figure 4-29 Analysis of fracture clusters in SVS. It start with splitting the fractures into set based on orientation, followed by the creation of a fracture intensity log in a specified step (e.g. every 10m along the borehole) and then analysing the fractures "well objects" within a range in the log. SVS allows for the creation of central object which may be used as representative for the calculation of a cluster's (e.g. fracture corridors) spacing.**

## 4.8 GN well by well fracture analysis in SVS

There are few wells with BHI in Ghaba North: a total of 7 wells with 1650m of BHI interval. Thus, I decided to present the data well by well in this section. This will not be the case in next chapter –the other field case example of Lekhwair- where the number of wells is much larger, hence there, well by well analysis will only be shown where it adds to the understanding of the fracture network.

### *4.8.1 GN16H1*

This vertical well was drilled in 1985 in the SW part of the field as an observation well –the well has never been produced. There is 20m of recovered core which is not available for this study. The BHI (FMS – 4 pads only) length is 76m with only 3 small fracture and 3 induced fractures observed. The FMS image is of low quality (Figure 4.30). The main observations are: The fracture picks are hard to see in the FMS; the orientation of the natural fractures is NW to WNW; and the orientation of the induced CI fractures is NE, found in the centre of Shuaiba Formation.

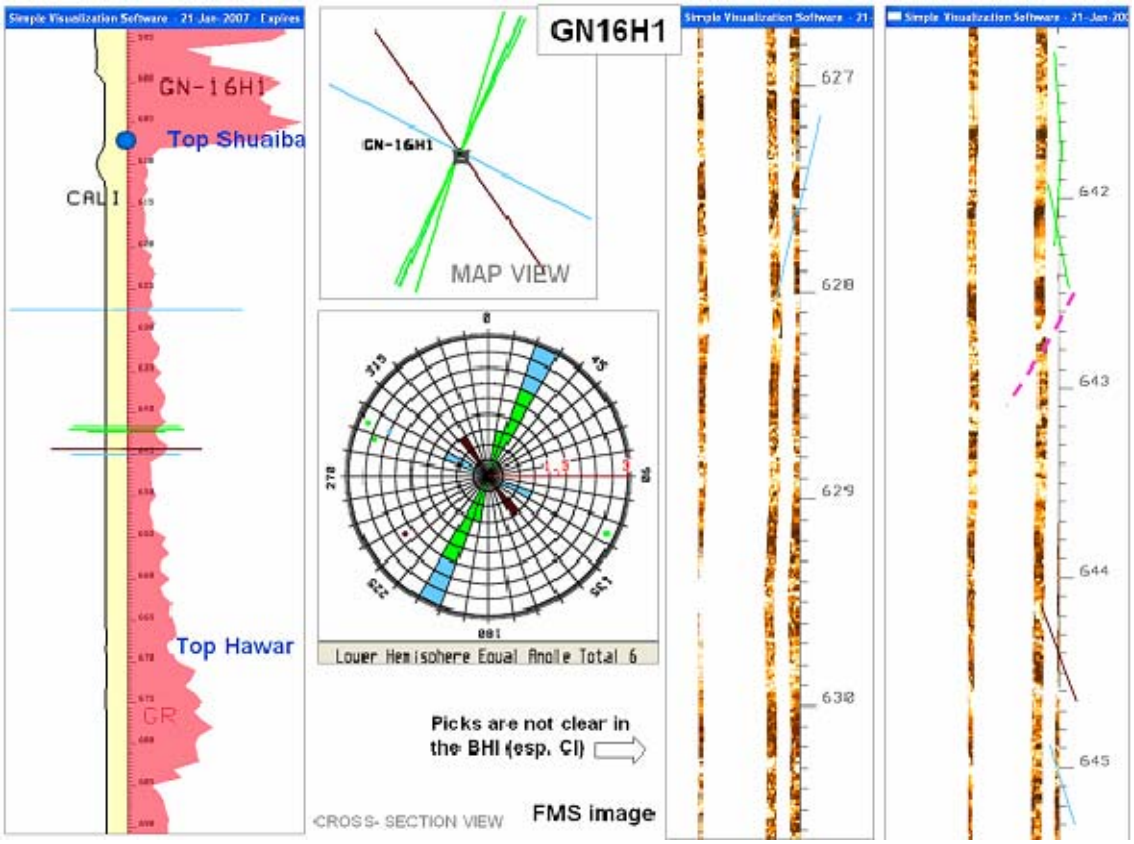


**Figure 4-30 GN-16H1 wellbore with GR log (red shade) and calliper log (light yellow) at Shuaiba interval showing fracture picks (horizontal colored lines); as well as rose-diagram showing fracture orientation; and snap shots of the FMS image available.**

### *4.8.2 GN17H1*

This vertical well was drilled in 1985 in the NE part of the field, in between GN-25H1 and GN-31H2, as an observation well – the well was never produced. The FMS interval length is 98m with 7 natural fractures picked and 18 induced fractures picked (Figure 4.31). The main observations are: Natural fractures are in the Kharaib Formation, only 1

fracture was picked in Shuaiba Formation; induced fractures occur mainly in the central part of Shuaiba; dominant fracture strike orientation is NE and NW. For the induced fractures (CI), the strike is NE. FMS image is poor but shows lithological variation in Shuaiba. Again because SVS does not allow for image enlargement, it is difficult to pick the fractures.

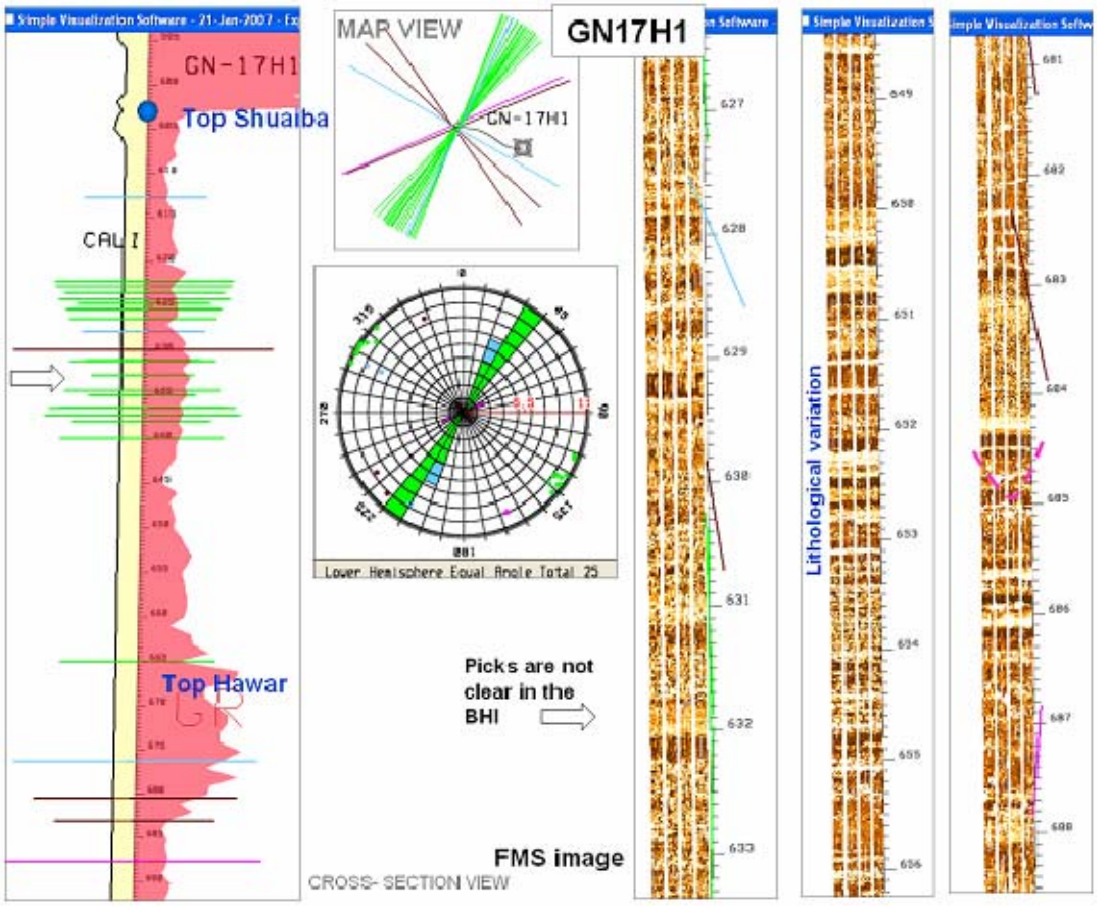


**Figure 4-31 GN-17H1 wellbore with GR log (red shade) and calliper log (light yellow) at Shuaiba interval showing fracture picks (horizontal colored lines); as well as rose-diagram showing fracture orientation; and snap shots of the FMS image available.**

### *4.8.3 GN21H1*

This vertical well was drilled in 1987, in the NE part of the field within the NE flank at about 100m east of the main fault "graben", as a producer for Gharif reservoir, but later converted to Shuaiba producer in June 1990. The well was shut in due to high water cut in 1994 and low gross rate (Figure 4.32), though its normalized gross rate is very low 21 km3/d. FMS interval length is 99m with 35 natural small BHI fractures and 2 undefined faults picked. The main observations regarding the BHI fractures are (Figure 4.33): the dominant strike orientations are NE and NW; majority of the fractures are small conductive; high fracture intensity is seen in top Shuaiba and top Kharaib (Hawar member); and the BHI image quality is poor, hence it is hard to pick fractures on it.

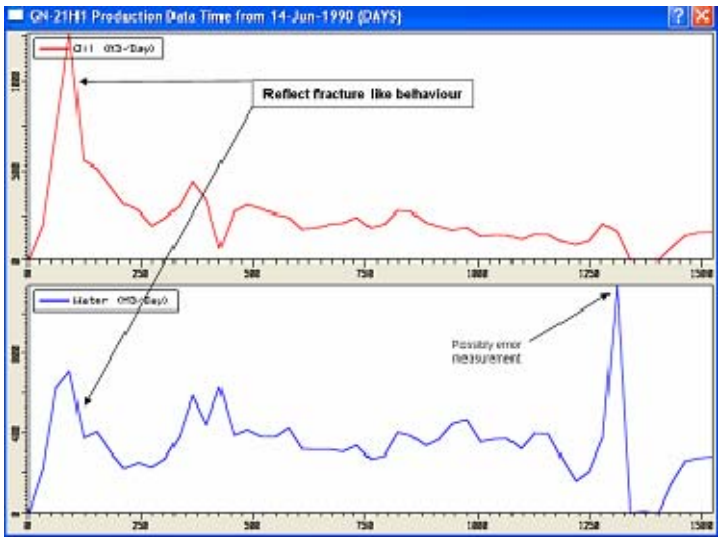


**Figure 4-32 GN21H1 production profile (red is produced oil rate and blue is produced water rate). The early high peak reflects fracture like behaviour.**

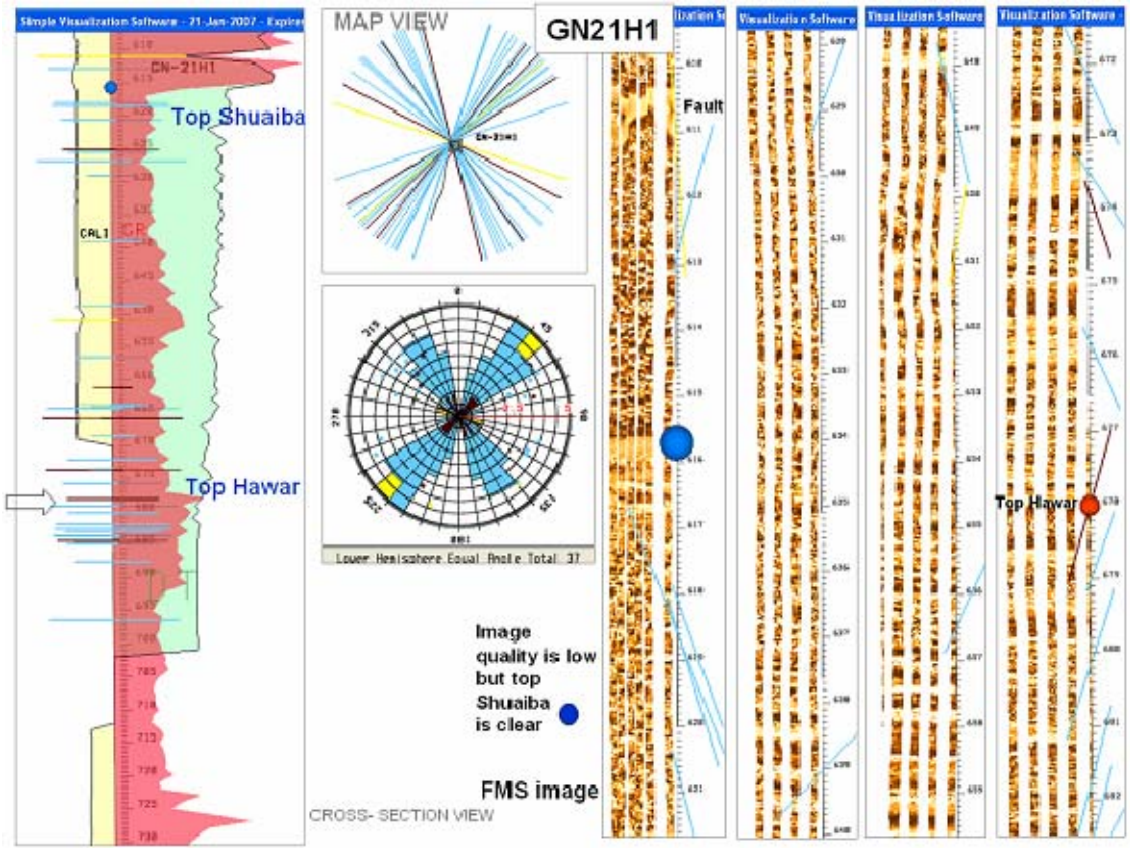


**Figure 4-33 GN-21H1 wellbore with GR log (red shade), DT sonic log (light green shade) and calliper log (light yellow) at Shuaiba interval showing fracture picks (horizontal colored lines); as well as rose-diagram showing fracture orientation; and snap shots of the FMS image available.**

### *3.8.4 GN23H1*

This vertical Gharif well was used to acquire 50m of core and logs for the Shuaiba interval. The well was drilled in the NE part of the field in the eastern flank at the main fault "graben". The core description was done by Fariz Srouji of UAE Core Laboratories in 1990. It indicates the presence of induced fractures and rubble zones (indicative of natural fracture though it can be related to lithology and coring mechanism) as well as the presence of tight layers, one about 15m below top Shuaiba

(Figure 4.34 and Figure 4.35). The main observations from the BHI image (Figure 4.36) are: there is a spread in the dominant strike orientation but in general NE and NW dominate; majority of the fracture are small conductive; high fracture intensity is present in middle Shuaiba and middle Kharaib; and again it is very difficult to pick fractures in BHI image due to its poor quality.

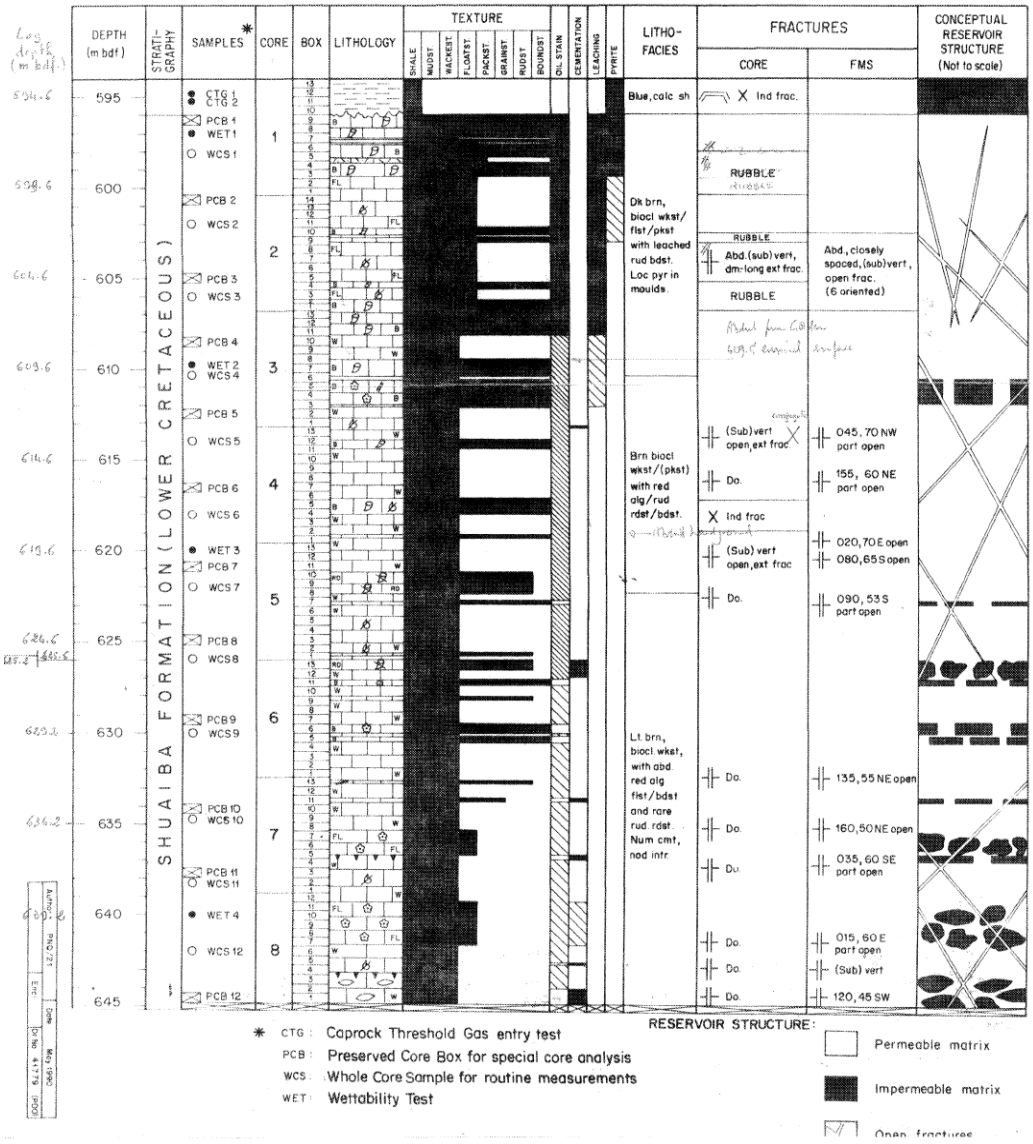


**Figure 4-34 GN23H1 Shuaiba core description showing fracture picks (last column).**

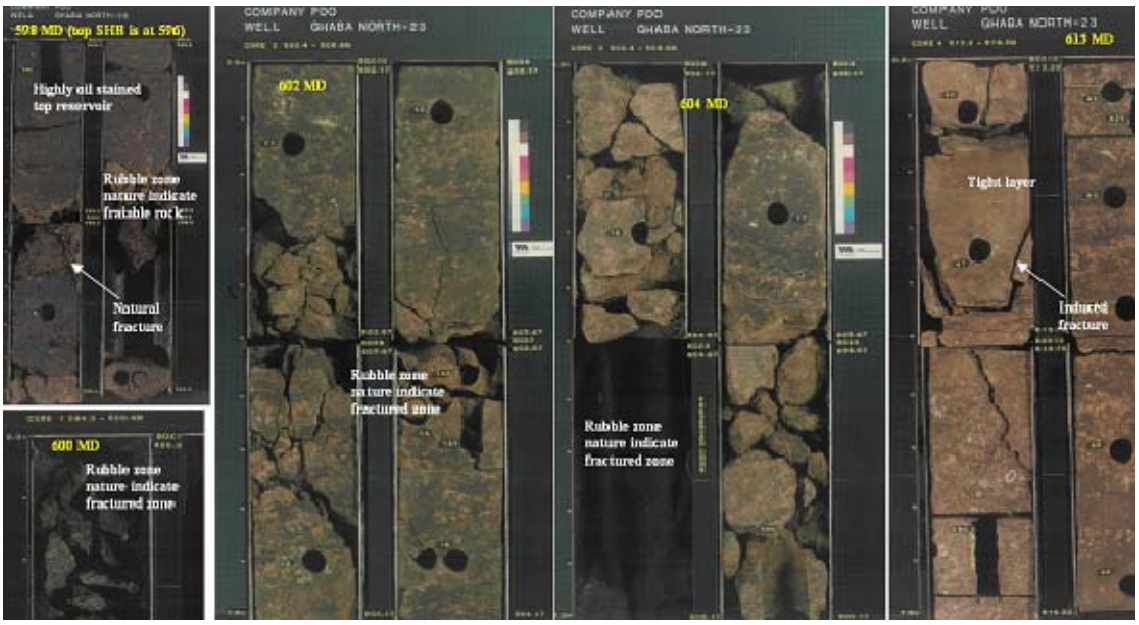


**Figure 4-35 Snap shots of GN23H1 Shuaiba interval core highlighting presence of fractures, rubbles and tight zones.**

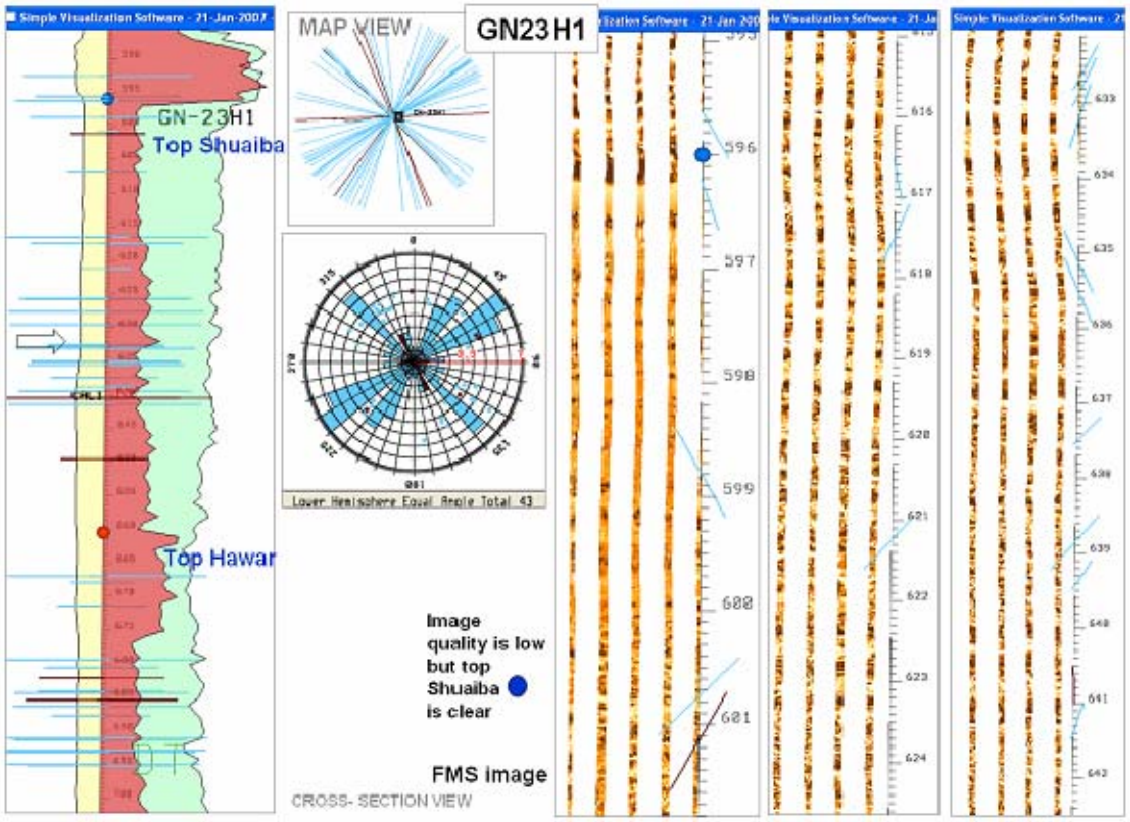


**Figure 4-36 GN-23H1 wellbore with GR log (red shade), DT sonic log (light green shade) and calliper log (light yellow) at Shuaiba interval showing fracture picks (horizontal colored lines); as well as rose-diagram showing fracture orientation and snap shots of the FMS image available.**

### *4.8.5 GN25H1*

This horizontal Shuaiba well was drilled in 1995 in the NE part of the field with a trajectory that is running NE to SW. The well is still producing with a very high normalized gross rate at 598 m3/d despite being closed in from late 1998 to 2000, when it was converted to ESP lift. There was a production allocation error in the whole of Qarn Alam area including Ghaba North field from 1998 to 2002, which has been

corrected. The production profile for the well is shown in Figure 4.37. It has 465m of BHI FMI interval within the upper part of Shuaiba, with 365 of natural fractures including large conductive and 53 induced fracture again striking NE (Figure 4.38 & Figure 4.39). The well encountered total losses during drilling. The main observations based on BHI fracture interpretation are: There is a dominant fracture strike orientations are NE and NW; conductive fractures dominate; fractures occur in clusters; fractures tend to correlate better with the 2001 study faults; and there is a weak relationship with curvature profile at trajectory level.

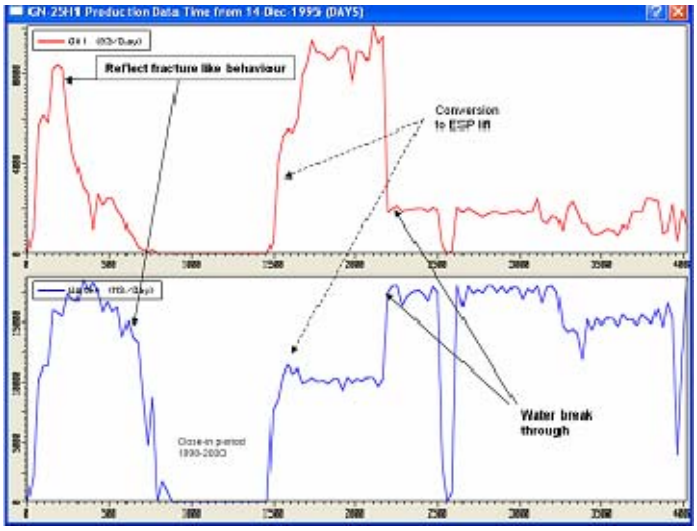


**Figure 4-37 GN-25H1 production profile (produced oil rate and produced water rate).**

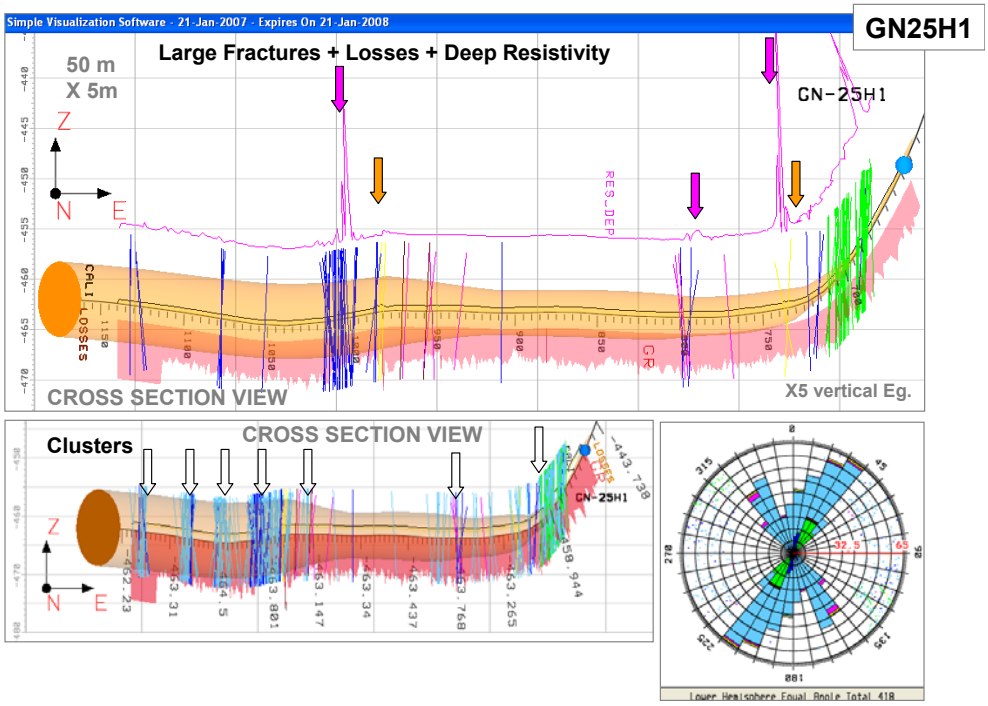


**Figure 4-38 GN-25H1 cross section view with BHI fractures and logs (losses, GR, calliper and deep resistivity pink) as well as rose-diagram with fracture strike and total count. Yellow lines- un identified faults, Green induced fractures, Blue conductive, Pink non conductive.**

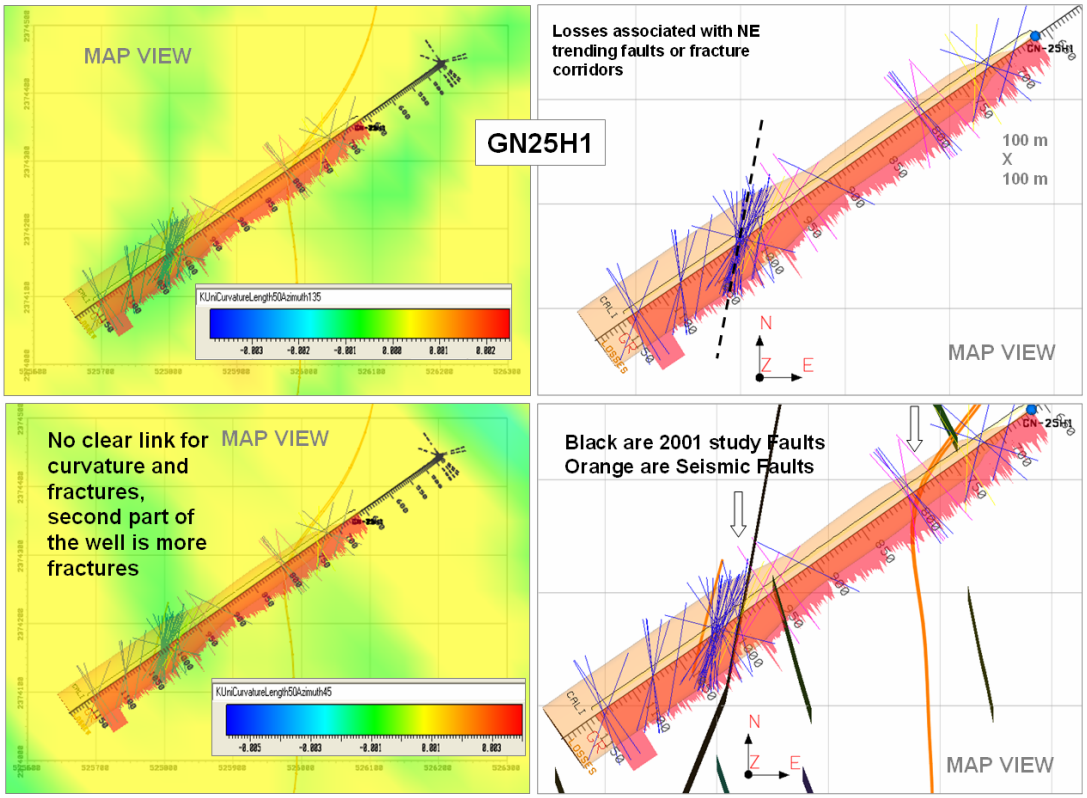


**Figure 4-39 GN-25H1 map view with BHI fractures and logs superimposed at small scale uni-direction curvature (azimuth is 135 top left & 045 bottom left) map (Kmax) of top Shuaiba; and faults (bottom right-black planes are 2001 study and orange planes are the sub-regional faults).**

### *4.8.6 GN26H4*

This horizontal Shuaiba well was drilled in 1997 in the SW part of the field with a trajectory that is running ENE to WSW. The well was shut-in in 1998 because of high water cut 98%; it has not produced for a long period. The normalized gross rate is very high at 478 m3/d, but still less than GN-25H1. The well has 310m of BHI FMI interval with 84 picked fractures, all of which are conductive, which fit with the high losses rate encountered. The main observations from BHI fracture analysis (Figure 4.40 & Figure 4.41) are the following: the fractures are conductive and strike NE with few running NW; fractures correlate well with the 2001 study fault picks; fractures occur mainly in clusters; and there is a weak correlation with curvature m

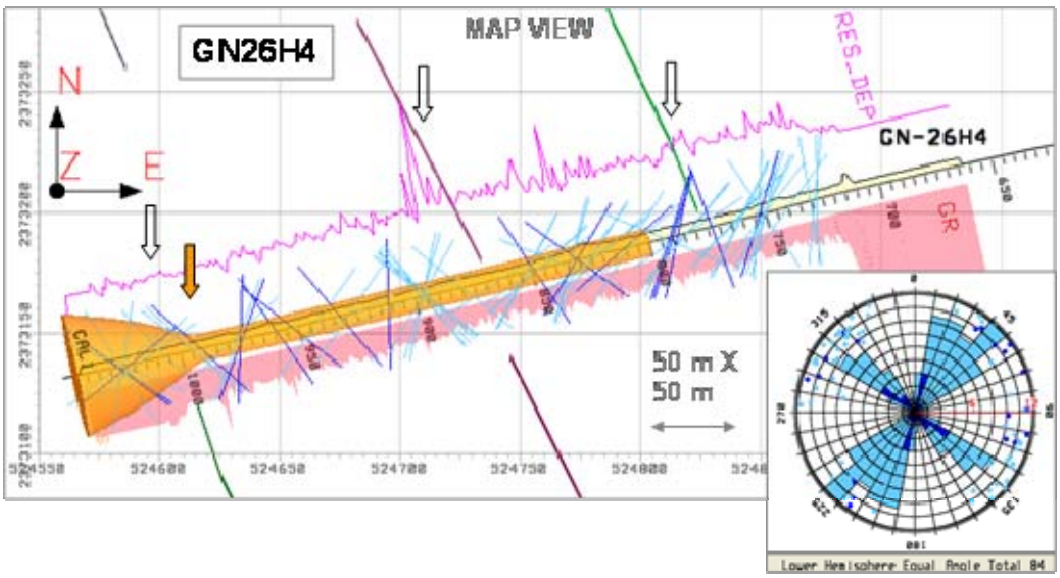


**Figure 4-40 GN-26H4 map view with BHI fractures and logs (yellow cone -losses, light red-GR, black line-calliper and pink line-deep resistivity) together with rose-diagram with fracture strike and total count (84 fractures in total), superimposed on 2001 study fault picks (large lines)**

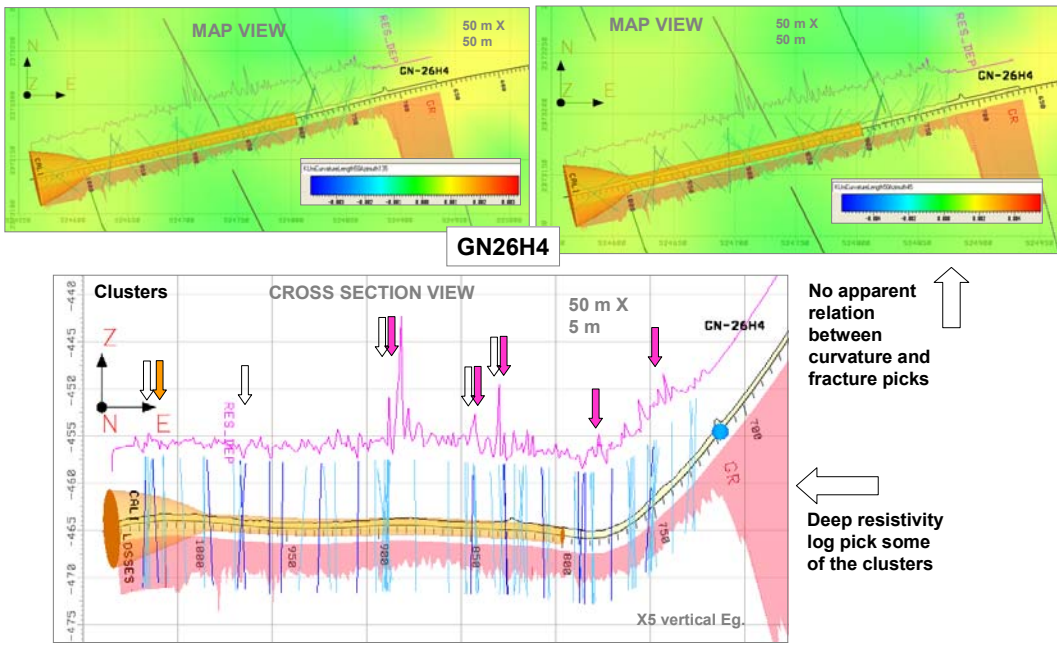


**Figure 4-41 GN-26H4 map view with BHI fractures and logs superimposed at small scale uni-direction Kmax curvature (135 azimuth top left & 045 azimuth top right). Bottom is a cross section view showing fracture clustering being picked by Deep resistivity log.**

### *4.8.7 GN31H2*

This recent appraisal horizontal Shuaiba well was drilled in 2006 as part of the on-going subsurface study, in the NE part of the field, with a trajectory that is running SE to NW. The vertical hole of the well GN31H1 has 80m of core with good recovery. There is NO available description of this vertical core, though core photos were visually inspected (Figure 4.42). GN-31H2 has 492m of BHI FMI interval with 85 picked fractures. The main observations from the BHI fracture analysis (Figure 4-43 & Figure 4.44) are: the majority of fractures are conductive, striking NE. This well might be biased in sampling the NW fracture set as it is striking ENE to WNW, though few NW striking non-conductive fractures were picked; the water flow log and deep resistivity log pick

individual fractures and fracture clusters, though it is more often reflect the clusters; and the first part of the leg is more fractured than second half and it correlates with curvature map (135 degree azimuth uni-directional).

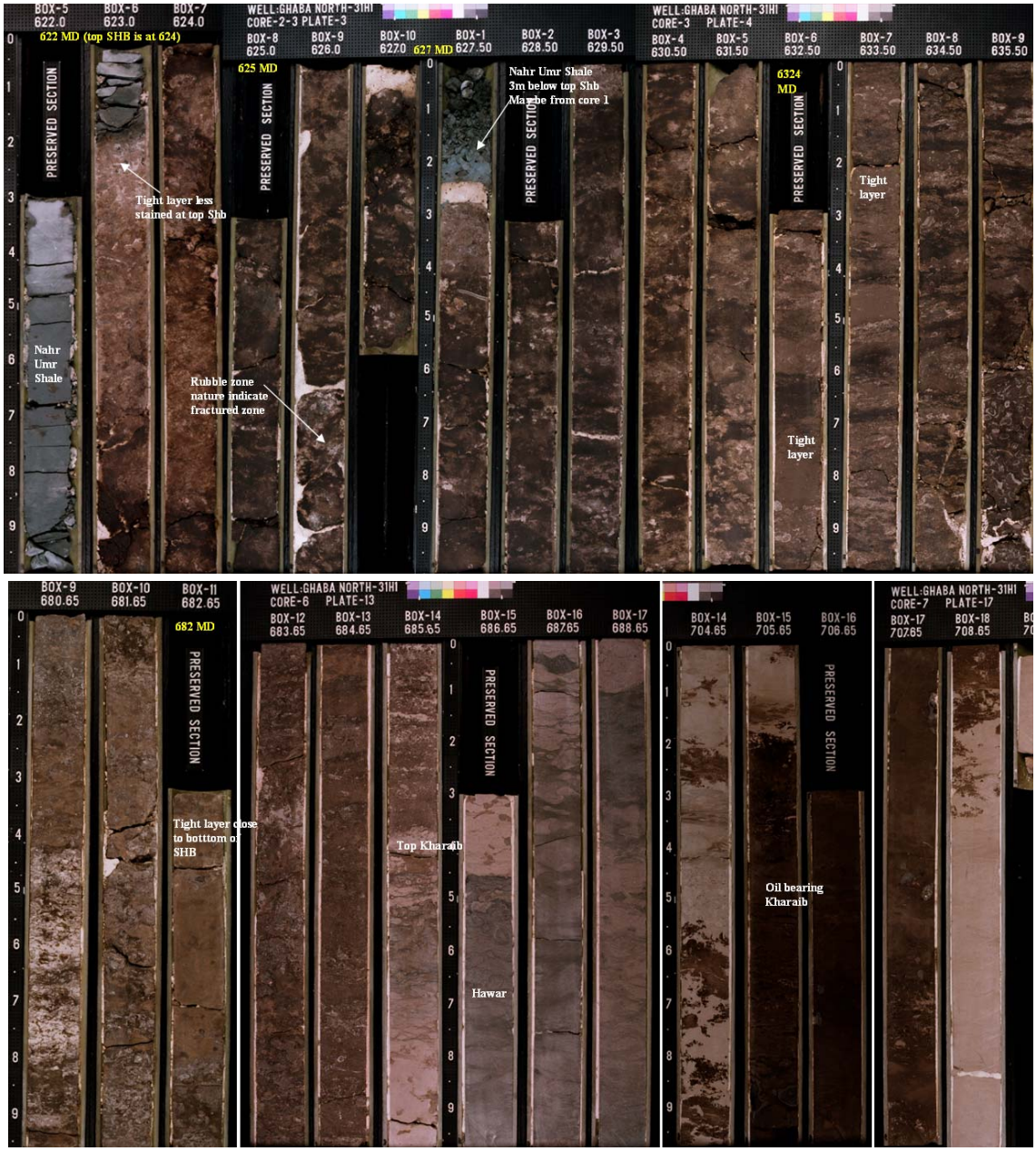


**Figure 4-42 GN-31H1 core photo shows no natural fractures and very few rubble zones.**

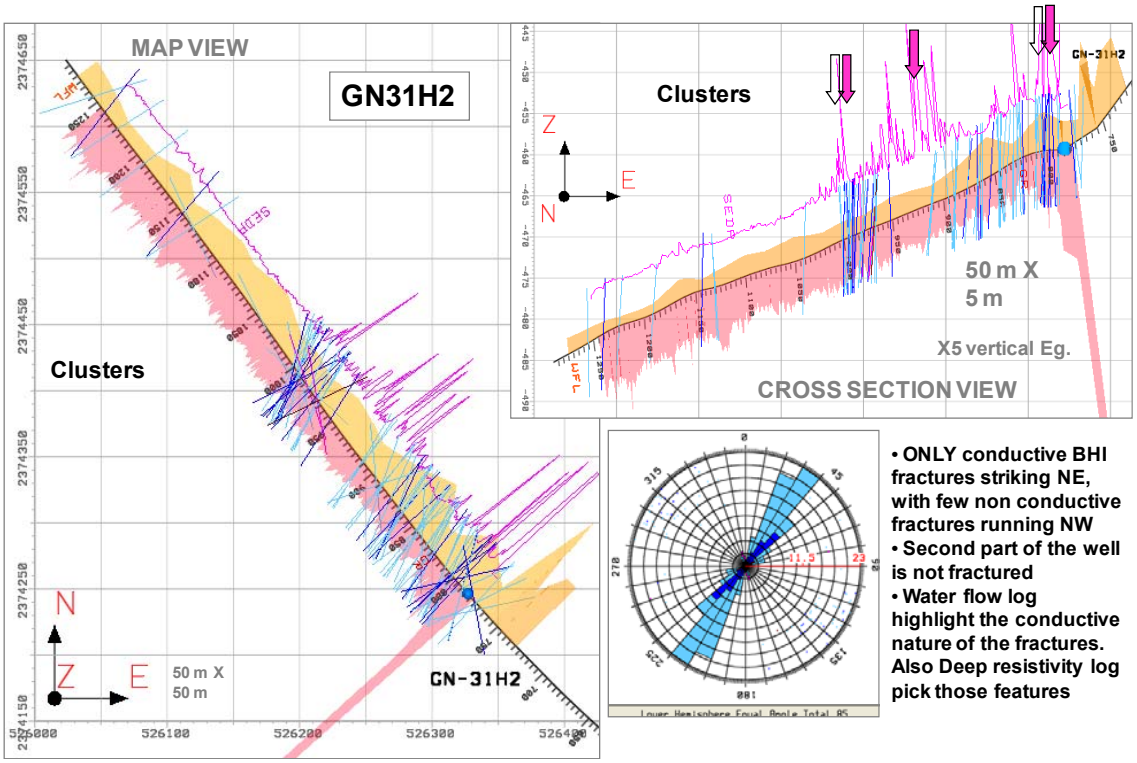


**Figure 4-43 GN-31H2 map view and cross section with BHI fractures and logs (GR, WFL and deep resistivity). Inserted in bottom left corner is a rose-diagram of fractures.**

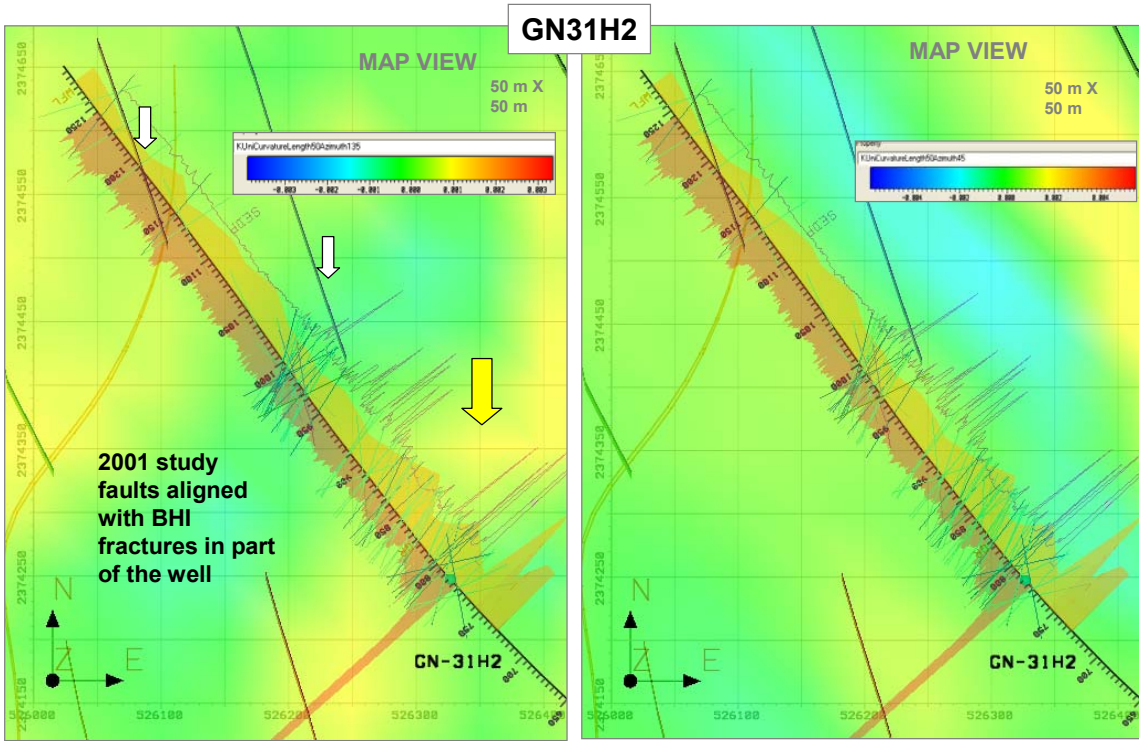


**Figure 4-44 GN-31H2 map view with BHI fractures and logs superimposed on top of a small scale 50m uni-directional curvature map Kmax (135 azimuth left & 045 azimuth right) as well as the 2001 study faults. Note the yellow arrow pointing to high curvature area with high fractures while white arrow points to fault picked next to BHI fracture cluster. This indicates a strong relationship between the faults and BHI fractures seen in the well.**

## 4.9 Statistical analysis of Ghaba North Shuaiba fractures

Statistical analysis of the BHI fracture picks can provide an indicator of fracture intensity (density); however the numbers have to be used with caution due to tool, data and interpretation limitations, which were mentioned in Chapter 1. A detailed statistical analysis of Ghaba North BHI picks had been done by Dhahab (Dhahab, 2002) up to GN-26H4. The main findings of that study were presented in Chapter 3. A summary of the statistical analysis of BHI fracture picks done during this research for Ghaba North Shuaiba and up to GN-31H2 is shown below (Table 4.3). The reader is advised to note the following while evaluating this table: (1) "All" in the table below stand for all the conductive and non conductive high and low confidence fractures, induced fractures un-identified faults for ONLY Shuaiba interval. Statistical analysis is based on SVS fractures spacing histograms (Figure 4.45). (2) Clusters calculations were done using a density log combined with visual inspections as shown below (Figure 4.46). (3) Background fractures spacing calculation is done using visual inspection, Figure 4.47.

| Object | Count | Average Spacing m |
|---|---|---|
| All [1] | 660 | 0.1 |
| Conductive all | 556 | 0.1 |
| Non-conductive all | 25 | 1, 10 & 50 |
| NE all | 420 | 10 |
| NE conductive | 332 | 0.3 |
| NE non-conductive | 10 | 1, 15 & 90 |
| NW all | 240 | 0.2 |
| NW conductive | 224 | 0.2 |
| NW non-conductive | 15 | 1, 4, 12 &50 |
| NE clusters [2] | 20 | 20-50 (200-300m) |
| NW clusters [2] | 11 | 20-50 (200-300m) |
| NE background [3] | - | 15-30 |
| NW background [3] | - | 20-30 |

**Table 4-3 Statistical analysis of GN Shuaiba BHI fracture picks**

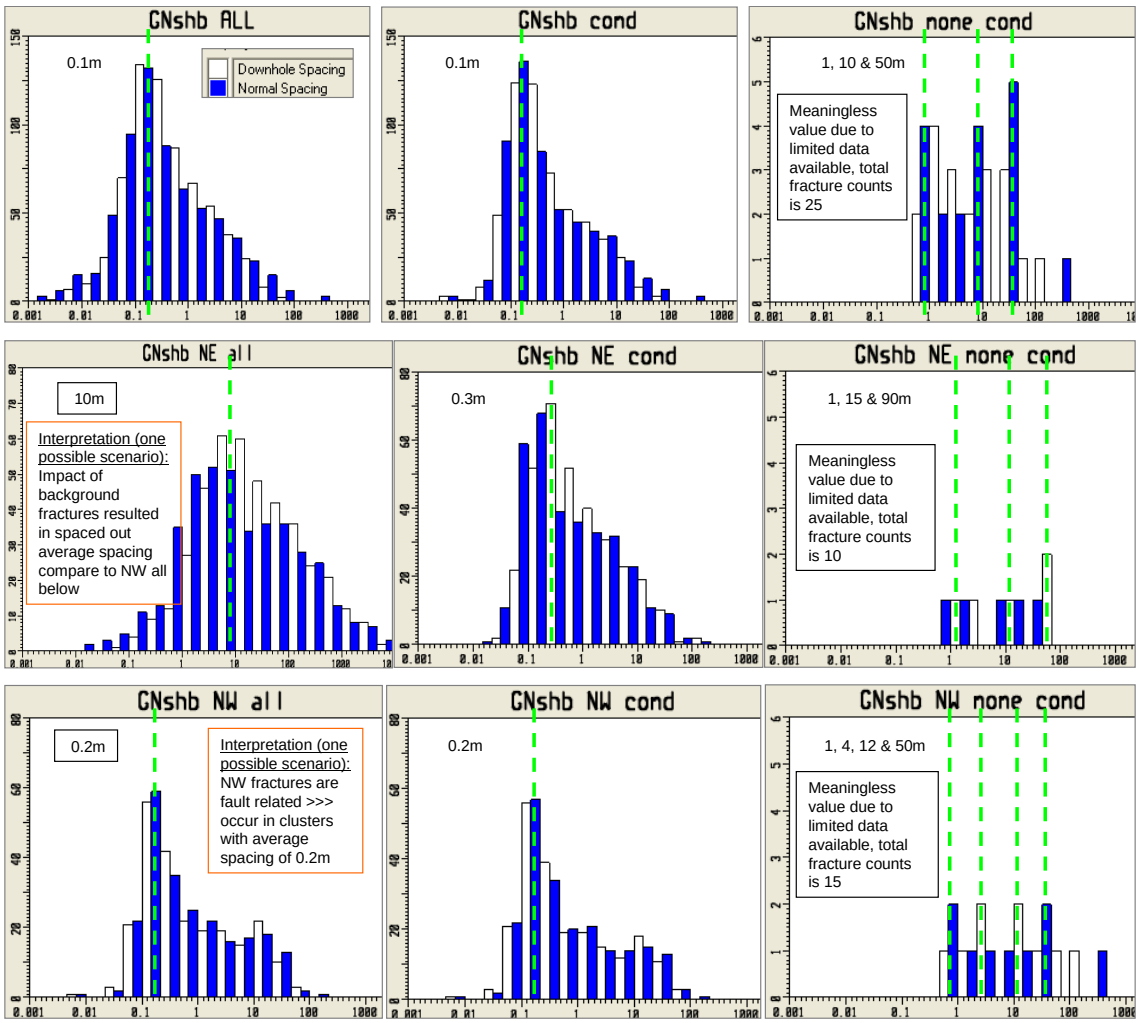


**Figure 4-45 SVS snap shot showing fracture spacing histogram (down hole and normal) per orientation per type (conductivity). NE fractures spacing is more spaced out compare to the NW, indicating possible impact of having more background fractures, while NW spacing is very tight, indicating clusters around fault or fracture corridors.**

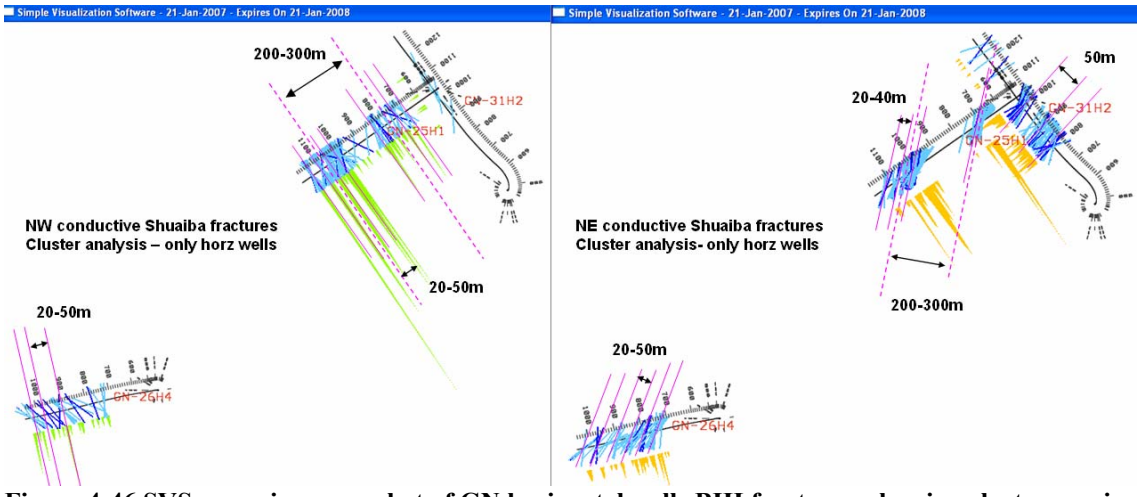


**Figure 4-46 SVS map view snap shot of GN horizontal wells BHI fractures, showing cluster spacing analysis. Yellow and green logs are fracture intensity logs. Pink lines are assumed to be cluster centre used to calculate the spacing.**

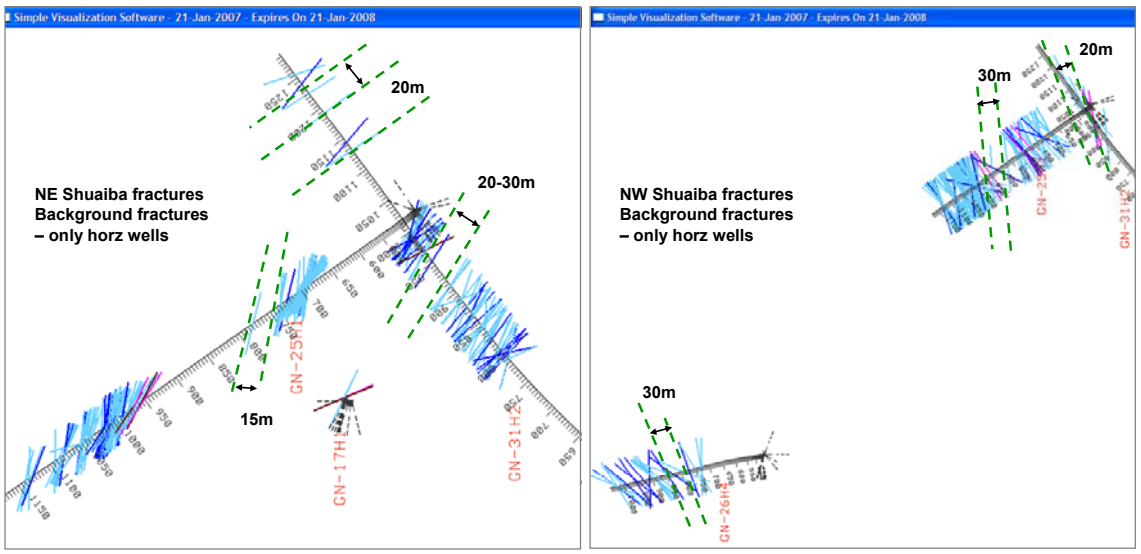


**Figure 4-47 Map view of GN horizontal wells BHI fracture picks, showing an attempt to calculate background fracture spacing. Note for the NW set (right) it is very hard to pick back ground fractures, whereas for the NE set the background fractures are clear at the tail of GN-31H2.**

## 4.10 Testing Fracture concepts for GN Shuaiba

This section investigates the potential fracture concepts for this field and cross check them against the available fracture related data to aid in creating a base case conceptual model for the GN Shuaiba. Table 4.4, table 4.5 and table 4.6 below list the proposed scenarios for the fracture network in Ghaba North Shuaiba based on the characterization done above at well and field scale.

| Scenario | For | Against |
|---|---|---|
| **NE crest and SW crest Only (Fold Model)** | **1-** High normalized gross rate profile for GN-5,GN-25 and surrounding crestal wells | **1-** Losses in flanks wells GN-13 & GN-21 *c.f.* No losses in GN-17 in the centre |
| | **2-** Large scale 500m multi-direction curvature map showing high strain, mainly for NE crest | **2-** GN-21 on NW flank, production profile showing high initial gross rate |
| | **3-** High BHI fracture intensity in GN-25 and GN-26 | **3-** Interference test between GN-10 & GN-13 in the southern flank, showing high connectivity |
| **Fault related fracture model with fracture corridors - possible sub-seismic faults - only (Fault only model)** | **1-** Over 80% of the BHI fractures occur in clusters | **1-** GN-5 is showing high normalized gross rate in area where there is NO faults* |
| | **2-** BHI fracture location coincide with possible fault location (2001 study fault interpretation) in GN-25, GN-26 and GN-31 | **2-** GN-23 is showing 0 losses in Shuaiba despite being on a NW trending fault |
| | **3- High initial production rate for GN-19 and GN-25 all hit by large fault "ZHarwi fault interp"** | |
| | **3-** High normalized gross rate profile for GN-4, GN-10, GN-12, GN-19,GN-25 &GN-26 all hit by large fault "ZHarwi fault interp" | |
| | **4-** Seismic semblance volume showing step change of acoustic impedance at and in the vicinity of fault traces | |
| **Fault related fracture model with fracture corridors combined with NE background fractures (Fault, FC and background)** | As above for fault model 1 to 4 | As above for fault model 1 * |
| | **5-** Background fractures seen in GN-31H2 tail | |
| | **6-** all most all the NW BHI fractures are coinciding with faults | |

**** GN5 high normalized gross rate could be attributed to diagenesis. Evidence for diagenesis is seen in GN-23H1 & GN-31H1 core: Facies are dominated by rudist which shows low leaching patches; also for GN-31H1 presence of Nahr Umr Shale 3m below top Shuaiba, though later could be related to drilling (coring) activities. In addition static images of the BHI for GN wells shows vuggy profiles***

**Table 4-4 Fracture network concept scenarios for Ghaba North Shuaiba reservoir based on the characterization presented in the sections above.**

| | For | Against |
|---|---|---|
| **On Mechanical Layering ML** | **1-** Core Photos of GN-23H1indicate presence of **rubble zones** below top Shuaiba | **1-** Lack sampling of Shuaiba interval. No deviated wells. Most of wells on top Shuaiba |
| | **2-** Core Photos of GN-31H1indicate presence of **rubble zones** "possible fractured layers" below top Shuaiba | **2-** GN-31H2, though sampled only 20m vertical interval of Shuaiba, showing no or slight hints of mechanical layering |
| | **3-** Core Photos of GN-31H1indicate presence of **tight layers "patches"** 10 m and 60 m below top Shuaiba | **3-** The core Phi and K data versus depth does not show a lot of deviation with depth |
| | **4-** GN-17 & GN-21 BHI static image showing facies variation and possible vuggy rock | |

**Table 4-5 Evidence for and against mechanical layering in Ghaba North Shuaiba reservoir.**

| **On conductivity** | |
|---|---|
| NE fracture are more conductive | **1-** Over 80% of conductive BHI fractures are striking NE |
| | **2-** Interference test profiles, showing highest connectivity between GN-10 and GN-13 in a NE direction |
| | **3-** WFL in GN-31H2 showing change when crossing a NE oriented fracture cluster |
| | **4-** Resistivity log spikes indication of conductivity when crossing NE BHI fractures in GN-25 and GN 26 |
| | |
| NW fracture are likely to be close | **1-** GN-23 is in the NW graben fault and showing NO losses in Shuaiba |
| | **2-** Non conductive BHI fracture are more in NW direction |

**Table 4-6 Fracture conductivity for Ghaba North Shuaiba reservoir.**

Based on the three tables above, a total of 16 fracture realizations have been created for Ghaba North Shuaiba, some as fracture density map, but the majority as a 3D discrete fracture network DFN models (Table 4-7).

| | | | | |
|---|---|---|---|---|
| **Fold only** | **No ML** | | **1** | |
| | **with ML** | | **2** | |
| **Fault only** | **No ML** | **ZHarwi fault** | **3** | **L** |
| | | **2001 study fault** | **4** | |
| | **with ML** | **ZHarwi fault** | **5** | |
| | | **2001 study fault** | **6** | |
| **Fault, FC & Background** | **2001 study faults** | **No ML** | **7** | |
| | | **with ML** | **8** | **M** |
| **Fault, FC & Background with Fold at NE crest** | **No ML** | **2001 study fault Medium** | **9** | |
| | **With ML** | **2001 study fault Medium** | **10** | **H** |

**ML = Mechanical layering**

**Realization No. 8 is perceived to be base case**

**Density fracture map** created for all realizations except for the one highlighted, where a **3D DFN** models were built

**DFN**

**Table 4-7 Fracture models built for GN Shuaiba, both 3D DFN and 2D fracture density maps.**

## 4.11 Building GN Shuaiba fracture models

In order to build a 3D discrete fracture network (DFN), confining upper and lower surfaces are needed. For the NO mechanical layering realization, these surfaces are **top Shuaiba THSU** and **top Kharaib THKH** (i.e. the reservoir, the abbreviation is out of PDO RUI data base, note that Shuaiba here is only Lower Shuaiba Formation). These surfaces, together with another 13 intermediate surfaces, were extracted, in SVS, out of an imported 3D Petrel binary grid called "GN_Ups_fine.opb" provided by PDO. When cross-checked against the available GR logs, the extracted surfaces "horizons" required a depth shift of up to 30m in GN-21H1 in the NW flank of the field (Figure 4.48).

To create realizations with mechanical layering, intermediate confining surfaces (bounding the highly fractured layers) have to be identified. A rationale is proposed below in picking up these surfaces since there are very few constraints available because of the very low sampling by deviated wells that are located in the upper reservoir only. Based on the core analysis it seems that the upper layer of Shuaiba is highly fractured. There is also a highly-fractured interval about half way through the Shuaiba. These are likely to coincide with the upper flow unit FU5, and FU3, which represents the top of the shoaling upwards sequences of the lower Shuaiba. Hence, the interval confined between **Surface 1 (THSU)** and **Surface 3** was picked for FU5, and the interval confined between **Surface 10** and **Surface 12** was also picked for FU3, as representing fracture bounded layers in Ghaba North Shuaiba.

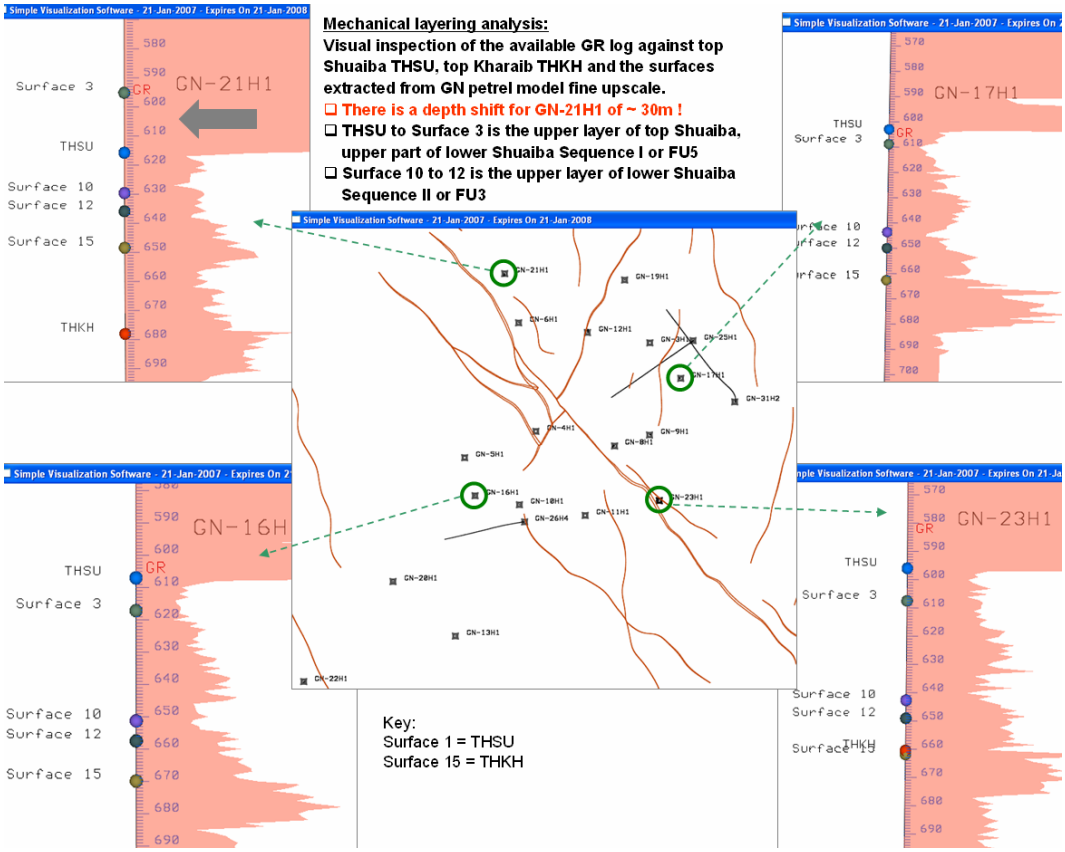


**Figure 4-48 Visual inspection of available GR against tops and surfaces markers (extracted from an imported Petrel GN project provided by PDO) to cross check horizons tops and to determine the bounding surfaces for the mechanical layers in Shuaiba reservoir.**

### *4.11.1 Fracture modelling approach*

*This section is applicable for next chapter.*

Two approaches are used for the creation of the fracture model: either building a 3D discrete fracture network model (3D DFN) or building a fracture intensity map termed Fracture Trend Map (FTM), both in SVS. In both cases the practical outputs consist of fracture geometrical properties (orientation and spacing). A 3D simulation grid or the same 3D geological cellular model (i.e. Petrel binary grid) is loaded to SVS and these static properties are exported into the cellular grid (or painted straight onto it in the case of the FTM), to be used to simulate flow and to assess the impact of fracture network. Thus, the 3D geological model is the common factor between the fracture characterization work and the reservoir simulation work (Figure 4.49). The creation of a 3D DFN, based upon the fracture characterization, is used to illustrate the understanding of the fracture network geometric characteristics. Some workers propose to use the 3D DFN as an input to flow simulation to derive effective flow properties. However, that approach requires specification of additional parameters such as fracture apertures, and can also require considerations of the interaction between fracture properties and the geomechanical state (including pore pressure evolution). Explicit fracture modeling is very demanding of computation resources especially if it is done at a field scale or at large sector scale in a highly fractured reservoir. In the approach illustrated here, the 3D DFN is used to derive fracture intensity characteristics for individual cells, which are then used as parameters to estimate flow properties for the cells. A choice needs to be made when creating a 3D DFN. The fractures can be simulated based upon a complete consideration of orientations (both strikes and dips), or the problem can be simplified by assuming that the fractures are approximately vertical (normal to layers). Since the use in this study is to derive proxy characteristics based on intensity measurements, it was decided to simulate the 3D DFN with vertical fractures. This choice saves time and is less demanding of the computation resources. The approach adopted here means that any consideration of dynamic fracture properties (fracture porosity and permeability) is handled in the simulation grid (i.e. in the dynamic world). Estimating fracture porosity and permeability from fracture aperture measurement obtained from BHI is unreliable, because the BHI tool is a pad tool, hence sensitive to borehole status (in gauge or not) and on drilling practice (pressure applied while drilling). In the dynamic world, fracture dynamic properties can be inferred from history matching of gross production, well test data, interference tests or from dynamic log analysis such as WFL or PLT.

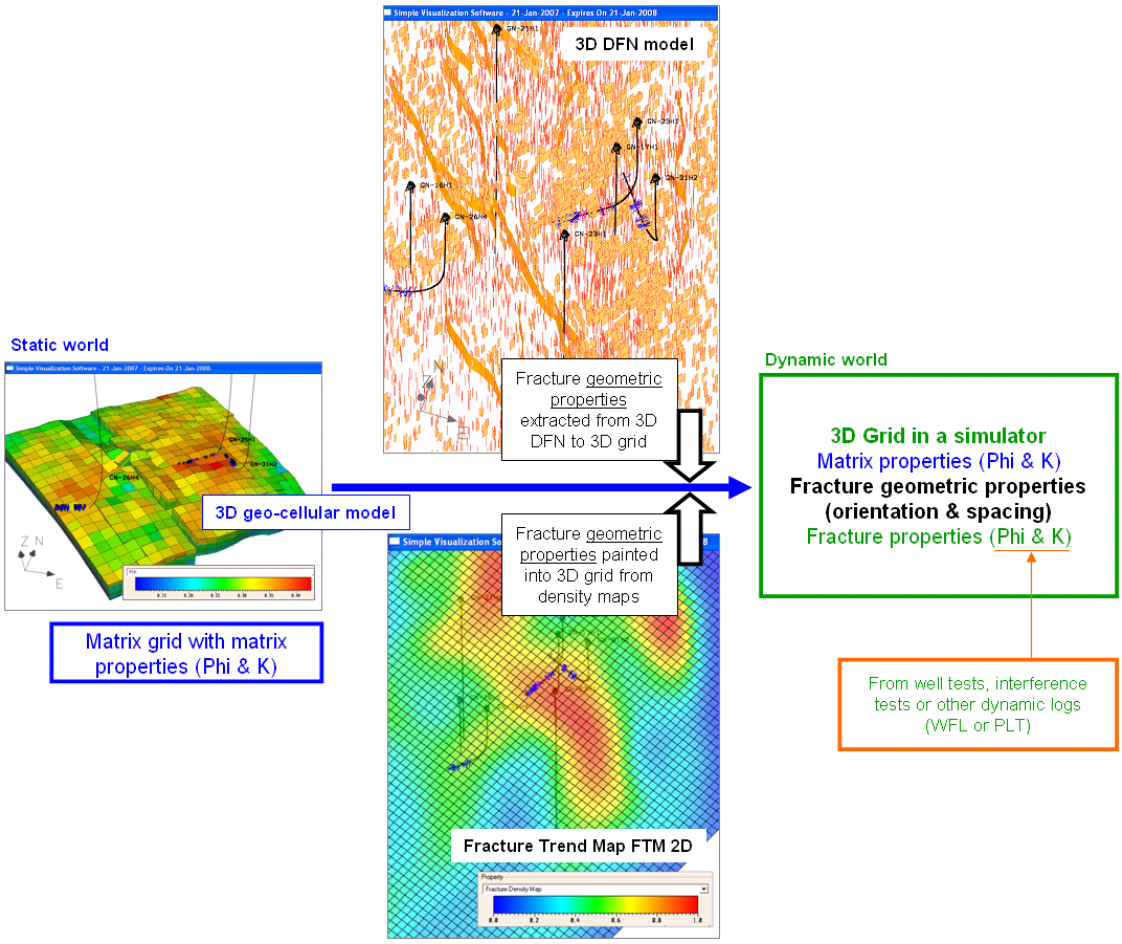


**Figure 4-49 Extracting fracture geometric properties to a 3D grid, from static to dynamic world.**

### *4.11.2 Fold ("curvature") related fracture models*

The fracture intensity in this model is based on the multi-direction curvature map Kmax of GN top Shuaiba at 500m wavelength, so to visualize the large-scale features. Basically it assumes that the crestal parts are more fractured especially the NE crest where GN-25 is located. The orientation of the fracture is inferred from a regional trend of a NE orientation as observed from BHI statistics, though it is aligned to fault orientation where ever a fault occurs.

A 3D DFN model was created for both with and without mechanical layering option (realization number 1 and 2 in table 4.7), with the parameters noted in Table 4.8 below, for further information on what each parameter mean refer to al Dhahab and O' Regan SVS manual (Dhahab and O' Regan, 2006). These models, with curvature only related fractures, and NO mechanical layering (Figure 4.50) or with mechanical layering (Figure 4.51), represent scenarios or realizations to be considered, even though the curvature-only situation is not perceived to be the most likely explanation (see arguments above), and hence is not a representative base case. Simple visual inspection of the created 3D DFN shows that the created fractures do not correlate with the actual wells BHI fractures.

| Model name | Fracture Set Vertical Fold ONLY |
|---|---|
| Total number of iteration | All 100, upper layer 40 & middle layer 30 |
| Delay | 1, 1, 1 |
| Step | 20, 10, 12 |
| Seeds Minimum | 1.00E-05, 0.0001, 0009 |
| Seeds Maximum | 1.00E-05, 0.0001, 0009 |
| Seeds Multiplier | 2, 4, 1 |
| FZ Width | 4, 2, 3 |
| FZ Projection | 10, 10, 10 |
| FZ Crossover | 10, 10, 10 |
| FZ Width To Length | 0.1, 0.1, 0.1 |
| Impedance Factor | 0.7, 0.7, 0.7 |
| Impedance Cut Off | 0.5, 0.5, 0.5 |
| Horizon 1 | topSHB, topSHB, S10 |
| Horizon 2 | topKHRB, S3, S12 |
| Orientation Map | Orientation Map Fold NE faults |
| Seed Probability Map | SeedProbability Map Fold |
| Propagation Impedance Map | PropagationImpedance Map Fold |
| Conditioning Lines | Conditioning Lines NE cond |

**Table 4-8 Curvature only 3D DFN model's parameters. Blue font text refers to the NO ML option.**

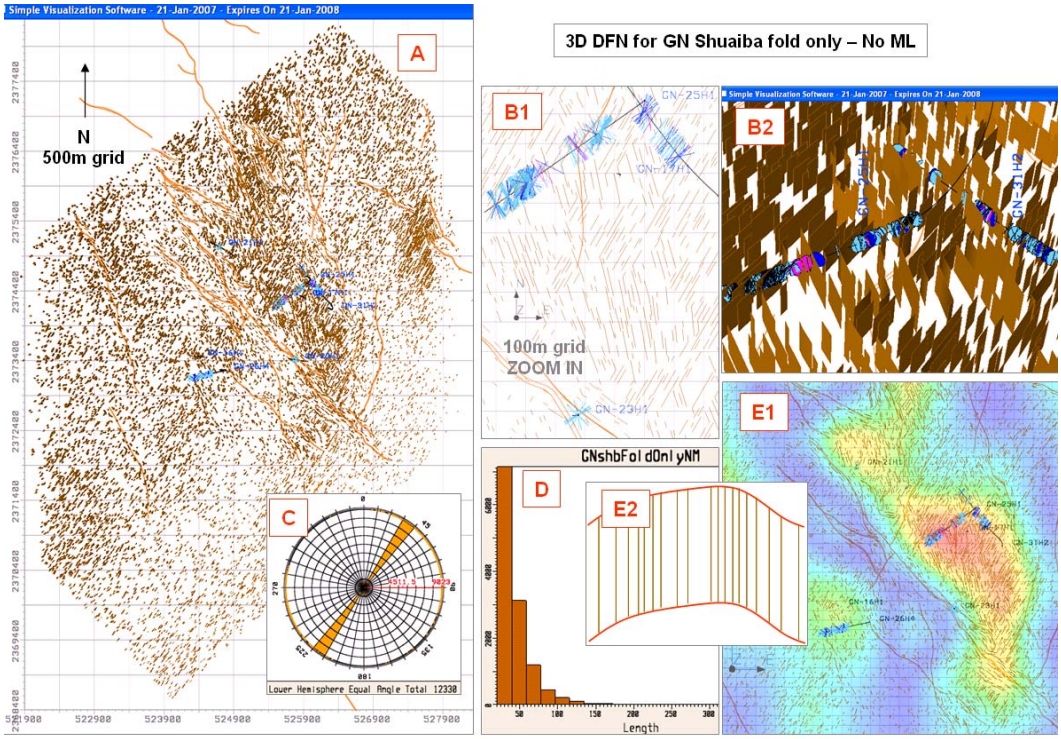


**Figure 4-50 SVS snap shot showing the Ghaba North Shuaiba curvature only with NO mechanical layering 3D DFN model at (A) full field scale and at (B) a zoom in scale with the orientation rose diagram (C) showing total number of fractures and length versus frequency histogram (D) for the 3D vertical fracture set created. The main input for fracture population is the curvature map (E1) shown with the 3D fracture set, with a simple concept model (E2) vertically exaggerated.**

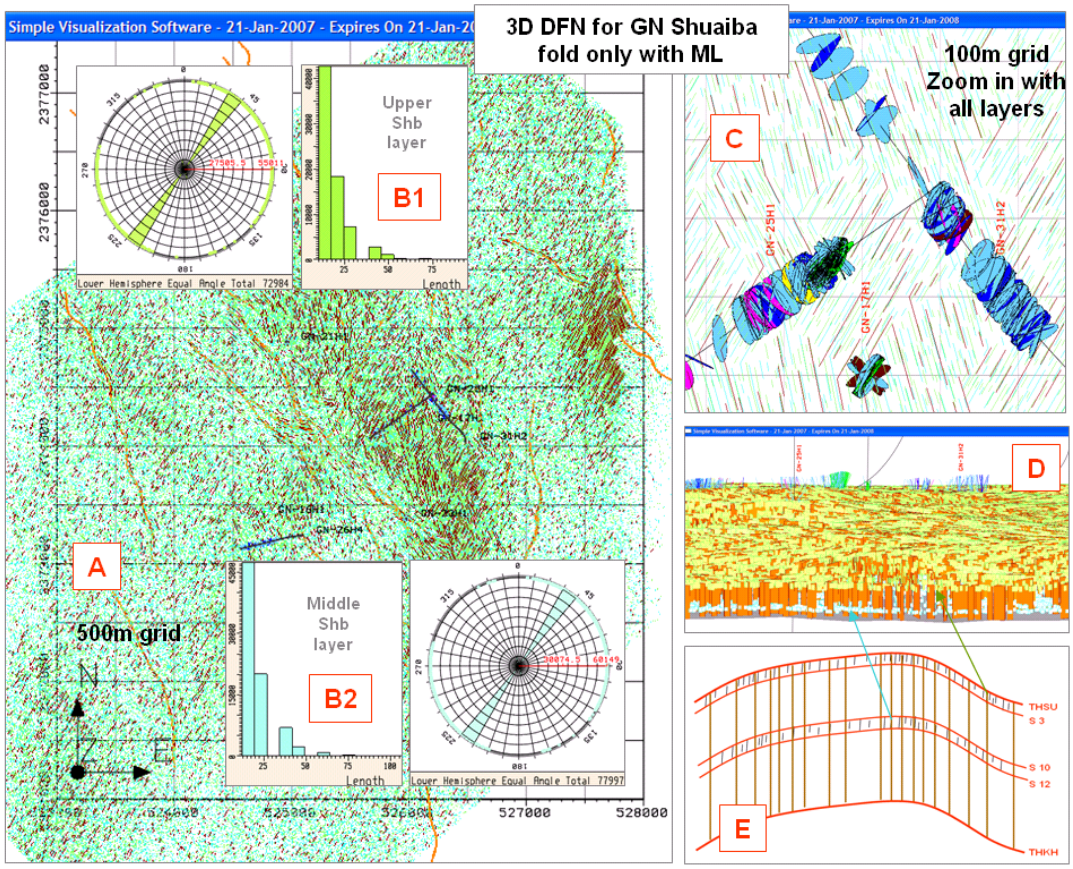


**Figure 4-51 SVS snap shot showing the Ghaba North Shuaiba curvature only with mechanical layering 3D DFN model at (A) full field scale with rose diagram and length histogram (B). A zoomed in shot is shown both areally (C) and vertically (D) with a simple concept of the layering shown in a sketch (E).**

### *4.11.3 Fault only -related fracture models*

The fracture intensity in this model is based on the seismically interpreted faults: the sub regional ZHarwi faults and the 2001 study conceptual faults. Basically the fractures are confined to the vicinity of the fault resulting in a fault damaged zones (Figure 4.52). A 3D DFN model was created for the fault-only related fracture realization with NO mechanical layering option (realization number 3 and 4 in table 4.7), with the parameters noted in Table 4.9 below. As with the curvature only model, the fault only DFN models do not reflects the BHI well observations. For instance, the fractures seen in GN-26H4 are not present in realization number 4 (fracture only occur in the vicinity of the ZHarwi faults), which can be thought of as the lowest case, i.e. least fractured scenario for Ghaba North Shuaiba. Visual inspection of both fault models indicate that the 2001 study conceptual faults are more representative than the ZHarwi sub-regional seismically interpreted faults. Though alone does not reflect the BHI fractures observed. Hence, it was decided to use the 2001 study conceptual faults for the other scenarios to reduce number of models created. For the fault related fracturing with mechanical layering realizations (realizations number 5 and 6 in table 4.7) a fracture trend map (FTM) were built in SVS and painted into the Petrel 3D geo-cellular grid using the following approach (Figure 4.53 and Figure 4.54): A Seed Probability Maps (SPM) were created and filled by the fault traces (the 2001 study conceptual fault and the sub-

regional "ZHarwi" seismically interpreted fault). 2D cell array grids were created out of the SPM, containing a fracture density values from 0 to 1 (i.e. 0% = no fracture to 100% fully fractured area). Surface grids (FTM) were created out of the 2D cell array grid. The Petrel 3D geo-cellular grid was imported to SVS and the layers were painted one by one using those surfaces (FTM). As with the fault only models with no ML, the created fracture trend maps also do NOT fit the observed BHI fracture picks. Moreover, it shows the NW striking graben to be the location of the highest fracture intensity which is in contrast with the little fractures observed in the vertical well GN-23 (albeit being vertical).

| Model name | Fracture Set Vertical Fault ONLY shb |
|---|---|
| Total number of iteration | 30, 30 |
| Delay | 1, 1 |
| Step | 5, 5 |
| Seeds Minimum | 0.0001, 0.0001 |
| Seeds Maximum | 0.0001, 0.0001 |
| Seeds Multiplier | 1, 1 |
| FZ Width | 0.01, 0.01 |
| FZ Projection | 1, 1 |
| FZ Crossover | 1, 1 |
| FZ Width To Length | 0.1, 0.1 |
| Impedance Factor | 0.7, 0.7 |
| Impedance Cut Off | 0.5, 0.5 |
| Horizon 1 | topSHB, topSHB |
| Horizon 2 | TopKHRB, topKHRB |
| Orientation Map | OM NE 2001 fault study, OM NE ZHarwi |
| Seed Probability Map | SPM 2001 fault study, SPM ZHarwi |
| Propagation Impedance Map | PIM 2001 fault study, PIM ZHarwi |
| Conditioning Lines | Conditioning Lines NE cond |

**Table 4-9 Fault only 3D DFN model parameters with NO ML option using both the 2001 study conceptual fault interpretation and the sub-regional seismically interpreted fault "ZHarwi.**

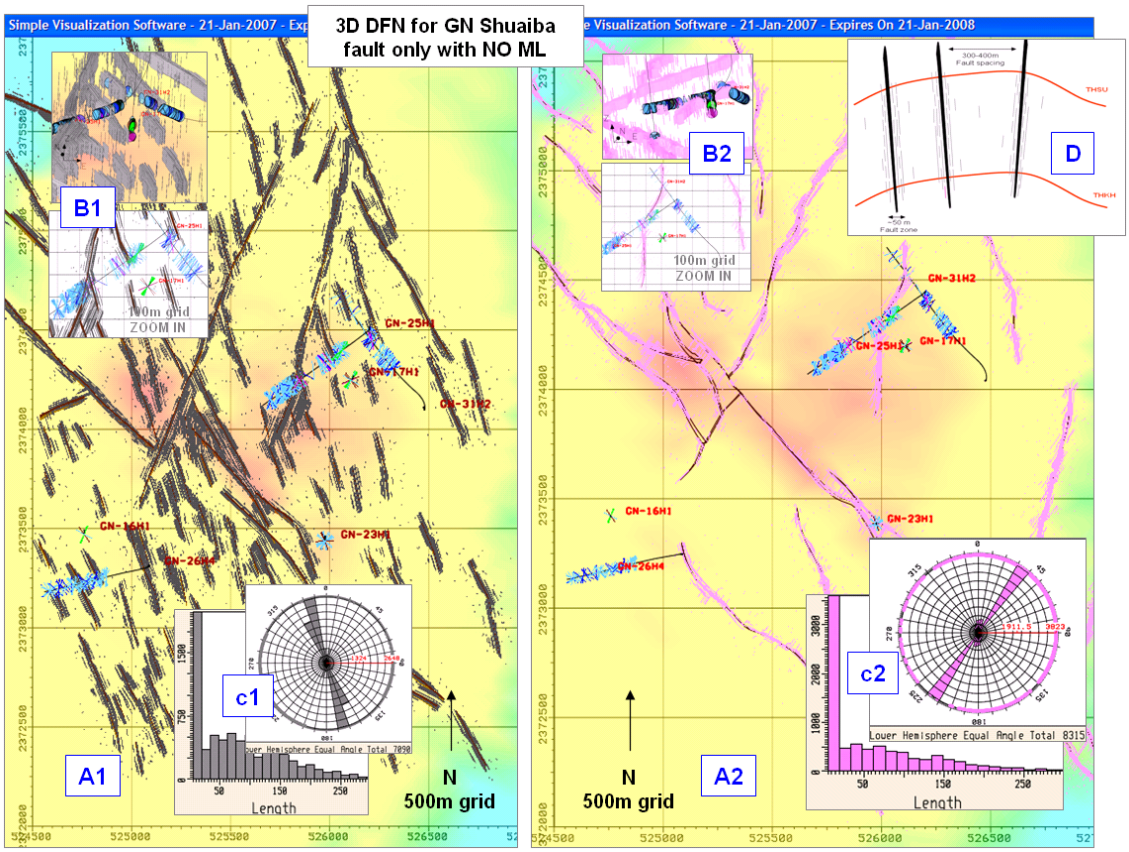


**Figure 4-52 SVS snap shot showing the Ghaba North Shuaiba fault only 3DFN models with NO mechanical layering for both the 2001 study conceptual faults (left 1) and the sub-regional ZHarwi faults (right 2) at (A) full field scale and (B) zoomed in scale both areally and vertically. Also shown their rose diagrams and length histograms (C) and a simple cartoon illustrating the concept of fault related fracturing (D). Note that the 2001 study conceptual faults (left) are more representative (reflect the observed BHI fracture picks) than the ZHarwi faults (right).**

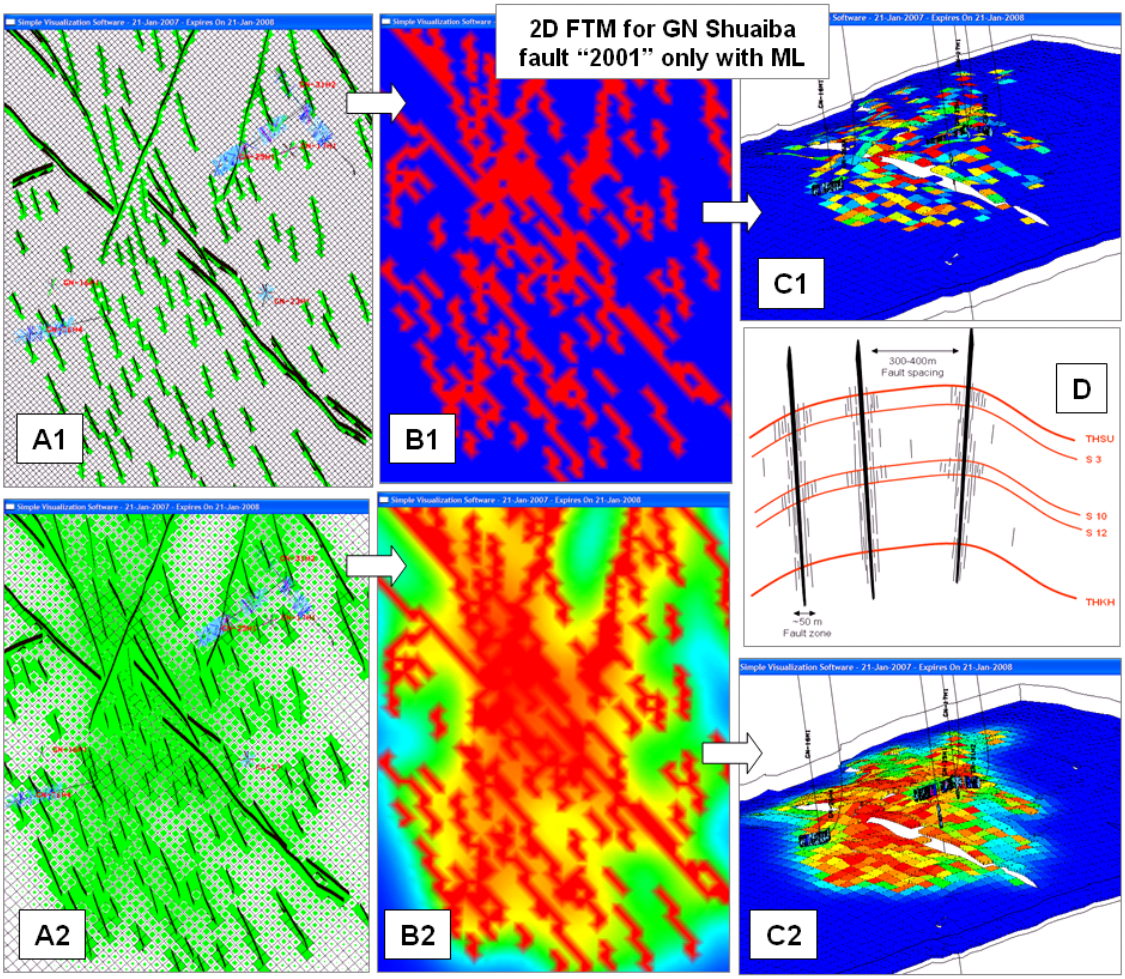


**Figure 4-53 SVS snap shot showing the Ghaba North Shuaiba fault "2001"only model with mechanical layering using FTM approach. (A) Seed Probability Map SPM filled using the fault traces (A1) expanded laterally away from the faults (A2) for the fractured layers (layer 1 &2 and layer 10 & 11). The SPM were converted to surfaces or Fracture Trend Maps FTM (B) as fracture density (red = 100% and blue 0% fractures). These FTM were later painted to the 3D Petrel geo-cellular grid as one property called "FTM 2001 fault" (C). A simple cartoon illustrating the concept of fault related fracturing with mechanical layering ML is shown (D).**

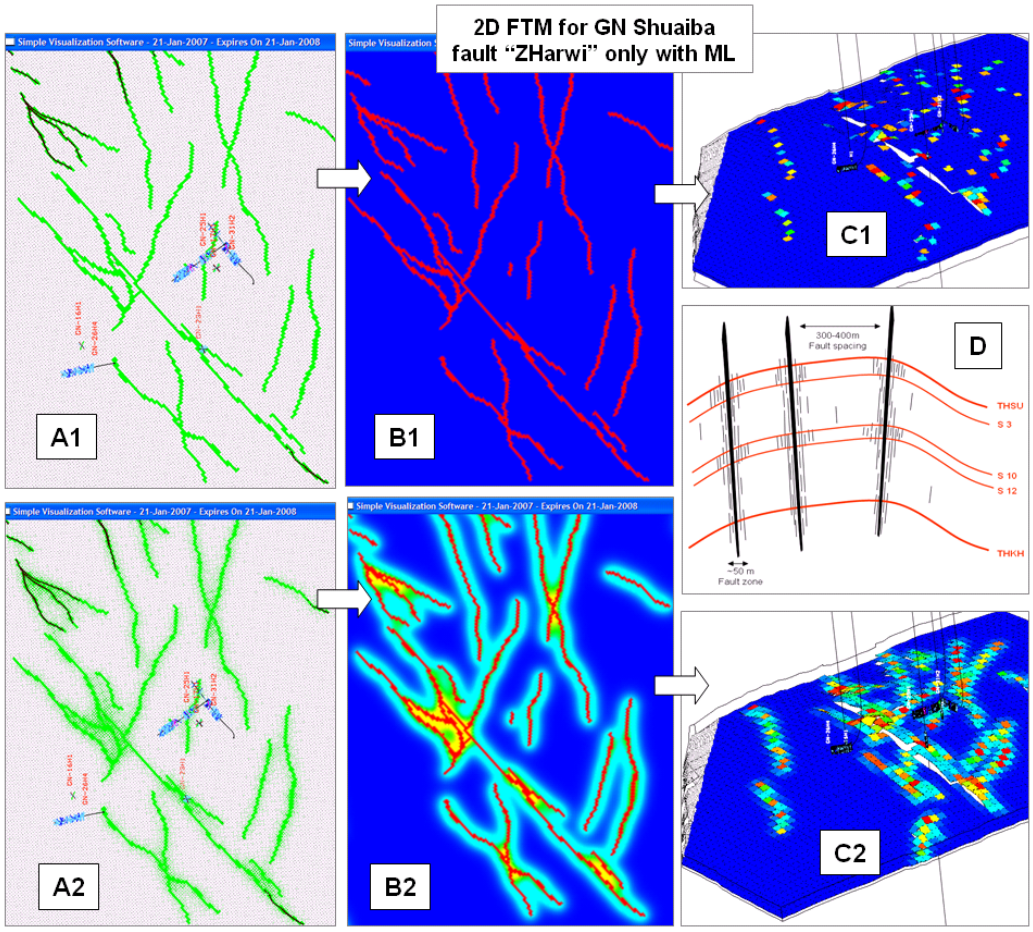


**Figure 4-54 SVS snap shot showing the Ghaba North Shuaiba fault "ZHarwi" only model with mechanical layering using FTM approach. (A) Seed Probability Map SPM filled using the fault traces (A1) expanded laterally away from the faults (A2) for the fractured layers (layer 1 &2 and layer 10 & 11). The SPM were converted to surfaces or Fracture Trend Maps FTM (B) as fracture density (red = 100% and blue 0% fractures). These FTM were later painted to the 3D Petrel geo-cellular grid as one property called "FTM ZHarwi fault" (C). A simple cartoon illustrating the concept of fault related fracturing with mechanical layering ML is shown (D).**

### *4.11.4 Fault, FC and background fracture models*

These are realizations number 7 and 8 in table 4.7 above. They are similar to the fault related fractures with the addition of the following: Fracture corridors based on the 50m length uni-directional Kmax curvature at 135 azimuth of GN Shuaiba horizon. This supported by the presence of fractures clusters seen in BHI, by interference tests and losses. Background fracture created to reflect the overwhelming NE striking trends, despite having majority of the fault orientated NW. A summary for the modelling parameters used for realization number 7 is presented in Table 4.10 below. For the ML realization number 8, the SVS parameters were changed (i.e. SVS fracture modelling was run twice for the upper and the middle layer). The resultant models are consistent with the fractures seen in BHI, though the intensity within the clusters seen in the BHI wells is more than those in the model. With respect to the orientation the dominant direction is the NE. A snap shot is shown in Figure 4.55 for the NO mechanical layering ML scenario, while figure 4.56 shows realization number 8, where additional bed bounded fractures were created in upper and intermediate layer of top Shuaiba (I.e. with mechanical layering).

| Model name | fsvFCfault |
|---|---|
| Total number of iteration | 20 |
| Delay | 1 |
| Step | 20 |
| Seeds Minimum | 0.0001 |
| Seeds Maximum | 0.0001 |
| Seeds Multiplier | 2 |
| FZ Width | 0.01 |
| FZ Projection | 1 |
| FZ Crossover | 1 |
| FZ Width To Length | 0.1 |
| Impedance Factor | 0.7 |
| Impedance Cut Off | 0.5 |
| Horizon 1 | topSHB |
| Horizon 2 | topKHRB |
| Orientation Map | OMfcFault |
| Seed Probability Map | SPMfc_fltML |
| Propagation Impedance Map | PIMfc_fltML |
| Conditioning Lines | Conditioning Lines NE cond |

**Table 4-10 SVS parameters used for the fracture corridors (FC) and Fault 3D DFN model parameters with no ML option using both the 2001 study conceptual fault interpretation.**

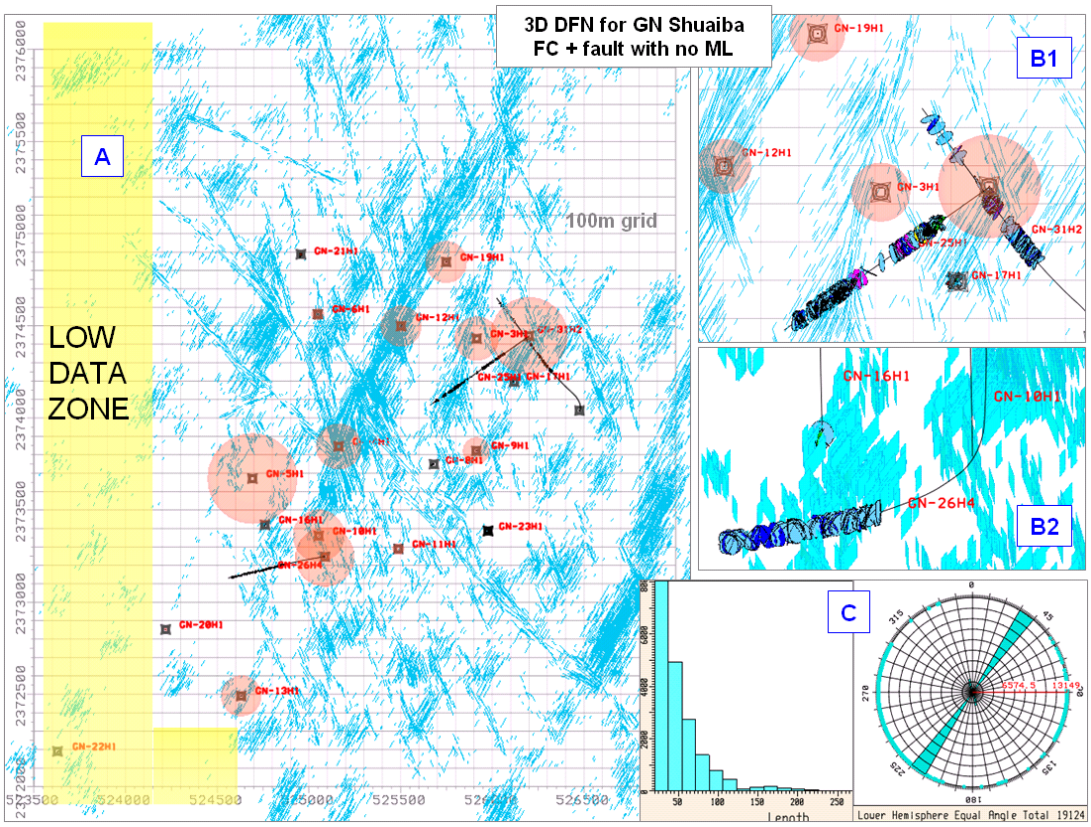


**Figure 4-55 SVS snap shot showing the Ghaba North Shuaiba Fracture Corridor and fault with NO mechanical layering 3D DFN model at (A) full field scale, (B1 & B2) zoomed in scale and showing the rose diagram and length histogram of the fractures (C). Red circles are normalized gross rate. The flank area (e.g. around GN-22) has low constraining data.**

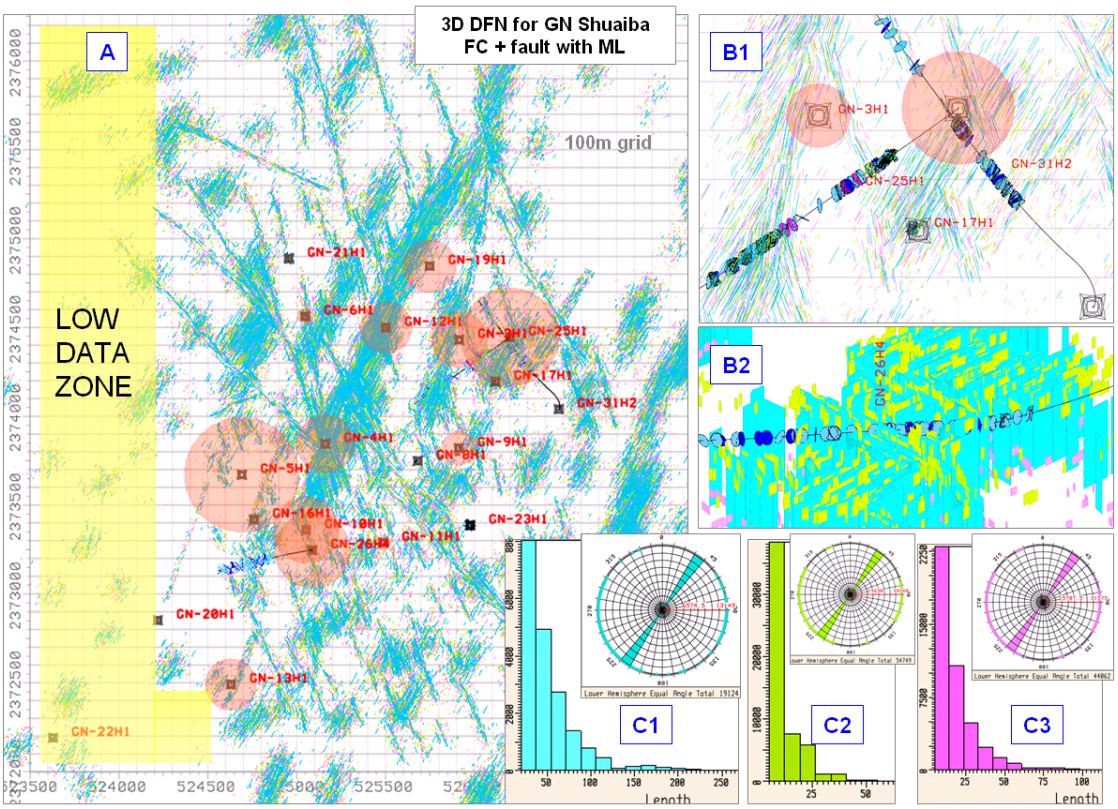


**Figure 4-56 SVS snap shot showing the Ghaba North Shuaiba Fracture Corridor and fault with mechanical layering 3D DFN model at (A) full field scale, (B1 & B2) zoomed in scale and showing the rose diagram and length histogram of the fractures (C1, C2 & C3). Red circles are normalized gross rate. This model is perceived to be the base case for Ghaba North Shuaiba.**

### *4.11.5 Fault, FC and background fracture with fold related fracture models*

These models (realizations 9 and 10 in table 4.7) represent a combination of the all the above realizations, using only the 2001 study conceptual faults with and without mechanical layering. A 3D DFN models were created for both realizations. The basis is a combination of all the above with manual edition using Seed Probability Map (SPM) in SVS. Figure 4.57 shows the result for the NO ML realization number 9. While Figure 4.58 shows the result for realization number 10, which is the same as realization number 9 but with ML at the upper layer and the intermediate layer of Shuaiba.

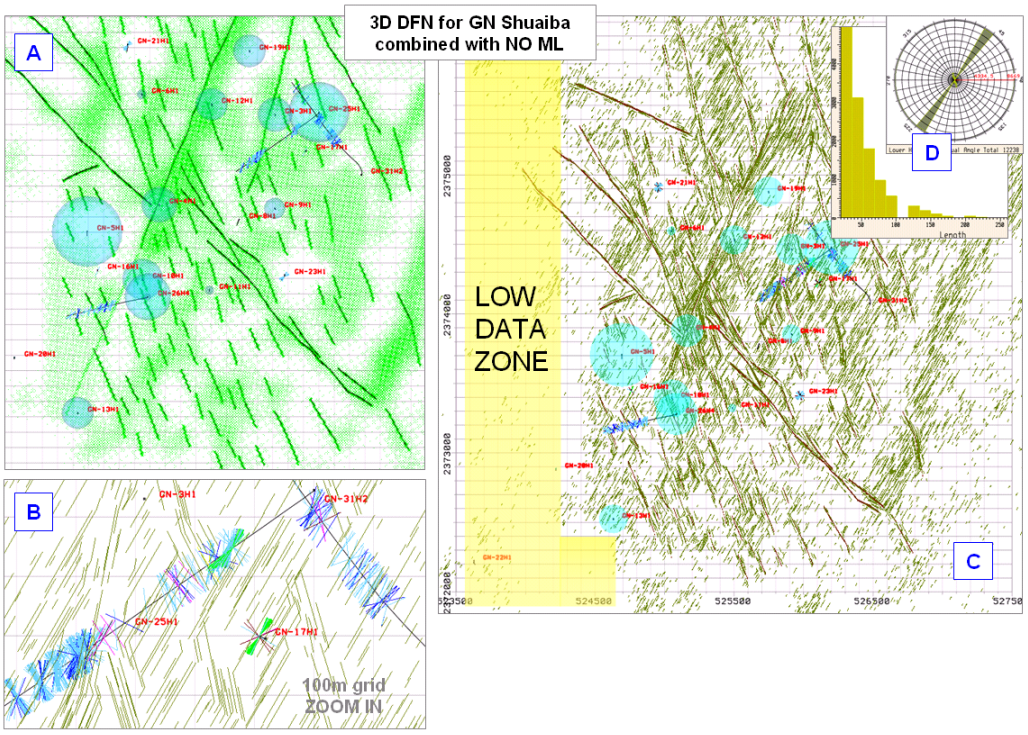


**Figure 4-57 SVS snap shot showing the Ghaba North Shuaiba combined fracture 3D DFN model with NO ML, showing the SPM for the full field (A) and the resultant fracture model (B) at zoomed in scale and (C) at full field scale, with the rose diagram and length histogram of the fractures (D). Blue circles are normalized gross rate.**

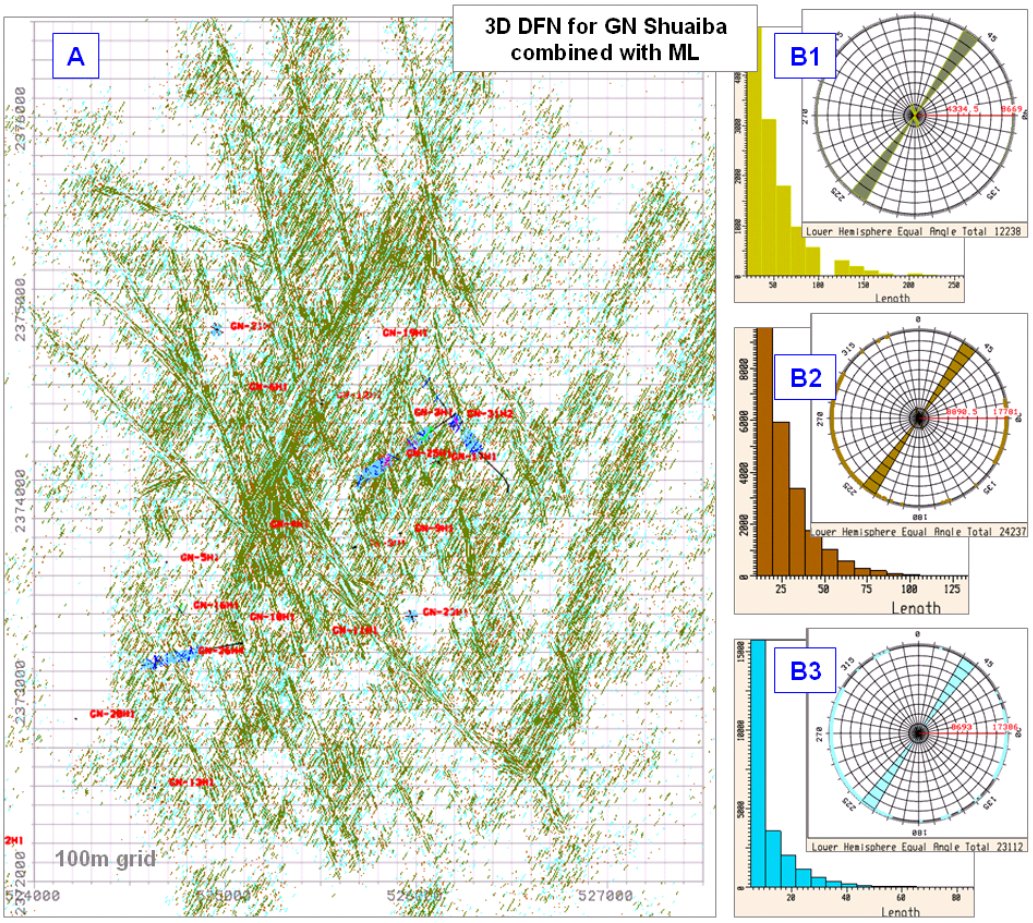


**Figure 4-58 SVS snap shot showing the Ghaba North Shuaiba combined fracture 3D DFN model with ML, showing the full field fracture model (A) and the rose diagram and length histogram of the fractures (B1 for all Shuaiba, B2 for upper layer and B3 for intermediate layer). This model is perceived to represent the high case realization for Ghaba North Shuaiba reservoir.**

### *4.11.6 Extracting fracture geometric properties to 3D geo-cellular grid*

*The first paragraph of this section is applicable for next chapter.*

The extraction of fracture geometric properties (basically fracture count and spacing) into a simulation grid is based on fracture counting between adjacent cells (cell n and cell n+1) parallel to the x and y direction of the grid. The approach is illustrated in Figure 4.59 extracted from Rawnsley and Dhahab Qarn Alam 3D fracture report (Rawnsley and Dhahab, 2005). The main output calculation is termed "Fracture Mean Apparent Spacing" in X, Y and Z direction of the 3D geo-cellular grid. Hence, the fracture spacing is a relative number which is dependent on grid orientation, grid cell size and method of calculating fracturing spacing. The criteria for picking a grid orientation for simulation in subsurface is governed by many elements such as well trajectory strike direction or dominant fault and fracture strike direction, etc. The issue becomes very complicated when there is two dominant fractures directions or because of the field development approach (e.g. water flooding or GOGD); the well orientation is oblique to fault direction, which result again on two main direction to pick from. In most cases however, reservoir engineers tend to align their grid (which normally originate from the geologist 3D geo-cellular grid), along well strike direction when they are horizontal to simplify flow calculations and avoid "zigzag" effect along a well.

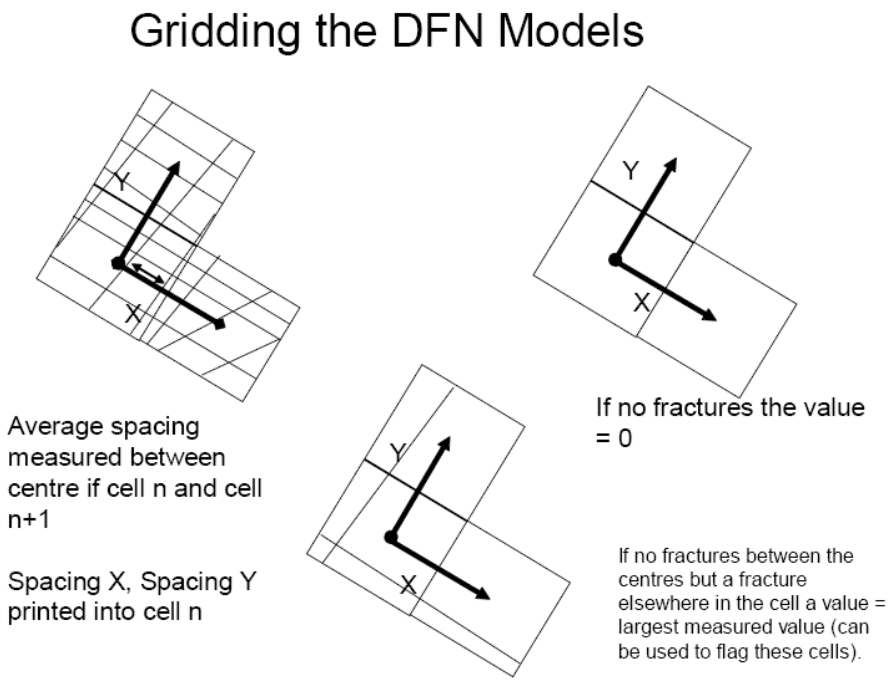


**Figure 4-59 Illustration of method used to extract fracture spacing from a DFN model to a simulation 3D geo-cellular grids (from Rawnsley and Dhahab, 2005).**

For Ghaba North Shuaiba, this decision and its justification were taken care of by PDO as the geo-cellular grid was provided by PDO with a NE orientation. This NE strike may be was chosen so that to have the 3D grid aligned with the NE fracture strike (the dominant fracture orientation seen in the BHI logs), or could be related to having GN25H1 and GN26H1 orientated toward the NE. Three realizations were chosen out of all the above models to represent a low, medium and high case for the fracture network in GN Shuaiba reservoirs. These are:

- Low case = realization 3: fractures occur only at or in the vicinity of ZHarwi sub-regionally seismically interpreted faults with NO mechanical layering
- Base case = realization 8: fracture occur at or in the vicinity of the 2001 study conceptual faults, and in the NE fracture corridors with some background fracturing also oriented NE, with ML.
- High case = realization 10: combined model where fractures occur at the faults, in the FC, in the strained NE folded (high curvature- Kmax) area and as background NE fractures, with ML.

In all the cases, the fracture geometrical characteristics (basically spacing and orientation) were extracted from the 3D DFN models to the 3D Petrel geo-cellular grid (which already include the matrix porosity and X-permeability) to be used for flow analysis to test the concepts.

SVS functionality allows for assessment “calibration” of fracture counts and spacing calculations at the full grid scale and along a specific well bore by showing only the cell intersected by the well bore. Thus, all the calculations for the low case, base case and the high case, were cross checked against the wells BHI objects. For the low case, it is clear that the model is very pessimistic, as it does not reflect the observed well BHI fractures around GN-26H4, for instance (Figure 4.60). Moreover, at the well scale (Figure 4.61), the fracture seen in the cells encountered by GN-25H1 and GN-31H2 does not reflect the fracture counts seen in the grid and more importantly the areas in between the faults has no fractures which does not fit with well observations (Figure 4.62). For the base case, the same assessment (visual inspection) was subjected to the extracted fracture geometrical properties. As expected the fractures are covering more cells away from the faults representing the FC and the background fractures (Figure 4.63). This was in turn reflected in the fracture spacing calculation averaging 25m in the fractured upper and middle Shuaiba layers and 40m in the remaining block of Shuaiba for the X grid direction with a total range from 2m to 150m (Figure 4.64). The fracture spacing in the Y direction is in a range of 2m to 650m. A visual inspection of the 3D DFN base case model against the grid is shown in Figure 4.65 for GN-25H1 and GN-31H2 area. As expected the 3D DFN fractures and their extracted geometric properties in the 3D grid (the cells) do agree with the observed BHI fractures along the wells (the ellipses). The high case scenario is similar to the base case in that the fracture are covering the areas in between the faults, but this time because of the FC, background

fracture and the folding (high curvature or strained areas). However, their intensity is almost double the base case (Figure 4.66) with an average of 60 fractures per cell. With respect to the fracture spacing along the grid X and Y direction, again the distribution resembles that of the base case but with closer spacing (Figure 4.67). The average fracture spacing along the X direction for the fractured layers is around 15m with a range of 2m to 150m. Whereas, for the bulk of Shuaiba, the average spacing along the grid X direction is around 25m. For the Y direction the average spacing is around 30m for the fractured layers with a range of 2m to 450m; and also 30m for the bulk of Shuaiba but with a range of 2m to 650m (the latter is in the NO data zone in the western flank of the field). A sector model from the low, base and high case scenarios is assessed for flow impact in Chapter 6.

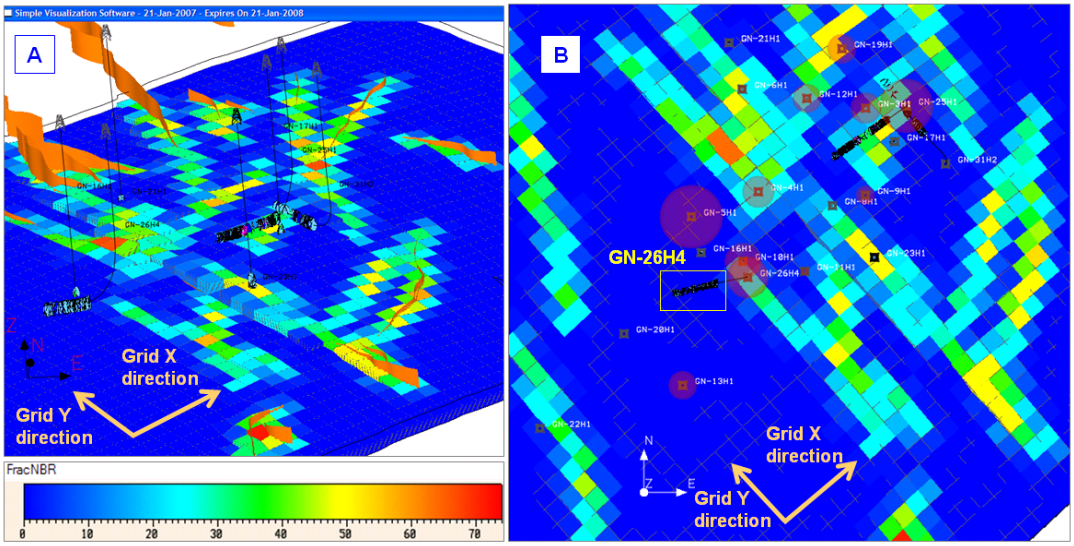


**Figure 4-60 3D cellular grid of GN showing fracture number extracted from low case (fault only) 3D DFN model into the 100m by 100m cells. An inclined view with ZHarwi fault traces (A) and in map view (B). The fracture number range from 0 in most part of the field to 70 at the vicinity of fault zones. The model is pessimistic as seen around GN-26H4, which shows many BHI fractures (black ellipses) while the grid is showing 0 fracture count (blue).**

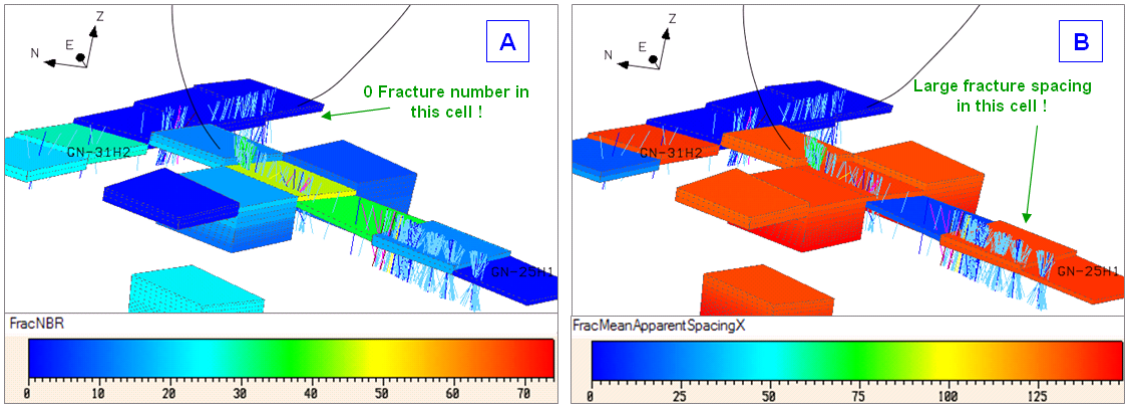


**Figure 4-61 Well scale assessment of the 3D geo-cellular grid with fracture count (A) and fracture spacing (B) properties. Note at the tail of GN-25H1, the fracture spacing is in the range of 125m, which is very pessimistic.**

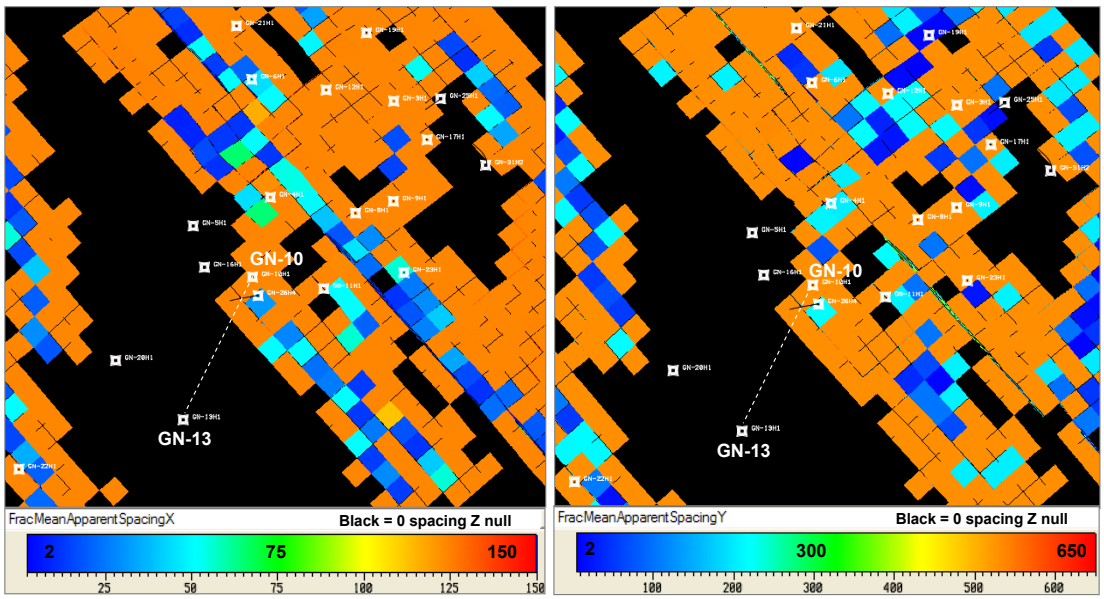


**Figure 4-62 Fracture spacing calculated in geo-cellular grid along its X (left) direction and Y (direction) showing areas in between the faults that have no fractures (black area) which does not fit with the observed well interference profile seen for instance in GN-13 to GN-10.**

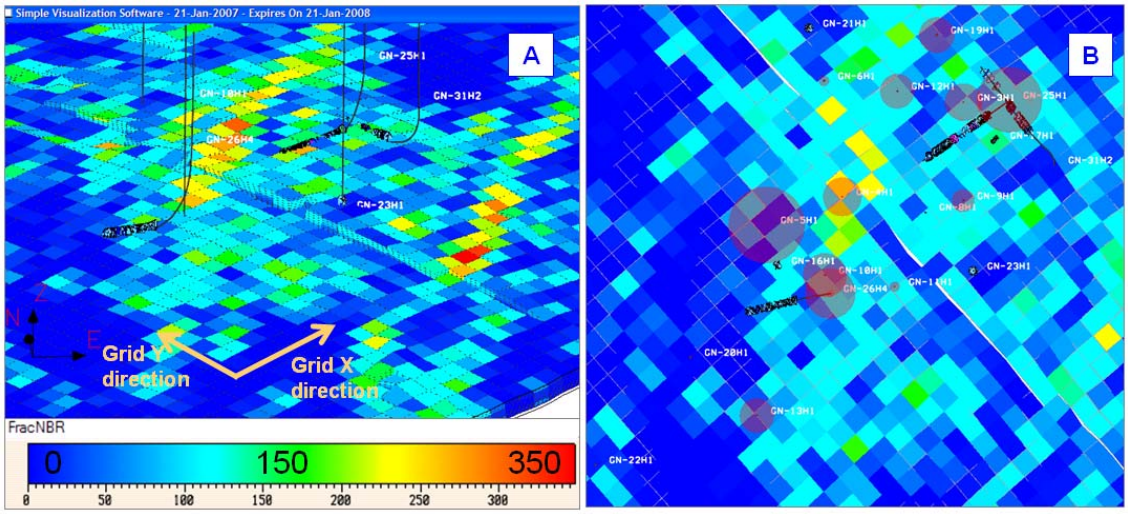


**Figure 4-63 SVS snap shot showing fracture number (count) calculation per cell for the proposed mid or base case scenario for GN Shuaiba. (A) Grid in an inclined view at the top fractured layer, and (B) showing a map view of a less fractured layer in Shuaiba. Red circles are gross production.**

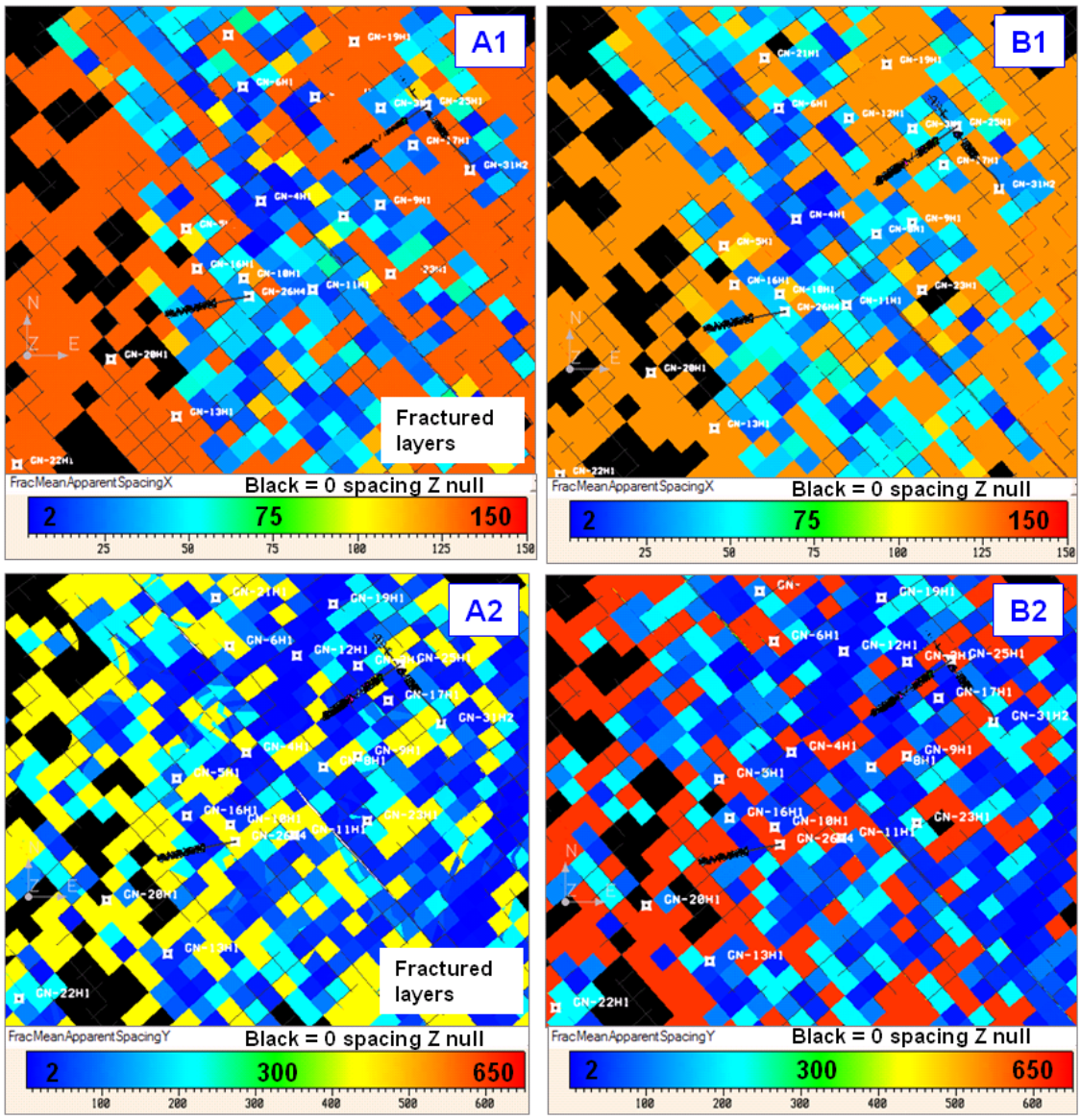


**Figure 4-64 SVS snap shot showing fracture spacing calculation along the grid X and Y direction for the proposed base case scenario. [A] is a fractured layer while [B] is the bulk of Shuaiba (i.e. less fractured layers). Wells with the BHI objects are shown superimposed on the grid.**

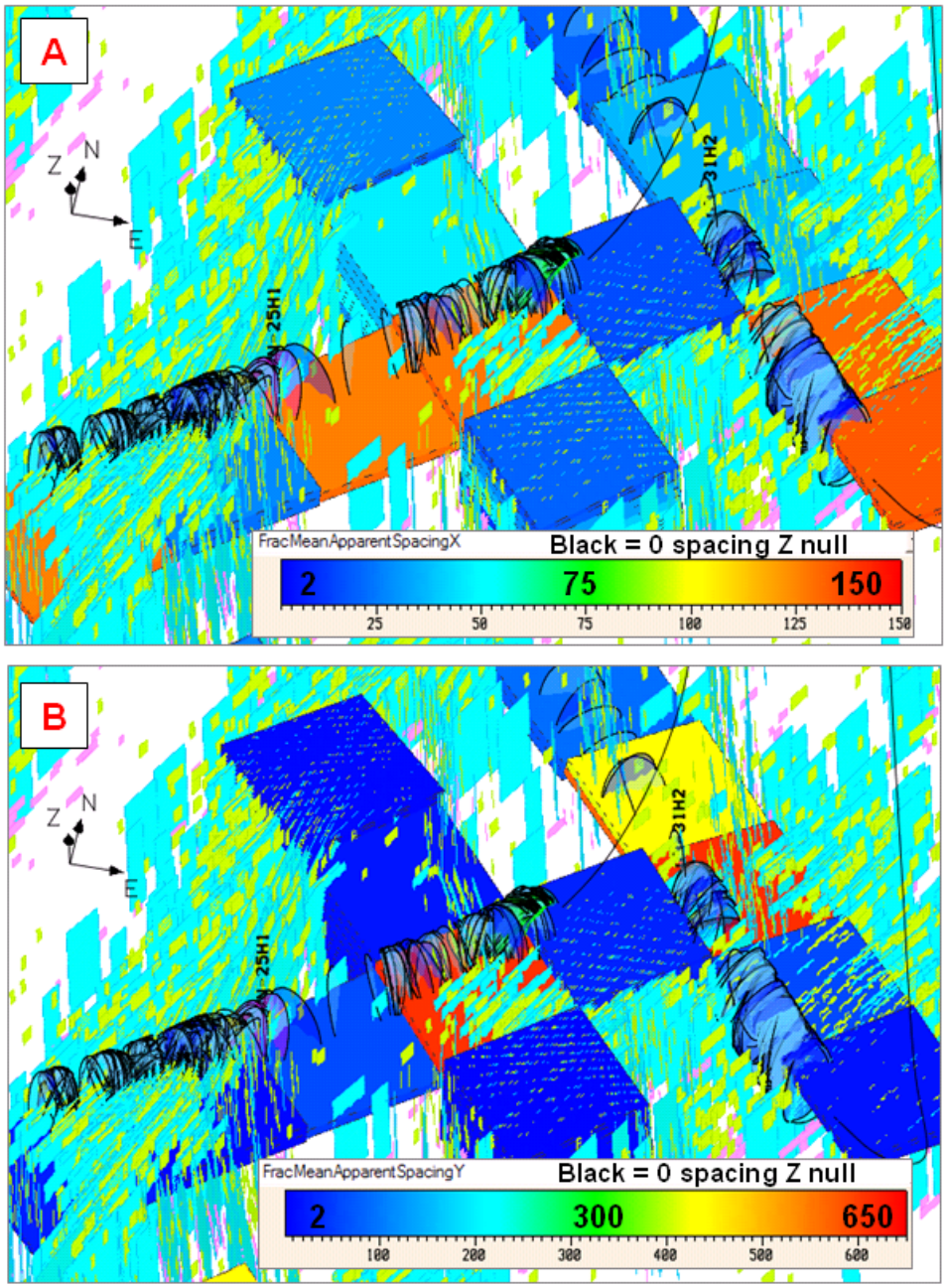


**Figure 4-65 SVS snap shot around GN-25H1 and GN-31H2 area showing proposed base case 3D DFN fractures (cyan crossing whole Shuaiba, yellow in top Shuaiba and pink in middle layer) and their extracted geometric properties in a 3D grid cells crossed by GN wells (spacing along the grid X direction [A] and along the grid Y direction [B]) together with well.**

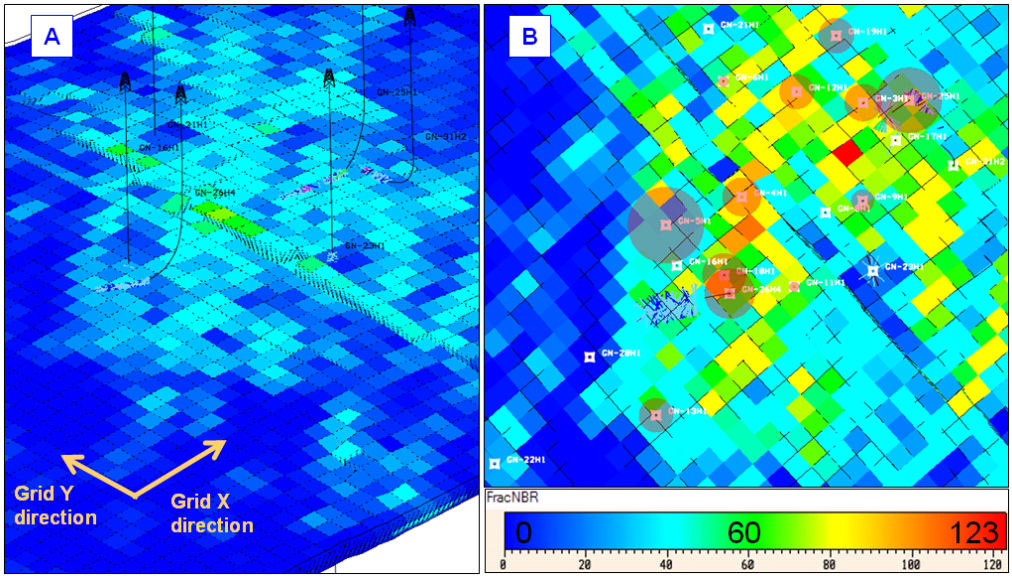


**Figure 4-66 SVS snap shot showing fracture number (count) calculation per cell for the proposed high case scenario for GN Shuaiba. (A) Grid in an inclined view at the bulk of Shuaiba, and (B) showing a map view at the fractured layer in upper Shuaiba. Red circles are gross production.**

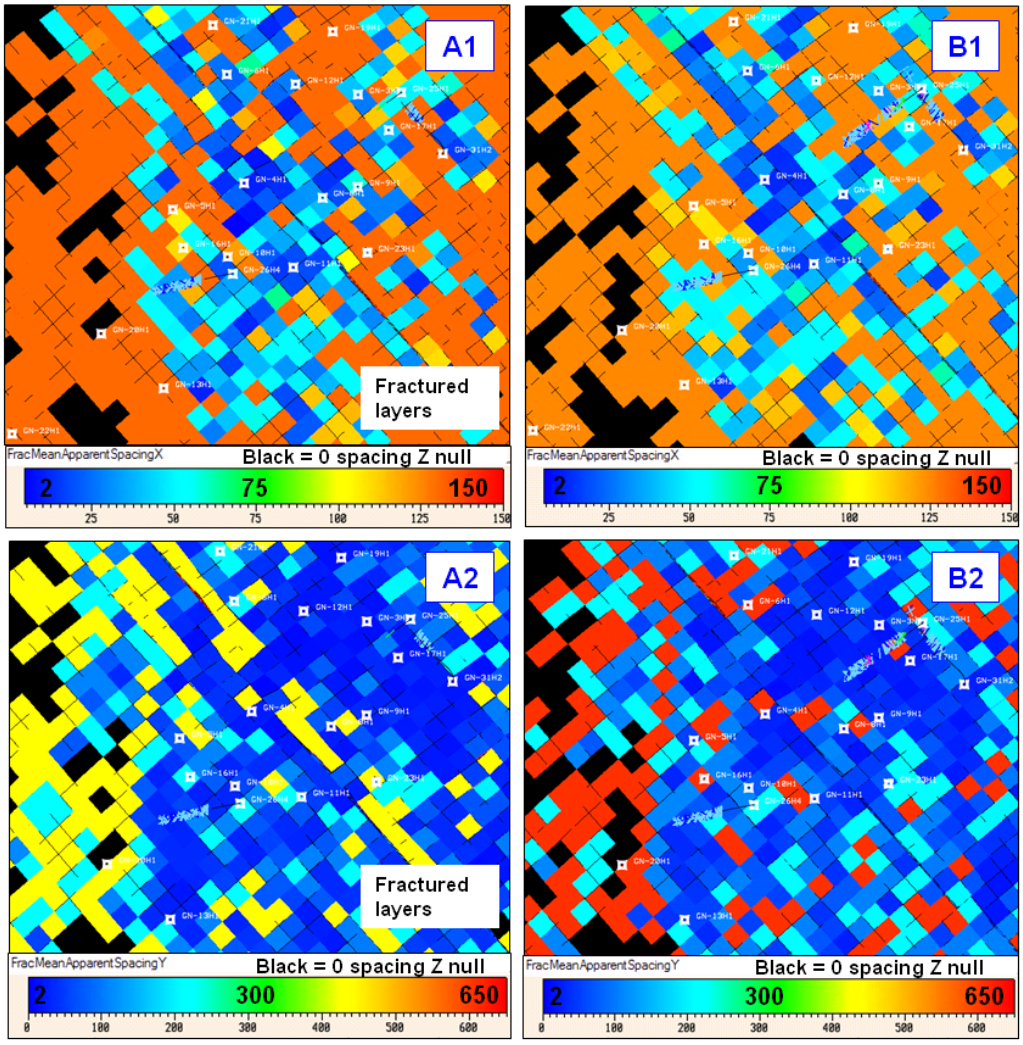


**Figure 4-67 SVS snap shot showing fracture spacing calculation along the grid X and Y direction for the high case scenario. [A] is a fractured layer while [B] represents the bulk of Shuaiba (i.e. less fractured layers). Wells with the BHI objects are shown superimposed on the grid.**

# Chapter 5– LEKHWAIR A NORTH (LAN) SHUAIBA

## 5.1 Field introduction

The Lekhwair cluster is located in the NW region of Oman close to the UAE. The cluster is made up of small fields donated Lekhwair A north LAN (focus of this chapter), Lekhwair A south LAS, Lekhwair B, Lekhwair C, Lekhwair D and Lekhwair East (Figure 5.1). As mentioned in Chapter 3, the cluster has 3 hydrocarbon bearing reservoirs: Upper Shuaiba split into 1 & 2, Lower Shuaiba split into A & B and Kharaib, with the Lower Shuaiba and Kharaib being the main commercial reservoirs. The Lekhwair area had been subjected to the main tectonic events (Cretaceous Alpine I and Tertiary Alpine II) seen elsewhere in the Oman Interior, though the area suffered huge uplift (in access of 1000m) at the end of the Cretaceous and erosion resulting in the removal of the whole of Fiqa Formation on crest of the field and the overlain Natih and Nahr Umr Formations above Shuaiba. Thus, Shuaiba is overlain directly by the Tertiary shale (Shammer) and carbonates (Figure 5.2). There is also a local tilting toward the NNE, by about 0.5-1.0 degree, seen in this area, which results in having the originally porous locations of a reservoir shifted SSW from the current structural crest.

The Lekhwair A north (LAN) is the oldest and largest field in this cluster. It produces from Lower Shuaiba (35m thick) and Kharaib (110m thick with 50m oil column), with the Hawar member acting as a baffle in between (Figure 5.3). Most of the wells have commingled completion. Upper Shuaiba has been mostly eroded in this part of the field. Available porosity and permeability measurements from core data of LAN field, show a matrix porosity of about 25% and a matrix permeability averaging in a range between 0.1 to 10 mD and as low as 0.01 mD for U Shuaiba (Figure 5.4). The trend of porosity with depth indicates a little change in rock competence within each reservoir unit (e.g. Lower Shuaiba). The focus of this chapter is on the L. Shuaiba and Kharaib (the main reservoir units). The field started production in 1976 with depletion drive. In 1984 a water injection pilot was introduced to sustain the efficiency of the reservoir as gross rate declined from 2500 m3/d to 600 m3/d. In 1992 water injection was implemented for the full field. A vertical infill wells campaign started in 2003 to minimize water production related to short circuiting. However, at the full field scale, the gradual increase in water cut is indicative of matrix-like behaviour. According to PDO field strategy note, there is a total of 286 active vertical wells out of 296; and 33 horizontal active wells, as of Jan 2005. These are split into 204 produces and 115 injectors. The estimated STOIIP is 159.10 mln m3. The water was initially injected at very high pressure (close to the perceived fracture condition at about 22500 kPa). This was later lowered to avoid water short circuiting along fracture network. The conclusion was derived from PLT analysis of the Lekhwair wells (Bait Muati, 2004). Recent static

pressure measurements for the field are shown in Figure 5.5 while the production history is shown in Figure 5.6.

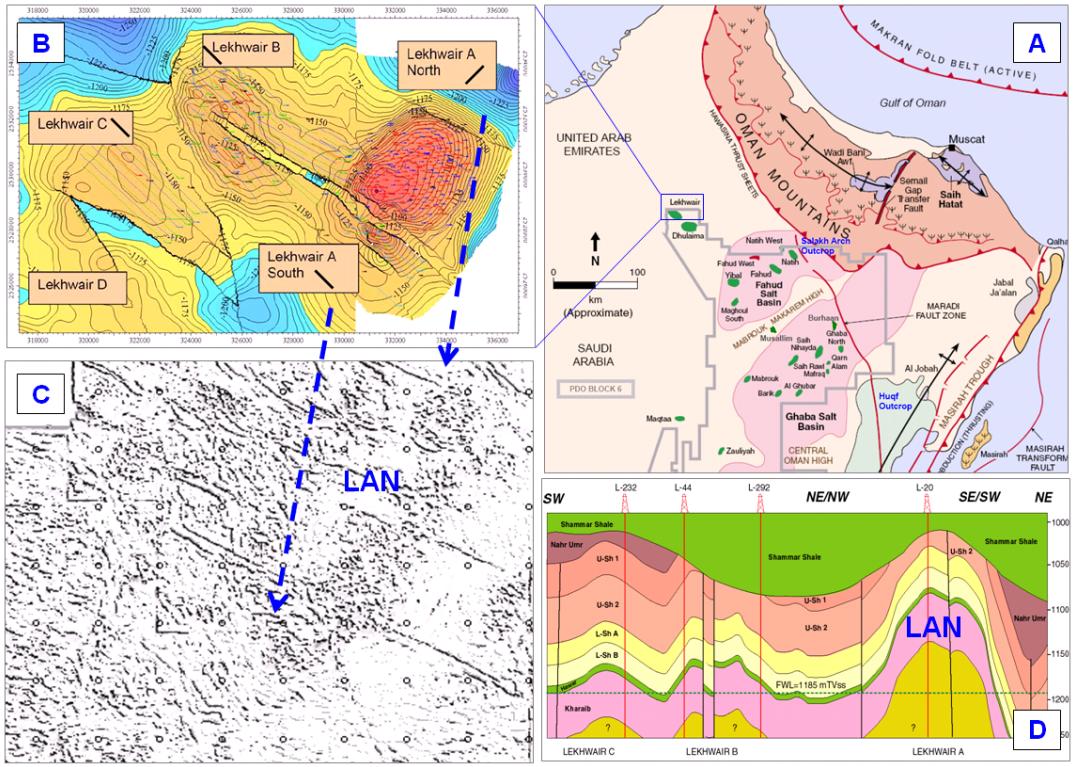


**5-1 A] Lekhwair field location map within north Oman (Filbrandt et al, 2006); B] Top Lower Shuaiba map for Lekhwair cluster with dominant well orientation (Poyser et al, 2005); C] Seismic coherency normalized semblance map at lower Shuaiba level over LAN (Yaarubi, 2006); D] Vertically exaggerated cartoon cross-section running SW-NE (Lekhwair team, PDO field strategy note for LAN, internal report, 2005).**

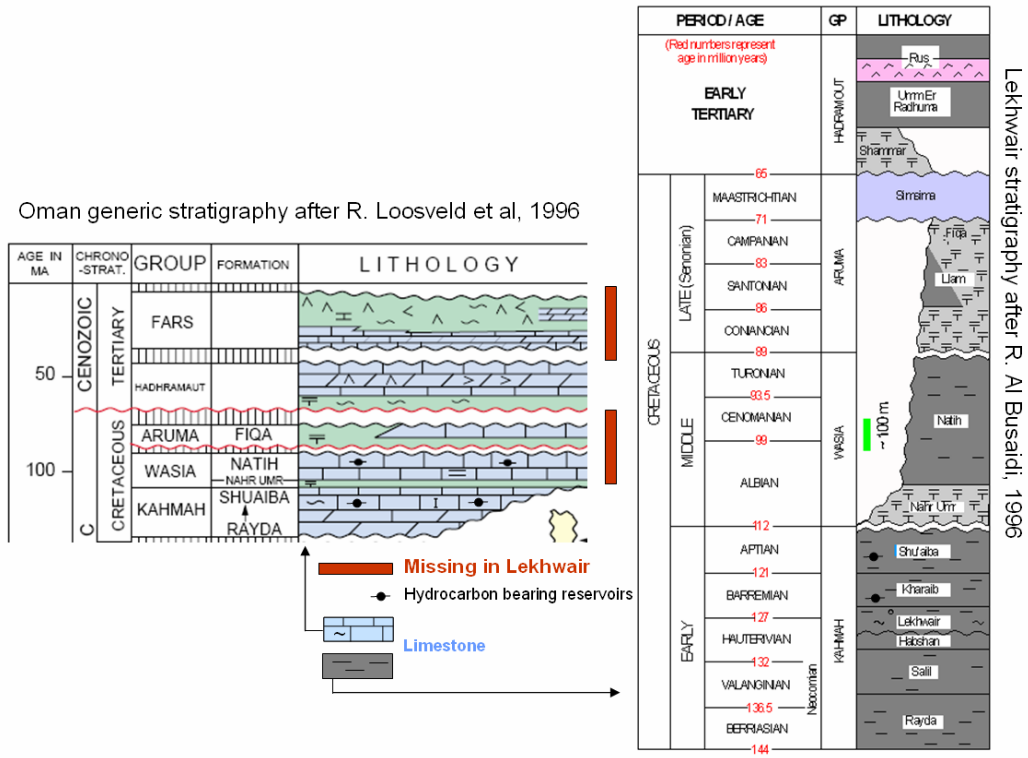


**Figure 5-2 North Oman regional stratigraphy compared to Lekhwair stratigraphy highlighting the major uplift and erosion associated with the Cretaceous deformation (modified from Loosveld et al, 1996 and Al-Busaidi, 1996).**

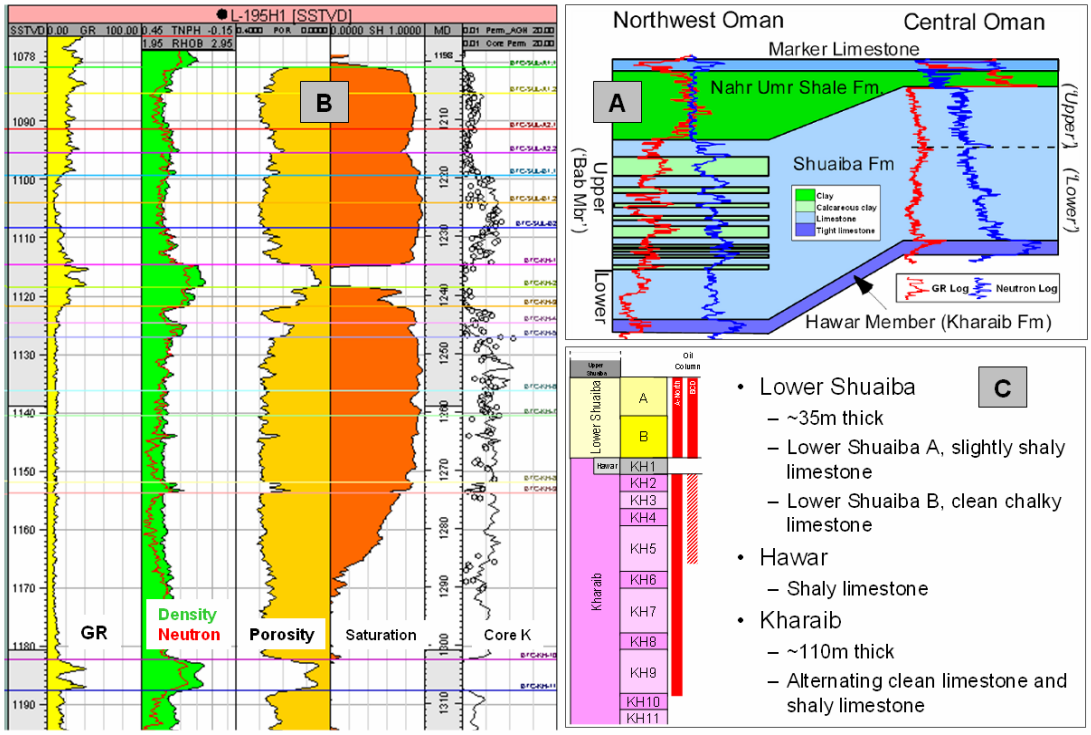


**5-3 A] Reminder of the stratigraphy of north Oman, Lekhwair in the NW area (from Droste, 2003). B] LAN type log for Lower Shuaiba and Kharaib and C] Sub-layering of LAN reservoirs (from Lekhwair team, PDO field strategy note, internal report, 2005).**

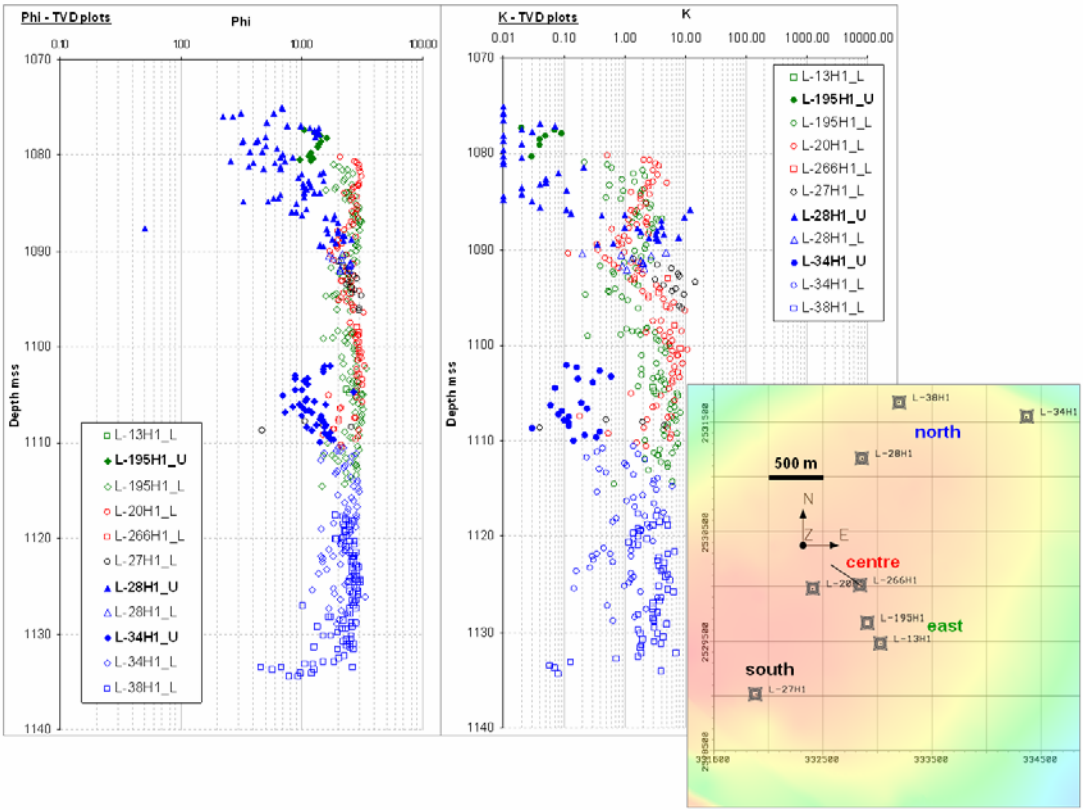


**Figure 5-4 LAN core data porosity (Phi) and permeability (K) versus depth, for both Upper Shuaiba (_U and solid colour) and Lower Shuaiba (_L and hollow colour) divided using colour into the north (blue), centre (red), east (green) and south (black) area as shown in top Lower Shuaiba map (right) for well location. Note how Upper Shuaiba has a lower "matrix" Phi & K compare to Lower Shuaiba. Also there little indications from Phi plot for Lower Shuaiba of change in rock competence with depth "mechanical layering".**

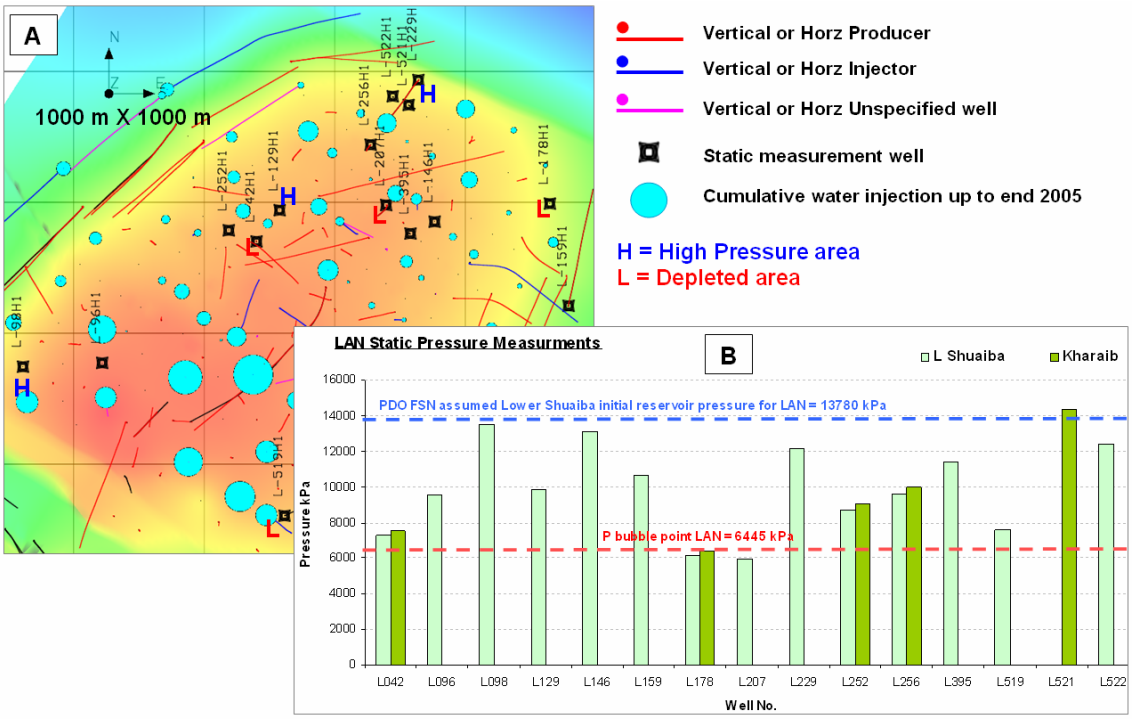


**5-5 LAN recent static pressure measurement indicate on average the reservoir's pressure is above the bubble point, thanks to water injection. Areas of high depletion are indicative of well connected network. Furthermore, areas of high pressure close to water injectors are also indicative of well connected network. A] Location of the wells with static measurement; B] Pressure readings.**

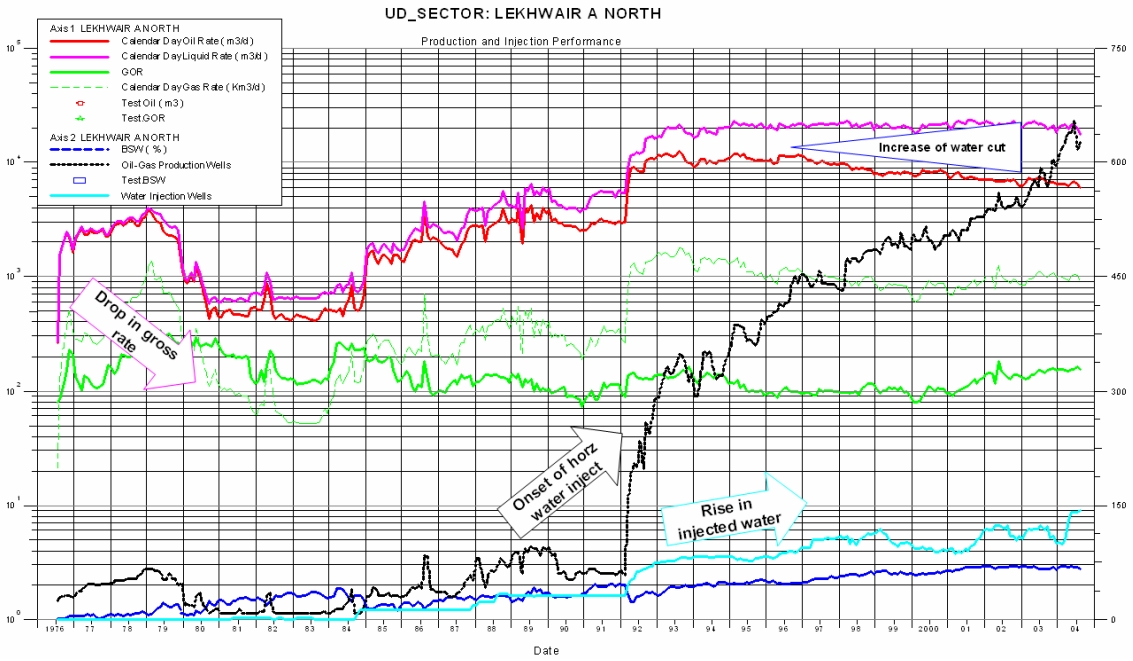


**Figure 5-6 LAN production rate and well drilling history from PDO field strategy note. Note the drop of gross rate few years after start of depletion development and increase of water cut at late 90s coinciding with rise in injected water.**

## 5.2 LAN Fracture related data

The workflow approach used in this chapter is similar to that stated in Chapter 1. In addition, the reader should refer to Chapter 4 for methods used for fracture characterisation. LAN field had been subjected to many detailed fracture characterization analysis by PDO, see Chapter 3, based mainly on BHI objects

"fracture" interpretations. Thus, a detailed fracture analysis related to BHI, at well scale, will not be undertaken here, to avoid any duplication. However, this chapter will focus on those fracture parameters that help in constructing conceptual fracture scenarios.

### *5.2.1 BHI fracture interpretation*

The BHI interpretation is normally done by Baker Atlas and in this research the interpretation has not been validated. The well data with BHI objects, provided by PDO in SVS format annotated "Lekhwair wells with good trajectories" is used (Figure 5.7). The latest well in this group is L-555H1 and BHI interpretation post date those used by Nelson in 2004, though two wells of Nelson report, were not used as they were not available for this research from the data base supplied by PDO (L-285H1 and L-3F28H1 – see wells written with red font in Figure 5.7 below to find their location). The well data set cover both LAN and LAS fields. As shown in the map of Figure 5.7, the areal coverage of the BHI logs is moderately good though there is few wells interpreted running NW-SE in LAN and visa versa in LAS. In addition, a visual inspection of the BHI data in SVS indicates a similar moderate coverage in the vertical dimension (Figure 5.8). Table 5.1 below provide a summary of the available BHI data per well together with other dynamic data. This is better illustrated in Figure 5.9 and figure 5.10 below. Table 5.2 provide a detailed summary of the BHI interpreted data for both LAN and LAS fields. A glance through the interpreted fracture data shows that conductive fractures represent about 82% of total data, compared to 70% with all the Lekhwair fields, though their dominant orientation is similar striking NW (Figure 5.11).

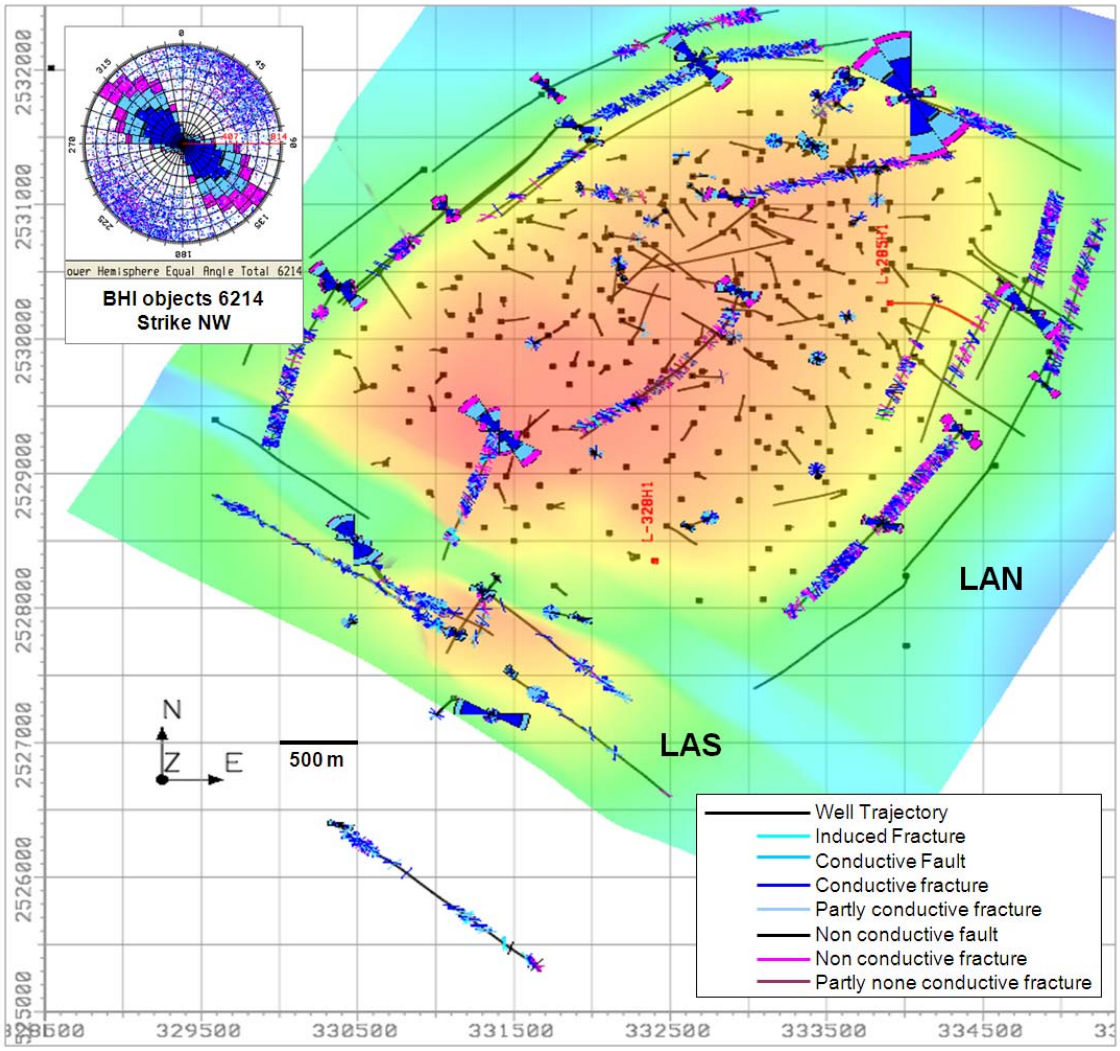


**Figure 5-7 Lekhwair A North (LAN) and A south (LAS) top Lower Shuaiba depth map (horizon extracted from PDO petrel grid), with all the wells provided by PDO in SVS format. BHI fracture objects are shown colour coded using PDO scheme (see insert) with standardized rose diagram showing the strike of the fracture. Wells with red trajectories (L-285H1 & L-328H1) were used by Nelson, 2004 fracture analysis, but were not available for this study.**

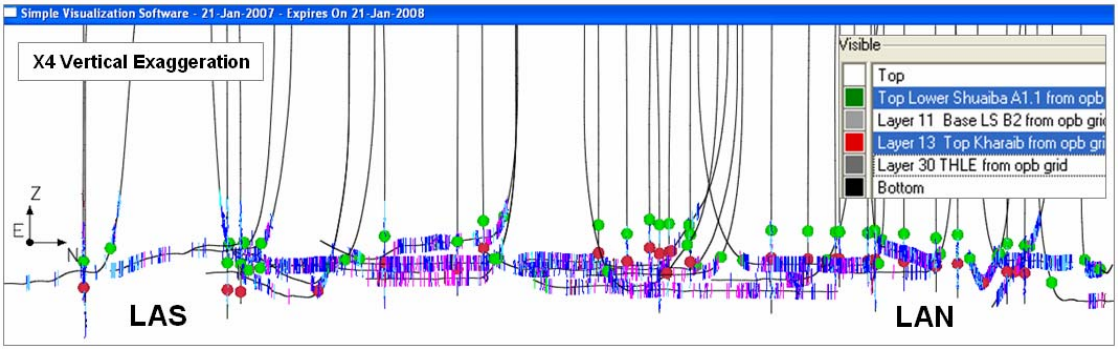


**Figure 5-8 Cross-sectional view of the BHI fractures per well for LAN and LAS fields, showing top L. Shuaiba and top Kharaib reservoirs as intersected from the horizons created from the petrel opb grid received from PDO.**

| Well | E | N | [A] Sum of BHI fractured objects | [B] Estimated BHI length | [C] Remarks: Wells in LAN unless specified - Cluster based on visual inspection | [D] frac/m (not cluster) | *[E] Normalized Gross Rate (Prod /Inj)* | [F] Losses |
|---|---|---|---|---|---|---|---|---|
| L-155H1 | 331909.21 | 2531576.47 | 204 | 763 | | 0.27 | *159* | 25 |
| L-159H1 | 334789.20 | 2530209.54 | 346 | 675 | | 0.51 | *323* | NA |
| L-181H1 | 334620.05 | 2530425.03 | 55 | 687 | | 0.08 | *118* | NA |
| L-182H1 | 331717.95 | 2531861.84 | 246 | 922 | clusters | 0.27 | *679* | NA |
| L-183H1 | 332666.97 | 2532070.99 | 412 | 591 | clusters | 0.70 | *273* | 100 |
| L-187H1 | 330373.97 | 2530394.10 | 358 | 898 | clusters | 0.40 | *85* | 25 |
| L-190H1 | 334895.00 | 2529658.98 | 198 | 1151 | clusters | 0.17 | *231* | NA |
| L-193H2 | 331065.94 | 2530965.93 | 162 | 566 | clusters | 0.29 | *48* | 100 |
| L-198H1 | 334361.92 | 2529310.80 | 225 | 721 | | 0.31 | *108* | 100 |
| L-198H2 | 334361.92 | 2529310.80 | 79 | 836 | | 0.09 | *129* | NA |
| L-200H1 | 333856.54 | 2528624.29 | 183 | 687 | clusters | 0.27 | *149* | 25 |
| L-205H1 | 331994.08 | 2531474.04 | 113 | 779 | clusters | 0.15 | *127* | 25 |
| L-212H1 | 331409.97 | 2529314.93 | 451 | 843 | clusters | 0.53 | *51* | 100 |
| L-215H1 | 332931.02 | 2530353.68 | 262 | 1357 | | 0.19 | *134* | 100 |
| L-218H1 | 331926.67 | 2531116.72 | 55 | 302 | clusters | 0.18 | *127* | NA |
| L-221H1 | 332883.90 | 2531049.97 | 283 | 1345 | | 0.21 | *224* | 25 |
| L-229H1 | 333639.61 | 2531934.36 | 103 | 283 | | 0.36 | *85* | 50 |
| L-234H3 | 331390.31 | 2528226.04 | 44 | 380 | LAS_cluster | 0.12 | *100* | NA |
| L-243H1 | 334200.72 | 2530300.13 | 59 | 580 | | 0.10 | *337* | NA |
| L-265H3 | 331300.03 | 2528130.22 | 129 | 1045 | LAS_cluster | 0.12 | *146* | NA |
| L-281H1 | 331125.04 | 2527810.08 | 143 | 1708 | LAS | 0.08 | *87* | NA |
| L-293H1 | 330477.78 | 2528509.15 | 287 | 654 | LAS_cluster | 0.44 | | NA |
| L-293H2 | 330477.78 | 2528509.15 | 272 | 727 | LAS_cluster | 0.37 | *853* | NA |
| L-298H2 | 331480.00 | 2527520.35 | 89 | 1160 | LAS_cluster | 0.08 | *140* | NA |
| L-323H2 | 330390.88 | 2526388.84 | 159 | 1587 | LAS_cluster | 0.10 | *159* | NA |
| L-368H1 | 333441.73 | 2529851.79 | 47 | 67 | vertical | 0.70 | *141* | 25 |
| L-376H1 | 332193.58 | 2530136.86 | 3 | 29 | vertical | 0.10 | *65* | NA |
| L-378H1 | 332640.30 | 2529726.37 | 3 | 9 | vertical | 0.33 | *134* | NA |
| L-382H1 | 333632.58 | 2530162.26 | 10 | 52 | vertical | 0.19 | *80* | NA |
| L-384H1 | 332119.15 | 2530772.76 | 7 | 54 | vertical | 0.13 | *62* | 25 |
| L-390H1 | 332881.58 | 2529974.77 | 15 | 87 | vertical | 0.17 | *242* | 25 |
| L-419H1 | 333828.56 | 2531238.80 | 17 | 57 | vertical | 0.30 | *90* | 25 |
| L-426H1 | 333410.87 | 2531436.93 | 111 | 59 | vertical | 1.88 | *68* | 50 |
| L-446H1 | 332009.45 | 2529149.25 | 12 | 41 | vertical | 0.29 | *253* | 50 |
| L-482H1 | 332200.75 | 2530449.80 | 41 | 80 | vertical | 0.51 | *255* | 25 |
| L-486H1 | 332536.80 | 2531316.38 | 9 | 22 | vertical | 0.41 | *15* | NA |
| L-489H1 | 332625.95 | 2531139.88 | 19 | 84 | vertical | 0.23 | *311* | NA |
| L-492H1 | 332644.71 | 2531208.04 | 4 | 57 | vertical & cluster | 0.07 | *244* | NA |
| L-498H1 | 331927.00 | 2527920.09 | 67 | 57 | LAS Graben_vertic | 1.18 | *50* | NA |
| L-502H1 | 331116.05 | 2527329.34 | 7 | 57 | LAS_vertical | 0.12 | *167* | NA |
| L-509H1 | 330469.72 | 2527898.80 | 28 | 58 | LAS_vertical | 0.48 | *74* | NA |
| L-510H1 | 331357.92 | 2527212.36 | 210 | 59 | LAS_vertical & clus | 3.56 | *26* | NA |
| L-511H1 | 332467.78 | 2530949.38 | 18 | 57 | vertical | 0.32 | *192* | 0 |
| L-515H1 | 333445.20 | 2528977.89 | 16 | 60 | vertical | 0.27 | *159* | NA |
| L-519H1 | 332615.12 | 2528606.17 | 41 | 114 | vertical | 0.36 | *355* | NA |
| L-520H1 | 333659.42 | 2530855.30 | 8 | 23 | vertical | 0.35 | *173* | NA |
| L-521H1 | 333564.80 | 2531743.59 | 11 | 51 | vertical | 0.22 | *53* | NA |
| L-522H1 | 333443.34 | 2531810.13 | 16 | 62 | vertical | 0.26 | *141* | NA |
| L-524H1 | 331719.96 | 2530026.09 | 11 | 51 | vertical | 0.22 | *150* | 50 |
| L-549H1 | 334038.55 | 2531804.69 | 566 | 377 | Hook | 1.50 | *470* | NA |

**[A] Sum of BHI objects: CI (induced fractures only 3 in L-243H1 & 3 in L-426H1), CF (conductive faults), CC (conductive fracture), CP (partly conductive fracture), NF (none conductive fault), NC (none conductive fracture) & NP (partly none conductive fracture)**
**[B] Estimated BHI coverage length based on the Measured Distance along hole from the last and first fracture**
**[C] Remark if the well is clustered or not and on the location of the well and type (vertical vs horizontal)**
**[D] Fracture intensity = total number of fracture / total BHI length. Used with caution whenever cluster exists**
**[E] Normalized production or injection rate = total volume of liquid produced or injected / number of days well on data obtained from nearby hole (e.g. L-549H1 data of L-549H2)**
**[F] Losses: assumed 0 for no losses, 25 for partial, 50 for medium and 100 for total losses; NA = Not Available**

**Table 5-1 Inventory of LAN and LAS BHI well data versus dynamic data.**

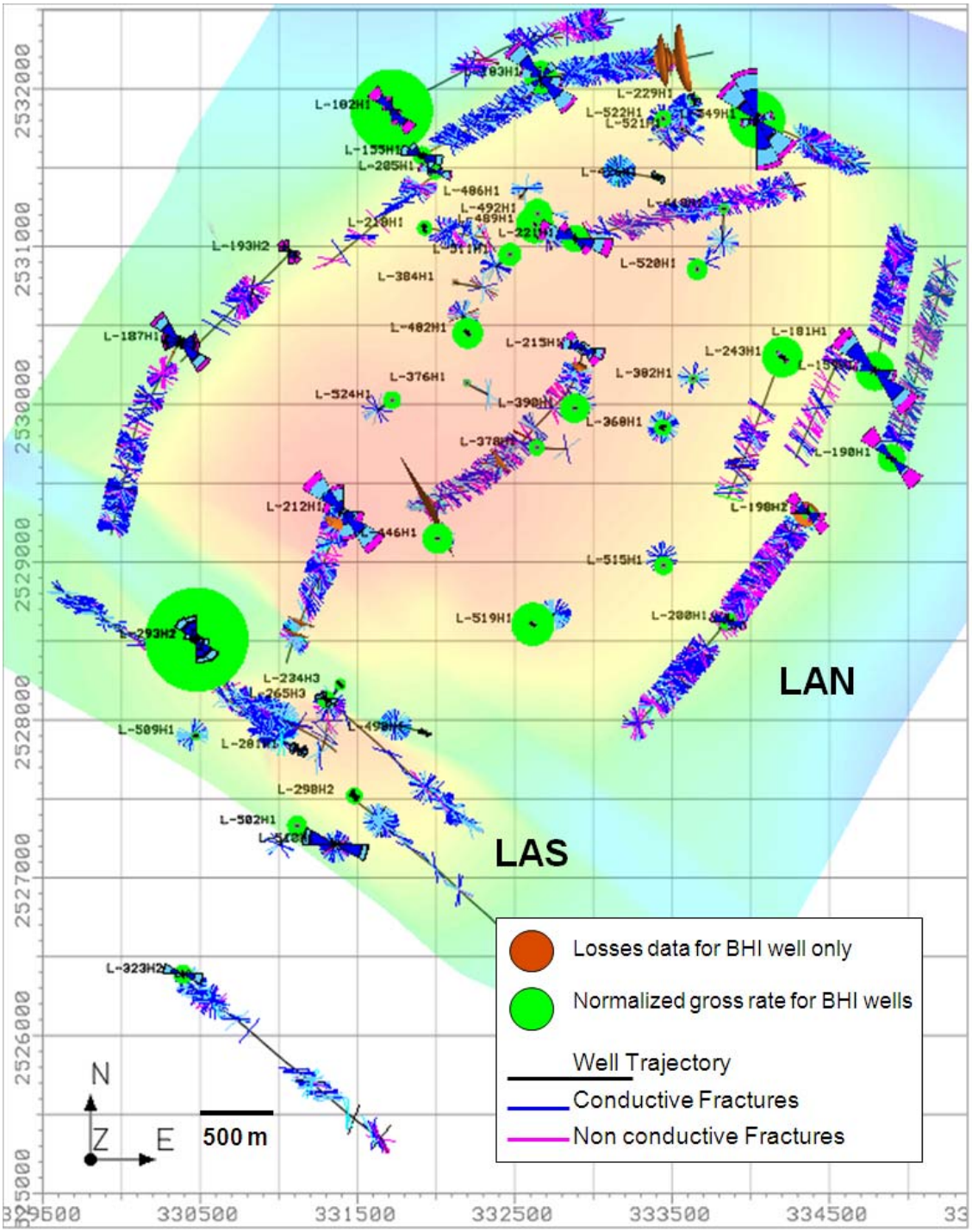


**Figure 5-9 LAN and LAS fields showing only BHI wells, drilling losses encountered and a normalized gross rate (total produced liquid / days on production or total injected water / days on injection) for those wells.**

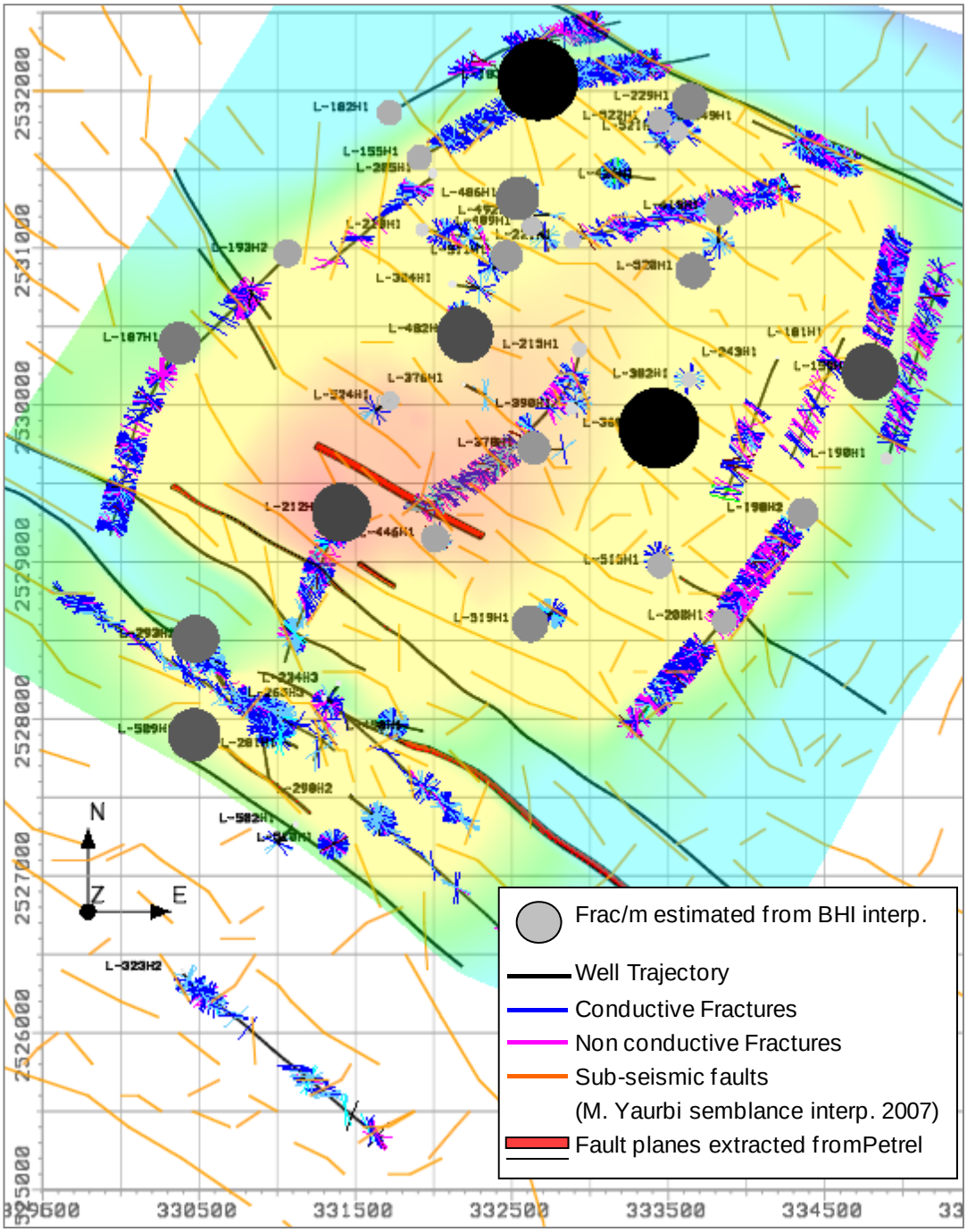


**Figure 5-10 Map view of top L. Shuaiba of LAN and LAS fields, with BHI fracture intensity (frac/m) with the removal of highly fractured wells due to being in a fault zone (LAS: L-510 & L498; LAN: L426 & L549) so that not to mask the areal distribution of the intensity.**

| Well | CI | CF | CC | CP | NF | NC | NP | Sum of BHI fractured objects |
|---|---|---|---|---|---|---|---|---|
| L-155H1 | 0 | 0 | 131 | 68 | 0 | 4 | 1 | 204 |
| L-159H1 | 0 | 1 | 213 | 66 | 1 | 62 | 3 | 346 |
| L-181H1 | 0 | 0 | 26 | 4 | 0 | 25 | 0 | 55 |
| L-182H1 | 0 | 1 | 151 | 14 | 0 | 74 | 6 | 246 |
| L-183H1 | 0 | 7 | 230 | 143 | 0 | 27 | 5 | 412 |
| L-187H1 | 0 | 4 | 233 | 55 | 2 | 56 | 8 | 358 |
| L-190H1 | 0 | 0 | 97 | 15 | 0 | 83 | 3 | 198 |
| L-193H2 | 0 | 0 | 85 | 10 | 2 | 63 | 2 | 162 |
| L-198H1 | 0 | 0 | 102 | 30 | 0 | 91 | 2 | 225 |
| L-198H2 | 0 | 1 | 14 | 8 | 0 | 51 | 5 | 79 |
| L-200H1 | 0 | 2 | 114 | 25 | 0 | 37 | 5 | 183 |
| L-205H1 | 0 | 0 | 57 | 38 | 0 | 16 | 2 | 113 |
| L-212H1 | 0 | 15 | 214 | 135 | 1 | 82 | 4 | 451 |
| L-215H1 | 0 | 9 | 120 | 77 | 0 | 51 | 5 | 262 |
| L-218H1 | 0 | 0 | 23 | 20 | 2 | 9 | 1 | 55 |
| L-221H1 | 0 | 6 | 147 | 55 | 1 | 71 | 3 | 283 |
| L-229H1 | 0 | 2 | 55 | 35 | 0 | 11 | 0 | 103 |
| L-234H3 | 0 | 1 | 22 | 10 | 0 | 11 | 0 | 44 |
| L-243H1 | 3 | 0 | 30 | 7 | 0 | 16 | 3 | 59 |
| L-265H3 | 0 | 2 | 61 | 60 | 0 | 6 | 0 | 129 |
| L-281H1 | 0 | 3 | 88 | 46 | 0 | 6 | 0 | 143 |
| L-293H1 | 0 | 4 | 179 | 92 | 2 | 8 | 2 | 287 |
| L-293H2 | 0 | 7 | 120 | 119 | 2 | 21 | 3 | 272 |
| L-298H2 | 0 | 2 | 37 | 43 | 3 | 4 | 0 | 89 |
| L-323H2 | 0 | 6 | 75 | 61 | 3 | 13 | 1 | 159 |
| L-368H1 | 0 | 0 | 15 | 28 | 0 | 4 | 0 | 47 |
| L-376H1 | 0 | 0 | 0 | 3 | 0 | 0 | 0 | 3 |
| L-378H1 | 0 | 0 | 1 | 2 | 0 | 0 | 0 | 3 |
| L-382H1 | 0 | 0 | 5 | 5 | 0 | 0 | 0 | 10 |
| L-384H1 | 0 | 0 | 2 | 3 | 0 | 1 | 1 | 7 |
| L-390H1 | 0 | 0 | 6 | 9 | 0 | 0 | 0 | 15 |
| L-419H1 | 0 | 0 | 6 | 10 | 0 | 1 | 0 | 17 |
| L-426H1 | 3 | 9 | 41 | 57 | 0 | 1 | 0 | 111 |
| L-446H1 | 0 | 0 | 5 | 6 | 0 | 0 | 1 | 12 |
| L-482H1 | 0 | 0 | 10 | 21 | 0 | 8 | 2 | 41 |
| L-486H1 | 0 | 0 | 2 | 7 | 0 | 0 | 0 | 9 |
| L-489H1 | 0 | 0 | 6 | 12 | 0 | 0 | 1 | 19 |
| L-492H1 | 0 | 0 | 1 | 3 | 0 | 0 | 0 | 4 |
| L-498H1 | 0 | 3 | 30 | 34 | 0 | 0 | 0 | 67 |
| L-502H1 | 0 | 0 | 4 | 3 | 0 | 0 | 0 | 7 |
| L-509H1 | 0 | 1 | 8 | 17 | 0 | 1 | 1 | 28 |
| L-510H1 | 0 | 2 | 147 | 51 | 1 | 8 | 1 | 210 |
| L-511H1 | 0 | 0 | 9 | 9 | 0 | 0 | 0 | 18 |
| L-515H1 | 0 | 0 | 13 | 3 | 0 | 0 | 0 | 16 |
| L-519H1 | 0 | 3 | 24 | 14 | 0 | 0 | 0 | 41 |
| L-520H1 | 0 | 0 | 6 | 2 | 0 | 0 | 0 | 8 |
| L-521H1 | 0 | 0 | 5 | 4 | 0 | 2 | 0 | 11 |
| L-522H1 | 0 | 0 | 15 | 1 | 0 | 0 | 0 | 16 |
| L-524H1 | 0 | 0 | 3 | 7 | 0 | 1 | 0 | 11 |
| L-549H1 | 0 | 9 | 286 | 185 | 0 | 75 | 11 | 566 |
| sum | 6 | 100 | 3274 | 1732 | 20 | 1000 | 82 | 6214 |

**Table 5-2 Detailed summary of the BHI fracture interpretation for LAN and LAS field wells.**

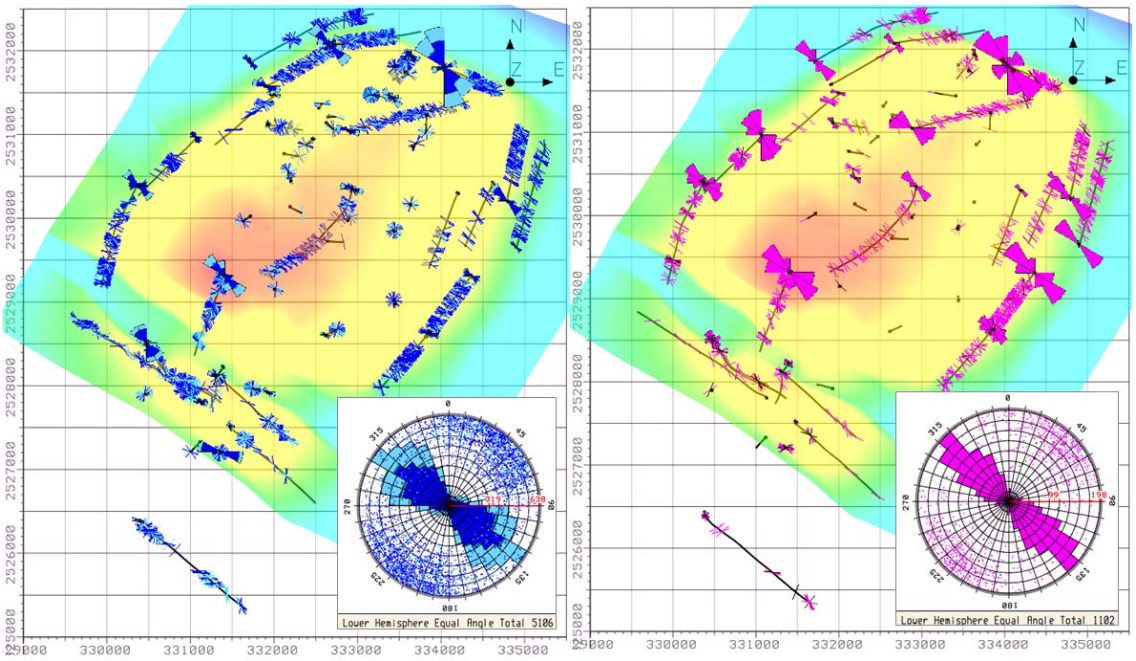


**Figure 5-11 BHI objects "fractures" conductive (blue –left) and non-conductive (pink –right) areal distribution in LAN and LAS fields superimposed on top of L. Shuaiba map.**

### *5.2.2 Seismically interpreted faults*

There are two set of faults interpreted by PDO for the LAN field (Figure 5.12): a detailed set of lineaments interpretation also provide by PDO, and a set that was extracted from the PDO matrix 3D geo-cellular petrel grid. The basis for the enhanced lineament interpretation is the usage of especially filtered semblance map by PDO (Yaarubi, 2006).

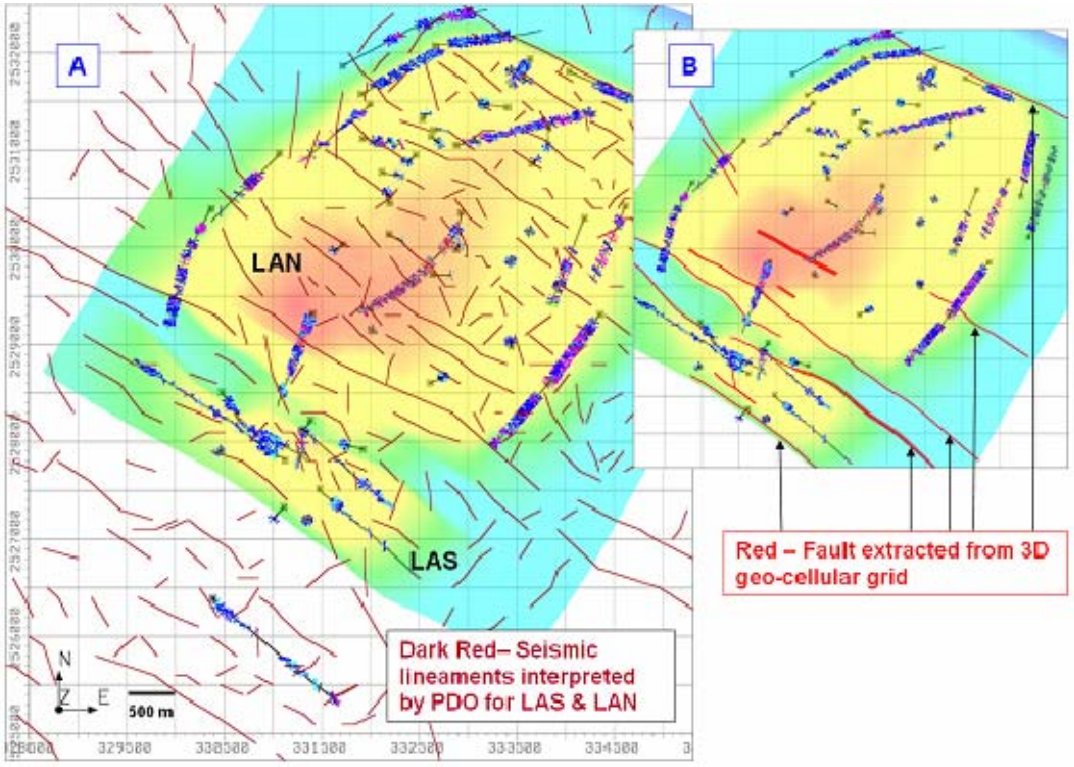


**Figure 5-12 LAN faults uploaded to SVS: A] Seismically interpreted lineaments and B] fault extracted from PDO 3D geo-cellular grid.**

### *5.2.3 Curvature analysis*

For background information on curvature analysis see Chapter 4.

The top L. Shuaiba horizon extracted from the PDO petrel 3D geo-cellular grid had been subjected to several curvature calculations at different scale and azimuth to check for any correlation between Kmax, BHI fractures ("objects") and the seismically interpreted faults and lineaments as well as normalized gross rate (Figure 5.13). Unidirectional curvature analysis at 500m and 100m parallel and perpendicular to the main fault trend (NE and NW) shows some interesting distribution (Figure 5.14).

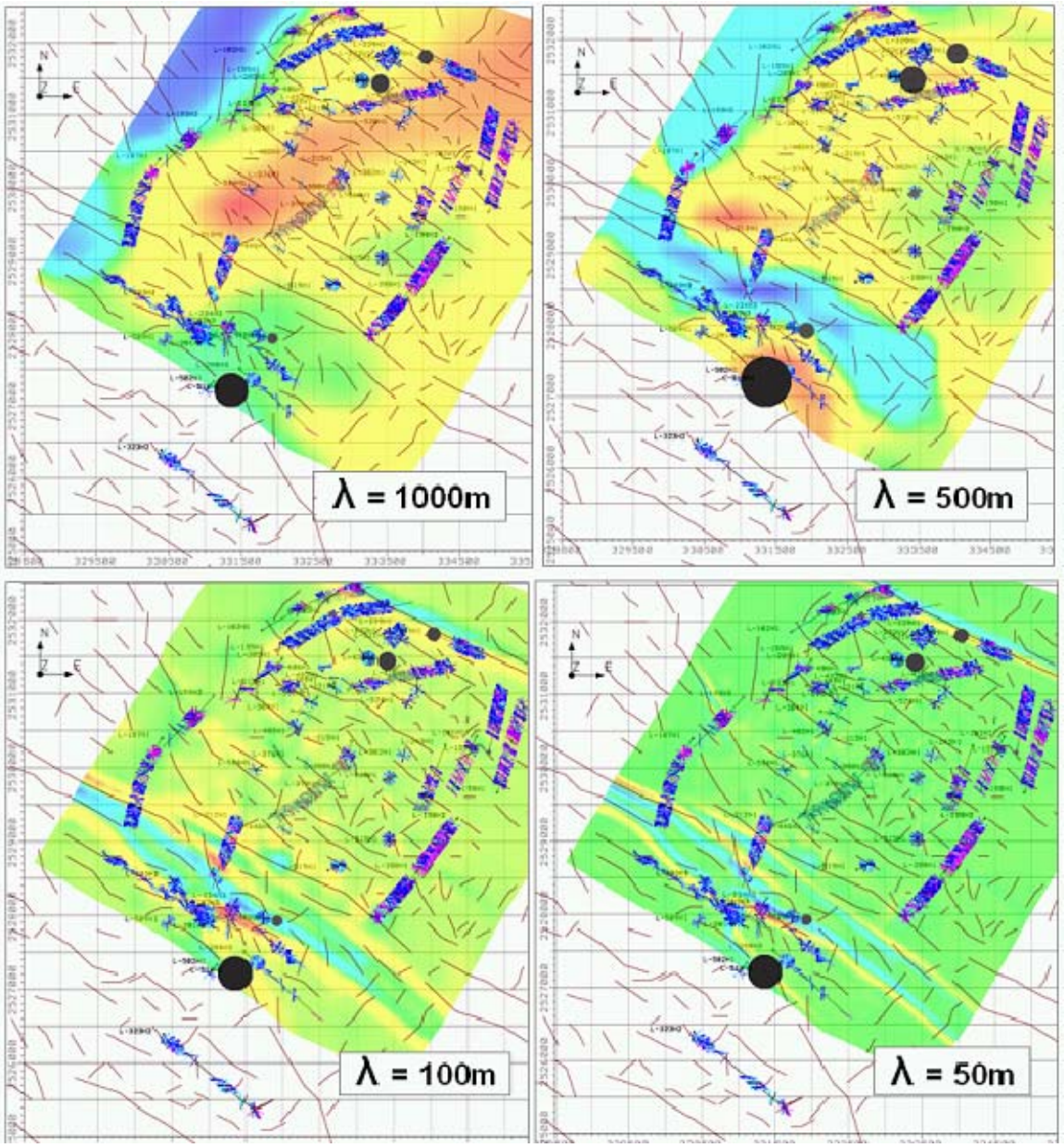


**5-13 Multi-directional Kmax curvature map of top L. Shuaiba for LAN/LAS, at different wavelength, integrated with BHI objects (blue conductive, pink non-conductive) and BHI fracture intensity per well (frac/m, white-small to large-dark grey circles in log scale) as well as, the seismic lineaments (brown). The low scale curvatures highlight the faults seen in the fields while the large scale indicates areas of high strain. The 500m scale seems to better fit the fracture intensity data.**

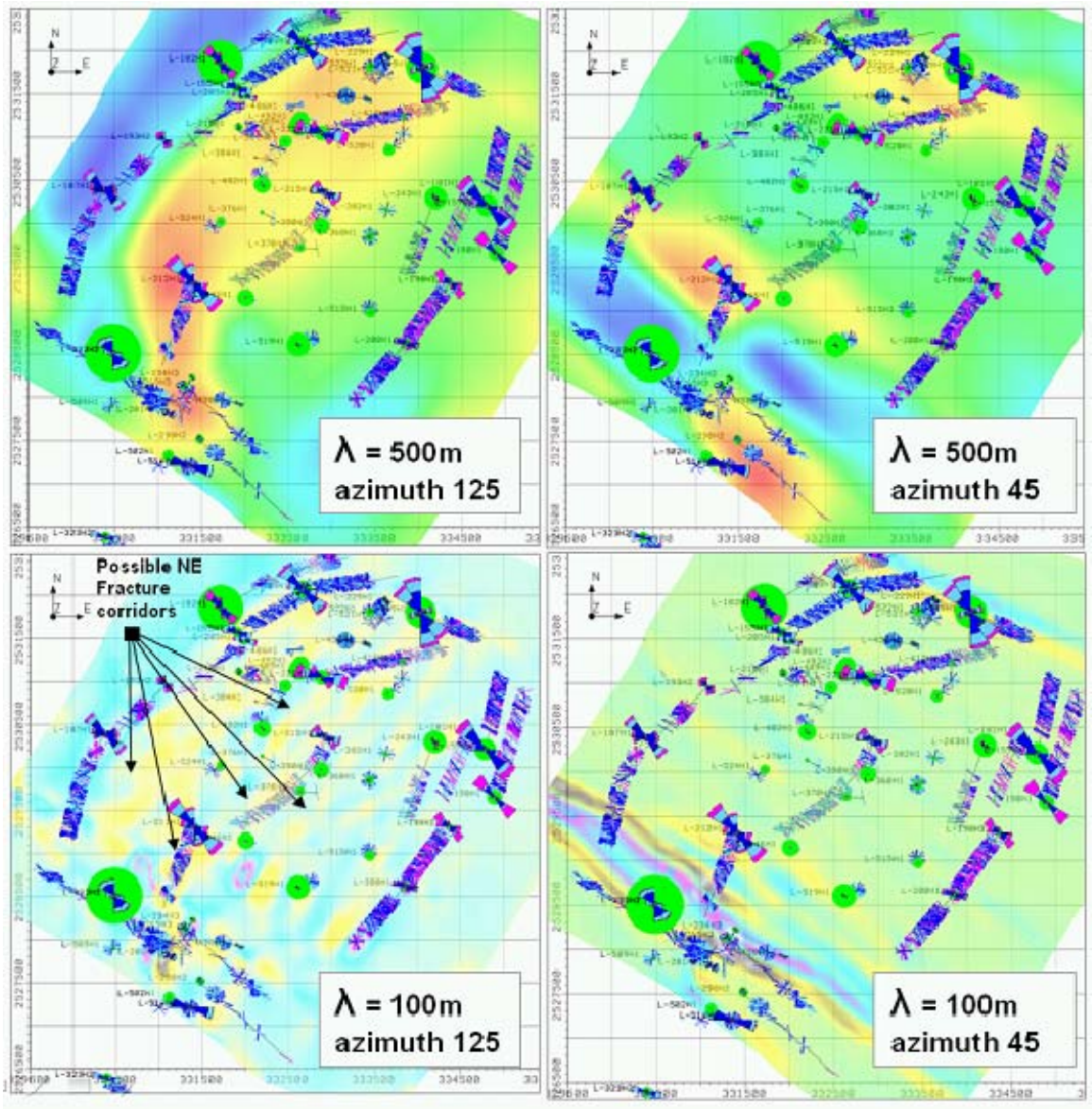


**Figure 5-14 Uni-directional Kmax curvature maps of L. Shuaiba for LAN and LAS fields, using 100m and 500m wavelength. Note how the 100m azimuth 125 highlight a potential NE fracture corridors, while the 500m with azimuth 125 seems to fit with the BHI fracture intensity except for the eastern wells. But Kmax maps do not fit with the BHI wells' normalized gross rate (green circle) though it thought to fit with LAN all wells normalized gross rate, see next section.**

### *5.2.4 Dynamic data calibration*

**Losses data:**

The drilling losses data provided by PDO at the reservoir interval were loaded to SVS to check for any areal variation (Figure 5.15). The losses seem to concentrate around the south western part of LAN field, coinciding with the large scale Kmax curvature map and the seismic lineaments seen in the field. Wherever a BHI log is run the losses occur around fracture clusters.

**Gross rate data:**

An analysis similar to that done for GN field was undertaken for LAN field to check if BHI fracture intensity and seismic faults (or lineaments) coincide with gross liquid rate.

The total production data and injection data per well were divided by the number of days wells were on production or on injection (Figure 5.16). The result indicates that the most connected area is likely to be the south western part of LAN field. There seems to be a good correlation with high matrix porosity areas (yellow in B of figure 5.15) as well as, the high curvature areas at large scale (yellow in C of figure 5.15).

**Well test data:**

Well tests are very complex to understand when executed in fractured carbonate reservoirs (Amri, 20065) because the whole process is governed by many factors that increase the level of uncertainties in the estimated results. These could be factors such as uncertainties in reservoir and fluid properties; uncertainties in production/injection history; and multiple matches (sometimes data can be matched against more than one single model). Other factors that are related directly to the testing process, which might also affect the results obtained, are: design of the test(s), proper execution of the designed test(s), data acquisition method(s), and interpretation method(s). Well test can either be **build-up test** for oil producers, or **fall-off test** for injectors. The latter is normally easier to interpret as there is NO gas to worry about in injectors (high GOR usually affect match quality). A pressure fall off test is the measurement and analysis of pressure data taken after an injector is shut in. It is a replay of the injection period but is less noisy because there is no fluid gain by the pressure gauge. The pressure derivative is essentially the rate change of pressure with respect to the superposition time function i.e. the slope of the semi-log plot. So, the basic idea of the derivative is to calculate the slope at each point of the pressure curve on the semi-log (superposition) plot, and to display it on the log-log plot (Figure 5.17). A long term high rate injection test was performed on L-54H1 where 450 m3/d of water was injected for two years: October 1988 to November 1990. Stofferis (Stofferis, 1991) reported connectivity along a consistent azimuth of 100-280 degrees (similar to the strike slip faults orientation seen in the field). In addition, water break through measured in the observation well L-068 occurred at a volume larger than theoretically calculated in most of the layers, indicating an elliptical flood front advance (Figure 5.18). In June 2006 Baker Atlas produced a report on a similar fall off and build up tests done on the following wells of LAN most likely in 2005 (Figure 5.19): injectors fall off test in L262, L390, L80 and L68; producers build up test in L266, L368, L296 & L83. Main findings are that all tests indicate linear flow except for L83; and effective permeability range of 0.3 to 5.8 mD is derived from the tests. Thus, all the data indicate homogenous reservoir behaviour except for L83, according to Baker Atlas report. Similar fall off test was recently (2006) done on L006, L177 and L276 injectors. The main findings are (Figure 5.20): L006 & L177 show water-flood under fracture dominated conditions in the southern part of LAN. L276 shows water flood under matrix dominated conditions in the central part.

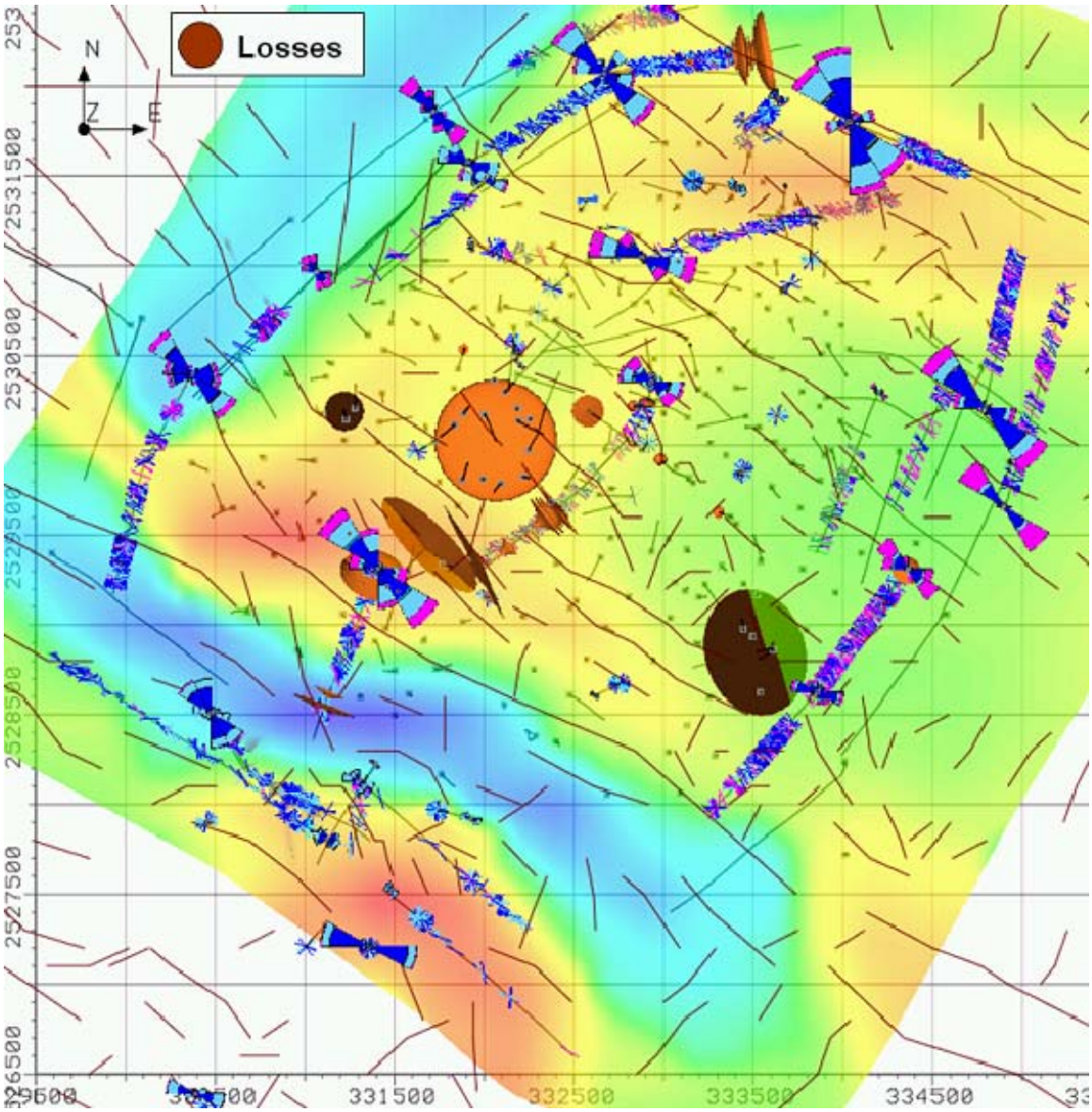


**Figure 5-15 All LAN field well losses areal distribution at reservoir level, shown integrated with BHI fractures, seismic lineament faults and curvature Kmax map of top Lower Shuaiba at 500m scale. Note how the losses concentrate in the south western side of LAN.**

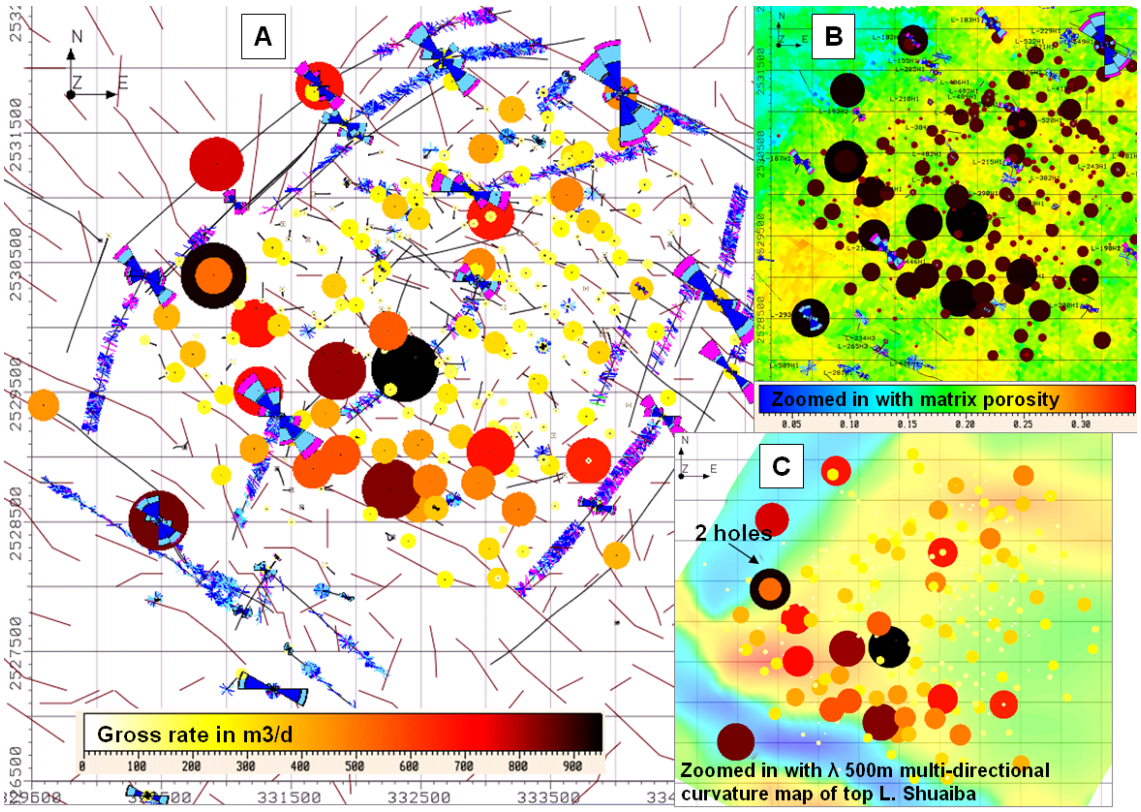


**Figure 5-16 A] map view of LAN and LAS field showing normalized gross rate per well (producers and injectors) as a point set data integrated with BHI objects and seismic lineaments. B] Same point set data at log scale on top of matrix porosity map and BHI objects. C] Same point set data but in linear scale on top of curvature map at L. Shuaiba. The most productive or most connected area is the south western part of LAN field and they seems to coincide with high porosity areas except for well in NW side of the field.**

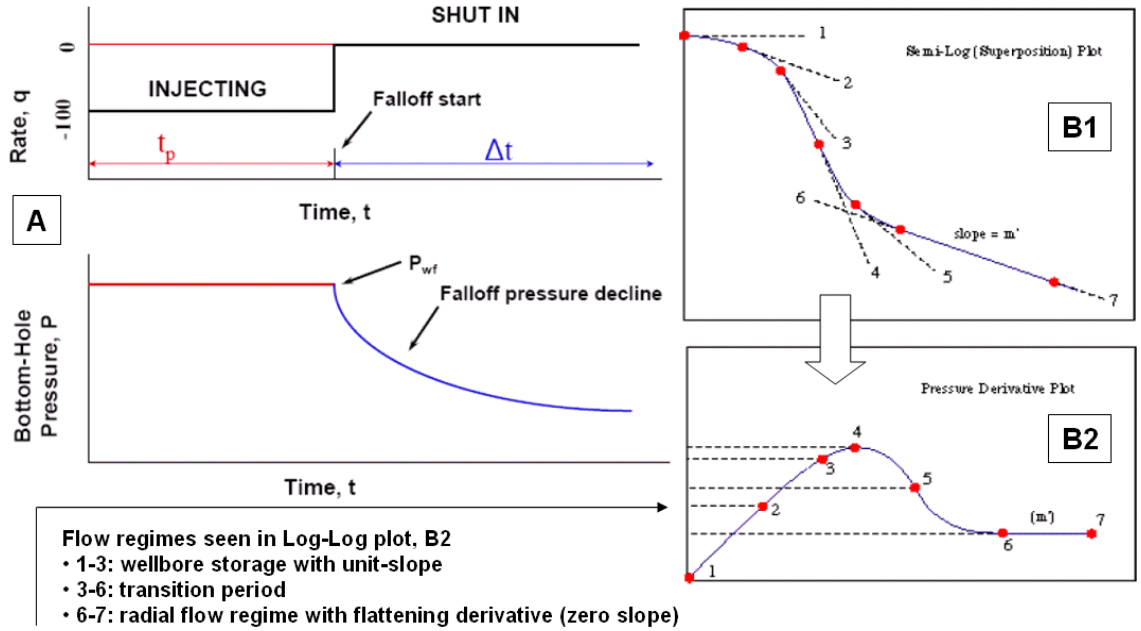


**Figure 5-17 A graphical plot to illustrate Fall off test [A], and the concept pressure derivative [B] used as the main diagnostic tool for determining flow regimes (Amri, 2006).**

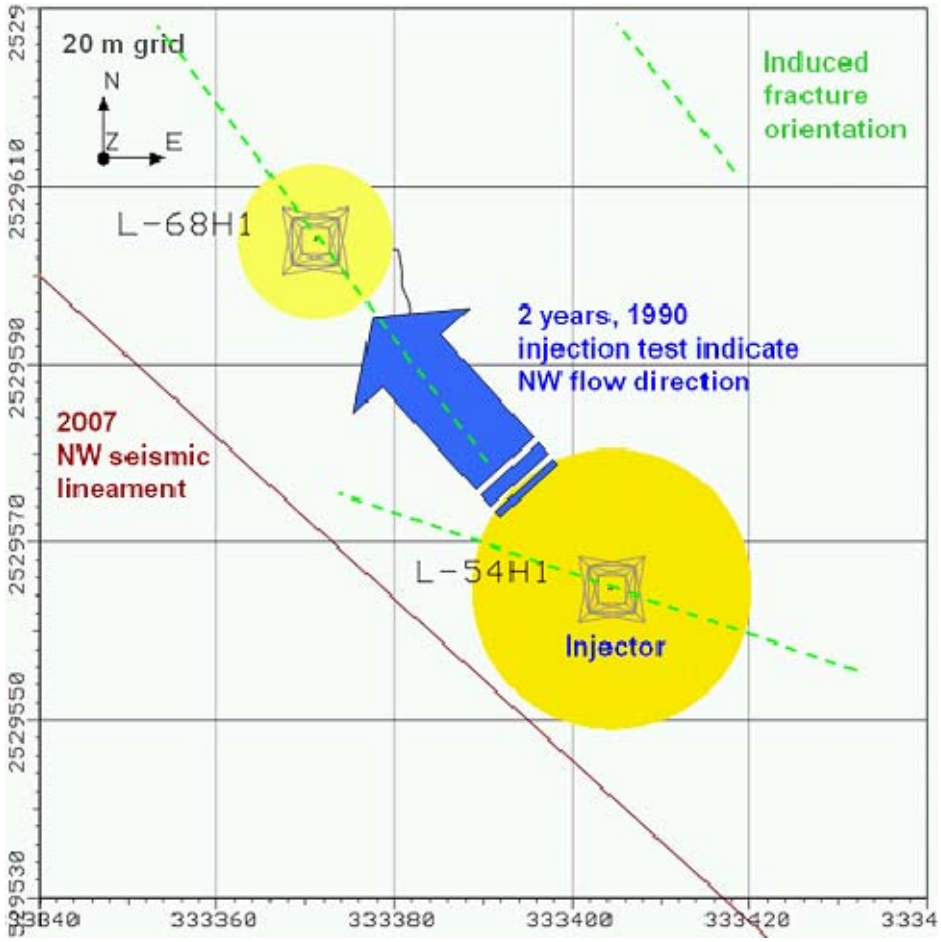


**Figure 5-18 Injection test in 1989 to 1990 indicated a NW preferential flow and NW induced fracture orientation.**

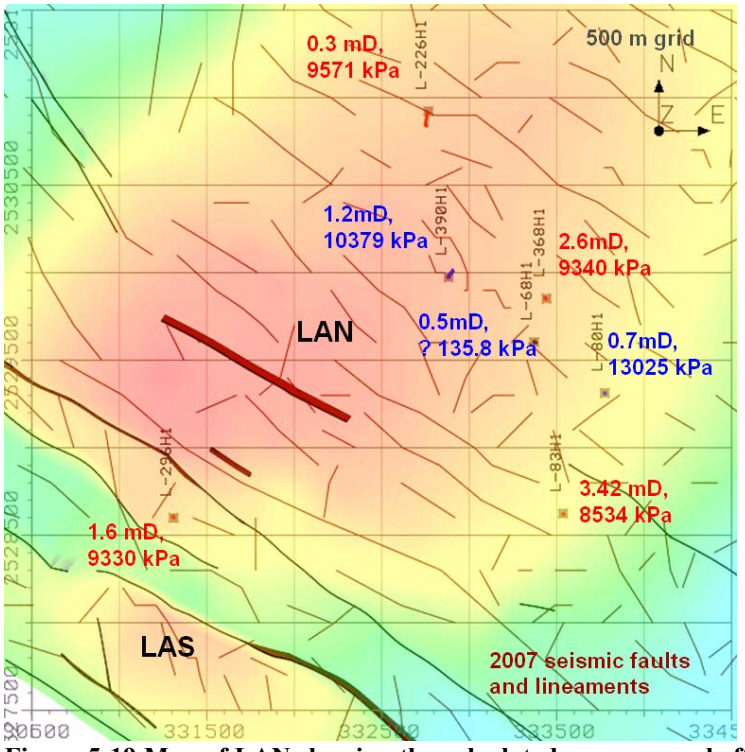


**Figure 5-19 Map of LAN showing the calculated pressure and effective permeability obtained from build up (red) and fall off (blue) test for Lekhwair wells, reported by Baker Atlas.**

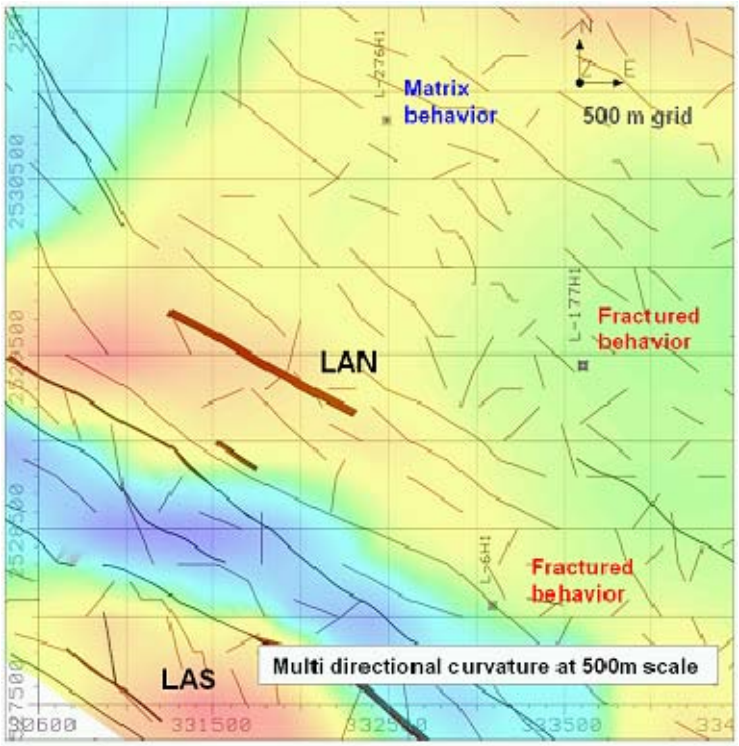


**Figure 5-20 Multi-directional curvature Kmax map of top L. Shuaiba, with 500m scale wavelength, integrated with well locations for the recent LAN fall off tests.**

### *5.2.5 Kinematics analysis*

The kinematics analysis for this field is extracted from the recently published paper of Filbrandt (Filbrandt et al, 2006) re-presented recently in an internal PDO report. It shows a regional transtensional deformation, driven by NW-SE maximum horizontal compression, indicated by the regional fish-net fault pattern (Figure 5.21).

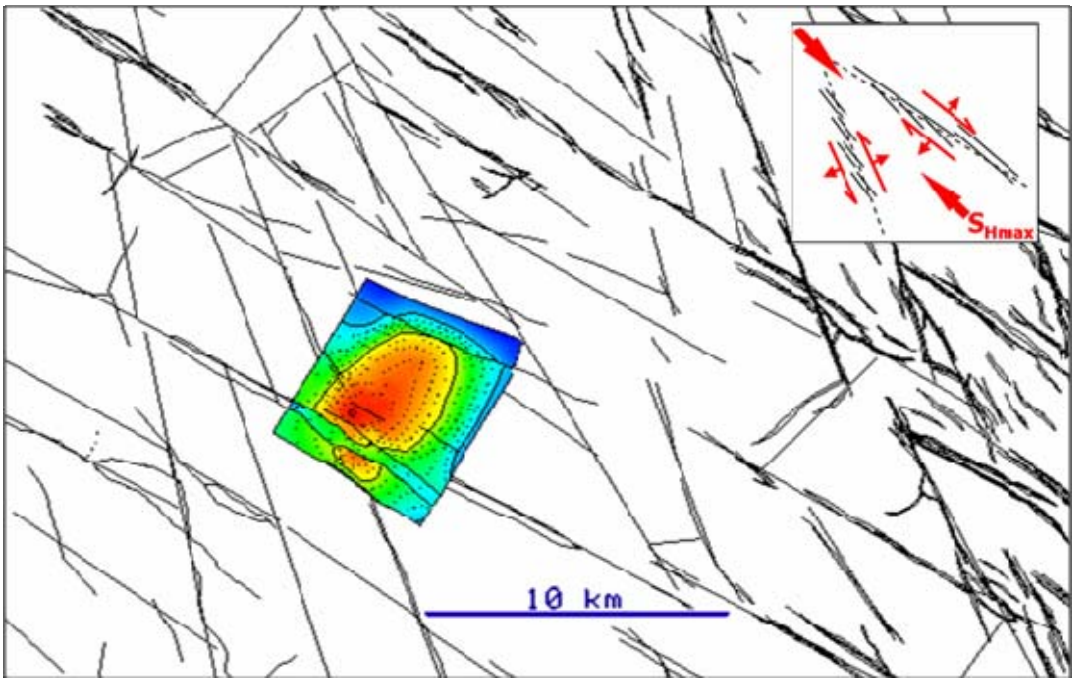


**Figure 5-21 Map view of Lekhwair cluster area showing Kharaib regional fault pattern. LAN and LAS fields are presented using a top structure map (coloured). Insert is a kinematics interpretation for the structural regime in the area based on the observed faults (Richard, 2007).**

## 5.3 LAN fracture characterization

LAN field had been subjected to detailed fracture characterization analysis by PDO based mainly on BHI objects ("fractures") interpretations. The latest study is an ongoing integrated fracture characterization by Baker Atlas and PDO. Thus, a detailed fracture analysis, at well scale, will not be undertaken here, to avoid any duplication. However, on top of what is presented above, this chapter will focus on those fracture parameters that help in constructing conceptual scenarios, hence 3D fracture models. Of particular interest to me are the following studies:

1. Nelson (Nelson, 2004) study covering U. Shuaiba, as well as L. Shuaiba and Kharaib in Lekhwair and Dhulaima cluster area. The main findings are presented in Chapter 3,
2. Bait Muati (Bait Muati, 2004) Lekhwair LAN Area-7 induced fractures review, PDO ONPL internal report, and
3. A 2006/2007 Baker-Atlas fracture study at well scale, see next section.

The above studies together with the specific analysis of few wells are the main inputs to the creation of the fracture models for LAN field.

### *5.3.1 LAN7 Induced Fracture study*

This study focused on understanding the induced fractures in LAN 7 area (at the north part of LAN field), however it provided a detailed review for most of fracture related data in Lekhwair field. The main related findings are: In 1998-99, a PLT campaign conducted in the fractured injectors showed that almost 90 % of the water was taken by fractures in Lower Shuaiba formation. A step rate test which was carried out on L-043U (upper Shuaiba) resulted in relatively constant and high injectivity index of about 1.0 m3/d/kPa, indicating that the well was already connected to a fracture network system. A review in 1994 of water flood performance (Al-Harthy and van Wunnik, 1994) in LAN showed that both Lower Shuaiba and Kharaib reservoirs have a dense network of water conductive features (distances ranging from 100 to 1000 m). These features are fault/fracture related, and this network is denser in Lower Shuaiba than in Kharaib. In addition, these two reservoirs are not connected except at a limited number of major faults and fractures. Analysis of producers' response to injectors in LAN7 shows no specific direction according to the author, though it seems that there is an overall NE impact, as shown in figure 5.22. Stofferis (Stofferis, 1991) reports on hydraulic fracture experiments with micro seismic acoustic measurements of the fracture growth directions. These were run in L-054 & L-068 in Lekhwair A North. Results indicate a maximum horizontal stress direction of 100 degrees azimuth for the L-054 and 160 degrees azimuth for L-068. These two wells are located only some 50 m from each other and even so they have developed induced fractures with a 60 degree difference in azimuth. These wells are also close to faults that run NW-SE which is expected to influence the induced fracture direction (see Figure 5.18).

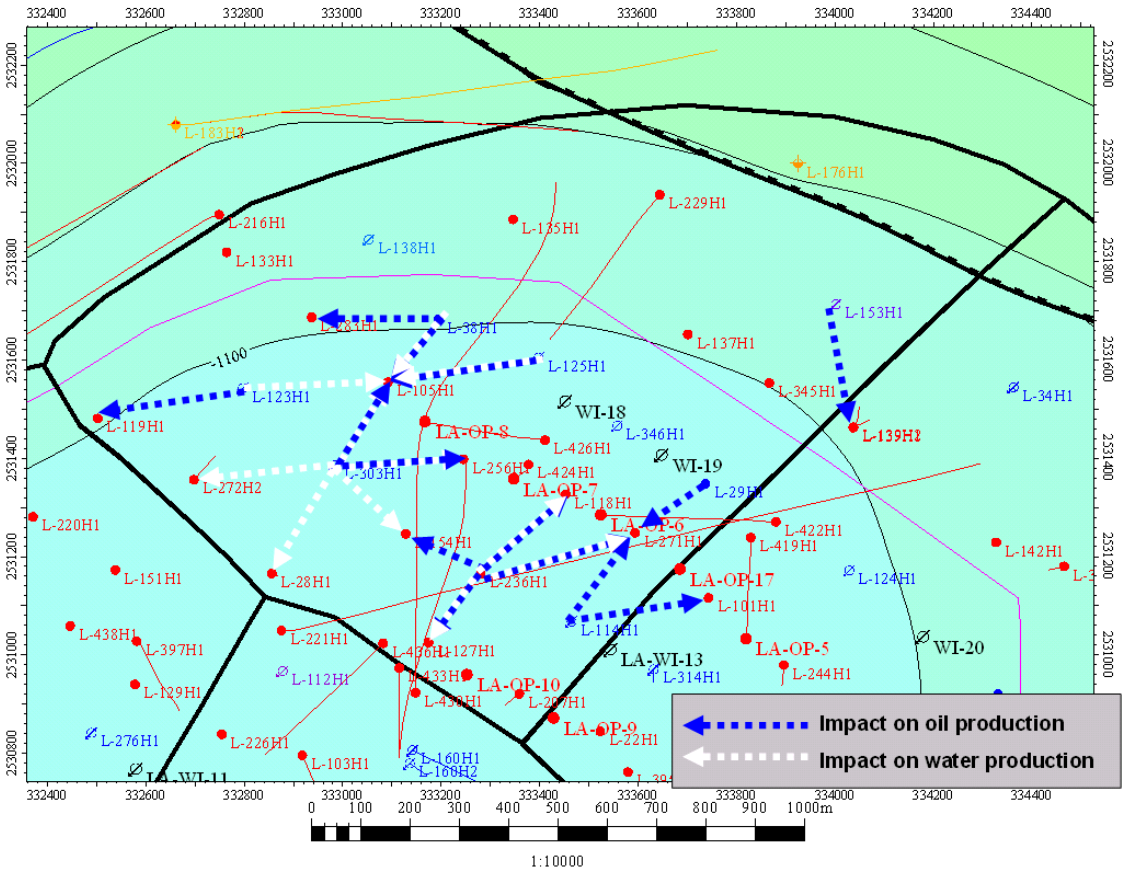


**Figure 5-22 Orientation of observed impact of injectors on producers in LAN7 (Bait Muati, 2004) showing a possible NE trend.**

### *5.3.2 Baker Atlas 2006/2007 LAN Fracture characterization study*

In Q4 2006, a detailed fracture characterization for the LAN field had been undertaken by Baker Atlas on behalf of PDO. In this on-going study, a well by well analysis has been done that resulted in the creation of a mega Excel spread sheet. The analysis covered the following fracture related data at well scale (Figure 5.23): Gross rate for producers; injection rate for injectors; BS&W; PLT and losses; and BHI fracture interpretations per well done by Baker Atlas. The analysis focused on data integration of the above parameters. Figure 5.24 shows the net result of the data integration for LAN by Baker Atlas work. The figure shows that the most connected area in the fields is in the far north and south of the field. This an important figure as it will be the basis for the base case fracture model for LAN. The spread sheet produces a SVS format output files donated “matrix” and “fractured” wells that is plotted as a point set (Figure 5.25).

| Dip Look-up | |
|---|---|
| H | 90 |
| L | 25 |
| M | 70 |
| NA | -999.25 |

| GROSS RATE LOOK UP |
|---|
| 0 LOW |
| 100 MOD |
| 150 HIGH |
| 300 V. HIGH |

| BSW LOOK UP |
|---|
| 0 LOW |
| 50 MOD |
| 80 HIGH |
| 90 V. HIGH |

| INJECTION RATE LOOK UP |
|---|
| 0 No Inj |
| 50 V. Low |
| 100 LOW |
| 200 MOD |
| 300 HIGH |
| 500 V. HIGH |

| Strike Look Up | |
|---|---|
| ENE | 67.5 |
| ESE | 222.5 |
| EW | 90 |
| NA | -999.25 |
| NE | 45 |
| NNE | 22.5 |
| NNW | 337.5 |
| NS | 0 |
| NW | 315 |
| SE | 135 |
| SN | 180 |
| SSE | 157.5 |
| SSW | 202.5 |
| SW | 225 |
| WE | 270 |
| WNW | 292.5 |
| WSW | 247.5 |

| Category Look Up | |
|---|---|
| A | fcplt |
| B | fcpta |
| C | fcbsw |
| D | fcgross |
| E | fcinj |
| F | fcloss |
| G | fcscuts |
| H | fcsweep |
| I | fcbhi |
| J | mplt |
| K | mpta |
| L | mbsw |
| M | mgross |
| N | minj |
| O | mloss |
| P | msweep |
| Q | mbhi |
| R | |
| S | |
| T | |
| U | |
| V | |
| W | |
| X | |
| Y | |
| Z | |

**Parameter investigated**

**Example – sweep analysis**

| WELL ID | AHD M | Cat | Dip | STRIKE | FRAC INTE | UTME | UTMN | TVDSS M | Dip | STRIKE | Cat | ALIGNM | SWEEP C/ | COMMENTS |
|---|---|---|---|---|---|---|---|---|---|---|---|---|---|---|
| L-412H1 | 1197.21 | msweep | 90 | -999.25 | HCM | 331001.5 | 2529572 | -1075.88 | H | NA | P | SINGLE | LSH SWP | |
| L-448H2 | 1235.63 | msweep | 90 | -999.25 | HCM | 332974.5 | 2529928 | -1080.77 | H | NA | P | SINGLE | FULLSWP | Low injection bright spot at 1530 kPa. Right next to the left 390 has moderate inj rate at 8500 kl |
| L-477H1 | 1229.9 | msweep | 90 | -999.25 | HCM | 331490.9 | 2530743 | -1101.97 | H | NA | P | SINGLE | NOSWP | No existing fc. Gross=86 m3/d bsw=26% |
| L-479H1 | 1232.75 | msweep | 90 | -999.25 | HCM | 331886.7 | 2530537 | -1090.88 | H | NA | P | SINGLE | FULLSWP | No existing FC. Especially lower sh is well swept |
| L-480H1 | 1283.8 | msweep | 90 | -999.25 | HCM | 332586 | 2530763 | -1085.16 | H | NA | P | SINGLE | FULLSWP | No existing fc. Inj rate =250 m3/d. ii=0.06 |
| L-488H1 | 1229.96 | msweep | 90 | -999.25 | HCM | 331898.8 | 2530965 | -1088.29 | H | NA | P | SINGLE | NOSWP | No existing fc. Gross=103 bsw=15 |
| I-489H1 | 1226.99 | msweep | 90 | -999.25 | HCM | 332708 | 2531069 | -1088.41 | H | NA | P | SINGLE | FULLSWP | No existing fc. Well never injected because of a fish. Nearby fc from 112 |
| L-497H1 | 1283.89 | msweep | 90 | -999.25 | HCM | 334639.4 | 2531084 | -1112.82 | H | NA | P | SINGLE | FNGR | No fc nearby LOW PROD |
| L-499H1 | 1302.84 | msweep | 90 | -999.25 | HCM | 332606.7 | 2530451 | -1079.25 | H | NA | P | SINGLE | NOSWP | QT=35 BSW=25.Open comingled |
| L-508H1 | 1215.35 | msweep | 90 | -999.25 | HCM | 333061.4 | 2529236 | -1094.19 | H | NA | P | SINGLE | NOSWP | fluctuation. Swept by fractor from 210. |
| L-511H1 | 1224.12 | msweep | 90 | -999.25 | HCM | 332377.2 | 2530877 | -1089.69 | H | NA | P | SINGLE | NOSWP | no existing fc. Inj rate from 300 to 200 m3/d.ii=0.04 m3/d/kPa. Be careful with the deviation |
| L-529H1 | 1204.03 | msweep | 90 | -999.25 | HCM | 332919.4 | 2530175 | -1081.56 | H | NA | P | SINGLE | NOSWP | QT=80 BSW=42 |
| L-530H1 | 1218.44 | msweep | 90 | -999.25 | HCM | 333836.1 | 2530798 | -1091.19 | H | NA | P | SINGLE | NOSWP | no fc nearby. ALL THESE WELLS could be in nice matrix area and water overriding in Lsh not i |

**Figure 5-23 Fracture related parameters used for the well by well fracture characterization of LAN by Baker Atlas, 2006/2007.**

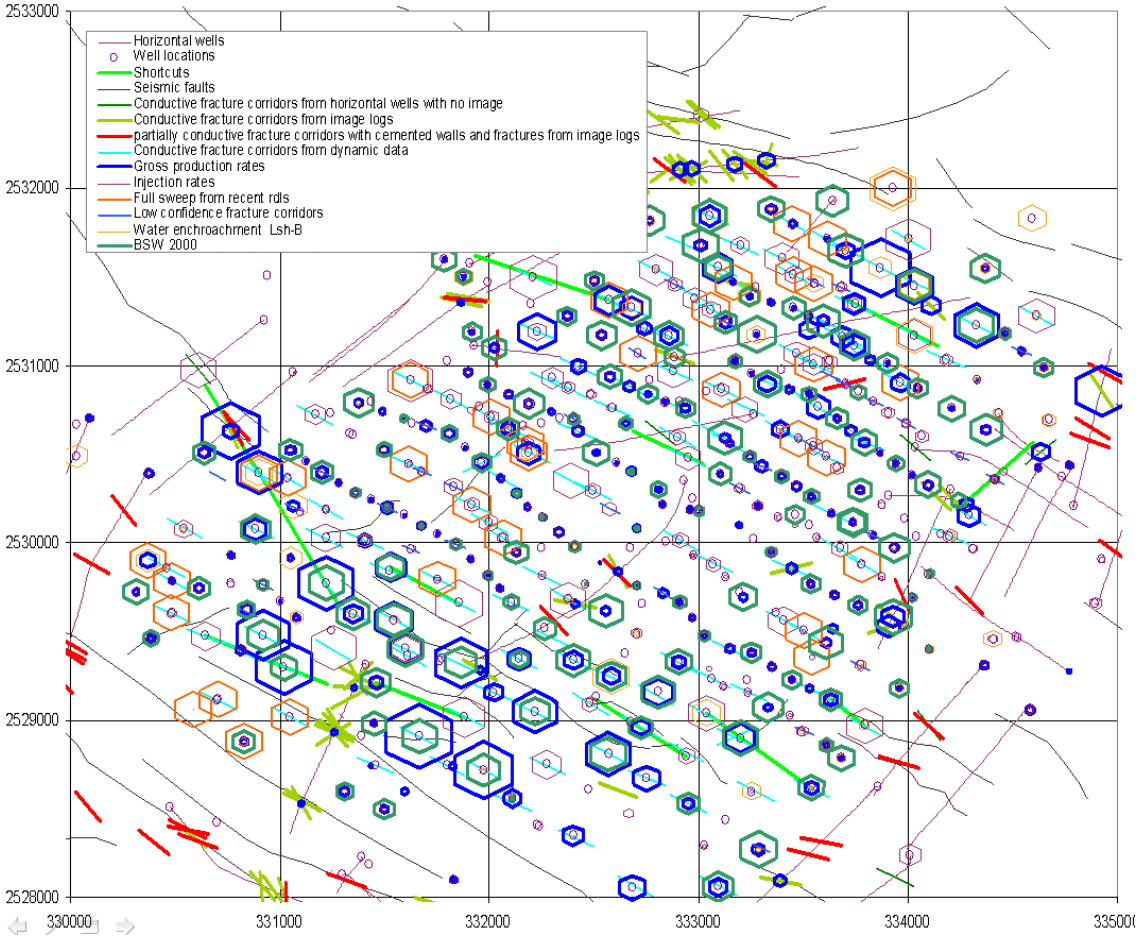


**Figure 5-24 A composite plot of all wells of LAN with the integrated fracture related data by Baker Atlas 2006/2007 LAN study. Note how the most connected wells (one with large polygons) occur in the south of LAN or far North.**

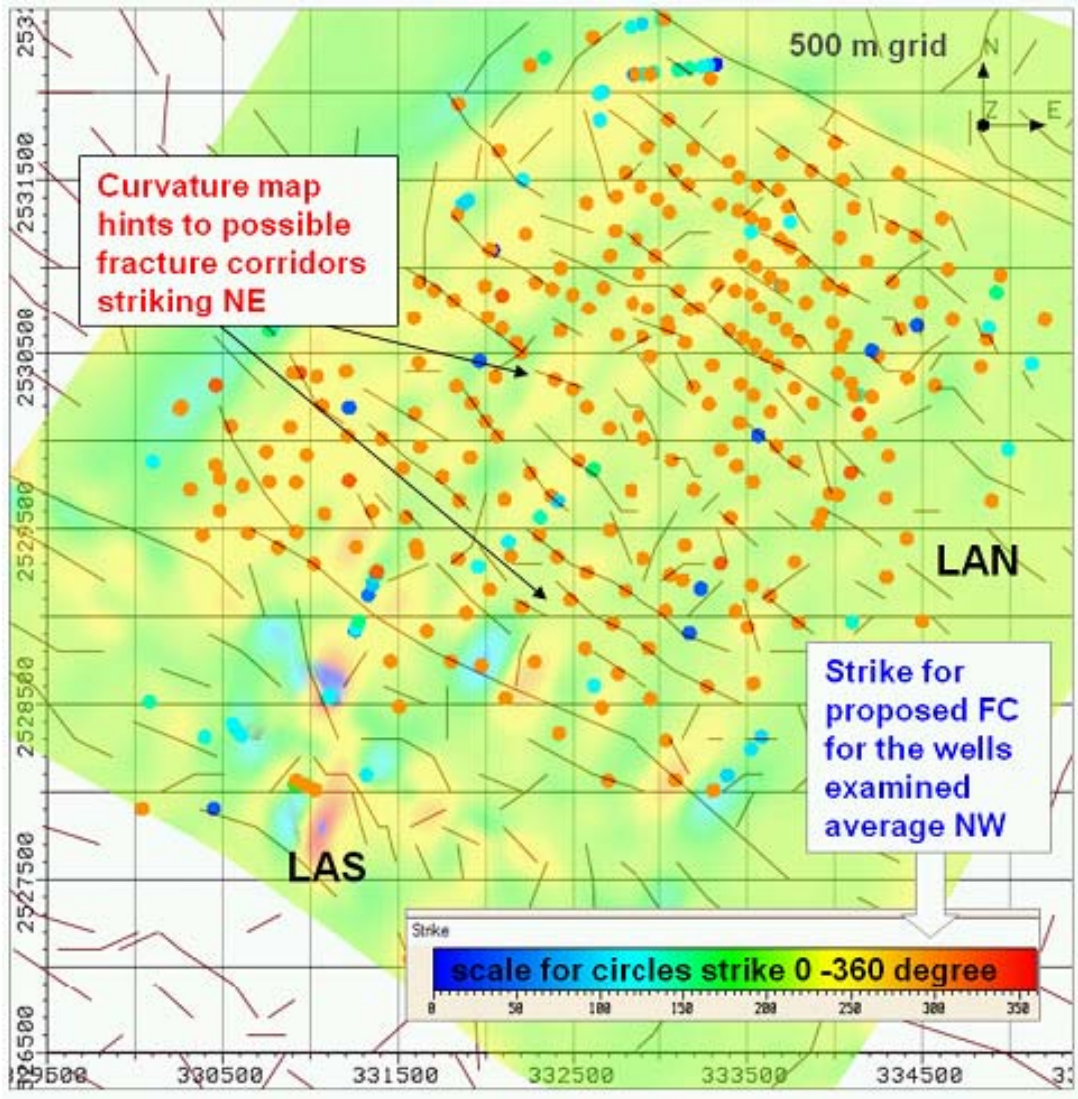


**Figure 5-25 LAN Baker "fractured" wells point set with FC strike (circles – average ~300 degree NW), integrated with seismic lineaments (brown lines) and a curvature Kmax map of top L. Shuaiba (uni-directional at 125 azimuth with 100m scale wave length). Note how the curvature map contradicts the fracture corridor strike, except where the blue circles occur.**

### *5.3.3 Specific well by well evaluation*

The following wells were chosen due to their location, trajectory orientation and the BHI fractures geometry seen in them (Figure 5.26) to better understand the areal variation (if any) in the LAN field.

**L-198H1 & L-198H2**

This well with two horizontal holes is located in the eastern flank of LAN. Both legs were targeting L. Shuaiba but one in the A and the other in the B member (Figure 5.27 and Figure 5.28). The main observations from this evaluation are: dominant fracture orientation is NW with high non-conductive fractures intensity, especially in the deeper interval, No clear correlation between curvature Kmax maps and BHI fractures, fractures occur in closely spaced clusters with large width zone, BHI visual inspection show low fracture picking, and Lower Shuaiba A is more fractured than B.

**L-549H1**

A horizontal well drilled in the northern region of LAN, very likely within a fault zone resulting in very high FI. Integration and visual inspection of the BHI fractures with other related data resulted in the following observations (Figure 5.29 and Figure 5.30): this well was drilled in or in the vicinity of a fault zone, NW fractures dominate compare to NE, but with few non-conductive fractures, clusters are closely spaced but with small width zone, and the hook shape design of the well allowed comparison of fracture intensity between different location of same layer and between layers: Fracture intensity increases in Kharaib layer compare to upper Lower Shuaiba; Non-conductive fractures are also more intense in Kharaib (or deeper intervals).

**L-215H1**

This is a very long horizontal well in the centre of LAN field, with a NE trajectory. The visual inspection of the BHI fractures (Figure 5.31) had shown that the dominate fracture strike orientation is WNW to NW for both conductive and non-conductive fractures, also clustering is very distinctive in this well showing a spacing of about 50m for small clusters, 200m for mega clusters and over 300m for the one associated with flow or mud losses.

**L-182H1**

This well is located in the NW part of LAN field and has a NE trajectory. It encountered the northern boundary fault. Visual inspection and integration analysis of the BHI fractures with other fracture related data (Figure 5.32) has shown that: NW fractures dominate (mainly due to encountering the fault), FC or sub-seismic fault related fracture cluster spacing is about 300m, and fault damaged zone is about 100m in width.

**L-212H1**

This well is located in the southern region of LAN field, area assumed to be highly fractured according to Baker Atlas analysis and so reflected in its fracture intensity (Figure 5.26 above). Analysis of BHI fractures integrated with other related data has shown the following (Figure 5.33): again dominate fracture orientation is NW for both conductive and non-conductive fractures, fault damage zone width is also about 100m, all the faults are associated with mud losses, and porosity log show a tight interval in between faults, which coincide with high fracture intensity (possibly ML or fault related cementation).

**L-293H1 & L-293H2**

This well, with its two legs, is located in the LAS field, but was analysed nonetheless to see fracture propagation with depth. The analysis (Figure 5.34) results are as follow: NW fractures again dominate with very few non-conductive fractures, cluster spacing range about 75 to 300m, and most of the fault related fractures cut through from one hole to another, with thin damaged zones but still there are layer bound fractures.

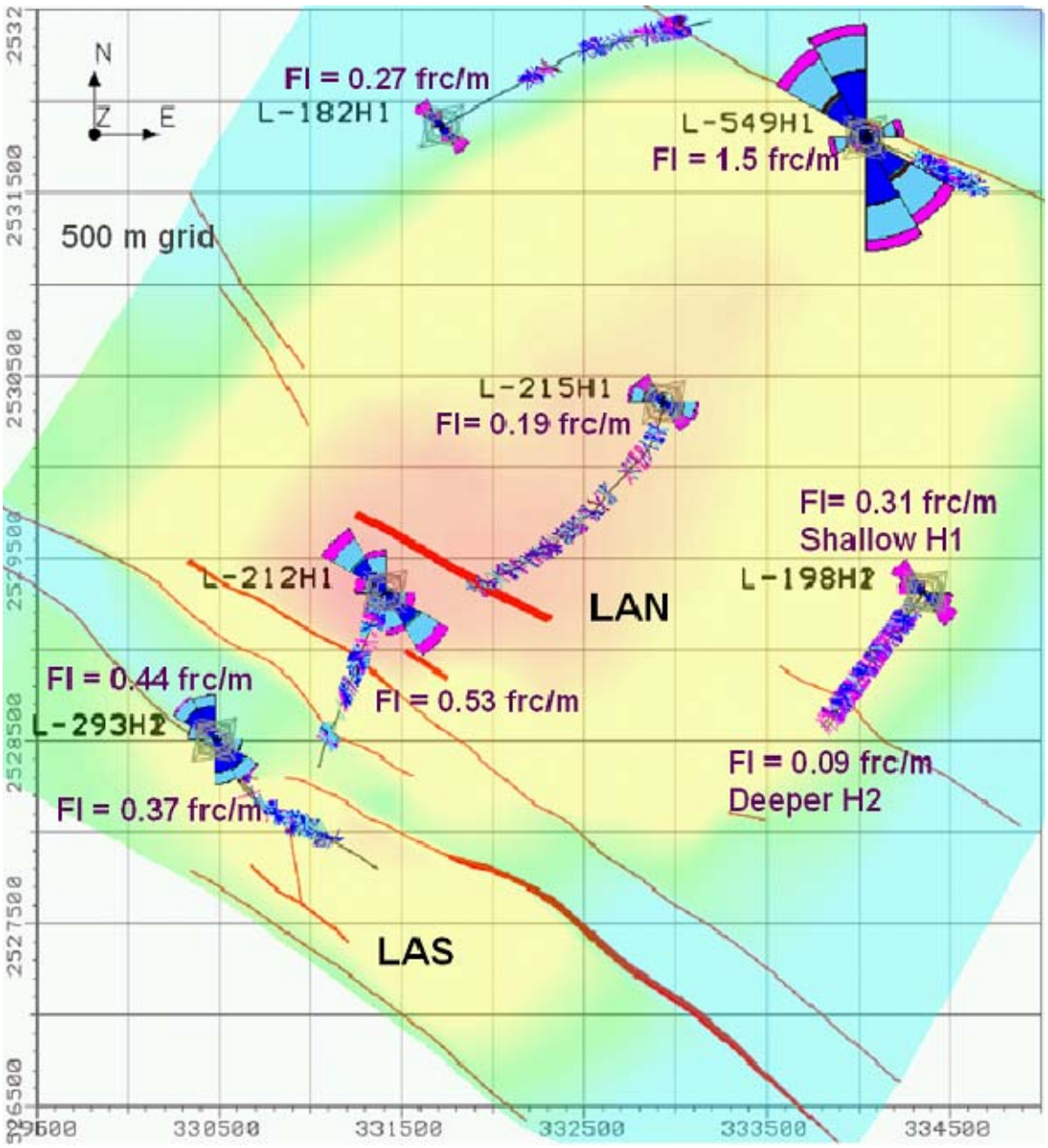


**Figure 5-26 Chosen wells from LAN and LAS fields for specific BHI analysis, shown with there BHI fracture intensity (FI) and main faults seen in the field.**

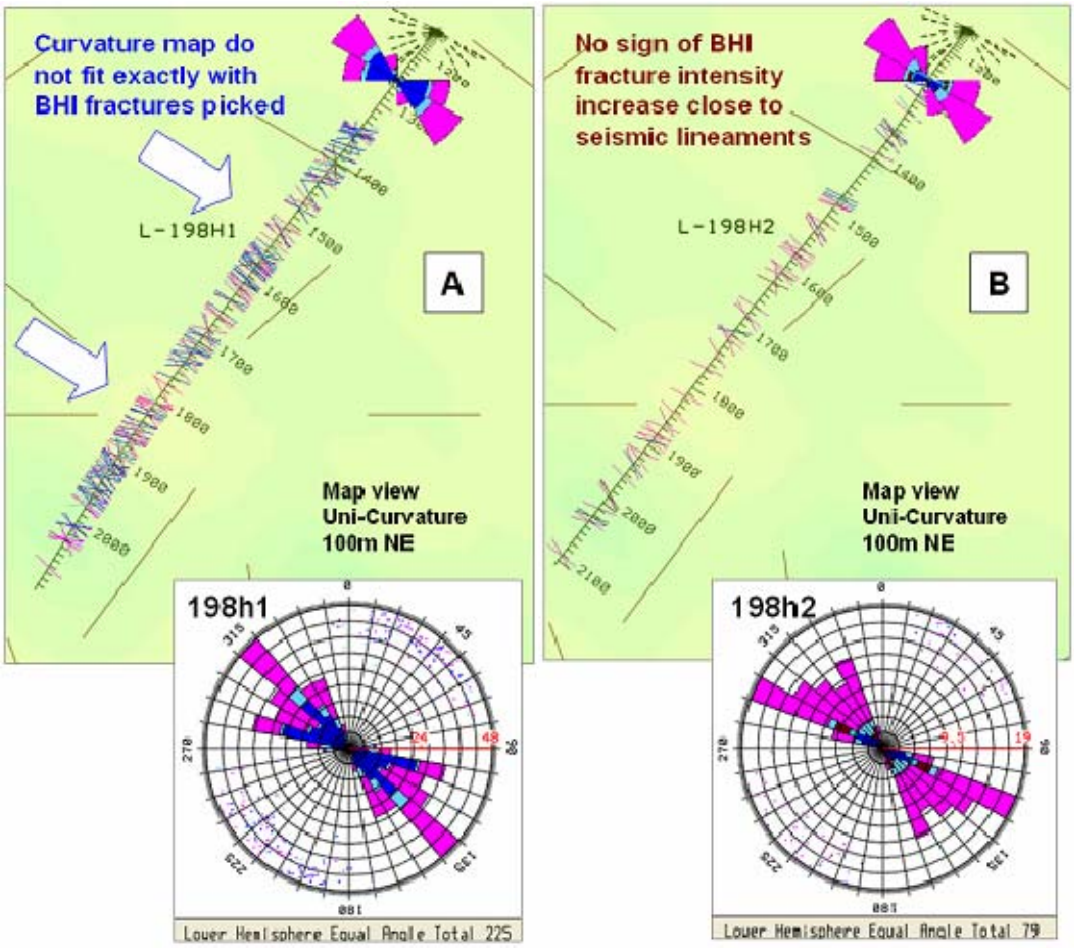


**Figure 5-27 Map view of L-198 H1 & H2 with BHI fractures (blue: conductive, pink: non-conductive) integrated with uni-directional curvature Kmax map of top L. Shuaiba, at 100m scale wavelength, with NE azimuth and seismic lineaments.**

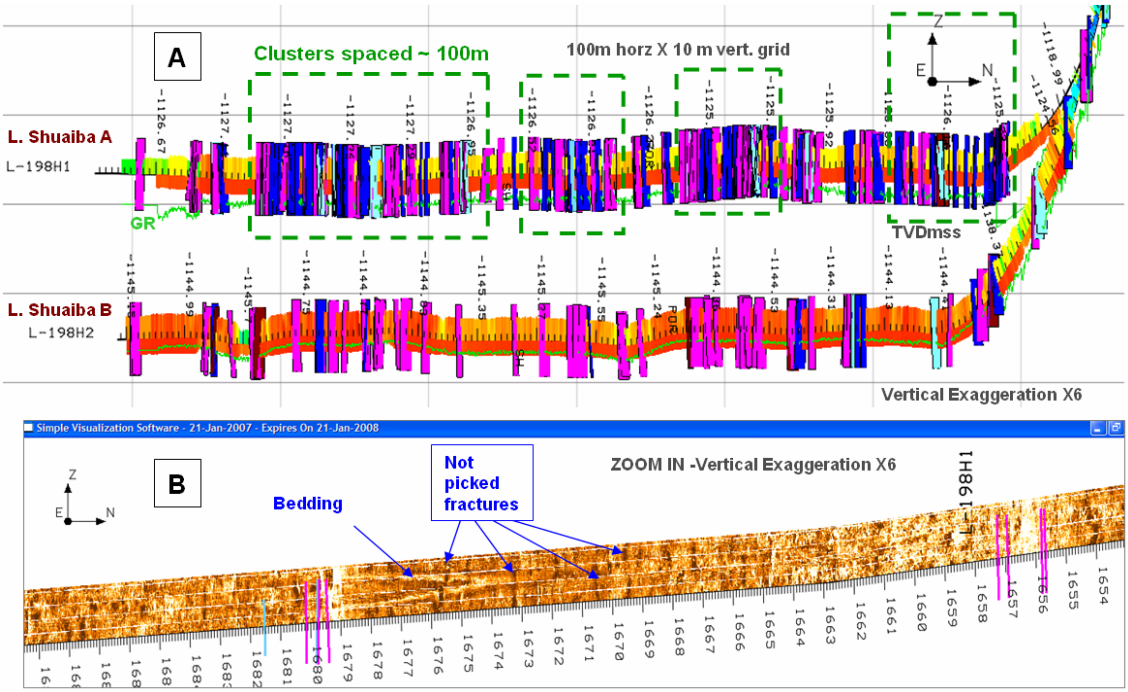


**Figure 5-28 A] Cross section of L-198 H1 & H2 with BHI fractures shown as planes. Note the variation in fracture intensity between top and lower leg hinting toward mechanical layering (ML), increase in non-conductive fractures wit depth (possibly related to approaching OWC) and the wide spread of cluster zones. B] Example of BHI image and the low picking of fractures, zoom-view cross section.**

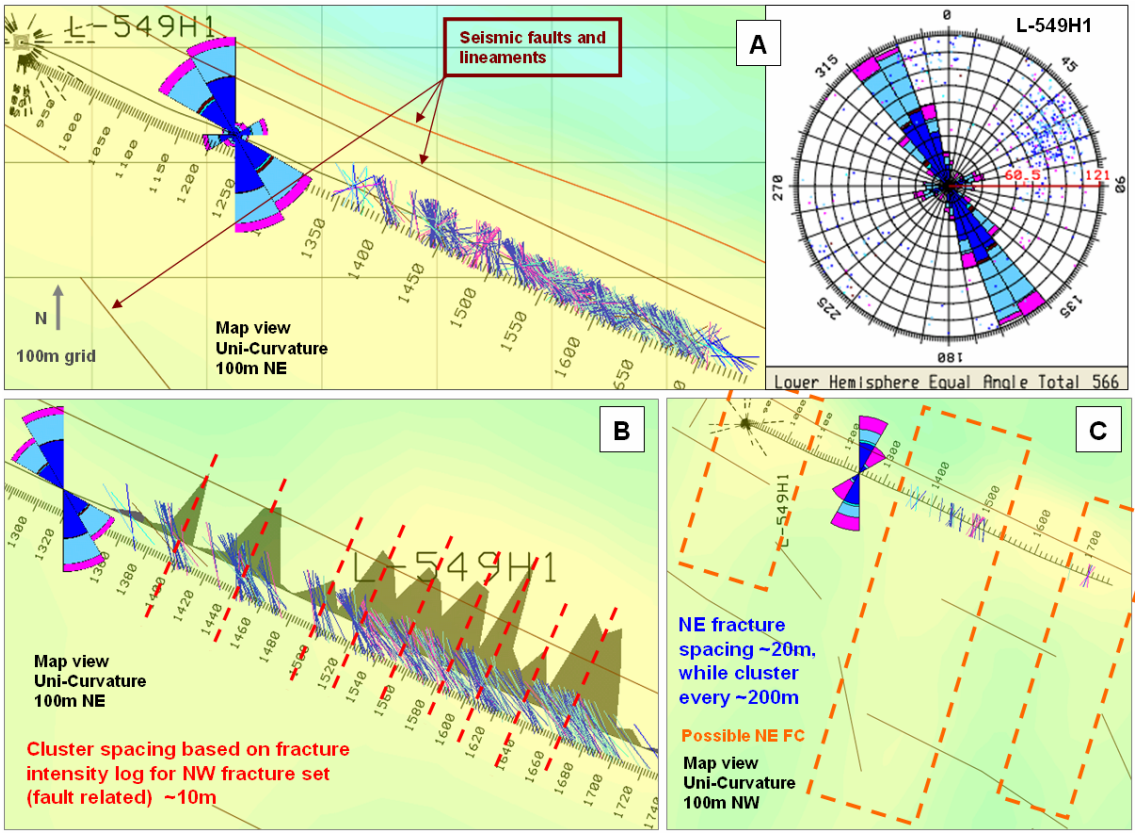


**Figure 5-29 A] L-549H1 BHI fractures all with their rose diagram. B] Only NW fractures with a fracture intensity log (dark olive) every 10m interval compared with C] NE fracture intensity. Note the latter were integrated with uni- curvature Kmax with 100m scale and NW azimuth.**

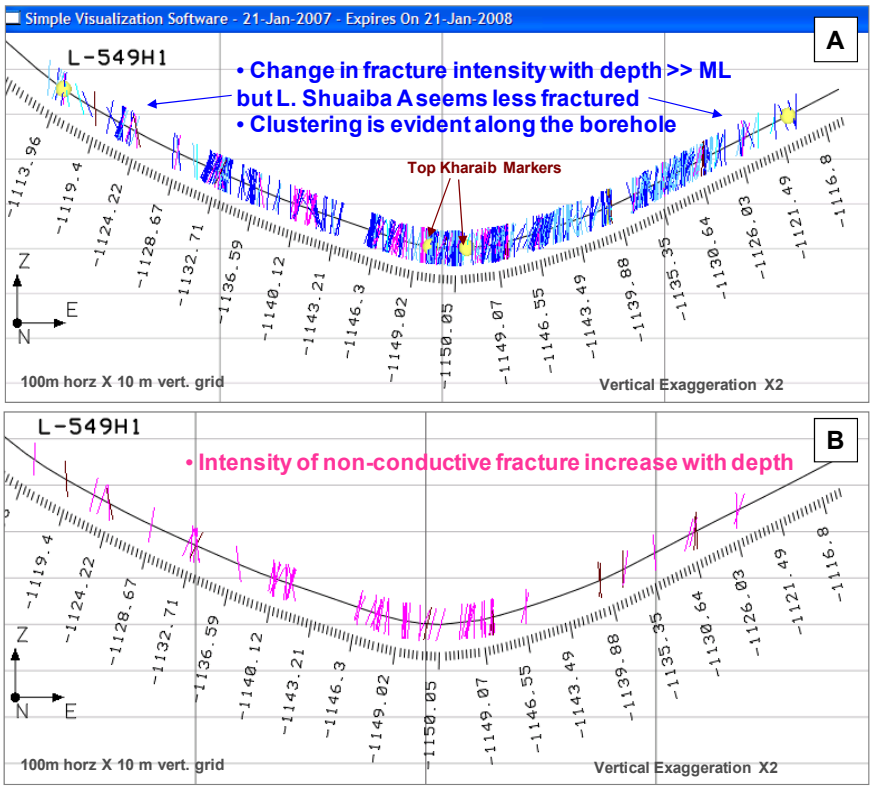


**Figure 5-30 Cross section of L-549H1 with BHI fractures A] all and B] Non-conductive only.**

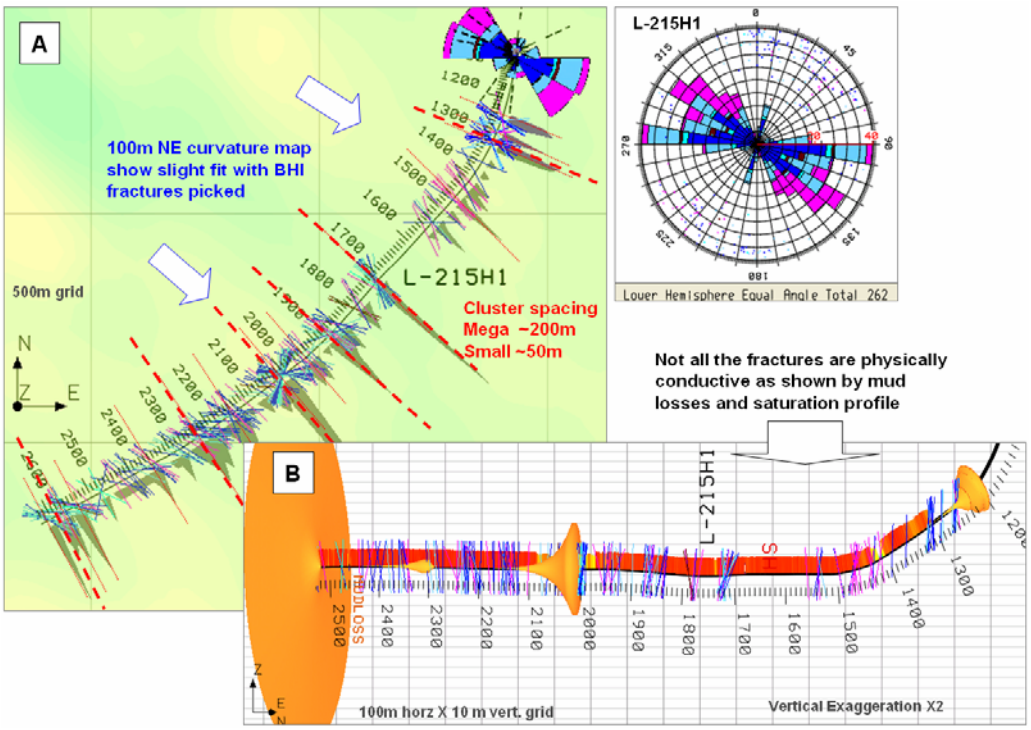


**Figure 5-31 A] Map view and B] Cross section of L-215H1 with BHI fractures integrated with curvature analysis (background in A) and saturation log (red in B) and mud losses (orange circles).**

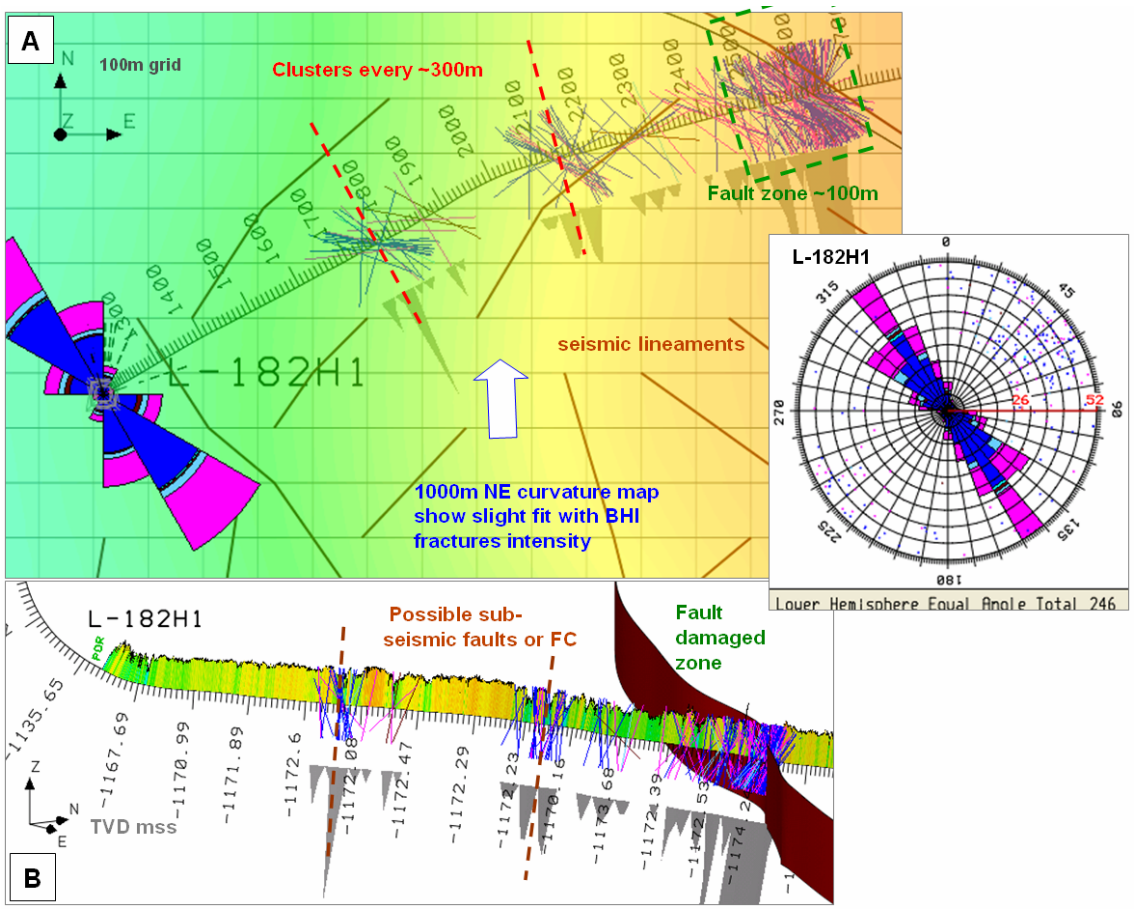


**Figure 5-32 L-182H1 map view A] and cross section B], shows fault damage-zone's length and sub-seismic fault related or FC cluster spacing.**

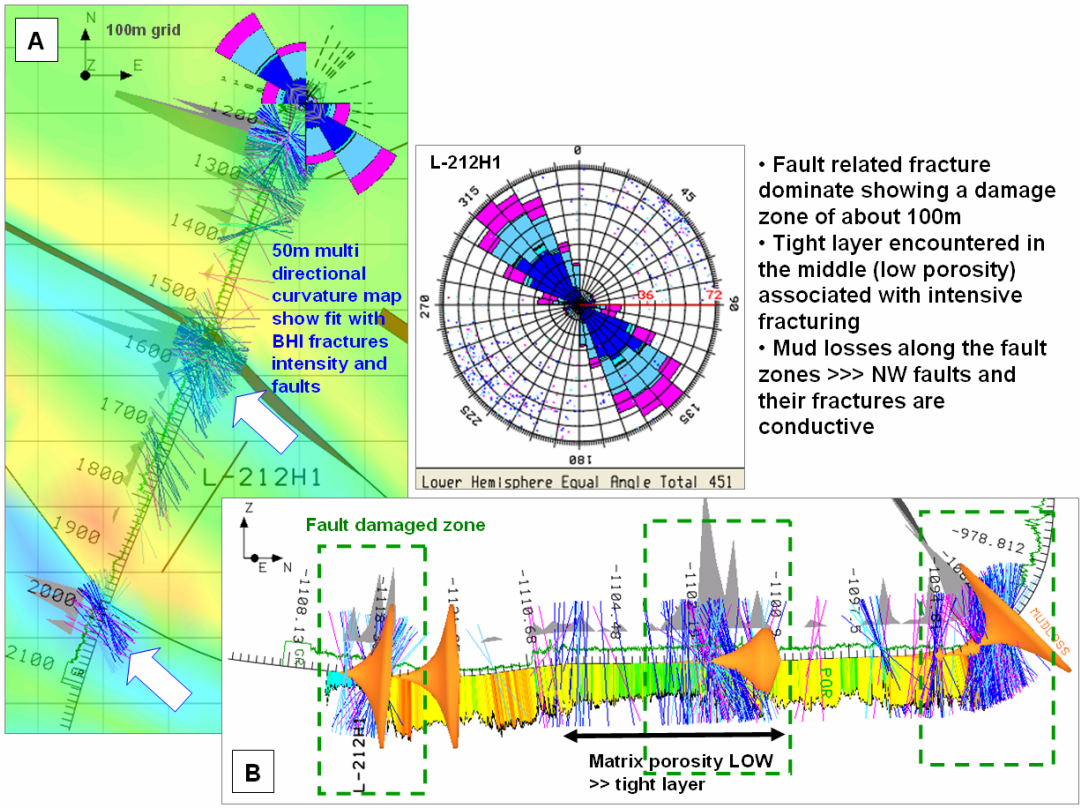


**Figure 5-33 L-212H1 BHI fracture analysis A] in map view and B] cross section.**

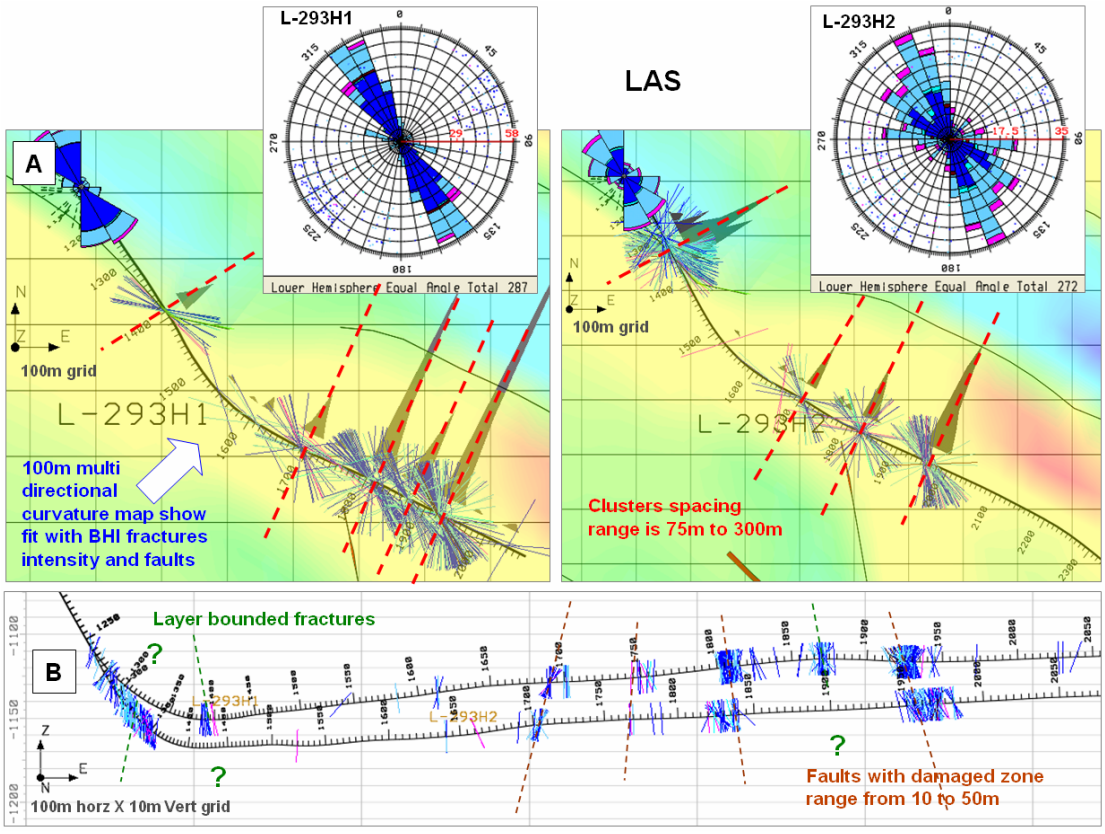


**Figure 5-34 L-293H1 & L-293H2 map view A] and cross section B] showing fault related fractures and possibly layer bound fractures.**

## 5.4 Fracture concepts for LAN

Based on the Baker Atlas 2006/2007 Lekhwair fracture analysis, the review of the existing studies (see Chapter 3) and the fracture related data analysis shown above in this chapter, a conceptual fracture model is presented below for Lekhwair Lower Shuaiba and Kharaib Formation. Upper Shuaiba is not included in this simple conceptual model as the emphasis was in the commercial reservoir for the time being. The illustration below summarizes this model (Figure 5.35). The matrix in table 5.3 below provides a summary of alternative scenarios and their supportive data.

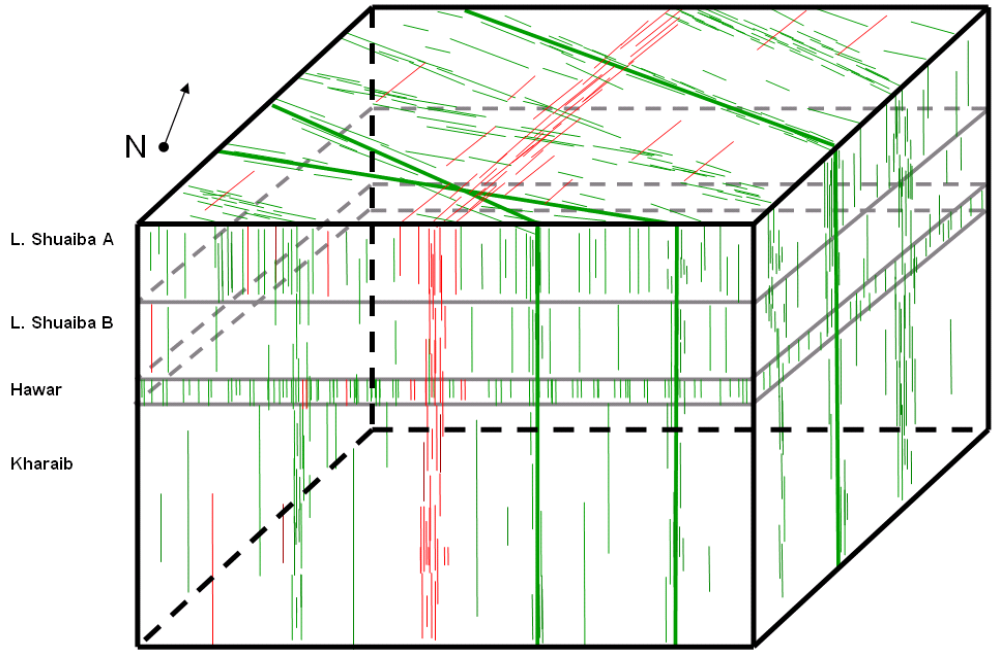


**Figure 5-35 Illustration of a conceptual fracture model for LAN field with NO relative depth.**

| Element of concept | Support |
|---|---|
| **Fault related fractures NW & WNW only** | 1- Fracture intensity increases as NW/WNW fault are approached (BHI visual inspection)<br>2- From 10 to few 100m of area of high BHI intensity next to fault planes<br>3- High gross rate and losses around faults |
| **FC or sub-seismic related fractures (Both NW and NE)** | 1- BHI clusters in area where there is NO faults (e.g. central part of LAN)<br>2- Curvature analysis at low wavelength (50 to 100m) show corridors of high strain striking NE & NW<br>3- Sudden changes in Shc log response coinciding with BHI fracture intensity where NO faults occur |
| **Fold related fractures** | 1- Higher strain in the southern part of LAN as seen from 500m scale multi-directional curvature map<br>2- Same area coinciding with high connectivity (gross rate and Baker Atlas detailed well analysis) |
| **Mechanical layering (ML)** | 1- Multi-lateral wells such as L-198 BHI log in LSA & LSB as well as existing studies<br>2- Core data inspection (Phi-K plot) show slight offset between LSA and LSB, as well as GR log |

| **Geological scenarios** | *All with ML: Fracture intensity in* *Hawar >> L. S A > Kharaib > L. S B* |
|---|---|
| **Low case** | **Fractures occur only in fault damaged zone of the Petrel major NW and WNW faults*** |
| **Base case** | **Combination of major NW & WNW faults; NW and NE FC based on curvature analysis as well as background fractures increasing in the southern part of LAN** |
| **High case** | **Similar to base case but fractures close to sub-seismic lineaments interpreted by PDO** |

**Table 5-3 LAN fracture modelling scenarios proposed after examining element of each concept. Only shown what is thought to be a geologically reasonable scenario.**

## 5.5 Building LAN fracture models

The 3D DFN models for LAN are based on the conceptual scenarios presented in the previous section (Figure 5.35 & Table 5.3 above). Only three 3D DFN realizations will be built for LAN. These are the low, base and high case. The horizons (confining surfaces) used for the 3D DFN realizations, to represent the mechanical layering, were extracted from PDO Petrel matrix grid (Figure 5.36).

For the low case scenario the seed probability map and the propagation impedance map were based on the Petrel faults, basically to create a fault damaged zone. The size of the zone around the major NW and WNW faults is up to 250m wide, representing a high end of low case scenario. Visual inspection of the output model indicate that it does not fit with the fracture indicators such as the BHI fracture intensity, seen in LAN wells, and the wells gross rate (Figure 5.37). The parameters used to create the 3D DFN realizations and their length histograms and rose diagrams are shown in Figure 5.38.

A total of 10 3D DFN sets were created to represent the base case. The reason behind the large number is that for every layer (L. Shuaiba A, L. Shuaiba B, all L. Shuaiba, Hawar and Kharaib) two orientation set were created: NW-WNW set representing the main fault related fractures, curvature related fractures and FC as well as background fractures; and the NE FC set seen by the small ratio of BHI fractures in the wells.The seed probability and propagation impedance maps were based mainly on the curvature maps (For the NW-WNW set: curvature “fold” set >>> using multi-directional curvature Kmax map at 500m scale and for the FC/fault related set >>> using uni-directional Kmax curvature map at 100m scale) and on the well data observation (mainly BHI data and gross rate data). Whereas, for the NE FC set the seed probability and propagation impedance maps were based only on the uni-directional curvature Kmax map at 100m scale (Figure 5.39). The total number of fracture per orientation per layer for the whole field, shown in figure 4.40, is as follow: L. Shuaiba NE (307), L. Shuaiba NW (2043); L. Shuaiba A NE (1177), L. Shuaiba A NW (11146); L. Shuaiba B NE (385), L. Shuaiba B NW (3925); Hawar NE (1318), Hawar NW (31426); and Kharaib NE (216), Kharaib NW (4779). This resulted in total of 56722 fractures for the whole field. The extraction of the 3D DFN geometric properties into a 3D geo-cellular grid was done only for the mid case scenario. The fracture number per cell (Figure 5.41) reflects what observed in the 3D DFN, i.e. higher fractures per cell in the northern and SW part of LAN as well as in the NW-WNW and NE Fracture corridors. The mean fracture spacing per cell reflects the effect of the grid orientation. When calculating the spacing along the grid X direction (Figure 5.42) the NE fracture corridors are very clear as they are perpendicular to the X direction. The average fracture spacing is around 110 though it can reach <20m inside the FC for the Shuaiba layer. In contrast, the average spacing per cell is around 50m in Hawar and Kharaib layers. The black cells are z null. On the other hand the Y spacing calculation shows a very homogeneous fracture

spacing (Figure 5.43) as it is calculating perpendicular to the main NW-WNW direction. The average spacing is around 30 to 50m.

The 3D DFN created for the high case realization is using both the major Petrel faults and the sub-seismic faults (seismic lineaments interpreted by PDO) as the main input, together with the curvature map to highlight high fracture intensity in the northern and SW side of LAN (Figure 5.44). The total number of fracture per orientation per layer for the whole field, shown in figure 4.44, is as follow: L. Shuaiba NE (242), L. Shuaiba NW (3428); L. Shuaiba A NE (3345), L. Shuaiba A NW (16960); L. Shuaiba B NE (1635), L. Shuaiba B NW (3921); Hawar NE (8692), Hawar NW (35064); and Kharaib NE (1009), Kharaib NW (8720). This resulted in total of 83016 fractures. The 3D geo-cellular grid with the extracted geometric properties of the fracture set, out of the mid case 3D DFN scenario will be given to Petroleum Development Oman reservoir engineers to test them and perform full dynamic calibration via history matching the well performance at sector scale.

**Way forward …**

The 3D geo-cellular grid with the extracted geometric properties of the fracture set, out of the mid case 3D DFN scenario will be given to Petroleum Development Oman reservoir engineers to test them and perform full dynamic calibration via history matching the well performance at sector scale.

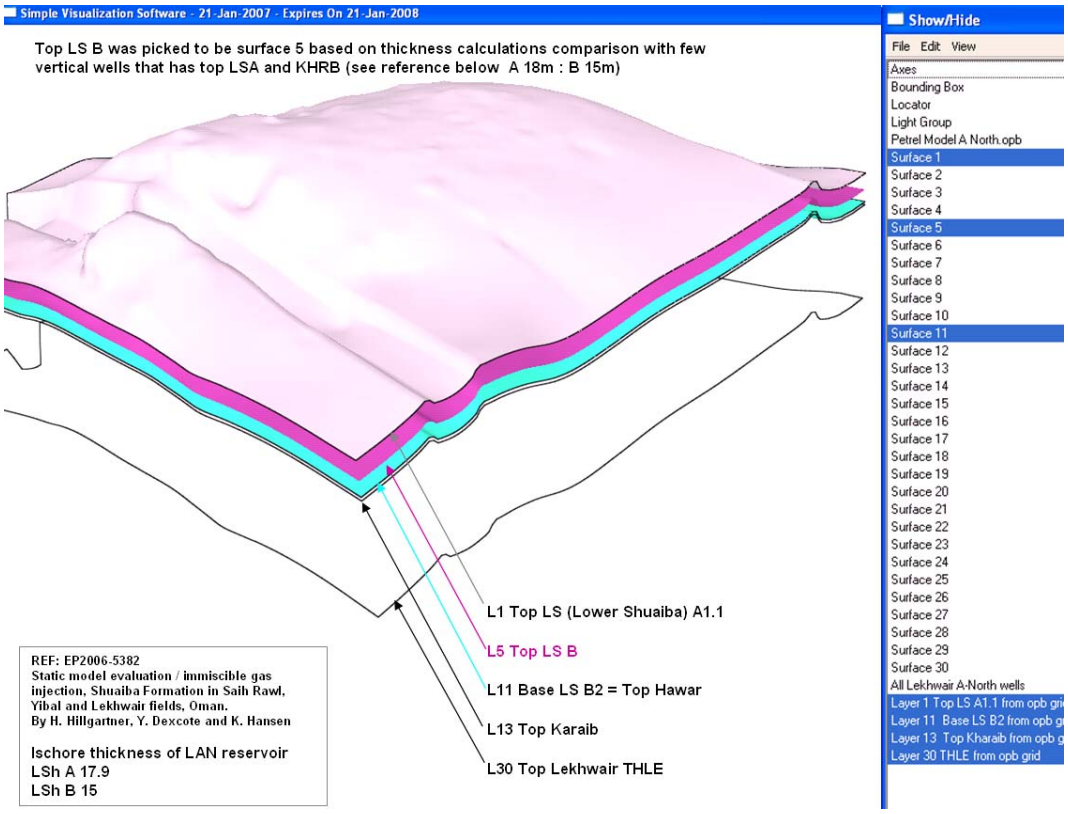


**Figure 5-36 the confining surfaces used for LAN 3D DFN models were extracted from PDO Petrel 3D grids based on layer thickness estimation.**

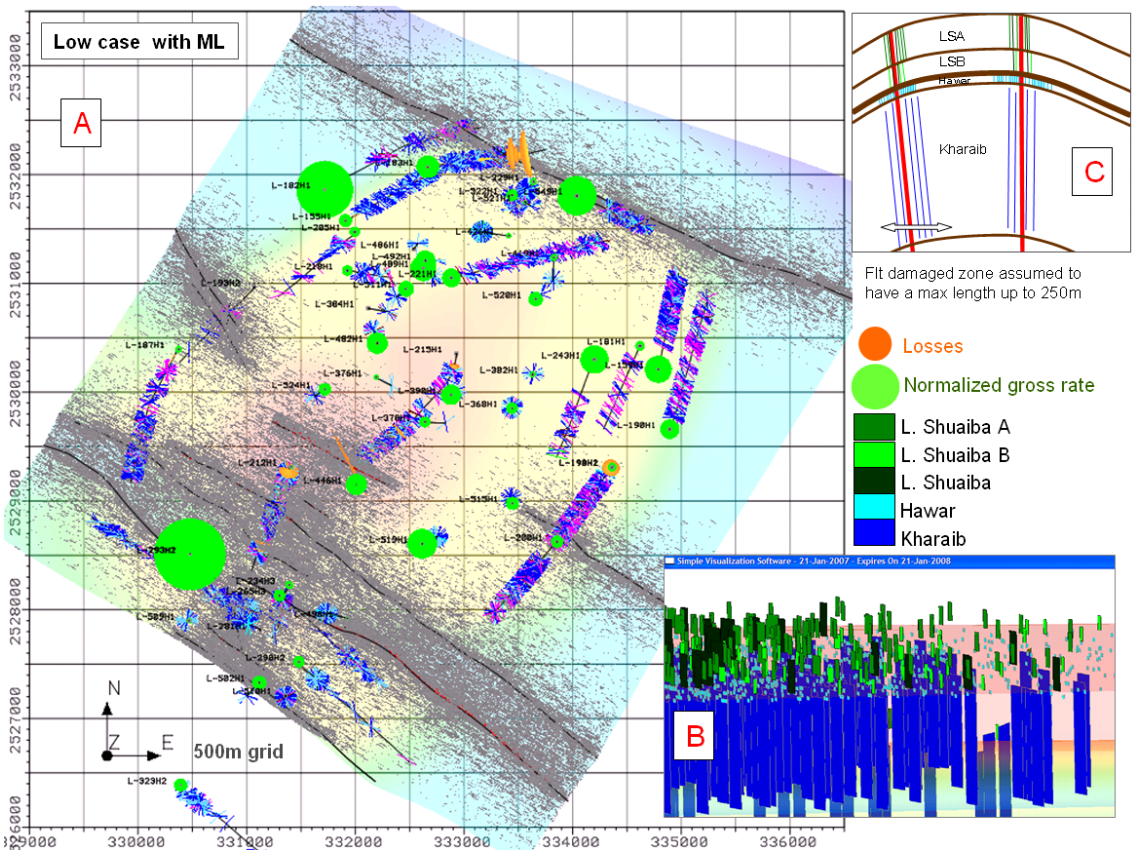


**Figure 5-37 Low case 3D DFN realization for LAN. Fractures occur in the vicinity of major NW & WNW faults. [A] Map view of full field with fracture created (grey lines), major faults (red to black lines), LAN BHI wells with both losses and normalized gross rate super imposed on top of Lekhwair map . Note how the realization does not fit with the BHI fracture data in the centre of the field. [B] A vertical snap shot highlighting the ML in the created fractures; and [C] a simplified cartoon to illustrate the concept used for the creation of these fractures.**

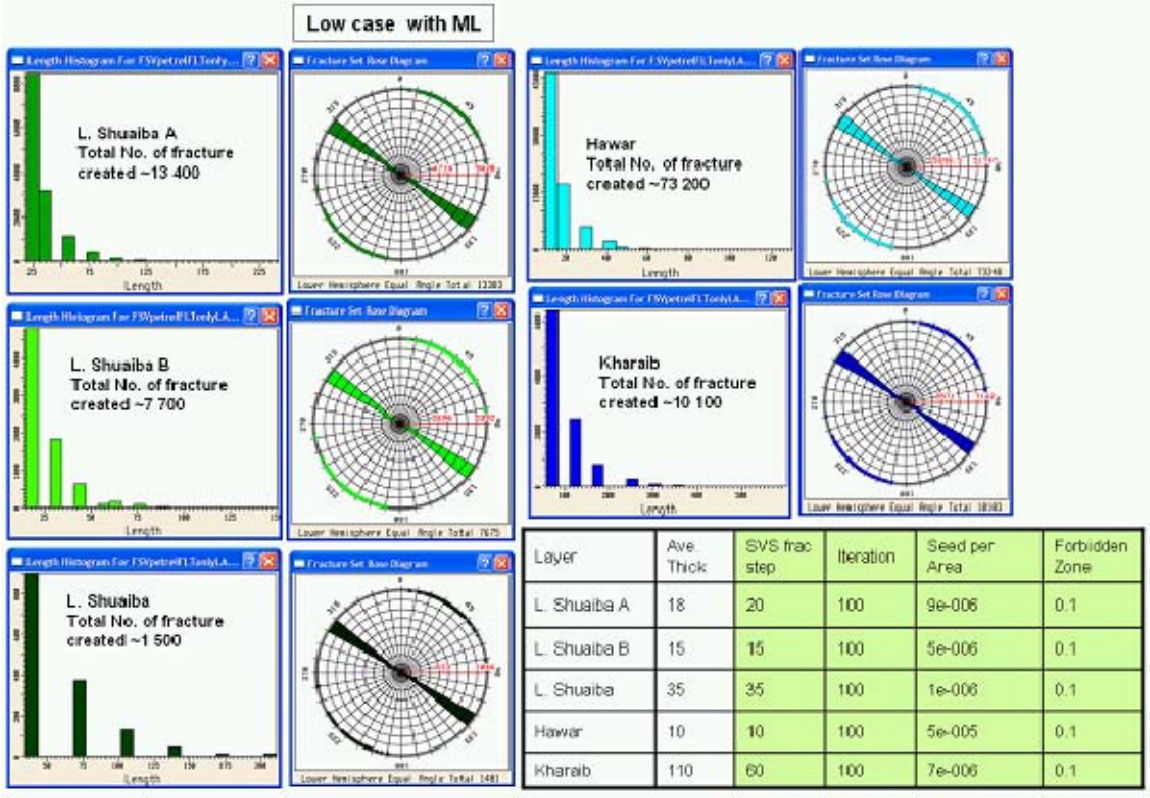


| Layer | Ave. Thick | SVS frac step | Iteration | Seed per Area | Forbidden Zone |
|---|---|---|---|---|---|
| L. Shuaiba A | 18 | 20 | 100 | 9e-006 | 0.1 |
| L. Shuaiba B | 15 | 15 | 100 | 5e-006 | 0.1 |
| L. Shuaiba | 35 | 35 | 100 | 1e-006 | 0.1 |
| Hawar | 10 | 10 | 100 | 5e-005 | 0.1 |
| Kharaib | 110 | 60 | 100 | 7e-006 | 0.1 |

**Figure 5-38 LAN low case 3D DFN realization parameters and total number of fracture created.**

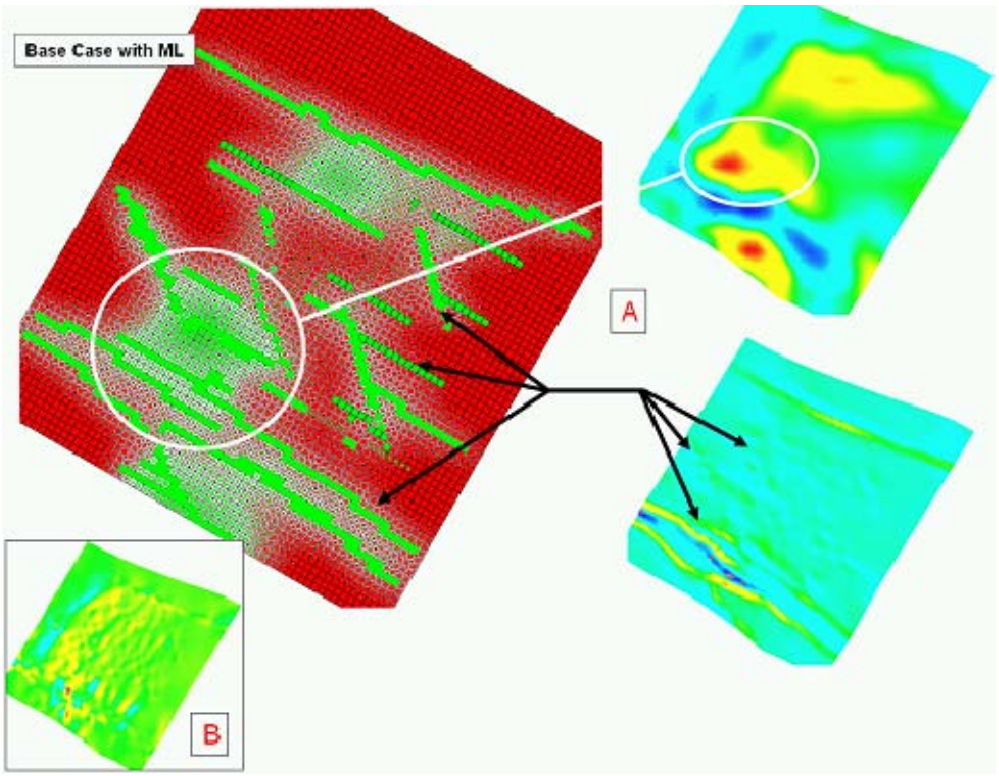


**Figure 5-39 SVS snap shot showing [A] the Seed probability map (green cells) and propagation impedance maps (red cells) used for the creation of the NW-WNW set, with the main input driver used for their creation: the curvature Kmax map at large scale and fine scale. [B] Show a snap shot of fine scale uni-directional curvature Kmax map, which was also used for the creation of the NE FC set's seed probability and propagation impedance maps not shown here.**

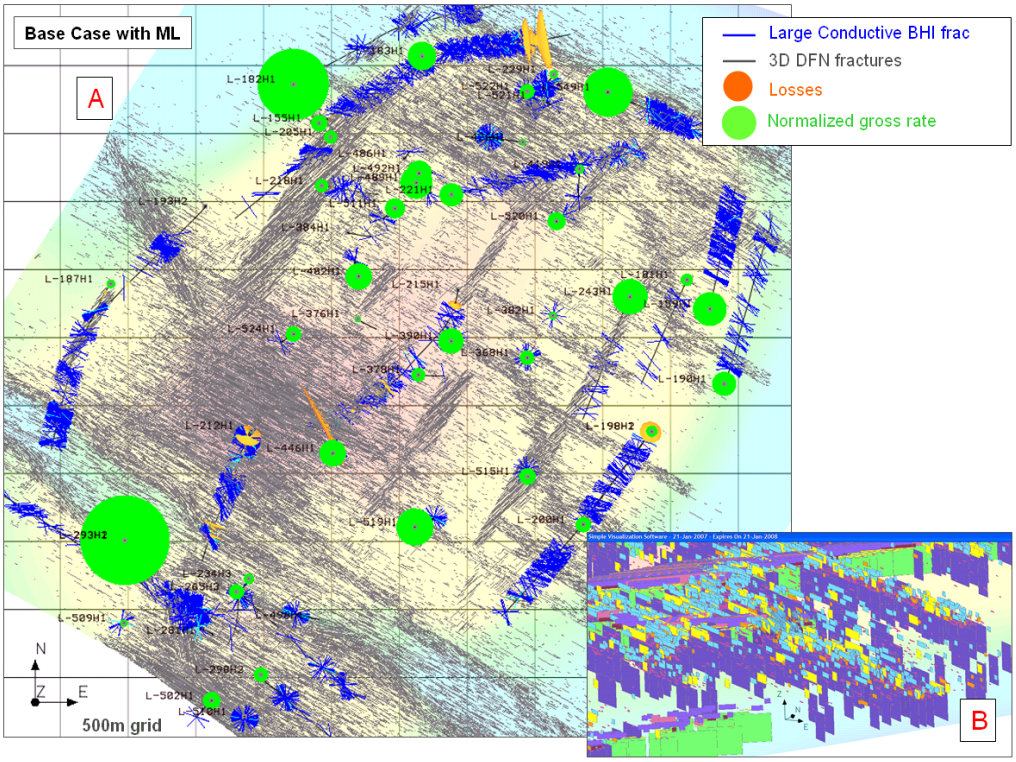


**Figure 5-40 SVS snap shot showing [A] map view of the total fractures created for the base case realization of LAN (note how fracture concentrate in FC or fault related fracture running NW-WNW and NE and also in highly strained areas in the north and SW regions of LAN). [B] Showing the same set but at zoomed-in inclined cross section to highlight the ML concept applied.**

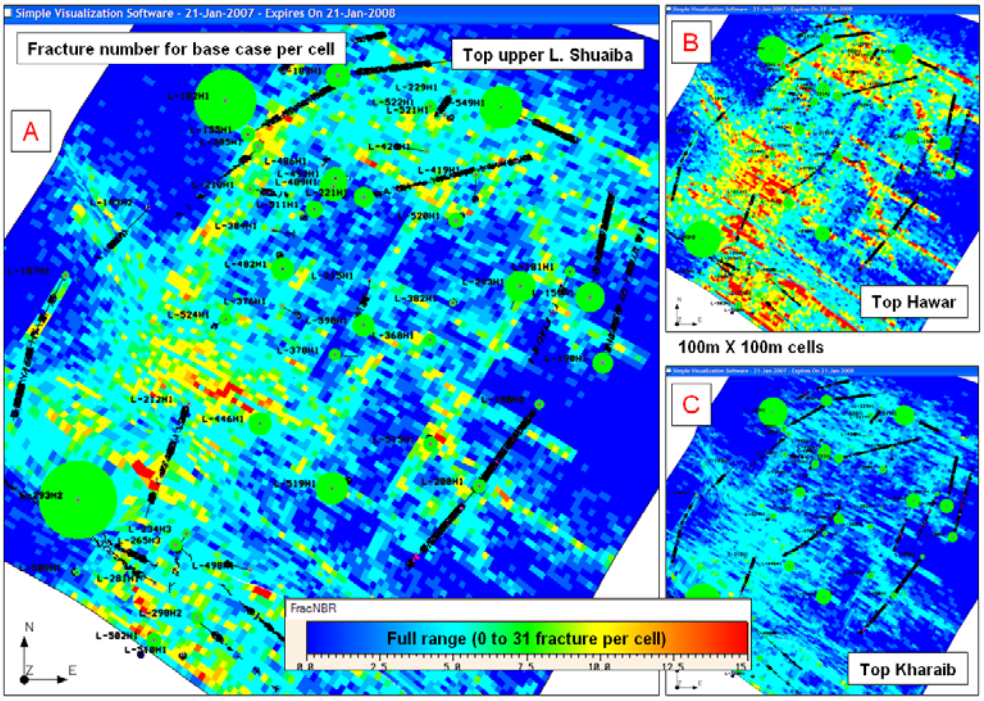


**Figure 5-41 SVS snap shot showing fracture number count per cell for LAN field for the base case. [A] At Upper Lower Shuaiba layer; [B] at Hawar layer; and [C] at Kharaib layer.**

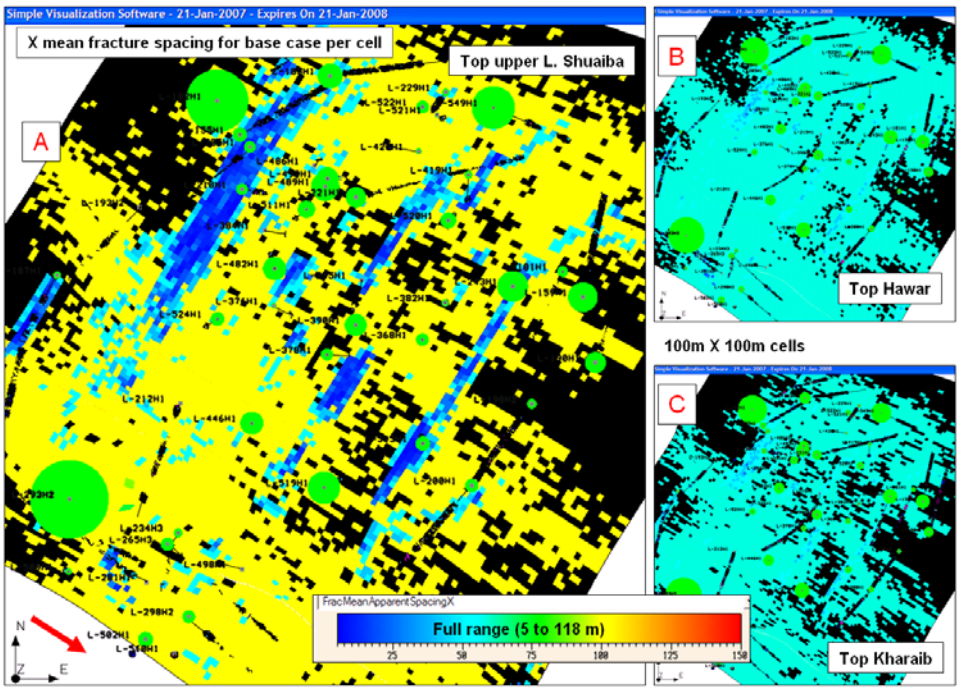


**Figure 5-42 SVS snap shot showing the mean apparent fracture spacing per cell along the grid X direction for LAN at upper Lower Shuaiba layer, Hawar and Kharaib layer for the base case. Note the effect of the spacing direction (red arrow at bottom left hand corner) on the results.**

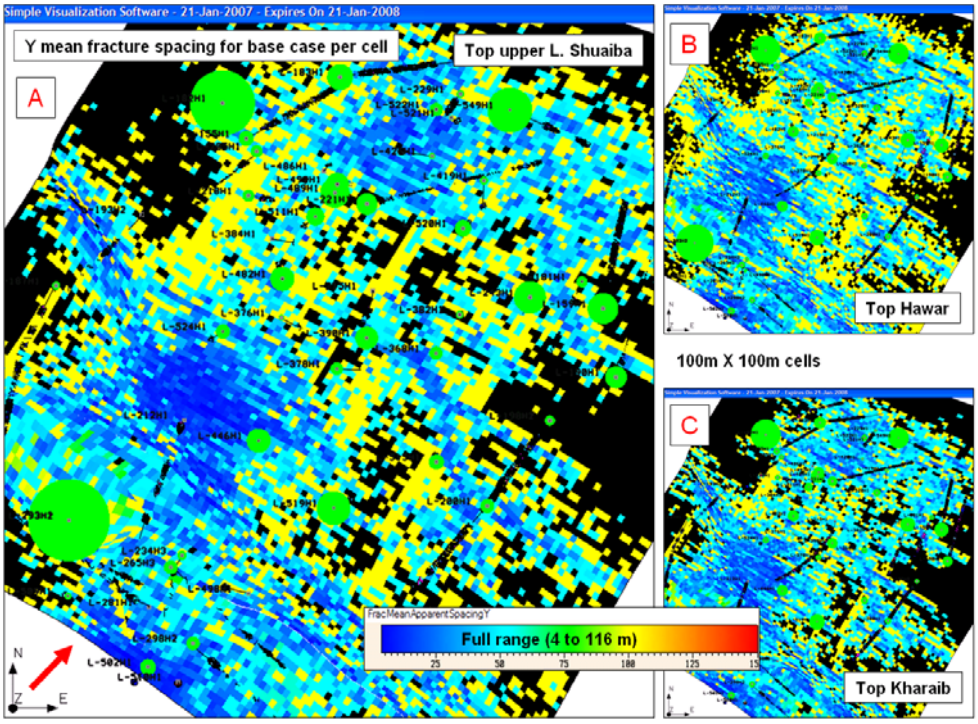


**Figure 5-43 SVS snapshot showing the fracture spacing per cell along the grid Y direction for upper Lower Shuaiba, Hawar and Top Kharaib for the base case. As the direction is perpendicular to the fractures NW-WNW main direction, the average spacing is much less than the X spacing. Black cells are z-null.**

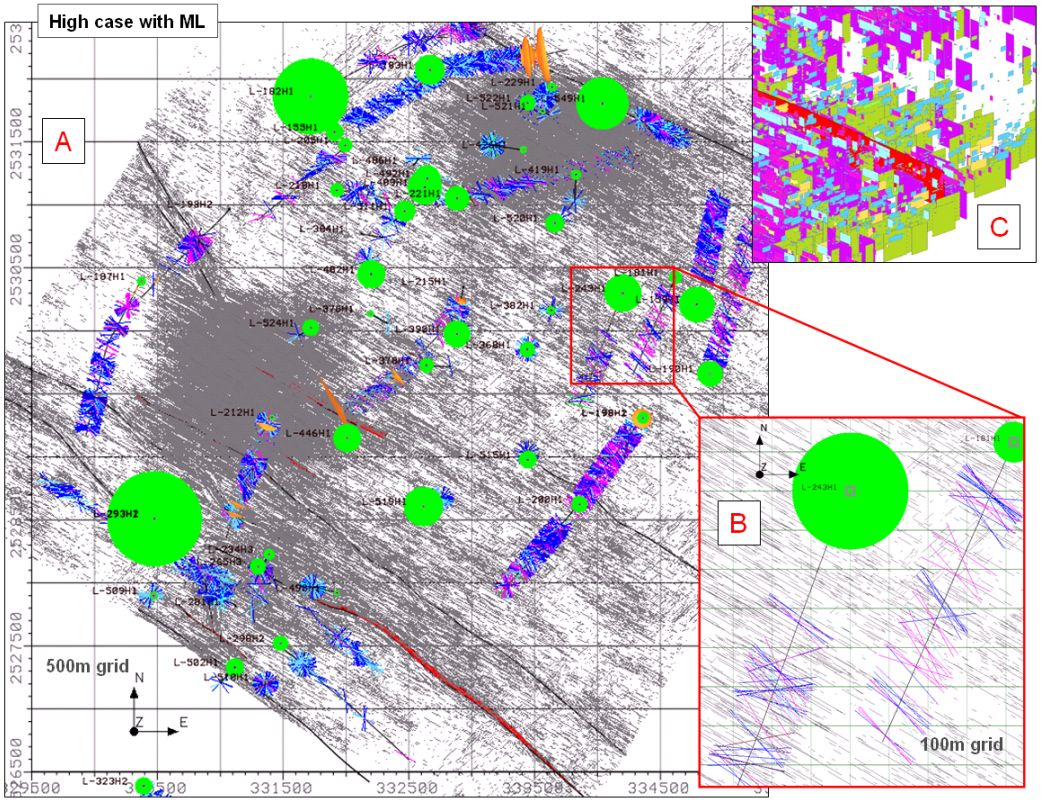


**Figure 5-44 SVS snap shot showing the 3D DFN created for the high case fracture scenario of LAN.**

# Chapter 6– FLOW ANALYSIS OF GN FRACTURE MODELS

This short chapter will present the method used and the result of a simple implicit simulation exercise done on the 3D DFN models created for the GN Shuaiba reservoir. The objective of the simulation is to show that the candidate understands the impact of each fracture scenario on the reservoir simulation process.
Simulation of naturally fractured reservoirs, where matrix provides the main storage volume and fractures provide the primary permeability ("flow path"), represents a significant challenge to petroleum engineers, because:

- Matrix properties have to be characterized,
- Fracture properties have to be characterized, and more importantly
- Flow interaction between fractures and matrix has to be defined.

The creation of 3D DFN models provides a good foundation for an alternative explicit fracture simulation, but it has to be done on a very fine-grid cells, which makes it impossible to be run on a large full field scale, as it consumes lots of computation power, even if the fine-grid cells are only in the heavily fractured zones (e.g. fault zones or fracture corridors). However, creation of several sector-size scenarios covering areas of perceived geometrical variation and/or flow characteristics variation in a field may be considered as an alternative. The normal approach used by petroleum engineers is to build implicit dual porosity models. These can be single permeability (where no matrix to matrix flow exist) or dual permeability. Such models are associated with many simplifying assumptions, but overall the main error in dual porosity models arises from the inaccurate definition of the flow interaction between fracture and matrix or the so called "transfer function". Eclipse software uses the Kazemi multi-phase dual-porosity model, which assumes a pseudo-steady-state flow and orthogonal fracture systems: continuous uniform fracture network oriented parallel to the principal axes of permeability (Sarma and Aziz, 2006).

## 6.1 Building GN simulation model

In this research, only the implicit simulation of Ghaba North fractured reservoir, was undertaken. This was done using a dual porosity dual permeability model on a sector grid that covers the central region of the field around GN-25H1 (Figure 6.1). A recap of the three DFN realizations used in the simulation is shown below (Figure 6.2). Note that they represent 3 three different concepts of fracture causation, although they are termed low, base and high cases here with respect to fracture intensity.

The sector grid used for the simulation, was cut out of the PDO 3D geo-cellular Petrel grid with a cell dimension of 100m by 100m in X and Y directions and 14 layers in Z direction covering Shuaiba and Kharaib Formations. The grid has a matrix porosity and matrix permeability in the X direction of the grid (Kmx). The matrix permeability in the

Y direction (Kmy) was assumed to be the same as in the X direction. In contrast, permeability in Z direction (Kmz) was calculated as 0.1 of Kmx, assuming a Kv/Kh ratio of 0.1 for normal layered carbonate reservoir. In addition, PDO/Shell EPT team also provided fluid and dynamic properties (e.g. relative permeability, pressure datum, etc) which were used in the Eclipse simulation. Fracture permeability in x, y and z directions were derived using the extracted fracture spacing in x, y, and z direction per cell, obtained from the 3D DFN created in SVS. The equation used to derive the permeability is:

$$K_f = A^3/12S \quad \textbf{(6.1)}$$

Where $K_f$ is fracture permeability, A is fracture aperture and S is fracture spacing per cell along the grid direction. Note: SI units are used here i.e. aperture in meters, permeability in $m^2$ (conversion: 1mD = 9.89 $10^{-16}$ $m^2$) and spacing in meter. The size of aperture (A) is very susceptible to nature of fracture, mechanical pressure and to mineralization, which makes it hard to define. In this research it was assumed to be 1.5 mm to represent an open fracture. The number was chosen based on what has been obtained from outcrop studies of Salakh Arch (Mercadier and Makel, 1989: quoting a range from 100μm up to 5cm); what was calculated by Nelson in Al Huwaisah field (Brown et al, 2002: quoting a high end of 0.58cm); and from reading in the internet literature (Georgia State University, Geological department, online geological presentation). Histograms of the calculated permeability per cell were cross checked against the effective permeability obtained from the interference tests done in GN Shuaiba, which gave a range of 10 to 60 Darcy. The fracture porosity was calculated in SVS by simple multiplication of a chosen uniform aperture into fracture dimension (cross-sectional area) per cell. The output was also cross checked by comparison to fracture porosity obtained from initial production rate profile (early rise in production in fractured reservoir is assumed to represent emptying of fracture network, thus fracture volume is determined and subsequently fracture porosity can be calculated). In most fields, the fracture volume amounts to 0.1% to 1% of bulk reservoir volume. In Ghaba North Shuaiba this was found to be 0.14% (Figure 6.3) compared to a calculated 0.2% for the nearby Qarn Alam field. The transfer function of Kazemi multi-phase dual-porosity model was used (Kazemi et al, 1976), represented in Eclipse by the key word ("sigma factor") and applied to the entire grid. It relates the matrix block size by this expression:

$$\sigma = 4\,[(1/L_x^2) + (1/L_y^2) + (1/L_z^2)] \quad \textbf{(6.2)}$$

Where, $L_x$, $L_y$, $L_z$ represent the dimensions of the matrix blocks, calculated to be 1580m, 1314.26m and 55.715m respectively. Hence $\sigma$ = 0.001292511 $m^{-2}$. A summary of the matrix and fracture parameters used in the Eclipse data file used for this simulation exercise are summarized in Table 6.1.

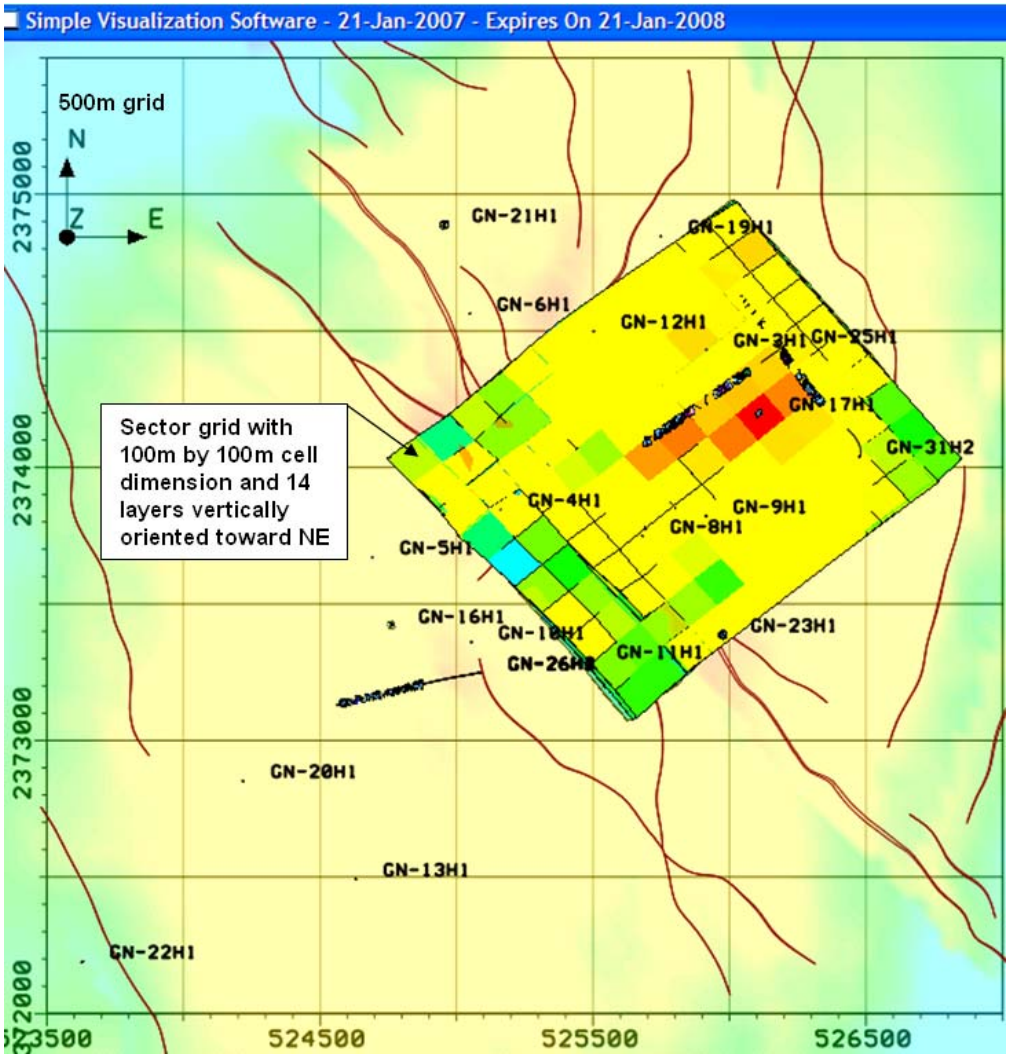


**Figure 6-1 Top Shuaiba map of GN, showing the location of the sector grid used for the simulation. Note the cell dimension of the grid is 100m by 100m in the X and Y direction and it is oriented toward the NE sub-parallel to the NE fracture set.**

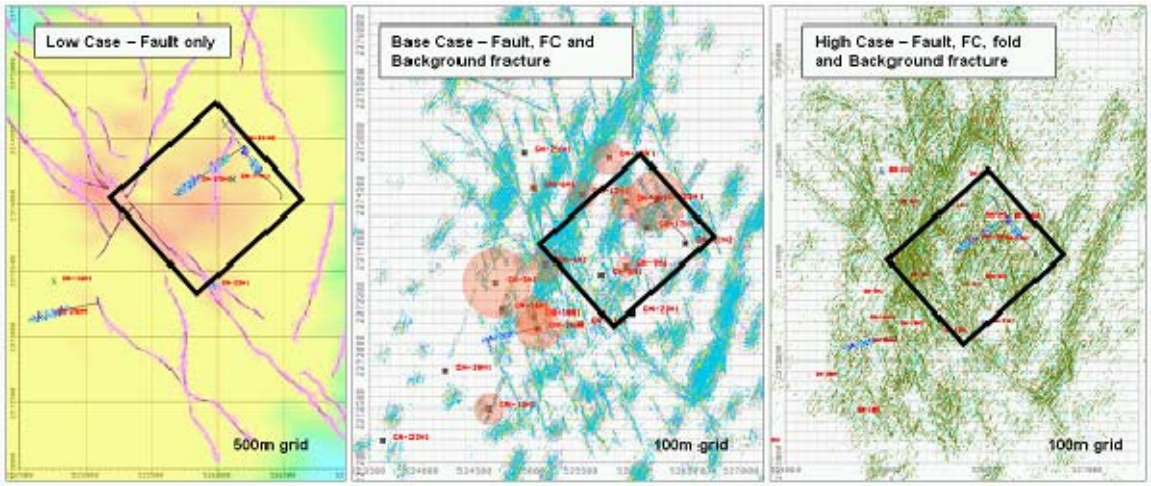


**Figure 6-2 A recap of the three DFN realizations used in the Eclipse simulation with a black outline box to show the rough location of the sector grid.**

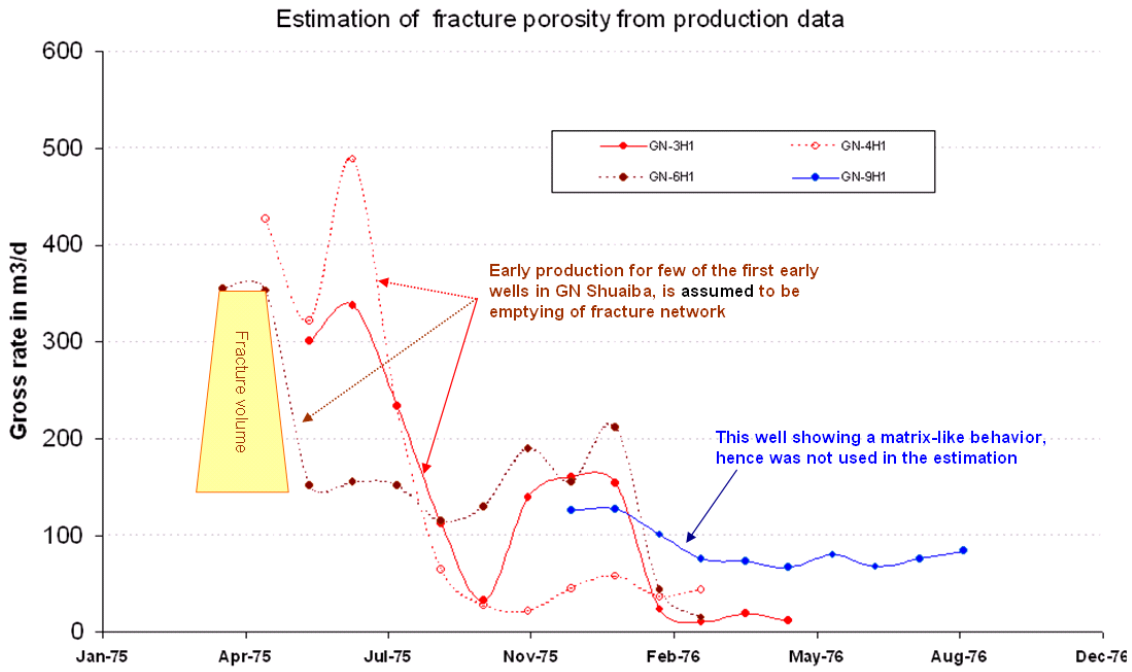


**Figure 6-3 A plot of GN Shuaiba early wells' gross rate obtained from PDO OFM data-base. These plots were used to estimate fracture porosity in the field assuming the early peak were related to emptying fracture network.**

| | | | | | | | Kmatrix X mDarcy | | | Kmatrix Y mDarcy | | | Kmatrix Z mDarcy | | | Matrix Poro (%) | |
|---|---|---|---|---|---|---|---|---|---|---|---|---|---|---|---|---|---|
| | | | | | | | Ave | Min | Max | Ave | Min | Max | Ave | Min | Max | Ave | Min |
| | | | | | | Low | 25.81 | 0.29 | 1198.74 | 25.81 | 0.29 | 1198.74 | 2.58 | 0.03 | 119.87 | 28 | 14 |
| | | | | | | Base | - | - | - | - | - | - | - | - | - | - | - |
| | | | | | | High | - | - | - | - | - | - | - | - | - | - | - |
| | X spacing | | | Y spacing | | | Kfrac x _mDarcy | | | Kfrac y_mDarcy | | | Kfrac z_mDarcy | | | Fracture Poro (%) | |
| | Ave | Min | Max | Ave | Min | Max | Ave | Min | Max | Ave | Min | Max | Ave | Min | Max | Ave | Min |
| Low | 85 | 0 | 148 | 172 | 0 | 577 | 4,578 | 0 | 52,600 | 3,604 | 0 | 65,426 | 4,578 | 0 | 52,600 | 0.004 | 0.000 |
| Base | 71 | 2 | 143 | 133 | 2 | 623 | 13,381 | 1,994 | 123,500 | 16,708 | 456 | 187,347 | 13,381 | 1,994 | 123,500 | 0.014 | 0.000 |
| High | 70 | 5 | 148 | 69 | 4 | 627 | 10,279 | 1,930 | 61,000 | 13,131 | 453 | 77,702 | 10,279 | 1,930 | 61,000 | 0.011 | 0.000 |

**Assumptions**

1) Fault transmissibility = 10
2) K matrix X = K matrix Y
3) K matrix Z = 0.1 * K matrix X (using Kv/Kh = 0.1)
4) Frac Porosity caclculated using sum of fracture area per cell * given aperture value (No range)
5) Fracture Permeability is calculated using Kfrac= A3/12S * 9.89 *10E-16 in mDarcy
   Where A is aperture in m and S is fracture spacing in m
6) Fracture K in z = Fracture K in x

**Table 6-1 Matrix and fracture parameters statistics used in GN Shuaiba simulation grid. Note how the X ("fracture") spacing for the base and high case are very similar. This is because the grid is oriented toward the NE, i.e. sub-parallel to the NE fracture set. Thus, the Y ("fracture spacing") is more representative. In addition, there is a negative effect to the large size of the cell X and Y dimension resulting in a large averaging for the spacing values. Since the fracture are vertical, SVS could not calculate fracture spacing in Z direction (as it used scan lines running from centre of one cell to the centre of the adjacent –consecutive- cell). Hence, fracture's permeability in the Z direction could not be calculated**

## 6.2 GN fracture simulation result analysis

In an ideal situation several simulation runs would be executed and iterations would take place between the geologist and the reservoir engineer. But because of time limitations and because of my limited knowledge of detailed simulation aspects, only one simple run was executed. The result of this simulation run was partly disappointing as it did not show the contrast between the three realizations, which was reflected in the static world (see Figure 6.2 above). The cumulative field production for the three cases

shows little difference (Figure 6.4). This similarity in flow can be attributed to several reasons, in order of importance:

1. Cell dimension (size) being large of 100m by 100m in X/Y direction,
2. Aperture value used for the calculation, which have impact on both fracture's permeability and porosity. A range should be used,
3. Grid orientation: being sub-parallel to the main NE fracture set,
4. Transfer function used to calculate flow from fracture to matrix,
5. Specific to this case: the absence of K matrix in Y and Z direction, and
6. The dynamic limitation (well constraint) used, in this case well bottom-hole pressure (WBHP) not to drop below the bubble point pressure (at 57.15 psi). This allowed very small delta pressure for flow as the initial reservoir pressure is just 61.9 psi at 426m datum (Figure 6.5).

Nonetheless, relative variation at well scale is seen within each model (Figure 6.6). For example the horizontal wells (GN-25H1 and GN-31H2) produced more oil. This is because they have a longer trajectory and greater contact with the reservoir. Hence horizontal wells can drain more oil and will intersect more fractures which will increase the flow rates and the amount of oil drained. In addition, vertical well GN-3H1 shows a high oil rate (WOPR) compared to GN-11H1, which fits with the normalized gross rate seen in the field (GN-3H1 has higher gross rate relative to GN-11H1, see Figure 3.16 in Chapter 3). Unfortunately, GN-17H1 which shows very high rate is an observation well and NO production data are available to cross check.

The general lack of differences between the three cases in the simulation world poses an important question: Is this outcome because of issues to do with the simulation approach, or does it suggests that fracture characterization is not worth doing? Based upon the considerable commercial and academic efforts that have been devoted to the study of fractured reservoirs, it seems unlikely that the in situ fracture distributions are not relevant. It is more likely that the simple simulation effort undertaken here was inappropriate to reveal the differences between the scenarios. The surprising uniformity of the flow responses underscores a need to undertake a further study to identify those simulation methods that will allow the asset teams to make distinctions between different DFN cases and thus to identify appropriate field management strategies.

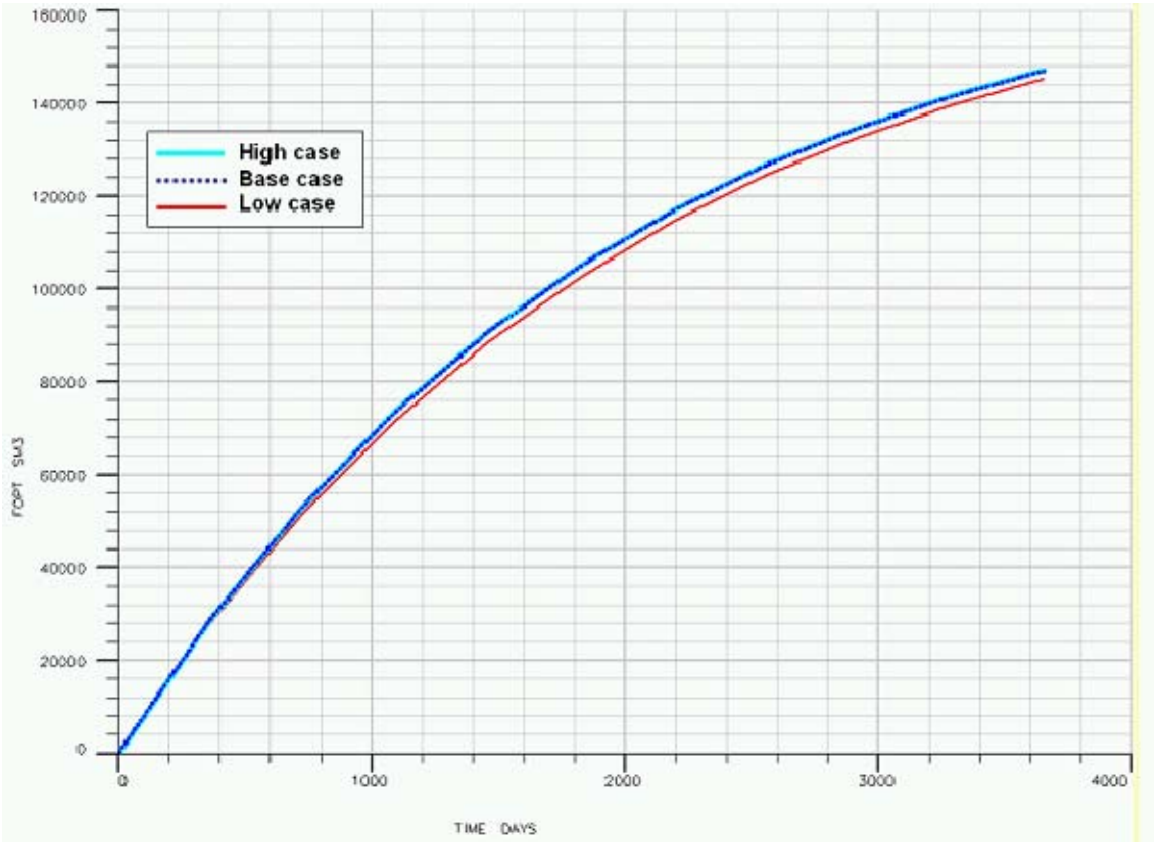


**Figure 6-4 Full field total oil production versus time for the three cases, showing little difference.**

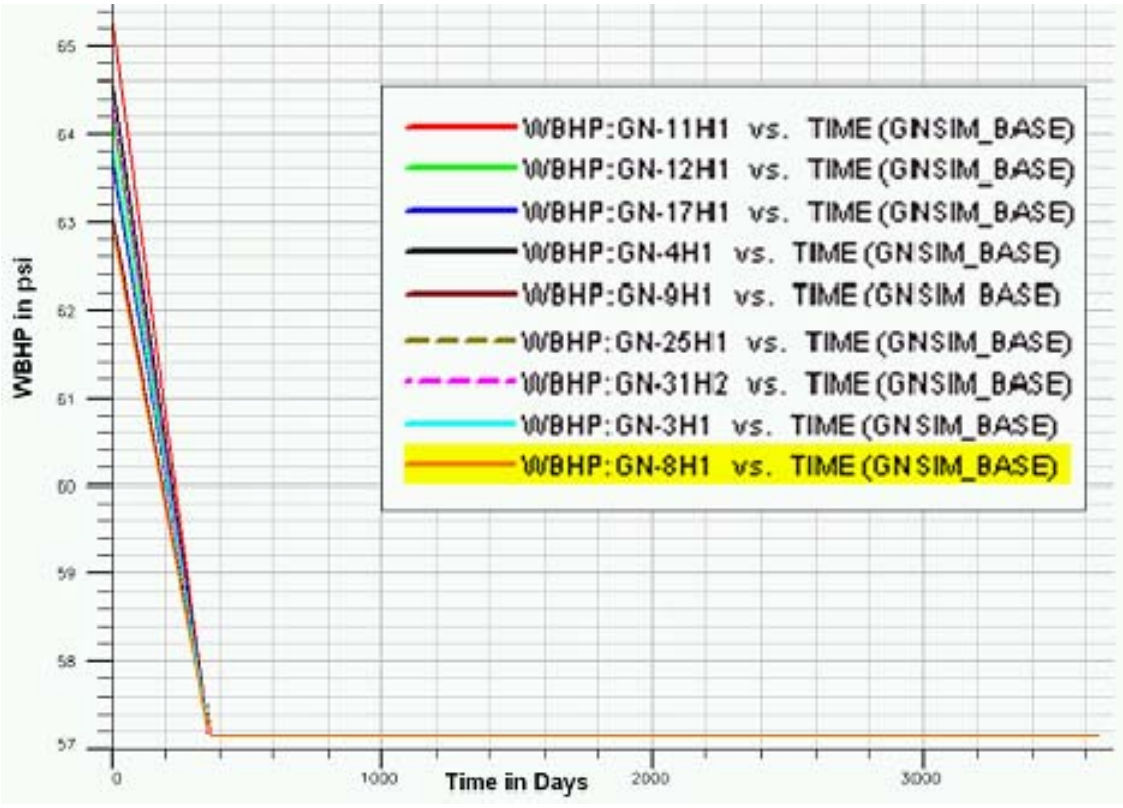


**Figure 6-5 Well bottom-hole pressure per each well versus time showing quick drop in pressure as there is no sufficient range of pressure for well to flow between the reservoir initial pressure and the constrain of no pressure drop below reservoir bubble point.**

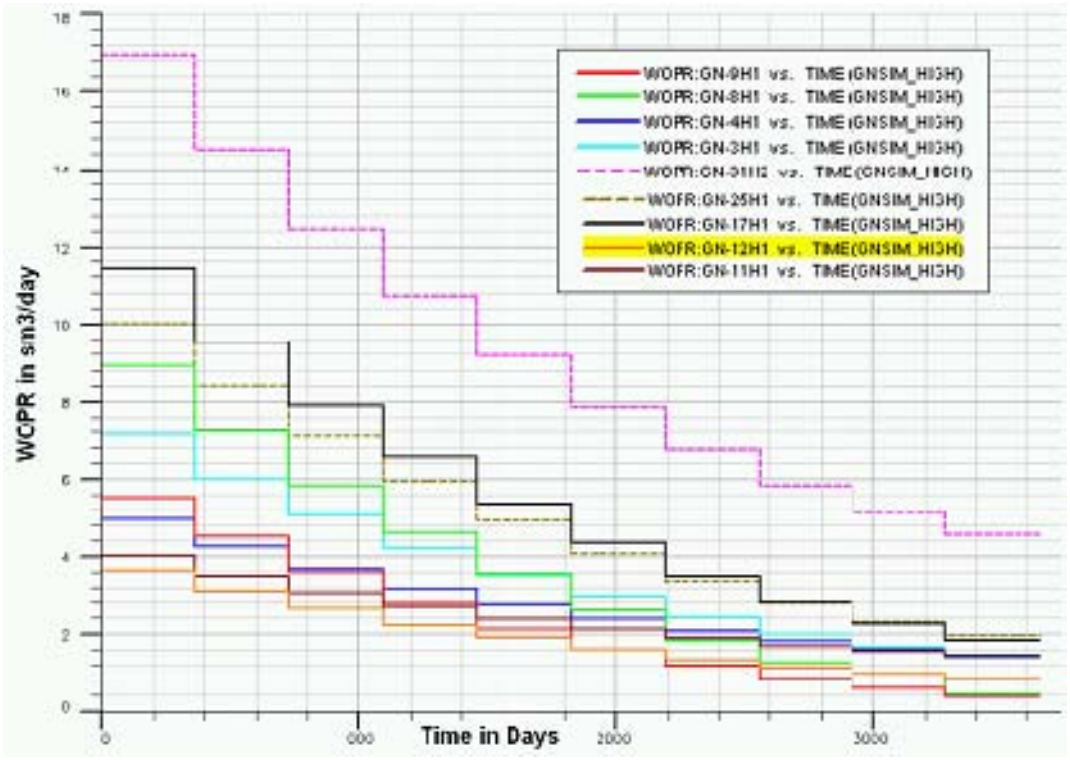


**Figure 6-6 Well oil production rate versus time per well. The objective is to see relative difference between wells, as the absolute values are incorrect. Note how the horizontal wells (dashed lines) produce more oil compare to the vertical wells.**

# Chapter 7– ANALYSIS

This chapter re-examines some of the critical fracture-related data described in the previous chapters and presents a coherent synthesis of the fracture network that occurs in the Cretaceous reservoirs of north Oman. It starts with a consideration of the role of the underlying geology, aiming to identify the relationship between the poroperm of the rocks (both those factors arising from primary deposition, and the effects of diagenesis, together creating the "matrix") and the flow impacts of the fracture network. This analysis is essential in enabling a clear identification of the role of fractures, since flow effects arising from aspects of the matrix can lead to similar reservoir behaviors. This analysis is then followed by a critical evaluation of the 3D DFNs that have been generated for GN. In addition to the types of model assessments that formed integral parts of the creation of the DFNs (such as comparisons between well trajectory summaries and model outputs), the analysis here considers dynamic data such as individual well flow rates. This sort of initial validation needs to be followed by detailed reservoir simulation and history-matching – a task that must be left to others.

## 7.1 Underlying Geology

The inter-relationships between matrix, fracture and diagenesis underpin the variations that have been described here in terms of the fracture network characteristics that distinguish the different types of north Oman fields. This statement is based on the premise that, at the time of a fracturing event, the intensity of fracturing, and the vertical extents of individual fractures, is controlled by the extant rock properties (which are the outcome of the prior depositional and diagenetic history). Diagenesis that occurs after fracturing may be spatially controlled as a consequence of the localized flow paths that are created by non-uniform fracturing. Thus, the heterogeneities of the reservoirs are determined by both primary and secondary factors that are themselves inter-related.

### *7.1.1 Matrix*

The lithological description of the Shuaiba of north Oman (see the stratigraphy section in Chapter 2) highlights the presence of different rock sequences that play a part in explaining the observed variations in fracture types and intensities seen in these fields. The initial depositional stacking geometries are very relevant to the presence or absence of bed-bounded fractures (i.e. mechanical layering). The fact that depositional sequences play this role is possible because of the lithological variation, which results in inter-layering of carbonate and shaley packages. Without the lithological changes (as in a carbonate-only sequence), the mechanical contrasts might not be great enough to lead to the sorts of variations seen across north Oman. Although these primary lithological effects are important relative to some of the fracture-distribution characteristics, it is clear that regional and local tectonic processes control the main variations in fracture distribution, with strong variances in intensity and geometry seen across north Oman (as

discussed below). The sequence stratigraphic framework proposed by Droste (Droste 2003) provides a conceptual model that is useful for explaining the variations in lithological controls that are associated with the original depositional history of this area. In general, the more southerly regions are less well-layered because of their palaeogeographic position closer to the basin edge, with a smaller degree of siliciclastic input. Carbonate buildups lead to very heterogeneous rocks, even if layering is not particularly strong. Those areas subjected to near-surface meteoric diagenesis, or to sequence-boundary leaching, can also be heterogeneous, with prominent high-perm streaks likely to be related to secondary processes (Figure 7.1).

These inherited depositional characteristics are reflected in the petrophysical data (e.g. plots of core porosity and permeability; Figure 7.2). In general, the northerly fields are more layered (and reveal vertical heterogeneity of properties), while the southerly fields are more uniform with depth. The notable anomalies in these trends (such as those in Yibal and Al Huwaisah) are related to the initial depositional heterogeneity and to later diagenesis that exploits those differences. Note that the depth-related petrophysical trends may also reflect the effect of burial diagenesis, but nonetheless the depositional signature is quite evident.

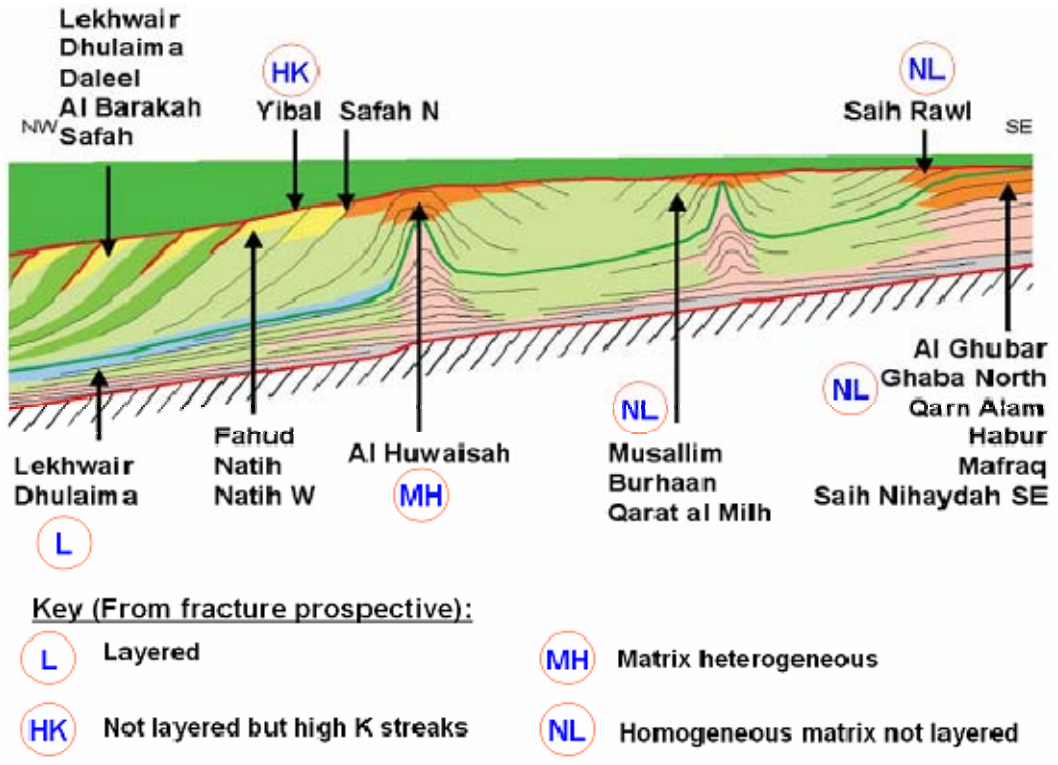


**Figure 7-1 Shuaiba sequence stratigraphic model showing the location of individual fields (from Droste, 2003) annotated with expected matrix characteristics from fracture prospective. Note how both the rock type and deposition morphology differ from SE, where only Lower Shuaiba member occur to the NW where both upper and lower members of Shuaiba are present.**

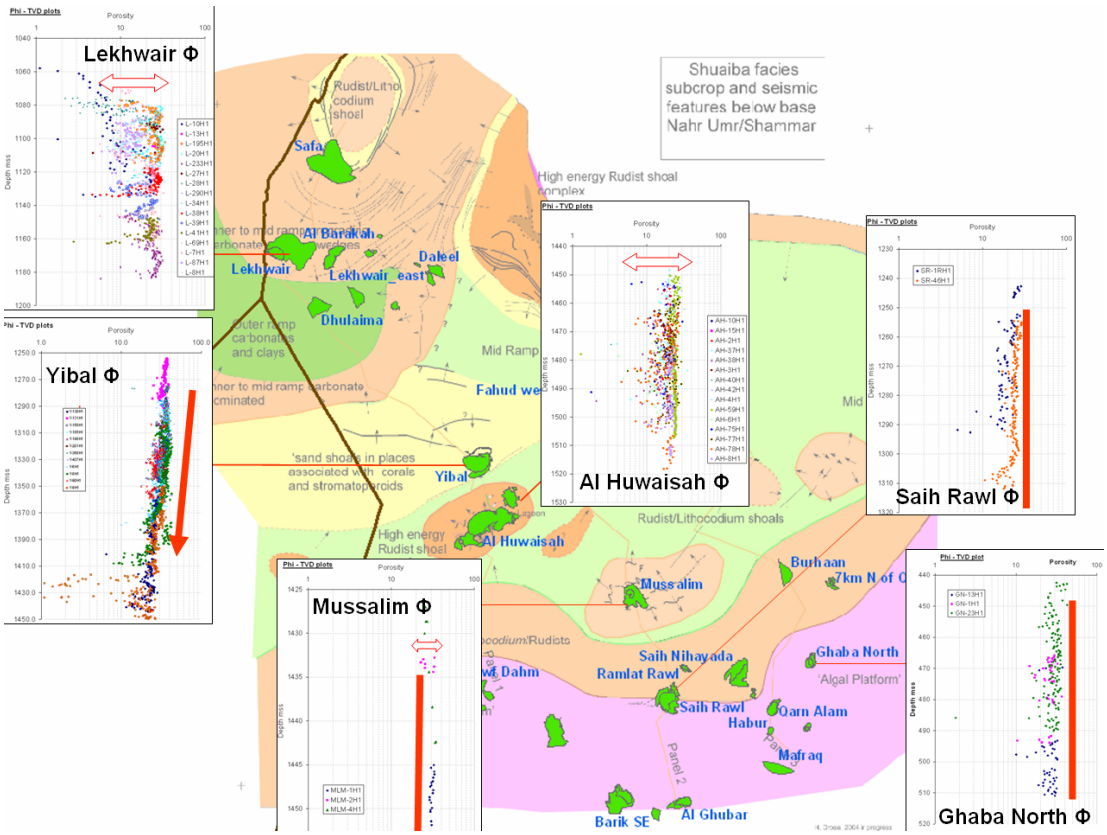


**Figure 7-2 Shuaiba fields porosity trends with depth superimposed on top of Shuaiba facies subcrop map created by Droste (Droste et al, 2003). Note how in the south-eastern fields around Qarn Alam, where only Lower Shuaiba is present, the porosity range with depth is much small compared to the north-western areas such as Lekhwair or local high areas such as Al Huwaisah where the porosity range is very large indicating variation of rock properties.**

The Bab Basin region (North):

In the northwestern region of north Oman (i.e. around the Lekhwair area), both the upper and Lower Shuaiba members are present within the Bab Basin. Amthor and Kerans (2004) propose that the outline of the Bab Basin extends all the way south from UAE to the rim of the Al Huwaisah fields (Figure 7.3). Droste stated that both early lowstand forced regression and transgressive system tracts are present in the Bab Basin. Thus, the area is characterized by both clean carbonate layers, and layers associated with sudden siliciclastic influx which possibly have extensive lateral continuity in the Lower Shuaiba but may have very poor lateral continuity where pinch-outs are common in the upper Shuaiba. The upper part of the sequence is susceptible to early fresh water diagenesis. The presence of both Shuaiba members with the interlayered siliclastic layers is evident from the large variation in the core porosity measurements from about 1% to over 33% (Figure 7.2). This variation affected the vertical distribution of fracture intensity. Upper Shuaiba BHIs where not analyzed in this thesis, but it is noted, in Chapter 2, that studies such as Nelson (2004), which examined upper Shuaiba, had documented evidence of mechanical layering (Figure 7.4). In addition, the detailed well by well examination of LAN (in Chapter 5) has summarized evidence of mechanical layering in this northern region, even within the Lower Shuaiba (Figure 7.5). This inherited variation in depositional lithology can be expected also to have affected the distribution of microfactures within the Lekhwair field reservoirs. Microfracturing (and

related stylolite analysis) is beyond the scope of this thesis as it requires the detailed examination of cores which, unfortunately, were not available to me. But note that, as mentioned earlier, the current practice is to represent the effects of microfractures as either an enhancement or degradation of matrix properties. Petroleum engineers working in this field should be cautious about this issue. Although the stratigraphic relationships have an impact on the vertical patterns of fractures, the lithology (resulting from the pre-fracturing geo-history) does not determine other aspects of the fracturing. Instead, as stated above, the regional tectonism is believed to be the major control on both the intensity of the fractures seen and their areal distribution. This is very clear when relating the matrix porosity at the top of the reservoir with both the BHI fractures and the normalized gross rate for each well in LAN. Wells with high BHI fracture intensity do not coincide with areas that have high matrix porosity (yellow areas). Also, wells with high normalized gross rates do not coincide with high matrix porosity (Figure 7.6). These relationships indicate two major conclusions: fractures play a major role in flow in the Lekhwair field reservoirs, and the main aspects of the fracture distribution there do not depend on the lithological details.

Further southeast, Yibal field is situated at the southeastern rim of the Bab Basin, and both upper and Lower Shuaiba members are again present. The matrix porosity trend of the field shows a gradual decline with depth (as shown in Figure 7.2), though high perm streaks have been observed. Figure 7.7 shows a typical log of a mature producer from Yibal (the well number is not known) obtained from the Shuaiba asset compilation report (Nicholls et al, 2003). The saturation log clearly indicates the presence of such high perm streaks. The genesis of these streaks is likely to relate to the susceptibly of upper Shuaiba to early meteoric diagenesis (based on its top-of-buildup location; see Fig. 7.1) although no evidence is presented here to support that conclusion. The impact of such layers on fracture distribution (presuming that they pre-dated fracturing) has not been examined in this thesis as the BHIs from Yibal were not available. However, the fracture analysis by Baker Atlas (Ozkays, 2003) indicates the presence of bed-bounded fractures in this field but they are probably not contributing to flow, as only the faults and the high perm layers were identified as the main contributors in that external report. Tectonism in Yibal field is the main driver for the areal distribution of the fracture network, similar to the Lekhwair area (see next section). The BHIs show high fracture intensity wells in the vicinity of or in faulted regions. From a flow prospective the best method to characterize such high k layers is by using a comparison between cased-hole and original open-hole saturation logs or 4D seismic. Their flow profile is envisaged to be different from that of fracture flow (see next section).

The nearby Al Huwaisah field is also located at the rim of the Bab Basin (Figure 7.3). According to the Droste sequence stratigraphy model (Figure 7.1); it is located in one of the local rudist mound areas where carbonate buildup processes flourished. Amthor and Kerans (Amthor and Kerans, 2004) also interpret the presence of both full Lower

Shuaiba and the base of upper Shuaiba, with the top of Lower Shuaiba being the main reservoir. The latter unit is by far the most complex sequence in terms of facies distribution, stratal geometry, and flow unit architecture within the Shuaiba of Oman (Figure 7.8). The reason behind this complexity is a combination of both depositional factors and matrix diagenesis. The complexity is reflected in the variation of matrix porosity with depth (Figure 7.2), ranging from less than 2% to over 30%, with several alternations evident from top to bottom of the unit. Yibal and Al Huwaisah present an opportunity to consider the flow effects of high perm streaks (see discussion below). The fracture intensity map created by Nelson (in Brown et al, 2002) indicates that there is an areal variation in the intensity of the fractures (Figure 7.9). This spatial pattern of intensities might be attributed to the lithofacies variation (e.g. Figure 7.8). However, the orientations of the fractures are likely to be controlled by tectonics (see next section). The BHI fracture cumulative frequency versus depth (Figure 7.9) does not show step changes with depth which suggests that mechanical layering is not very strong in this field. In order to test these suggestions, additional data is needed. The sub-horizons of Shuaiba can be used to assess BHI fracture intensity variation with lithofacies layers. Unfortunately, the local Al Huwaisah top reservoir map and Shuaiba sub-layer maps are not available for this study, so the suggestions need to be tested via future work.

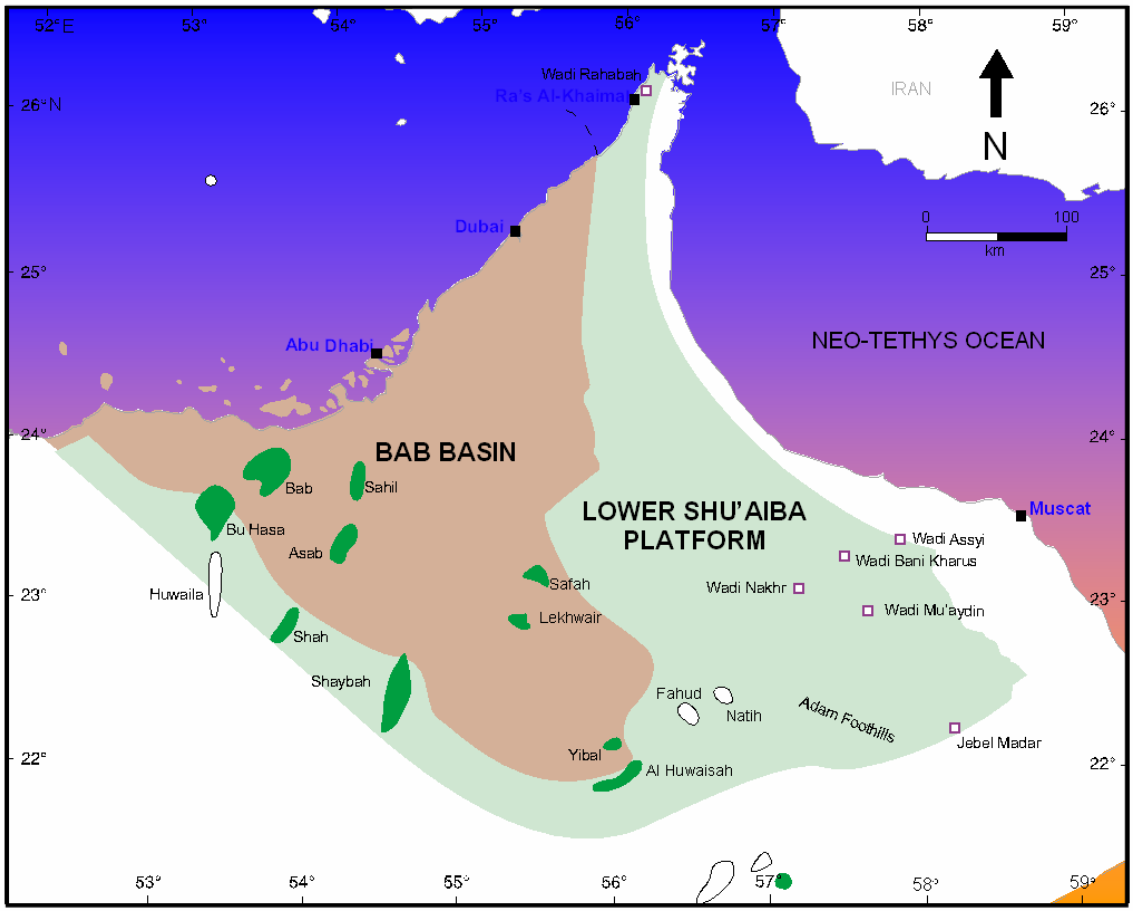


**Figure 7-3 The outline of the Shuaiba Bab Basin covering both north-western part of Oman and majority of the UAE oil fields (Amthor and Kerans, 2004). Note that it is not clear whether Al Huwaisah is out or just at the rim of the Bab Basin. The Cretaceous reservoirs within the basin are characterized by the presence of both Upper and Lower Shuaiba members.**

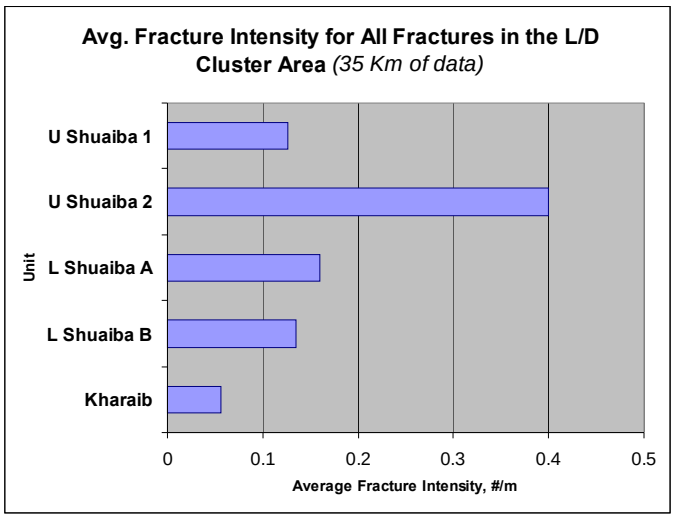


**Figure 7-4 Average BHI fracture intensity for Lekhwair – Dhulaima cluster per layer (Nelson, 2004). Note how the BHI fracture intensity in U Shuaiba is much more compare to Lower Shuaiba indicating mechanical layering.**

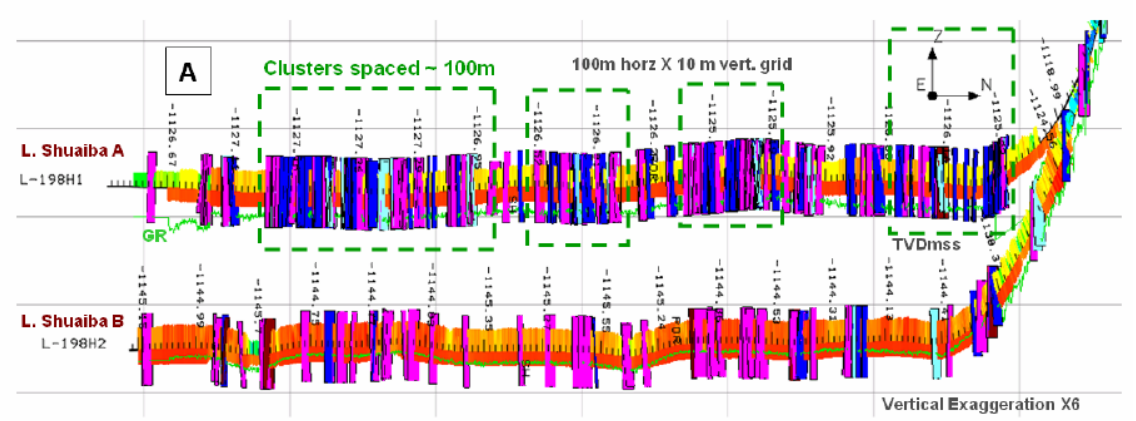


**Figure 7-5 Cross-section view showing the two legs of L-198 targeting Lower Shuaiba A and B. Note how the fracture intensity is much less in B and the intensity of non-conductive fractures (pink planes) is more in B. The non-conductivity will be discussed in the fracture diagenesis section later.**

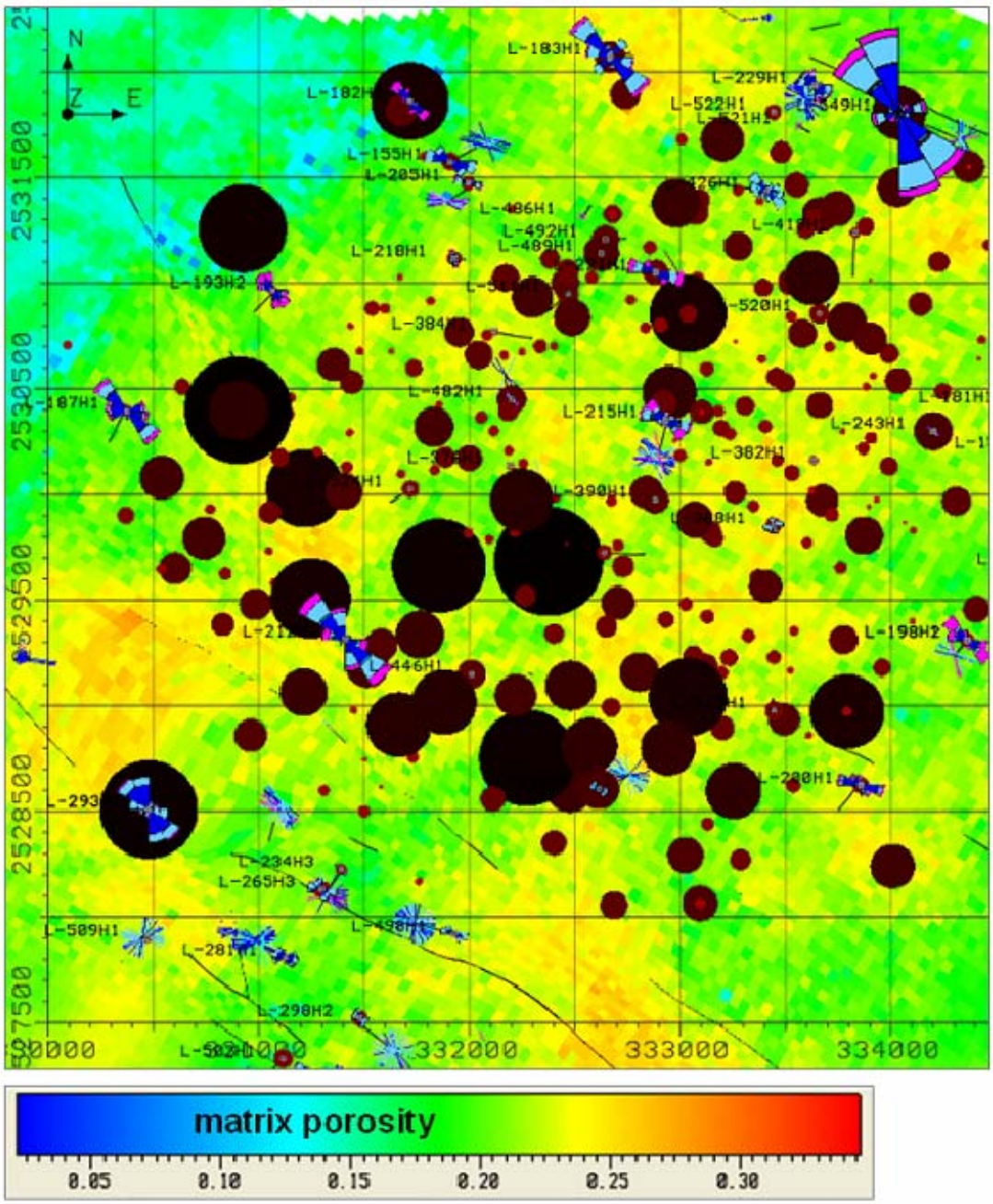


**Figure 7-6 BHI fractures rose diagram per wells (blue/pink roses) and normalized gross rate per wells superimposed on the matrix porosity map of top Shuaiba in LAN. Note how the high porosity areas colored yellow do not coincide with high BHI fracture intensity or high normalized gross rate.**

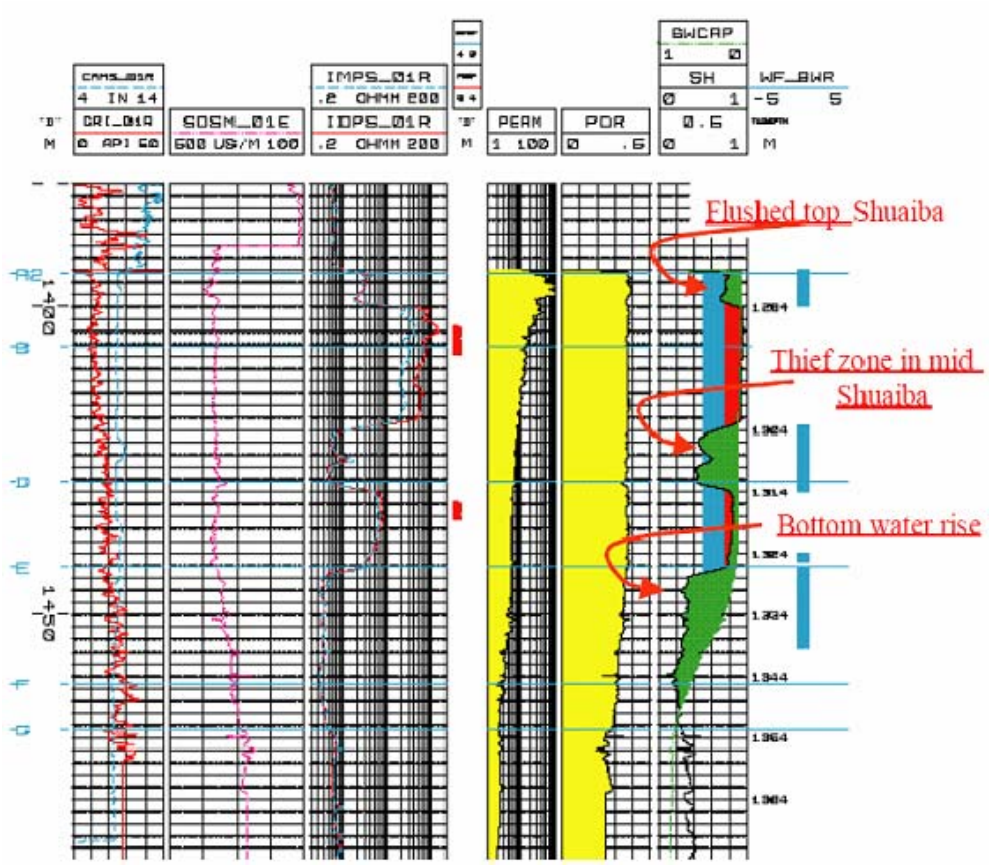


**Figure 7-7 A type log from Yibal field of a mature producer (well number is not known, Nicholls et al, 2003) showing position of possible high K layers within Shuaiba at the top and close to the middle of the reservoir. These together with main faults and associated fracture damaged zone are thought to be the main contributors to flow conductivity.**

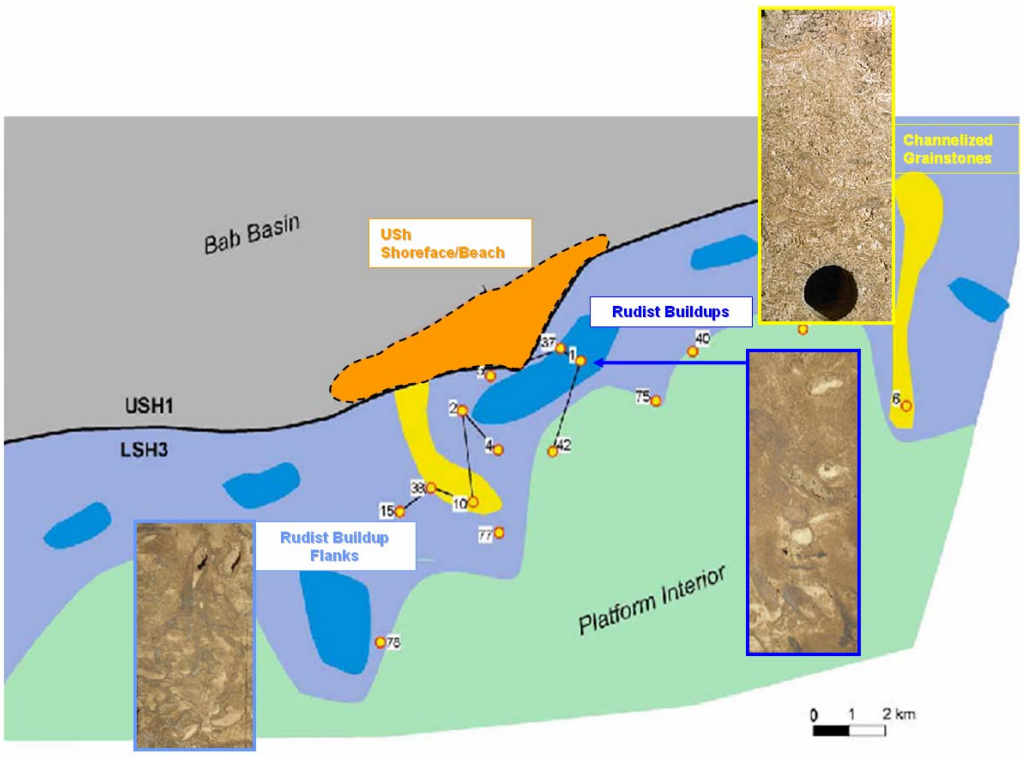


**Figure 7-8 Deposition and facies model for the top Lower Shuaiba and upper Shuaiba layers with example of rock types seen in Al Huwaisah (from Amthor and Kerans, 2004). Note the complexity of the matrix and its diagenesis (vuggy rudists seen in the core images). This had an impact on the distribution of the fractures in the field.**

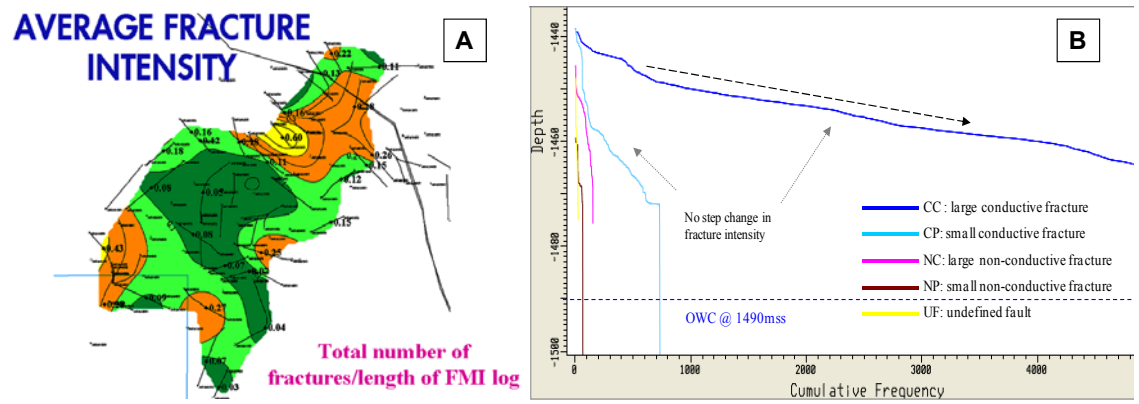


**Figure 7-9 A] Average BHI fracture intensity for Al Huwaisah field (from Nelson, 2002) showing areal variation that might be dictated by the lithofacies in the field. B] Cumulative BHI fracture intensity per type versus depth, not showing a very clear step changes with depth (i.e. not hinting toward a very evident mechanical layering).**

Central region:

Saih Rawl, Musallim and, to some extent, Burhaan Shuaiba fields are termed the carbonate pancakes of north Oman. The fields are very flat, although Droste (2003) reports the presence of internal clinoforms (picked from regional seismic analysis) with a dip of less than 1 degree. Only Lower Shuaiba is present, though deposits from both the high-stand systems tract and the trangressive systems tract occur, with the latter being dominant (Figure 7.1). The thickness of the oil column is thin in these fields (less than 20m for Musallim, and less than 30m for Saih Rawl) compared to the thickness of the reservoir (around 80m). The rock competence seems to be vertically and horizontally homogenous, at least from a fracture prospective. Recent attempts to subdivide the reservoir, based on sedimentology, into three sequences using the Huqf outcrop as an analogue do NOT reveal an impact on the distribution of the fractures vertically (areally the distribution is governed by tectonism and to some extent by matrix diagenesis associated with tilting – see next section). This homogeneity is supported also by the GR logs that show a constant range of readings with depth, seldom exceeding 20 API in value (Figure 7.10).

It is not possible to confirm that there is no impact on fracture distribution with depth in Saih Rawl and Musallim, as all the deviated wells are confined to the upper part of the Shuaiba and the sampling of the fractures by vertical wells is very low. However, in the Qarn Alam fields (also only the Lower Shuaiba is present), deviated appraisal wells were drilled but did not show any large variation in fracture density with depth within the Lower Shuaiba Formation. Nevertheless, for Musallim and Saih Rawl, core descriptions have recorded the possible presence of a thin (less than 1m) tight layer. It is not clear whether this layer is continuous (though one would think so, as the Lower Shuaiba layers are seen in Huqf outcrop to be of high lateral continuity – I traced a 30 cm layer in Huqf Lower Shuaiba Formation for over 2 km). This tight layer, which is likely to be fractured, is reported in the Baker Atlas BHI fracture characterization of Musallim field, and might be encountered both within the OWC and below it in some wells. This is because of the lateral change in the OWC datum of the field (with

differences of up to 12m) which is probably attributed to capillary pressure. Matrix diagenesis on the other hand, does play a role in the areal distribution of the fractures in Musallim (see next section), but the overall characteristics of the fracturing is again controlled by the tectonism (fault distributions).

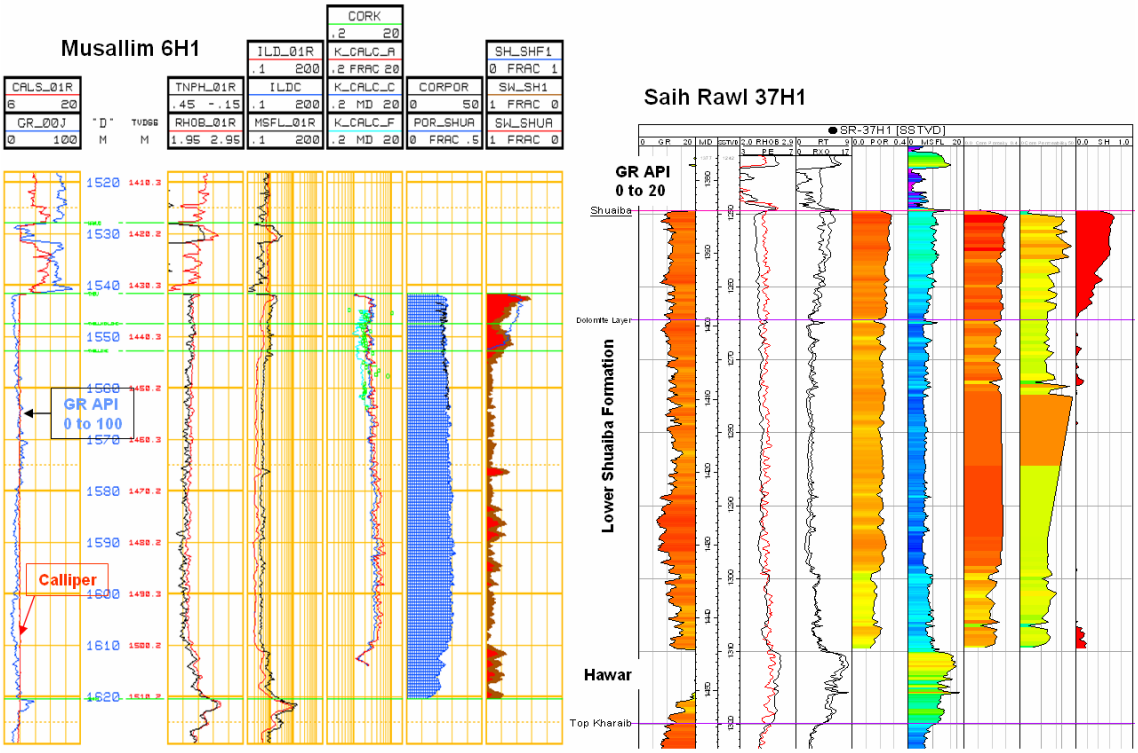


**Figure 7-10 Type logs from Musallim and Saih Rawl fields. Note how the GR logs are at all time Lower than 20 API indicating a clean carbonate rock. Also note how the calliper value is constant with depth in MLM-6H1 indicating a straight unfractured hole.**

Southeastern region:

Qarn Alam, Habur, Al Ghubar and Ghaba North are the southeastern oil fields of Shuaiba in north Oman. Their oil is moderate (Al Ghubar and Ghaba North) to heavy. Habur and Qarn Alam produce from both Shuaiba and Kharaib (stratigraphically lower), with oil column thicknesses of 80m and 120m, respectively. These fields are highly faulted and fractured to the point that the Hawar member (between Shuaiba and Kharaib) does not act as a real baffle to flow. In all of them, only the Lower Shuaiba is present and it is homogenous, except for Habur, where patches of rudists are seen. Habur field has only three wells in it, so proper correlation and modeling of these rudist patches is not yet established. As mentioned above, the matrix is subdivided into sub-layers based on the Huqf outcrops. The physical differences between these sub-layers are subtle, as shown from the narrow spread in the porosity with depth (see Figure 7.2) and the low GR profile, not exceeding 20 API variance in value (Figure 7.11).

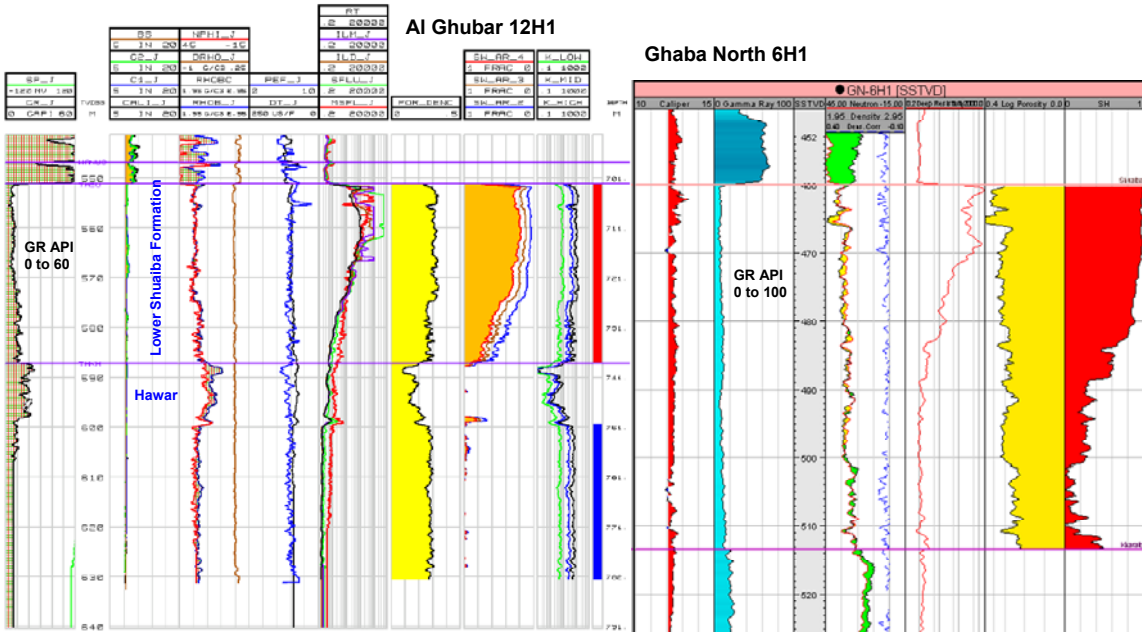


**Figure 7-11 Type logs of Al Ghubar and Ghaba North Shuaiba fields. Note how the GR value is very low indicating clean carbonate and its trend with depth is almost constant.**

Natih Formation:

The Natih Formation is the commercial reservoir for Fahud and Natih fields in the NE and Al Ghubar field in the SE. The layered nature of the Natih, which possibly has been intensified by early diagenesis, dramatically impacts the vertical distribution of the fractures, resulting in the most intense mechanical stratigraphy recorded in the Cretaceous reservoirs of north Oman (Figure 7.12). These layers (or "members", termed G to A from the base to the top), each start with a thin mixed carbonate/shale unit that is overlain by a thick carbonate. Outcrops show much more intense fracturing within the sub-layers of the Natih members compared to what has been picked by the BHI in the subsurface. As mentioned earlier, this is related to the issue of resolution. Integrating fracture-related data, such as wireline logs and BHIs, does help in recognizing these layer-bounded fractures. From experience, the best logs to use to assess mechanical stratigraphy are GR, Density and Caliper (Figure 7.13). Outcrop analysis (de Keijzer et al, 2004) has shown that the vertical persistence of the fractures is controlled by rock composition (clay content exerts a major control), texture, bed style, nodularity and rock stiffness. For instance, bed-bounded fractures are generally terminated at sharp stratigraphic discontinuities that have a textural or mineralogical change, whereas unit-scale mechanical boundaries occur where there is a change in texture and/or composition, and, additionally, a change in bedding style across the boundary. Formation-scale boundaries (or fractures) are clearly controlled by the change in clay content and the thickness of the clay/marl interval adjacent to the boundary.

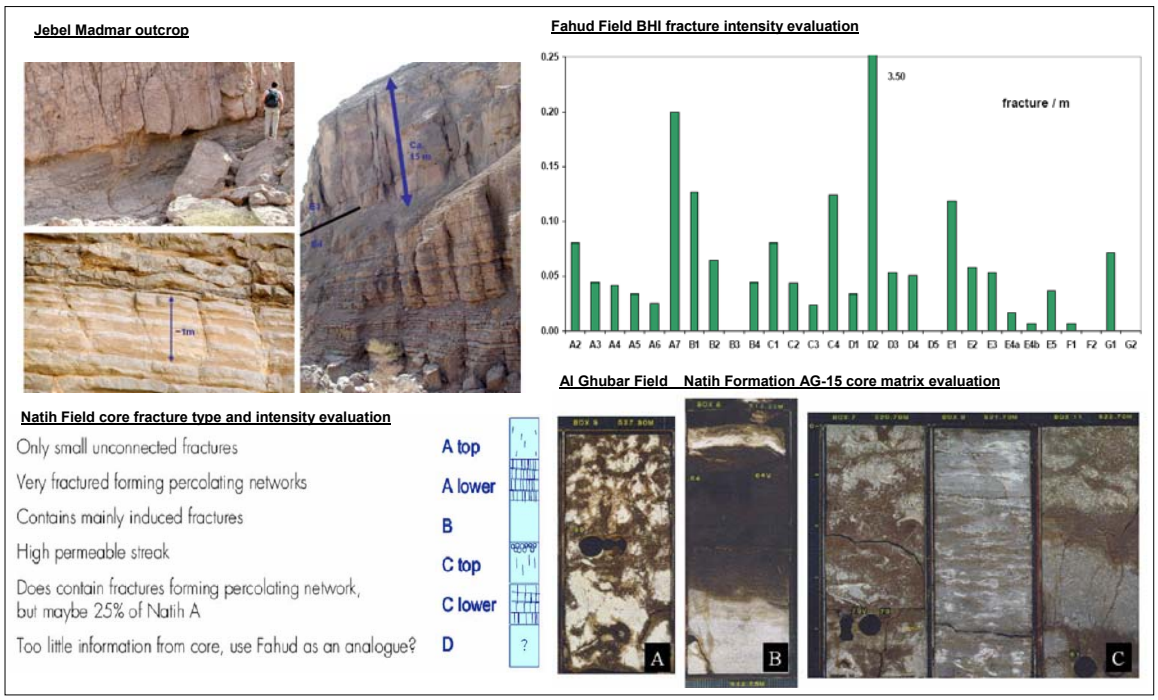


**Figure 7-12 Example of impact of matrix lithology on fracture distribution in the Natih Formation. In Jebel Madmar outcrop (de Keijzer et al, 2004) the fracture are bed bounded, unit bounded or Formation bounded. Evaluation of Natih field's core (Roeterdink, 2004) shows strong mechanical layering with intense fracturing in the base of Natih A member and no natural fractures in the clay rich Natih B. Analysis of the BHI fractures of Fahud fields also showed strike change in fracture intensity between the members of the Natih Formation. Core evaluation of Al Ghubar Natih E (Konijnenburg et al, 1999) indicates change in the rock type within this member that would had surely affected the distribution of the fracture network.**

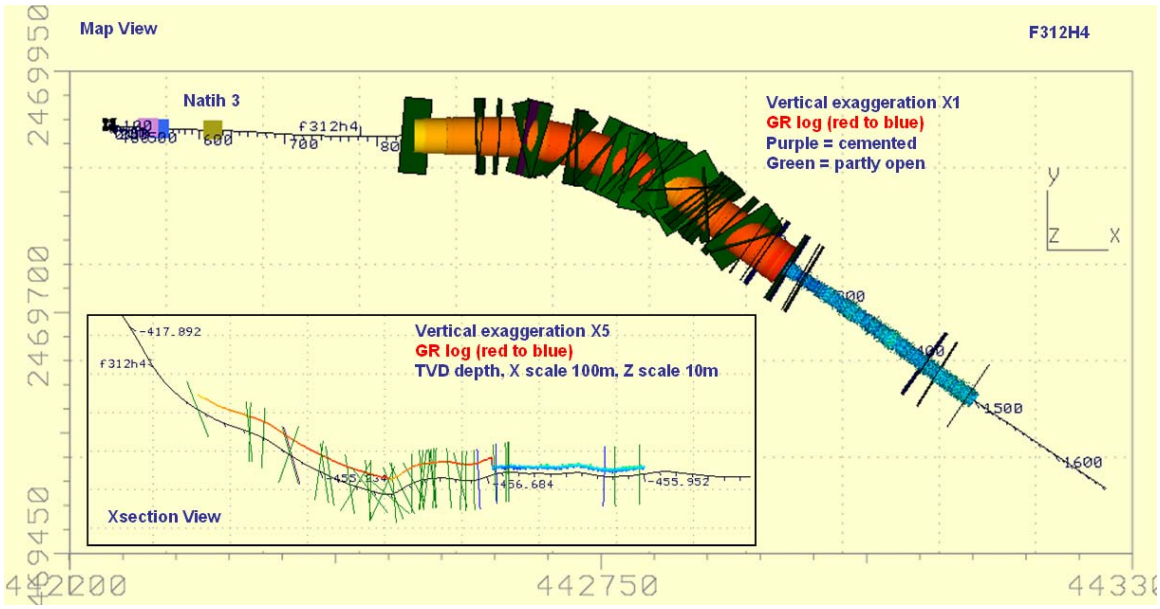


**Figure 7-13 Fahud 312H4 legs showing a dramatic drop in BHI fracture intensity that coincide with a drop in GR log p most likely reflecting change in rock competence "lithology".**

### *7.1.2 Diagenesis*

This section describes the distribution of diagenetic changes in both time and space. These alterations of the rock matrix impact the reservoir properties in three ways: (1) directly, by changing the porosity and permeability; (2) indirectly, by altering the pre-fracturing mechanical properties of the rocks, and hence affecting the fracture

distribution and thereby the fluid flow; and (3) by adding cement to fractures or by dissolving previously-cemented fracture fillings. Thus, diagenesis has the potential to be as important, for reservoir performance, as are the primary deposition and the fracturing. Although there is evidence (given below) that supports these possible effects from diagenesis in north Oman, there has been very little direct work aimed at constraining the timing or conditions of diagenesis based on petrographic data, dating, or fluid-inclusion studies. If the diagenetic history was to be fully examined, the conclusions of that work could help to constrain the fracture story. Wagner (in Droste et al, 2004; shown in Figure 2.44) provides a regional foundation for this analysis.

In order to facilitate the description of diagenetic events, it is useful to define how certain terms are used herein. It is commonly assumed (Hasiuk and Lohmann, 2008; Mark et al, 2007; Sattler et al, 2005) that carbonate rocks experience an initial lithification event within a few meters of the depositional surface, and that concept is accepted here as having general applicability (although there is no direct evidence arising from diagenetic studies of these rocks). Because carbonate sediments can fill their accommodation space, slight changes in sea level can lead to subaerial exposure and the influx of meteoric waters. Thus, meteoric diagenesis may occur, and will generally be represented by leaching of the less-stable mineral components. Meteoric diagenesis can extend into the subsurface, depending on the hydrogeological regime. During burial, additional leaching and cementation can occur as the stability of mineral constituents is altered due to thermal changes and alterations of the porefluid chemistry. Burial diagenesis can therefore produce either increases or decreases in the petrophysical properties. During continued burial, warmer porefluids from depth can migrate towards shallower regions, with the possibility for moderate or large temperature differences. The fluids are often not in equilibrium with their new host rocks, and leaching can occur during such hydrothermal diagenesis. Finally, after fracturing, minerals can precipitate within fracture openings, leading to post-fracture cementation.

Southeastern region:

This area includes Qarn Alam, Habur, Ghaba North and Al Ghubar fields. In this region, as noted above, only Lower Shuaiba is present, and the impact of early meteoric diagenesis is minimal. However diagenesis (both leaching and cementation) is quite strong in this region. The leaching is most common along intensely-fractured fault zones and in fracture corridors (Figure 7.14). The zones affected by diagenetic alterations are normally wider at the top of the Shuaiba, indicating that they formed at a time that post-dates the deposition of overlying Nahr Umr. It is convenient to suppose that the leaching is due to hydrothermal fluid that rose along the conductive fracture networks to the top of the reservoir where it encountered the shale and spread laterally to a greater distance. Some of the faults and corridors are affected by this leaching, while others are not, as shown from the evaluation of the BHI of Qarn Alam fields

(Chapter 3: Figure 3.53). One possible explanation for the occurrence of leached and not-leached cases is that the fracturing (or faulting) occurred at different times, pre- and post-dating a single porefluid expulsion event. It is likely that the leaching indicates preferential flow paths. That circumstance could be caused by larger-scale connectivity issues, but it could also be related to self-organization in the fluid flow. Studies of basin-scale hydrogeological systems (Raffensberger, 1996; Fleming et al, 1998) suggest that buoyancy-driven flows (even at small temperature differences) can choose certain of the available flow paths to achieve better efficiency in terms of thermal transfer. It would be good to examine these concepts in terms of their potential applicability to the cases observed in the southern region of north Oman. An example of this leaching was noted in the top 10m of the Shuaiba of Qarn Alam field (Vahrenkamp et al, 2000). In those cases the leaching was interpreted to be a karstification implying an exposure event. However, a re-examination of the borehole data suggests that the leaching is more likely to be of the hydrothermal type and not due to karst processes. The basis for this view is that there is no consistent pattern of top-Shuaiba leaching in this field. For example, consider BHIs from wells located close to one another (e.g. QA-16H1 and QA-20H1, which are less than 40m apart) that do not have the same leaching evidence, and where the putative karst zone is not correlatable, even on wireline logs for additional nearby wells (Figure 7.15). In addition, recent work (Hadhrami et al, 2006) has shown that karst is not present in the nearby Huqf outcrop. Furthermore, the cuttings from around 800m of AG-16HST2, a horizontal well drilled within the top 5m of the reservoir (Dhahab, 1998), showed a soft oil-stained limestone that is probably leached alternating with a tighter unstained limestone. These all hint to a lack of correlatability of any leaching, and instead support a leaching concept based on hydrothermal fluid using faulted and fracture corridor zones. This burial leaching can be very extensive and might explain the high losses encountered in the fractures seen in Ghaba North, where in GN-26H4, over 60m3 mixed mud and LCM (coarse mica – losses treatment) together with over 20 sacks of calcium carbonate were pumped down hole to close the fractures yet this treatment failed. This well was shut in straight away because of high water cut over 98% indicting connection to the water aquifer.

There is also another phase of diagenesis, which reflects a cementation of most of the fractures near and below the OWC. The cementation may cover both the matrix and the fractures, but it is readily noted in the fractures. With respect to the matrix, this diagenetic event results in a slight degradation of the matrix porosity with depth in all those fields shown in Figure 7.2. In terms of the fractures, the cementation is very evident in Qarn Alam where most of the deep fractures are cemented (Figure 7.16).

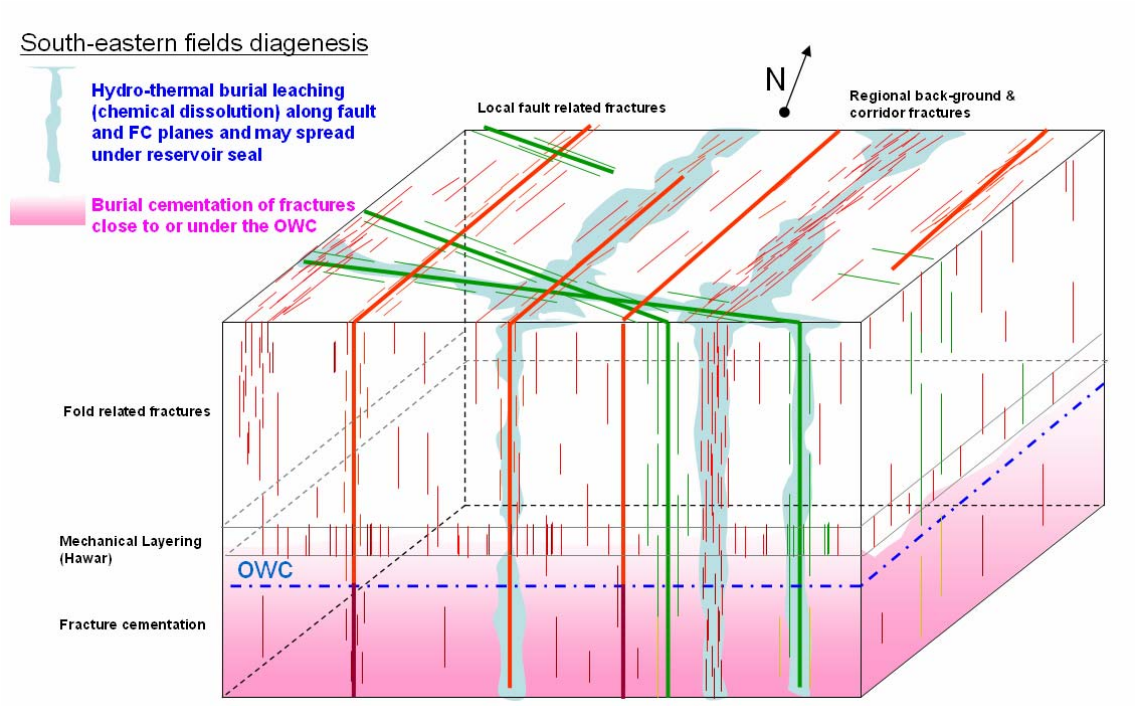


**Figure 7-14 A schematic cartoon proposed the morphology and nature of the diagenesis seen in south-eastern fields of north Oman. A burial leaching along intense fault planes (light blue) and a burial cementation below the OWC (light pink).**

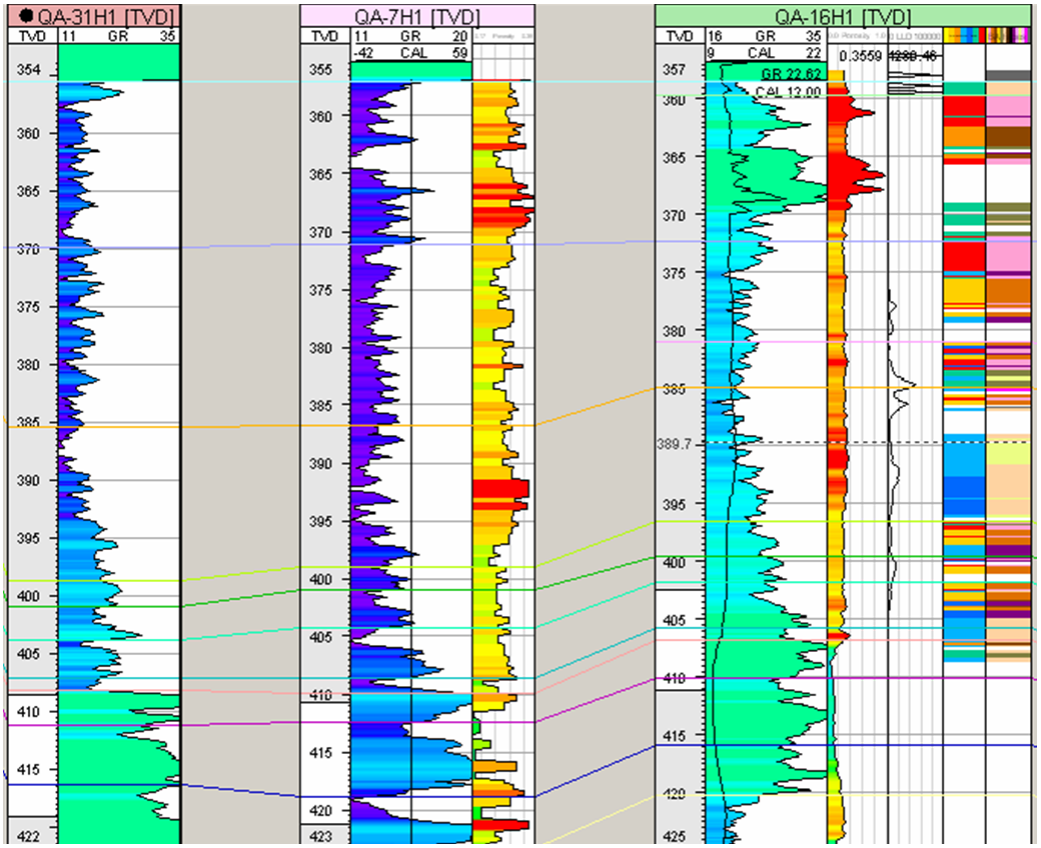


**Figure 7-15 GR logs of crestal wells in QA showing no correlation with at top reservoir, dismissing a top karst continuous layer in the top of Lower Shuaiba. Note how the lack of correlation in GR as the kast was assumed to result in having traces of the Nahr Umr Shale dropped in and hence slight increase in its value as the case of QA16H where those traces had been seen in the core and picked up by the rise in GR at the top of the reservoir.**

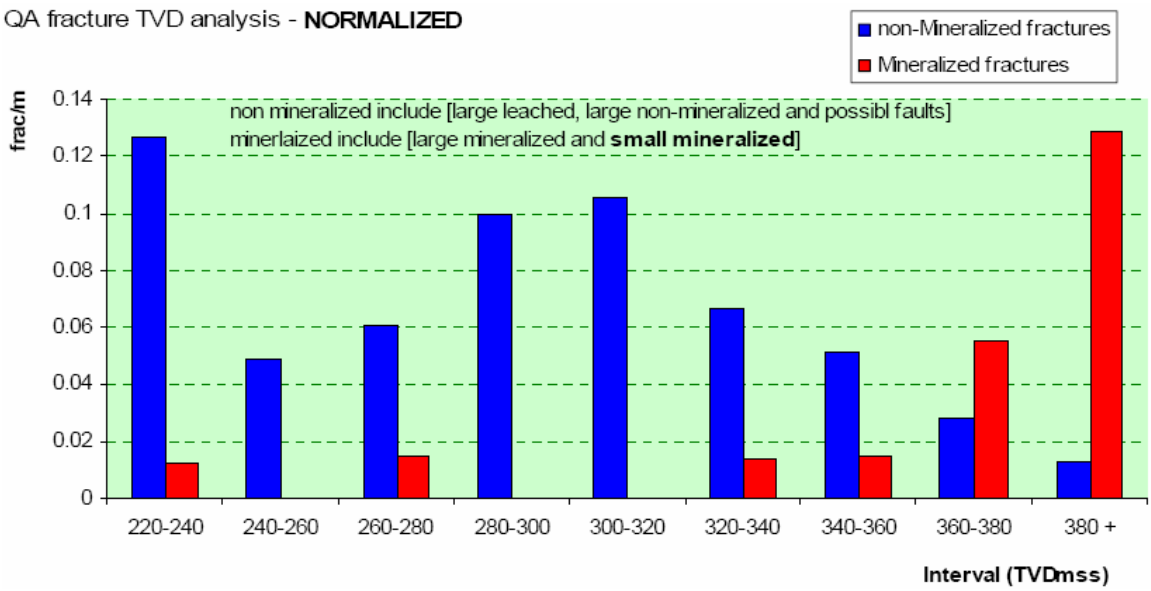


**Figure 7-16 Sudden rise in BHI non-conductive "mineralized" fractures with depth in Qarn Alam Shuaiba indicating burial cementation of the fractures below the OWC at 368mss.**

Central region:

This area includes Musallim in the Makarm High, Saih Rawl and Burhaan to some extent. Again in all these fields, only the Lower Shuaiba is present. The diagenetic alterations in this area are rather simple, and, according to Wagner (see Chapter 2), only meteoric diagenesis is present in the Makarm high area. The diagenesis affects the fracture network in that it resulted in the cementation of most of the NW-WNW faults and their associated fractures. A clear example of this is in Musallim field (MLM-2HST) where the well trajectory encountered a NW- WNW fault. MWD and cuttings showed that the fault zone consists of a cemented fractured zone whose width is close to 200m (Chapter 3: Figure 3.87). In addition, sub-regional seismic amplitude maps usually reveal this fish-net pattern of NW-WNW faults due to their cementation, which makes them denser than the nearby matrix and hence leads to variations in acoustic properties. Another effect is related to a possible control on the lateral distribution of the fractures due to the pre-fracture matrix diagenesis. This is perceived to have happened at the high structural crest of the reservoir before it was tilted. Now, in these central fields (even reported in Al Ghubar field), the high matrix porosity areas are offset to the southwest of the crest of the fields as the case in Musallim (Figure 7.17). Warrlich and Richard (2004) observed that the wells in the less porous areas are characterized with a greater number of large conductive fractures and high water cut but low gross production (e.g. MLM-4H2), compared to the more productive high porosity areas (e.g. MLM-2), which contain smaller numbers of large conductive fractures.

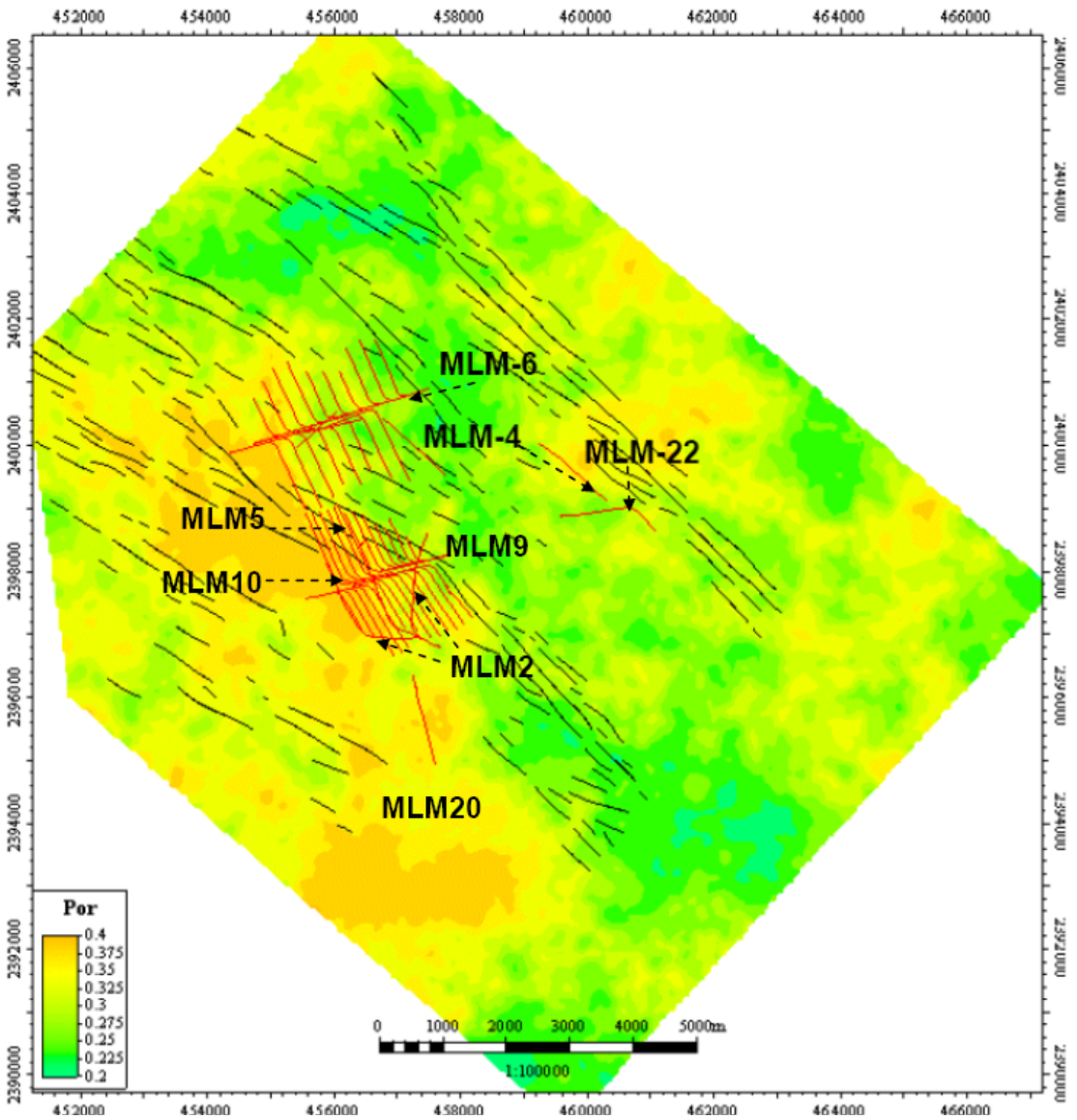


**Figure 7-17 Musallim Field, average porosity of the top 5m of Shuaiba reservoir, showing the NW-WNW faults (Warrlich and Richard, 2004) and the offset of the high matrix porosity areas SW of the crest of the field.**

The Bab Basin region (north):

The effect of diagenesis in the northern region is intensified due to the presence of the strongly-layered Shuaiba. The region suffered a complex meteoric leaching followed by burial leaching and cementation. The impact on the fracture network at Yibal cannot be assessed here as NO BHI data is available. For Al Huwiasah, the impact of diagenesis on the matrix is very distinctive but complex. It resulted in the creation of a large area with very vuggy rocks within the northwestern flanks of the fields. These were picked from BHI and cores. It is not possible to analysis and assesses the impact of diagenesis on fractures in Al Huwaisah due to the unavailability of data. Lekhwair and Dhulaima fields, which probably experienced the same diagenesis processes as Yibal and Al Huwaisah, but with more intensive burial leaching due to their proximity to the center of the Bab Basin, reveal that at least two phases of diagenesis has occurred. The first is the possible leaching of the cemented NW-WNW faults and their associated fractures. This may explain the odd situation of having the NW-WNW faults conductive in these

fields and being non-conductive in the central Makarm high area. The other type of fracture related diagenesis is the possible cementation of the fractures close to the OWC (Figure 7.18), as noted above for the southern area. This cementation is inferred from a few wells seen in LAN and the BHI fracture cumulative frequency versus depth plot for the whole of Lekhwair fields.

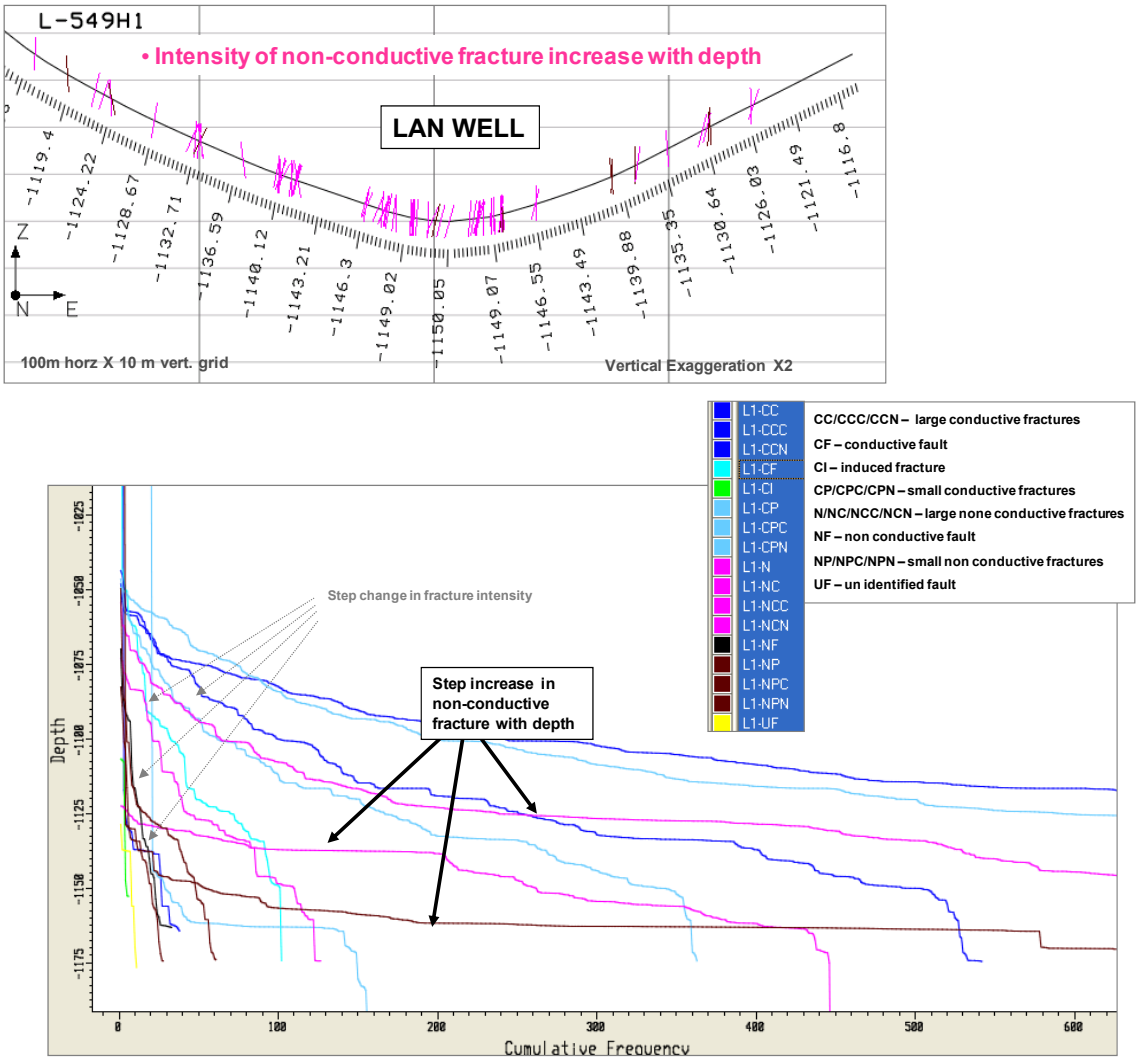


**Figure 7-18 L-549H1 shows possible increase in non-conductive fractures with depth together with cumulative BHI fracture frequency versus depth plot for the whole of Lekhwair A/B/C/D fields showing similar trend of rise of non-conductive fractures with depth.**

Natih Formation:

There are few data available to me to assess the impact of diagenesis on the fracture network of Fahud, Natih and Al Ghubar Natih E fields. However, as mentioned by Wagner, burial hydrothermal leaching is evident along fault planes in all these fields. In addition, as shown in Figure 7.12, cementation of both matrix and fractures might have happened in these fields. The conductive nature of most of the NE fractures of north Oman can be attributed to the diagenesis process (burial leaching), but also the role of having a NE orientated maximum horizontal stress in the region nowadays may had helped in making these fractures mechanically open.

Figure 7.19 is an attempt to summarize the impact of both matrix and matrix diagenesis on the vertical and lateral distribution of the fracture network of north Oman Cretaceous reservoirs. It is essential to mention that these effects are much less than the main controlling factor on the fracture network distribution and intensity, which is the tectonism of the region.

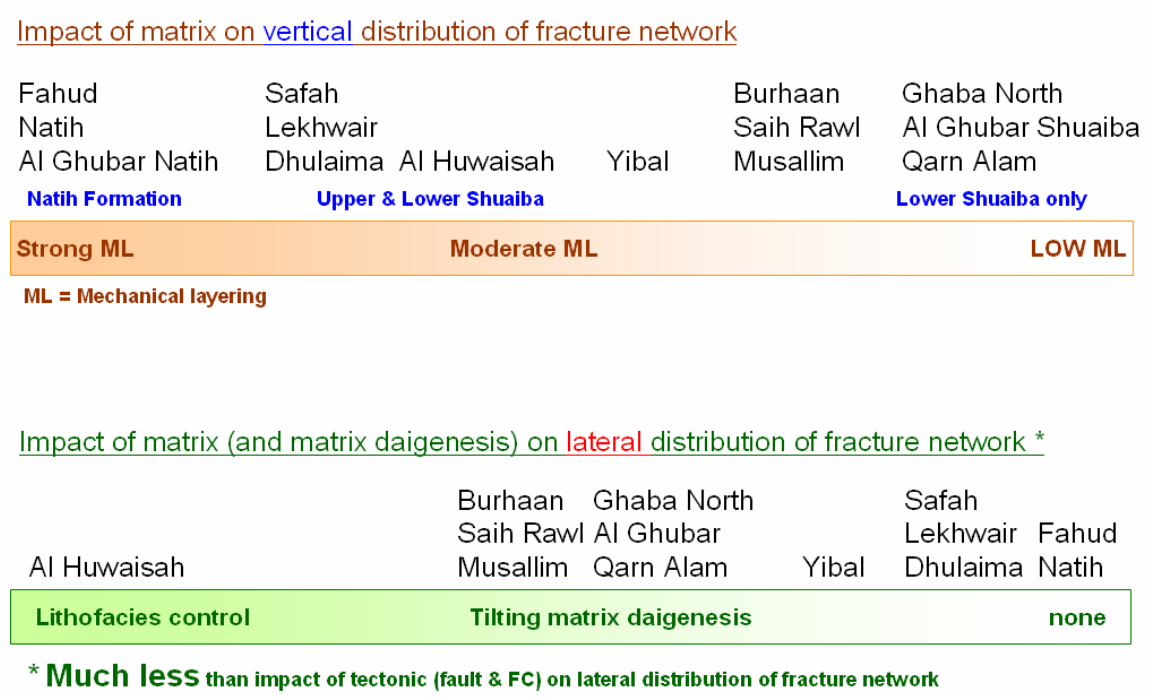


**Figure 7-19 An attempt to qualitatively summarize the impact of both matrix and matrix's diagenesis on the vertical and lateral distribution of the fracture network.**

## 7.2 Fracture network genesis

The main controlling feature on the distribution and the intensity of the north Oman Cretaceous fracture network is the tectonism. This is basically the result of the Alpine I Cretaceous deformation and the Alpine II Tertiary deformation.

The Cretaceous deformation has resulted in the generation of a regional set of NW-WNW strike slip faults (Filbrandt et al, 2006) extending from the Huqf area all the way to UAE. In addition, in areas where there is salt (e.g. the Ghaba North salt basin), the complexity allowed by salt detachment has resulted in intensified faulting and the creation of fault patterns that are not only orientated NW. The fracture BHI data of all the Shuaiba Formation fields support the presence of the NW-WNW sets, best examples are from the Makarm High (Musallim) and Lekhwair region. The NW-WNW fault-related fractures occur in damage zones with variable width, some reaching 200m as the case in MLM-2HST (Figure 7.20). The large faults are picked readily in seismic data but for the smaller ones, technique such as dip-azimuth maps and coherency may help in finding their locating them.

The Tertiary Alpine II deformation has resulted in the creation of most of the NE fractures. These occurred mainly as fracture corridors along with a level of background fractures. There are virtually no faults with this NE orientation (except in the salt region and Natih Field; see below), which makes it difficult to identify a clear tectonic process for the formation of the fractures. It is therefore not clear why the fracturing has been concentrated into fracture corridors or why they have the spacing that is observed. One possible scenario is to link their location to already existing basement or deeper faults or they just could have picked a simple discrepancy in the properties of the rocks representing a weak point, but that explanation simply introduces another question that does not have an answer (or data). The best evidence for these NE fracture corridors is seen in Fahud, though my analysis of the curvature of the local top Shuaiba map of Lekhwair A North indicate their possible presence there (Figure 7.21). One would suspect that these curvature anomalies are responsible for the fractures seen in Al Huwaisah too, where the fracture orientation (NE) is at odds with the NW fault orientation seen in the field (Nelson, 2002). This Alpine II deformation is also responsible for the creation of local NE faults seen in the salt based fields (e.g. Al Ghubar and Qarn Alam) and their associated fractures. The high intensity of NE fractures in Qarn Alam is possibly different from that of the Fahud fields. The latter reflects the presence of fracture corridors, which is most likely due to the Tertiary deformation as the Fahud field is much closer to the Oman Mountains. Whereas, in Qarn Alam the fractures are mainly caused by local faults related to salt movement related to the Cretaceous and Tertiary deformation (Figure 7.22). Nonetheless, presence of a few NE fracture corridors in Qarn Alam is possible. However, in both fields (over 200 km apart) background diffused NE fractures exist. These two sets of fractures – the NE and the NW-WNW – have also been reported in the Cretaceous reservoirs (Thamama Formation) in nearby fields of UAE (Gibson et al, 1993; Williams et al, 2000; Sirat et al, 2007). Figure 7.23 shows an example of an outcrop fracture corridor and how it may appear in the subsurface, thus providing a dimensional perspective of these features.

The last type of fracturing which can be attributed to tectonics is the fold-related group. As most of the Cretaceous fields are not usually highly folded, the percentage of this type of fracture is much less compared to the fault-related fractures or fracture corridors. The best examples of the fold-related types of fractures are seen in at the north-western and south-eastern edges of Fahud fields (see Figure 7.21) and in Natih field (Figure 7.24). Curvature analysis at large scale wavelength can help in picking the location of these fractures as seen in Qarn Alam, LAN and Ghaba North (Figure 7.25).

Based on the evaluation the BHI images detailed in Chapter 3 and the analysis above the current envisaged conceptual models for each the fields is as shown below (Figure 7.26). The fault-related fractures (mainly NW-WNW except in the southeast where it could be N to NE) dominate the north Oman fracture network in the subsurface. These

are followed by fracture corridors (mainly NE) more clearly seen in the northeastern region and most likely attributed to the late Tertiary deformation. Mechanical stratigraphy in these fields is dictated by the lithofacies but in general plays a major role in Natih Formation and the Bab Basin fields, where the upper Shuaiba member is present. The least common fractures are the fold-related fractures. This is attributed to a lack of extensive folding compared to what is seen for instance in the Oman Mountain outcrops.

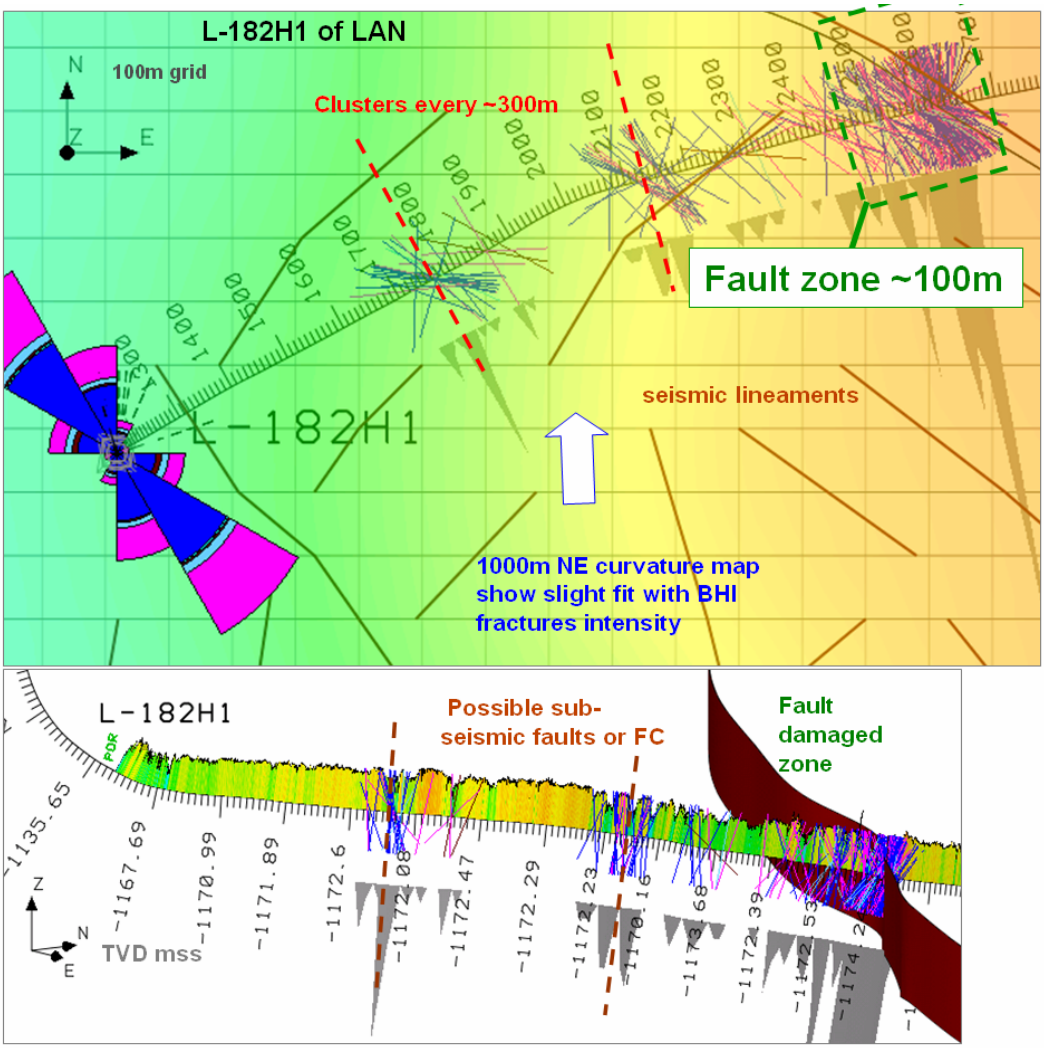


**Figure 7-20 Fault related fractures associated with the NW-WNW strike slip regional faults of north Oman, example from LAN (map view and cross section of L-182H1). Note how the damage zone width is variable: 100m in the large seismic faults and few meters in the sub-seismic faults.**

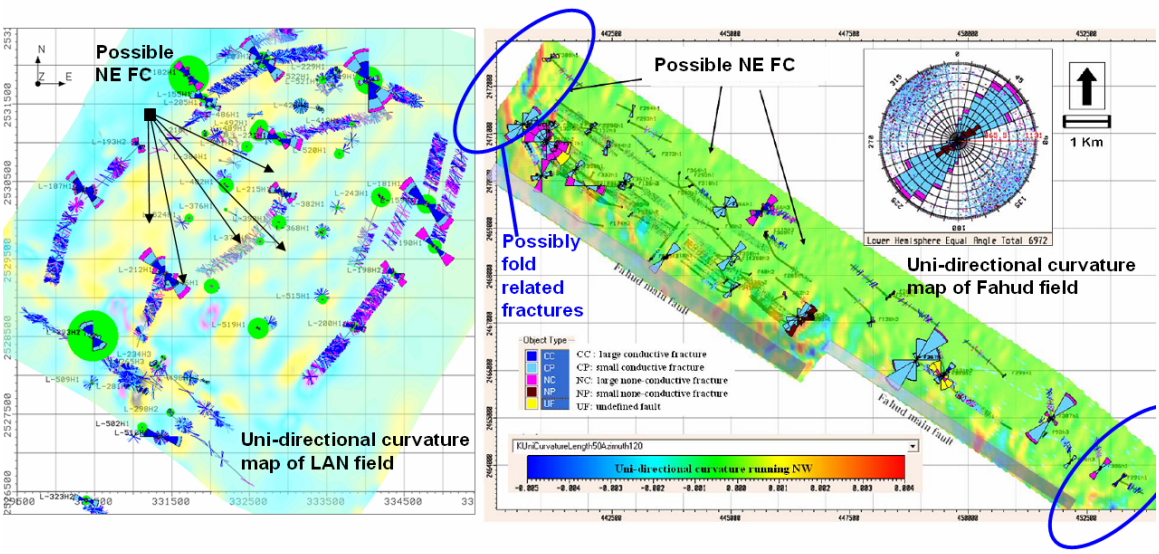


**Figure 7-21 Uni-directional curvature maps at small wavelength value helps a lot in picking possible locations of NE fracture corridors (FC). The left image show that even in the NW-WNW dominated fault and associated fractures of Lekhwair A North (LAN), NE fractures do exist and possibly occur in FC. Whereas, in Fahud (right image), where the main fault trend is NW (e.g. the southern bounding main fault), the fractures are running NE and well data analysis hints toward FC and the curvature map shown above may help in picking the location of these FC. These two fields are more than 200 Km apart.**

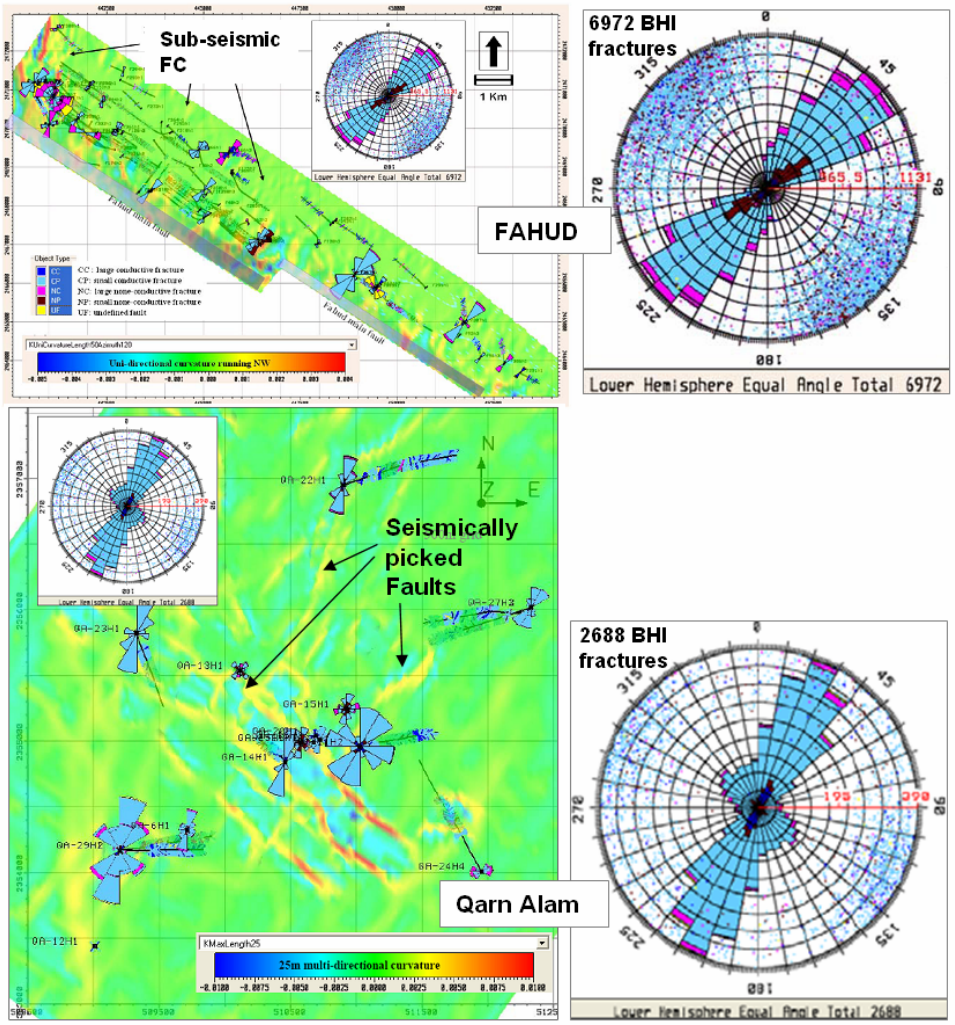


**Figure 7-22 The NE BHI fractures of Fahud fields are mainly fracture corridors whereas the NE BHI fractures seen in Qarn Alam are mainly fault related fractures.**

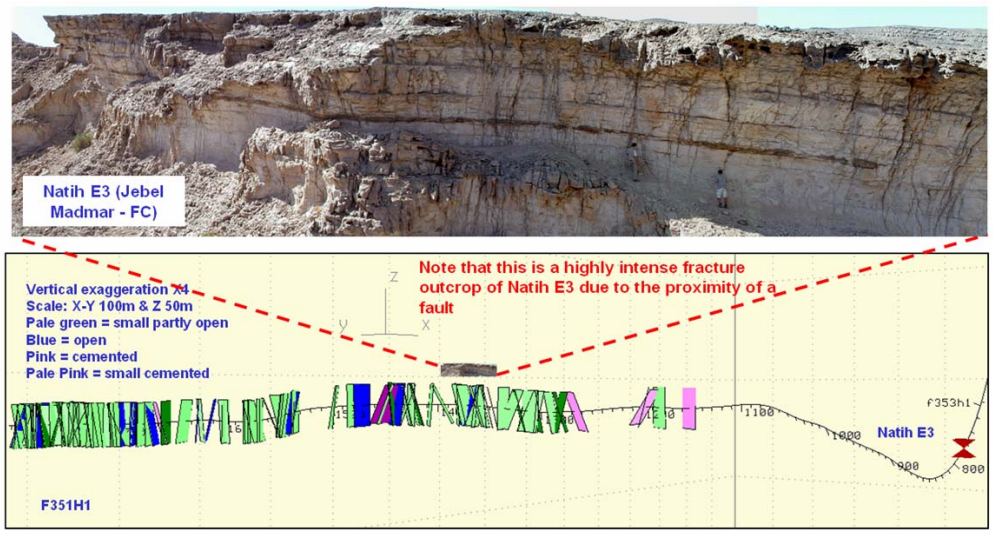


**Figure 7-23 FC picked in Jebel Madmar and how it may look in the subsurface BHI picks. This highlights the issue of resolution also when comparing core to FMI. In other word outcrop and cores see much more fractures than those picked in BHI.**

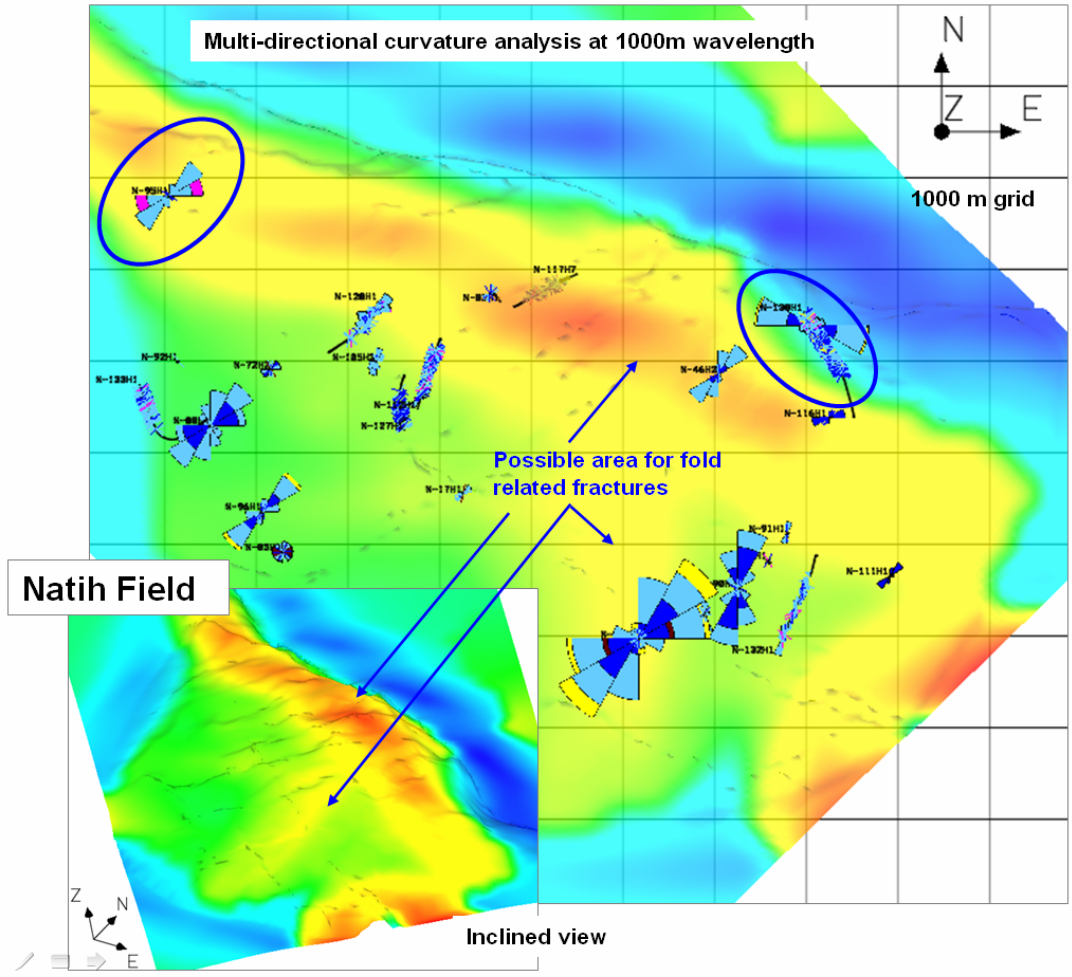


**Figure 7-24 Natih Field with a curvature map at large scale of top reservoir indicating possible area of fold related fractures close to the crest of the field.**

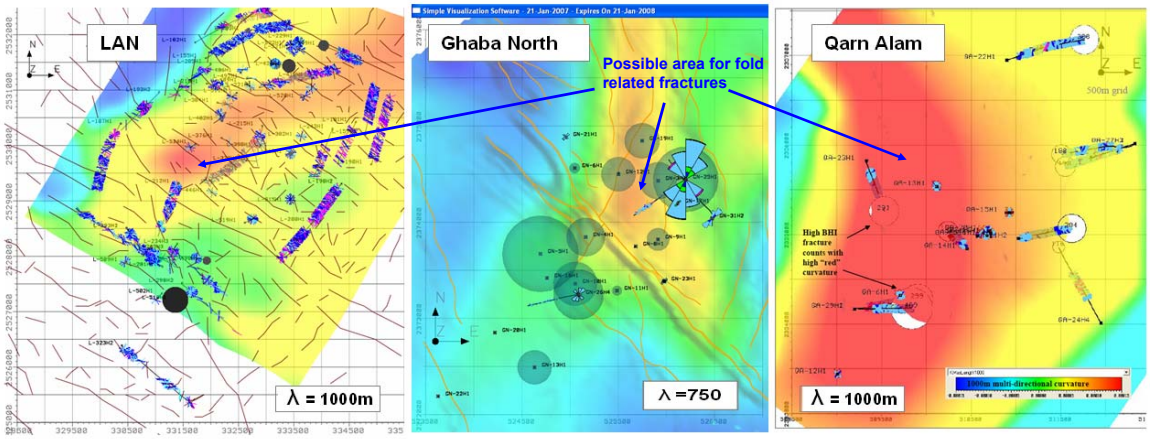


**Figure 7-25 Large scale curvature analysis can help in finding the locations for fold related fractures. In Qarn Alam field (right image) wells drilled in the western flank of the fields encountered more BHI fractures compare to the north flank even compare to the centre.**

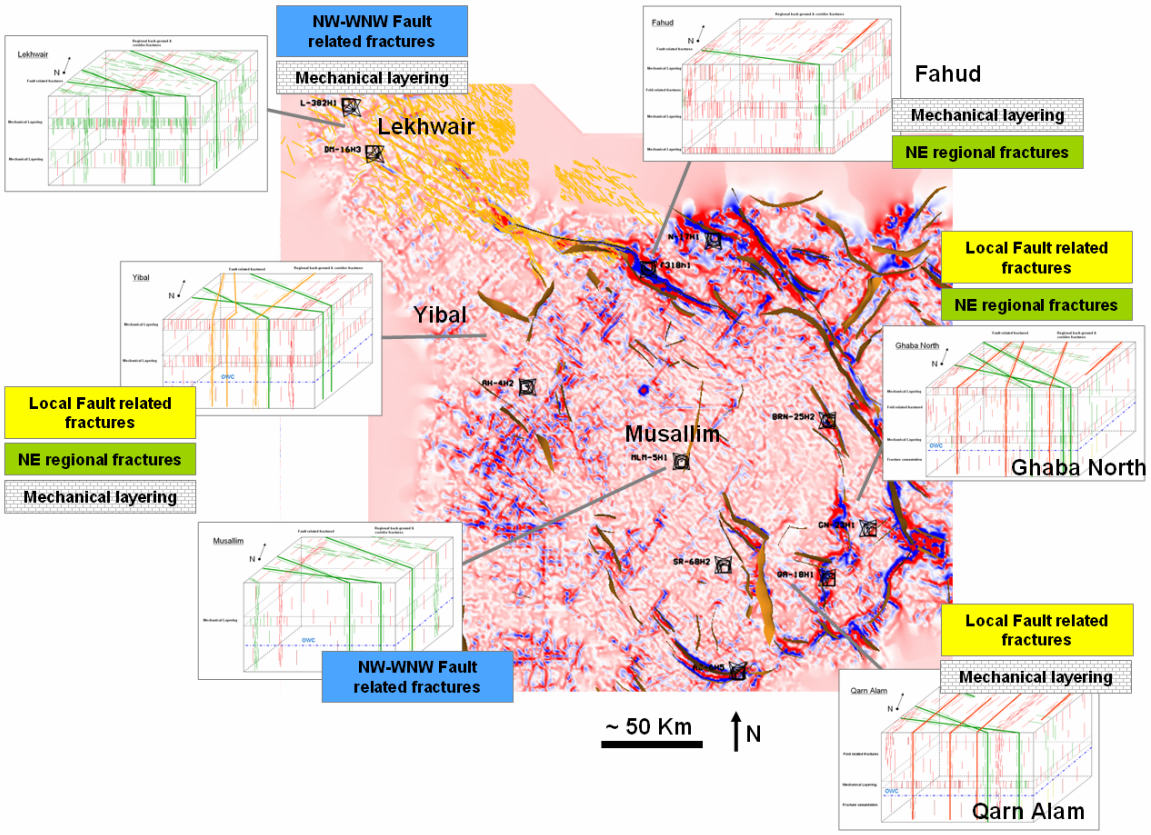


**Figure 7-26 Proposed conceptual model for the fracture network geometry seen in north Oman Cretaceous reservoirs per field, highlighting the main driving mechanism in each field or region (see APPENDIX II for enlarged image)**

In consideration of the above analysis, the following sequence of geological events (Figure 7.27) is proposed for the north Oman Cretaceous reservoirs. After the deposition of each of these reservoirs (i.e. Shuaiba and Natih) an early meteoric diagenesis occurred. Then after a period of time, and deposition of the younger Cretaceous overburden, the Alpine I deformation took place. This resulted in the creation of the NW-WNW faults, and their related fractures. A period of cementation occurred later on, that mineralized all these NW faults and fracture in the whole region. In the Tertiary the second phase of deformation took place (Alpine II), which had a number of effects: (1)

possible reactivation of some of the NW-WNW faults; (2) reactivation of salt-cored structures – which in turn generated local faults, some of which strike NE (as in south-eastern region of north Oman); and (3) the creation of NE-striking background "diffuse" fractures and, more importantly, NE-trending fracture corridors. The Alpine II event was strongest in Natih and Fahud fields. Deep-seated hydrothermal diagenesis followed which resulted in enlarging and enhancing the conductivity of the faults and fracture swarms around Fahud and Natih and in the south-eastern region around the Qarn Alam area. It also resulted in the opening of the previously-cemented NW faults and fractures in the Lekhwair area. Hydrocarbon charge probably started after the Alpine II event, as all the north Oman fields occur close to major faults as seen in the geological setting chapter. It is likely that the hydrocarbon charge needed the fault zones to be open in order to reach these reservoirs. A very late cementation process may have taken place after the hydrocarbon charge. Even-later tilting to the northeast, so not associated with foredeep flexure, resulted in offset of the high porosity areas to the SW of the structural high "crest" (presumably by a short-distance re-migration of the accumulations) in some of the fields in the central and southern regions of north Oman. This proposed sequence of events can be further refined with detailed diagenesis studies (e.g. fluid inclusions) and local detailed field based data.

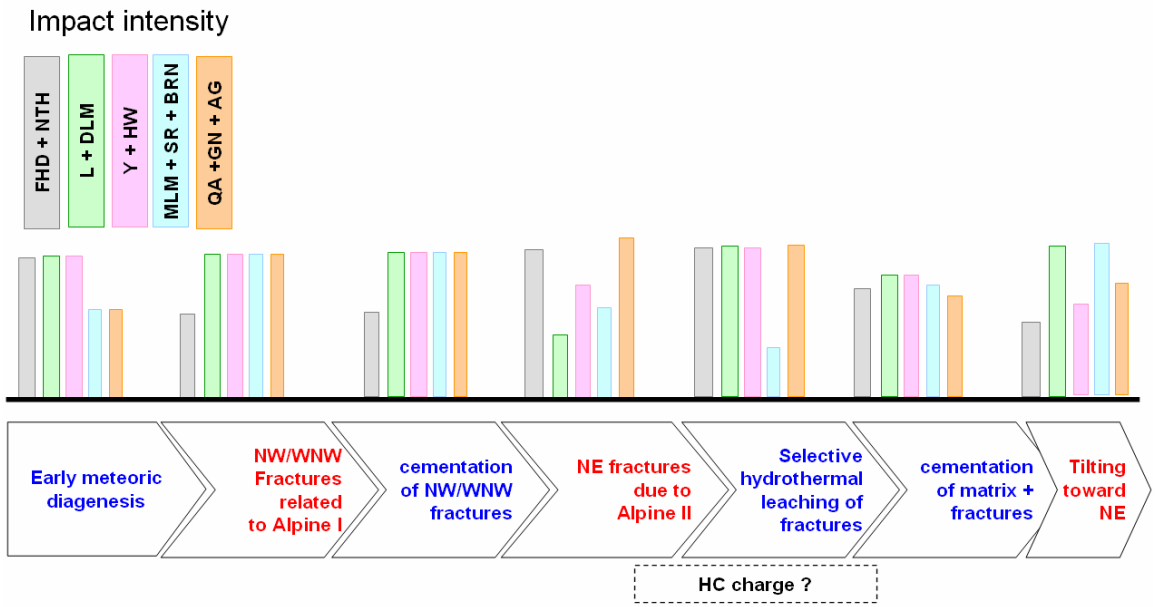


**Figure 7-27 Proposed geological sequence of events for north Oman Cretaceous reservoir together with a simplified chart showing relative intensity of impact of each even on each region (FHD + NTH = Fahud and Natih; L + DLM = Lekhwair and Dhulaima; Y + HW = Yibal and Al Huwaisah; MLM + SR + BRN = Musallim, Saih Rawl and Burhaan; QA + GN + AG = Qarn Alam, Ghaba North and Al Ghubar).**

## 7.3 Flow analysis

The section focuses on the dynamic (e.g. by considering flow responses) analysis of the interpreted fracture networks, with an emphasis on fracture characterization and correlation with observed flow responses more than on numerical simulation.

### *7.3.1 Full field production data*

The shape of the curve that depicts the full-field production rate versus time can be used as a first pass screening tool for fracture characterization. Of course, this after-production classification does not assist in the appraisal stage of a single-field development, but it does play a role in supporting a regional synthesis that is intended to underpin decisions concerning long-term exploitation schemes. In terms of these production profiles, fractured reservoirs usually exhibit a high initial oil rate (reflecting a phase in which the fracture network itself is emptied), followed by a sustained oil plateau rate that (reflecting matrix contributions to the production). In both stages, the fractures provide the essential permeability (thus, this response indicates a type II reservoir in Nelson's classification). If the fractures connect all the way down to an aquifer, then the decline in oil rate is usually followed by an influx of water, leading to a high cut and uneconomic operation (Figure 7.28). Due to the rise of water in the fracture system, the saturation distribution can be complex, with separate OWCs in matrix and fractures, as seen in the Natih and Fahud -Natih E and Qarn Alam fields. This assessment has been applied to the production profiles of the north Oman Cretaceous fields. It shows that it is possible to argue that the majority of the fields in north Oman are affected by fractures to a greater or lesser extent. There is, of course, a spectrum of responses, with the end-members being represented by Qarn Alam and Saih Rawl (Figure 7.29). In Qarn Alam, other field data such as seismic and BHI indicate the presence of faults and fractures (as described previously in this thesis), but the picture is complicated by the occurrence of leaching. Whereas, in Saih Rawl other field data such as seismic and BHI does indicate presence of intense faulting and open natural fractures. The digital production data for only the specific fields (i.e. Ghaba North Shuaiba and Lekhwair A North) are available for the thesis, for all the other fields I managed only to obtain view graphs of the total production history. The early stage gross production profile can be analyzed to estimate the fracture porosity. This approach assumes that the high flow rates of an initial spike are associated only with fluids located in the fractures, and that the volume produced then provides an approximation of the initial fracture storage. This method can be used to also estimate fracture apertures (see below), once fracture intensity is independently estimated.

Another way of identifying heterogeneity (such as fractures) is to examine the relative contribution to total flow for each well in a field. In an infinite and homogeneous reservoir, each additional well would increase the total production by an equal increment. If plotted on a percent-of-wells versus percent-of-flow diagram, that hypothetical case would indicate a straight line. In reality, that case would never exist, because reservoirs are finite, and due to incremental wells tapping into an already-depleted reservoir. Nevertheless, there is value in creating such plots for the whole region in order to gain a better understanding of the degree of heterogeneity of fields, from which inferences can be made about the role of fractures (if matrix heterogeneity can be separated).

For the north Oman Shuaiba reservoirs, an evaluation of reservoir heterogeneity has been completed during the Shuaiba asset study by Matsuura (Nicholls, 2003). Figure 7.30 shows the results of this evaluation. It indicates that Saih Rawl is the least heterogeneous (which can be interpreted as being closest to matrix-like production), and Al Huwaisah is the most heterogeneous reservoir. (Note that Qarn Alam data were not available for the Shuaiba asset study). For Al Huwaisah field, this heterogeneity is attributed mainly to the matrix. Thus, simple indicators of heterogeneity do not prove very useful for characterizing the importance of fractures in this region.

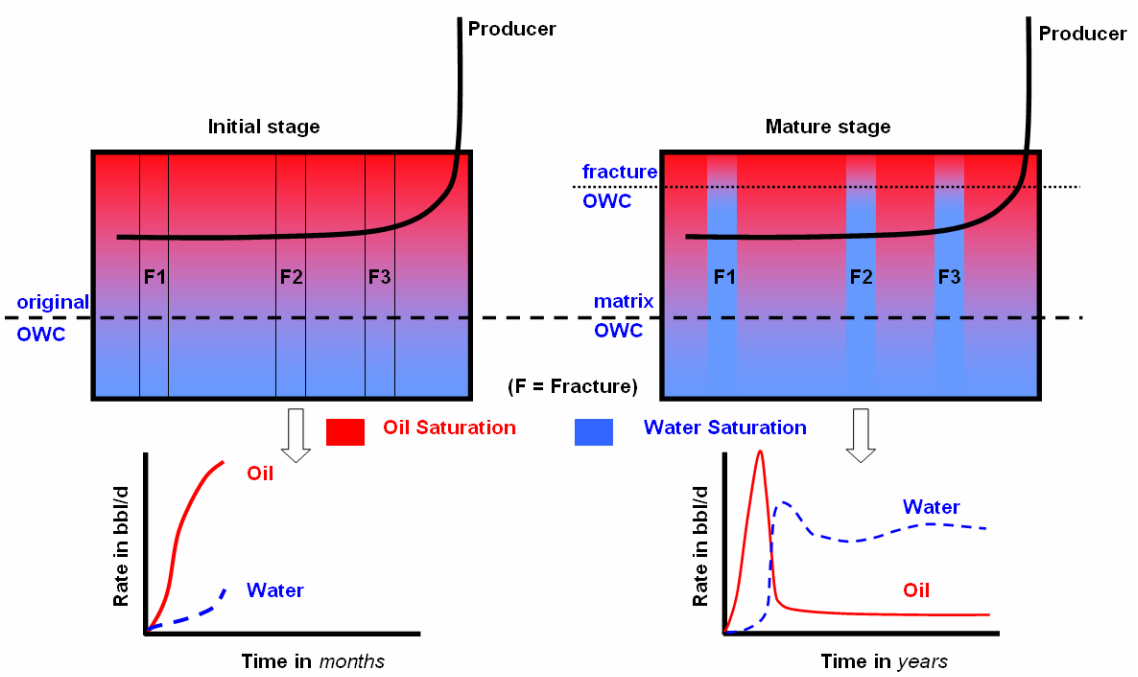


**Figure 7-28 A simplified cartoon illustrating impact of fractures on a reservoir's performance. Note that the width of the fractures had been exaggerated for the sake of illustration. At the initial stage the oil comes out of the fracture much quicker than the matrix (though matrix contribution is not zero) but once the fractures are empty the oil is produced from the matrix. If the fractures are connected all the way to the aquifer water rate will increase sharply. At this mature stage the amount of oil rate produced depend on matrix poroperm characteristics in a pure depletion development scenario.**

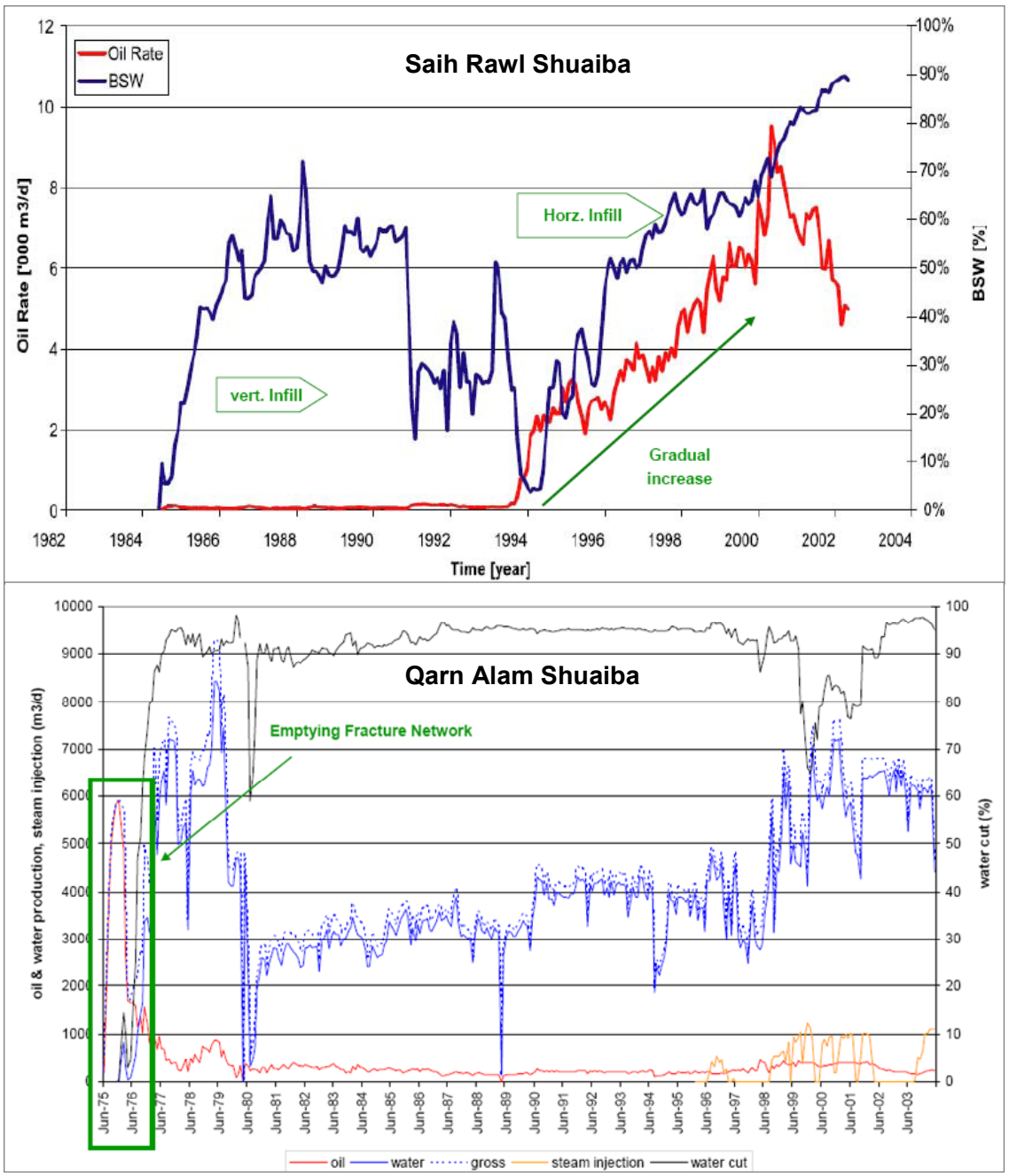


**Figure 7-29 Full field production profile for Saih Rawl showing a matrix like behaviour with gradual increase in oil rate, compare to a fracture like behaviour in Qarn Alam with high surge at the initial stage of production, followed by a long plateau.**

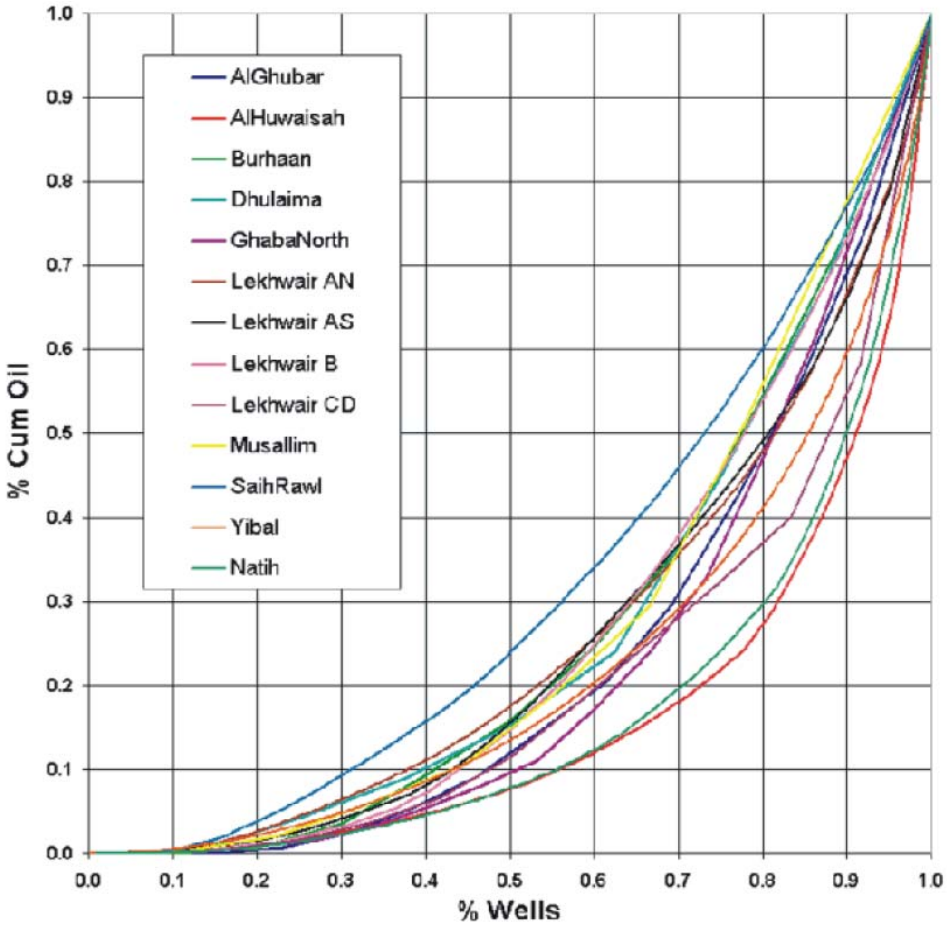


**Figure 7-30 Heterogeneity plots of Shuaiba reservoirs per field in north Oman. The curves show that Al Huwasiah represents the most heterogeneous field. Note that Qarn Alam is not included. From Matsuura, part of the Shuaiba Asset Study Phase I appendixes – These heterogeneity plots was first proposed as an approach for fracture analysis by Nelson, 2001.**

### *7.3.2 Well scale dynamic data*

The analysis approach involving flow rates is applicable at both full field scale and also at the well scale (i.e. individual well performance). The flow rates are likely to be easier to interpret at the well scale, since the full field scale flow responses are normally complicated by operational patterns, and potentially more heterogeneity and the resulting curves may not be as easily interpreted in terms of the type examples. Fewer of these issues should affect single-well analysis, but it can be challenging to obtain good records. In the case of the Cretaceous carbonate reservoirs of north Oman (and possibly as a common issue); the effects of diagenesis can lead to leached and vuggy regions whose flow responses can be difficult to distinguish from those caused by fractures. Unfortunately, data on individual well flow rates is not always available, and that is the case here, so it has not been possible to assess whether the production profiles of these fields could be interpreted in terms of local fracture systems. It is perhaps easier to assess fracture network contributions using dynamic data at the well scale as the area of investigation is more local and hence uncertainty on rock and fluid characteristics is narrowed. The best tool to be used for such analysis is the well test, as this investigates a moderate volume around the borehole. There have been many reports on how to

distinguish fracture behavior using well test results, such as that by Wei (Rawnsley et al, 2007) and Heber (1996). The assessment is much easier in the case of a fall off test in an injector as is the case represented for Lekhwair A North in Chapter 5. One of the main difficulties with well test information is that it needs a prolonged time to pick up fracture signatures in most fractured reservoirs. This is the reason, why most of the well test results from this region are inconclusive. Bubble maps are very useful in visualizing how the dynamic data from individual wells is spatially related to matrix and fracture characteristics, and in assessing the connectivity at different parts of a field. In this thesis these plots have been useful in understanding the connectivity network of Lekhwair and Ghaba North (Figure 7.31).

A good practice is to plot the normalized gross rate, i.e. the total (both oil and water) well production or injection volume divided by the duration the well was on stream. This normalization helps in making direct comparisons between wells, and eliminates the effects of operational interference such as shut in. For LAN the data have been useful in highlighting that the inter-well connectivity is high at the southern part of the field, and whenever a well crosses a fault (in this case NW to WNW trending faults). Whereas, for GN, the data – when integrated with other fracture related data – have shown that some of the production may not be associated with faulting and fracturing (as in the case for GN-5, which was drilled in a relatively tectonically relaxed area). These results suggest that matrix diagenesis and fracturing play roles in explaining the high normalized gross rates seen. The other well-scale dynamic data useful for fracture analysis is the pressure interference test. Flow results from these investigations can show the geometrical characteristics (mainly connectivity) of the fracture network. An interference test conducted in Ghaba North supported the NE orientation of the main fracture connectivity. This NE orientation is also seen in Thamama Formation in UAE (Gibson et al, 1993; Figure 7.32). Chemical tracers can also help in assessing fracture connectivity, although it is normally hard to reach a unique interpretation of the outcomes. This approach can only identify the direction of the most connective path, but it cannot quantify the properties. In PDO, tracer tests are hardly ever executed. Only one example is known to me, and that is from Fahud (shown in Chapter 3).

Production logs such as PLT/WFL and water saturation monitoring (e.g. TDT pulsed neutron log) are useful in determining high-k intervals in a well. These intervals can be caused by high fracture intensity, or by matrix effects (depositional or diagenetic). If the logs are integrated with other dynamic data, such as losses, and static data such as BHI analysis or wireline logs (e.g. resistivity logs, PEF log in water based mud and/or caliper), it can be possible to relate the high-k zones to fracturing. In PDO, PLT/WFL logs are not a common tool to run. In addition, they are limited by rig tank capacity, which can make it difficult to assess the full reservoir unit. Usually PLT can identify the first few fractures which contribute almost all the pumped fluid, thus the contribution of the subsequent fractures is hard to define. In Qarn Alam field (Figure 7.33, Dhahab, 2000) the WFL profile picked fractured zones that were seen in the BHI image for QA23 well, which is situated in a possibly highly strained area as shown from large

wavelength curvature map, which serves as a proxy for strain. For Ghaba North (GN), this integration of WFL log data with other fracture related data (BHI picks and wireline logs) has shown that the NE fractures are usually conductive (Figure 7.34). Water saturation monitoring in a mature field helps in identifying a fractured interval, but it is difficult to interpret this in isolation (i.e. the saturation data needs to be integrated with other fracture related data such as BHI). One way to differentiate between fractures and leached "vuggy" zones or simple depositional layers porous lithofacies using a TDT log, is to examine the general profile of the log (Figure 6.35). A continuous increase in sweep is characteristic of a leached matrix, while an erratic increase in saturation is more likely to be caused by fractures. However, in most cases high-k layers are usually thin, and some of the fractures, when occurring in a zone, will mimic the effect of such layers. When water injection is the main recovery mechanism, one additional dynamic log that might be useful in detecting fractures is the temperature log, assuming that there is a difference between the injected water temperature and reservoir temperature. The cooler water can advance rapidly along a fractured interval, thus disturbing the temperature profile. This effect has been seen in Saih Rawl (shown in Chapter 3).

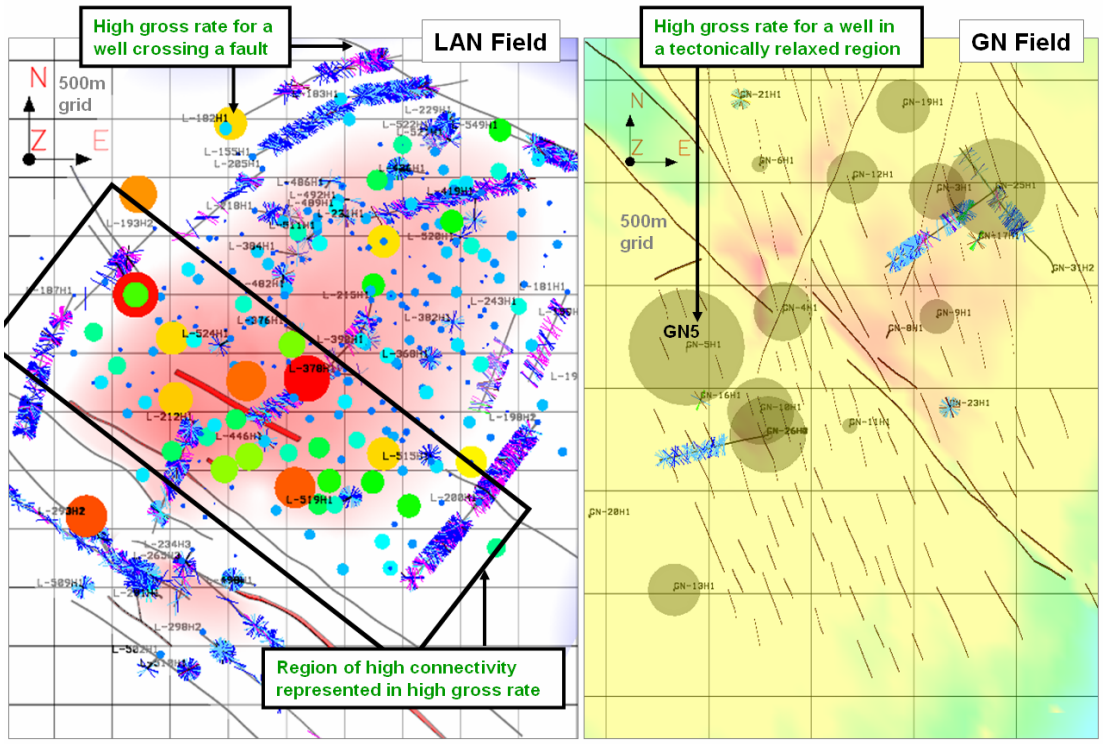


**Figure 7-31 Normalized gross rate (bubble "circles" seen in both snap shots) for Lekhwair field helped in finding regions of high connectivity and in confirming connectivity of some of the NW/WNW fault related fractures. For GN the integration of the dynamic data with static data such as faults map and BHI fractures had shown that some of the production might not be attributed to fracturing as the case for GN5, which was drilled in tectonically relaxed area.**

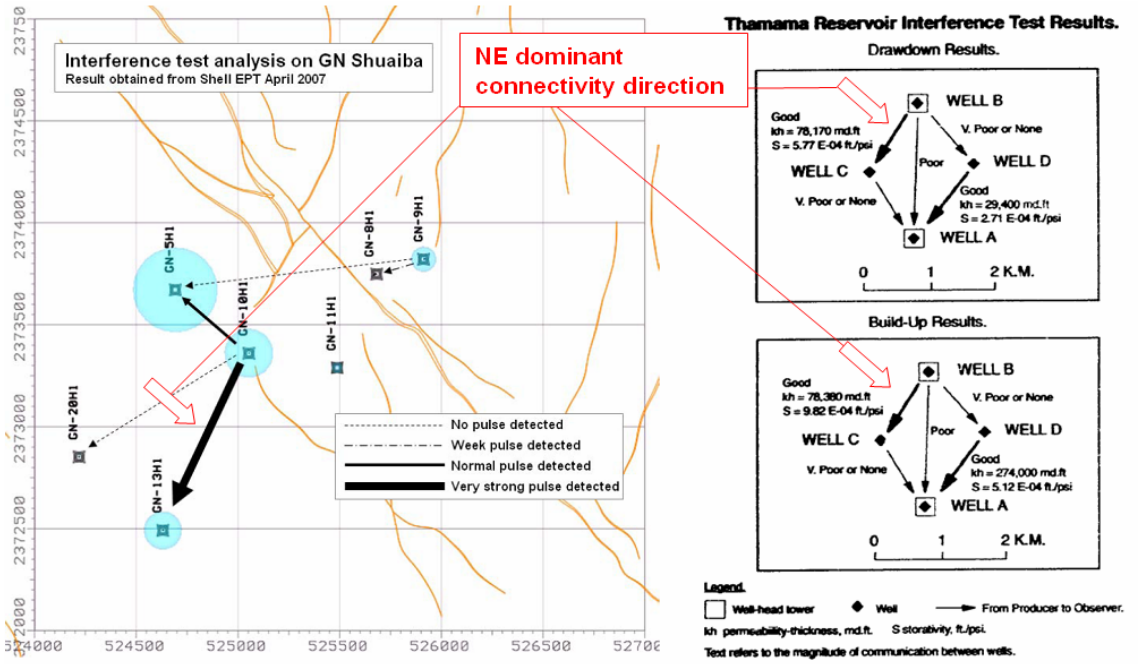


**Figure 7-32 Result of interference test in Cretaceous reservoirs of Ghaba North Shuaiba (Left) and in Thamama of a UAE field (right –Gibson et al, 1993), both indicating a NE dominant connectivity direction.**

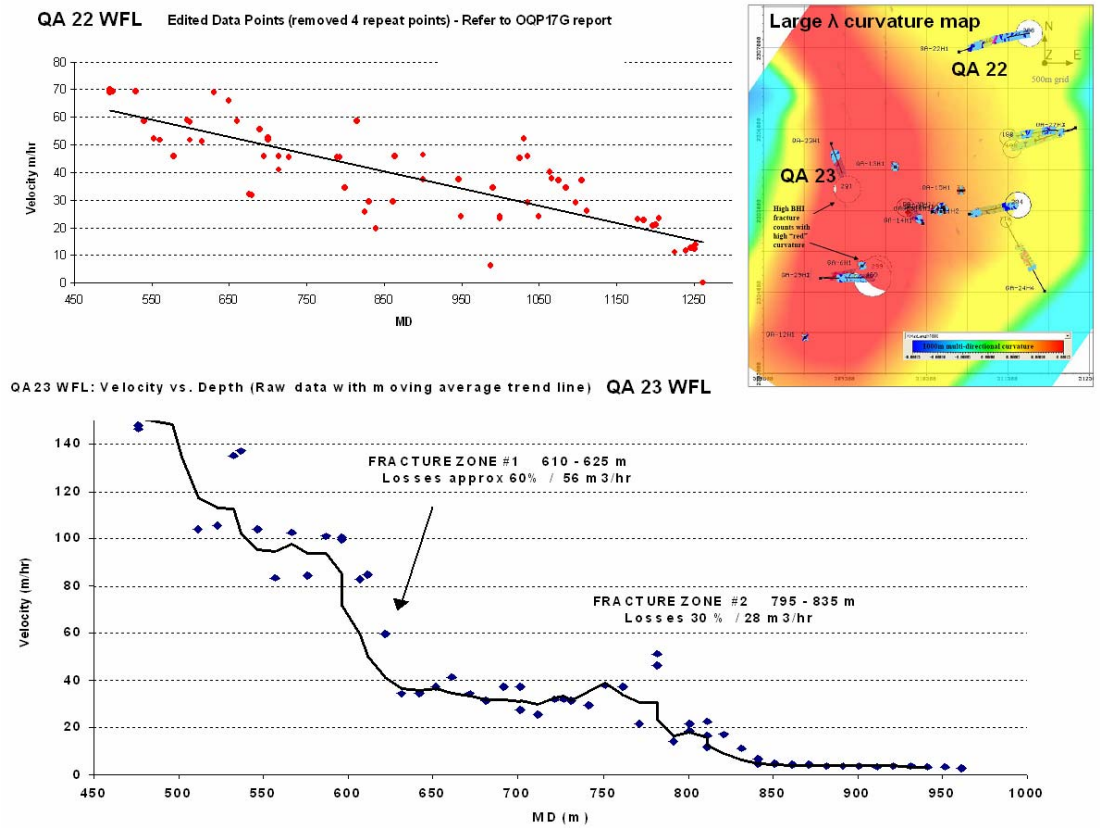


**Figure 7-33 QA22 and QA23 WFL profile hinting toward presence of fracture zone which resulted in sharp decline of velocity for QA23. For QA22 the WFL is hinting toward matrix profile (gradual decline). The logs were integrated with losses data and BHI images. Also shown (top right) curvature map at large wavelength as a proxy to highly strained area, predicting that the western flank of the field is more strained and hence more fractured.**

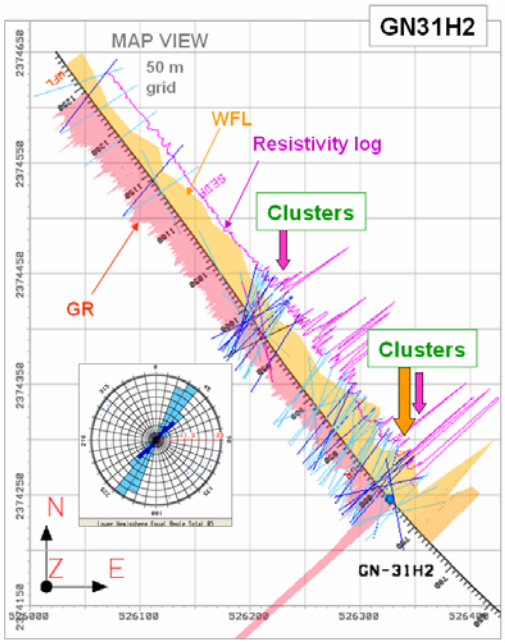


**Figure 7-34 Integration of WFL with resistivity log together with BHI fracture picks in GN31 is showing that NE fracture clusters are usually conductive**

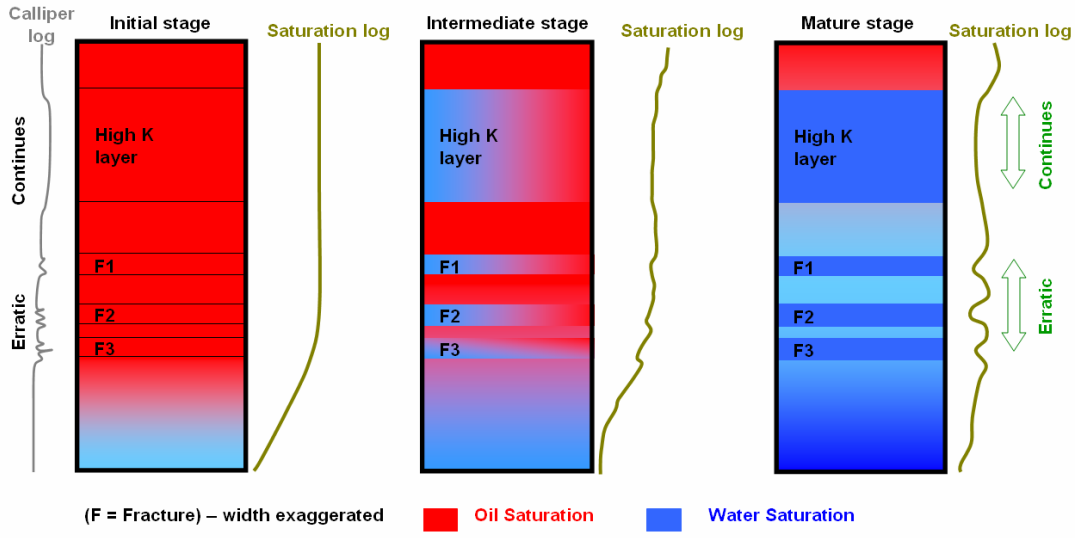


**Figure 7-35 A simplified cartoon illustrating impact of fractures on saturation logs at different stage of reservoir's life. It also illustrates a possible way to distinguish fractures from matrix response (high k streaks).**

### *7.3.3 North Oman fracture apertures*

In order to make use of a DFN, in terms of predicting flow responses, it is necessary to assign apertures to the fractures, thus allowing the calculation of an effective permeability. There are several approaches to obtain an estimate of aperture size in a fracture network. Overall, the methods can be divided into two: static based data (e.g. outcrop, core and BHI), and dynamic based data (e.g. well test, interference test and production logs). The aperture is controlled by both mechanical and chemical processes that took place at previous times, and by the current mechanical state. The mechanical process relates to the stresses that developed and these states might be different from one fracture type to another. For instance, extensional fractures might have different

apertures compare to shear fractures, and fractures with different orientations could also have different causative states. The chemical process relates to diagenesis and can either result in a reduction of aperture size in case of cementation; or enlargement of the size in case of dissolution or leaching. It is also worth noting that cementation can partially fill a fracture so that its aperture remains propped open in conditions where that would not otherwise be expected. Outcrop, core and BHI experience has shown that a single fracture usually does not have a constant aperture along its length. In the case of chemical process this is amplified when more than one diagenesis process takes place.

There are many limitations associated with determining aperture size based on static data (Bai, et al, 2000; Olson, 2003). In north Oman, the Salakh Arch and Huqf outcrops have undergone slightly different tectonic history compared to the subsurface oil fields of the Interior. For instance, uplift is much stronger in these outcrops compared to the subsurface. Hence the mechanical stress history experienced by the outcrops is different and subsequently the size of fracture apertures there. If outcrop data were to be used to estimate subsurface apertures, then errors might occur. Furthermore, most if not all the fractures in these outcrops are mineralized (Figure 6.36), which make it hard to determine whether the current aperture size would be the same, if there was no mineralization. As mentioned earlier, Mercadier and Makel (Mercadier and Makel, 1989) reported a variation in aperture size from less than 100 microns to 5 cm.

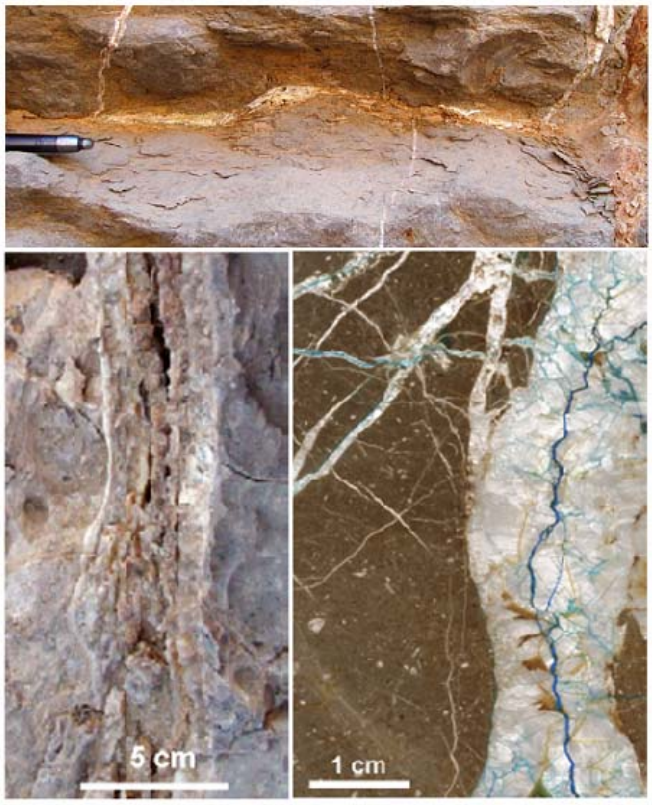


**Figure 7-36 Example of fracture aperture seen in Jebel Madmar Natih Formation outcrop (de Keijzer et al, 2004). Note how the size differs for every different fractures and how generations of fractures have been mineralized (bottom right).**

The BHI evaluation for fracture aperture also has its limitations. Since it is a pad tool there is a tendency to overestimate fracture apertures due to pressure applied by the tool on the rock surface while logging. Nonetheless, for the north Oman BHI evaluation, mainly done by Baker Atlas and Schlumberger, the BHI-interpreted apertures show large variations from less than 1mm to close to 1m (Figure 7.37). Another observation is that bed bounded fractures have smaller fracture aperture compared to possibly unit or formation bounded fractures in the Natih Formation (Figure 7.38). This could be also applicable for the Shuaiba Bab Basin fields which are strongly-layered reservoirs. A critical limitation for both core and BHI fracture aperture size determination, is the fact that it is not possible to know whether a large open fracture will continue being open over a large distance from the borehole, or if it will die out away from the wellbore.

On the other hand, dynamic-based fracture aperture determination can be of better value as these tests the actual connectivity of the fractures and their effective properties. However, deducing fracture aperture from a connectivity analysis is basically a backward mathematical calculation, where a certain relationship is assumed to link permeability to aperture. There are different equations addressing different reservoir architecture (Tiab et al, 2007; Leckenby et al 2005) but they all assume that the aperture is constant in size. An example of such a relationship is described in the simulation chapter:

$$K_f = A^3/12S \qquad (7.1)$$

Where $K_f$ is fracture permeability, A is fracture aperture and S is fracture spacing per cell along the grid direction. Note: SI units are used here i.e. aperture in meters, permeability in $m^2$ (conversion: 1mD = 9.89 $10^{-16}$ $m^2$) and spacing in meter. As seen from the evaluation of Ghaba North's interference tests (see Figure 7.32), the predicted connectivity on the test wells for the reservoir range from tens of mD in the E-W direction up to 60D in NE direction (between GN10 to GN13). In contrast, for Lekhwair A North, the well tests (build up and fall off tests) show an overall low effective permeability ranging from less than 1 to a few mD (Figure 7.39). The latter values may reflect the matrix properties more than the fractures noting that they had been acquired in the eastern flank of the field which is likely to be less fractured and more critically because in LAN the fractures are mainly fault related and hence if a fault zone is missed then the reading will be low. Furthermore, it is not clear from the report available whether or not these tests had been run for a sufficient time to see the effects of fracturing.

In summary, integration of dynamic data with other fracture related data can be a very useful diagnostic tool for fracture characterization. It is usually more complex while examining full field production data and off course less beneficial at an appraisal stage. However, at a well scale can be valid at both appraisal and mature stage of field development. At well scale, fracture's dynamic characterization tools have different

depth of investigation: Well tests gives deeper penetrating information compare to PLT logs or losses. It is normally quite hard to distinguish between high K thin matrix layers and fracture zones from dynamic data alone, but this distinction can be made easier if static data such as BHI are integrated. Fracture aperture is very heterogeneous in nature and seldom in constant size. The variation can be related to the origin of fracture (i.e. nature of fracture type such as extensional versus shear fractures); or due to the stress applied on the fractures (current stress and paleo); and due chemical processes (diagenesis) that affect the fracture over time. The latter normally result in having partially open fractures. Estimating fracture aperture from static based data is usually less reliable compare to dynamic data. These because the static data normally examine fractures at the well bore and assume a constant size away from the borehole. Though, the dynamic approach is a backward mathematical calculation, where a certain relationship is assumed to link permeability to aperture. As a recommendation both approaches should be used and tested as a sensitivity analysis.

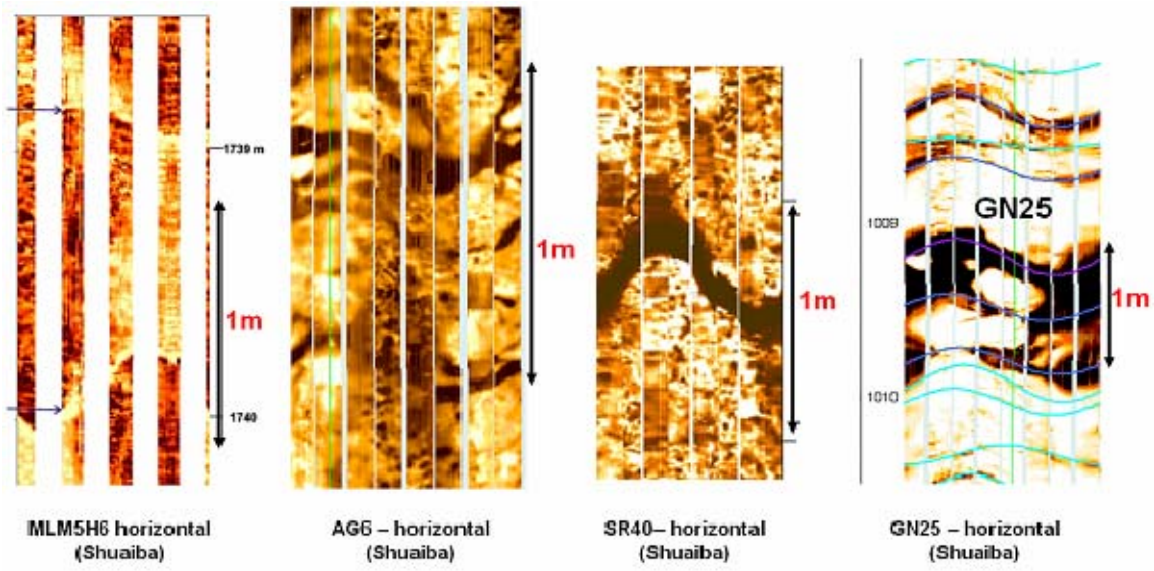


**Figure 7-37 BHI of several Shuaiba reservoirs in north Oman showing a large variation in aperture size. This variation is also seen even in individual wells within one field.**

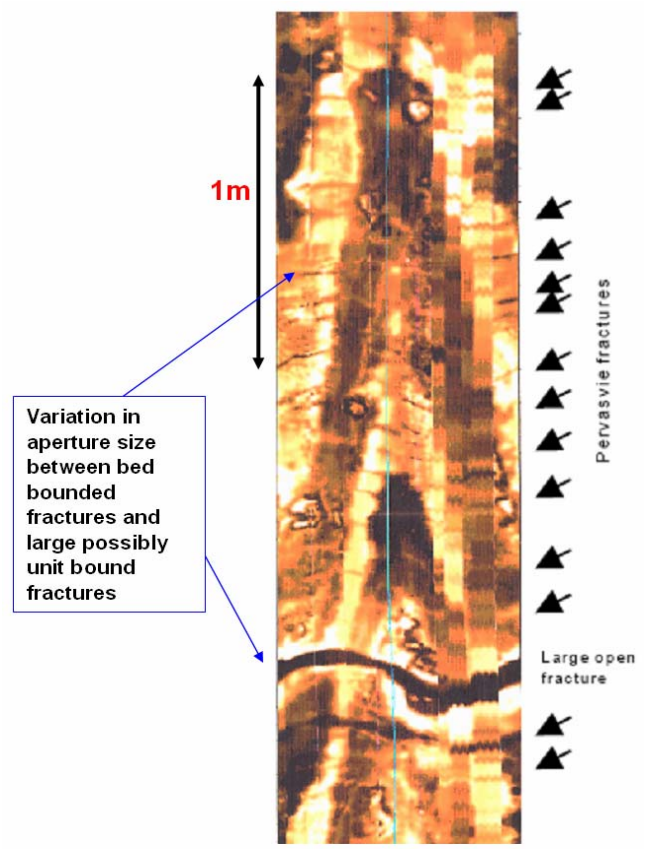


**Figure 7-38 BHI image showing different fracture aperture size for different type of fractures in Natih Formation in Fahud field.**

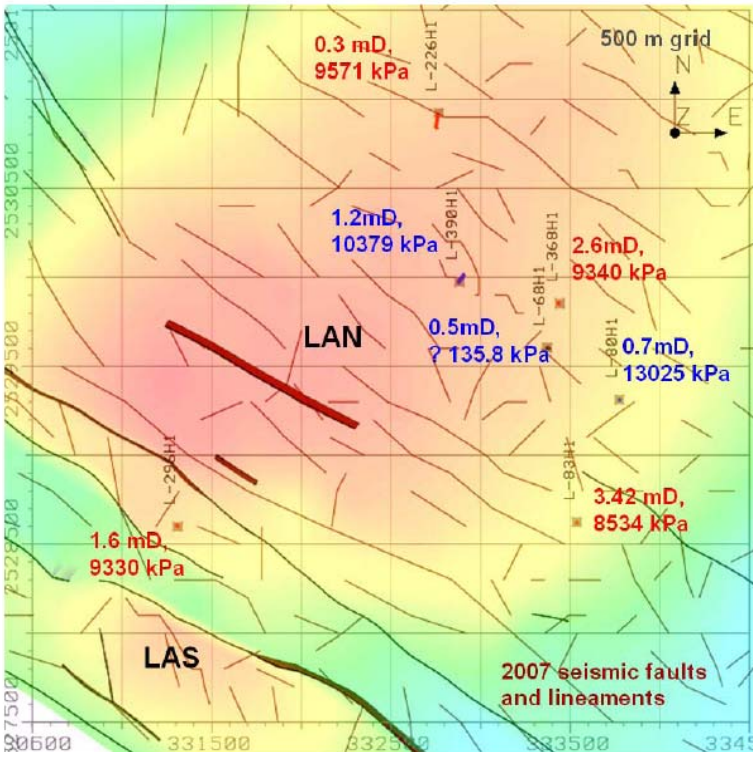


**Figure 7-39 Map of LAN showing the calculated pressure and effective permeability obtained from build up (red) and fall off (blue) test for Lekhwair wells, reported by Baker Atlas.**

## 7.4 Fracture 3D modeling analysis

The section focuses on the analysis of the 3D models created using both static and dynamic data, with emphasis on the latter.

### *7.4.1 Creation of 3D DFN in SVS*

The approached used in SVS to create discrete fracture network is based primarily on geological conceptual modeling. The conceptual model itself is based on detailed fracture characterization which uses integration of static and dynamic constraints. These can be data such as BHI or core fracture listing (fracture depth, azimuth and dip list), losses, well production data, well tests, wireline logs, core, curvature maps, seismic, etc; or concept such as sand box models and understanding of uplifts or outcrop analogue data, which can be uploaded to SVS as pictures.

The main objective is to reach geologically representative realizations and avoid data based stochastic modeling. Data based stochastic modeling normally honor well data and even simulation at full field scale, but it quickly collapsed when challenged with operational practices (e.g. where to encounter a fracture zone while drilling a highly deviated well with a specific orientation). In addition, it does not represent what is seen on outcrops. A good example of such data driven stochastic model is that of Qarn Alam field produced using ResFrac and NAPSAC in 2000 based on fracture drivers and indicators (Zellou et al, 2003). The model fitted the well data correctly but did not represent what is normally seen in outcrop (Figure 7.40) and did not highlight the fracture network heterogeneity.

In SVS the basis for the 3D DFN are the confining surfaces “horizons” which determine the upper and lower limitation of the vertical extent of the created fractures, as well as the orientation map, which determine the strike direction of the created fractures in each area. The area is normally represented by cells (Figure 7.41). Seed probability and propagation impedance maps dictates where the fracture seeds fall and get populated (Figure 7.42). The seed probability maps are normally filled either by painting for instance in case of fault related fracture, the faults and deciding on the width of the damaged zone; or can be filled, for instance from large scale wavelength curvature maps to represent fold or highly strained area in a field; or can even be filled manually. The orientation maps can also be filled by fault painting to let the created fracture follow the direction of the faults or manually or by using other lineaments.

The other controlling factors that decide the shape and intensity of the fracture outcome are specific input numbers: these include number of fracture per seed cell, fracture width zone “forbidden zone”; number of iteration for the seed population to take place, the length of each fracture, etc. To further explain this methodology, below is an illustration of how a fracture damaged zone is created in SVS. Let’s assume that the seismic faults are available, then the seed probability map can be filled by these faults,

and also the propagation impedance map (to stop fracture from growing outside the fault damaged zone). Now the width of the zone in such scenario is a function of the seed cell size, which can be altered manually by picking a different size or simple refining an existing seed map's cell size. By smoothing the seed map, the probability of fracture growing outside the faults is declined in a linear relationship with distance away from the fault, though one could simple just stick with the original painting without smoothing, hence having a sharp decline in fracture occurrence away from a fault zone (Figure 7.43). Another approach is to fill the probability from curvature maps at very low wavelength as shown in figure 7.42 fault example. The seed per unit area determine the intensity of fracture thrown in this high probability area, whereas the single fracture width zone "the forbidden zone" dictates the spacing between fractures within the damaged zone. The user can either create a single fracture set per orientation per layer per type (e.g. fault related fracture) or can create a combination. Normally it takes several iterations before landing on a fracture set that fulfill the requirement or represent the scenario needed. In addition, usually users end up with more than at least 10 realizations reflecting the uncertainty of the data available and the concept models they started with (Figure 7.44).

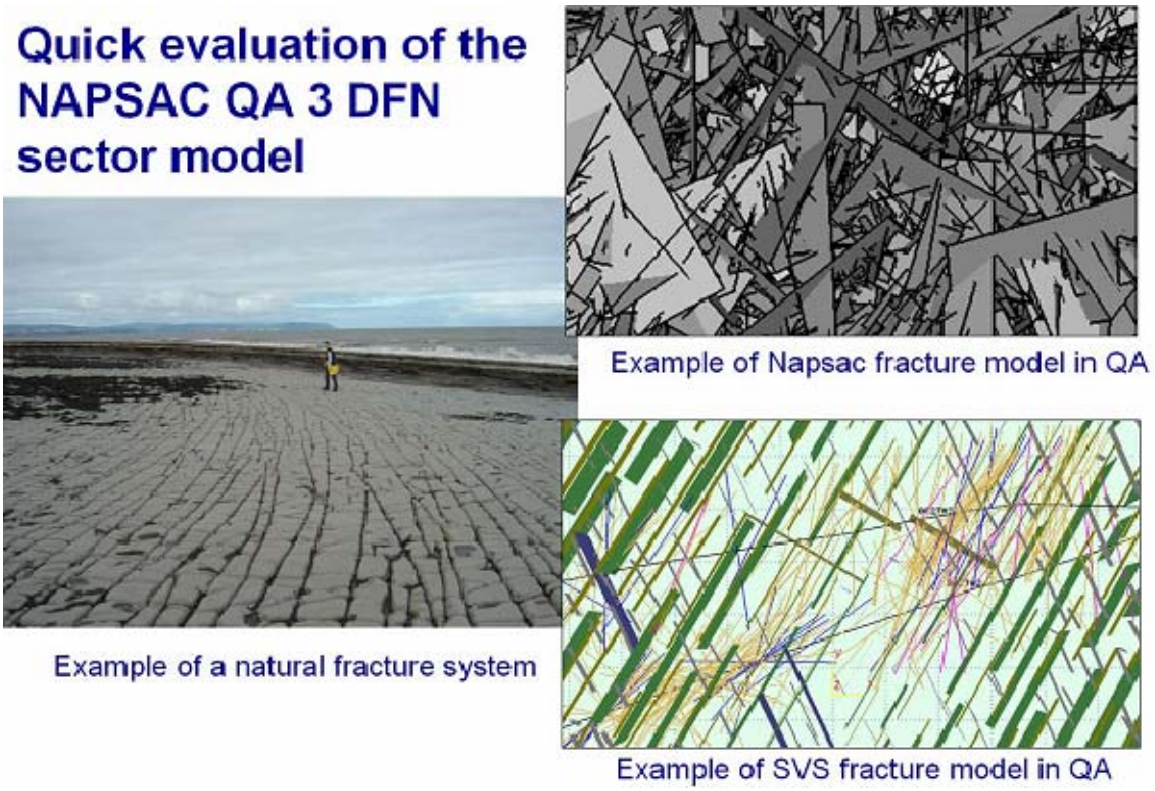


**Figure 7-40 A snapshot of Bristol Channel fracture outcrop (left) to compare with the 3D DFN created by ResFrac/Napsac and that of SVS for Qarn Alam field.**

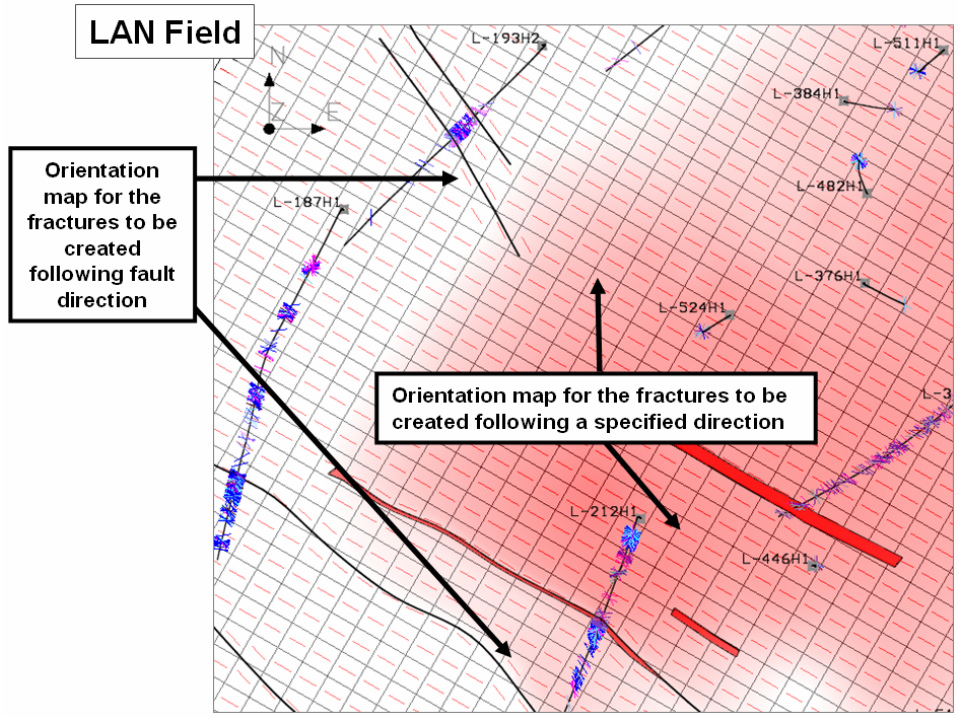


**Figure 7-41 Example of an orientation map (small red lines) used to control the direction of the fractures to be created. In this case of LAN field, it is based on a specific value (a NW direction) that changes once approaching a fault to be parallel to it.**

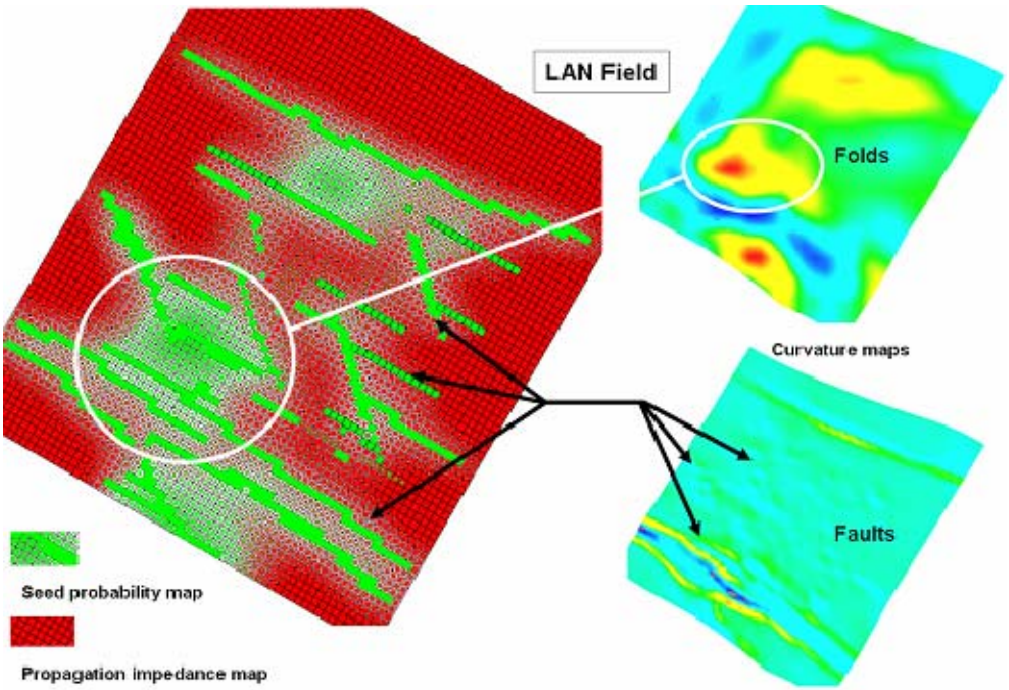


**Figure 7-42 Example of a seed probability and propagation impedance maps based on faults and folded area.**

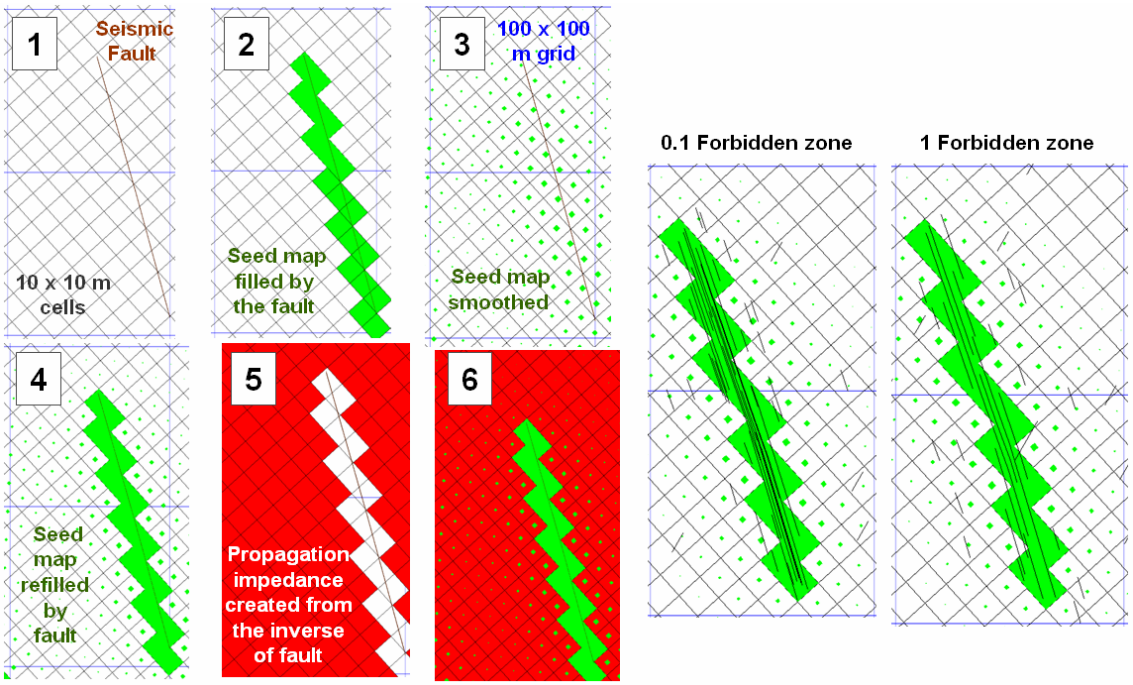


**Figure 7-43 An example of a workflow showing how to create a fault related fracture or fracture corridor. Note how the forbidden zone (basically the width between each fractures) determine the intensity of the fracture generated inside the zone together with the seed per unit area.**

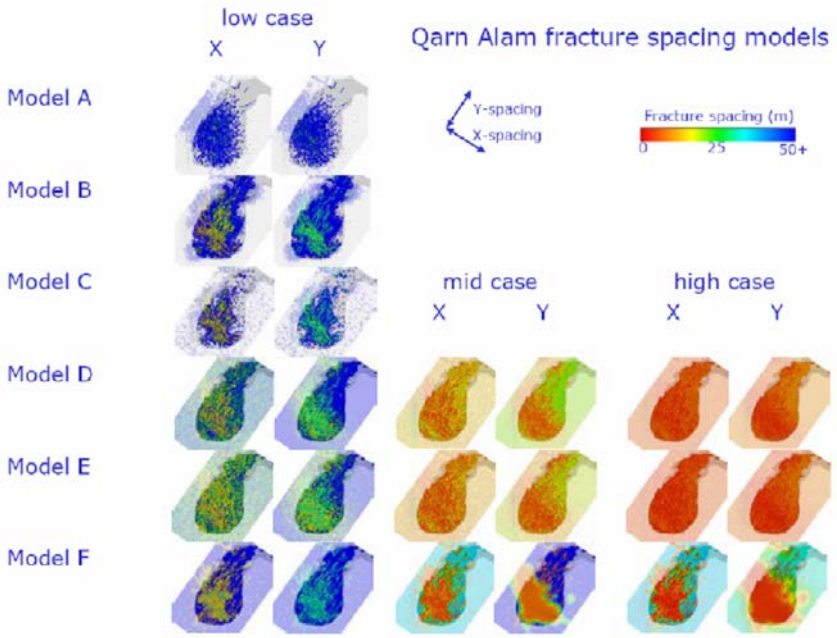


**Figure 7-44 Example of SVS 3D DFN models created for Qarn Alam Shuaiba reservoir. Each model represents a different concept (e.g. model C is a fault only scenario while model E is fault + diffused fractures + strong mechanical layering scenario), Rawnsley and Dhahab, 2005.**

### *7.4.2 Analysis of the created 3D DFNs*

This sub-section summarizes the analysis done on 3D DFNs as part of the workflow. Ghaba North field's DFN realizations (3 scenarios only) will be used an example for this analysis. In principal there are two approaches to critically asses 3D DFNs: First is by cross checking the output against the input data and the geological basis (i.e. the conceptual model used); the second is by forward dynamic simulation either at full field scale or well to sector scale and history matching with well production. Both approaches incorporate iterations, until certain realization or realizations is or are achieved. The

objective is to minimize uncertainly with respect to the nature of the fracture network in a field and its impact on flow performance; and to arrive at an appraisal strategy that would minimize the uncertainty of fracture network distribution. In the case of forward 3D simulation, processes such as experimental design can help in accelerating the analysis. For instance in Fahud field, experimental design had helped in reducing the time used for the fracture characterizations by eliminating certain parameters early on the modeling stage based on flow impact (Wei et al, 2005).

The first approach does involve history matching too, but is done by analyzing individual well performance and comparing it with the expectation, based on the heterogeneity of the fracture network at different location in a field. Though, this conceptual model which is the basis of the created 3D implicitly contains the understanding of the flow performance in it. The second approach is more time consuming as it involves dynamic simulations. In addition, errors might be introduced due to uncertainty related to dynamic parameters used in simulations. These are capillary pressure used, relative permeability used, aquifer strength, which are normally hard to define for fractured reservoirs. As mentioned in the quick simulation Chapter 6 above, 3D implicit simulation (e.g. dual porosity dual permeability) represents a significant challenge to petroleum engineers, because matrix properties have to be characterized, fracture properties have to be characterized, and more importantly flow interaction between fractures and matrix has to be defined.

For the Ghaba North, the created 3D DFN were based on the conceptual scenarios that were derived from data analysis represented in Table 4.4, 4.5 and 4.6. The two scenarios to be further investigated here are shown in Figure 7.45 below.

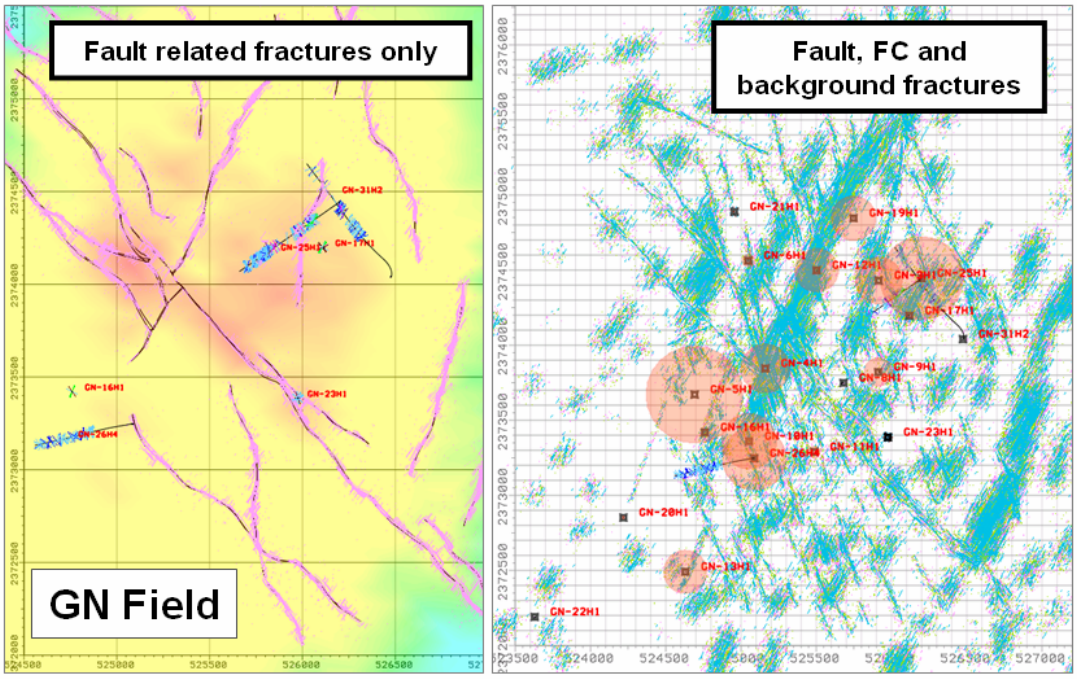


**Figure 7-45 Example of GN 3D DFN to be analysed in this section. A fault related fracture only scenario (left); and fault related fracture with fracture corridors and background fractures (right).**

Fault –only related fracture scenario:

As mentioned in Chapter 4, the main reason behind this unlikely realization is to show the lowest fracture scenario envisaged in order to estimate impact on field development, if such cases do exist. Thus, it is like the worst scenario for GOGD development and the best scenario for pure depletion recovery or water flooding.

Cross-checking the generated 3D DFN against wells' performance and BHI fracture intensity (Figure 7.46), role out the probability of such scenario. Furthermore, detail examination of the production profile for GN3H1, show a classical fracture flow, with high initial rate followed by sustained plateau of low oil production coinciding with sharp rise in water influx (Figure 7.47). This well is drilled in an unpracticed area according to this fault only model.

Fault, FC and background fracture scenario:

This middle case scenario seems to honor the fracture dynamic and static data (Figure 7.48). Wells with high normalized gross rate production seems to occur in zones of intense fractures in the DFN. Now the fracture like behavior in the production data for GN3H1 can be explained. GN-5H1 does not fit the DFN model, and I reckon, for this wells there is two possible scenarios why is that the case: One is that the nearby fractures after some time connect to the well and result in high connectivity, hence will see low initial gross rate followed by sharp increase; or it could be related to matrix diagenesis and in such cases the gross rate will be high from the start. The production profile of this well supports the latter interpretation (Figure 7.49). Furthermore this proposed mid case scenario also honor the interpretation of the interference test done in GN (Figure 6.50) in having a strong NE conductivity, with a normal to week NW conductivity.

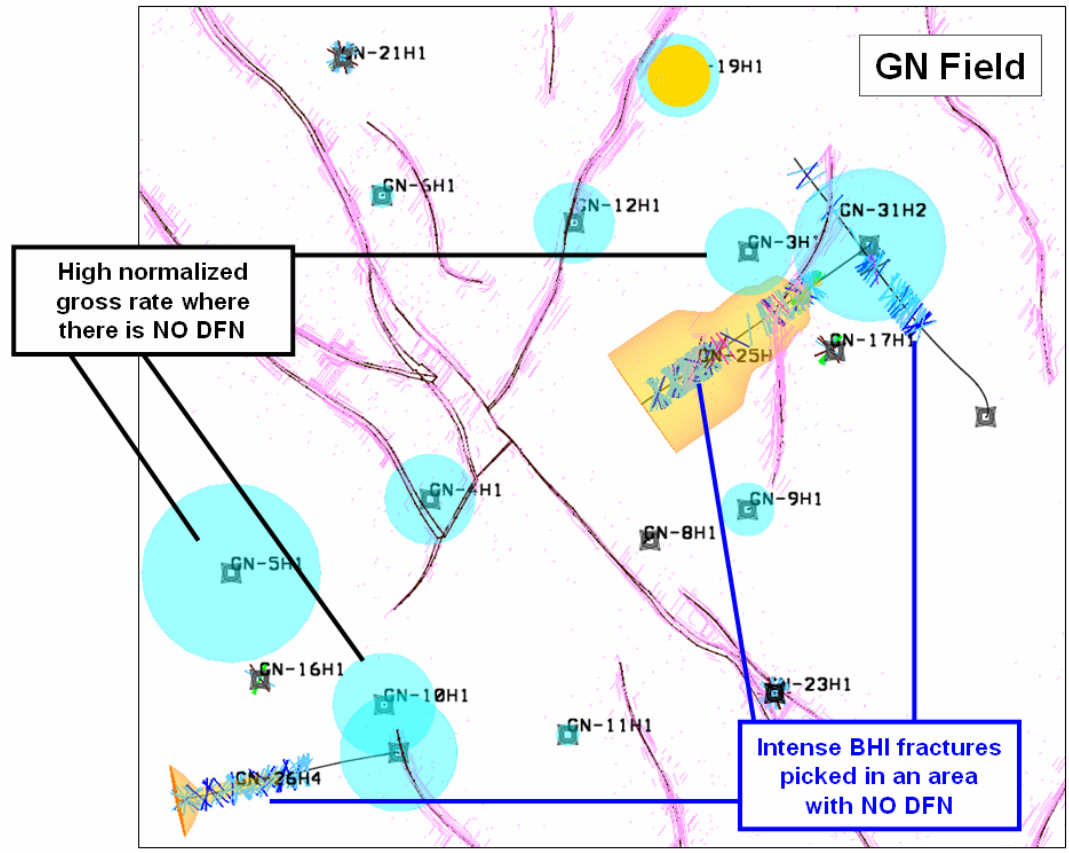


**Figure 7-46 A snap shot of ZHawari fault related DFN. Note how BHI fractures (blue/pink lines along wellbores) in the horizontal wells (GN31H2/GN26H4/GN25H1) contradict the model. In addition the normalized gross rate per well for GN10H1, GN5H1 and GN3H1 showing high rate again in a no fractured area.**

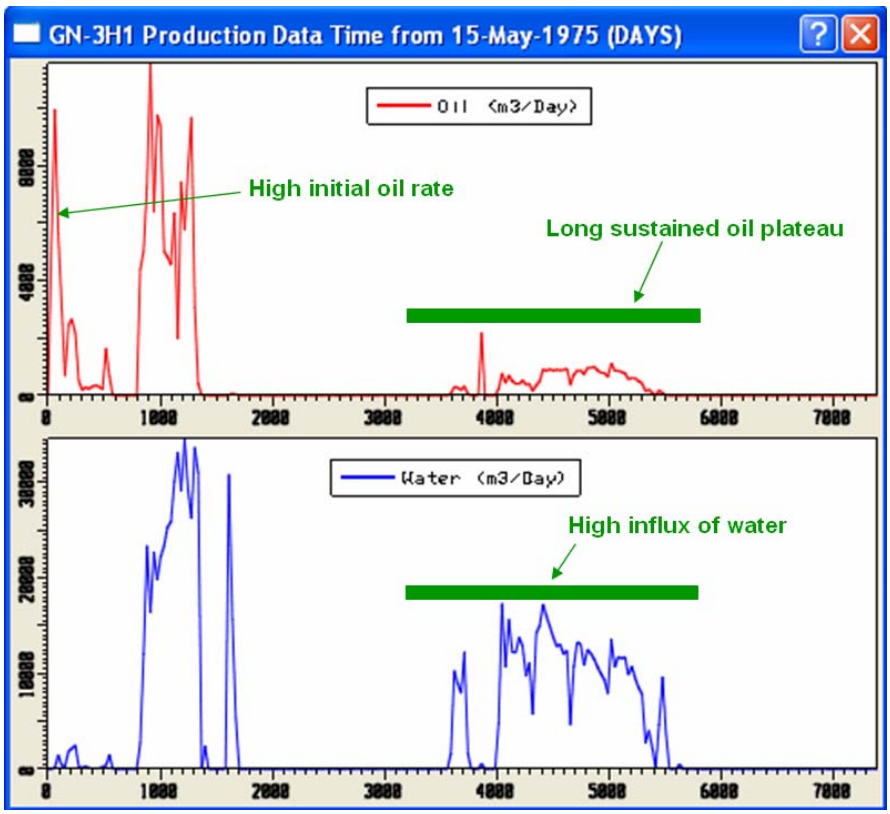


**Figure 7-47 GN3H1 production profile indicating a fracture like behaviour. In the fault only model, the created DFN indicate that the well is drilled in non-fractured area, which contradicts this flow performance.**

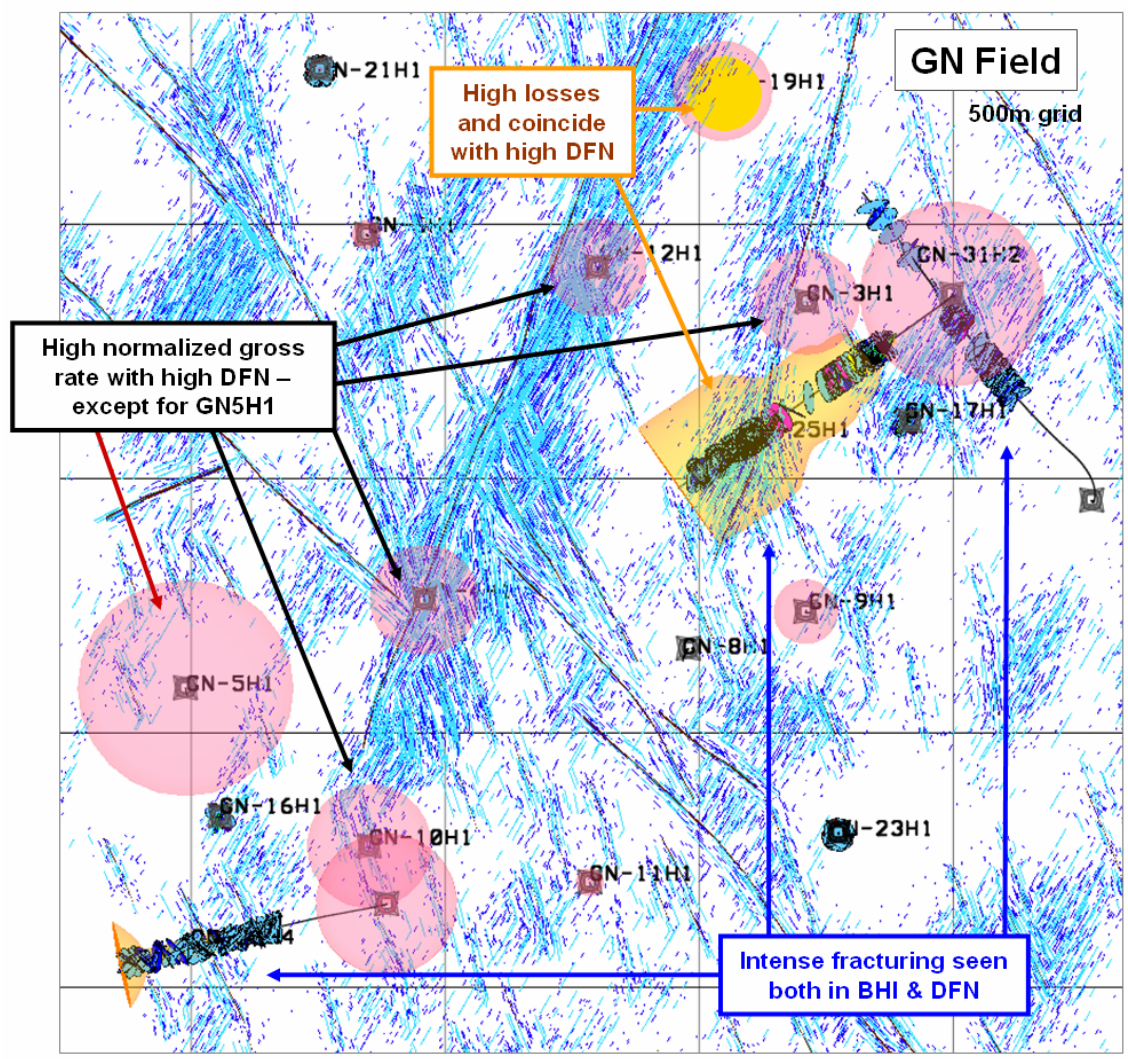


**Figure 7-48 A snap shot of the 3D DFN for Ghaba North Shuaiba with fault related fracturing, fracture corridors and background fractures. Note how the DFN model fit with the well BHI fracture intensity data, with the losses data and with well flow performance (the normalized gross rate). GN5H1 seems to differ with high rate than expected, but this can be explained.**

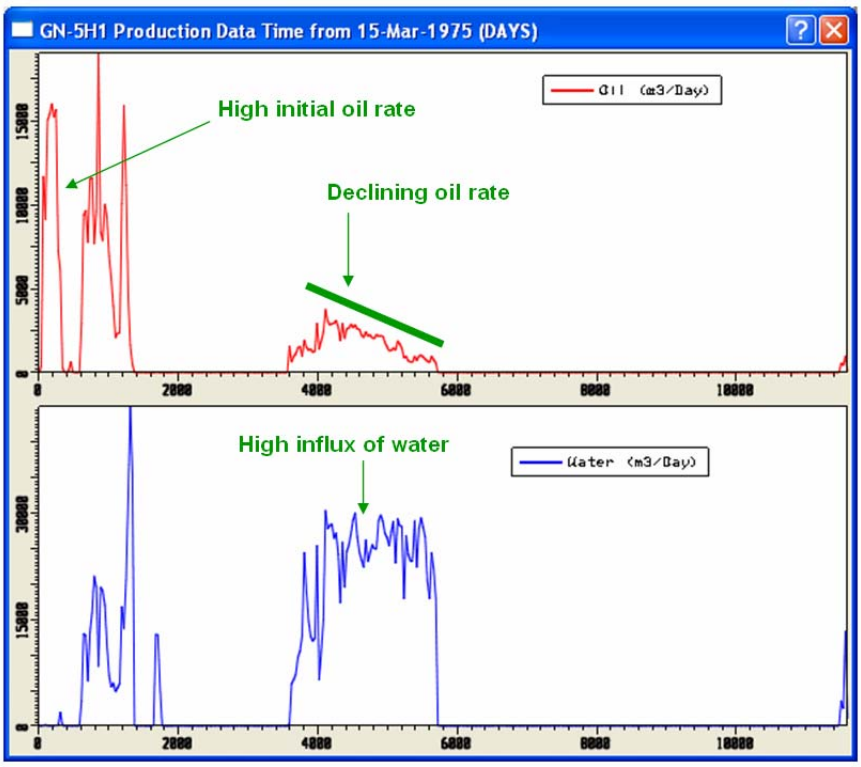


**Figure 7-49 GN5H1 production performance indicating a connective network. This could be attributed to matrix diagenesis more than due to nearby fractures impact on the flow, as the latter profile should start with low gross followed by high gross influx.**

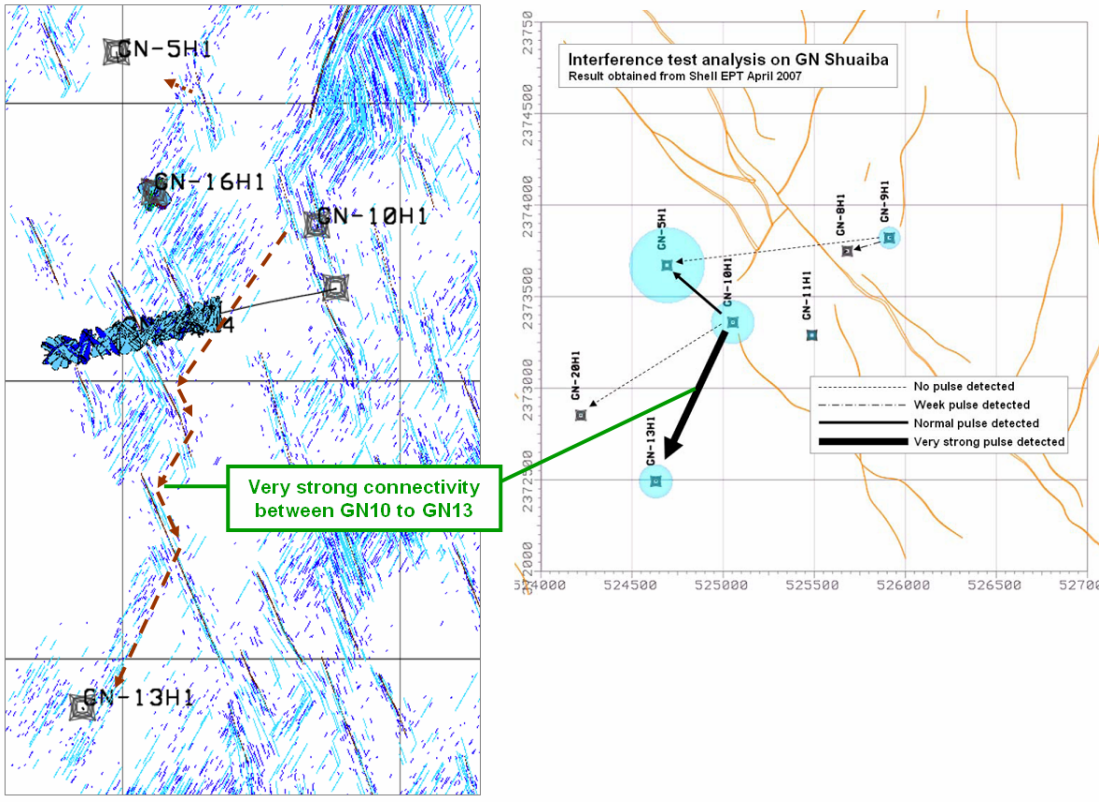


**Figure 7-50 Snap shot of GN 3D DFN showing a possible path between GN10 and GN16 which honour the observed interference test data.**

# Chapter 8– SUMMARY

More than one third of Oman oil, currently ~800,000 bbl/day, is reservoired in the Cretaceous Natih and Shuaiba limestone Formations. Traditionally, the fields' reservoirs have been classified into either matrix reservoirs such as Yibal, Lekhwair, Musallim and Saih Rawl, or fractured reservoirs (in relation to flow) such as Qarn Alam, Fahud, Natih and Al Ghubar. However, almost all have shown fracture behavior to some extent. Thus, understanding fracture network present, is a key enabler for the development of these reservoirs. This research presents a coherent descriptive fracture characterization for the Cretaceous reservoirs of north Oman with a detailed evaluation of two specific fields: the Shuaiba Ghaba North and Lekhwair A North.

## 8.1 North Oman regional fracture evaluation

The inter-relationship between tectonic, matrix and diagenesis, control the north Oman Cretaceous fracture network geometric distribution and conductive properties. Tectonisim manifested in faults and regional stress is the main dominant factor controlling the lateral distribution of the fractures, as most of the fractures examined are either fault related fractures or fracture corridors that occur in clusters. The fault related fractures can be split into two groups: fractures that are associated with the NW-WNW striking regional faults probably created as a result of the late Cretaceous deformation; and fractures that are associated with local faulting resulting mainly from a combination of regional deformation and presence of local salts. On the other hand, fracture corridors, mainly striking NE as seen in Fahud field, are probably associated with the late Tertiary deformation. These fault related fractures and fracture corridors normally occur as cluster with a width of 25-100m, a fracture spacing of less than 1m within them and are 50m-100s of meter apart. On the other hand, the intensity, and impact on production, of the diffused background fracturing and fold related fractures is minimal compare to the fault related fractures and fracture corridors. These diffused and fold related fractures are closer spaced (few meters apart).

From a fracture prospective, the matrix-diagenesis inter-relationship controls mainly the mechanical layering seen in the Cretaceous reservoir, thus impacting the vertical distribution of the fracture network. The impact is low for most of the southern fields of north Oman, where only lower Shuaiba is present. However, the impact intensifies in the northwestern fields, where upper Shuaiba is present. Furthermore, mechanical layering plays a major role on vertical fracture distribution for the Natih Formation, which is present in Fahud, Natih and Al Ghubar field as a commercial hydrocarbon reservoir. An attempt to summarize fracture network distribution for the north Oman Cretaceous reservoirs is presented in conceptual illustrations below (Figure 8.1).

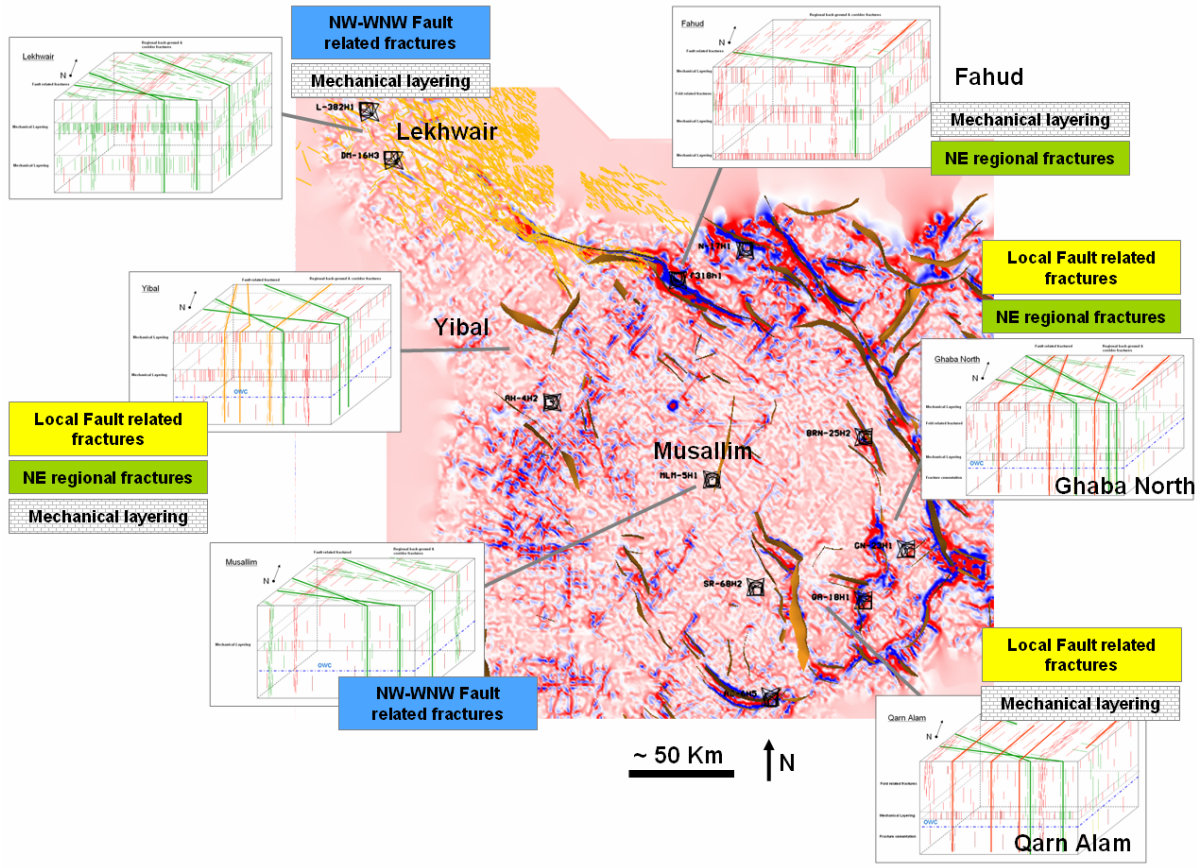


**Figure 8-1 Proposed conceptual model for the fracture network geometry seen in north Oman Cretaceous reservoirs per field, highlighting the main driving mechanism in each field or region (see APPENDIX II for enlarged image).**

On top of its impact on the fracture vertical distribution (mechanical layering), diagenesis is also a major control on the conductivity of the fracture network seen in these reservoirs. To date there has been very little detailed studies on diagenesis characterization for the Cretaceous reservoirs of north Oman. The only available regional work is that of Wagner in (Droste et al, 2004). Based on the analysis of the fracture network in north Oman fields, at least two phases of diagenesis can be readily distinguished. A burial cementation phase that had resulted in rise of non-conductive fracture with depth (close to OWC) as well as the cementation of the NW-WNW faults (mainly in the central area) and their associated fractures; and a possibly thermal leaching that had resulted in re-opening of existing fault related fractures and fracture corridors. A sequence of geological events based on the analysis of the tectonic-matrix-diagenesis interaction is shown in Figure 8.2 for the north Oman Cretaceous reservoirs. This proposed sequence of events can be further refined with detailed diagenesis studies (e.g. fluid inclusions) and local detailed field based data.

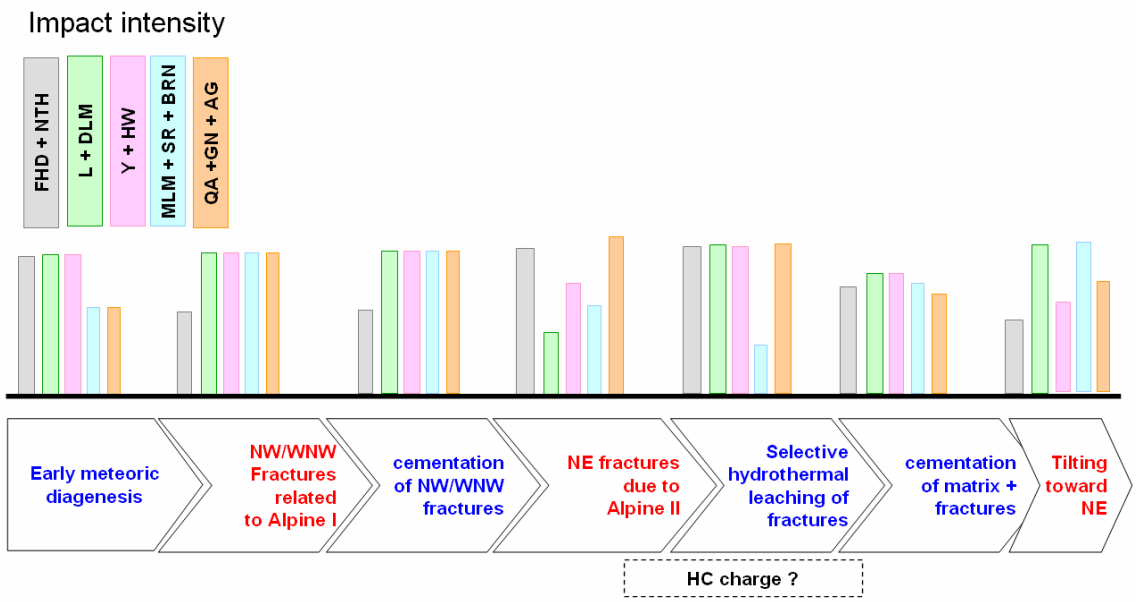


**Figure 8-2 Proposed geological sequence of events for north Oman Cretaceous reservoir together with a simplified chart showing relative intensity of impact of each even on each region (FHD + NTH = Fahud and Natih; L + DLM = Lekhwair and Dhulaima; Y + HW = Yibal and Al Huwaisah; MLM + SR + BRN = Musallim, Saih Rawl and Burhaan; QA + GN + AG = Qarn Alam, Ghaba North and Al Ghubar).**

## 8.2 Generic static fracture evaluation

From a generic prospective, integration of all the available fracture data helps in reducing single source data errors and helps in developing a better understanding of a fracture network in a reservoir. Fractures seen in outcrops or in core are normally much more intense than those observed in a BHI log. This is due to the resolution limit of the BHI tool. There are also other issues that limit the usage of the BHI log, but nonetheless it is still the most critical fracture-related data available in PDO. Fractures should be split per type (single or in cluster; conductive or non-conductive), per orientation, and, if possible, per origin (e.g. fault related or bed-bounded), before embarking on fracture statistical analysis (i.e. fracture spacing calculation). Usage of dynamic data for fracture characterization helps understanding fracture connectivity network. These includes plots of simple gross rate, productivity index, pressure interference test, analysis of well test, production logs (PLT/WFL) plots or even losses profile along a well bore. Again, these should be plotted with the static data to better understand fracture network. The integration and detailed analysis of these fracture data should enable the creation of a geologically based conceptual scenario for the fracture network examined, that may be later used to create either fracture density map or discrete fracture network (DFN) (Figure 8.3). The main objective is to reach geologically representative realizations and avoid data based stochastic modeling. Data based stochastic modeling normally honor well data and even simulation at full field scale, but it quickly collapsed when challenged with operational practices (e.g. where to encounter a fracture zone while drilling a highly deviated well with a specific orientation). In addition, it does not represent fracture seen in outcrops.

If a 3D discrete fracture network DFN is not modeled "simulated" explicitly, then the geometrical properties, and their extraction into a 3D geo-cellular grid, should be done

with caution. In other word, errors may arise from extraction of fracture count and fracture spacing calculation in a 3D grid due to the method of calculation used for the extraction, due to the orientation of the fracture set relative to the grid orientation and due to the grid cell size. Simulation of naturally fractured reservoirs represents an ample challenge to petroleum engineers. Implicit dual permeability -porosity models are normally oversimplified using many assumptions especially with regard to the interaction between matrix and fracture in the case of non-uniform fracture networks. Regardless, which approach is used for simulation, fracture aperture (hence storage and conductivity) will always be difficult to estimate. Fracture aperture is very heterogeneous in nature and seldom in constant size. The variation can be related to the origin of fracture (i.e. nature of fracture type such as extensional versus shear fractures); or due to the stress applied on the fractures (current stress and paleo); and due chemical processes (diagenesis) that affect the fracture over time. The latter normally result in having partially open fractures. Estimating fracture aperture from static based data is usually less reliable compare to dynamic data. These because the static data normally examine fractures at the well bore and assume a constant size away from the borehole. Though, the dynamic approach is a backward mathematical calculation, where a certain relationship is assumed to link permeability to aperture. As a recommendation both approaches should be used and tested as a sensitivity analysis.

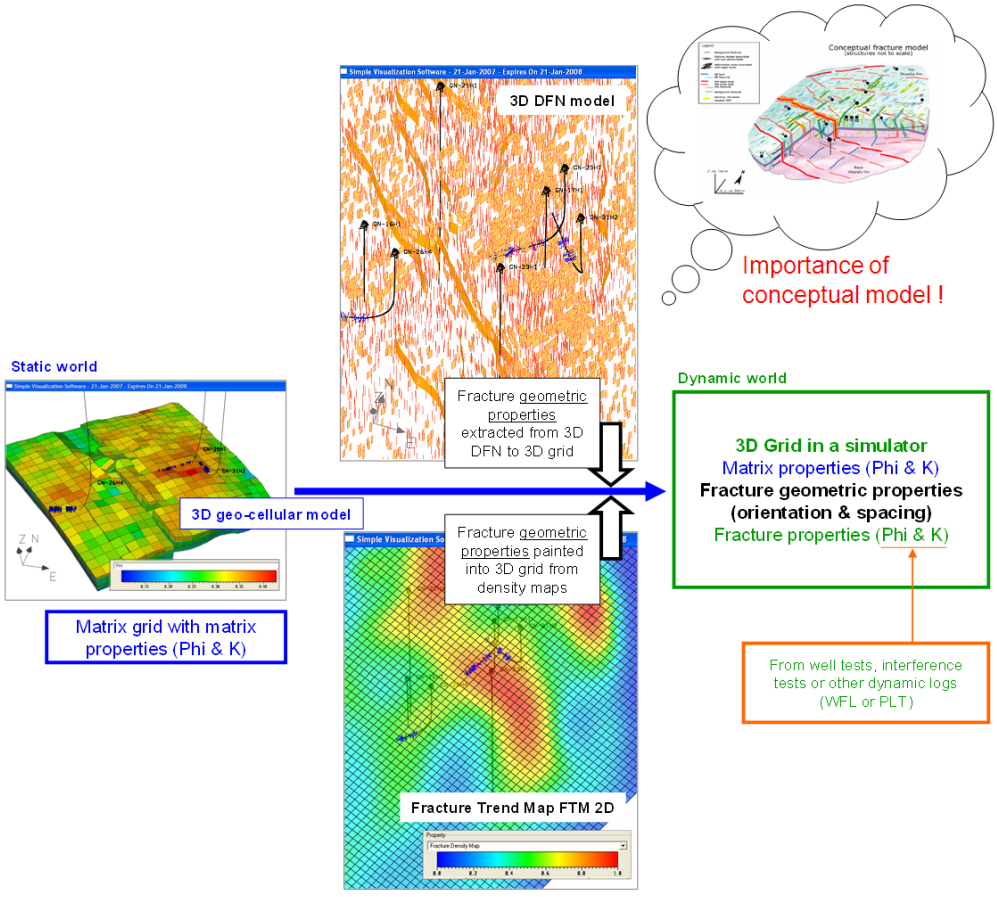


**Figure 8-3 Approach of extracting fracture static properties (spacing and orientation) into a geo-cellular grids, note the importance of having a geologically based conceptual model before embarking on DFN or FTM.**

## 8.3 Ghaba North Shuaiba fracture network evaluation summary

The well data available for this field is very limited (only three horizontal wells). Fault geometry and BHI fracture geometry, together with interference test analysis indicate a dominant NE striking fracture network, though NW striking fracture are present. Most of the BHI fractures are conductive (ratio of all conductive to non-conductive is 20:1) and occur in clusters, which are averagely spaced at 20-50m and 200-300m (Figure 8.4).

Estimation of fracture vertical distribution is limited as most of the deviated/horizontal wells are confined to the upper most part of the reservoir. However, it is proposed here that the impact of mechanical layering is minimal as only Lower Shuaiba is present in this field and the core porosity trend with depth does not show substantial change that may cause a variation in fracture density across the layers.

Based on the detailed fracture analysis three main scenarios were considered for Ghaba North fracture network (Table 8.1): Fold related fracture scenario; fault and fracture corridor fracture scenario and a combination scenario. The fault and fracture corridor fracture scenario is the more likely one (i.e. base case).

Several 3D models discrete Fracture Network (DFN) and Fracture Trend Maps (FTM) were built for this reservoir based on the conceptual understanding of the fracture characterization. All the models were subjected to static calibration and to some extent dynamic calibration, both during the creation and after the extraction of fracture geometrical properties of the DFNs into 3D grid (Figure 8.5).

Simple dual porosity dual permeability analysis were run on some of these realizations but additional future work may consider a detailed simulation analysis to test each of the reasons given in the simulation chapter for the similarity in the flow output between the proposed 3D DFN realizations. Such work may involve further simulation of the fracture network using different approaches such as explicit dynamic modeling and may involve refinement of the fracture realizations.

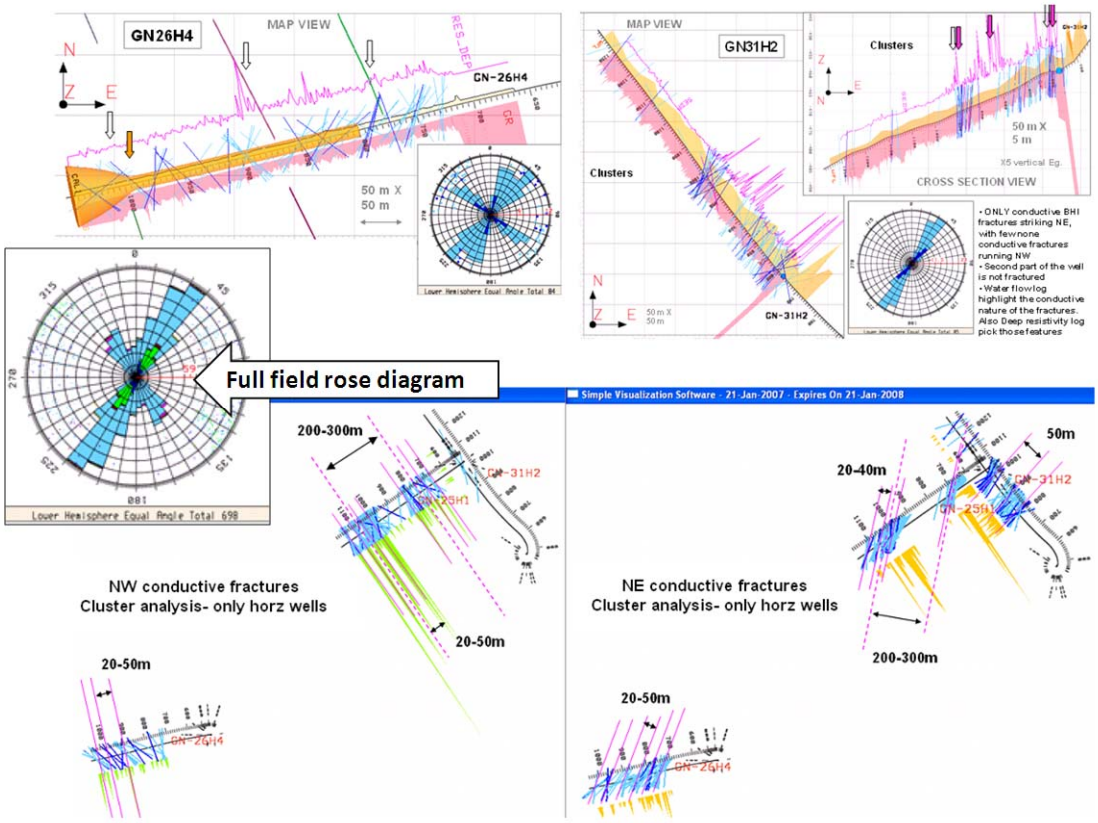


**Figure 8-4 Ghaba North Shuaiba BHI fractures (blue lines are conductive fracture picks). Note how the dominant NE striking fractures affect the resistivity logs (pink lines) and the WFL (light orange shadow log) in GN31H2 (right hand- top). Lower side is showing simple manual cluster spacing analysis for both the NW and NE BHI fracture picks.**

| Scenario | For | Against |
|---|---|---|
| NE crest and SW crest Only (Fold Model) | 1- High normalized gross rate profile for GN-5,GN-25 and surrounding crestal wells | 1- Losses in flanks wells GN-13 & GN-21 *c.f.* No losses in GN-17 in the centre |
| | 2- Large scale 500m multi-direction curvature map showing high strain, mainly for NE crest | 2- GN-21 on NW flank, production profile showing high initial gross rate |
| | 3- High BHI fracture intensity in GN-25 and GN-26 | 3- Interference test between GN-10 & GN-13 in the southern flank, showing high connectivity |
| Fault related fracture model with fracture corridors - possible sub-seismic faults - only (Fault only model) | 1- Over 80% of the BHI fractures occur in clusters | 1- GN-5 is showing high normalized gross rate in area where there is NO faults* |
| | 2- BHI fracture location coincide with possible fault location (2001 study fault interpretation) in GN-25, GN-26 and GN-31 | 2- GN-23 is showing 0 losses in the reservoir despite being on a NW trending fault |
| | **3- High initial production rate for GN-19 and GN-25 all hit by large fault "ZHarwi fault interp"** | |
| | 3- High normalized gross rate profile for GN-4, GN-10, GN-12, GN-19,GN-25 &GN-26 all hit by large fault "ZHarwi fault interp" | |
| | 4- Seismic semblance volume showing step change of acoustic impedance at and in the vicinity of fault traces | |
| Fault related fracture model with fracture corridors combined with NE background fractures (Fault, FC and background) | As above for fault model 1 to 4 | As above for fault model 1 * |
| | 5- Background fractures seen in GN-31H2 tail | |
| | 6- all most all the NW BHI fractures are coinciding with faults | |

** GN5 high normalized gross rate could be attributed to diagenesis. Evidence for diagenesis is seen in GN-23H1 & GN-31H1 core: Facies are dominated by rudist which shows low leaching patches; also for GN-31H1 presence of overlain Shale 3m below top reservoir, though later could be related to drilling (coring) activities. In addition static images of the BHI for GN wells shows vuggy profiles*

**Table 8-1 Fracture network concept scenario building for Ghaba North Shuaiba.**

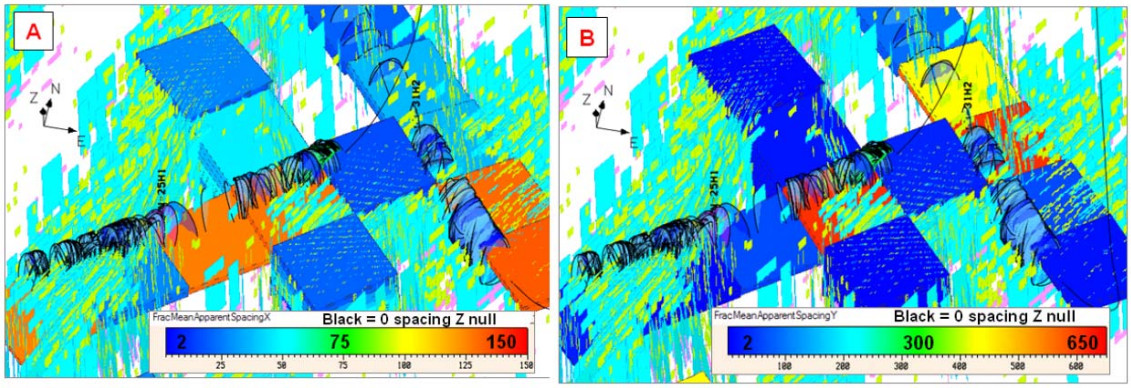


**Figure 8-5 Ghaba North SVS snap shot around GN-25H1 and GN-31H2 area showing proposed base case 3D DFN fractures (cyan crossing whole reservoir, yellow in top layer and pink in middle layer) and their extracted geometric properties in a 3D grid cells crossed by GN wells (spacing along the grid X direction is shown A and along the grid Y direction is shown in B) together with well BHI fracture objects interpreted (ellipses). Note how the model agrees with the BHI observation (large fracture spacing in the area where NO BHI fractures occur).**

## 8.4 Lekhwair A North (LAN) fracture network evaluation summary

The evaluation in this field concentrated on the Lower Shuaiba Formation and the Kharaib Formation. The areal and vertical coverage of BHI logs is moderately good with the majority of the fractures are striking NW to WNW (Figure 8.5).The ratio of all FMI's interpretation conductive fractures to non-conductive fractures is 5:1.

The current PDO fault map show few faults striking NW to WNW bounding the field at the NE and SW, however a recent lineament interpretation by PDO based on seismic coherency analysis, indicates possibly much more intense faulting. This is also supported by uni-directional curvature analysis at low wavelength (Figure 8.7).

A detailed fracture characterization analysis per well (based primarily on integration of BHI/FMI log fracture interpretation with other fracture related data) were undertaken by Baker Atlas. It results, in the creation of an Excel based data base with summary map views (Figure 8.8). Based on the Baker Atlas 2006/2007 LAN fracture study, review of other existing studies and the fracture related data analysis undertaken on the whole field and on specific wells in this research, several element of conceptual fracture scenarios were examined (Table 8.2).

Out of the concepts examined, three geologically constraints scenario were considered and converted to low, base and high case 3D DFN realizations for the LAN field to illustrate the variation of the fracture network per model. The base case fracture geometry was extracted into 3D geo-cellular grid to be further analyzed in PDO using dynamic simulation.

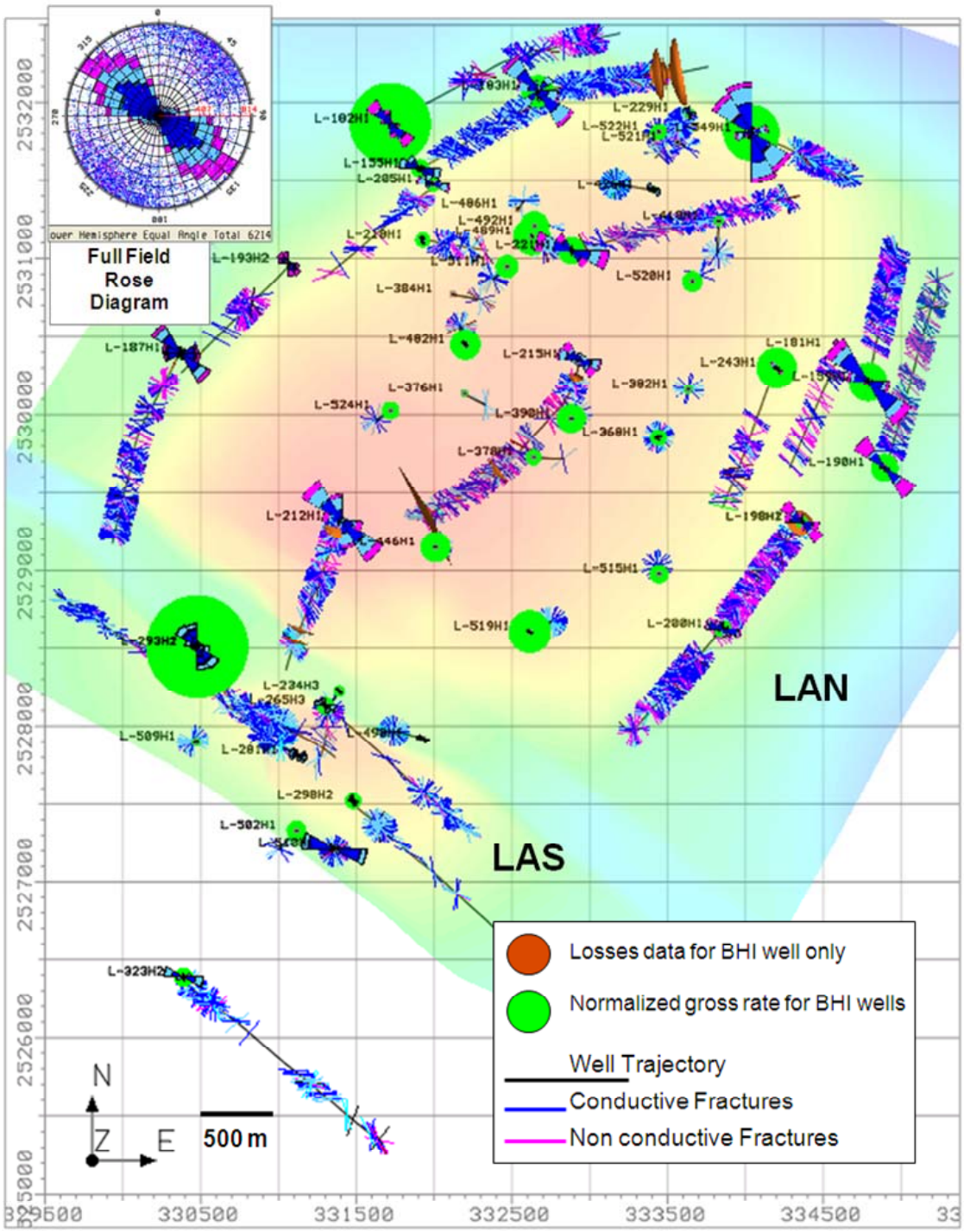


**Figure 8-6 LAN and LAS fields showing only BHI wells, drilling losses encountered and a normalized gross rate (total produced liquid / days on production or total injected water / days on.**

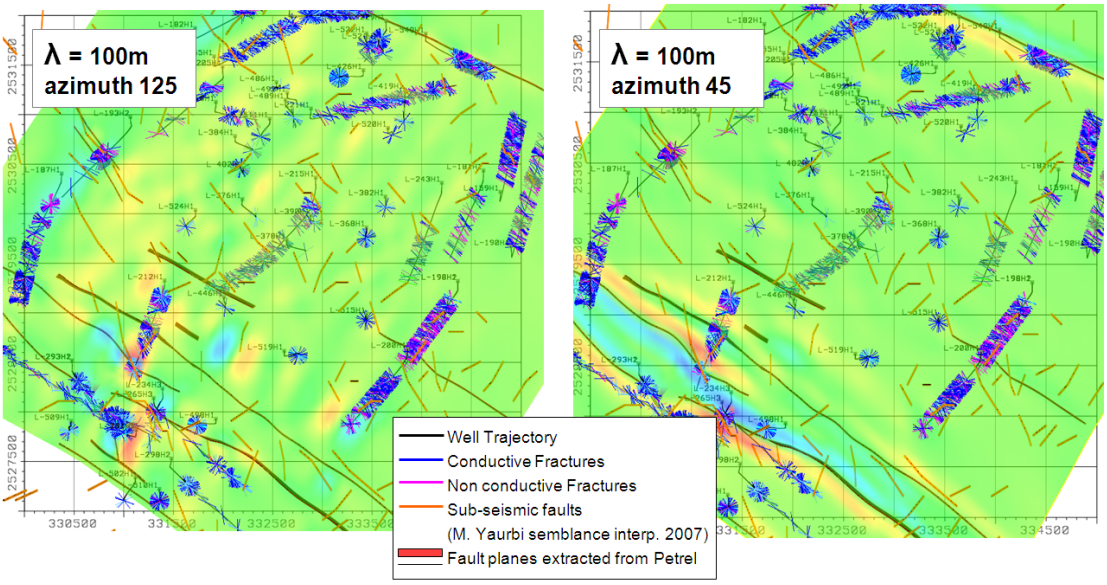


**Figure 8-7 LAN and LAS fields showing only BHI wells, fault plane (continuous lines), fault lineaments (discontinuous orange lines). The lineaments "sub-seismic" faults and the curvature show possibly more intensive faulting than what is currently seen.**

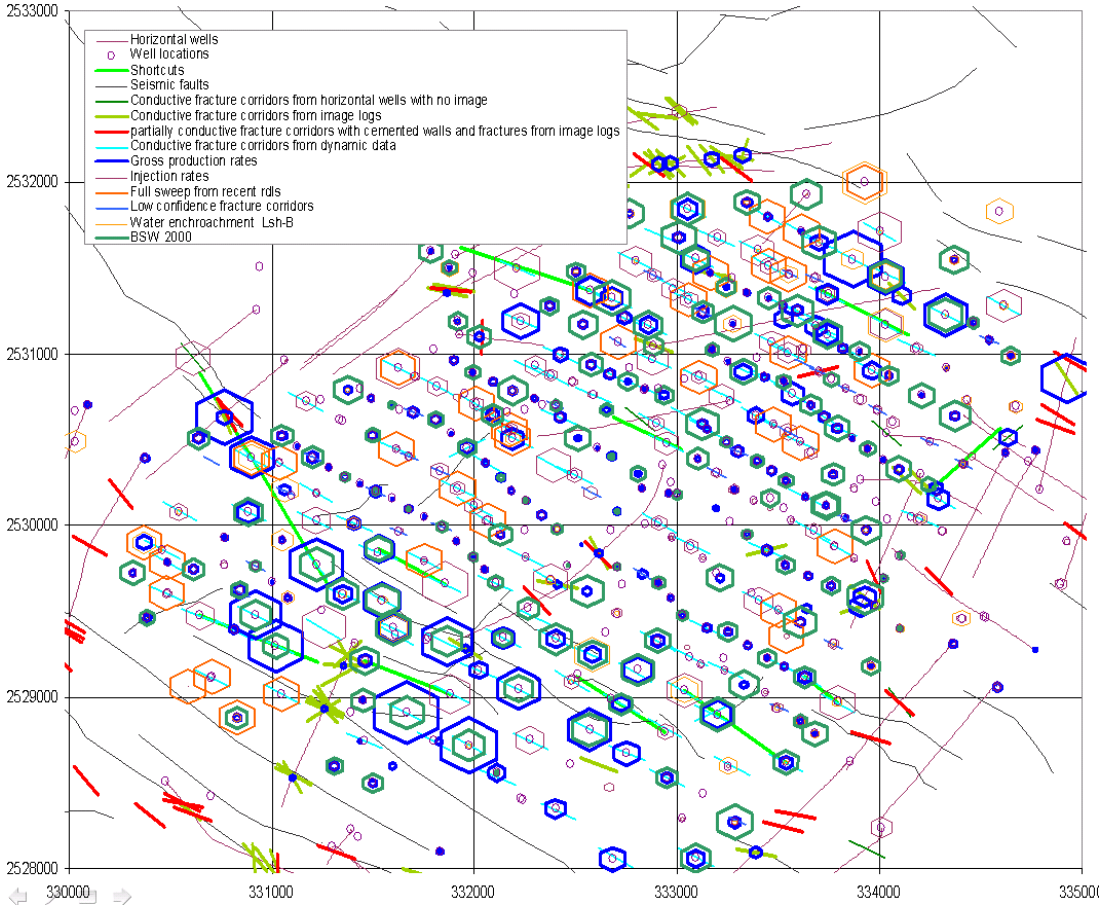


**Figure 8-8 A composite plot of all wells of LAN with the integrated fracture related data by Baker Atlas 2006/2007 LAN study. Note how the most connected wells (one with large polygons) occur in the south or the far North of LAN field.**

| Element of concept | Support |
|---|---|
| **Fault related fractures NW & WNW only** | 1- Fracture intensity increases as NW/WNW fault are approached (BHI visual inspection)<br>2- From 10 to few 100m of area of high BHI intensity next to fault planes<br>3- High gross rate and losses around faults |
| **FC or sub-seismic related fractures (Both NW and NE)** | 1- BHI clusters in area where there is NO faults (e.g. central part of LAN)<br>2- Curvature analysis at low wavelength (50 to 100m) show corridors of high strain striking NE & NW<br>3- Sudden changes in Shc log response coinciding with BHI fracture intensity where NO faults occur |
| **Fold related fractures** | 1- Higher strain in the southern part of LAN as seen from 500m scale multi-directional curvature map<br>2- Same area coinciding with high connectivity (gross rate and Baker Atlas detailed well analysis) |
| **Mechanical layering (ML)** | 1- Multi-lateral wells such as L-198 BHI log in LSA & LSB as well as existing studies<br>2- Core data inspection (Phi-K plot) show slight offset between LSA and LSB, as well as GR log |

| **Geological scenarios** | *All with ML: Fracture intensity in* *Hawar >> L. S A > Kharaib > L. S B* |
|---|---|
| **Low case** | **Fractures occur only in fault damaged zone of the Petrel major NW and WNW faults*** |
| **Base case** | **Combination of major NW & WNW faults; NW and NE FC based on curvature analysis as well as background fractures increasing in the southern part of LAN** |
| **High case** | **Similar to base case but fractures close to sub-seismic lineaments interpreted by PDO** |

**Table 8-2 Fracture network concept scenario building for LAN field.**

## 8.5 Recommendation

In order to further refine the understanding of the fracture network of north Oman Cretaceous reservoirs, presented in this research, PDO will need to drill appraisal wells that cut through the Cretaceous reservoir at deviated angles to assess the mechanical layering, this is very crucial in fields such as Musallim and Saih Rawl where the current development dictates the design of well trajectories (in this case producers are confined to the upper parts of the oil window of Shuaiba and injectors are drilled below the OWC, hence no appraisal of the intermediate Shuaiba layers). In addition, acquiring and interpreting well test data is of great value to the fracture characterization, here. Thus, such tests should be executed whenever possible; especially in fields were the development scenario is dependent on understanding of the fracture network. PDO should continue acquiring dynamic fracture related data (PLT or WFL) in new wells with BHI logs. This integration is key enable to the understanding of the connectivity of fracture network.

Furthermore, new seismic processing and interpretation (e.g. coherence cubes analysis) should be undertaken on existing seismic volumes with the objective to enhance fracture detection. There are very few deviated and horizontal cores available for the Cretaceous reservoir of north Oman. These cores should be acquired especially in appraisal wells, but more critically their fracture network should be described quantitatively, if possible.

A detailed fracture diagenesis studies should be done for the north Oman carbonate reservoirs. Such studies are currently the main missing pillar of the fracture story. They are critical to differentiate the impact of diagenesis compared to mechanical stress in fracture connectivity, as well as their impact on the deposition lithofacies “layering”, which will on-turn dictate the fracture density distribution vertically (i.e. mechanical layering).

The work done in this research sets the scene for the understanding of the fracture network of north Oman using a descriptive approach based mainly on well data and available seismic data linked to regional tectonic understanding. Further work would be helpful to refine the understanding of the genesis of the Cretaceous fracture network of north Oman using geo-mechanical mathematical stress-strain simulations.

## APPENDIX I

A3 Enlarged image- showing the proposed conceptual model for the fracture network geometry seen in north Oman Cretaceous reservoirs per field, highlighting the main driving mechanism in each field or region.

# REFERENCES

Al Busaidi, R. Lekhwair field stratigraphy type log, *Petroleum Development Oman, Internal Presentation* (1996).

Al Dhahab, S. Ghaba North field - Shuaiba Formation geo-statistical analysis of fracture, *Petroleum Development Oman, Internal Report* OQP/02/018NFF (2002).

Al Dhahab, S. Al Ghubar 16 ST2 end of well report, *Petroleum Development Oman, Internal Report* OQP/98/003R (1998).

Al Dhahab, S. Qarn Alam - QA21, QA22 & QA23 wells review, *Petroleum Development Oman, Internal Report* OQP/00/021NFF (2000).

Al Dhahab, S. and Regan, P. Shell 3D fracture software SVS - Simple Visualization Software Manual, *Shell EP Technology Report* 5306 (2006).

Al Dhahab, S., de Keijzer, M. and Richard, P. Shuaiba asset study: 2002 & 2003 structural and tectonic framework, *Shell EP Technology Report* EP5273 (2003).

Al Salhi, M., Wei, L., Van Rijen, M., Alias, Z., Visser, F., Dijk, H., Lee, H., Timmerman, R. and Upadhyaya, A. Reservoir modelling for redevelopment of a giant fractured carbonate field, Oman: Experimental design for uncertainty management and production forecasting, *International Petroelum Technology Conference-10537* (2005).

Al Harthy, S. and van Wunnik, J. Performance review of the water flood in Lekhwair A-North field, *Shell EP Technology Report* (1994).

Amri, B. Pressure fall off test in Lekhwair A North field, *Petroleum Development Oman, ONPL Internal Report* (2006).

Amthor, J. and Kerans, C. Stratigraphy and facies of a shelf-margin rudist reservoir - Al Huwaisah Shuaiba Field, North Oman, *Geo-Arabia Conference, Oral Presentation* (2004).

Bai, T., Maerten, L., Gross, M. and Aydin, A. Orthogonal cross joints: do they imply a regional stress rotation, *Journal of Structural Geology*, vol. 24, p 77-88 (2002).

Bai, T., Pollard, D. and Gross, M. Mechanical prediction of fracture aperture in layered rocks, *Journal of Geophysical Research*, vol. 105, p 707–721 (2000).

Bait Muati, M. Lekhwair AN-7 induced fractures review, *Petroleum Development Oman*, *ONPL Internal Report* (2004).

Barree, R. and Woodroof, R. A practical guide to hydraulic fracture diagnostic technologies, *SPE 77442* (2002).

Bazalgette, L., Beintema, K., Bettembourg, S., Swaby, P., Al Dhahab, S., de Keijzer, M. and Rawnsley, K. Fault, fracture corridor detection and fracture modelling using SVS curvature analysis tools, *Shell EP Technology Journal* , p. 7001-09 (2007).

Bergbauer, S., Mukerji, T. and Hennings P. Improving curvature analyses of deformed horizons using scale-dependent filtering techniques, *AAPG Bulletin*, vol. 87, p. 1255-1272 (2003).

Bizarro, P. Upper Shuaiba fractured reservoir characterization of Lekhwair cluster, *Petroleum Development Oman, Internal Report* DSC2/05/017N (2005).

Boadu, F. and Long, L. The fractal character of fracture spacing, *Journal of Rock Mechanics Mining Science & Geo-chemistry,* vol. 31, p. 127-134 (1994).

Boerrigter, P., Pingo-Almeida, M., Rodriquez, A. and Janssen, L. Natih oil rim lowering study - dynamic modelling report, *Shell EP Technology Report* EP5020 (2004).

Bourbiaux, B., Basquet, R., Daniel, J., Hu, L., Jenni S., Lange, A. and Rasolofosaon, P. Fractured reservoirs modelling- a review of the challenges and some recent solutions, *First Break,* vol. 23 (September 2005).

Caine, J., Evans, J. and Forster, C. Fault zone architecture and permeability structure, *Geological Society of America Journal,* vol. 24, p. 1025-1028 (1996).

Couples, G. and Lewis, H. Strain partitioning during flexural-slip folding, *Geological Society of London*, *Special Publications,* No. 127, p. 149-165 (1998).

Couples, G., Stearns, D. and Handin, J. Kinematics of experimental forced folds and their relevance to cross-section balancing, *Tectonophysics,* vol. 233, p. 193-213 (1994).

Da-lil, G., Xiao-hui, Z., Jin-zhou, Z. and Ci-qun, L. Model and method of well test analysis for wells with vertical fracture, *Applied Mathematics and Mechanics*, vol. 26, p. 571-578 (2005).

De Keijzer, M., and al Dhahab, S. Fahud field fracture characterization, part of Fahud field development plan, *Shell EP Technology, Internal Report* (2004).

De Keijzer, M. and Richard P. Qarn Alam field fracture study, *Shell EP Technology Report* EP5746 (2000).

De Keijzer, M., Hilgartner, H., Rawnsley, K., Al Dhahab, S., Heesbeen, B., Taberner, C., Rejas, M., Esteban, M. and Alfonso, P. North Oman fault and fracture exposed - Jebel Madmar study, *Shell EP Technology Report* EP-5401/5402/5403/5404/5405 (2004).

Droste, H. Shuaiba asset study 2002 & 2003 sequence stratigraphy framework, *Shell EP Technology Report* EP5272 (2003).

Droste, H. and van Steenwinkel, M. Stratal geometries and patterns of platform carbonates - the Cretaceous of Oman, *AAPG Memoir* 81, p. 185-206 (2004).

Droste, H., Richard, P., Al Dhahab, S., Wagner, P. and Ochs, S. North Oman Shuaiba regional synthesis, *Shell EP Technology Report* 5473(2004).

Engelder, T. and Peacock, D. Joint development normal to regional compression during flexural-flow folding - the Lilstock buttress anticline Somerset England, *Journal of Structural Geology,* vol. 23, p 259-277 (2001).

Everts, A. and Leinster, R. Fractured carbonate reservoirs modelling of Lekhwair field north Oman, *Shell EP Technology Report* SIEP5015 (1997).

Fachri, M. Fault-related fracture characterizations - A quantitative approach in naturally fractured reservoir characterization, *Proceedings of Indonesian Petroleum Association 28th Annual Convention and Exhibition* (2001).

Filbrandt, J. , Al Dhahab, S. , Al Habsy, A., Harris, K., Keating, J., Mahruqi, S., Ozkaya, S., Richard, P. and Robertson, T. Kinematics interpretation and structural evolution of north Oman Block 6 since the Late Cretaceous and implications for timing of hydrocarbon migration into Cretaceous reservoirs, *Geo-Arabia,* vol. 11, p. 97-140 (2006).

Fleming, C., Couples, G. and Haszeldine, R. Thermal effects of fluid flow in steep fault zones, *Geological Society of London Special Publications,* vol. 147, p. 217-229 (1998).

Frese, D. Ghaba North petrophysics status and handover, *Shell EP Technology Report* EP5254 (2006).

Geo-Mechanics International, Provision of in situ stress magnitude interpretation and modelling services, *Petroleum Development Oman, Internal Report* (2004).

Georgia State University website, Fracture intensity termination interconnectivity, in http://www2.gsu.edu/~geohab/courses/Geol%204008-6008/1%20Lectures%20-%20Powerpoint%20slides/11-20Fracture%20Intensity%20termination%20interconnectivity.ppt

Gibson, A., Al Kaioumi, Q. and El-Amin, A. An assessment of natural fracturing in the Thamama Formation by reservoir surveillance, *SPE 25628* (1993).

Gillespie, P., Howard, C., Walsh, J. and Watterson, J. Measurement and characterization of spatial distributions of fractures, *Tectonophysics,* vol. 226, p. 113-141(1993).

Glennie, K., Boeuf, M., Hughes-Clarke, M., Moody-Stuart, M., Pilaar, W. and Reinhart B. Geology of the Oman Mountains, *Verhandelingen Koninklijke Nederland Geologisch Mijnbouwkundig Genootschap,* vol. 31, pp. 423 (1974).

Gross, M., Bahat, D. and Becker, A. Relations between jointing and faulting based on fracture-spacing ratios and fault-slip profiles - A new method to estimate strain in layered rocks, *Geology,* vol.25, p. 887-890 (1997).

Haiqing, W. and Pollard, D. An experimental study of the relationship between joint spacing and layer thickness, *Journal of Structural Geology,* vol. 17, p. 887 -905 (1995).

Harwijanto, J. Seismic evaluation report Al Ghubar and Ghaba North Fields, Oman, *Shell EP Technology Report* EP5459 (2005).

Hasiuk, F. and Lohmann, K. Mississippian Paleo-ocean chemistry from biotic and abiotic carbonate Muleshoe Mound, Lake Valley Formation New Mexico, *Journal of Sedimentary Research,* vol. 78, p. 147-164 (2008).

Heber, C. Well test analysis for naturally fractured reservoirs, *JPT SPE 31162* (1996).

Heesbeen, B. Semi-quantitative fracture analysis Shuaiba Formation Jabal Madar, Oman, *Vrije Universiteit Amsterdam unpublished report* 1110926 (2002).

Hickman, S. and Zoback, M. The interpretation of hydraulic fracturing pressure-time data from in-situ stress determination in hydraulic fracturing stress measurements, *National Academy Press Washington*, p. 44-54 (1983).

Hitchings, V. and Potters, H. Production and geological implications of the Natih 9C3D seismic survey, *Geo-Arabia*, vol. 5, No. 4 (2000).

Hoogerduijn Strating, E. The present-day stress for the fields in central Oman, *Petroleum Development Oman, Internal Note for File* OQP/02/025NFF (2002).

Hughes Clarke, M. Stratigraphy and rock unit nomenclature in the oil-producing area of interior Oman, *Journal of Petroleum Geology,* vol. 11, p. 441-456 (1988).

IFP. Fractured reservoirs simulation and modelling Part I introduction on fractures, *Internal IFP training course material* (2004).

Immenhaauser, A., Hillgartner, H., Bertotti, G., Schoepfer, P., Homewood, P., Vahrenkamp, V., Steuber, T., Masse, J., Droste, H., van Koppen, J., van der Kooij, B., van Bentum, E., Verwer, K., Hoogerduijn Strating, E., Swinkels, W., Peters, J., Immenhauser-Potthast, I. and Al Maskery, S. Barremian-lower Aptian Qishn Formation of the Haushi-Huqf area, Oman, a new outcrop analogue for the Kharaib/Shuaiba reservoirs, *Geo-Arabia,* vol. 9, p. 153-212 (2004).

Ita, J. and Richard, P. Ghaba North Shuaiba subsurface study, *Shell EPT and Petroleum Development Oman, Internal Report* (2002).

Johson, C., Al Minhali, S., Bin Sumaidaa, S., Sabin, B. and West, B. Structural style and tectonic evaluation of onshore and offshore Abu Dhabi, *UAE IPTC* 10646 (2006).

Jones, C. and Loosveld, R. Extensional fractures in the Natih field and Salakh Arch, Oman - comparison of surface and subsurface, *Shell EP Technology Report* RKGR 94.126 (1994).

Joshi, S. Horizontal Well Technology, *PennWell Pub. Co. Tulsa, USA*, 535 pp (1991).

Kazemi, H., Merrill, J., Porterfield, K. and Zeman, P. Numerical simulation of water-oil flow in naturally fractured reservoirs, *SPE Journal,* vol. 16, p. 317-326 (1976).

Kindi, M. Structural evolution and fracture pattern of Salakh Arch, *University of Leeds School of Earth and Environment,* PhD thesis (September 2006).

Konijnenburg, J., Kraaijveld, M. and Mauduit, T. Al Ghubar asset study report, Part 4 geology and static model of the Al Ghubar Natih E reservoir, *Shell EP Technology Report* SIEP5804 (1999).

Konning, M. Structural framework building with VOICE workflows - application in the Yibal field, Oman, *Shell EP Technology Report* EP5223 (2004).

La Pointe, P. A method to characterize fracture density and connectivity through fractal geometry, *Int. Journal of Rock Mech. Min. Sci. Gemech*, Abstract 25, p 421-429 (1988).

Laurence, R., Brown, C., Cleneay, G., Cocksworth, K., Grondin, C., Hsu, G., Janssen, R., Nelson, J., Noe, J. and O'Bannon, P. Al Huwaisah historical well performance and fracture investigation, *Shell EP Technology Report* (2002).

Leckenby, R., Sanderson, D., and Lonergan, L. Estimating flow heterogeneity in natural fracture systems, *Journal of Volcanology and Geothermal Research,* vol. 148, p. 116-129 (October 2005).

Lee, G. The geology and tectonics of Oman and parts of south eastern Arabia, *Quarterly Journal of the Geological Society London*, vol. 84, p. 585-670 (1928).

Lekhwair A North subsurface team, Field strategy note for Lekhwair A North field, *Petroleum Development Oman, Internal Report* (2005).

Li, Z., and Sun, Z. Criterion for mixed mode fracture initiation of rock, *Journal Cent. South Inst. Min. Metal*, vol. 19, No. 4 (1988).

Loosveld, R., Bell, A. and Terken, J. The tectonic evolution of interior Oman, *Geo-Arabia*, vol. 1, p. 28–51 (1996).

Lorenz, J., Teufel, L. and Warpinski, N. Regional fractures - a mechanism for the formation of regional fractures at depth in flat-lying reservoirs, *AAPG Bulletin*, vol. 75 p. 1714 (1991)

Mark, R., Frank, T. and Andres, M. Early diagenetic controls on porosity distribution in a carbonate mound, *AAPG Bulletin,* vol. 9, p. xxx (2007).

Marzouk, I. and Sattar, M. Implication of wrench tectonics on hydrocarbon reservoir, UAE, *SPE 25608* (1993).

Mercadier, C. and Makel, G. Fracture pattern of Natih outcrops at Jebels Nihayda, Qusaybah and Salakh, north Oman, relevance to the Natih field and development implication, *Petroleum Development Oman Internal Report* PE/89/181(1989).

Montenat, C., Barrier, P. and Soudet, H. Aptian faulting in the Haushi-Huqf Oman and the tectonic evolution of the southeast Arabian platform-margin, *Geo-Arabia*, vol. 8, No. 4 (2003).

Narr, W. Estimating average fracture spacing in subsurface rock, *AAPG Bulletin*, vol.80, p. 1565-1586 (1996).

Nelson, R. Geologic Analysis of Naturally Fractured Reservoirs, *Gulf Professional Publishing Butterworth-Heinemann, Houston*, 332 pp (2001).

Nelson, R. Natural fracture quantification and visualization leading to discrete fracture modelling in the Lekhwair/Dhulaima cluster area, north Oman, *Shell EP Technology Report* EP3200 (2004).

Nelson, R. Natural fracture system description and classification, *AAPG Bulletin*, vol. 63, p. 2214-2232 (1979).

Nicholls, C. Shuaiba asset study 2002 & 2003 summary of carbonate research status on Shuaiba, *Shell EP Technology Report* EP5271 (2003).

Ochs, S., Taylor, P. and al Kindy, S. A fresh look at north Oman's charge history & fluid distribution, *Petroleum Development Oman Exploration Geo-Solution Team Internal Presentation* (2004).

Olson, J. Sublinear scaling of fracture aperture versus length - An exception or the rule, *Journal of Geophysical Research*, vol. 108, p. 2413-2426 (2003).

Ozkaya, I. Yibal BHI review fracture study, *Baker Atlas Report of Service Project for Petroleum Development Oman* (2003).

Ozkaya, I., Swindells, E. and Ghezai, Y. Fracture analysis from borehole image logs of Musallim field, *Baker Atlas Report of Service Project for Petroleum Development Oman* (2004).

Peters, J., Filbrandt, J., Grotzinger, J., Newall, N., Shuster, M. and Al-Siyabi, H. Surface-piercing salt domes of interior north Oman and their significance for the Ara carbonate stringer hydrocarbon play, *Geo-Arabia,* vol. 8, No. 2 (2003).

Poyser, L., Pöppelreiter, M., Talbott, C., Tsin, B., van Alebeek, H., Anson, G., Sumrow, M., Nelson, R., Clay, H., Wigley, P., Moranville, M. and Pelechaty, S. Lekhwair South field development plan, *Shell EP Technology Report* EP3201 (2005).

Price, S. Al Ghubar field development plan, *Shell and Petroleum Development Oman Internal report* (2008).

Price, S. Ghaba North Shuaiba field development plan, *Shell and Petroleum Development Oman Internal Report* (2008).

Raffensberger, J. Numerical simulation of basin-scale hydro-chemical processes, in *Advances in Porous Media, Elsevier,* vol. 3, p. 185–305 (1996).

Rao, Q., Sun, Z., Stephanssson, O., Li, C., and Stillborg, B. Shear fracture (Mode II) of brittle rock, *International Journal of Rock Mechanics and Mining Sciences,* vol. 40, p. 355-375(2003).

Rawnsley, K, de Keijzer, M, Wei, L., Bettembourg, S., Asyee, W., Massaferro, J., Swaby, P., Drysdale, D. and Boettcher, D. Characterizing fracture and matrix heterogeneities in tight gas fields, *World Oil Magazine,* vol. 228, No. 10 (2007).

Rawnsley, K. Fault and fracture characterization of the Natih E Fahud Field Oman - Part 5 of Fahud asset study, *Shell EP Technology Report* EP5612 (2001).

Rawnsley, K. and Al Dhahab, S. Qarn Alam steam fracture service project - QA reservoir 3D fracture modelling, *Shell EP Technology Report* EP5327 (2005).

Richard, P. Burhaan NW field fracture modelling, *Petroleum Development Oman Internal Report*, live link document (2003).

Richard, P. North Oman salt diapers - Fault interpretation and kinematics model, *Petroleum Development Oman Exploration Internal Note for File* No.199 (November 1997).

Richard, P. Sand box model for Ghaba North and an analogue field offshore UAE, Image from *Shell –PDO sandbox model illustrations* personal communication (2007).

Richard, P., Al Dhahab, S. and Bettembourg S. Saih Rawl field fracture modelling, *Petroleum Development Oman Internal Report*, live link document (2003).

Richard, P., Al Dhahab, S., Hillgartner, H., de Keijzer, M. and Bettembourg, S. Qarn Alam steam fracture service Qarn Alam sequence stratigraphy and fracture analysis, statistical analysis, *Shell EP Technology Report* EP5336 (2004).

Roeterdink, R. Natih field oil rim lowering study - fracture characterization, *Shell EP Technology Report* EP5013 (2004).

Rohrbaugh, M., Mauldon, M. and Dunne, W. Estimating fractures trace intensity, density, and mean length using circular scan lines and windows, *AAPG Bulletin,* vol. 86, p 2089–2104 (2002).

Sarma, P. and Aziz, K. New transfer functions for simulation of naturally fractured reservoirs with dual-porosity models, *SPE 90231*(2006).

Sattler, U., Immenhauser, A., Hillgartner, H. and Esteban, M. Characterization, lateral variability and lateral extent of discontinuity surfaces on a carbonate platform - Barremian to Lower Aptian, Oman, *Journal of Sedimentology*, vol. 52, p. 339-361 (2005).

Sims, D., Morris, A., Ferrill, D., Wyrick, D., Tamura, Y. and Takanashi, M. Simulation of fault patterns of offshore oil fields of the Arabian Gulf, *AAPG Annual Convention Abstracts,* vol. 14, p. A129-44 (2005).

Sirat, M., Salman, S., and Bellah, S. Fracture mechanism and fracture system analysis of fractured carbonate reservoir from Abu Dhabi, UAE, *SPE 111397* (2007).

Stofferis, M. Well test analysis of Lekhwair field, *Petroleum Development Oman Note for File* APY/91/011R -EP91-1505 (1991).

Stuart-Smith, P. and Romine, K. Integrated potential field interpretation of the tectono-stratigraphy of Oman, *SRK Consulting Report for Petroleum Development Oman*, SRK code PO701 (2003).

Stuart-Smith, P., Romine, K., Aitken, R., Archer, J. and Fryberger, S. North Oman Haima-Huqf tectono-stratigraphy study - Part 1, *SRK- Badley Ashton Consulting report for Petroleum Development Oman*, SRK cod PO704 (2004).

Terken, J. The Natih Petroleum System of north Oman, *Geo-Arabia*, vol. 41, p. 157-180 (1999).

Terzaghi, R. Sources of error in joint surveys, *Geotechnique*, vol.15, p. 287–304 (1965).

Tiab, D., Igbokoyi, A., and Restrepo, D. Fracture porosity from pressure transient data, *SPE – IPTC* 11164 (2007).

Tindall, S. and Davis, G. Joint spacing and distribution in deformation band shear zones, *Geol. Mag. Cambridge University Press*, No. 140/1, p.1-9 (2003).

Vahrenkamp, V, al Kharusi, L. and al Maamari, M. Review of the deposition and diagenesis of the Shuaiba Formation at Qarn Alam field, *Petroleum Development Oman Internal Note for File* OQP/01/002R (November 2000).

Van Buchem, F., Razin, P., Homewood, P., Oterdoom, H. and Philip, J. Stratigraphic organisation of carbonate ramps and organic-rich intra-shelf basins - Natih Formation middle Cretaceous, *AAPG Bulletin*, vol. 86, p. 21-54 (2002).

Warrlich, G. and Richard, P. Fracture characterization and conceptual model development, Musallim field, *Shell EP Technology Report* EP5392 (2004).

Wilkins, S., Gross, M., Wacker, M., Eyal, Y. and Engelder, T. Faulted joints - kinematics displacement, length scaling relations and criteria for their identification, *Journal of Structural Geology*, vol. 23, p. 315-327 (2001).

Williams, P., Maddock, R., Sapru, A. and Lawrence, M. Analysis of a fractured carbonate reservoir of Thamama Group using borehole images from horizontal well, offshore UAE, *SPE* 87303 (2000).

Yaarubi, M. Recent breakthrough in Lekhwair cluster seismic fault interpretation, *Petroleum Development Oman Lekhwair Subsurface Team Internal Presentation* (2006).

Yang, D. Experimental study on fracture initiation by pressure pulses, *SPE* 63035 (2000).

Zellou, A., Hartley, L., Hoogerduijn-Strating, E., Al Dhahab, S., Boom, W. and Hadrami, F. Integrated workflow applied to the characterization of a carbonate fractured reservoir, Qarn Alam field, Oman, *SPE* 81579-MS (2003).